

IAEA-TECDOC-697

# ***Fission gas release and fuel rod chemistry related to extended burnup***

*Proceedings of a Technical Committee Meeting  
held in Pembroke, Ontario, Canada, 28 April–1 May 1992*



INTERNATIONAL ATOMIC ENERGY AGENCY

IAEA

FISSION GAS RELEASE AND FUEL ROD CHEMISTRY  
RELATED TO EXTENDED BURNUP  
IAEA, VIENNA, 1993  
IAEA-TECDOC-697  
ISSN 1011-4289

Printed by the IAEA in Austria  
April 1993

**PLEASE BE AWARE THAT  
ALL OF THE MISSING PAGES IN THIS DOCUMENT  
WERE ORIGINALLY BLANK**

## FOREWORD

At the invitation of the Government of Canada, the Technical Committee Meeting on Fission Gas Release and Fuel Rod Chemistry Related to Extended Burnup was held in Pembroke, from 28 April to 1 May 1992. It was jointly organized by the International Atomic Energy Agency and the Atomic Energy of Canada Limited (AECL) and included a technical visit to Chalk River Laboratories.

Fifty-five participants from 16 countries and one international organization attended the meeting. These proceedings contain the 28 papers presented in five sessions as well as summaries of the sessions and recommendations prepared by the participants.

The purpose of the meeting was to review the state of the art in fission gas release and fuel rod chemistry related to extended burnup. Previous IAEA meetings on this topic were held in Erlangen and Karlsruhe (Germany) in 1979 and 1985 respectively, and in Preston (United Kingdom) in 1988.

To determine progress in the area of fuel behaviour, it was instructive to look back to the Technical Committee Meeting on Water Reactor Fuel Element Computer Modelling in Steady State, Transient and Accident Conditions held in Preston in 1988 (IWGFPT/32). The topics covered at that meeting were:

- Transient fission gas release (FGR),
- Axial gas mixing,
- Degradation of  $\text{UO}_2$  thermal conductivity,
- Enhancement of fission gas diffusion co-efficient, and
- Chemistry effects.

In the summary of the Preston meeting it was said: "It is clear that we are some way off a mechanistic model for FGR", and "the processes involved are complex and improperly understood."

Important recommendations were made on the following aspects:

- The "right" level of complexity in fuel codes;
- The ability to simulate in-reactor data with out-reactor tests;
- The necessity for specialized microstructural examination of irradiated  $\text{UO}_2$ ;
- "Single effects" tests to quantify chemical effects; and
- Generate data from instrumental out-reactor tests to establish degradation of  $\text{UO}_2$  thermal conductivity.

The present meeting was held at a time when several national and international programmes on water reactor fuel irradiated in experimental reactors were still ongoing or had reached their conclusion (e.g. AECL, Risø, Halden) and when lead test assemblies had reached high burnup in power reactors and been examined. At the same time, several out-of-pile experiments on high burnup fuel or with simulated fuel were being carried out. As a result, significant progress has been registered since the last meeting, particularly in the evaluation of fuel temperature, the degradation of the global thermal conductivity with burnup and in the understanding of the impact on fission gas release. This was due largely to important developments in programmes carried out at national and international levels.

The IAEA wishes to express its gratitude to Dr. R. Hatcher, President and Chief Executive Officer of AECL, and to the local organizing committee for their support and to the session chairmen and all participants for their contributions.

## **EDITORIAL NOTE**

*In preparing this material for the press, staff of the International Atomic Energy Agency have mounted and paginated the original manuscripts as submitted by the authors and given some attention to the presentation.*

*The views expressed in the papers, the statements made and the general style adopted are the responsibility of the named authors. The views do not necessarily reflect those of the governments of the Member States or organizations under whose auspices the manuscripts were produced.*

*The use in this book of particular designations of countries or territories does not imply any judgement by the publisher, the IAEA, as to the legal status of such countries or territories, of their authorities and institutions or of the delimitation of their boundaries.*

*The mention of specific companies or of their products or brand names does not imply any endorsement or recommendation on the part of the IAEA.*

*Authors are themselves responsible for obtaining the necessary permission to reproduce copyright material from other sources.*

## CONTENTS

Summary of the Technical Committee Meeting .....	7
Opening address: The energy dilemma .....	19
<i>S.R. Hatcher</i>	
<b>EXPERIMENTAL I (Session 1)</b>	
Fission gas release and fuel temperature during power transients in water reactor fuel at extended burnup .....	25
<i>P. Knudsen, C. Bagger, M. Mogensen, H. Toftegaard</i>	
Fission gas release below 20 kWm <sup>-1</sup> in transient tested water reactor fuel at extended burnup .....	32
<i>M. Mogensen, C. Bagger, H. Toftegaard, P. Knudsen, C.T. Walker</i>	
Experimental assessment of a temperature threshold for thermally induced fission gas release in transient tested water reactor fuel with extended burnup .....	38
<i>C. Bagger, M. Mogensen</i>	
Fission gas release behavior of high burnup fuels during power ramp tests .....	44
<i>T. Aoki, S. Koizumi, H. Umehara, K. Ogata</i>	
Fission-gas release in fuel performing to extended burnups in Ontario Hydro nuclear generating stations .....	53
<i>M.R. Floyd, J. Novak, P.T. Truant</i>	
<b>EXPERIMENTAL II (Session 2)</b>	
Fission gas release of high burnup fuel .....	63
<i>R. Manzel, R.P. Bodmer, G. Bart</i>	
Fission gas release enhancement at extended burnup: Experimental evidence from French PWR irradiation .....	68
<i>C. Forat, B. Blanpain, B. Kapusta, P. Guedeney, P. Permezel</i>	
The effect of fuel pellet variants on fission gas release following power ramps .....	75
<i>D.A. Howl, I.R. Topliss</i>	
FP gas release behaviour of high burn-up MOX fuels for thermal reactors .....	82
<i>K. Kamimura</i>	
<b>FUEL ROD CHEMISTRY AND RELATED PROPERTIES (Session 3)</b>	
Fission gas release from high burnup PWR fuels under transient conditions .....	91
<i>H. Kanazawa, H. Sasajima, K. Homma, K. Ichise, T. Fujishiro, T. Yamahara</i>	
Fission product behaviour and fuel rod chemistry at extended burnup: Results, models and programmes of analytical experiments carried out at the CEA, Grenoble .....	98
<i>M. Charles, L. Caillot, P. Dehaudt, C. Lemaignan</i>	
Impact of systematic stoichiometry differences among BWR rods on fission gas release .....	103
<i>B. Grapengiesser, D. Schrire</i>	
Rim effect observations from the third Risø fission gas project .....	111
<i>N. Kjaer-Pedersen</i>	
Experimental techniques and results related to high burn-up investigations at the OECD Halden Reactor Project .....	118
<i>W. Wiesenack</i>	
Review of Studsvik's international fuel R&D projects .....	124
<i>M. Grounes, S. Djurle, G. Lysell, H. Mogard</i>	

Methodology of in-pile experiments including experimental studies of VVER-1000 refabricated fuels at the MIR research reactor .....	130
<i>Yu.K. Bibilashvili, A.V. Grachev, V.V. Novikov, V.P. Smirnov, A.V. Smirnov</i>	
Some experimental results of investigations on the nuclide composition and burnup fraction of VVER-1000 standard fuel .....	133
<i>A.V. Smirnov, A.P. Chetverikov, V.V. Novikov, V.N. Proselkov</i>	

#### **MODELLING AND MODELLING SUPPORT I (Session 4)**

Hot cell fission gas release studies on UO <sub>2</sub> .....	145
<i>M. Coquerelle, D. Bottomley</i>	
Fission-product release kinetics from CANDU and LWR fuel during high-temperature steam oxidation experiments .....	153
<i>D.S. Cox, Z. Liu, P.H. Elder, C.E.L. Hunt, V.I. Arimescu</i>	
Thermal conductivity and gas release from SIMFUEL .....	165
<i>P.G. Lucuta, R.A. Verrall, H. Matzke, I.J. Hastings</i>	
Intergranular fission gas bubbles and solid precipitates in UO <sub>2</sub> irradiated at high burnup in various conditions .....	172
<i>M. Charles, G. Eminent, C. Lemaignan</i>	
FGR model improvement for high burnup fuel analysis .....	176
<i>K. Mori, H. Ikeda, N. Furuya</i>	
Modeling CANDU-type fuel behaviour during extended burnup irradiations using a revised version of the ELESIM code .....	183
<i>V.I. Arimescu, W.R. Richmond</i>	
Improvement of ELESIM CANDU fuel performance analysis code: Fission product gas release, fuel densification and neutron flux depression .....	193
<i>H.C.Suk, W. Hwang, B.G. Kim, K.S. Sim, Y.H. Heo</i>	

#### **MODELLING AND MODELLING SUPPORT II (Session 5)**

Evaluation of measured high burnup fuel temperature at Risø project phase 3 .....	205
<i>S. Kitajima, M. Kinoshita</i>	
A simple fission gas release/gaseous swelling model .....	211
<i>T. Kogai</i>	
An approach to modelling fuel behaviour using data from some international high burnup fuel programmes .....	219
<i>L-Å. Nordström, C. Ott</i>	
Fuel performance modeling of high burnup fuel .....	225
<i>S.H. Shann, L.F. van Swam</i>	
Discussion between S.H. Shann and M. Mogensen .....	231
List of Participants .....	233

# SUMMARY OF THE TECHNICAL COMMITTEE MEETING

## EXPERIMENTAL I

### Session 1

Chairmen: M. Coquerelle (CEC)  
H.C. Suk (Republic of Korea)

#### Summary

Improvements in fuel utilization have led to a growing interest in extending the burnup of thermal power reactors. Fission gas release (FGR) could be a life limiting factor under either steady irradiation conditions or moderate transient conditions. Incentives for a better understanding of the release mechanisms exist and various international or national programmes are targeting the influence of the different parameters which can play a role in FGR.

Three papers from Denmark (M. Mogensen et al.) reported on the Third Risø Fission Gas Project. This project aimed at continuous monitoring of FGR from  $\text{UO}_2$  during power transients ( $< 400 \text{ W/cm}$ ) conducted in the Risø reactor by irradiating prefabricated fuel rod segments instrumented with pressure transducers and thermocouples. Furthermore, a detailed study of the fuels before and after the power transients allows a correlation between FGR and fuel restructuring.

$\text{UO}_2$  fuel was supplied by American Nuclear Fuel (ANF) (42 MW.d/kg U, grain size =  $6 \mu\text{m}$ ), General Electric (GE) (15-44 W.d/kg U, 16-21  $\mu\text{m}$  grain size) and Risø (44-48 MW.d/kg U, 10  $\mu\text{m}$  grain size) and used for the transient tests. The major results can be summarized as follows:

- These transient tests allow a determination of FGR as a function of centreline fuel temperature and display the existence of a threshold temperature of about  $1200^\circ\text{C}$  at which fission gas release occurs. This onset temperature is independent of burnup;
- No grain size effect on FGR could be determined by comparing tests on fuels with increasing grain size and supplied by a same vendor (GE);
- An unexpected release was determined at low power transients (125-170 W/cm, ANF fuel); this result was confirmed by radiochemical analysis and could be explained by a release of gas contained in large pores (diameter 20-50  $\mu\text{m}$ );
- The results from the ANF fuel were attributed to a typical fuel structure.

T. Aoki (Japan) reported on the ramp behaviour of Zr-liner fuels, with emphasis on the correlation between fission gas release and pellet microstructural changes.

The fuels tested were of two different types, which were base-irradiated up to 20 and 40 GW.d/t U, respectively.

The power ramp tests were performed at the Japan Material Test Reactor (JMTR) and at the R2 reactor in Sweden: in JMTR, power was held for a maximum of four hours at a ramp terminal level of 60 W/cm maximum; in Sweden, power was

cycled between 220 and 440 W/cm, where the number of cycles was 100 and 1000. The accumulated hold time at ramp terminal level was 25 and 200 hours for the two types of test.

Experimental investigations show that the fission gas release is proportional to the ramp terminal level and also to the square root of the accumulated hold time at ramp terminal level. The following conclusions were drawn:

- (1) The power ramp fission gas release mechanism is essentially the same as the fission gas release from steady state fuel.
- (2) The two major control mechanisms are considered to be:
  - (a) The tunnel formation that depends on gas diffusion to the grain boundaries; growth and connection of the grain boundary bubbles;
  - (b) Gas diffusion from the grain after tunnel formation.
- (3) The tunnel formation process might be determined by the gas accumulation on grain boundaries. Therefore, the burnup dependency might appear in the fission gas release of power ramp tests.
- (4) Power cycling effect on FGR is expected to be small because of extended time operation.
- (5) A short time power increase, as in an abnormal transient, is not expected to induce additional FGR.

Mr. Floyd (Canada) reported on investigations on CANDU 37-element bundles irradiated in the Bruce NGS-A reactor. Stress corrosion cracking (SCC) related defects have been observed in ramped bundles having a burnup < 450 MW.h/kg U, and under steady-state conditions at higher burnup. Only a few bundles are involved. It was noted that graphite-based CANLUB coating decreases SCC susceptibility, but also seems to inhibit the inner surface of the sheath from acting as a getter for liberated oxygen. The retention of graphite CANLUB coating is greatly reduced above a burnup of 400 MW.d/kg U. Hence, guidelines are suggested for power ramping.

Extended burnup fission gas release was not predicted by low burnup fuel modelling code extrapolations. This is believed to be primarily due to a reduction in  $UO_2$  thermal conductivity, not accounted for in the models. The presence of solid fission products is at least in part responsible for this. More work needs to be concentrated on the possible onset of hyperstoichiometry and any possible link with CANLUB and sheath oxidation behaviour.

## Recommendations

Incentives for a better understanding of FGR mechanisms still exist and the interest in more detailed, sophisticated studies is growing. Future studies should focus on the following points:

- FGR determination on fuel rods irradiated at very high burnup (> 60 000 MW.d/t) should be envisaged;
- Determination of the thermal conductivity of irradiated  $UO_2$  for example, via thermal diffusivity, heat capacity, etc. must be carried out for high burnup;

- The chemical variations of irradiated  $\text{UO}_2$  must be analysed by means of hot-cell techniques (Knudsen cell, solid state chemistry, annealing techniques);
- The experimental determination of the fission gas retained in the rim must be carried out by means of methods other than emp or X ray fluorescence.

Additional effort needs to be concentrated on the possible onset of hyperstoichiometry (O/U ratio), and any possible link with graphite coating and sheath oxidation.

Developments and studies similar to those detailed above (particularly instrumented ramp tests) should be launched in the field of MOX fuel.

The influence of burnup on the threshold of FGR should be more precisely determined.

## EXPERIMENTAL II

### Session 2

Chairmen: M. Mogensen (Denmark)  
M. Yamawaki (Japan)

#### Summary

Participants from Germany and France reported on experience with high burnup lead test assemblies. R. Manzel (Germany) reported that fuel rods designed for high target burnups (high U-235 enrichment of 3.8 to 4.2%) and operated under realistically high power conditions to high burnups show higher FGR compared to the older, lower enriched standard rods. Under these high power conditions the initial fuel clad gap has a pronounced influence on FGR. This influence remains visible up to high burnup, but the difference in FGR due to the different initial gap decreases. Under high release conditions maximum fission gas release usually occurs at intermediate burnups with a tendency to saturation at high burnup.

C. Forat (France) reported that two families of 17 x 17 FRAGEMA assemblies were irradiated for 5 cycles in commercial PWRs; post-irradiation examinations performed on rods extracted after each cycle showed interesting features linked to the different power levels the two families experienced. Particularly, the evolution of the fuel microstructure made it possible to single out the contribution of the thermal process. The development of realistic "high burnup" models needs a correct evaluation of the thermal conductivity deterioration and the lowering of the gas release threshold as burnup proceeds.

D. Howl (United Kingdom) reported on on-line measurements of rod internal pressure following power ramps made on 12 rods containing different fuel pellet variants. The results confirmed the expected benefits from large grain fuel, including niobia-doped fuel, and from an annular pellet design. The increase of fission gas release following the ramp did not saturate within several hundred hours after the ramp, for all the fuel types tested. The ENIGMA code predicted well the magnitude and the kinetics of the release.

Y. Kamimura (Japan) reported on experience with MOX fuel. The fission gas release behaviour of MOX fuel rods to the high burnup level of 41 GW.d/t MOX (47 GW.d/tM) was analysed by the Power Reactor and Nuclear Fuel Development Corporation (PNC) with the irradiation test data of IFA-514/565 in the Halden reactor.

The following observations were made:

- (1) The Vitanza threshold for UO<sub>2</sub> fuel is applicable to predict the onset of significant fission gas release for not only solid but also hollow MOX fuel.
- (2) There was no significant difference in fission gas release between PNC MOX fuels and UO<sub>2</sub> fuel.
- (3) The fission gas release fraction from hollow pellets might have been smaller than that of solid pellets, according to the in-pile data.

## **Recommendations**

The participants support the already planned national and international programmes which will provide data, for example, on thermal conductivity degradation with increasing burnup. Data should be carefully analysed before undertaking any further programmes.

Additional work should be performed to determine the relationship between the temperature of onset of significant fission gas release and burnup, and, particularly, it should be extended to higher burnups.

In order to obtain more useable data on high burnup fuel (average of 60-70 MW.d/t U), experiments should be done with realistic powers and power histories (high linear power). The analysis of development of fuel microstructure and porosity should be emphasized.

# FUEL ROD CHEMISTRY AND RELATED PROPERTIES

## Session 3

Chairmen: D.A. Howl (U.K.)  
R. Manzel (Germany)

### Summary

H. Kanazawa and H. Sasajima (Japan) reported on tests on fission gas release (FGR) of high burnup PWR fuels, showing that rapid release occurred at temperatures ranging from 1800°C to 1900°C in the annealing test and in the RIA transient test. FGR was much higher than in normal reactor operation and FRAP-T6 code predictions.

Among analytical experiments carried out at the CEA, France (M. Charles), to study fuel behaviour at high burnups, special mention should be made of the study of the effects of moderate transients on fission gas release (importance of cracking associated with power variations), and SEM examination of fracture surface of various fuels (analysis of bubble populations and precipitates of associated metallic fission products).

Several factors must be considered when analysing the results: radial specific power profile and its thermal effect, fission gas creation, oxygen balance, density and open porosity, gaseous swelling. This paper describes the principle of various tools (calculations or experiments) used to obtain information on all these points.

Finally, a brief discussion is given of the study programmes relating to the effect of O/M ratio on fuel behaviour and to the major problem of caesium retention.

The paper by Grounes et al. (Sweden) gave a general review of Studsvik's international fuel R&D projects, which have produced many fission gas release data.

In Sweden, observations on BWR fuel (B. Grapengiesser) show that strict physical arguments suggest considerable scatter in material properties among BWR rods of similar burnup within an assembly. Improved modelling of FGR should result from introducing a stoichiometry-dependent diffusion enhancement factor. It would be valuable to strengthen the experimental support for the suggested O/M effects by appropriate PIE and irradiation experiments with strictly identical powers. The BWR assembly, if carefully characterized, can be looked upon as an interesting laboratory for materials of different properties, as O/M ratio automatically varies among rods at high burnup.

The paper on modelling of H. Kjaer-Pedersen (USA), had the objective to understand and model the "squared" temperature profile in the Risø experiments. As a result, a new porosity and burnup dependent expression for UO<sub>2</sub> thermal conductivity, emphasizing "rim porosity", which reasonably predicts the squared temperature profile, was produced. A separation of the "rim effect" from the "regular" burnup effect, will allow benchmarking at 45 MW.d/kg U of the burnup dependency in general.

The paper from Norway (W. Wiesenack) gave an overview on sensors, re-instrumentation techniques and irradiation rigs that have been developed and applied at the Halden Project, allowing tests to be conducted at extended burnup with high data quality. The Halden fission gas release threshold gives good predictions of FGR onset also at high burnup. Evaluations of temperature data point to a UO<sub>2</sub> conductivity degradation effect of about 35% at 50 MWd/kg UO<sub>2</sub> and 600°C.

A paper on a programme of full-scale investigations of WWER-1000 fuel assemblies to determine nuclide composition by mass spectrometry and radiochemical methods, and fission product distribution over the length and radius of the fuel was given by A.V. Smirnov and V.N. Proselkov (Russian Federation). Fuel assemblies from Novo-Voronezh Nuclear Power Plant and South-Ukrainian NPP were investigated after burnups of 45 MW.d/kg U and ~37 MW.d/kg U. A dependence of Cs-137, Cs-134, Nd-145 and Nd-146 accumulation was shown with burnup. Analysis of the distribution of Pu-isotopes resulted in the conclusion suggesting a similarity of operating conditions along the fuel rod length.

## **Recommendations**

Heat conductance through the pellets needs further investigation, taking into account, for example, the effect of:

- degradation of thermal conductivity due to accumulation of fission products;
- O/M changes (integral and locally);
- the influence of porosity developed during irradiation at the pellet rim, and
- micro-and macro-cracking.

This addresses the need to predict radial temperature profiles inferred from work reported in Session 1.

Experimental techniques are available to at least study the overall influence of these effects, and it is suggested to apply these techniques to high burnup fuel.

International programmes have greatly contributed to an understanding of ramping behaviour and it may be considered to extend these programmes to higher burnup.

# MODELLING AND MODELLING SUPPORT I

## Session 4

Chairmen: M. Grounes (Sweden)  
N. Kjaer-Pedersen (USA)

### Summary

The session consisted of 7 papers, three experimental ("modelling support"), one "physical modelling", and three strictly modelling papers.

The experimental papers by M. Coquerelle (CEC), D.S. Cox (Canada) and M. Charles (France) contributed to the effect on gas release of burnup, grain size, and oxygen potential. They unanimously concluded that increasing burnup lowers the temperature threshold for gas release. Increasing oxygen potential has the same effect, possibly due to an increase in the diffusion coefficient. Increasing grain size in itself tends to lower the level of gas release, but may increase intergranular swelling. However, the structure of the grain boundaries may provide a separate parameter for fuel characterization. This parameter, when varied, may override the effect of a varying grain size. The grain structure determines the nature of the network of tunnels that may form along the grain edges, providing the ultimate escape path for the fission gas. The tunnels are formed by grain boundary bubbles that diffuse along the grain surfaces to the grain edges and finally into larger bubbles. Coalescence and tunnel formation occurs at about 1400-1500 °C.

The paper on SIMFUEL, by P.G. Lucuta (Canada), presented an out-of-pile method of measuring thermal conductivity at high burnup. The burnup is simulated by built-in inventories of solid elements that occur dominantly as fission products. The method shows good potential for expanding the data-base or burnup degraded thermal conductivity. However, the method needs to be benchmarked against the high burnup data.

Modelling: Papers presented by K. Mori (Japan), W.R. Richmond (Canada) and H.C. Suk (Republic of Korea), dealt with improvements to existing models in the areas of gas release and thermal conductivity. The primary effect elected for modelling improvement was the "second stage" of gas release, i.e., the boundary stage. Studies of bubble configurations on the grain boundaries show potential for improved predictions.

### Recommendations

The session concludes that the influence of burnup, oxygen potential and grain size on fission gas release and fuel swelling should be the subject of further investigations and modelling. The second stage of the gas release mechanism in (the grain boundary configuration, bubble coalescence, tunnelling, etc.) is particularly important.

All too often in this field experimentalists and computer modellers are unaware of each other's work. Significant progress could be made if these two groups were brought together in the same forum. Consequently, the session recommended that future activities in the field should involve both experimentalists and computer modellers whenever possible.

## MODELLING AND MODELLING SUPPORT II

### Session 5

Chairmen: M. Charles (France)  
F. Iglesias (Canada)

#### Summary

A thermal conductivity degradation model was presented by S. Kitajima (Japan). It combines the effects of microgaps and fission products in solid solution. The model successfully predicts the high burnup fuel temperature and the dynamic temperature variation of the Risø project phase 3.

A simple fission gas release/gaseous swelling model has been developed in Japan (T. Kogai). The model's feature lies in the treatment of gas release from the grain boundary to the rod free volume. The model considers a hypothetical tube, in which gas atoms flow. The gas flow conductance of the tube is a function of the bubble radius and the tensile stress in pellet. The former describes the steady-state release with bubble interlinkage, and the latter describes the abrupt gas release resulting from a transient. Both mechanisms compete, and the model is able to simulate both steady-state and transient releases.

Well defined fuel rod tests from the international research programmes, Tribulation and HBEP, were used by L.A. Nordstroem (Switzerland), for verification and validation of different FGR models, implemented in the TRANSURANUS fuel behaviour code. In a first phase, the model parameters were adjusted in order to reproduce the measured EOL clad dimensional changes. The agreement was very good. The experimental FGR was then compared with the values predicted by the URGAS (TRANSURANUS standard), Halden Threshold and a FRAMATOME model. A significant discrepancy was found not only between the different models but also with the measured fission gas release values. The results were discussed and some conclusions on the use of these models for high burnups were drawn.

It was shown by S.H. Shann (USA) that, with modifications of fuel thermal conductivity, rim effect and fission gas release models, the application range of a fuel performance code has been extended to high burnup. Various aspects of the code were validated with HBEP data. The validation results indicated that the modified code accurately accounted for the rim effect and fission gas release to high burnup.

#### Recommendations

The consensus of the participants was that meetings like this one in which both experimental results and computer models are combined are very important. In addition, specific points were highlighted:

- (1) More information is necessary concerning fabrication irradiation and post-irradiation details for the experiments used in the database.
- (2) The uncertainties associated with the results should be given whenever possible.

(3) Additional data are required on:

- (a) Fuel temperature. Temperature measurements on fuel with simple power histories. Radial temperature profile data;
- (b) Measurements as a function of burnup of fuel thermal conductivity, thermal diffusivity, specific heat;
- (c) Fuel stoichiometry as a function of fuel radius and burnup;
- (d) Fuel microstructural changes at high burnup including porosity, micro-cracking, rim effect;
- (e) Measurements of releases of radioactive isotopes in addition to the stable gases, to provide licensing data, and to elucidate the timing and mechanism of release.

## CONCLUSIONS AND RECOMMENDATIONS

I.J. Hastings (Chairman of Meeting)  
P. Chantoin (Scientific Secretary)

### CONCLUSIONS

In advance of this meeting, fission gas release and fuel chemistry were identified as important factors in determining high burnup fuel behaviour, and the ability to improve prediction of such fuel behaviour through refined modelling and further development of calculational methods were key points. These items will assist safety of reactor operations and contribute to licensing procedures. However, the models require the establishment of reliable databases, and these, in turn, need well grounded programmes in research reactors and in the laboratory.

Participants acknowledged the progress made in the evaluation of fuel temperature, degradation of the global thermal conductivity with burnup and an understanding of the impact on fission gas release. This progress was due largely to the strong development of national and international parametric studies and to examination of high burnup lead test assemblies.

### RECOMMENDATIONS

Further needs exist to explore the area of even higher burnup fuel with realistic linear power rates and histories, and to accumulate additional macroscopic observations and improved mechanistic understanding of FGR associated with the thermal behaviour of the fuel and burnup.

For **macroscopic** observations, we need additional observations on:

- (a) Onset of FGR at high burnup, dependent on temperature and burnup.
- (b) Well characterized experiments to determine the degradation of global thermal conductivity, and its evolution when burnup increases.

Instrumented ramp tests with good characterization of the base pre-and post-ramp state may still be justified, particularly in the area of MOX fuel.

In the area of **mechanistic understanding** further needs have been identified in the following areas:

- (a) Experimental determination of fuel thermal conductivity, thermal diffusivity and thermal capacity of irradiated fuel, as a function of burnup;
- (b) Chemical evolution of the fuel with burnup (fission product evolution, stoichiometry, etc.), especially evolution of the grain boundary structure;
- (c) O/M variation with burnup, influence on diffusion, cladding oxidation and, in the case of CANDU fuel, on the graphite coating;
- (d) Confirmation and quantification of the importance of the "thermal" process of FGR;

- (e) Formation mechanism, kinetics and influence on properties of porosity observed in the fuel rim ("rim effect");
- (f) Confirmation of the influence of grain size and/or the fabrication "process" on FGR.

It was stressed that MOX fuel should be studied in the same way as UO<sub>2</sub> fuel, to confirm similarities and differences in behaviour.

The FUMEX co-ordinated research programme, developed by the IAEA has many components that satisfy the recommendations that evolved from this meeting. FUMEX will contribute substantially to increasing the understanding of the processes involved in fuel behaviour and modelling.

## Opening address

### THE ENERGY DILEMMA

S.R. HATCHER

President and Chief Executive Officer,  
Atomic Energy of Canada Limited

During the past 50 years, there has been a remarkable increase in the availability of energy to fuel economic and industrial growth. The question that I want to address with you tonight is "How much energy will be needed in the future, and how will it be generated?". The answer has immense implications for the environmental well-being of the globe and presents us with the "dilemma" of my title. Huge energy demands on the one hand. Concerns about a healthy environment on the other hand. Let's look at the size of the global challenge.

The developed nations have a collective population of about 1.1 billion people. According to the United Nations, that population is projected to rise to approximately 1.9 billion by the middle of the next century. The developing nations, by contrast, have a collective population of about 4.4 billion people. By the middle of next century, that population is projected to rise to approximately 9.5 billion. These projections of a doubling of world population to 11.4 billion have staggering implications. For example, the massive growth in population is projected to occur mainly in those countries where the average per capita energy consumption is about one fifth that of the developed countries and many are one tenth.

Now think about that in terms of economic and social sharing among the world's populations. In this global village of instant visual communication... the developing countries know exactly how we live. They want that way of life for themselves. And they will go for it by industrializing their economies as rapidly as they can. That means finding ample and reliable energy, particularly electricity. If 11.4 billion people used energy at the rate of the developed nations, global consumption would increase by a factor of about six, and that means a surge in global pollution.

Even if we have a heroic drive for energy efficiency and the developed nations cut their per capita consumption by a factor of two, and if that because the global standard, the world would consume two to three times as much energy as it does today.

Right now, there are four principal sources of energy. The biggest is fossil fuels. About 75 percent of the world's energy is supplied by burning coal, oil and natural gas. The second is... surprisingly... still wood, 15 percent of the world's total energy supply. In North America, by contrast, fuel wood makes up less than one percent of our energy usage. Next comes hydro-electricity at about five percent of the world's energy supply.

Finally, there is nuclear power. Nuclear power contributes almost five percent of the world's energy supply. There are 420 commercial nuclear reactors, with a further 76 under construction; 12 countries depend on nuclear for at least 25% of their electricity. In 1991 in Canada, 20 reactors produced 17% of the electricity and in the US, 111 reactors produced 22% of their electricity.

In some European nations, as you well know, the reliance on nuclear power for electrical energy is much higher -- ranging from 45 percent in Sweden to 75 percent in France.

So we have is a situation where the emerging economies rely heavily on combustion for their energy; coal, oil, wood and almost anything else that will burn. And, the biggest concern in the global mix of energy sources is -- pollution, primarily the acid gases and carbon dioxide. After all, pollutants... once in the atmosphere... recognize no political or economic boundaries. As you well know, there are still many uncertainties regarding global warming, but many scientists believe that unless we do something soon to offset the burning of fossil fuels, the global environmental damage will be irreversible.

Now, there is no doubt that the world will continue to rely on fossil fuels for most of its energy production, even with efficiency and conservation. The burning of coal... as well as oil and gas... will expand dramatically in Asia, India, Africa, South America and other heavily-populated areas of the world seeking a better way of life. Coal and other fossil fuels make sense to these emerging nations because they are readily accessible... relatively economical to produce using off-the-shelf technology... and they are abundant. With a more than doubling of current demand from 400 to 1,000 EJ in the future, fossil fuels will still provide 60% of the needs. And this assumes massive conservation and efficiency.

What about other energy sources to reduce reliance on the burning of fossil fuels in the future? These are less well defined, but biomass might produce another 10%, hydro electric power, 5%, and the renewables - fuel wood, solar and wind - also 5%. Only one proven source - nuclear energy - is able to supply the balance of 20%, up from the current 5%. And in West Germany, the government is specifically linking carbon dioxide targets to nuclear acceptance, an approach we should continue to support vigorously.

Whatever the energy supply mix, two points are clear. First, we cannot meet the realistic energy needs of the developing nations for a sustainable standard of living without turning to alternatives such as nuclear power. Second, if we don't chose alternatives to a massive increase in the burning of fossil fuels, future generations will pay the environmental penalty. And I don't have to enumerate the comparative environmental consequences of fossil and nuclear to a group such as this, either operationally or from the point of view of back-end waste. In such a comparison, I would not condemn coal - or natural gas - which also contributes substantially to the greenhouse effect. Rather I seek to provide an environmental perspective. Both will continue to fuel energy needs in a significant way.

And I should also touch on the importance of the architecture of these future global energy systems - "looking at the building as well as the bricks", as it was put in a recent study by the U.S. Energy Association and the Energy Council of Canada. The example I show is urban transportation in personal vehicles. If the end use alternatives are small combustion-driven cars and electric cars, there are a number of fuels, from oil to alternative automotive fuels, through to the use of coal and nuclear to generate electricity for electric cars. The environmental impact goes far beyond the fuels themselves to such things as the fate of the millions of electric batteries if electric cars are used. Clearly parameters such as environmental effects, resource requirements, economic consequences and timing, of different energy architectures.

To illustrate the broad impact of electricity production in developing countries, let's look at China, currently building three nuclear generating plants. Over the next 25 years, it will expand its nuclear power capability five-fold. But... even then... nuclear power will provide only 6.5 percent of China's total electrical generation. Coal will still be the driving force behind China's electrification program. And it is projected that by 2015 China's coal burning will contribute more than 50 percent of the world's projected CO<sub>2</sub> emissions.

The seriousness of this situation from a global perspective cannot be underestimated. Yet, there is a massive gap between public expectations and industrial reality on this point. Many people in the developed world believe that the world is poised to reduce polluting emissions of carbon dioxide. But this belief flies in the face of the projections for industrial growth among the developing nations. On the one hand, the expectation of a less contaminated global environment. On the other hand, the reality of escalating energy requirements coupled to demands among the poorer nations for a better standard of living. Even in the developed nations, the consumption of fossil fuels will continue to increase. Climate change... acid rain... urban air quality... and other environmental problems... have all been linked to the consumption of coal, oil and natural gas. Yet... these fuels are the very basis of the world economy. Obviously the developed world has got to improve its energy efficiency and practice conservation.

But, frankly, it is virtually impossible to cap global CO<sub>2</sub> emissions in the next half century. Realistically... when there are more than 10 billion people walking this earth in the middle of the next century... they will not be persuaded by talk of environmental integrity.

But nothing will be gained by pessimism and despair. Indeed, the challenge gives rise to opportunity within the nuclear industry. We must foster an orderly growth in electrical power... based on a mix of energy sources, but emphasizing nuclear power. Can it be done? Let's look at Korea. In less than 20 years, Korea has established nine operating nuclear units that supply more than 50 percent of the country's electricity needs. And during those 20 years, Korea has experienced a phenomenal increase in national prosperity... and continues to do so.

Consider the desperate plight of Eastern Europe. Western energy expertise is one form of assistance that can help these nations attain a new economic and political dignity. As well as new nuclear plants, there are opportunities in retrofit, rehabilitation, safety studies and waste management, in what is estimated as a \$50 billion challenge.

Let me use Canada's presence in Romania as an example of what can be done. We are completing a CANDU project there that will provide 30 percent of that nation's electricity. The reliability of that capacity will do much to bolster the people's faith in the new and struggling market economy. It will contribute to improvements in the standard of living. It will create confidence in the fledgling democracy.

There are political benefits to exporting nuclear generating expertise... as a catalyst for economic growth. The rise of an affluent middle class from economic expansion brings with it a commitment to democracy and political stability. And,, short of international famine and pestilence, the only effective long-term way shown to limit the birth rate is through a more affluent society. That too means a greater chance of sustainable international peace.

But we still have the underlying dilemma of political and personal perceptions vs the reality of the world. So let me summarize the major points:

- an inexorable increase in the world population, primarily in the developing countries
- the aspirations of those countries for improved living standards, leading to massive industrialization
- the energy issue in Eastern Europe
- the major continuing influence of fossil fuels
- and, through all this, the key role to be played by nuclear, with the opportunity for people like yourselves to provide the leadership.

**EXPERIMENTAL I**

**(Session 1)**

**Chairmen**

**M. COQUERELLE**

Commission of the European Communities

**H.C. SUK**

Republic of Korea

# FISSION GAS RELEASE AND FUEL TEMPERATURE DURING POWER TRANSIENTS IN WATER REACTOR FUEL AT EXTENDED BURNUP

P KNUDSEN, C. BAGGER,  
M MOGENSEN, H TOFTEGAARD  
Risø National Laboratory,  
Roskilde, Denmark

## Abstract

Data on transient fission gas release and fuel temperature have been obtained with refabricated test fuel pins that were instrumented with pressure transducers and centre line fuel thermocouples. Major test variables were fuel type, burnup, transient power history, fill gas, refabricated/unopened fuel segments. The previously irradiated test fuels (15-48 MWd/kgU) were provided by ANF, GE and Risø.

A total of 15 transient tests were performed. The maximum power was usually around 350 - 400 W/cm. The hold time at maximum power ranged from a few hours to six days. The test fuels were characterized extensively after base irradiation and after transient testing.

These investigations were carried out in the framework of the Third Risø Fission Gas Project. The paper presents an overview of the experiments and of the major results thus obtained.

## 1. INTRODUCTION

The desire to improve fuel utilization has created a growing interest in extending the burnup of water reactor fuel. As a result, fuel performance data are needed at burnup levels well in excess of 30,000 MWd/tU. Fission gas release is one of the important factors, especially for power increases (transients) late in life, because even moderate increases can then lead to important releases. In addition to the detailed knowledge of transient fission gas release as a function of time, it is also highly desirable to know the fuel temperature during the power transient. Such data are required for the general assessment of fuel performance for the validation of fuel performance codes and for the formulation of more adequate models for transient fission gas release.

Two Risø projects (Refs 1-2) have already generated comprehensive data sets in this area with high-burnup fuel. Part of these data is detailed descriptions of transient

fission gas release as a function of time. In addition, detailed characterizations are provided of local fission product distributions and fuel structures resulting from the power transients.

At the time of the first two Risø projects, techniques did not exist for direct measurement of the fuel temperature during a power transient, using fuel that has been previously irradiated to significant burnup in a power reactor. Risø consequently developed a technique to instrument irradiated fuel segments with fresh thermocouples.

In the Third Risø Fission Gas Project, previously irradiated power reactor fuel was refabricated into test fuel pins that were instrumented with pressure transducers and fuel thermocouples. This enabled continuous monitoring of fission gas release and fuel temperature during power transients. In addition, extensive hot cell examinations provided detailed, local data on fission gas release and fuel structure.

This paper presents an overview of the experiments and of the major results obtained from these investigations.

## 2. THE EXPERIMENTS

Major test variables in this project were fuel type, burnup, transient power history, fill gas, refabricated/unopened fuel segments. The following fuel types were used:

- ANF fuel, manufactured by Advanced Nuclear Fuels (now Siemens Nuclear Power Corporation) and base irradiated in a PWR to a burnup of 42 MWd/kgU,
- GE fuel, manufactured by General Electric and base irradiated in BWR's to 15-44 MWd/kgU,
- Risø fuel, manufactured by Risø and base irradiated in the OECD Halden Reactor (HBWR) to 44-48 MWd/kgU.

Details of these fuels are shown in Table 1. During base irradiation, the fission gas release was 0.1-0.3% for the ANF and GE fuels and 5-15% for the Risø fuel.

A total of 15 transient tests (bump tests) were performed in the DR3 reactor at Risø. For 11 of the tests, the fuel was refabricated and instrumented at Risø. The ramp

Table 1  
Test Fuel Summary

Fabrication by Reactor		ANF Biblis-A	GE Quad Cities-1	GE Quad Cities-1	GE Millstone-1	Risø HBWR
Pellet						
Diameter	mm	9.0	10.4	10.4	10.9	12.6
Height	mm	6.9	10.4	10.4	12.4	13
End shape		dished	flat	flat	flat	dished
		+ chamfered	+ chamfered	+ chamfered	+ chamfered	
Powder route		ADU	ADU + UPS <sup>(a)</sup>	UPS <sup>(a)</sup>	Dry route <sup>(a)</sup>	ADU
Sinter temperature	°C	1780	1780	1780	1750	1675
Sinter time	h	3	4	4	4	2
Density	%TD	93.7	95.2	96.2	95.7	94.7
Density increment in resinter <sup>(b)</sup>	%	0.18	0.37	0.34	0.7	1.5
Open porosity	%	0.07	03-05	02-14	01-08	0.02
Grain size (2-D)	μm	6	12	21	12	10
Enrichment	% <sup>235</sup> U	2.95	3.0	2.6	2.89	5.078
Cladding						
Alloy		Zr-4 <sup>(c)</sup>	Zr-2 <sup>(c)</sup>	Zr-2 <sup>(c)</sup>	Zr-2 <sup>(d)</sup>	Zr-2
Outer diameter	mm	10.8	12.3	12.3	12.5	14.0
Wall thickness	mm	0.8	0.8	0.8	0.7	0.6
Pin						
Stack length	mm	540	750	750	750	1670
Gap (diametral)	mm	0.19	0.22	0.23	0.23	0.21
Fill gas	bar He	25	3	3	17	1
Burnup <sup>(e)</sup>	%FIMA	4.3	3.8-4.5	2.3	1.5-2.4	4.3

(a) Including use of pore former

(b) 1700°C, 24h

(c) With a Zr liner

(d) With a Nb "buned" barrier

(e) Pin average

approach to the bump terminal level (usually around 350-400 W/cm) was mostly made in small steps, generally 20 W/cm, to obtain extensive measurements of fuel temperature. Most of the tests had a total duration of three days, with a few lasting only a few hours and others up to six days. The tests are summarized in Table 2. The type of data obtained during the transient testing are illustrated by Figs. 1-3.

Extensive hot cell examinations were performed to characterize the test fuels after base irradiation and after bump testing. In the investigations, the emphasis was on local (radial, axial) data on fission product release and fuel structure. These examinations were carried out in the hot cells at Risø and at the Transuranium Institute at Karlsruhe (JRC/FRG). The various hot cell examinations are listed in Table 3. Examples of the hot cell data are shown in Figs. 4-7

Table 2  
Risø-FGP3 Transient Tests

Name	Test Type	Fuel Pin	Burnup %FIMA	Rating at BTL		CLT <sup>(1)</sup> °C
				Pin Average W/cm	at TC W/cm	
AN1	P	CB9-2R	4.4	398	—	—
AN2	Unopened	CB6	4.3	390 <sup>(3)</sup>	—	—
AN3	TP	CB8-2R	4.4	407	365	1425
AN4	TP	CB7-2R	4.4	407	370	1500
AN8	Unopened	CB10	4.3	298 <sup>(3)</sup>	—	—
AN10	TP	CB13-4R	4.4	344	321	1225
AN11	Unopened	CB11	4.4	169 <sup>(3)</sup>	—	—
GE2	TP	ZX114-3R	4.6	405	405	1625
GE4	TP	XW104-3R	2.4	433	411	1640
GE6	TP	ZX113-4R	4.5	379	363	1520
GE7	Unopened	ZX115	4.4	355 <sup>(3)</sup>	—	—
II2	TP	STR024-2R	2.8	428	381	1500
II3	TP	STR014-3R	1.6	447	438	1575
II1	T	M72-2-2R	4.8	403	448	1880
II5	TP	M72-2-7R	5.3	401	373	1525

Fill gas	Power hist. <sup>(2)</sup> /hold time	FGR %	Time of Test	Purpose	Test Name
15 He	Ax /42h	36.5	Feb-88	Effect of refabrication	AN1
25 He	B /62h	29.7	Nov-87	Power history / effect of refabrication	AN2
15 He	Ax /42h	35.5	Jan-88	Fill gas / effect of refabrication	AN3
1 Xe	Ax /42h	40.9	Dec-87	Fill gas	AN4
25 He	B /4h	13.7	Jan-89	Power history / fuel type / GB gas / low-power release	AN8
5 He	Bx /40h	26.9	Feb-89	Power history / low-power release	AN10
25 He	B /4h	5.1	Nov-89	Release at low power	AN11
5 He	Ax /41h	23	Mar-88	Burnup / power history	GE2
5 He	Ax /34h	27.8	Apr-88	Burnup / large grain size	GE4
5 He	Bx /140h	25.5	May-89	Power history	GE6
3 He	B /4h	13.7	Mar-89	Power history / fuel type / GB gas	GE7
5 He	B /2h	Failed	Sep-87	Burnup / link to FGP2	II2
5 He	Ax /36h	17.4	May-88	Burnup / link to FGP2	II3
1 Xe	A/24h	16.0 <sup>(3)</sup>	Aug-87	Link to FGP2	II1
5 He	Axy/24h	10.6 <sup>(4)</sup>	Apr-89	Burnup / link to FGP2	II5

(1) Stable center line temperature before first dip (or failure, II1)

(2) See power history types below

(3) Large axial form factor, peak ratings (W/cm). 450(AN2), ~500(AN8), 206(AN11) and 530(GE7)

(4) Base irradiation release 12-16%

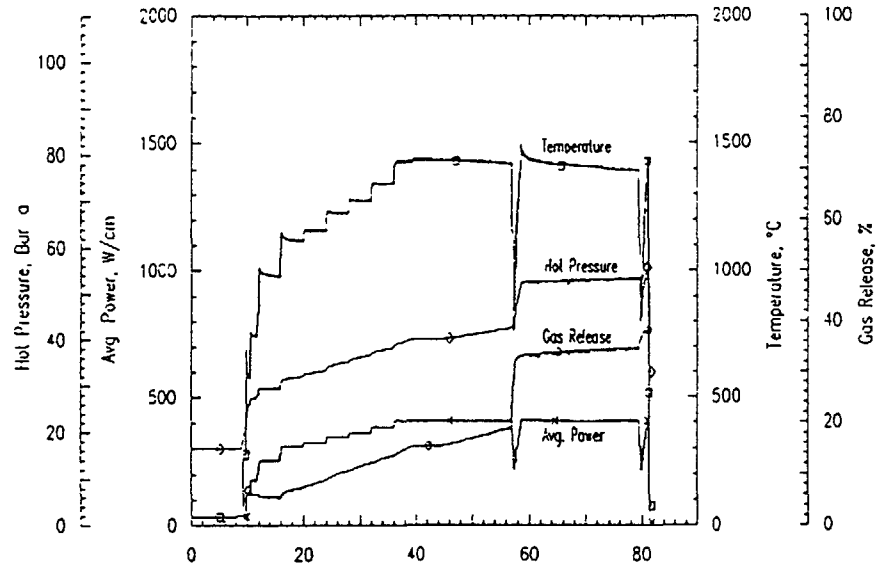


Fig. 1a. Bump test history of ANF TP-test AN3

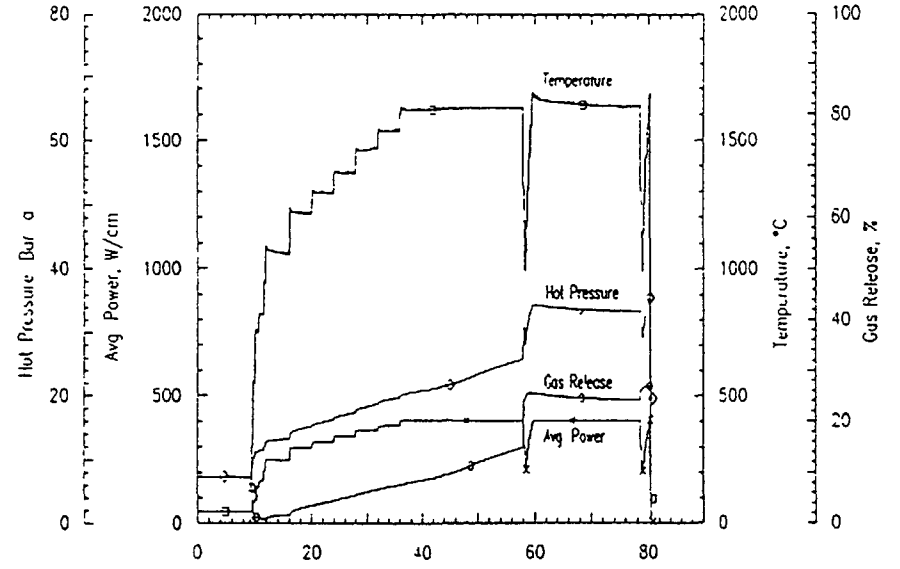


Fig 2a. Bump test history of GE TP-test GE2.

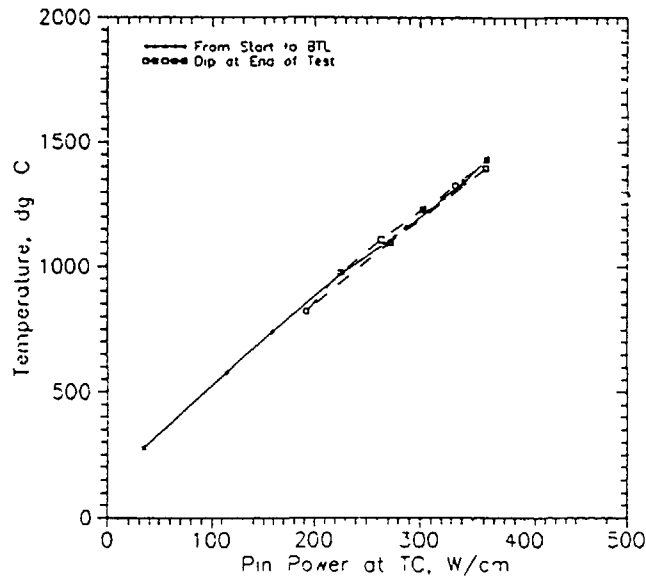


Fig 1b Fuel centre temperature vs local power at the thermocouple in ANF test AN3

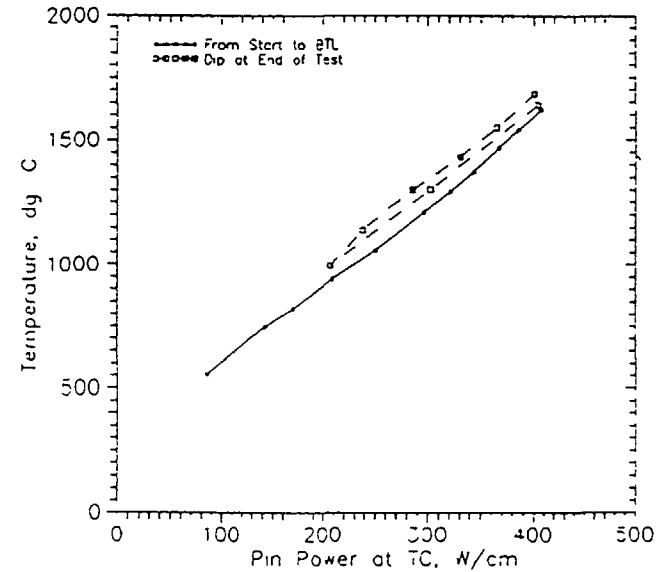


Fig 2b Fuel temperature vs local power at the thermocouple in GE test GE2

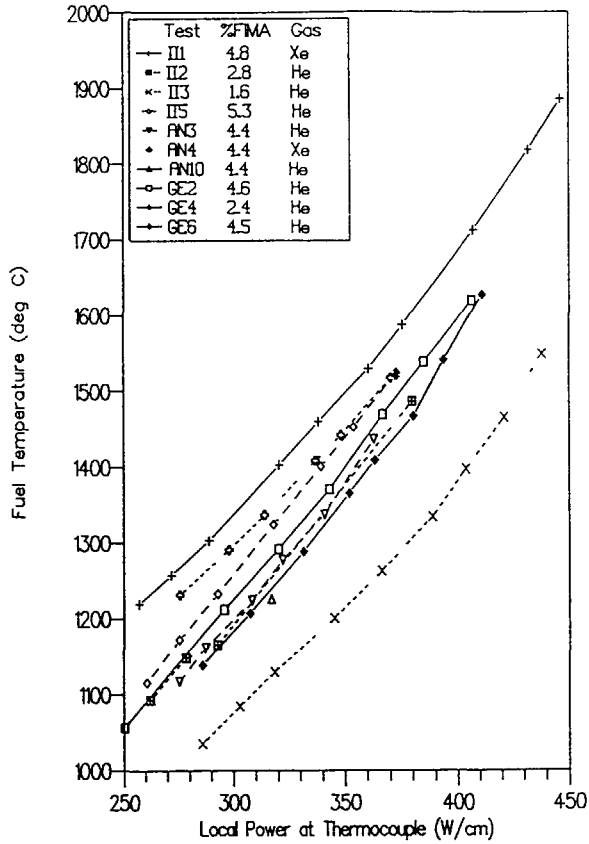


Fig 3 Fuel temperature vs local power for all TC-tests from first approach to transient terminal level

3. MAJOR RESULTS

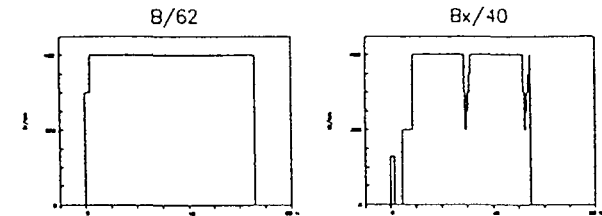
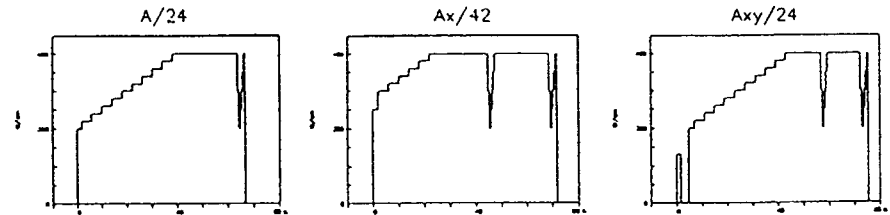
Generally speaking, comprehensive data sets were obtained from the combination of (i) monitoring of fuel temperature and internal pin pressure during the bump testing (ii) the extensive pre-/post-test examinations in the hot cells

These data sets are well suited for the benchmarking of fuel performance codes Furthermore, such data are useful in the understanding of and development of models for the calculation of fuel temperature and fission gas release

Table 3  
List of Hotcell Examinations

NDE Technique	Observation
Axial gamma scanning	Local, relative power and burnup
Profilometry	Diameter change
DE Technique	Observation
Puncturing	Analysis of released fission gases
X ray fluorescence analysis (XF)	Diametral Xe distribution (total gas content)
Electron probe micro analysis (EP) <sup>(a)</sup>	Radial Xe and Cs distribution (in matrix and small bubbles)
Micro gamma scanning (MG)	Diametral <sup>137</sup> Cs distribution
Optical microscopy <sup>(b)</sup>	Fuel structure, especially pore and grain (size, shape, distribution)
Replica electron microscopy (REM) <sup>(a)</sup>	Fuel structure, especially pore and grain (size, shape, distribution)
Scanning electron microscopy (SEM) <sup>(a)</sup>	Fuel structure, especially pore and grain (size, shape, distribution)
Transmission electron microscopy (TEM) <sup>(a)</sup>	Fuel structure, especially pore and grain (size, shape, distribution)
Burnup and heavy isotope analysis (IA) <sup>(b)</sup>	Burnup, basis for calculation of fission gas generated
Retained gas measurement (RG)	Isotopic composition of retained fission gas

(a) at TU  
(b) at Riso as well as at TU



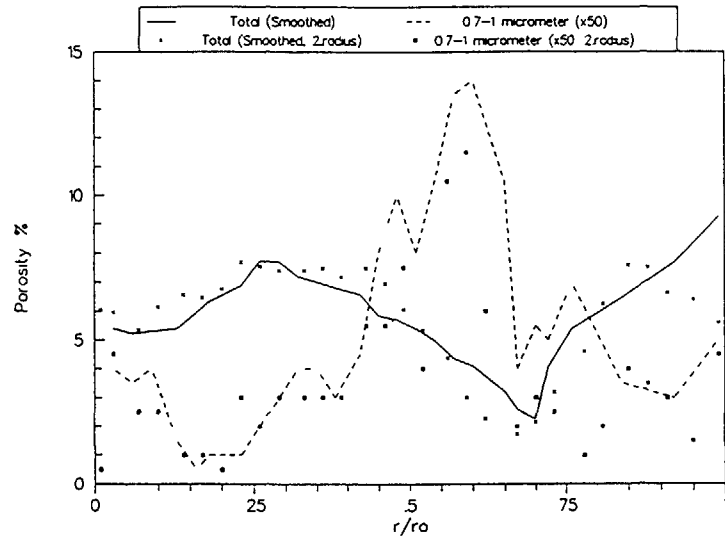


Fig. 4a. Test AN3. Radial distribution of porosity at 395 W/cm (42h)(CB8-2R-9A) A full diameter was measured and is shown in the figure as two radii

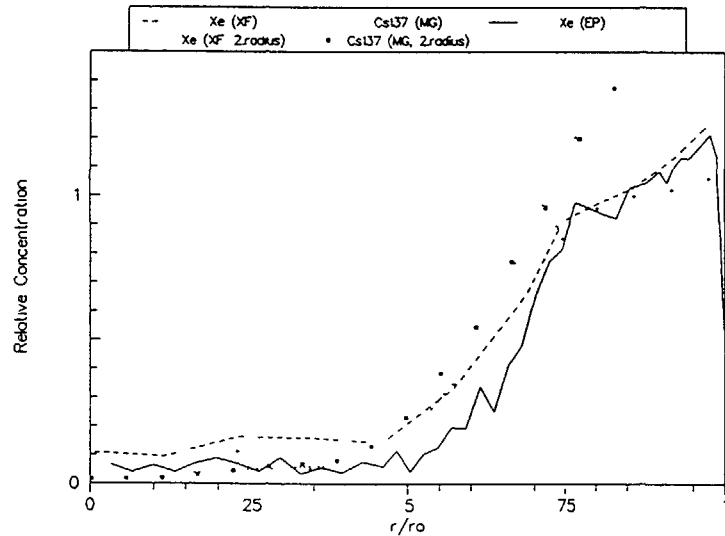


Fig 4b Test AN3 Radial distribution of Xe by EP (410 W/cm, CB8-2R-3), by XF (413 W/cm, CB8-2R-5) and of <sup>137</sup>Cs by MG (415 W/cm, CB8-2R-7) Full diameters were measured by XF and MG Each diameter is shown as two radii in the figure

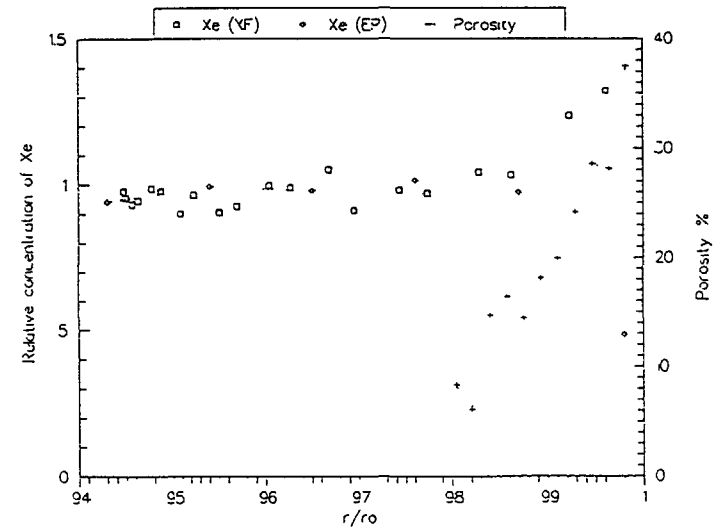


Fig 5 Rim of base irradiated ANF fuel At the top is shown a x400 micrograph of the fuel rim showing development of small porosity The graphs below (same radial magnification as the micrograph) give total porosity and Xe profiles (the latter from bump tested samples of AN4 (CB7-2R-12 (XF), -5 (EP)), but assumed representative for base irradiated fuel in the cold fuel zone) The porosity developed (approaching 40% in total) contains Xe, released from the grains



- (g) In the transient testing, the ANF fuel exhibited an unexpected release of 5-7% during a transient from power levels of 30-60 W/cm to levels of 125-170 W/cm. It is proposed that the high ramp rate during the transient test is the cause of release at the low powers. Ref. 4 discusses this in detail.
- (h) The release behaviour was not affected by refabrication of Ge fuel without fuel drilling (for thermocouple insertion) nor by refabrication of ANF fuel with or without fuel drilling.

- 3. C. Bagger and M. Mogensen, "Experimental Assessment of a Temperature Threshold for Thermally Induced Fission Gas Release in Transient Tested Water Reactor Fuel with Extended Burnup", paper presented at the IAEA Technical Committee. Meeting on Fission Gas Release and Fuel Rod Chemistry Related to Extended Burnup, Pembroke, Ontario, April 27 - May 1, 1992.
- 4. M. Mogensen, C. Bagger, H. Toftegaard, C.T. Walker and P. Knudsen, "Fission Gas Release Below 20 kWm<sup>-1</sup> in Transient Tested Water Reactor Fuel at Extended Burn-up", *ibid.*

### ACKNOWLEDGEMENTS

The achievements of the investigations reported in this paper resulted from the work of many staff members at Risø, the Transuranium Institute, Advanced Nuclear Fuels, General Electric and the OECD Halden Reactor Project. The authors gratefully acknowledge the dedicated efforts and collaboration of all these people.

The work performed within the scope of the Third Risø Fission Gas Project was supervised by a project committee representing the sponsors of the project: ABB Atom (S), Advanced Nuclear Fuels (USA), AEA Technology (UK), British Nuclear Fuels (UK), Central Research Institute of Electric Power Industry (J), Electric Power Research Institute (USA), General Electric Company (USA), Hitachi (J), Institute for Energy Technology (N), Institute for Transuranium Elements (JRC/FRG), Nippon Nuclear Fuel Development Company (J), Nuclear Electric (UK), Studsvik (S), Swedish Nuclear Power Inspectorate (S), Swedish State Power Board (S), Technical Research Centre of Finland (SF), Toshiba (J), Risø National Laboratory (DK).

### REFERENCES

- 1. Per Knudsen, Carsten Bagger, Hans Carlsen, Ib Misfeldt and Mogens Mogensen, "Fission Product Behaviour in High-Burnup Water Reactor Fuel Subjected to Slow Power Increases", *Nucl. Tech.*, vol. 72, March 1986, pp. 258-267.
- 2. P. Knudsen, C. Bagger, H. Carlsen, B.S. Johansen, M. Mogensen and I. Misfeldt, "Fission Gas Release in High-Burnup Fuel During Power Transients", *Proc. ANS Topical Meeting on LWR Fuel Performance*, April 17-20, 1988, Williamsburg VA, pp. 189-203.

## FISSION GAS RELEASE BELOW $20 \text{ kWm}^{-1}$ IN TRANSIENT TESTED WATER REACTOR FUEL AT EXTENDED BURNUP

M. MOGENSEN, C. BAGGER, H. TOFTEGAARD, P. KNUDSEN  
Risø National Laboratory,  
Roskilde, Denmark

C.T. WALKER  
Institute for Transuranium Elements,  
Commission of the European Communities,  
Joint Research Centre, Karlsruhe

### Abstract

One of the fuel types transient tested in the Third Risø Fission Gas Project released 5-7% of its fission gas in the power range  $3.6$  to  $17 \text{ kWm}^{-1}$  during the ramp. Isotopic analysis revealed that compared with fission gas released at powers above  $30 \text{ kWm}^{-1}$  this gas contained lower concentrations of  $^{85}\text{Kr}$  and  $^{131}\text{Xe}$ . This suggests that it had left the  $\text{UO}_2$  matrix during the base irradiation and had been for a long period isolated from the rest of the gas generated. It is proposed, therefore, that the gas released at low power had emanated from large pores, which were vented when the fuel cracked during the ramp.

### 1. INTRODUCTION

Athermal gas release is generally considered to be a phenomenon of relatively little significance. Under transient conditions, when such release is most likely to occur due to the high ramp rate, it usually amounts to not more than a few tenths of a percent. However, new results from the Third Risø Fission Gas Project Ref. [1] suggest that at high burn-up, athermal release from certain fuel types may be higher than previously expected. Fuel supplied to the Project by the Advanced Nuclear Fuel Company (ANF; now, Siemens Nuclear Power Corporation) released 5-7% fission gas in the low power interval  $3.6$ - $17 \text{ kWm}^{-1}$  during the ramp. This contrasts with the usual finding that under transient conditions the release of fission gas from  $\text{UO}_2$  starts at a linear power of  $30 \pm 2 \text{ kWm}^{-1}$  Refs. [2,3].

In the Third Risø Project, seven transient tests were carried out on ANF fuels. Four tests were made on refabricated fuel segments fitted with either a pressure transducer or central thermocouple, or both. The remaining three tests were performed on uninstrumented (not refabricated) pins. In addition eight other transient tests were carried out on GE and Risø fuels. Two of these (GE6 and II5) were instrumented tests which incorporated one or more holds of 1h duration at  $10$ - $14 \text{ kWm}^{-1}$  with the objective of ascertaining whether these fuels also released gas at low power.

Athermal release was detected in five of the transient tests on ANF fuel; that is, in all the tests in which detection was possible. The athermal release level of 5-7% was

relatively small compared with the total percentage release in the tests (27-41%). Virtually no athermal release was recorded in the tests on the GE and Risø fuels. Even in the tests GE6 and II5, which were designed to investigate the occurrence of athermal release, less than 0.5% of the fission gas inventory was released at powers below  $20 \text{ kWm}^{-1}$ .

This paper offers an explanation for the athermal release of gas from the ANF fuel. Briefly, it is claimed that the fission gas released at low power in the transient tests had left the fuel matrix during the base irradiation and had been stored for a long time in large pores which were a prevalent feature of this ANF fuel microstructure. The proposal is based on results for the radial distribution of xenon in the base irradiated fuel and fuel that had been transient tested at low power, on the isotopic composition of the gas released at low power and on the microstructure of the ANF fuel.

### 2. FUEL TYPE AND IRRADIATION HISTORY

The PWR fuel supplied to the Third Risø Fission Gas Project by ANF was not of a standard type. It possessed a special structure, which consisted of areas of dense fuel  $200$ - $800 \mu\text{m}$  in size separated by wide veins of porosity. Located within these veins were numerous highly porous islands  $50$ - $100 \mu\text{m}$  in size (see fig. 1). Relevant pellet and pin design characteristics of the ANF fuel are listed in table 1.

The ANF fuel was base irradiated in the Biblis-A reactor in Germany and subsequently transient tested in the DR3 reactor at Risø. The base irradiation spanned four reactor cycles beginning on July 10th 1982 and ending on October 3rd 1985. At the end of this period the pin average burn-up was 4.3 to 4.4% FIMA. The highest linear power seen by the fuel ranged from  $24.1$  to  $26.7 \text{ kWm}^{-1}$ . Powers of this magnitude were recorded at the beginning of the second and fourth reactor cycle. Power changes within each cycle were made at a rate slower than  $24 \text{ kWm}^{-1}\text{h}^{-1}$ . Fission gas release in the base irradiation was very low. Only 0.2-0.3% release was measured when 4 pins were punctured.

The transient tests in DR3 were carried out in a water cooled high pressure rig (HP1) under PWR conditions (system pressure  $15.3 \text{ MPa}$ ). The relevant test parameters are given in table 2. It is seen that in all the tests except AN11 and AN8 the power form factor was close to 1.0. The form factor was large in these two tests because full length pins were employed and these were exposed to the steep decline in the neutron flux in the upper part of the reactor core.

### 3. POST-IRRADIATION EXAMINATION

All the fuels were examined by electron probe microanalysis (EPMA), X-ray fluorescence analysis (XRF) and ceramography. In addition, the isotopic composition of the fission gas retained in the base irradiated fuel and fission gas that had been released to the fuel plenum was measured by mass spectrometry.

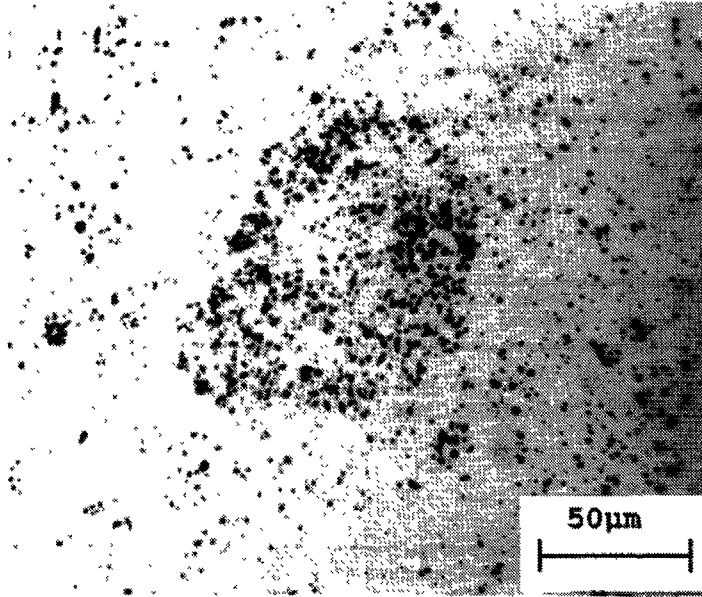


Figure 1

Photomicrograph showing an island of high porosity in unirradiated ANF fuel.

TABLE I. ANF PELLETT AND FUEL PIN DESIGN CHARACTERISTICS

Pellet Dia. (mm)	9.0
Pellet Density (% TD)	93.7
Open Porosity (%)	0.07
2D Grain Size ( $\mu\text{m}$ )	6
Enrichment (% $^{235}\text{U}$ )	2.95
Fill Gas <sup>a)</sup>	He (2.5)
Diametrical Gap (mm)	0.19
Cladding Material	Zircaloy-4 <sup>b)</sup>
Cladding Thickness (mm)	0.8
Stack Length (mm)	540

a) Figure in parenthesis is the pressure in MPa.

b) With a Zr liner.

TABLE II. THE TRANSIENT TESTS ON ANF FUEL

Test	Type <sup>a)</sup>	Fuel Pin	Rating at TTL <sup>b)</sup> ( $\text{kWm}^{-1}$ )	Form Factor <sup>d)</sup>	Hold Time (h)	Fill Gas <sup>d)</sup>	Percentage Release
AN1	P	CB9-2R	39.8	1.06	42	He (1.5)	36.5
AN3	TP	CB8-2R	40.7	1.03	42	He (1.5)	35.5
AN4	TP	CB7-2R	40.7	1.04	42	Xe (1.0)	40.9
AN8	U	CB10	29.8	1.58	4	He (2.5)	13.7
AN10	TP	CB13-4R	34.4	1.05	4	He (0.5)	26.9
AN11	U	CB11	16.9	1.19	4	He (2.5)	5.1

a) P, pressure transducer; T, central thermocouple; U, unopened.

b) Transient Terminal Level. Pin average power is quoted.

c) Peak pin power/average pin power.

d) Figure in parenthesis is the gas pressure in MPa.

Electron probe microanalysis was carried out at the Institute for Transuranium Elements, using the procedure reported in refs. [4,5]. X-ray fluorescence analysis was carried out at the Risø National Laboratory. Information about this technique, such as the experimental setup, can be found in ref. [6]. Isotopic analysis of the fission gas extracted from the ANF fuel pins by puncturing was also carried out at Risø as was ceramography. A brief description of the techniques used in the determination of the isotopic composition of the fission gas can be found in ref. [7]. For ceramography, standard preparation techniques were employed.

## 4. RESULTS

### 4.1. The evidence for low power release

Figure 2 shows the pin power, fuel centre temperature and percentage of gas released at the start of the transient test AN10. It is seen that during the second power step which began after 10.5h the temperature increased dramatically from 293 to 735 °C before stabilising at 640°C. At about the same time as the temperature stabilised a gas release of about 6% was registered by the pressure transducer. The temperature spike is evidence that gas was released during the second power step. The spike results from a momentary drop in gap conductivity caused by local release of xenon into the gap and subsequent mixing with the plenum gas (He). The delay in detecting the released gas with the pressure transducer (approx. 7 min.) is due to the response time of the device.

Data on release at low power gathered from the instrumented transient tests on the ANF fuel and from test AN11 (an unopened pin) are collected in table 3. It is seen that gas release was 5-7%. This represents at the most one fifth of the gas released when the fuel was transient tested to about 40  $\text{kWm}^{-1}$  (cf., release figures in tables 2 and 3). Release occurred when the power was raised from 4 or 5  $\text{kWm}^{-1}$  to about 13

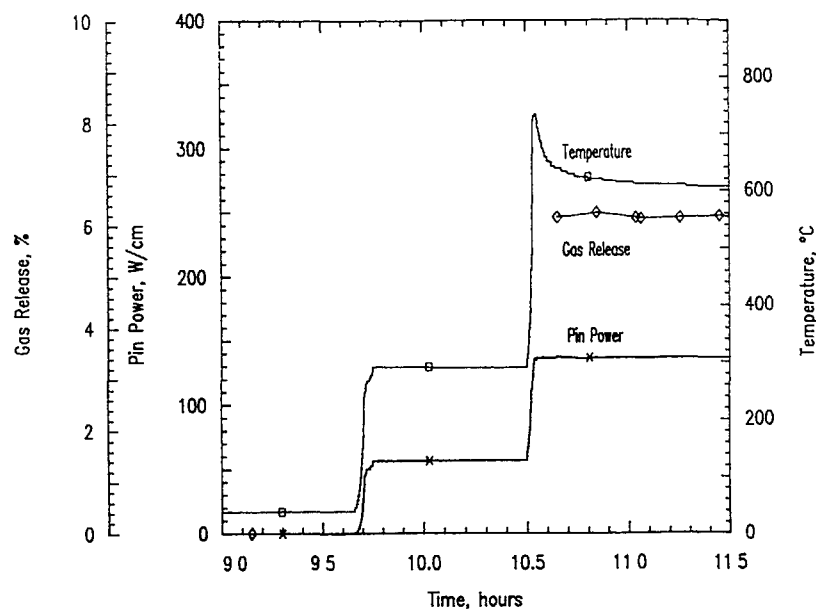


Figure 2

Average pin power, fuel centre temperature and percentage gas release at the beginning of the transient test AN10. Gas is released in the power step from 57 to 137 kWm<sup>-1</sup> after 10.5 h

TABLE III LOW POWER RELEASE DATA GATHERED FROM THE INSTRUMENTED TRANSIENT TESTS ON ANF FUEL AND FROM TEST AN11

Test	P <sub>in</sub>	Power Interval kWm <sup>-1</sup>	Ramp Rate <sup>a)</sup> kWm <sup>-1</sup> h <sup>-1</sup>	Percentage Release	Centre Temp <sup>b)</sup> °C
AN1	CB9-2R <sup>c)</sup>	4.1-13.3	136.8 (162)	7	-
AN3	CB8-2R	5.4-13	282.0 (630)	7	278,689
AN4	CB7-2R	5.1-13	100.8 (348)	6	448,804
AN10	CB13-4R	5.7-13.6	238.8 (444)	6	293,735
AN11 <sup>d)</sup>	CB11	3.6-17	133.8 (174)	5.1	-

- a) Average value for the pin in the power interval quoted. Figure in parenthesis is the maximum ramp rate  
 b) Measured temperature at the beginning and end of the power step  
 c) Fitted with a pressure transducer only  
 d) Uninstrumented test

TABLE IV LOW POWER RELEASE DATA FOR THE INSTRUMENTED TRANSIENT TESTS, GE6 (GE FUEL) AND II5 (RISØ FUEL)

Test	P <sub>in</sub>	Power Interval kWm <sup>-1</sup>	Ramp Rate <sup>a)</sup> kWm <sup>-1</sup> h <sup>-1</sup>	Percentage Release	Centre Temp <sup>b)</sup> °C
GE6	ZX113-4R	9.7-15.0	73.8 (233)	0	480,680
II5	M72-2-7R	6.1-11.6	124.8 (230)	0	328,565
		12-16.7	336 (422)	0.2	560,780

- a) Average value for the pin in the power interval quoted. Figure in parenthesis is the maximum ramp rate  
 b) Measured temperature at the beginning and end of the power step

TABLE V THE RATIOS <sup>83</sup>Kr/<sup>84</sup>Kr AND <sup>131</sup>Xe/<sup>132</sup>Xe IN DIFFERENT SAMPLES OF FISSION GAS TAKEN FROM ANF FUEL

Gas Sample	%FGG <sup>a)</sup>	Isotope Ratio	
		<sup>83</sup> Kr/ <sup>84</sup> Kr	<sup>131</sup> Xe/ <sup>132</sup> Xe
Retained gas from base irradiated fuel (CB7-10)	99.8	0.324 ± 0.001	0.333 ± 0.001
Puncture gas from base irradiated fuel	0.2-0.3	0.262 ± 0.015	0.253 ± 0.003
Puncture gas from all transient tests but AN11	13.1-39.3	0.312 ± 0.006	0.321 ± 0.009
Puncture gas from AN11 <sup>b)</sup>	5.1	0.291 ± 0.003	0.283 ± 0.001

- a) Fission Gas Generated  
 b) Composition Kr + Xe, 19.8 cc, He, 134 cc

kWm<sup>-1</sup> at an average ramp rate of 100.8 to 283 kWm<sup>-1</sup>h<sup>-1</sup>. At 13-14 kWm<sup>-1</sup> (the upper limit of the second power step in the instrumented tests) the highest temperature measured at the fuel centre was 804°C.

Table 4 lists the low power release data for the tests GE6 and II5 which were carried out on GE and Risø fuel, respectively. As seen from the table, these fuels released hardly any gas at low power, although the maximum ramp rates in the tests were faster than 162 kWm<sup>-1</sup>h<sup>-1</sup>, the maximum rate in test AN1 which produced 7% release at low power (see table 5).

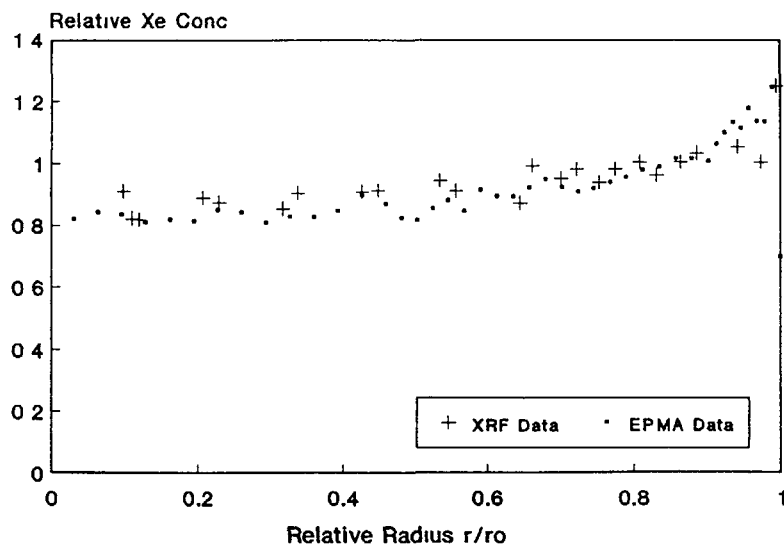


Figure 3

Radial distribution of retained xenon in the ANF fuel at the end of the base irradiation. Fuel sections CB7-8 (XRF) and CB7-9 (EPMA), burn-up 4.4 and 4.3% FIMA, respectively. The profiles are accurate to better than  $\pm 3\%$

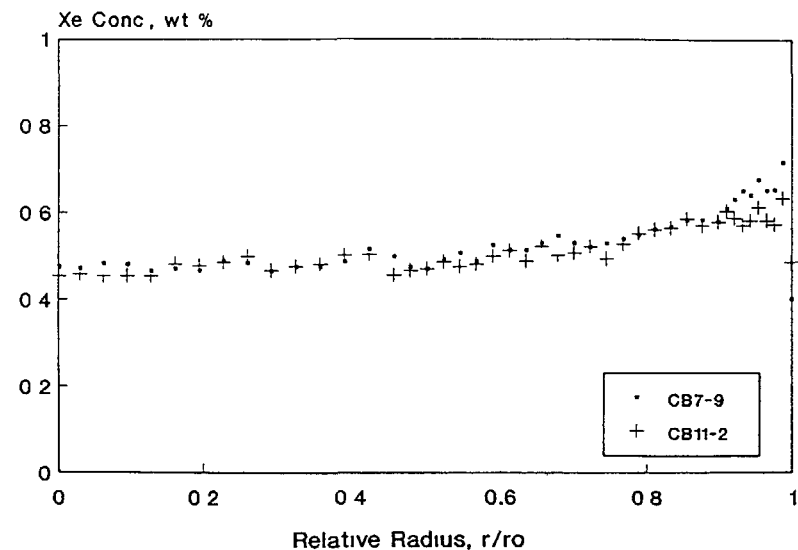


Figure 4

Radial distribution of retained xenon at the end of the base irradiation (section CB7-9, burn-up 4.3% FIMA) and following a power transient to  $20 \text{ kWm}^{-1}$  (section CB11-2, burn-up 4.4% FIMA) as revealed by EPMA. The relative error derived from the statistics of X-ray counting is  $\pm 2\%$

#### 4.2. Radial distribution of xenon in the base irradiated fuel and in fuel transient tested at low power

In the search for the source of the gas which was released at low power, XRF and EPMA was used to look for evidence of the accumulation of xenon on the grain. In the search for the source of the gas which was released at low power, XRF and EPMA was used to look for evidence of the accumulation of xenon on the grain boundaries in the base irradiated fuel and for evidence of thermal release in the fuel from the low power test AN11

The radial distribution of xenon in base irradiated fuel from pin CB7 is shown in fig 3. It is seen that in the body of the fuel XRF detects slightly more gas than EPMA when the data are plotted on a relative scale (both normalised to 1 at  $r/r_0 = 0.85$ ). It has been argued that difference in the local concentration of xenon measured by XRF and EPMA corresponds to the amount of gas on the grain boundaries [5]. Thus, the disparity in the data for CB7 may be interpreted as indicating that about 3% of the retained gas was present on the grain boundaries. The small difference in the XRF and EPMA profiles for CB7, however, may also be explained by point to point variations

in the local xenon concentration and by the fact that XRF and EPMA were carried out on different fuel section (albeit adjacent ones)

In fig 4 the EPMA radial concentration profile for retained xenon in CB11 (section 2, transient terminal level (TTL)  $20.4 \text{ kWm}^{-1}$ ) from the low power test AN11 is shown together with the EPMA profile for the base irradiated fuel CB7. It is seen that slightly less xenon was measured in the centre of CB11 out to  $r/r_0 = 0.16$ , and close to the fuel surface between  $r/r_0 = 0.92$  and the pellet rim. As gas bubbles were found on the grain faces in the centre of CB11, thermal release must have occurred in this region. Locally, 4% of the gas inventory is missing which corresponds to an integral release value for the cross-section of just 0.1%. Probably this gas was released at the beginning of the fourth cycle of the base irradiation and not during the transient test

Burn-up variations and not gas release are apparently responsible for the difference in the concentrations of xenon measured at the surface of CB11 and CB7. The xenon profile for CB7 shows the customary sharp increase in concentration arising from the fission of plutonium created by neutron capture, whereas CB11 does not. None of the other transient tested ANF fuel sections analysed by EPMA exhibited such a small change in xenon concentration at the pellet surface

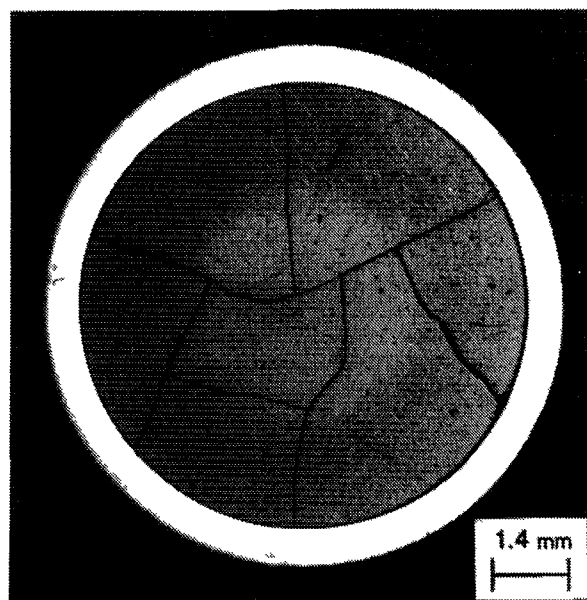


Figure 5

Photomicrograph of base irradiated ANF fuel. Numerous large pores are scattered throughout the fuel.

#### 4.3. Microstructure of the base irradiated fuel and fuel transient tested at low power

Figure 5 shows a photomicrograph of the base irradiated ANF fuel. It is seen that the fuel contained numerous large pores ( $>50 \mu\text{m}$ ). Similar features were not found in the base irradiated GE and Risø fuels. It is assumed that the pores had developed from the islands of high porosity which were scattered throughout the unirradiated ANF fuel pellets (see fig.1).

Ceramography of fuel (section CB10-3A) which had been transient tested to  $15.5 \text{ kWm}^{-1}$  in test AN8 showed that significant crack formation occurred at low power. In fact, three distinct types of crack had formed in the fuel during the test; short hair-line radial cracks, short circumferential cracks and fine intergranular cracks inclined  $30$  to  $45^\circ$  to the pellet axis. These cracks were mainly confined to the cold outer half of the pellet radius. Few radial and circumferential cracks were found, but a number of oblique intergranular cracks were observed.

#### 4.4. Age of the fission gas released at low power

Table 5 gives the  $^{83}\text{Kr}/^{84}\text{Kr}$  and  $^{131}\text{Xe}/^{132}\text{Xe}$  isotope ratios in the gas retained in the base irradiated fuel (pin CB7) and in puncture gas from all of the tests on ANF fuel except test AN11, from pin CB11 (test AN11) and in puncture gas from base irradiated fuel pins. It is seen that the  $^{83}\text{Kr}/^{84}\text{Kr}$  and  $^{131}\text{Xe}/^{132}\text{Xe}$  ratios in these gas samples are noticeably different. The significance of this variation becomes clear when the neutron capture cross-sections of the two krypton isotopes and the two xenon isotopes are considered. The neutron capture cross-section of  $^{83}\text{Kr}$  is 200 barn, whereas the capture cross-section of  $^{84}\text{Kr}$  is only 0.13 barn. Similarly, the neutron capture cross-section of  $^{131}\text{Xe}$  is 90 barn while that of  $^{132}\text{Xe}$  is just 0.39 barn. Hence, when a given mixture of  $^{83}\text{Kr}$  and  $^{84}\text{Kr}$  or of  $^{131}\text{Xe}$  and  $^{132}\text{Xe}$  is exposed to a neutron flux,  $^{83}\text{Kr}$  will gradually transform to  $^{84}\text{Kr}$  and  $^{131}\text{Xe}$  to  $^{132}\text{Xe}$ . Thus, the ratio of  $^{83}\text{Kr}$  to  $^{84}\text{Kr}$  and of  $^{131}\text{Xe}$  to  $^{132}\text{Xe}$  become smaller with time; that is to say, with increase in the neutron fluence.

It is apparent from table 5 that the  $^{83}\text{Kr}/^{84}\text{Kr}$  and  $^{131}\text{Xe}/^{132}\text{Xe}$  isotope ratios were highest in the retained gas in the base irradiated fuel and lowest in the puncture gas from this fuel. Most importantly, however, it is also evident from the table that the  $^{83}\text{Kr}/^{84}\text{Kr}$  and  $^{131}\text{Xe}/^{132}\text{Xe}$  isotope ratios in the puncture gas from pin CB11 were much lower (i.e. contained less  $^{83}\text{Kr}$  and  $^{131}\text{Xe}$ ) than in the gas extracted from the other ANF pins that were transient tested to higher power levels.

## 5. DISCUSSION

As seen from table 3 a low power release of 6-7% was recorded in the instrumented tests on the ANF fuel. The gas was released during the ramp from  $4.1$ - $5.7$  to  $13$ - $13.6 \text{ kWm}^{-1}$  (see fig.2). In the low power test AN11 on the uninstrumented pin CB11, 5.1% release was measured in the power interval  $3.6$  to  $17 \text{ kWm}^{-1}$ . This confirms that the gas released at low power in the instrumented tests was indeed fission gas and not gas arising from the refabrication of the pins; e.g.,  $\text{H}_2$  from reacted moisture. The slightly lower release obtained in test AN11 could be because the fuel at the top of the pin did not reach the power required to initiate release.

All the evidence indicates that the mechanism of gas release was athermal. In the instrumented tests, at the time of release the highest temperature measured at the centre of the fuel ( $804^\circ\text{C}$ ) was well below  $1100$ - $1200^\circ\text{C}$  at which thermal gas release begins [8,9]. The absence of significant thermal release at the low power levels under consideration is also confirmed by the EPMA results for section CB11-2 (TTL,  $20 \text{ kWm}^{-1}$ ). The radial xenon profile shown in fig. 4 indicates that while thermal release had evidently occurred in the vicinity of the fuel centre it did not constitute more than 0.1% of the total cross-section inventory.

Isotopic analysis of the gas released in test AN11 revealed that on average it was older than the retained gas in the base irradiated fuel. The concentrations of  $^{83}\text{Kr}$  and  $^{131}\text{Xe}$  in the gas indicated that it was younger than the puncture gas from the base irradiated fuel, but much older than the gas released in all the other transient tests on

ANF fuel (see section 5.4.). These results are interpreted as showing that the gas released in the low power test AN11 had left the  $\text{UO}_2$  matrix during the base irradiation and had for a long period been isolated from the rest of the gas generated.

It is deduced from this finding that the gas released from the ANF fuel at low power had probably been stored in the large pores which were scattered throughout the base irradiated fuel. Any gas contained in these pores would not have been detected by XRF because their size ( $>50 \mu\text{m}$ ) was larger than the depth from which the xenon X-ray signal was collected (about  $20 \mu\text{m}$ ), and hence those pores lying within the region of X-ray excitation would have been vented during specimen penetration.

The assumption that the gas released at low power had been stored in large pores is consistent with the fact that the GE and Risø fuels, which did not contain large pores, barely released any gas at low power even though they were exposed to fast ramp rates (table 4). Presumably the large pores in the ANF fuel were vented when the fuel cracked during the ramp. A number of new hair-line cracks were seen in section CB10-3A which had been transient tested to  $15.5 \text{ kWm}^{-1}$ . Most of these were situated in the cold outer part of the fuel and were quite short. This indicates that many of the pores in the central region of the fuel were not vented at low power and that the large radial and circumferential cracks which remained from the base irradiated constituted important escape paths for the gas. Since most of the cracks that formed at low power during the ramp appear to have been small they could only have acted as links between the pores and larger cracks.

Compared with the ramp rate, the linear power was of secondary importance as far as the athermal release was concerned. Only 0.2-0.3% of the fission gas inventory was released in the base irradiation although the linear power at which athermal release occurred in the transient tests had been greatly exceeded (see section 2). Significantly, in the base irradiation power changes were made at a much slower rate ( $<24 \text{ kWm}^{-1}$ ) than in the transient tests and only a few large cracks formed as a result.

An alternative source for the gas released at low power is the grain boundaries. Clearly, if the grain boundaries crack during the ramp any gas which has accumulated there in the base irradiated will be released. However, the evidence for the presence of grain boundary gas at the end of the base irradiation is inconclusive. The difference between the XRF and EPMA profiles shown in fig. 3 may be interpreted as indicating that up to 3% of the retained gas was present on the grain boundaries of the ANF fuel at the end of the base irradiation. This is, however, too small a percentage to account for the release at low power. Moreover, the possibility that the gas originated from the grain boundaries seems to be incompatible with it having been isolated from the rest of the retained gas for a long period during the base irradiation.

## 6. SUMMARY AND CONCLUSIONS

The ANF fuel transient tested in the Third Risø Project released 5-7% of its fission gas in the power range  $3.6$  to  $17 \text{ kWm}^{-1}$  during the ramp. GE and Risø fuels transient

tested using comparable ramp rates did not show low power release. The gas released at low power contained lower concentrations of  $^{85}\text{Kr}$  and  $^{131}\text{Xe}$  than that released at powers above  $30 \text{ kWm}^{-1}$ . This suggests that it had left the  $\text{UO}_2$  matrix during the base irradiation and had been for a long period isolated from the rest of the gas generated. It is considered that the gas released at low power had been stored in large pores greater than  $50 \mu\text{m}$  in size. These pores were dispersed throughout the ANF fuel but were scarce in the GE and Risø fuels. Presumably, the pores were vented when the fuel cracked during the ramp. In the relevant power interval,  $4.1$ - $13.6 \text{ kWm}^{-1}$ , the ramp rate was in the range  $162$  to  $444 \text{ kWm}^{-1}\text{h}^{-1}$  which is much faster than the rate at which power changes were made in the base irradiation.

## REFERENCES

- [1] KNUDSEN, P., BAGGER, C., MOGENSEN, M., TOFTEGAARD, H., Fission gas release and fuel temperature during power transients in water reactor fuel at extended burn-up (in these proceedings).
- [2] KNUDSEN, P., BAGGER, C., CARLSEN, H., MISFELDT, I., MOGENSEN, M., Fission product behaviour in high burn-up water reactor fuel subjected to slow power increases, Nucl. Technol. 72 (1986) 258-267.
- [3] KNUDSEN, P., BAGGER, C., CARLSEN, H., JOHANSEN, B.S., MOGENSEN, M., MISFELDT, I., Fission gas release in high burn-up fuel during power transients. LWR Fuel Performance (Proc. ANS Topical Mtg. Williamsburg, 1988) ANS, La Grange Park (1988) 189-203.
- [4] WALKER, C.T., Measurement of retained xenon in advanced fuels by microprobe analysis, J. Nucl. Mater. 80 (1979) 190-194.
- [5] WALKER, C.T., MOGENSEN, M., On the rate determining step in fission gas release from high burn-up water reactor fuel during power transients, J. Nucl. Mater. 149 (1987) 121-131.
- [6] MOGENSEN, M., ALS-NIELSEN, J., ANDERSEN, N.H., Determination of Fission Products in Irradiated Fuel by X-ray Fluorescence, Rep. Risø M-2599, Risø National Laboratory, Roskilde (1986).
- [7] LARSEN, E., EGSGAARD, H., MOGENSEN, M., Mass spectrometric measurement of fission gas from nuclear fuel, Int. J. Mass Spectroscopy and Ion Phys. 48 (1983) 385-388.
- [8] VITANZA, C., KOLSTAD, E., GRAZIANI, U., Fission gas release from  $\text{UO}_2$  pellet fuel at high burn-up, Light Water Reactor Fuel Performance (Proc. ANS Topical Mtg. Portland, 1979). ANS La Grange Park (1979) 361-366.
- [9] SONTHEIMER, F., MANZEL, R., STEHLE, H., Transiente spaltgasfreisetzung und  $\text{UO}_2$ -Mikrostruktur bei Leistungsrampen, J. Nucl. Mater. 124 (1984) 33-43.

## EXPERIMENTAL ASSESSMENT OF A TEMPERATURE THRESHOLD FOR THERMALLY INDUCED FISSION GAS RELEASE IN TRANSIENT TESTED WATER REACTOR FUEL WITH EXTENDED BURNUP

C BAGGER, M MOGENSEN  
Risø National Laboratory,  
Roskilde, Denmark

### Abstract

In-pile measurements of gas release and fuel temperature in The Third Risø Fission Gas Project show that onset of fission gas release during mild power transients takes place at a fuel temperature close to 1200°C. Evaluation of PIE results together with the temperature measurements confirms the temperature level and indicates that the onset temperature is independent of fuel type, burnup and hold time. The radial location of the 1200°C isotherm moves towards the rim with increasing burnup and constant linear power, assumably because of formation of a thermal barrier at the rim. Consequently the fractional fission gas release increases with burnup. For one of the fuel types investigated fission gas release is complete after 42h at 1525°C. The results suggest that the radial temperature distribution changes gradually from a parabola towards a square with increasing burnup.

### 1. INTRODUCTION

Fission gas release may become a life limiting factor for water reactor fuel. It is therefore of special interest to obtain detailed knowledge of transient fission gas release at extended burnup.

This paper describes, how a temperature threshold for fission gas release was assessed by simultaneous measurement of internal pin pressure and fuel centerline temperature. Features such as bubble precipitation, start of fission gas release and completion of release were correlated with temperature on a purely experimental basis. This made it possible to sketch a rough radial temperature profile.

Experimental data from The Third Risø Fission Gas Project show that thermal fission gas fractional release increases with burnup. The results indicate, that this is caused by a change in the radial temperature profile. The fuel volume with temperatures above the thermal release threshold expands with burnup for a fixed linear heat rating.

### 2. EXPERIMENTAL

As part of the Third Risø Fission Gas Project (Ref. 1), 9 previously irradiated light water power reactor fuel sections were refabricated into test fuel pins. All were instrumented with pressure transducers (P-tests), 8 were additionally instrumented with thermocouples, mounted in the fuel centerline (TP-tests). 4 sections were used in the unopened condition. The fuel types were:

-ANF fuel (3 TP, 1 P and 3 unopened AN-tests), manufactured by Advanced Nuclear Fuels, base irradiated to 4.4%FIMA (42 MWd/kgU) in Biblis-A (PWR) with a maximum pin power of 270 W/cm and a fission gas release around ~0.2%

-GE fuel (5 TP and 1 unopened GE-tests), manufactured by General Electric, base-irradiated to 1.6-4.6%FIMA (15-44 MWd/kgU) in Quad Cities-1 or Millstone-1 (BWRs) with maximum pin power of 300 W/cm or lower. The fission gas release after base-irradiation was at maximum 0.3%.

The mounting of fuel center thermocouples involved removal of fuel (Ref. 1). A center hole with diameter 2.5 mm was produced by drilling and clad on the inside by a molybdenum tube, inside which a W/Re thermocouple was positioned. The measured temperatures are therefore representative for a hollow pellet, where ~8% fuel has been removed from the center (ANF-fuel). The center hole thus extends to  $r/r_o=0.28$  with an ANF pellet diameter of 9.05 mm.

The refabricated fuel pins and 4 unopened fuel sections were transient tested in the DR3 reactor under BWR or PWR conditions as appropriate. The test pins were taken through a stepped approach to full power in the range 169-447 W/cm pin average with ramp rates in the range 7-54 W/cm/min and held at full power over a period in the range 4-140h. Fuel temperature and hot fission gas pressure were monitored continuously throughout the test, where applicable, the fuel pin power was monitored calorimetrically. The hot pressure was converted to cold pressure, using an empirical correlation. The temperature of the cladding surface was in both cases determined by surface boiling, when the fuel linear heat rating was above 200 W/cm, giving cladding temperatures of app. 339°C (PWR) and 289°C (BWR).

In a comprehensive PIE programme detailed analysis of <sup>140</sup>La axial distributions was used to determine relative power distributions. Combination of the relative power distributions with the calorimetric measurements produced test power histories for fuel samples, taken for destructive testing, and for the fuel sections containing the hot junction of thermocouples.

The maximum local test linear power seen by destructively examined samples spanned 150-490 W/cm. Analyses on cross sections included determination of diametral distributions of <sup>137</sup>Cs by micro gamma scanning, of element Xe by X-ray fluorescence analysis and of porosity (for 10 pore size intervals covering the range 0.7-128µm). The measurement techniques (Ref. 2) generally covered 100% of the diametral or radial sample strips examined.

### 3. RESULTS

#### 3.1. Temperature Threshold for Thermal Gas Release

Transient testing of ANF fuel gave 5-7% athermal fission gas release below 150 W/cm, Ref. 3. This phenomenon is, however, easily separated from thermal release, which occurred above 250 W/cm.

Table 1 shows fuel temperatures at 4 power levels for 3 ANF fuel tests with fill gas compositions/pressures as indicated. The burnup was 4.4%FIMA for all tests. The temperatures refer to the end of the 4h holding time spent at each power step towards target power. The values in the table were calculated by linear interpolation between actually measured combinations of temperatures and power levels to facilitate intercomparison. Fig. 1 shows the power/temperature correlation obtained from test AN3 during approach to maximum power.

Using the in-pile measured hot pressure, converted to fission gas release, the power levels bracketing the first significant thermal gas release (1%) has been determined; the power at the highest rated pellet before and after the release has been calculated (Table 2). Using the temperature data of Table 1, the power values have been converted to temperatures, still assuming hollow pellets (Table 2).

Substantial release occurred in the three He-filled tests when the maximum power level was stepped between the values indicated. Test AN4 (Xe-filled, 1bar) similarly showed substantial fission gas release, when the power was changed from 270 to 317 W/cm (Fig. 2), but prior to this ~1% release occurred over 4h at 270 W/cm.

Test AN1 was equipped with a pressure transducer, only. The power levels of AN1, bracketing the fission gas release, have been converted to fuel temperatures using the power/temperature correlation determined for test AN3 (Fig. 1), which had similar test parameters.

TABLE 1. Power levels at thermocouple hot junctions and corresponding temperature readings after 4h hold time. Determined by linear interpolation between actual levels to enable intercomparison.

Power at TC W/cm	Test AN3 Fill gas 15b He	Test AN4 Fill gas 1b Xe	Test AN10 Fill gas 5b He
200	880°C	1050°C	870°C
250	1040°C	1170°C	1020°C
300	1200°C	1300°C	1170°C
350	1380°C	1450°C	1330°C <sup>1</sup>

<sup>1</sup> Linear extrapolation from max level at TC position 336 W/cm

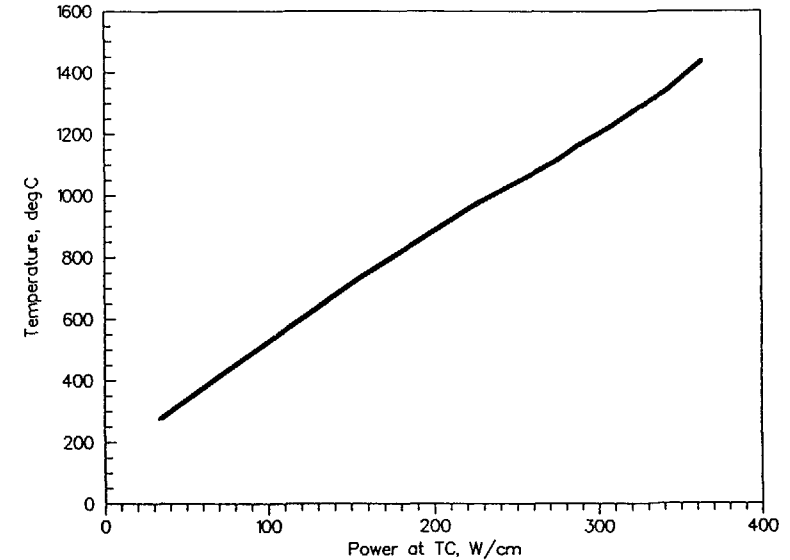


Fig. 1. Measured fuel temperature versus local axial heat rating at the thermocouple position PWR fuel, He-filled, 4.4%FIMA

TABLE 2. Maximum fuel pellet rating at power steps before and after first significant gas release. Corresponding fuel temperatures (valid for pellets with a center hole) according to Table 1.

Test	Maximum pellet power, W/cm		Max pellet temperature, °C (assuming hollow pellet)	
	Before start of release	After start of release	Before start of release	After start of release
AN1	270	304	1060 <sup>1</sup>	1170 <sup>1</sup>
AN3	267	325	1100	1290
AN4	270	317	1200	1350
AN10	220	360	920	1350

<sup>1</sup> Test AN1 was equipped with a pressure transducer, only. The temperatures were taken from the power/temperature relation measured from test AN3 (Fig. 1), as fuel pin parameters, test irradiation conditions and post-test puncturing results were identical

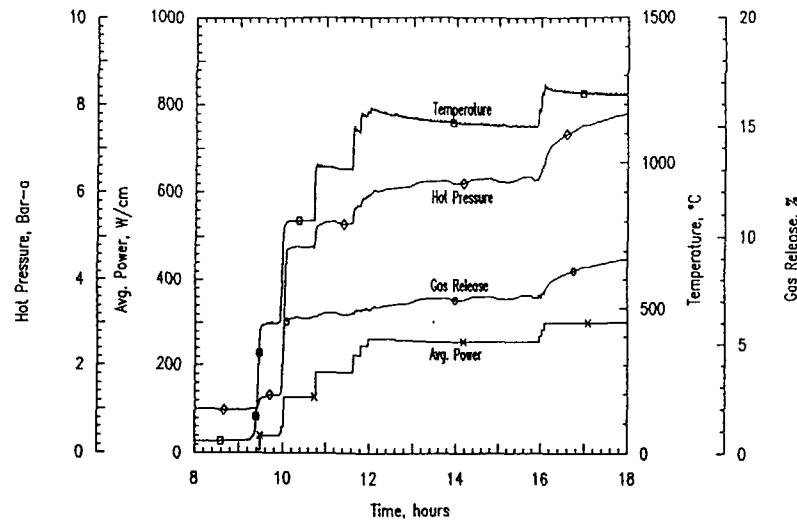


Fig. 2. In-pile measured average linear heat rating, fuel temperature, hot pressure and calculated gas release of a PWR test fuel pin (Xe-filled, 4.4%FIMA) during stepped upramp. Detail from the time of the initial fission gas release. The local power at the thermocouple is 91% of the test average value.

The local fission product release in samples, taken for destructive analysis by diametral micro gamma scanning ( $^{137}\text{Cs}$ ) and by diametral X-ray fluorescence analysis (Xe) was determined. This was carried out by volume integration of the difference between profiles obtained from transient tested samples and from base-irradiated samples. Radial distributions as well as volume integrated release values of  $^{137}\text{Cs}$  and of Xe are generally very similar when allowing for differences in power rating between neighbouring samples. For short test fuel pins with low axial power form factor there was found good agreement between local release values (from as well Cs as Xe) and results from puncturing (Ref. 1). The local release values from all ANF fuel samples (constant burnup) have been assembled in Fig. 3. No release occurred during 62h at 265 W/cm whereas 4% release occurred during 4h at 280 W/cm. Extension of the hold time from 42h to 62 h did not increase the fission gas release.

In summary, the experimental observations show, that transient thermal fission gas release in ANF fuel at 4.4%FIMA started in the narrow interval 260-280 W/cm; the corresponding fuel temperature (in hollow pellets) was between 1070 and 1200°C.

### 3.2. Radial Temperature Markers

It seems reasonable to assume that the onset position for thermal fission gas release can be used as a temperature marker, at least for a given fuel type at given burnup

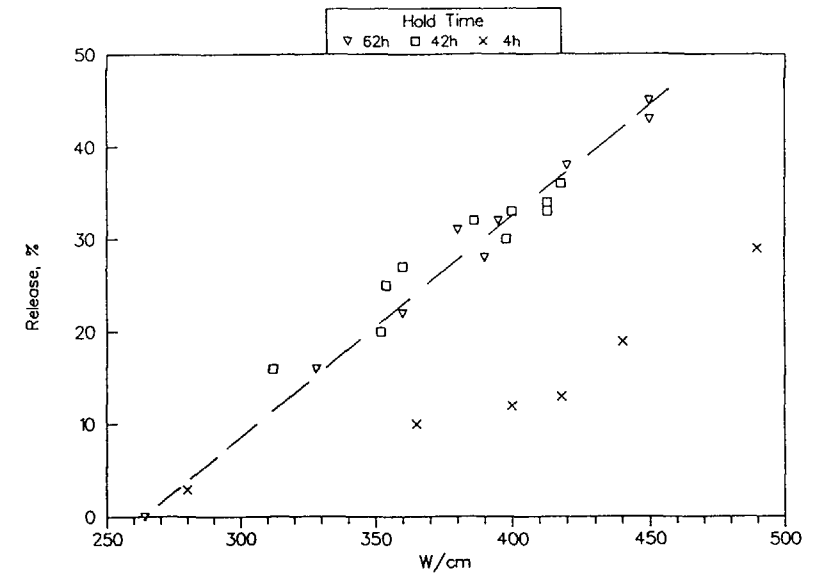


Fig. 3. Local release values measured after indicated hold times and linear heat ratings. PWR-fuel, 4.3-4.4%FIMA.

and hold time. Another marker which is closely associated to gas release is the onset of gaseous swelling.

Data from The Third Risø Fission Gas Project showed, that Cs behaved similarly to Xe with respect to release during power transients. Radial shapes as well as integrated releases were usually little different. Radial positions for start of Cs-release and completion of Cs release are therefore regarded as equivalent to start and completion of fission gas release.

An example of diametral porosity distribution (0.7-4 $\mu\text{m}$  pore size interval) is shown in Fig. 4. Moving from the rim towards the center the porosity is observed to decrease, reaching a minimum at  $r/r_o=0.76$  before a steep rise. The rise in porosity inside  $r/r_o=0.76$  is due to pores growing beyond the lower resolution limit of the light microscope, so the radial position of the minimum corresponds to the position for start of visible swelling, SBS (fractional radial position for Start of Bumptest related Swelling, pore size range indicated by suffix).

SBS<sub>0.7-1 $\mu\text{m}$</sub>  has been determined for all samples examined by porosity measurements. The number of pores in the interval 0.7-1 $\mu$  is usually small close to the start of swelling position and may therefore lead to some inaccuracy in the determination of SBS. Determination of SBS for the extended pore size interval 0.7-4 $\mu\text{m}$ , SBS<sub>0.7-4 $\mu\text{m}$</sub> , have

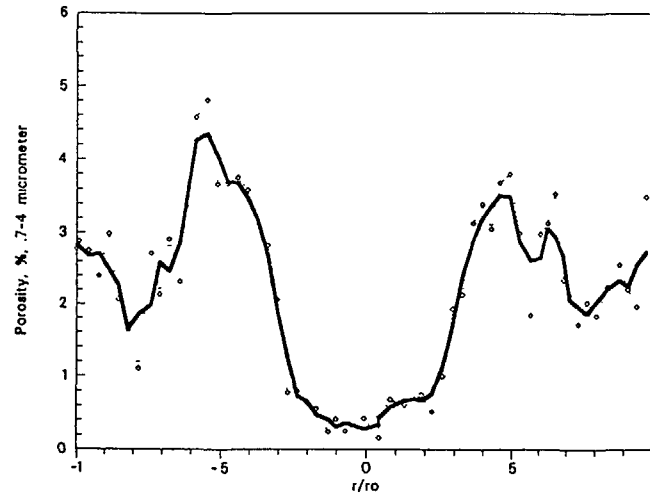


Fig. 4. Diametral distribution of porosity, as-measured (dotted line) and smoothed (3-point smoothing). Pore size interval 0.7-4 $\mu$ m. PWR fuel, 4.4%FIMA, transient tested to 450W/cm.

been made for the ANF samples, too. While the number of pores in the extended group size range is much larger, and the determination of  $SBS_{0.7-4\mu m}$  accordingly, more precise, the contribution of pores from the smallest size group remains low.  $SBS_{0.7-4\mu m}$  may therefore indicate start of swelling too close to the fuel center.

Fig. 5 shows fractional radial positions for start of fission gas release. for start of visible swelling (average of  $SBS_{0.7-1\mu m}$  and  $SBS_{0.7-4\mu m}$ ) and for completion of fission gas release. Each radial position is plotted against the local power of the sample, which provided the information. No points corresponding to completion of release after 4h were included, as Fig. 3 shows that completion did not occur within the short hold time.

Fig. 5 illustrates, that within the experimental error given by the width of the scatterband ( $\pm 0.04$ ) fission gas release started in the same radial position as transient test related swelling, visible by the light microscope. The temperature markers in Fig. 5 thereby delineate 3 isotherms:

- Isotherm A, corresponding to start of release/start of swelling with 4h hold time
- Isotherm B, corresponding to start of release/start of swelling with 42-62h hold time
- Isotherm C, corresponding to completion of release after 42-62h hold time

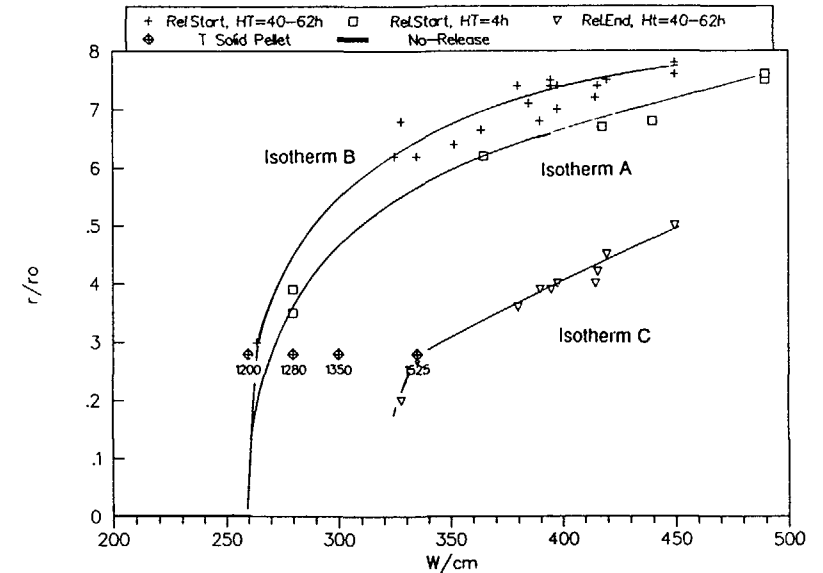


Fig. 5. Radial positions for start of release (measured after 4h at constant power, A, after 42-62h, B) and for completion of release (measured after 42-62h at constant power, C) plotted versus local power. The discrete temperature points were measured (hollow pellets) and converted to solid pellet temperatures (see para. 4.). PWR fuel, 4.3-4.4%FIMA.

Fig. 5 include PWR-data with little variation in burnup. Less numerous data were obtained with BWR-fuel at three burnup levels. Fig. 6 shows isotherm B of Fig. 5 together with comparable BWR fuel values covering the burnup interval 1.6-4.6%FIMA.

#### 4. DISCUSSION

The initial thermal fission gas release occurred from pellets without a centerhole at a linear heat rating in the interval 260-280 W/cm. In a hollow pellet rated to 260 W/cm the temperature at the inside of the hole (at  $r/r_o=0.28$ ) is 1070 $^{\circ}$ C, according to the measured temperature-power relation (AN3, Table 1). For a solid pellet with the same linear heat rating, the fuel center temperature will be higher, because 8% of the heat generation is moved to the volume inside  $r/r_o=0.28$  and, accordingly, has to be transported over a larger radial distance.

In order to assess the magnitude of the difference between fuel temperatures at  $r/r_o=0.28$  in hollow ( $T_{holl, 0.28}$ ) and solid ( $T_{sol, 0.28}$ ) pellets, equation 11.86.1 of Ref 4 was applied to both pellet types with appropriate dimensional parameters. The calculation

showed that  $T_{\text{sol}, 0.28}$  at a given linear heat rating corresponds to  $T_{\text{holl}, 0.28}$  in a pellet with a linear heat rating 17% higher than that of the solid pellet.  $T_{\text{sol}, 0.28}$  for 260 W/cm would thus correspond to  $T_{\text{holl}, 0.28}$  at 304 W/cm. According to the measured power/temperature relationships for He filled test fuel pins (Table 1)  $T_{\text{holl}, 0.28}$  at 304 W/cm is 1214° (AN3) and 1183° (AN10). A temperature difference at  $r/r_o=0.28$  of the order of 100-150°C is thereby indicated between hollow and solid pellets at similar linear heat ratings close to the power threshold for fission gas release.

The temperature at  $r/r_o=0.28$  in the solid pellets giving the first thermal release observed from the in-pile measurements has accordingly been quite close to 1200°C. The temperature in the fuel center might have been somewhat higher, although evaluation of the radial temperature profile indicates a flat temperature distribution close to the fuel center. The amount of gas available for release from the center part of the short axial fuel section with maximum rating is small, so a significant amount of fuel need to be enveloped by the release threshold isotherm to enable detection.

Isotherm A of Fig. 5, delineated by 4h hold time data points, may be calibrated by the in-pile measurements, which were made after a 4h conditioning period at constant power. On the figure is indicated a number of temperatures at  $r/r_o=0.28$ , as measured from the He-filled test AN3. The temperatures were read from Fig. 1 ( $T_{\text{holl}, 0.28}$  vs. power) at the power levels indicated with an addition of 17% to obtain the temperature of a solid pellet,  $T_{\text{sol}, 0.28}$ , as described above. The isotherm need to be steep in the interval 267W/cm-280W/cm, because 62h at 267 W/cm did not produce release, whereas release at 280W/cm occurred at  $r/r_o=0.33$  after 4h. The isotherm intersects  $r/r_o=0.28$  at a point, corresponding to a temperature in the range 1200-1280°C.

Isotherm B of Fig. 5 also has to include a point at  $r/r_o=0$  above 267 W/cm. Within the experimental accuracy this point is shared with isotherm A, strongly indicating that the temperatures of the two isotherms are the same. Consequently the release frontier moves towards the rim with hold time. The thermal release threshold temperature is accordingly little if at all affected by hold time.

Isotherm C corresponds to completed fission gas release. A temperature in the vicinity of 1525°C is indicated by the evaluated temperatures at  $r/r_o=0.28$ . Similar to isotherm B isotherm C represents a hold time of 42-62h, while the discrete temperature values given correspond to 4h hold time. The actual terminal power levels gave temperature readings close to 1525°C in several tests. The temperature was largely constant with hold time at these terminal power levels, showing that isotherm C did not move towards the rim with time. Isotherm C is therefore representative for as well 4h hold time as 42-62h hold time.

The PWR data discussed so far do not include a burnup variation. This is achieved with BWR-data, which cover a burnup interval between 1.6 and 4.6 %FIMA (GE-fuel). In Fig. 6 the radial positions for start of swelling/start of release from the few samples available (hold time 36-140h) have been plotted together with isotherm B of Fig. 5, which had corresponding hold times (42-62h). A difference of  $r/r_o \approx -0.06$  is seen

between radial positions for release in high burnup PWR and BWR fuel having fuel radii of 4.52 mm and 5.2 mm, respectively. The figure shows expansion of the fuel volume above the release threshold with burnup. With a release threshold of  $\sim 1200^\circ\text{C}$  in high burnup ANF fuel as argued above and a release threshold in fresh fuel (different fuel types) of about 1200°C (Ref. 5,6) it is reasonable to assume, that the release temperature threshold at intermediate burnup levels is independent of burnup and fuel types, too. KWU results pointing at 1200°C as the temperature for start of release at 2.5%FIMA (Ref. 7) supports the assumption. Fig. 6 thereby indicates the radial shift of a fixed release temperature isotherm with burnup. With an axial power level of 400 W/cm the change from 1.6%FIMA to 4.5%FIMA will increase the volume of fuel inside the release temperature threshold by a factor of two. This is illustrated in Fig. 7a, where a rough sketch of the outer part of the radial temperature profiles at 400 W/cm (solid pellets) is given for BWR fuel at three burnup levels, 1.6, 2.5 and 4.6%FIMA. The temperature at the outside is the temperature of the coolant. Onset of fission gas release is indicated at 1200°C.

SBS was measured on a number of hollow pellets from a diameter including the thermocouple hot junction. Fig. 7b shows coarse radial temperature profiles for two BWR pellets with 4.6 and 2.5%FIMA. The sketch uses 1) the coolant temperature, 2) the radial position for SBS which according to the above corresponds to approximate-

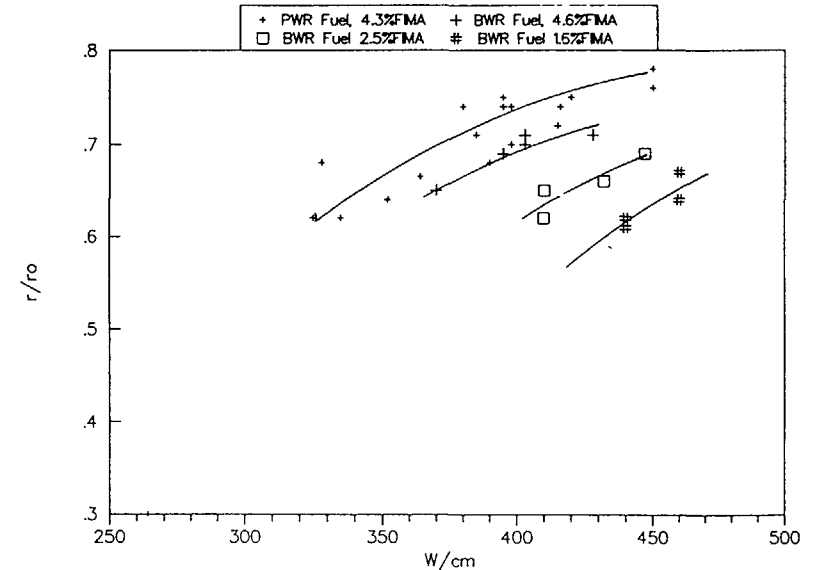


Fig. 6. Radial position for start of release, measured after 36-62h a constant power, plotted versus local power. PWR and BWR fuel at different burnup levels, as indicated.

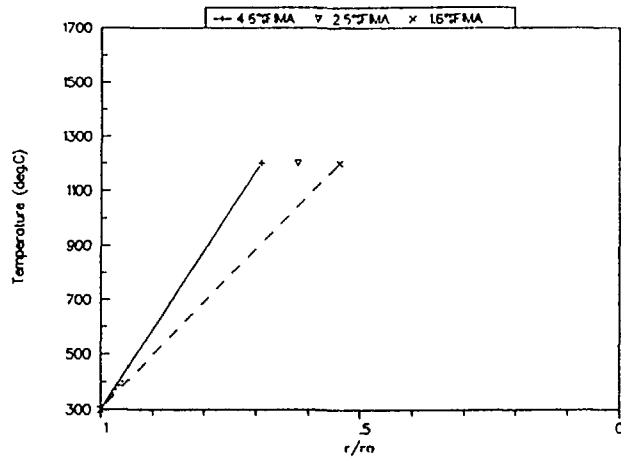


Fig 7a Coarse sketch of radial temperature distributions in non-releasing BWR fuel (without center hole) at three burnup levels. Straight lines connect the coolant temperature and the radial location of the 1200°C isotherm.

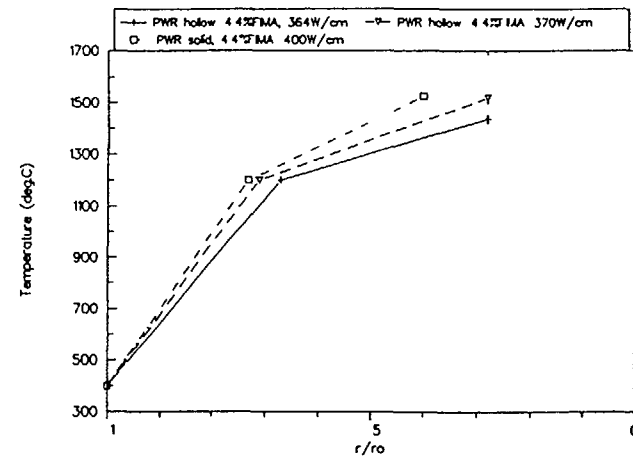


Fig 7c Coarse sketch of radial temperature distributions in hollow and solid PWR pellets at the same burnup (4.4% FIMA). The temperature distributions for the hollow pellets were obtained as in Fig 7b (including measured center temperatures); the profile for the solid pellet was inferred from Fig 5 (radial locations of the 1200°C and the 1525°C isotherms).

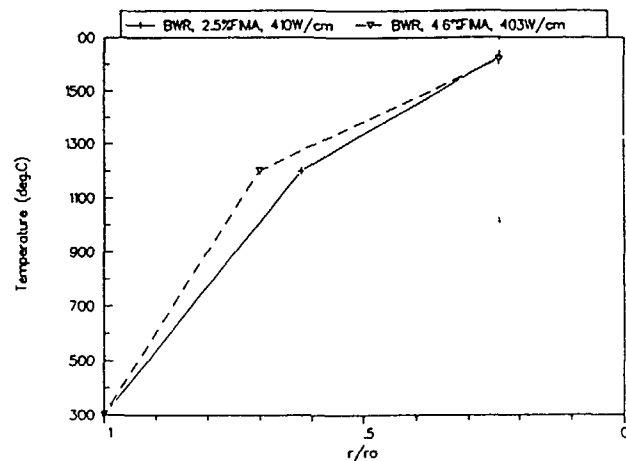


Fig 7b Coarse sketch of radial temperature distributions in hollow BWR fuel at two burnup levels. Straight lines connect coolant temperature, radial locations of the 1200°C isotherm and measured temperatures at the surface of the center hole.

ly 1200°C and 3) the actual thermocouple readings during the 42h hold time which produced SBS. Fig 7c shows coarse radial temperature profiles for two PWR hollow pellets (364 and 371 W/cm, respectively) and for a solid pellet (400 W/cm). Similar to Fig 7b the sketches use 1) the coolant temperature, 2) the radial location of the 1200°C isotherm and 3) the actual temperature measurements (hollow pellets) or the radial location of the 1525°C isotherm (solid pellet).

The data which are solely based upon experimental observations, indicate that accumulation of burnup creates a gradually increasing thermal barrier. Fig 6 shows that the barrier is situated outside  $r/r_o = 0.8$  and leads to increasingly steep temperature profiles in an outer, non-releasing ring of fuel (Fig 7). It is suggested, that the thermal barrier is established by the burnup dependent build-up of Pu at the rim by epithermal neutron capture and subsequent enhanced burnup of the layer.

## 5. CONCLUSIONS

Experimental evidence from in-pile measurements of fission gas release and fuel temperature shows that a fuel temperature close to 1200°C is required to produce thermal fission gas release in fuel with a burnup of 4.3% FIMA.

Release of as well Xe as Cs started at radial sample positions where swelling porosity grew beyond the lower resolution limit of the light microscope (0.5-0.7 μm). Xe and

Cs show similar release behaviour during power transients. Cs must therefore be on gaseous form at temperature levels resulting in release.

The onset temperature for thermal transient fission gas release is not dependent of hold time.

The onset temperature for thermal transient fission gas release appears independent of burnup and fuel type.

The radial location of the constant thermal transient fission gas release threshold temperature moves towards the fuel rim with burnup at constant power. The movement is assumably caused by gradual development of a thermal barrier at the fuel rim, related to buildup of Pu and locally enhanced burnup. Raising of the temperature gradient at the rim envelops an increasing amount of fuel by the constant release threshold isotherm, causing burnup enhancement of the transient fission gas release.

Completion of thermal release has been effected in the ANF fuel after 40h at approximately 1525°C.

#### REFERENCES

1. Knudsen,P., Bagger,C., Mogensen,M. Toftegaard,H.:Fission Gas Release and Fuel Temperature during Power Transients in Water Reactor Fuel at Extended Burn-Up. (In these proceedings).
2. The Third Risø Fission Gas Project, Final Report: The Methods. RISØ-FGP3-FINAL, Pt.2. March 1991.
3. Mogensen,M., Bagger,C., Toftegaard,H., Knudsen,P. and Walker,C.T.:Fission Gas Release Below 20kWm<sup>-1</sup> in Transient Tested Water Reactor Fuel at Extended Burn-Up. (in these proceedings).
4. Glasstone, S.: Principles of Nuclear Reactor Engineering. D. Van Nostrand Company, INC., 1955, p 662.
5. Lewis,W.B., McEwan, J.R., Stevens, W.H. and Hart, R.G.: Fission-Gas Behaviour in UO<sub>2</sub> Fuel, Proc. 3rd International Conference on Peaceful Uses of Atomic Energy, 1954, Vol. 11, pp 405-413
6. Notley, M.J.J.: A Computer Program to Predict the Performance of UO<sub>2</sub> Fuel Elements Irradiated at High Power Outputs to a Burnup of 10,000 MWd-tU, Nucl. App. Tech., Vol. 9, pp 195-200, 1970.
7. Sontheimer, F., Manzel, R. and Stehle, H.: Transiente Spaltgasfreisetzung und UO<sub>2</sub>-Mikrostruktur bei Leistungsrampen. J.Nuc.Mat. 124 (1984) pp 33-43

#### FISSION GAS RELEASE BEHAVIOR OF HIGH BURNUP FUELS DURING POWER RAMP TESTS

T. AOKI  
Nuclear Power Engineering Center,  
Tokyo

S. KOIZUMI  
Toshiba Corporation,  
Yokohama

H. UMEHARA  
Hitachi Limited,  
Hitachi, Ibaraki

K. OGATA  
Nippon Nuclear Fuel Development Company Ltd,  
Oarai, Ibaraki

Japan

#### Abstract

The Nuclear Power Engineering Test Center (NUPEC) conducted the MITI-sponsored Verification Test Program on High Performance Fuel to investigate the ramp behavior of Zr-liner fuels. This paper discusses fission gas behavior by correlating gas release data and pellet microstructural changes.

For the ramp tests were utilized segment fuels of burnup of ca. 20 and 40 GWd/tU, which were assembled into a standard BWR bundle and irradiated for 2 and 4 cycles, respectively, under normal BWR operation conditions. The ramp tests were carried out at the JMTR reactor in Japan and R-2 reactor in Sweden. The program was comprised of two types of tests, one in which power was held for a certain time (max.4 hours) at a ramp terminal level (RTL ; max.600 W/cm), and the other in which power cycling was executed between 220 and 440 W/cm. The number of cycles amounted to 100 and 1000, and the accumulated hold time at RTL did 34 and 200 hours, respectively.

The non-destructive measurement of  $\gamma$  ray intensity of Kr-85 at a plenum region revealed that fractional gas releases (FGRs) before the ramp tests were less than several percents for all the fuels supplied for the program. After the ramp tests, FGR was obtained via puncturing tests, and an extensive examination on pellet microstructural change was accomplished.

FGRs of the fuels which underwent 4-hour power hold at RTL increased approximately in proportion to RTL, and the maximum FGR was ca.40%. FGRs of 4-cycle irradiated fuels were greater than those of 2-cycle ones. That the FGR in a relatively short while of 4hours increased with burnup implies that released fission gas in the tested fuels consisted mainly of gas atoms accumulated at grain boundaries. Extension of burnup brings about a greater gas atom concentration at grain boundaries, resulting in more gas release due to the degradation of grain boundaries.

Plotting FGR data of power cycled fuels as a function of the accumulated hold time at RTL revealed that FGR was proportional to  $\sqrt{t}$  until several ten hours after reaching RTL. This shows that fission gas release after the burst release at the initial power increase was governed by diffusive flow of gas atoms from grain interior to grain boundaries. On the other hand, FGR digressed from the  $\sqrt{t}$  dependency after ca.200 hours. This implies that most of the gas atoms in a hotter region of pellet were released in the above time duration.

## 1. Introduction

Zr liner fuels are used in Japanese BWRs as a standard fuel. In order to demonstrate the good performance of Zr liner fuels against rapid power change events, Nuclear Power Engineering Corporation (NUPEC) has been carrying out "VERIFICATION TEST ON HIGH PERFORMANCE FUEL" sponsored by MITI. In this program, Zr liner fuels have soundly been power-ramp tested with various ramp modes. Fission gas release (FGR) mechanism during the power ramp tests is discussed based on the FGR data measured after the power ramp tests.

## 2. Outline of Power Ramp Tests

"VERIFICATION TEST ON HIGH PERFORMANCE FUEL" is aiming at verification of the excellent resistance of Zr liner fuels against PCI failures. Four test fuel assemblies equipped with some segment rods were fabricated by Japan Nuclear Fuel Co., Ltd. (JNF) and well precharacterized during the fabrication. The design specifications of the segment rods are basically the same as those of the current fuels for commercial use, except their length and the installation of neutron flux depressors in the plenums. Their design parameters are listed in table 1.

The four fuel assemblies were loaded at the medium power positions in the core of Fukushima Daiichi No.3 Unit, the Tokyo Electric Power Company, in 1984. They were irradiated under the normal BWR conditions and each one was respectively discharged after one, two, four and five cycle irradiations. Their achieved burnups are as follows:

<u>Assembly ID</u>	<u>Irradiated Cycles</u>	<u>Burnup</u>
F3GT1	1	6Gwd/t
F3GT2	2	15Gwd/t
F3GT4	4	32Gwd/t
F3GT3	5	40Gwd/t

They were transported to a hot laboratory of Nippon Nuclear Fuel Development Co., Ltd. (NFD) for detailed PIE. The segment rods were dismantled from the assemblies and subjected to nondestructive tests, as visual observation, dimensional measurement, eddy current test, gamma scanning, Kr-85 measurement at the plenum position to confirm the condition of the fuels before the power ramp tests.

Table 1 Pertinent Design Parameters of the Segment Fuel Rod

Pellet Diameter	10.3 mm
Pellet Length	10.3mm
Pellet Material	Sintered UO <sub>2</sub>
Pellet Density	95 %TD
Cladding Outer Diameter	12.27mm
Cladding Thickness	0.86mm
Cladding Material	Zircaloy-2 with Zr Liner
Rod Length	512mm
Pellet Stack Length	360mm
He Pressure	3 ata

Power ramp tests have been carried out mainly on the fuels irradiated for two and four cycles in Japan Material Test Reactor (JMTR) and STUDSVIK R2 reactor. The tests on the five cycle fuels are now under way.

Typical power ramp test modes for Zr liner fuels are shown in figure 1. One is a step ramp mode in which the power is rapidly increased to the terminal and is kept there for four hours. Another one is a power cycling mode in which the power is repeatedly changed for 100 and 1000 cycles between 220W/cm and 440W/cm.

After the power ramp tests the segment rods were returned to the hot laboratory for nondestructive and destructive examinations.

## 3. Test Results and Discussion

### 3.1. Fission Gas Release During Normal Operation

FGR mechanism was discussed in the previous paper(1). The results obtained on the standard fuel rods in this study appear to support the discussion in it.

The FGR data obtained in this study are represented in figures 2 and 3 with the previous ones. Figure 2 shows that the FGR rates at the burnup range lower than 15Gwd/t are very low. On the contrary, some fuels show high FGR rates and the scattering of the data increases suddenly at a higher burnup side. However, there are many fuel rods which keep their FGR rates very low as a few% at high burnup over 40Gwd/t. This implies that FGR does not depend only on the burnup, but on the other parameters.

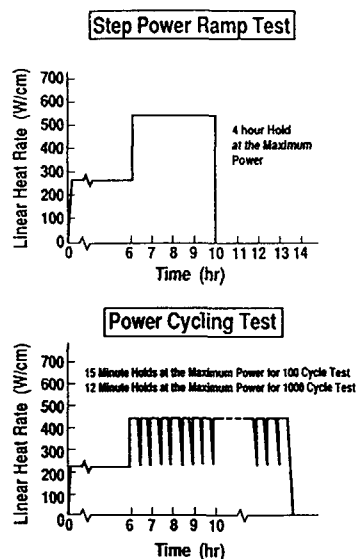


Fig. 1 Power Ramp Test Modes

The FGR data can well be correlated with the maximum power experienced at the burnup higher than 10GWD/t, as shown in figure 3. The FGR rate increases in proportion to the power when it exceeds over about 300W/cm. This implies that there exists a threshold power, may be a threshold temperature, in the FGR behavior.

The FGR rates of the full length fuel rods in this study are relatively low because most of them were irradiated at the power less than 300W/cm. Most of the data are not greater than a few%, however, one rod irradiated for four cycles and one rod irradiated for five cycles showed FGR rate of 19% and 10% respectively, even their experienced powers differed little from the others. This large data scattering can be considered to have caused by the positive feed back effect of FGR phenomena through gap conductance deterioration.

Radial distributions of typical fission product (FP) species and microstructural changes in the pellets were studied. Radial distributions of all FP species in a low FGR rate pellet shaped almost the same as that of local burnup; that means little fission gas was released from there. No remarkable microstructural changes were observed in low FGR rate pellets.

The concentration distributions of xenon and cesium in a high FGR rate pellet are shown in figure 4. They indicate that

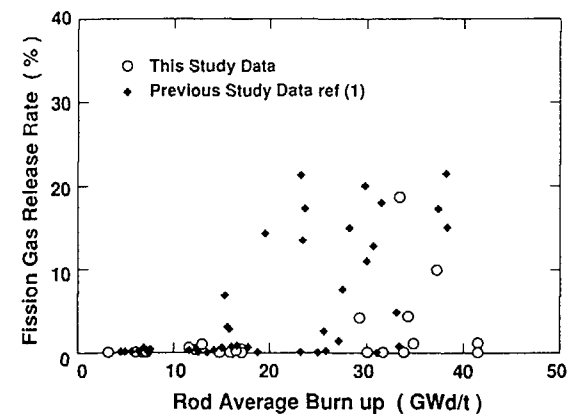


Fig. 2 Fission Gas Release Rate v.s. Burn up

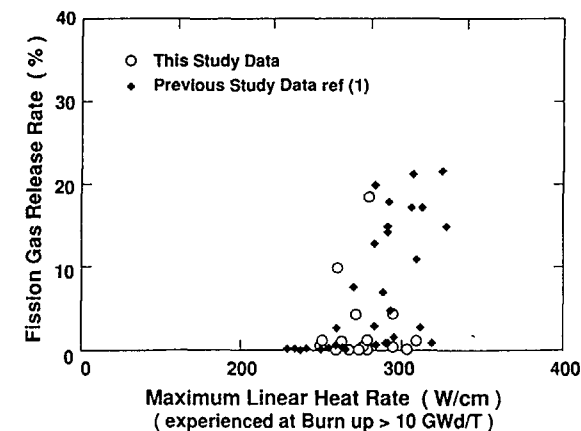


Fig. 3 Fission Gas Release Rate v.s. Maximum Linear Heat Rate

local FGR rate was close to 100% at the center region, on the contrary, almost 0% at the outer region. Between the two regions, there existed a narrow band where local FGR rate changed from 0% to 100%. The narrowness of this transition band seems to indicate that the FGR is not controlled by a continuously changing phenomena with the temperature, but by a suddenly changing thing.

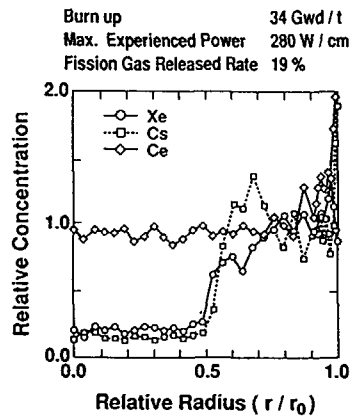


Fig. 4 Radial Distributions of Typical Fission Products in a Fuel Pellet Normally Operated in BWR (Example of High Fission Gas Release Rate Rod)

Microscopic observations revealed that the gas bubbles on the grain boundaries initiated to form tunnels, connecting each others in the FGR transition band.

Based on the above observations the FGR phenomena during normal operation is considered to step the following processes and the decisive one may be the tunnel formation on the grain boundaries;

- a) Formation of intra- and intergranular gas bubbles.
- b) Growth of the grain boundary bubbles and reduction of the intragranular bubbles because of their equilibrium pressure difference.
- c) Tunnel formation to open space by connecting the grain boundary bubbles.
- d) Accelerated FGR from the grains through the tunnels.

### 3.2. Tests before Power Ramp Tests

The segments were examined to confirm their condition before the shipment to JAERI-JMTR and Studsvik R2. Visual examination and eddy current test did not show any anomalies on them. Krypton-85 gamma intensities measured at their plenums showed their FGR rates were very low and that most of them were less than a detectable level.

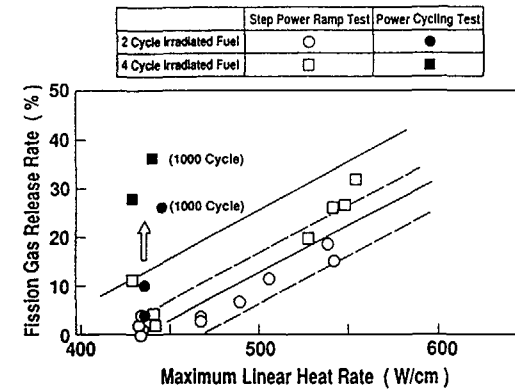


Fig.5 Fission Gas Release Rate v.s. Maximum Linear During Power Ramp Test

### 3.3. Examinations after Power Ramp Tests

The segment rods were confirmed their integrity with eddy current test and punctured to measure the FGR rates. The obtained data are shown in figure 5, relating with the terminal power at the ramp tests.

The FGR data from the fuels subjected to the step ramp tests (four hour holding) showed a tendency to increase with the terminal power rises. However, the maximum FGR rate of the fuels irradiated for two cycles was 19%, though some of them were ramped to about 550W/cm. This value is less than the maximum of the commercial fuels shown in figure 2. The maximum of the fuels irradiated for four cycles was 33%. The fuel was similarly ramped to 560W/cm.

Fairly large difference was noticed between the data of two and four cycle irradiated fuels. As shown in figure 3, burnup showed very little influence on the FGR in commercial use fuels. However, the data obtained from the ramp test fuels in this study suggested that the FGR during ramp tests had a relatively large dependency on burnup.

The fuel rods tested with a power cycling mode showed a tendency that the FGR rate increases with the number of the power cycling. The fuel, irradiated for two cycles, showed 27% of the FGR rate after 1000 time power cycling, that is greater than the maximum FGR rate of the fuels step ramped to 550W/cm.

Figure 6 shows the concentration distributions of typical FPs in the pellets after the ramp tests, measured by EPMA. They had been irradiated for two cycles and their burnups range from 17 to 19Gwd/t. The distributions of xenon and cesium concentration in the pellets before the ramp tests could be

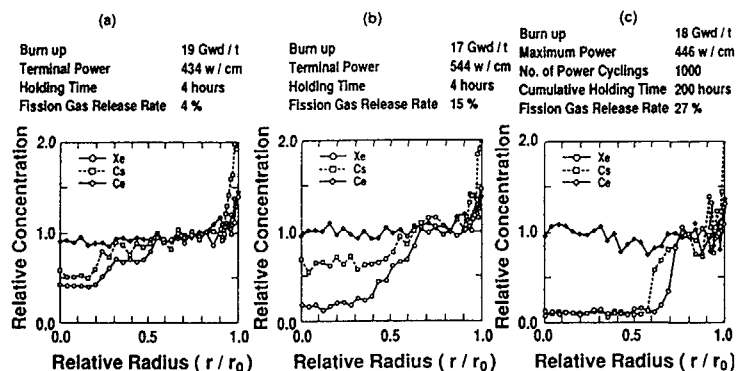


Fig. 6 Radial Distributions of Typical Fission Products after Power Ramp Tests (2 Cycle Irradiated Fuels)

assumed to be flat at the center, because they had been confirmed that their FGR rates were very low. After the ramp tests all the pellets appeared to have released pretty amount of xenon and cesium from the center.

The fuels tested with a step ramp mode showed different FP concentration distributions from that of the fuels steadily irradiated in commercial BWRs (figure 6(a),(b) v.s. figure 4). A distinctive difference is obscurity of the FGR transition band; the concentration in the former pellet changed gradually from the center to the mid-radius position, in contrast with the abrupt change of the latter one. The relatively large concentration difference was also noticed between xenon and cesium at the center of the former pellets. On the contrary, coincidental distributions have been observed in the fuels used in commercial BWRs.

The FP concentration distributions in the pellet experienced 1000 power cyclings, as shown in figure 6(c), appeared to have approached to that of the fuels steadily irradiated in commercial BWRs. Xenon and cesium concentration distributed similarly in it and both changed abruptly at the pellet mid-radius position. The xenon concentration level at the pellet center region indicates that the local FGR rate was almost 100% there.

Figure 7 shows comparison of the distributions in the fuel ramped to 440W/cm with that of the fuel experienced 100 power cyclings at the same power level. Both fuels were irradiated for four cycles and their burnups are 35 and 38GWd/t. The step ramped fuel represented basically the same distributions as that of the two cycle irradiated fuels, similarly ramped, as shown in figure 6(a). However, the local FGR rate appeared to

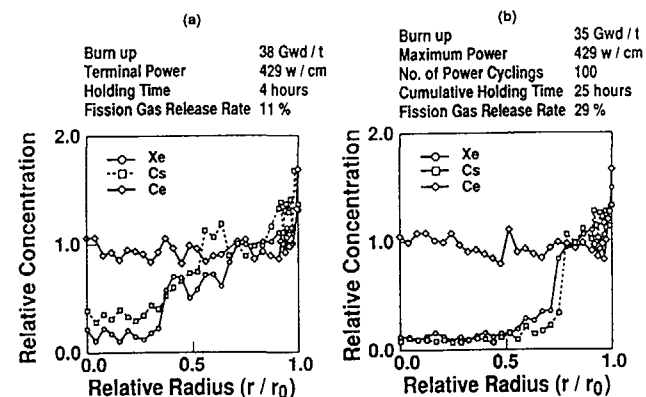


Fig. 7 Radial Distributions of Typical Fission Products after Power Ramp Tests (4 Cycle Irradiated Fuels)

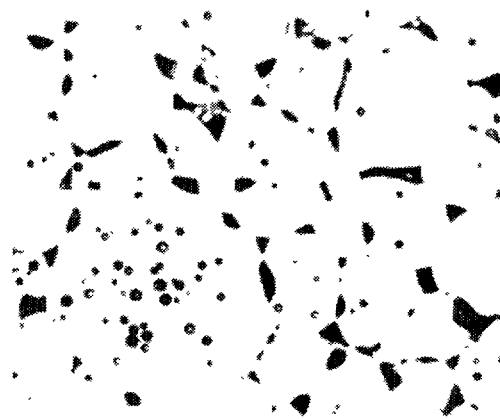
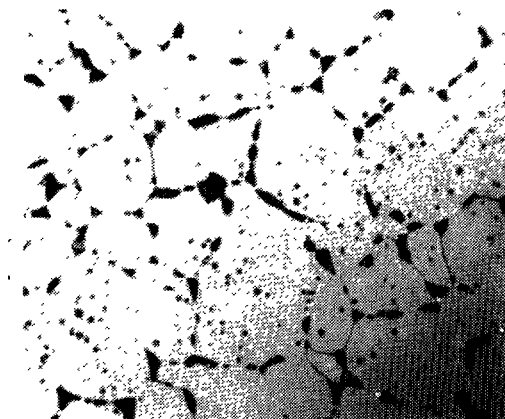
have much increased at the pellet center. The distribution of the power cycled fuel showed that it had also approached to that of the steadily operated fuels, as shown in figure 6(c), though the cycling number was 100. These two cases indicate that the higher the burnup is, the faster the FGR rate increases and approaches to the condition of the steadily operated fuels.

Photo 1 shows typical parts of the pellets after the power ramp tests. One was a two cycle irradiated fuel and ramped to 544W/cm (the same fuel of figure 6(b)) and the other was a four cycle irradiated fuel and ramped to 530W/cm. Photo 2 shows the typical fractography of the same pellet shown in photo 1. Observed microstructural features appeared in the fuels power-ramped are summarized as follows;

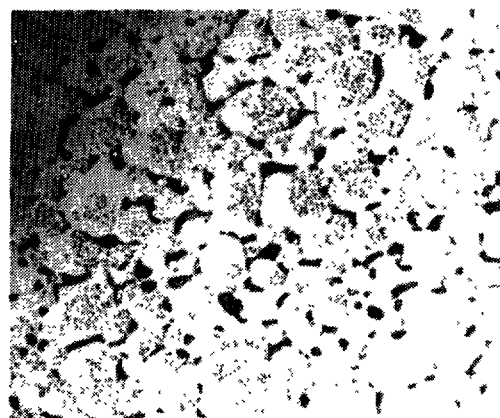
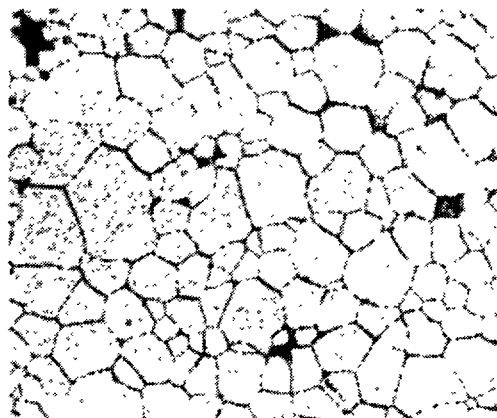
- No remarkable changes from as-fabricated were found at the outer low-temperature region, seemed retaining almost of fission gas.
- Huge number of very fine bubbles were observed at the vicinal area to the outer boundary of the FGR transition band. They seemed to have appeared due to a rapid temperature increase.
- The bubbles, especially on the grain boundaries, showed a tendency to grow more toward the center. Pearl necklace structure of bubbles was noticed at the grain boundaries in the outer side area of the FGR transition band.
- The grain boundary bubbles formed the tunnels to open space, connecting each other. The intragranular bubbles had disappeared from the surface regions of the grains.
- The grains grew gradually with further temperature increase.

50  $\mu$ m

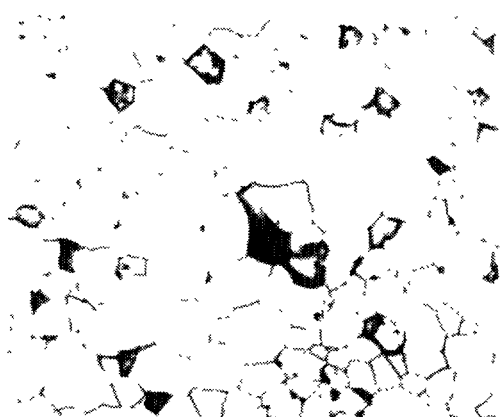
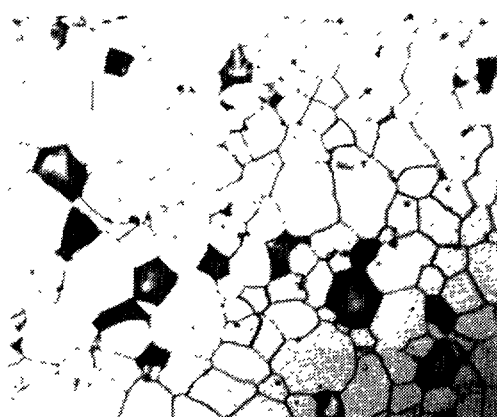
Center  
( $r / r_0 = 0$ )



Mid - Radius  
( $r / r_0 = 0.5$ )



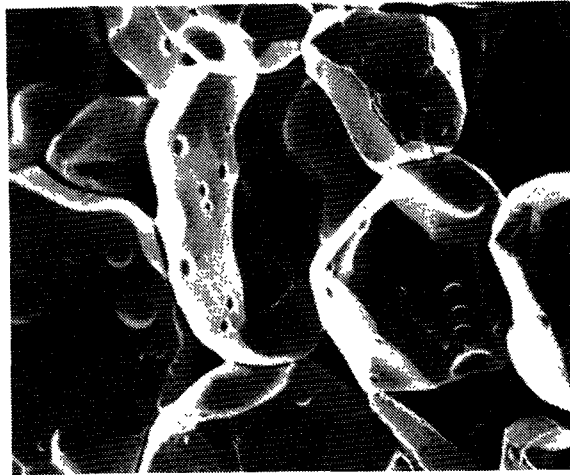
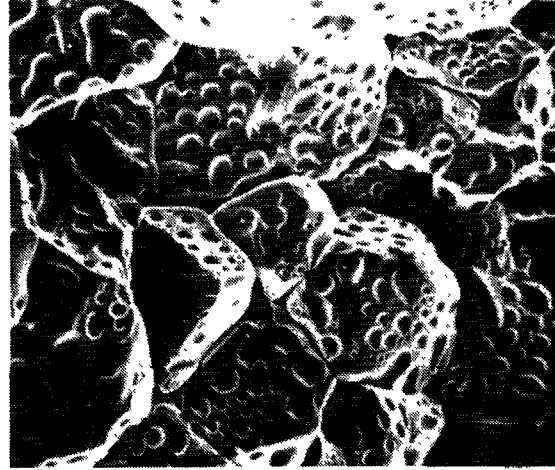
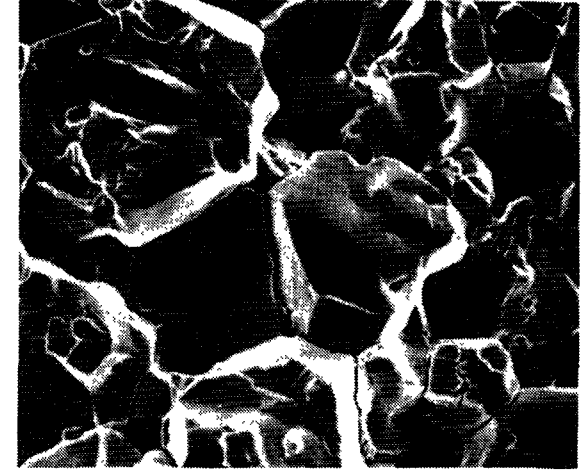
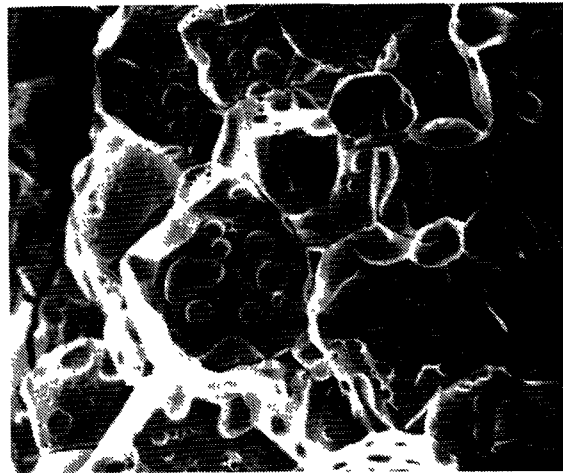
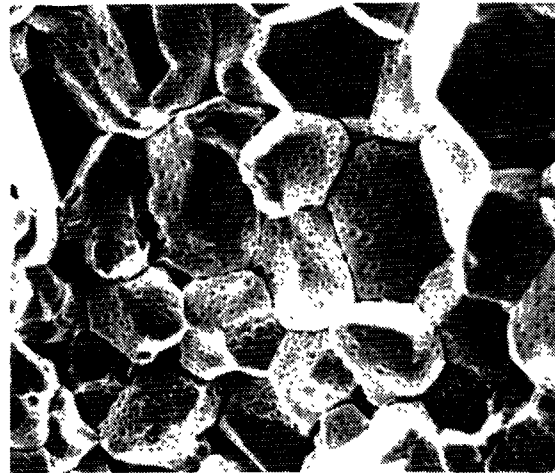
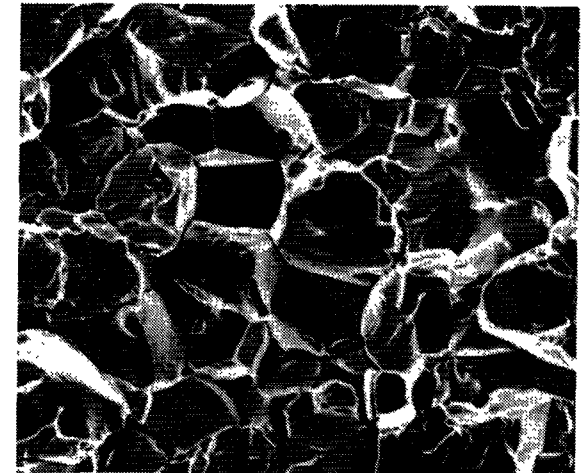
Pheriphery  
( $r / r_0 = 0.95$ )



Burnup 17 GwD / t  
Terminal Power 544 w / cm  
Holding Time 4 hours  
Fission Gas Release Rate 15%

Burnup 35 GwD / t  
Terminal Power 530 w / cm  
Holding Time 4 hours  
Fission Gas Release Rate 20%

Photo 1 Typical Pellet Ceramographs  
After Power Ramp Tests


 $r/r_0 = 0$ 

 $r/r_0 = 0.5$ 

 $r/r_0 = 0.7$ 

 $r/r_0 = 0.4$ 

 $r/r_0 = 0.6$ 

 $r/r_0 = 0.9$ 

 15  $\mu\text{m}$ 

Burn up 17 Gwel / t, Terminal Power 544w / cm, Holding Time 4 hours, Fission Gas Release Rate 15%

Photo 2 Typical SEM Pictures Showing Grain Boundary Bubble Formation

### 3.4. Fission Gas Release Mechanism during Power Ramp Tests

The results obtained in this study suggest that the FGR mechanism during the power ramp tests is basically the same as that already discussed in 3.1. The latter seems to describe the completely equilibrated condition, however, the former does on the transient situation, on the way to the latter's equilibrium condition.

When the fuel was irradiated at a temperature lower than the threshold that was discussed in 3.1, the pellet can retain fission gas in the matrix beyond the solubility. A fuel behavior analysis code predicted the threshold temperature as  $1100 \pm 150^\circ\text{C}$ . When a large temperature rise beyond the threshold occurs, over-saturated fission gas seems to precipitate into very fine bubbles, due to the increase of the gas diffusion rate and to the softening of the matrix. An abrupt temperature rise makes the bubble precipitations distributed homogeneously and in a high number density.

The pressure of each bubble is equilibrated with the static pressure and the surface tension. Surface tension is proportional to the curvature of the bubble, consequently, it decreases rapidly with bubble growth. The larger the bubble size is, the lower the equilibrium pressure is. When a temperature rise occurs, gas bubbles will be formed, gathering gas from the surrounding. The gas quantity that each bubble can accumulate for a time may be constant. This might be the reason that lots of bubbles develop in a uniform size.

The grain boundary bubbles have the lower equilibrium pressure than the intragranular bubbles do, because the former has a lenticular shape. Therefore, the grain boundary bubbles, especially the larger ones, have a tendency to grow faster, absorbing gas from the surrounding smaller ones. When they grow enough to connect each other, they will make tunnels to open space. Once the tunnels developed, fission gas stored in them will be released instantaneously and the gas concentration there will be lowered much. This increases the intra- and intergranular concentration difference and gas diffusion flow from the grains will be accelerated. The intragranular gas bubbles will become unstable, when the gas concentration level is lowered slightly. This might partly contribute to the zonal disappearance of the intragranular bubbles from the grain surfaces.

The following two processes are considered important in the FGR mechanism during power ramp tests.

#### a) The tunnel formation

A certain quantity of gas is required to have been accumulated on the grain boundaries. This process will be affected by burnup that determines absolute fission gas concentration.

#### b) Gas release from the grains after the tunnel formation

This process seems to depend much on a temperature. However, the pellet, ramped to  $550\text{W/cm}$  and held for four hours, seemed to retain pretty amount of fission gas in its center part. The center temperature was estimated as over  $1800^\circ\text{C}$ . This suggests that relatively long time is necessary to release fission gas completely from the grains after the tunnel formation, even at a such high temperature.

Figure 8 shows the relation of FGR rate and the maximum experienced power both of steady operations and of power ramp tests. The observation that local FGR rate changes from 0% to 100% in a narrow band, possibly corresponding to the threshold temperature, seems to indicate that the FGR rate can reasonably be estimated with the pellet volume fraction which temperature exceeds the threshold. The extrapolated curves of steadily operated fuel's data in figure 8 show the equivalent FGR rates, evaluated by the above method. These curves predict the FGR rates of the fuels steadily operated at  $440\text{W/cm}$  and  $550\text{W/cm}$  as about 40% and 50%, respectively.

Figure 9 shows the relation between the FGR rates and the cumulative holding time at the terminal power. This figure suggests that the FGR rate increases with the cumulative holding time, approaching to 40% that was guessed as the steady operation data in figure 8. The increase rate of the FGR rate is proportional to  $\sqrt{t}$ . This implies that the FGR at this stage is ruled by the gas diffusion, possibly from the grains to the

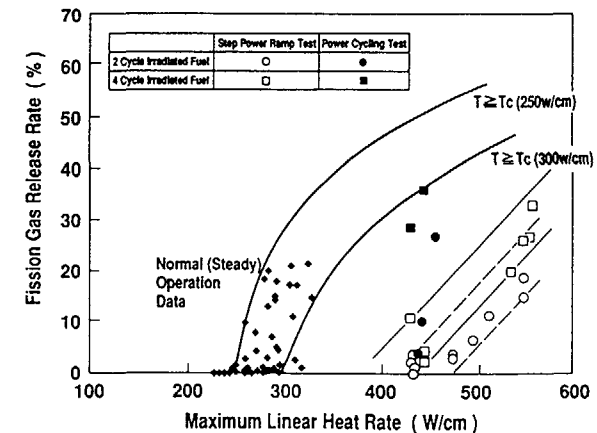


Fig.8 Fission Gas Release Rate v.s. Maximum Linear Heat Rate (Commercial BWR Fuels and Power Ramp Tested Fuels)

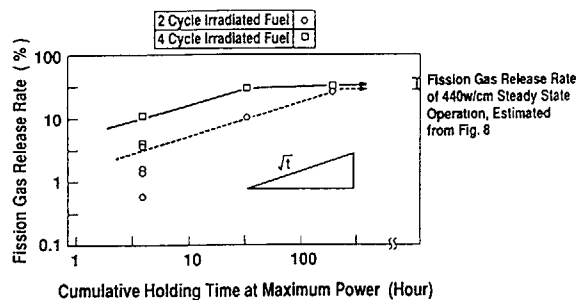


Fig.9 Fission Gas Release Rate v.s. Cumulative Holding Time at Maximum Power

tunnels. It also indicates that a few days or a few months are necessary to attain the equilibrium condition, depending on the burnup and the power ramp condition.

Power cycling has been reported to affect on FGR behavior, however, figure 9 seems to suggest that its effect becomes small when the operation time is long enough.

The FGR data of the power ramped fuels in this study showed the dependencies both on the terminal powers and on the burnups, i.e. the higher the burnup is, or the higher the terminal power is, the shorter time it is necessary to attain the equilibrium condition. However, in the case of 38GWD/t burnup fuel, which was power-ramped to 550W/cm, four hour holding was not enough to reach the equilibrium. It suggests that the additional FGR is not necessary to take into account during the short time power increase transients.

#### 4. Conclusion

FGR behavior during the power ramp test was studied on high burnup fuels to 40GWD/t. The results obtained in the study can be summarized as follows;

- 1) The FGR mechanism during the power ramp test is essentially the same as that of the steady irradiation.
- 2) The process substantially control the FGR behavior during the power ramp test is considered as follows;
  - a) The tunnel formation that depends on gas diffusion to the grain boundaries, growth and connection of the grain boundary bubbles.
  - b) Gas diffusion from the grains after the tunnel formation
- 3) The tunnel formation process might be determined by the gas accumulation on the grain boundaries. Therefore, the burnup dependency might appear on the FGR data of power ramp tests.
- 4) Power cycling effect on FGR is expected to be small in commercial BWR fuels, because they will be operated for long time.
- 5) A short time power increase, as an abnormal transient, is expected not to induce additional FGR.

#### Reference

- (1) Koizumi S., et al., "STUDY IN FISSION GAS RELEASE FROM HIGH BURNUP FUEL" IAEA Meeting on FUEL PERFORMANCE AT HIGH BURNUP FOR WATER REACTORS, held in STUDSVIK, SWEDEN, 5-8 June 1990, IWGFPT/36 p102

# FISSION-GAS RELEASE IN FUEL PERFORMING TO EXTENDED BURNUPS IN ONTARIO HYDRO NUCLEAR GENERATING STATIONS

M.R. FLOYD\*, J. NOVAK, P.T. TRUANT  
Nuclear Operations Central Division,  
Ontario Hydro,  
Chalk River, Ontario,  
Canada

## Abstract

The performance of 37-element fuel at extended burnups is of interest to reactor operators who desire a better understanding of the limits of operation, particularly for fuel resident in fuel channels that cannot be refuelled for an extended period of time.

The average discharge burnup of CANDU fuel is about 200 MWh/kgU. A significant number of 37-element bundles have achieved burnups in excess of 400 MWh/kgU. Some of these bundles have experienced failures related to their extended operation.

To date, hot-cell examinations have been performed on fuel elements from nine 37-element bundles irradiated in Bruce NGS-A that have burnups in the range of 300-800 MWh/kgU. Most of these have declining power histories from peak powers of up to 59 kW/m.

Fission-gas releases of up to 26% have been observed and exhibit a strong dependence on fuel power. This obscures any dependence on burnup.

The extent of fission-gas release at extended burnups was not predicted by low-burnup code extrapolations. This is attributed primarily to a reduction in fuel thermal conductivity which results in elevated operating temperatures. Reduced conductivity is due, at least in part, to the buildup of fission products in the fuel matrix. Some evidence of hyperstoichiometry exists, although this needs to be further investigated along with any possible relation to CANLUB graphite coating behaviour and sheath oxidation.

Residual tensile sheath strains of up to 2% have been observed and can be correlated with fuel power/fission-gas release. SCC-related defects have been observed in the sheath and endcaps of elements from bundles experiencing declining power histories to burnups in excess of 500 MWh/kgU. This indicates that the current recommended burnup limit of 450 MWh/kgU is justified. SCC-related defects have also been observed in ramped bundles having burnups <450 MWh/kgU. Hence, additional guidelines are in place for power ramping extended-burnup fuel.

## 1. INTRODUCTION

Thirty-seven element CANDU<sup>1</sup> fuel bundles irradiated in Ontario Hydro Nuclear Generating Stations consist of three concentric rings of elements about a central element (Figure 1). Each element contains natural UO<sub>2</sub> (0.7 wt% U-235) and has a length of approximately 0.5 m and a diameter of 13 mm. The inner surface of outer and intermediate elements of CANDU 37-element bundles are coated with a graphite-based coating called "CANLUB". This coating has been shown to enhance power-ramp performance by decreasing the susceptibility to SCC.<sup>2</sup> These bundles are typically irradiated for 12-16 months to burnups of 200 MWh/kgU,<sup>3</sup> achieving peak powers of up to 60 kW/m. Refuelling of the reactor is accomplished on-power.

Approximately 400 000 thirty-seven-element bundles have been successfully irradiated. The cumulative bundle defect rate is 0.1%. On an element basis, the defect rate is significantly lower (<0.01%). Most of the failures can be attributed to manufacturing and debris fretting. Approximately 10% of the failures are related to PCI.<sup>4</sup>

Approximately 210 thirty-seven-element bundles have achieved burnups in excess of 400 MWh/kgU in Bruce Nuclear Generating Station reactors. The majority of these bundles have not been inspected in the irradiated fuel bay or examined in hot cells because they showed no evidence of having failed in-reactor (Bruce reactors have on-power failed-fuel monitoring systems). Of those bundles inspected/examined, four have exhibited PCI-failures and high fission-gas releases. Thus, the PCI defect rate for 37-element bundles at burnups greater than 400 MWh/kgU is approximately 2%.

The performance of CANDU fuel is of interest to reactor operators who desire a better understanding of the limits of operation, particularly for fuel resident in fuel channels that cannot be refuelled for an extended period of time. Currently, the recommended burnup limit for fuel irradiated in Ontario Hydro Nuclear Generating Stations is 450 MWh/kgU.

## 2. EXTENDED-BURNUP FUEL EXAMINATIONS

To date, hot-cell examinations have taken place at Chalk River Laboratories (AECL Research) on fuel elements from nine 37-element bundles that have been irradiated to extended burnups in Bruce NGS-A. Operational data and examination results are summarized in Table I. Element burnups are in the range of 300-800 MWh/kgU, most having been determined chemically by HPLC.<sup>5</sup>

1. CANada-Deuterium-Uranium; registered trademark
2. Stress-Corrosion Cracking
3. 240 MWh/kgU = 10 GWD/TeU
4. Pellet-Clad Interaction
5. High-Performance-Liquid-Chromatography<sup>(1)</sup>

\* Attached to Chalk River Laboratories (AECL Research).

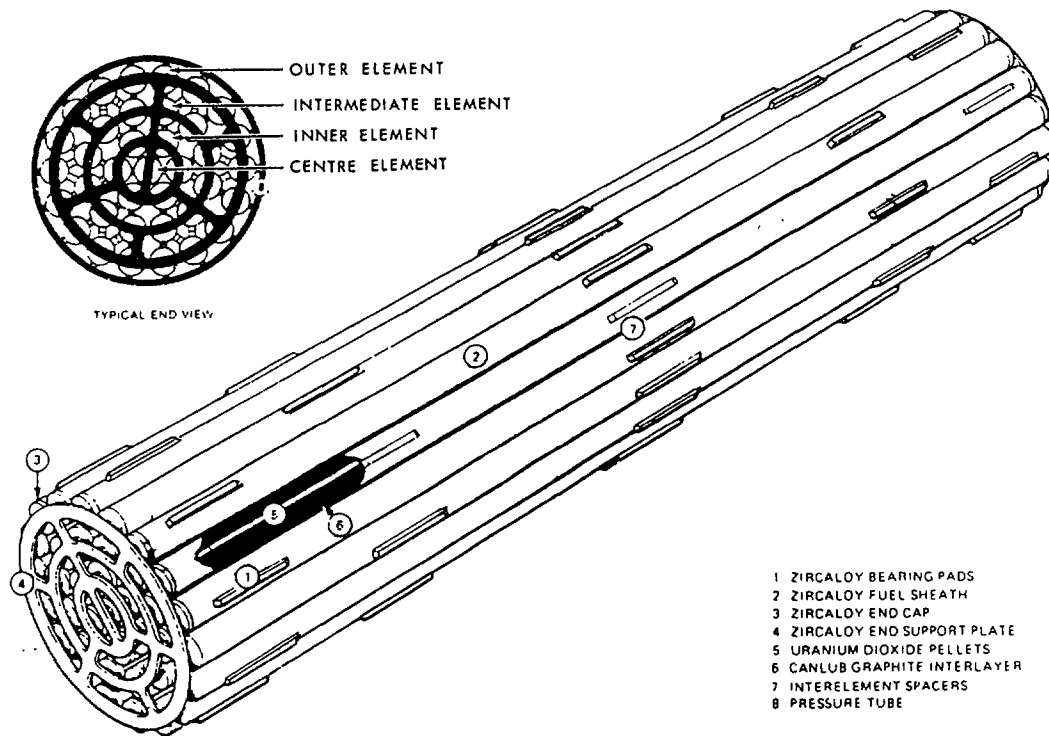


FIGURE 1: CANDU 37-element bundle irradiated in Ontario Hydro Nuclear Generating Stations. Each element contains natural  $UO_2$  (0.7 wt% U-235) and has an approximate length of 0.5 m and diameter of 13 mm. Note concentric geometry, which results in differential powers/burnups.

TABLE I: DATABASE FOR ONTARIO HYDRO 37-ELEMENT FUEL EXAMINED IN HOT CELLS AT CHALK RIVER LABORATORIES

Bundle	Power History Type <sup>a</sup>	Element Type <sup>b</sup>	Discharge Burnup (MWh/kgU)	Peak Linear Power (kW/m)	% Fission Gas Release	Average Grain Size ( $\mu m$ )		Average <sup>d</sup> CANLUB Retention(%)	Sheath ID Oxide Thickness( $\mu m$ ) <sup>e</sup>	Peak Sheath Strain <sup>f</sup> (%)	PCI Defects ?	
						Initial	Final <sup>c</sup>					
F04857C	Declining	Outer	570 <sup>g</sup>	51	3-10	8	20	20	1	0.0	no	
		Intermediate	456 <sup>g</sup>	42	-	8	-	-	-	-	no	
		Inner	400 <sup>g</sup>	36	0.1-0.2	8	8	-	-	-	no	
J24518C	Constant	Outer	458 <sup>g</sup>	24	0.1-0.2	7	7	73	<1	0.2	no	
		Intermediate	371 <sup>g</sup>	19	-	7	7	78	<1	0.2	no	
		Inner	348 <sup>g</sup>	18	-	7	7	-	6-8	0.0	no	
J24533C	Declining	Outer	772 <sup>g</sup>	52	24-26	6	21	-	-	0.9	yes	
		Intermediate	624 <sup>g</sup>	42	1.4-1.9	6	10	-	-	0.7	no	
		Inner	568 <sup>g</sup>	38	-	7	9	-	-	0.5	no	
J24546C	Declining	Outer	757 <sup>g</sup>	51	23-24	6	14	6	1-2	1.5	yes	
		Intermediate	615 <sup>g</sup>	41	0.5-0.8	6	7	60	<1	0.7	no	
		Inner	559 <sup>g</sup>	38	0.2-0.3	5	6	-	1-8	0.1	no	
J64703C	Ramped	Outer	441 <sup>g</sup>	42	12-14	9	13	88	<1	1.9	yes	
		Intermediate	357 <sup>h</sup>	34	<0.3-0.5	9	19	88	<1	0.8	no	
		Inner	335 <sup>h</sup>	32	<0.3	10	12	-	3-11	0.3	no	
J64728C	Ramped	Outer	323 <sup>h</sup>	47	11-12	10	-	-	-	-	yes	
J98315C	Declining	Outer	583 <sup>g</sup>	57	-----all outer elements failed (PCI)-----							yes
		Intermediate	474 <sup>g</sup>	47	4-5	9	12	63	1-5	2.0	no	
		Inner	432 <sup>g</sup>	42	0.1-0.3	9	10	-	6-10	1.4	no	
		Centre	402 <sup>g</sup>	40	0.1	9	11	-	6-10	0.7	no	
J98324C	Declining	Outer	605 <sup>g</sup>	56	-	-	-	-	-	-	yes	
J03311V	Declining	Outer	544 <sup>g</sup>	59	23-24	8	27	62	<1	2.0	no	
		Intermediate	447 <sup>g</sup>	48	2.5-2.7	9	15	63	2-3	0.3	no	

Notes: a - see Section 2.1 and Figures 1-3  
b - see Figure 1  
c - pellet-centre  
d - only outer and intermediate elements are CANLUB-coated  
e - most of the oxides >1  $\mu m$  were discontinuous (patches)  
f - the value quoted is the highest average midpellet strain observed on any of the elements  
g - chemically-determined by HPLC<sup>(1)</sup>  
h - calculated

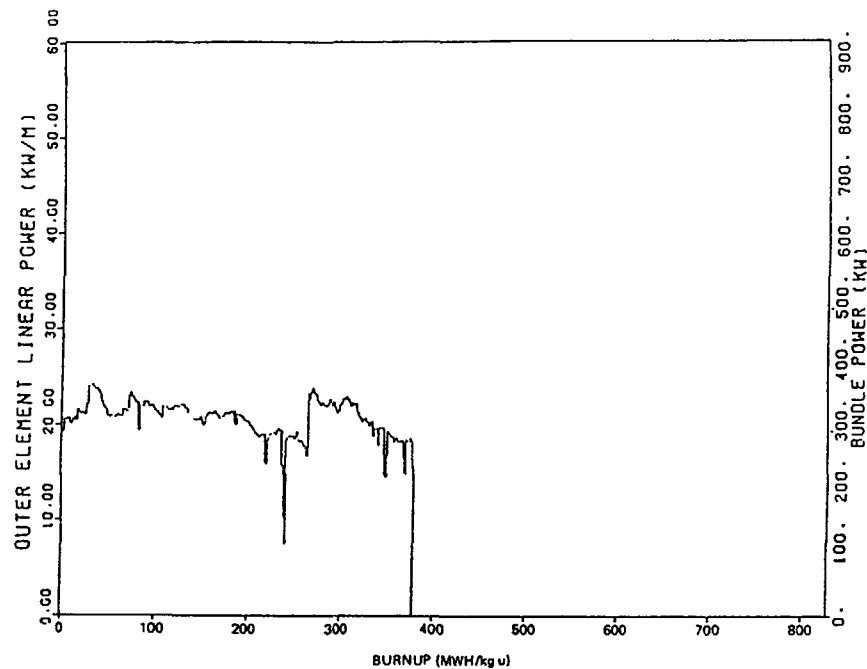


FIGURE 2: "Constant" power history of bundle J24518C.

## 2.1 POWER HISTORIES

The irradiation histories of the nine bundles can generally be categorized as either constant, declining or ramped. Figure 2 shows the outer element linear power (kW/m) vs average bundle burnup (MWh/kgU) for bundle J24518C. This irradiation history is characterized by a relatively low constant power (average = 21 kW/m). Figure 3 shows the irradiation history for bundle J03311W, which achieved a high power (59 kW/m) at low burnup (<100 MWh/kgU) and then experienced a decline in power proportional to the decline in fissile atoms. Five other bundles in the database experienced similar declining power histories (F04857C, J24533C, J24546C, J98315C, and J98324C). Figure 4 shows the irradiation history of bundle J64703C, which was irradiated at low power to a burnup of ~300 MWh/kgU, at which time it was ramped to higher power. Bundle J64728C experienced a similar ramped power history.

A thermal-flux shielding effect is experienced in all 37-element CANDU bundles such that the inner rings of elements achieve lower powers and burnups than the outer ring of elements (Table I).

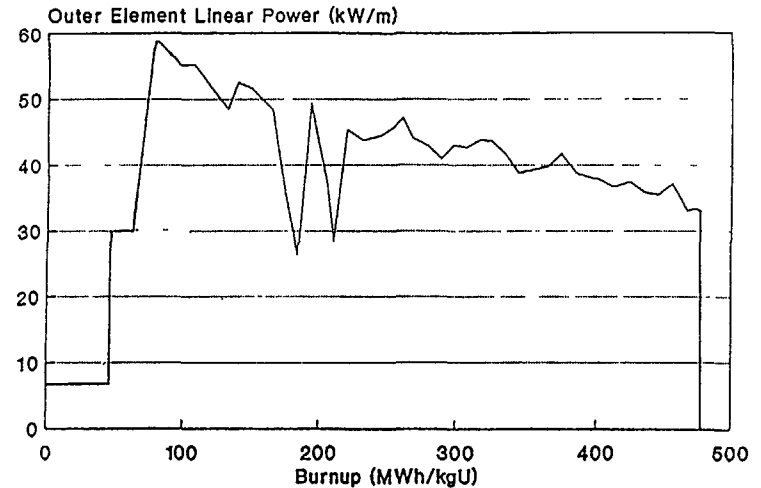


FIGURE 3: "Declining" power history of bundle J03311W typical of that for F04875C, J24533C, J24546C, J98315C, and J98324C.

## 2.2 FISSION-GAS RELEASE: RESULTS AND DISCUSSION

Table I summarizes the fission-gas releases calculated from gases collected from intact elements at ambient hot-cell temperatures. Figure 5 shows that fission-gas release exhibits an exponential dependence on fuel power. At peak powers less than 40 kW/m, fission-gas releases are low (<1%). In the range of 40-50 kW/m, fission-gas releases are generally in the range of 1-10%. At powers in the range of 50-60 kW/m, releases of up to 26% have been observed. This strong thermal dependence obscures any burnup dependence (Figure 6).

Generally, extrapolations using fuel modelling codes verified with low-burnup fuel irradiations have underpredicted fission-gas release at extended burnups,<sup>[2]</sup> particularly for fuel irradiated at high powers (peak powers above 50 kW/m). It has been postulated that higher-than-predicted fuel temperatures have been achieved at extended burnups as a result of a reduction in fuel (U<sub>2</sub>) thermal conductivity and/or a degradation in fuel-to-sheath heat transfer.<sup>[3]</sup>

The thermal conductivity of fission gases (predominantly xenon) is significantly lower than helium, which is present as a filling gas from the time of fabrication. As a result, the release of fission gas into the fuel-to-sheath gap may result in a degradation in gap conductance. The timing and extent of degradation depends on the gap size and the ratio of gas species present. LWR rods with large gaps have demonstrated a sensitivity to fission-gas "poisoning"; however, those with small gaps do not.<sup>[4]</sup> CANDU fuel elements exhibit a high degree of PCI (Section 2.5) and hence, fuel-to-sheath gaps are relatively small. For this reason, elevated fuel temperatures in CANDU fuel at extended burnups is not primarily attributed to a degradation in gap conductance.

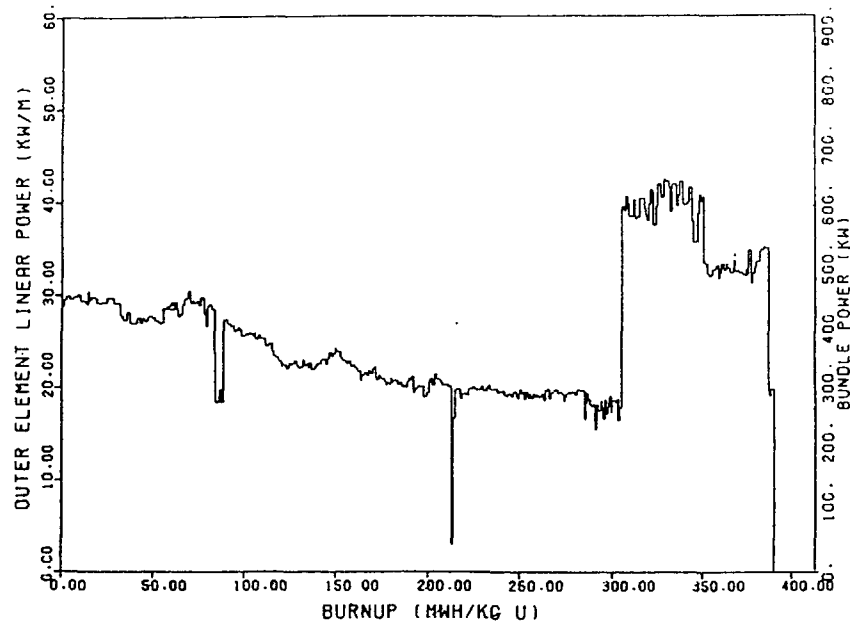


FIGURE 4: "Ramped" power history of bundle J64703C, typical of that for J64728C.

There is significant evidence to suggest that a reduction in fuel ( $UO_2$ ) thermal conductivity is primarily responsible for the elevated fuel temperatures and fission-gas release at extended burnups. Lucuta et al.<sup>(5)</sup> have performed extensive measurements on SIMulated high-burnup nuclear FUEL (SIMFUEL). The results show that the presence of solid fission products in  $UO_2$  results in a reduction in thermal conductivity. It is estimated that a typical CANDU fuel element irradiated at a constant linear rating of 45 kW/m will experience an increase in central fuel temperature from 1500 K (at zero burnup) to 1700 K (at 675 MWh/kgU), due to the buildup of solid fission products. This does not account for the presence of fission-gas bubbles and cracks, which will result in a further reduction in fuel conductivity.

Some evidence suggests that the onset of  $UO_2$  hyperstoichiometry may also be responsible (to a degree) for a decrease in thermal conductivity. Figure 7 shows a transverse section through an intact CANDU element irradiated to a burnup of 757 MWh/kgU. Much of the periphery of the pellet has experienced preferential etching of the grain boundaries and, as a result, many of the grains "pull-out" during etching and polishing. This is typical of fuel that has experienced oxidation at the grain boundaries. More analysis (such as O/U determinations) needs to be performed to confirm whether oxidation is the cause of this effect. If it is, it may be linked to the observed behaviour of sheath oxidation and CANLUB coatings described in Section 2.3.

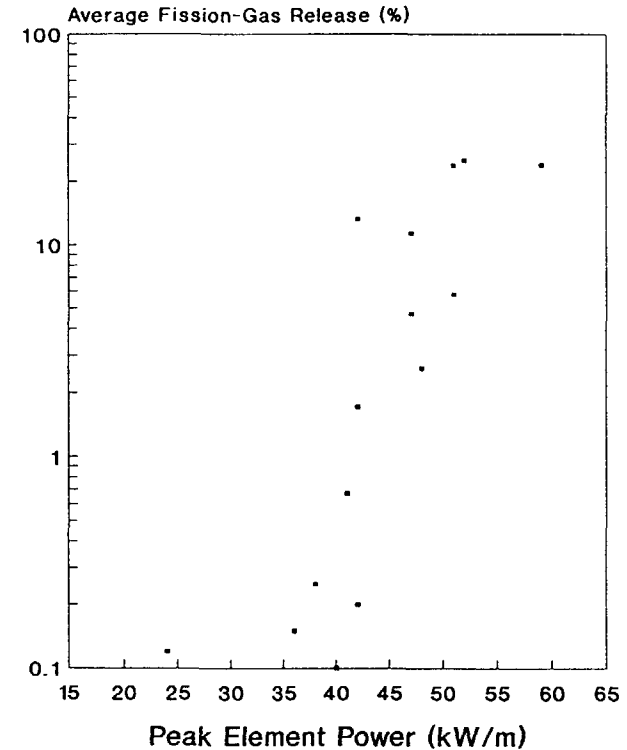


FIGURE 5: Fission-gas release versus peak power for extended-burnup Ontario Hydro 37-element fuel.

### 2.3 SHEATH OXIDATION AND CANLUB COATING BEHAVIOUR

The behaviour of the CANLUB coating on the inner surface of the sheath is important to fuel performance. Figure 8 shows that the retention of the CANLUB layer between the fuel and the sheath is greatly reduced between burnups of 400 and 700 MWh/kgU. At burnups <400 MWh/kgU, more than 75% of the layer can be accounted for visually (usually adhering to the fuel). At burnups >500 MWh/kgU, 40-100% of the CANLUB may be visually unaccounted for. The cause of the apparent "disappearance" is unknown.

Table I shows that there is an interesting correlation between CANLUB and the oxidation of the sheath inner surface:

1. Inner and Centre elements which are not CANLUB coated exhibit oxide patches up to 11  $\mu\text{m}$  in thickness. These patches (on the sheath inner surface) are generally associated with radial fuel cracks.

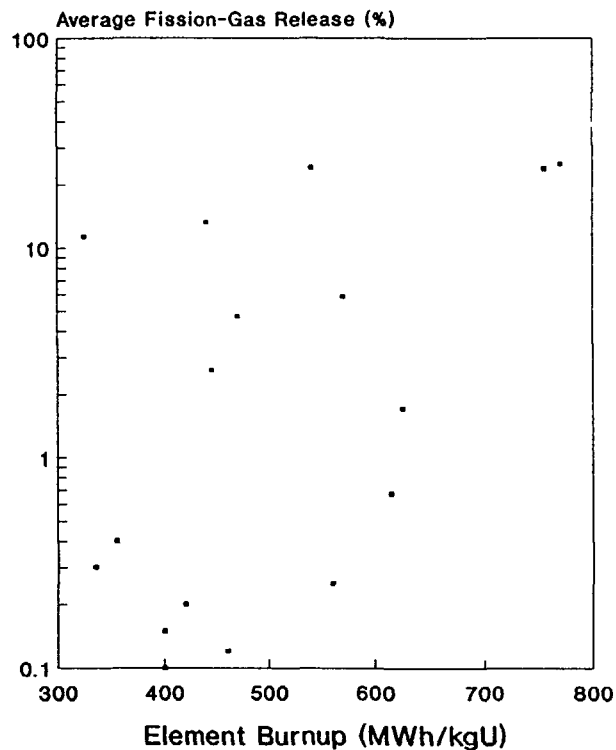


FIGURE 6: Fission-gas release versus element burnup for extended-burnup Ontario Hydro 37-element fuel.

2. Outer and Intermediate elements with high values of CANLUB retention exhibit no visibly detectable oxide on the sheath inner surface ( $<1 \mu\text{m}$ ).
3. Outer and Intermediate elements with low values of CANLUB retention exhibit thin oxide films of 1-2  $\mu\text{m}$ .

This suggests that CANLUB inhibits the sheath from acting as a getter for liberated oxygen. The CANLUB-oxygen interaction may also be linked to grain-boundary effects observed in the periphery of the fuel (discussed in Section 2.2.2).

#### 2.4 GRAIN GROWTH

Both fission-gas release and grain growth are thermally activated processes and generally correlate with one another. Table I shows the initial and final pellet-centre grain sizes measured for 37-element CANDU fuel irradiated to



FIGURE 7: Transverse section through intact outer element 10 from bundle J24546C. Note dark band at the pellet periphery on top-left, caused by preferential etching of the grain boundaries. (A18-G4 x 7)

extended burnups. Initial grain sizes were in the range of 5-10  $\mu\text{m}$ . Up to a factor of four has been observed in average pellet-centre grain growth (up to 30  $\mu\text{m}$  in final grain size). Figure 9 shows the relation between fission-gas release and average final pellet-centre grain size. At low fuel temperatures ( $<40 \text{ kW/m}$ ), no grain growth is observed and fission-gas releases are low ( $<1\%$ ). Generally, significant grain growth ( $\geq$  a factor of two) is accompanied by significant fission-gas releases (up to 26%). One of the intermediate elements of the ramped bundle J64703C exhibited significant grain growth, but fission-gas release remained low. This behaviour is not yet understood.

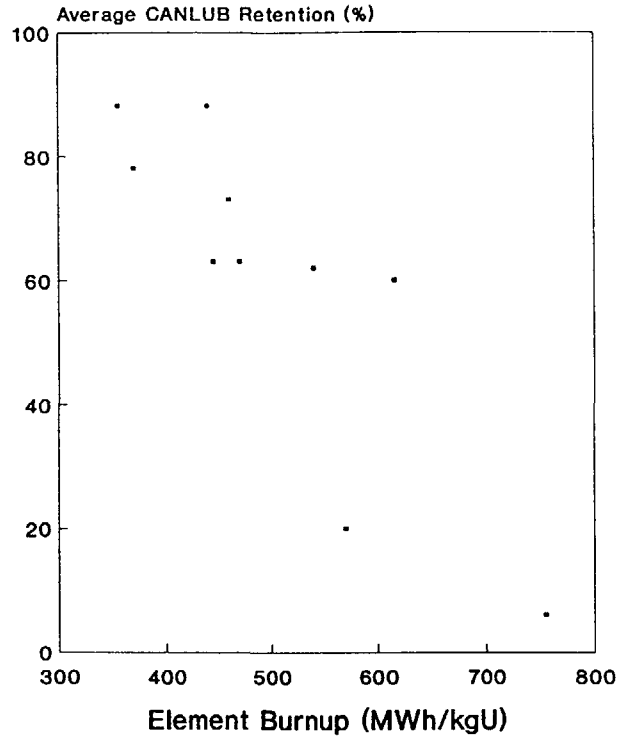


FIGURE 8: Graphite CANLUB-coating retention versus burnup for extended-burnup Ontario Hydro 37-element fuel.

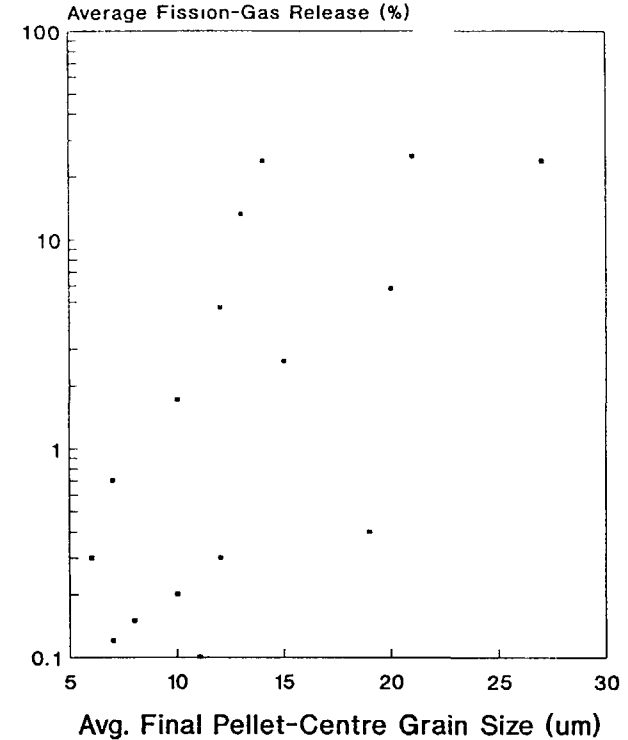


FIGURE 9: Fission-gas release versus final pellet-centre grain size for extended-burnup Ontario Hydro 37-element fuel. Initial grain sizes were in the range of 5-10  $\mu\text{m}$ .

### 2.5 PELLETT-CLAD INTERACTION (PCI)

Table I illustrates that residual tensile sheath strains of up to 2% are observed in 37-element fuel irradiated to extended burnups. The highest strains are exhibited in elements that operated at high power and exhibited significant grain growth and fission-gas release.

SCC-related defects have been observed in the sheath and endcaps of outer elements of four bundles that have experienced declining power histories to average bundle burnups >500 MWh/kgU (e.g., J98315C, J98324C, J24533C and J24546C, Table I). This would indicate that the recommended burnup limit of 450 MWh/kgU that is in place is justified. However, ramped bundles such as J64703C and J64728C have exhibited SCC-related failures at burnups of <450 MWh/kgU; hence, additional guidelines are in place for power-ramping extended-burnup fuel.<sup>[6]</sup>

### 3. SUMMARY

1. Fission-gas releases of up to 26% have been observed in CANDU fuel elements that have declining power histories from peak powers of up to 59 kW/m to discharge burnups of up to 772 MWh/kgU (32 GWh/TeU). This was not predicted by low-burnup code extrapolations.
2. Elevated fuel temperatures, caused primarily by a decrease in fuel thermal conductivity, are believed to be responsible for the higher-than-expected fission-gas releases. A reduction in fuel thermal conductivity can be attributed, at least in part, to the buildup of solid fission products.
3. Further investigation is needed into the possible onset of hyperstoichiometry. This may be linked with the presence of CANLUB coatings and sheath oxidation.

4. SCC-related defects have been observed in the sheath and endcaps of outer elements, which have experienced declining power histories to average bundle burnups >500 MWh/kgU. This indicates that the recommended burnup limit of 450 MWh/kgU for 37-element fuel in Ontario Hydro Nuclear Generating Stations is justified. Additional guidelines are in place for power-ramping extended-burnup fuel.

#### ACKNOWLEDGEMENTS

The authors are indebted to V.I. Arimescu (IAEA Fellow, attached to AECL Research from Romania), G. Brenciaglia (Ontario Hydro, Canada), T.J. Carter, P.J. Fehrenbach, I.J. Hastings, P.G. Lucuta (AECL Research, Canada) and M.J.F. Notley (Consultant to Ontario Hydro, Canada) for their assistance.

#### REFERENCES

- [1] CASSIDY, R.M. et al., "Dynamic Ion Exchange Chromatography for the Determination of Number of Fissions in Uranium Dioxide Fuels", Anal. Chem., 1986, 58, 1181-1186 (AECL Report, AECL-9121, 1986 May).
- [2] ARIMESCU, V.I. and RICHMOND, W.R., "Modelling CANDU-Type Fuel Behaviour During Extended Burnup Irradiations Using a Revised Version of ELESIM Code", paper presented at this meeting.
- [3] NOVAK, J. and HASTINGS, I.J., "Ontario Hydro Experience with Extended-Burnup Power-Reactor Fuel", paper presented at the ANS/ENS International Topical Meeting on Light Water Reactor Fuel Performance, Avignon, France, 1991 April 21-25 (AECL Report, AECL-10388, 1991 July).
- [4] KOLSTAD, E. et al., "In-Reactor Thermo-Mechanical Measurements on LWR Fuel Rods in the High Burnup Range", proceedings of the Technical Committee Meeting Organized by the International Atomic Energy Agency on Fuel Performance at High Burnup for Water Reactors, Studsvik, Sweden, 1990 June 5-8 (IWGFPT/36, pp. 140-146).
- [5] LUCUTA, P.G. et al., "Thermal Conductivity and Gas Release from SIMFUEL", paper presented at this meeting.
- [6] DASILVA, R.L., "CAPE - A Probabilistic Model for Predicting CANDU Fuel SCC Power-Ramp Failures", Ontario Hydro Report No. CPS-N-37000-0003, 1990 August.

## EXPERIMENTAL II

(Session 2)

### **Chairmen**

**M. MOGENSEN**

Denmark

**M. YAMAWAKI**

Japan

# FISSION GAS RELEASE OF HIGH BURNUP FUEL

R MANZEL  
Siemens AG,  
KWU Group,  
Erlangen, Germany

R P. BODMER  
Kernkraftwerk Gösgen-Däniken AG,  
Däniken, Switzerland

G. BART  
Paul Scherrer Institute,  
Villigen, Switzerland

## Abstract

Fission gas release data are presented for PWR fuel rods with an enrichment of 3.8 w/o to 4.2 w/o U-235 designed for high burnup. These fuel rods were operated up to 4 cycles under realistic power conditions to target burnups of 54 MWd/kgU.

As expected, the fission gas release of fuel rods of higher enrichment was generally higher compared to that of fuel rods of lower enrichment. However, whilst the fractional fission gas release of lower enriched fuel rods shows a tendency to increase with increasing burnup, the fractional release of higher enriched rods passes through a maximum at intermediate burnups, and then shows a tendency to saturate.

The highest fractional fission gas release of about 10% was measured on fuel rods with large initial diametrical gaps between fuel and cladding, the lowest release values were found on fuel rods with small initial diametrical gap. These fuel rods showed a behaviour similar to that of the lower enriched fuel rods.

The fission gas released in general originates from the center region of the pellets. The diameter of this region is dependent on fuel center temperature. However, microstructural examinations do also show an increase with increasing burnups in spite of decreasing fuel temperatures. The microstructural features observed can be correlated with distinct steps in fission gas release.

## 1. Introduction

Fission gas release is an important aspect in the analysis of the thermal and mechanical design of LWR fuel rods especially at extended burnup. The majority of data on fission gas release of LWR fuel rods stem from standard fuel assemblies that were irradiated

beyond their prospective design burnups. Fission gas release of these fuel rods was generally low and did not exceed 5% of the amount generated [1].

However, in order to achieve the prospective high burnup target with complete reloads higher fuel enrichments are necessary. As a consequence fuel rods are operated at higher average power over a longer period of time and hence higher fuel temperatures. Fuel assemblies with the appropriate high enrichment of 3.8 to 4.2 w/o U-235 were irradiated in a commercial pressurized water reactor (PWR) under realistic power conditions. Irradiation and fuel performance evaluation were done in close cooperation with the utility.

This paper presents fission gas release measurements on fuel rods removed from these fuel assemblies at various burnups. The fission gas release measurements are supplemented by detailed microstructural and microanalysis. The data are compared with those obtained from standard fuel rods of lower enrichment.

## 2. Fuel Rod Characteristic and Irradiation History

The fuel rods were arranged in a 15x15 rod array. All fuel rods measured were precharacterized. Zry-4 was used as cladding material and the UO<sub>2</sub>-fuel was produced by the AUC-process [2]. Characteristic fuel rod data are given below.

Fuel rod length	= 3842 mm
Fuel rod diameter	= 10.75 mm
Fuel / clad diametrical gap	= 163 to 220 μm
He fill gas pressure	= 22.5 bar
Fuel density	= 10.40 g/cm <sup>3</sup>
Fuel grain size (linear intercept)	= 6.5 – 7.5 μm
Initial enrichment (U-235)	= 3.8 and 4.2 %

The fuel rods were operated for up to four consecutive cycles to a maximum rod average burnup of 53.5 MWd/kgU. Cycle average linear heat generation rates (LHGR) for these rods were in the range of

265 to 295 W/cm	1st cycle
260 to 280 W/cm	2nd cycle
215 to 230 W/cm	3rd cycle
175 to 180 W/cm	4th cycle

After the second, third and fourth cycle corresponding to 636, 969 and 1296 EFPD respectively, fuel rods were withdrawn from fuel assemblies and shipped to Hot Cell laboratories for post-irradiation examinations.

### 3. Experimental Techniques

The fuel rods examined covered a wide range of initial fuel/clad gaps. Since the fuel/clad gap is an important parameter in fission gas release evaluation the cold gap between fuel and cladding was measured non-destructively [3] at regular intervals along the axis of the fuel rods.

Standard fuel rod puncturing techniques and mass spectrometric analysis were applied to determine the integral amount and the composition of fission gases released into the free rod volume.

Basis for a more detailed analysis of the fission gas release behaviour was the optical microscopy on ceramographic cross sections.

In order to quantitatively determine the radial distribution of fission gases and other fission products in the fuel pellet an electron microprobe was used. The electron probe microanalysis (EPMA) was carried out on the shielded electron microprobe at the European Institute for Transuranium Elements [4]. The radial distributions of xenon retained in single  $UO_2$  grains was determined by point analysis at intervals between  $50\ \mu\text{m}$  and  $150\ \mu\text{m}$  along the radius. This gave the concentration of gas dissolved in the grains and of gas trapped in intragranular bubbles. The point analyses were made away from grain boundaries in order to avoid a contribution from gas contained in intergranular bubbles.

Fractional Fission Gas Release

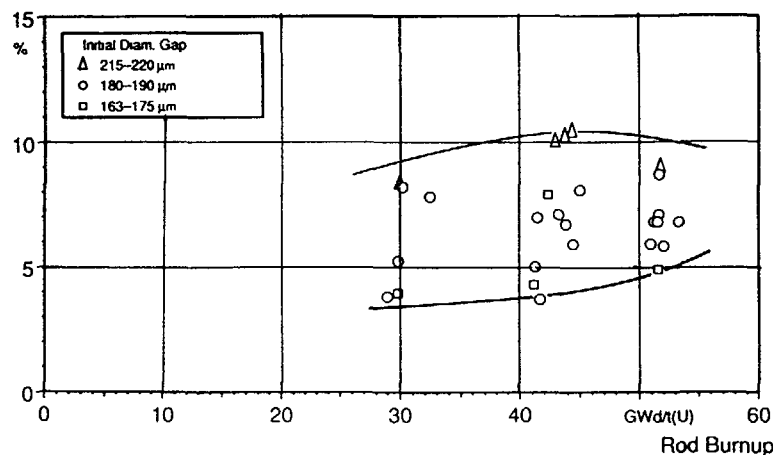


Fig 1

Fractional Fission Gas Release of PWR Fuel Rods with U-235 Enrichment of 3.8 – 4.2 w/o

### 4. Results

The results of the standard puncturing and mass spectrometric analysis are plotted in fig. 1 as fractional fission gas release as a function of rod average burnup. As expected, the fission gas release of fuel rods with higher enrichment is generally higher compared to that of fuel rods with lower enrichment, shown in fig. 2. But there are also distinct differences in the evolution of fission gas release visible. The fractional release of the higher enriched rods passes through a maximum at intermediate burnups, and shows a tendency to saturate at high burnup for most of the rods. The fractional fission gas release of the lower enriched rods passes through a maximum at lower burnups, followed by a decrease at intermediate burnups and a further increase at high burnups.

The data obtained on the high enriched fuel rods show a distinct dependence of fission gas release on the initial diametrical fuel/clad gap. The highest fractional fission gas release of about 10 % was measured on fuel rods with large initial gaps between fuel and cladding, the lowest release values of about 4 % were found on fuel rods with small initial gaps.

This pronounced influence of the diametrical gap size on fission gas release must be discussed in terms of fuel pellet center temperatures. At a given LHGR the fuel pellet center temperature is governed by the temperature gradient across the effective fuel/clad gap which in turn depends on the initial gap size. This influence of the gap size is most

Fractional Fission Gas Release

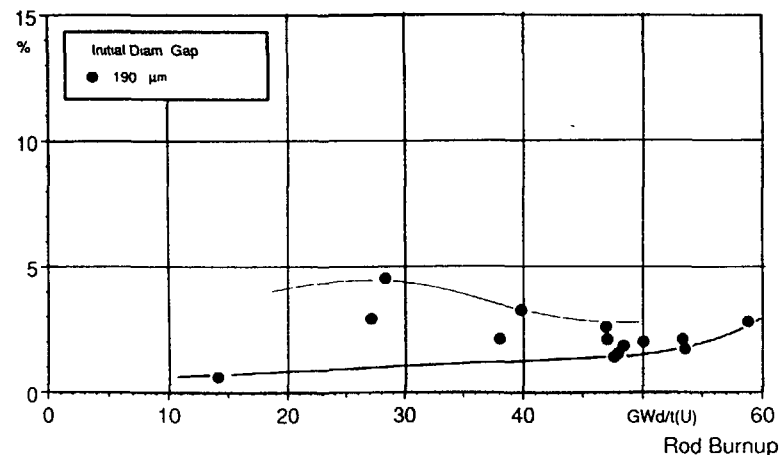


Fig 2

Fractional Fission Gas Release of PWR Fuel Rods with U-235 Enrichment  $\leq 3.2$  w/o

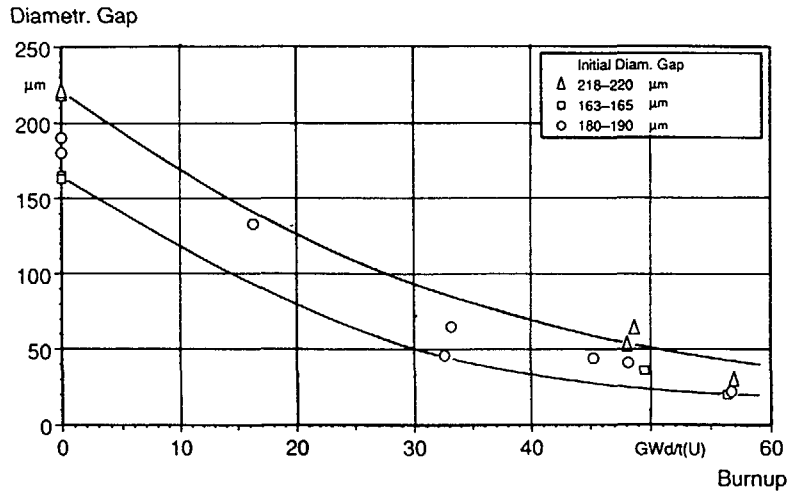
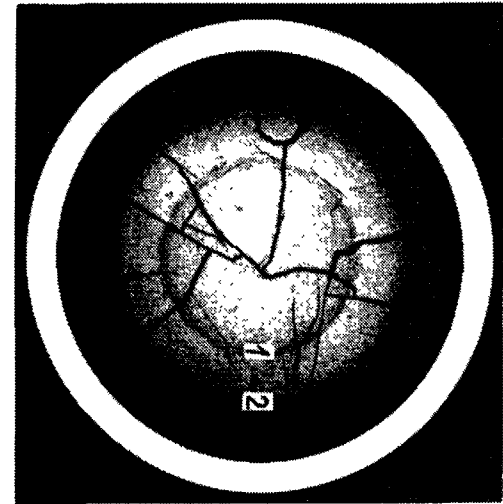


Fig. 3 Hard Diametrical Gap of PWR Fuel Rods

pronounced at low and intermediate burnups and decreases at higher burnups, a fact that is not surprising, since the initial gap decreases in size due to the combined effects of cladding creep and fuel swelling under irradiation. As shown in fig. 3 the decrease in gap size is more pronounced for fuel rods with large initial gaps than for fuel rods with small initial gaps. Consequently, initial differences in gap size diminish at higher burnup and fuel center temperatures approach each other at the lower level. This explains the tendency of the fractional fission gas release in fuel rods with large initial gaps, to saturate at high burnup.

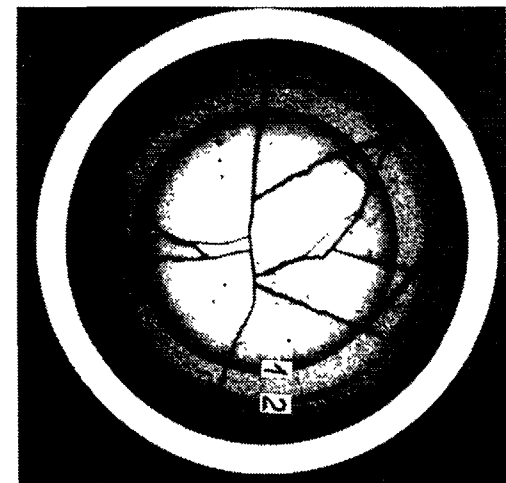
On the other hand, the increase in fractional fission gas release of fuel rods with small initial gaps with burnup is attributed to a release from pellet zones radially further outward. With increasing burnup the saturation level for fission gases within the fuel lattice will be reached even in these outer zones of the pellets [5]. If during steady operation the saturation temperature is exceeded fission gas release will start from these zones. In fuel rods with large initial gap these zones have contributed to fission gas release already early in life because of the higher fuel temperatures of those rods.

Such a release mechanism is clearly supported by the results of the microstructural examinations. Fig. 4 shows typical ceramographic cross sections of a 2-cycle and a 4-cycle fuel rod. Apart from the usual crack pattern of the pellets grain growth was observed in the pellet center, and the pellet rim shows a zone of heavily distorted grain



Local Burnup  
32.8 MWd/kg

2 mm



Local Burnup  
56.2 MWd/kg

Fig. 4 Typical Ceramographic Cross Sections of a 2-cycle and a 4-cycle Fuel Rod

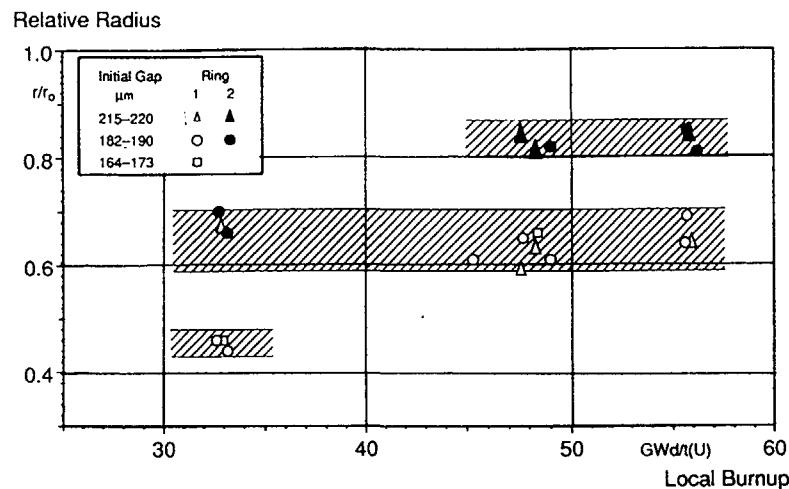


Fig. 5  
The Development of Rings in  $\text{UO}_2$ -Pellets at Different Relative Radii Marking the Onset of Fission Gas Release as a Function of Burnup

structure with bubbles homogeneously distributed. The width of this rim zone increases with burnup but even at burnups of about 60 MWd/kgU is still confined to less than 200  $\mu\text{m}$ .

In addition, two distinct dark rings (marked 1 and 2 in the figure) at different radii are clearly visible. It has been proven earlier [5] that these rings contain a large number of fission gas bubbles precipitated within the grains. These rings mark the onset of fission gas release from the fuel grains. The development of two rings is considered as a clear indication that fission gas release occurred at two distinct periods of time. An evaluation of all relevant cross sections with regard to the number of rings and their relative radii as a function of pellet burnup is shown in fig. 5. The evaluated data fall into different subsets and can be classified according to their initial fuel/clad gap size.

After two cycles (burnup - 33 MWd/kg/U) the first ring is formed at a relative radius ( $r/r_0$ ) of about 0.45. For the fuel rod with a small initial gap this is the only ring formed, and as a consequence fission gas release is low. In fuel rods with medium gap size a second ring has developed at relative radii between 0.65 and 0.70, causing medium to high fission gas release. Again, only one ring at a relative radius of about 0.67 was formed in the fuel rod with a large initial gap leading to high fission gas release.

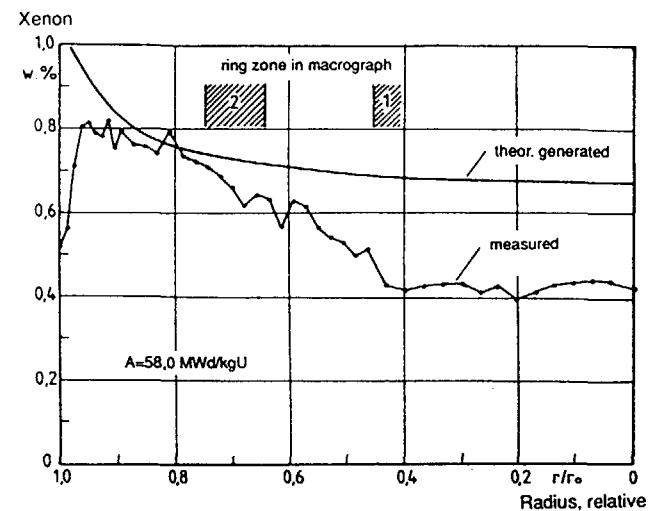


Fig. 6 Radial Xenon Distribution in a PWR Fuel Pellet vs. Relative Radius, EPMA-Measurement on Individual Grains

After three cycles (burnup 44 MWd/kgU) the rings at a relative radius of about 0.45 have disappeared. It is suggested that grain boundary sweeping by grain growth is causing this restructuring. Fuel rods with small initial gaps now show one ring only at relative radii of 0.6 to 0.7. In fuel rods with medium and large initial gaps a second ring now appears at relative radii between 0.8 and 0.85 resulting in high fractional fission gas releases between 8 % to 10 %. This picture is preserved during the fourth cycle (burnup 56 MWd/kg) with the consequence that the fractional fission gas release during that cycle remained constant or even decreased.

In contrast, the fractional fission gas release of the rod with small initial gap, although small in magnitude, increased during the fourth cycle. Based on previous examinations it can be expected that in this rod a second ring at a relative radius of about 0.8 developed during the fourth cycle.

The stepwise release of fission gases described above has been confirmed by EPMA. For example, fig. 6 shows the EPMA results of retained Xe in the grains as a function of relative radius. The analysis was performed on a pellet with a burnup of 58 MWd/kgU. This pellet stems from a fuel rod with low fission gas release equivalent to those of a rod with small initial fuel/clad gap. Comparing the amount of xenon retained within the grains with that theoretically generated yields a high release of fission gas from the center region

of the pellet within the radius of the first ring. A drop in the release at the edge of the first ring can be observed, and the analysis reveals a medium release between the first and the second ring. No release from the grains outside the second ring has been observed. The deficiency at the pellet rim will not be considered here and has been discussed elsewhere [5].

Based on rod power history it is concluded that the inner, first ring bounds the area where fission gases were released from early in life (cycle 1 and 2) at high power and consequently high temperature. The second ring as an indication of additional fission gas release from the area further outward should have developed later in life in spite of steadily decreasing rod power and hence fuel temperature.

## 5. Conclusions

The fission gas release of higher enriched PWR fuel rods (3.8 w/o to 4.2 w/o U-235) operated under typical power conditions to high burnup is generally higher than that of lower enriched standard rods.

The fuel rods examined comprise a variety of initial diametrical fuel/clad gaps in the range of 165  $\mu\text{m}$  to 220  $\mu\text{m}$  resulting in different fuel temperatures and consequently different fission gas release.

Fuel rods with a large initial fuel/clad gap show an increasing fractional fission gas release of up to 10 % after three cycles of operation (41 – 44 MWd/kg burnup), but no further increase during the 4th cycle.

The fuel rods with medium gap size reveal a wide variation in fractional fission gas release between 4 % and 8 % after three cycles. During the 4th cycle a trend towards a saturation under high release conditions but a further increase under low release conditions has been observed.

The fractional fission gas release values of the rods with small initial gap size fall into the lower part of the range measured on fuel rods with medium size gap, and they also show a further increase during the 4th cycle. The data suggest that during further operation to even higher burnups the differences in fission gas release due to different initial gap sizes will be reduced.

Microstructural examinations have been performed to analyse this different behaviour. Fission gas release in general occurs from the center region of the pellet. The diameter of that region and the amount of fission gases released is determined by the local temperature. However, the microstructural features clearly indicate that the diameter of that region is also dependent on burnup. With increasing burnup more and more pellet regions

at lower temperature become saturated with fission gases. Exceeding the saturation temperature in the course of burnup will result in an additional release of fission gases even at decreasing power as the burnup increases.

## References

- [1] R. Manzel, F. Sontheimer and H. Stehle, "Fission gas release of PWR fuel under steady and transient conditions up to high burnup", Proc. ANS Topical Meeting on LWR Fuel Performance, Orlando, Florida, April 21–24, 1985.
- [2] H. Aßmann and W. Dörr, "Microstructure and density of UO<sub>2</sub> pellets for Light Water Reactors as related to powder properties", Ceramic Powders, edited by P. Vincenzini, Elsevier Scientific Publishing Comp., Amsterdam 1983, p. 707–718.
- [3] Olshausen, "How to determine residual gaps in irradiated fuel rods", Paper presented at EMPG–Meeting, Sanderstølen, Norway, March 1976.
- [4] C. T. Walker, "Measurement of retained xenon in advanced fuels by microprobe analysis", J. Nucl. Mat. 80 (1979).
- [5] R. Manzel and R. Eberle, "Fission gas release at high burnup and the influence of the pellet rim", ANS/ENS Intern. Topical Meeting on LWR Fuel Performance, Avignon, France, April 21–24, 1991.

## FISSION GAS RELEASE ENHANCEMENT AT EXTENDED BURNUP: EXPERIMENTAL EVIDENCE FROM FRENCH PWR IRRADIATION

C. FORAT, B. BLANPAIN

Fragéma/Framatome Fuel Division,  
Lyon

B. KAPUSTA, P. GUEDENEY

Commissariat à l'énergie atomique,  
Centre d'études nucléaires de Saclay,  
Gif-sur-Yvette

P. PERMEZEL

Service Etudes et projet thermiques et nucléaires,  
Electricité de France,  
Villeurbanne

France

### Abstract

Two families of 17X17 FRAGEMA assemblies were irradiated for five cycles in French PWR, post-irradiation examinations performed on rods extracted after each cycle showed interesting features linked to the different power histories the two families experienced. Particularly, the evolution of the fuel microstructure made it possible to single out the contribution of the athermal process, including the "rim effect", and the thermal process. The development of "high burnup" realistic models needs a correct evaluation of the thermal conductivity deterioration and the lowering of the gas release threshold as burnup proceeds.

Key words High burnup, Fission gas release, Experimental results

### 1 - Introduction

There is still no complete understanding of the dependence of fuel chemistry evolution, thermal conductivity and therefore fission-gas release on burnup. Due to the complexity of the involved phenomena, more investigations concentrated on high burnup effects are needed to get a general consensus on this subject.

Important facts such as the degradation of the thermal conductivity as burnup proceeds and the behavior of the cold outer pellet rim are to be clarified and quantified for fuel rod performance and design modelling.

Usually, fuel rods irradiated up to very high burnups and examined in hot cells present significant fission-gas release due mainly to the high linear heat generation rate they experienced during their irradiation in experimental reactors. Examination of these very high burnup fuel rods shows intragranular bubbles as well as grain boundary bubble networks developing in the hot inner part of the pellets and also a pellet rim new population of gas bubbles. However, it is quite difficult for modelling purposes to discriminate between these phenomena and to evaluate the influence of each of their contributions on the overall fractional release in the fuel rod.

In order to get a better understanding of the high burnup effect and to validate the data gained from experimental irradiations, FRAGEMA, EDF and CEA launched an important examination programme on fuel rods irradiated up to 5 cycles in French EDF reactors (1,2). The present paper summarizes and discusses the main results obtained so far.

### 2 - Experimental investigations

Two families of 17X17 fuel assemblies designed by FRAGEMA were irradiated during 5 cycles:

- five 3.1% U235 fuel assemblies, in the FESSENHEIM power station (FSH) from 1977 to 1984, several fuel rods were extracted after 2, 4 and 5 irradiation cycles and examined in the hot laboratories of CEA/Saclay. The maximum average burnup achieved by these rods was 55 MWd/kgU.

- two 4.5% U235 fuel assemblies in the GRAVELINES power station (GRA) from 1983 to 1989, several fuel rods were extracted and examined after 2, 3, 4 and 5 cycles in the same laboratories. The highest average burnup reached by those rods was 58 MWd/kgU.

All these fuel rods were clad with CWSR zircaloy 4 and filled with UO<sub>2</sub>-IDR pellets of 95% TD characterized by a low in-pile densification and a very low open porosity (0.1 vol%).

	Initial enrichment %U235	Average rod burnup MWd/kgU	Representative LHGR W/cm
FSH			
2cy	3.1	31.7	190,165
4cy	3.1	45.8	120,185,150,125
5cy	3.1	54.9	130,185,155,125,125
GRA			
2cy	4.5	25.8	195,235
3cy	4.5	36.1	160,235,200
4cy	4.5	49.0	200,235,200,170
5cy	4.5	57.5	200,235,200,165,160

Figure 1 - Irradiation conditions

The main irradiation characteristics of the examined rods are displayed in Figure 1.

### 3 - PIE Examinations

#### 3-1 Overall rod behaviour

The examined fuel rods presented a sound behavior after 5 irradiation cycles (3). Rod length changes show a roughly linear dependence with burnup. In both cases, the relative length changes range 0.95-1.00% after 5 cycles. The fuel stack growth, however, is greater for the GRA rods ( 1.1% after 5 cycles) compared to the FSH rods ( 0.80% after 5 cycles).

Examination of the interpellet ridging seems to indicate that the fuel-cladding contact occurred during the second irradiation cycle for both rod series.

The evolution of the rod fractional gas release of the two fuel families as a function of burnup is illustrated in Figure 2. After two irradiation cycles they show a similar behavior despite the fact that the GRA rods

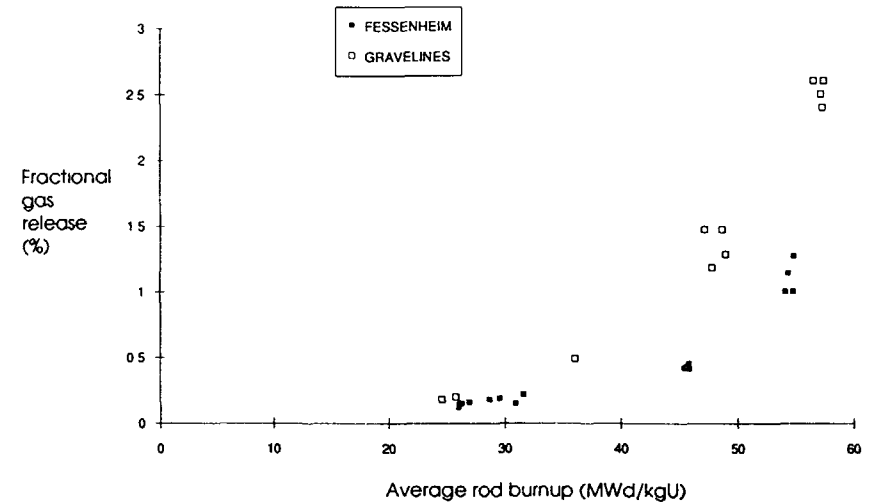


Figure 2 - Global fission gas release versus burnup

experienced a somewhat higher power level. Afterwards they show a differing behavior as irradiation proceeds, with a higher FGR enhancement for the GRA fuel rods. However, in both cases the FGR has been doubled between fourth and the cycles: 0.5% to 1.2% and 1.4% to 2.6% for the FSH and the GRA rods respectively.

#### 3-2 Microstructure analysis and EPMA

- Ceramographic examination of FSH fuel does not show noticeable fuel microstructural evolution up to 5 cycles: a normal fracturing aspect and no fuel restructuring or grain growth are observed. Evidence of fuel-cladding interaction on 2-cycle fuel (observed after local burnup from 27 MWd/kgU) is noted. From the fourth cycle, the pellet periphery appears to be quite different from the rest of the pellet; this region is characterized by a large increase in porosity, presence of fine metallic inclusions and a loss of definable grain structure. This feature, typical of high burnup fuel, is more pronounced after the fifth cycle: image analysis of the microphotographs was performed to estimate the pore volume fraction in different regions of the fuel For the 4-cycle fuel

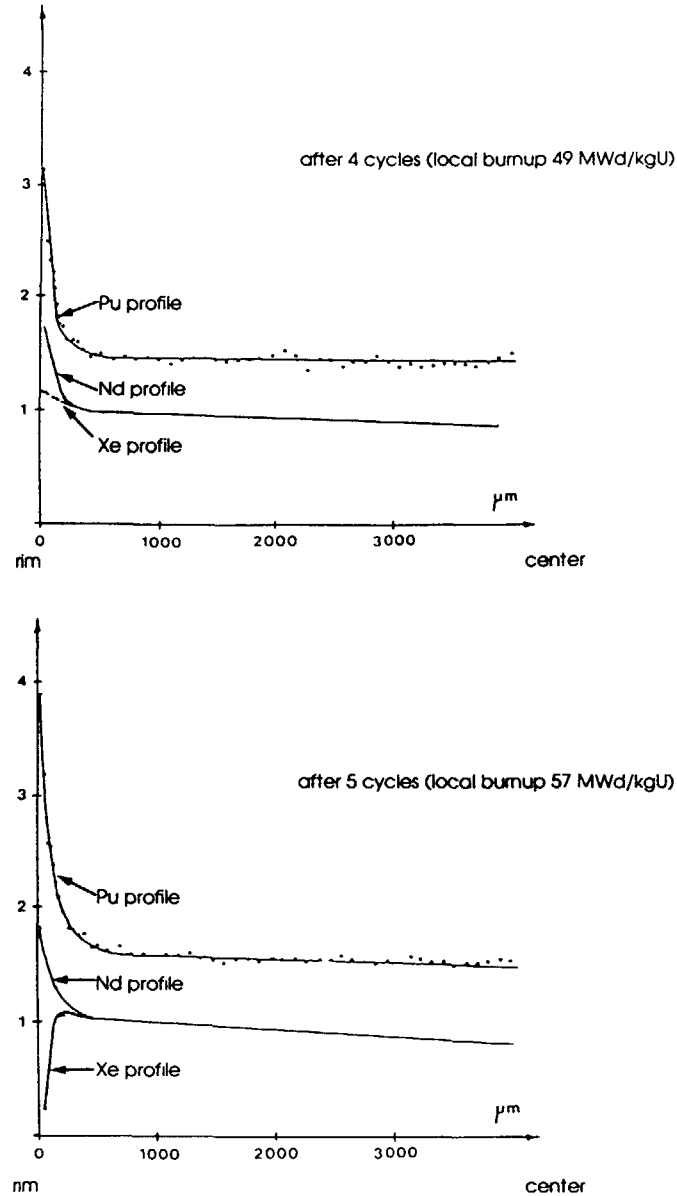


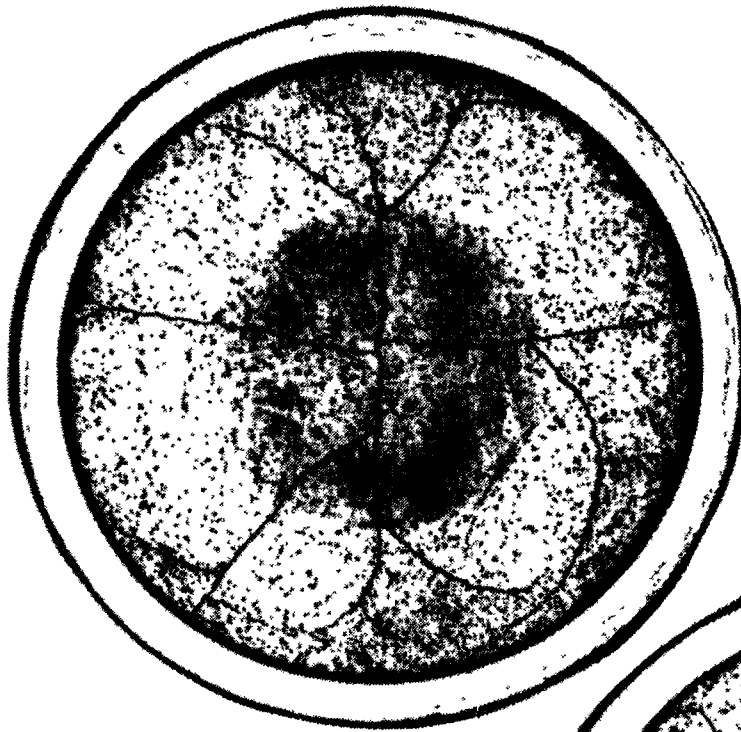
Figure 3 - EPMA radial analysis for FESSENHEIM fuel

(local burnup 49 MWd/kgU) the porosity in central and intermediate zones is estimated respectively at 4.5 and 6.6% and 10% for the rim, after 5 cycles (local burnup 57 MWd/kgU), the volume fraction for the rim region reaches 13% while it is estimated at 5% in central and intermediate regions

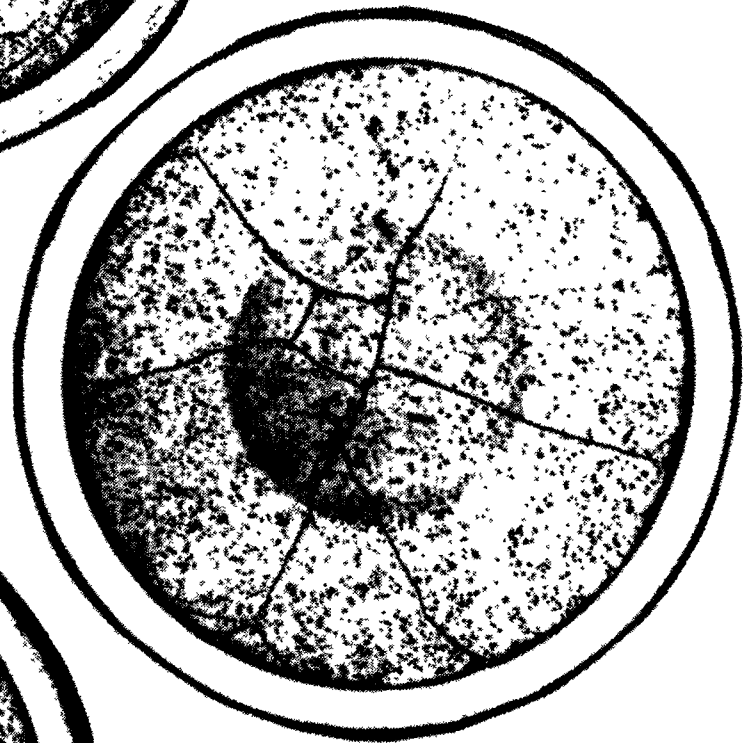
EPMA observations (Figure 3) are consistent with metallographic observations, the xenon concentration profile is not disturbed in the center of the fuel even for local burnup of 57 MWd/kgU and xenon depletion in the rim region is noticeable from the fourth cycle, but well much pronounced in the 5-cycle fuel

- For the GRA rods, metallographic observations performed on 2, 3, 4 and 5-cycle fuels show a significant microstructural evolution with burnup after the second irradiation cycle as-fabricated microstructure is still observed, but incipient fission gas bubble precipitation at grain boundaries is seen after the third cycle. Furthermore, the 4 and 5-cycle fuel centerline is characterized by a massive precipitation of intragranular gas bubbles and also by an increase of intergranular porosity and interlinkage, this feature being observed to a greater extent after 5 cycles. The relative radius of the incipient intragranular bubble precipitation varies with the axial location of the examined fuel section: the relative radii are 0.23 and 0.52  $r/r_0$  for local burnups of 59 and 65 MWd/kgU respectively (Figure 4). A slight grain growth is measured in the fuel centerline region after 5 cycles: 15 μm (mean linear intercept) compared to 10-12 μm for the as-fabricated fuel. The pellet outer rim is characterized by a very high porosity and metallic inclusions as well.

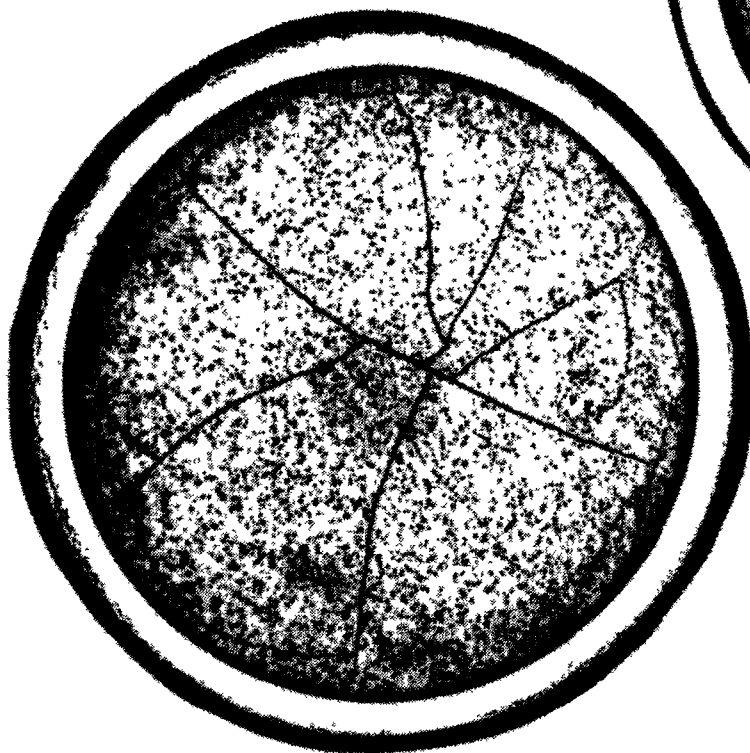
EPMA radial measurements performed on 3, 4 and 5-cycle fuel show xenon depletion in the pellet fuel centerline (Figure 5). For the observed cross sections the measured xenon depletion radii correspond to the grain boundary bubble precipitation radii as observed on ceramographies. Compared to the Nd profile a lack of xenon concentration is observed at pellet periphery for the 4-cycle and 5-cycle fuels. Evaluation of the matrix concentration of xenon in that region is quite doubtful due to the scattering of the data.



local burnup : 64.6 MWd/kgU  
 $d_{\text{central ring}}/d_{\text{pellet}} : 0.52$   
ZrO<sub>2</sub> thickness : 35 $\mu$ m



local burnup : 64.4 MWd/kgU  
 $d_{\text{central ring}}/d_{\text{pellet}} : 0.49$   
ZrO<sub>2</sub> thickness : 88 $\mu$ m



local burnup : 59.3 MWd/kgU  
 $d_{\text{central ring}}/d_{\text{pellet}} : 0.23$   
ZrO<sub>2</sub> thickness : 98 $\mu$ m

Fig. 4 Radial macrographies for GRA fuel after 5 cycles.

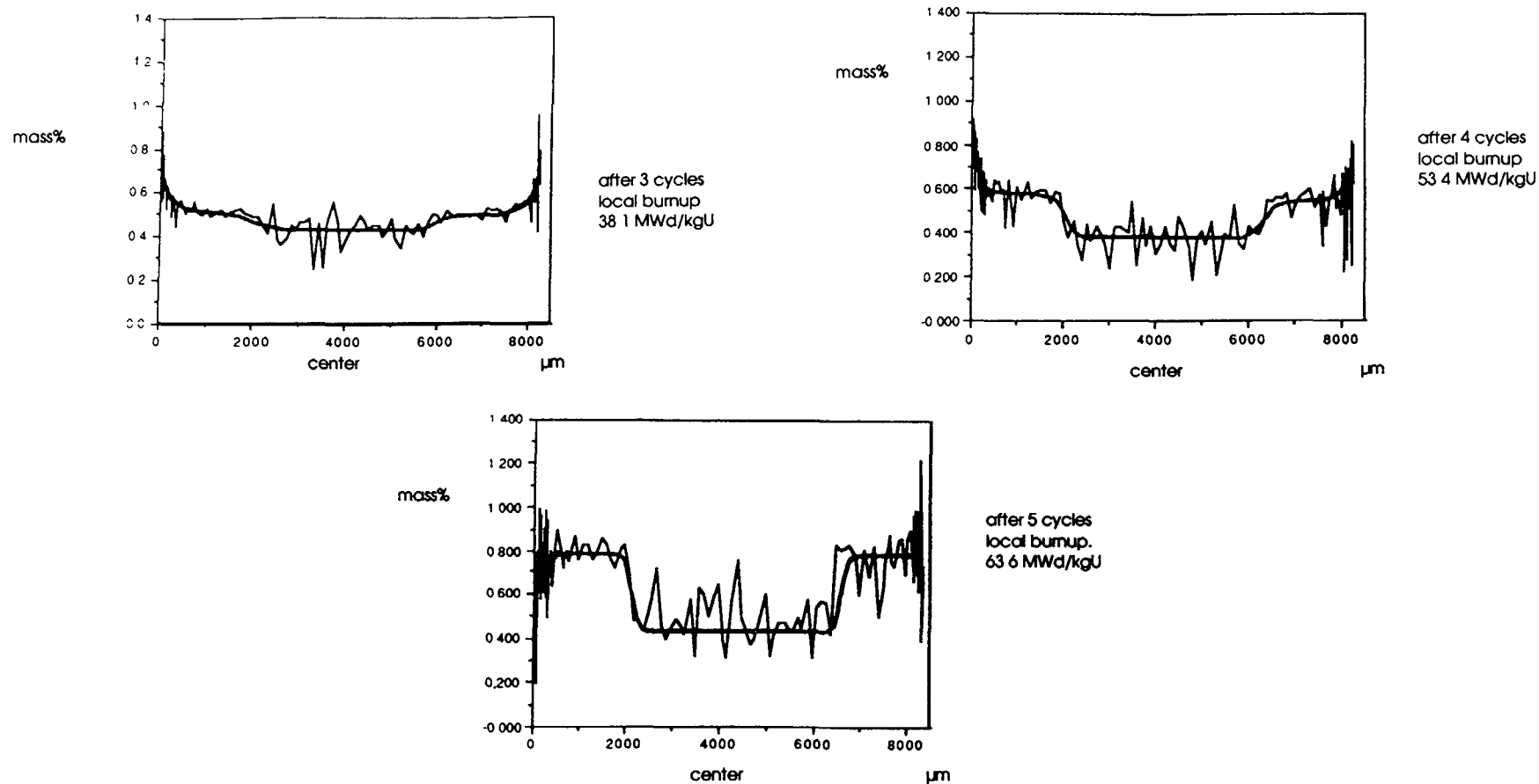


Figure 5 - EPMA xenon profile for GRAVELINES fuel

#### 4 - Discussion

The extent of the particular features observed at the pellet rim resulting from high fission density due to plutonium buildup is similar for both rod families, that phenomenon being independent of the irradiation conditions (power and temperature). Fission gas saturation and bubble precipitation which appeared during the fourth and increased during

the fifth irradiation cycles is likely to be responsible for the measured acceleration of the global fractional release.

The fractional release of the FSH fuel rods, even after five irradiation cycles, did not result from a thermal process as demonstrated by the absence of fuel restructuring in the pellet centerline region. The fractional release measured during different irradiation steps and at EOL thus came from the combination of the athermal process

(knockout and recoil effects) and potential contribution of the pellet rim. The lack of xenon as measured by EPMA in that zone is incontestably higher after the fifth than after the fourth irradiation cycle. However, because of the detection limit of EPMA (detection of xenon only present in the UO<sub>2</sub> matrix and in closed porosity within 1 μm of the surface (4)), this method is not completely adequate to correctly evaluate the total retained or released xenon, especially in the very high porosity rim region. For that reason, the "rim effect" contribution in global release of the rod is not easily determined, and further investigations could be necessary.

However, when modelling fission gas release, if we consider that the release from the rim exists and if we express this phenomenon in a global "athermal" term versus burnup, the results obtained for this family of rods are very useful for its quantitative validation.

Concerning the fractional release of the GRA fuel rods, the low values measured after the second cycle compare with those of the FSH fuel rods and are consistent with the absence of microstructural evolution. That behavior is consistent with the irradiation conditions in terms of burnup and temperature experienced by the examined rods during the first and the second cycle, which correspond to an incubation period.

After three irradiation cycles the relative rod fractional release acceleration corresponds to experimental indications of the start of intergranular pores formation at pellet centerline and of a weak xenon depletion in the UO<sub>2</sub> matrix, as measured by EPMA in that fuel region. These observations indicate that the fuel achieved the burnup as well as the temperature conditions needed to reach the so-called HALDEN fission gas release threshold which corresponds to the precipitation limit of fission gases, which then diffuse out of the grains. During the fourth and particularly during the fifth cycle the evolution of fuel restructuring and of xenon depletion in the fuel central zone clearly indicate the continuation of that thermal process.

The thermal contribution to fission gas release when burnup proceeds can be evaluated by comparing global fractional release for the two families of rods. Since the initial U<sup>235</sup> enrichment is different in the two fuel families, the plutonium buildup at pellet periphery is expected to

evolve differently as burnup proceeds. At equivalent pellet burnup the Pu buildup and thus the "rim effect" should be higher for the lower enriched FSH fuel. However, as the mean EOL burnup of the GRA fuel rods is slightly higher than the FSH fuel rods, we can consider in a first approximation that, at EOL the sum of the contributions of the rim effect and of the athermal process on fractional release is equivalent for the two fuel families. With this hypothesis, the difference between the measured fractional releases of the two rod families roughly gives the thermal contribution on gas release of the GRA fuel rods: 0.9% after 4 cycles and 1.4% after 5 cycles.

This thermal contribution to gas release increases with burnup although the linear power was slightly lower during the fifth irradiation cycle. This observation is consistent with the microstructural evolution observed on the microphotographs.

Two different explanations are usually proposed to understand this phenomenon:

- the deterioration of fuel thermal conductivity at high burnup, which leads the fuel temperature to exceed the gas release threshold at EOL;
- the lowering of the gas release threshold with burnup as suggested by various authors. This feature can be explained by the augmentation of intragranular diffusion coefficient resulting from the irradiation induced effects.

Gradual degradation of UO<sub>2</sub> thermal conductivity with exposure, compared with the values for unirradiated fuel, is more and more widely acknowledged. Data reported by the Halden Project (6) suggest this degradation in the range 6-8% per 10 MWd/kgU at temperatures below 700°C. Many experiments are underway with the aim to verify these observations and to quantify this degradation with temperature and burnup. However, an experimental argument in favor of high temperature regime during the fifth cycle in GRA fuel is the grain growth observed in the pellet central zone.

On the other hand, isothermal annealing tests performed on irradiated fuel show a significant decrease at high burnup (60 MWd/kgU) of the threshold at which fission gas release occurs compared to low burnup.

(25 MWd/kgU); this feature is verified under reducing and oxidising atmospheres (7).

These experimental evidences suggest that the deterioration of the thermal conductivity and the lowering of the gas release threshold with burnup have to be taken into consideration. The observations made on the GRA fuel rods likely result from a combination of the two phenomena.

In order to discriminate between these effects for modelling purpose, an experimental and quantitative evaluation of each of them is necessary. The data available to date are still insufficient.

By correlating the centerline temperature estimation and the release observed in the hot center of the pellet for the GRA rods, one can estimate the curve of the threshold temperature of fission gas release evolution with burnup. With the extreme hypothesis of no thermal conductivity degradation with burnup, the curve obtained is slightly above the threshold temperature for a 1% rod integral fission gas release curve proposed by reference (5), and shows a tendency of flattening at high burnup (Figure 6).

With the hypothesis of a constant gas release threshold with burnup after the incubation period, the obtained curve should be similar to the one proposed by Vitanza (8), but this implies a serious deterioration of the thermal conductivity with burnup.

### 5 - Conclusion

The results of postirradiation examinations made at different steps of the irradiation of two fuel rod families irradiated in PWR during five cycles showed interesting features linked to the different power histories the two families experienced.

Particularly, the evolution of the fuel microstructure and of the fractional gas release made it possible to single out the contribution of the athermal process, including the "rim effect", and the thermal process.

The development of "high burnup" realistic models needs a correct evaluation of the fuel thermal conductivity deterioration with burnup on the one hand, and of the lowering of the gas release thermal threshold on the other.

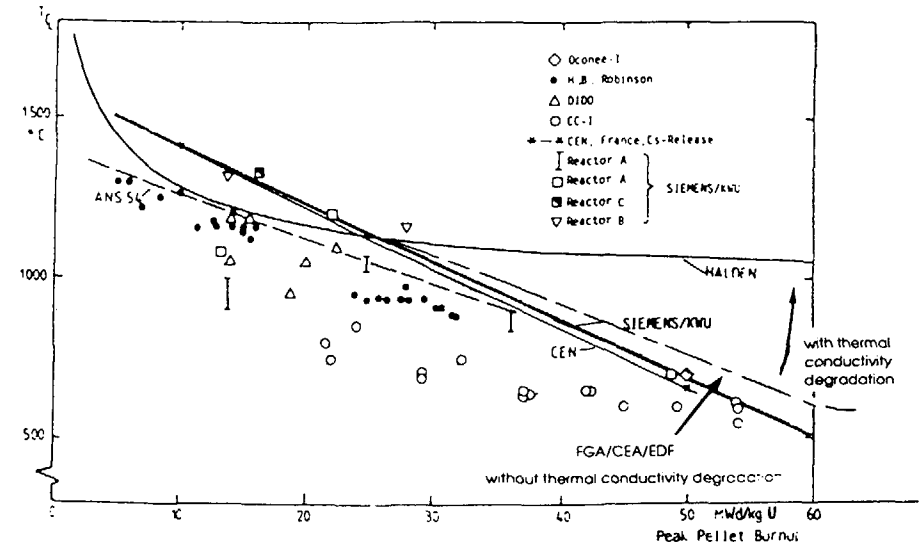


Figure 6 - Threshold temperature for 1% integral fission gas release (issued from (5))

Several national or international programmes are devoted to these fundamental subjects. In France, two new projects are currently being studied in order to increase the knowledge of the very high burnup fuel: refabrication and instrumentation of a GRA 5-cycle fuel rod for central temperature measurement under irradiation and also, the reirradiation of the same fuel to extended burnup.

### REFERENCES

- (1) BARON, D., and al., "Experience on Fission Gas Release in High Burnup Fuel Rods Operating in Power Plants", IAEA Technical Meeting on Fuel Internal Chemistry and Fission Products Behaviour, Karlsruhe (1985).
- (2) MOREL, M., and al., "FRAGEMA Fuel Behaviour at High Burnup", IAEA Technical Committee Meeting on Performance at High Burnup for Water Reactors", Nyköping (1990).

(3) GUEENEY,P and al, "FRAGEMA Fuel Rod Behaviour Characterization at High Burnup", ANS/ENS International Topical Meeting on LWR Fuel Performance, Avignon (1991)

(4) BARNER,J O ,and al "Relationship Between Microstructure and Fission Gas Release in High Burnup UO<sub>2</sub> Fuel with Emphasis on the Rim Region", ANS/ENS International Topical Meeting on LWR Fuel Performance, Avignon (1991)

(5) MANZEL,R, EBERLE,R , "Fission Gas Release at High Burnup and the Influence of the Pellet Rim", ANS/ENS International Topical Meeting on LWR Fuel Performance, Avignon (1991)

(6) KOLSTAD,E, VITANZA,C , "Fuel Rod and Core Materials Investigations Related to LWR Extended Burnup Operation", EMRS Fall Meeting, Symposium E, Strasbourg (1991)

(7) COQUERELLE,M , BOTTOMLEY,D , "Hot Cell Fission Gas Release Studies on UO<sub>2</sub>", this meeting

(8) VITANZA,C , and al , "Fission Gas Release from in-pile Pressure Measurements", Paper presented at the EHPG Meeting , Loen (1978)

## **THE EFFECT OF FUEL PELLET VARIANTS ON FISSION GAS RELEASE FOLLOWING POWER RAMPS**

D A. HOWL, I R TOPLISS  
British Nuclear Fuels plc,  
Springfields, Preston,  
United Kingdom

### **Abstract**

Results are presented of fission gas release inferred from on-line rod internal pressure measurements for several fuel variants which were subjected to a power ramp after irradiation to 18 MWd/kgU. The variants were standard and large grain solid fuel, and niobia-doped and undoped large grain annular fuel. The rates of fission product release, which did not saturate in 20 - 70 days following power ramps to 38 - 45 kW/m, are well predicted by the ENIGMA fuel performance code.

The experiments also included on-line measurements of rod diameter, enabling the evolution and relaxation of ridging to be determined. Examples are given in the paper.

These experiments were jointly funded by British Nuclear Fuels plc and the Electric Power Research Institute.

### **1. INTRODUCTION**

A series of experiments has been conducted in the Halden HBWR to investigate the effects of several different fuel pellet variants on the behaviour of fuel at power ramps. The principal objective of the work was to point the way to a fuel pellet design which had improved Pellet-Clad Interaction (PCI) performance. Fuel rods, each containing pellets of a different design, were subjected to power ramps to rating levels which might be reached during reactor faults. On-line measurements were made of the clad diameter, showing the formation and relaxation of ridging, and of internal pressure, showing the rate of fission gas release following the power ramps.

This paper will concentrate on the results obtained for the fission gas release and the comparison of these results with calculations using the ENIGMA fuel performance code<sup>(1)</sup>. An outline of the ridging results, together with ENIGMA calculations, will also be given.

### **2. FUEL PELLET VARIANTS**

The fuel pellet variants tested were

- (a) Standard solid pellets
- (b) Solid pellets with large grain size
- (c) Annular pellets with large grain size

- (d) Annular pellets doped with 0.25% niobia  
 (e) Annular pellets doped with 0.45% niobia

In all cases the pellets were made from powder produced by the Integrated Dry Route (IDR) and contained a pore former (CONPOR) to achieve a density of 95%. The pellet dimensions were outer diameter 10.59 mm, inner diameter (for the annular pellets) 3.39 mm, and length 10.8 mm. The grain sizes are given in Table 1.

TABLE 1 : FUEL GRAIN SIZES

FUEL TYPE	GRAIN SIZE ( $\mu\text{m}$ )
Standard solid pellets	15
Solid pellets with large grain size	47
Annular pellets with large grain size	45
Annular pellets doped with 0.25% niobia	20
Annular pellets doped with 0.45% niobia	37

Twelve fuel rods, each with a stack length of about 450 mm and each containing one of the pellet variants, were fabricated. The cladding was cold-worked and stress-relieved Zircaloy-2 with outer diameter 12.54 mm and inner diameter 10.80 mm. The rods were filled with helium at 0.1 MPa. Each rod was fitted with a bellows-type pressure transducer after the base irradiation, enabling the internal pressure to be measured on-line. The rods were assembled in two 6-rod clusters in the Halden rigs IFA-437.5 and IFA-415.4 (see Fig. 1).

### 3. IRRADIATION AND POWER RAMPING

The fuel rods were irradiated in IFA-437.5 and IFA-415.4 to a burn-up of about 18 MWd/tU. The irradiation history for IFA-415.4 is shown in Fig. 2, the history for IFA-437.5 was similar. Calculations with the ENIGMA fuel performance code indicated that the fuel temperatures were always below the Vitanza threshold<sup>(2)</sup> for 1% fission gas release, and very low release values (less than 0.5%) were predicted. An example of the ENIGMA prediction of fuel centre temperature is given in Fig. 3.

At the end of the period of base irradiation, the rods were ramped in groups of three to power levels of 38 – 45 kW/m in the Halden IFA-550 rig. The ramp imposed on the rods is shown schematically in Fig. 4. The purpose of the reduction in the rating from 31 to 25 kW/m followed by a short conditioning period (1 – 5 days) was to ensure relocation of pellet fragments following the transfer of the rods between rigs, previous experience at Halden had indicated the necessity for this.

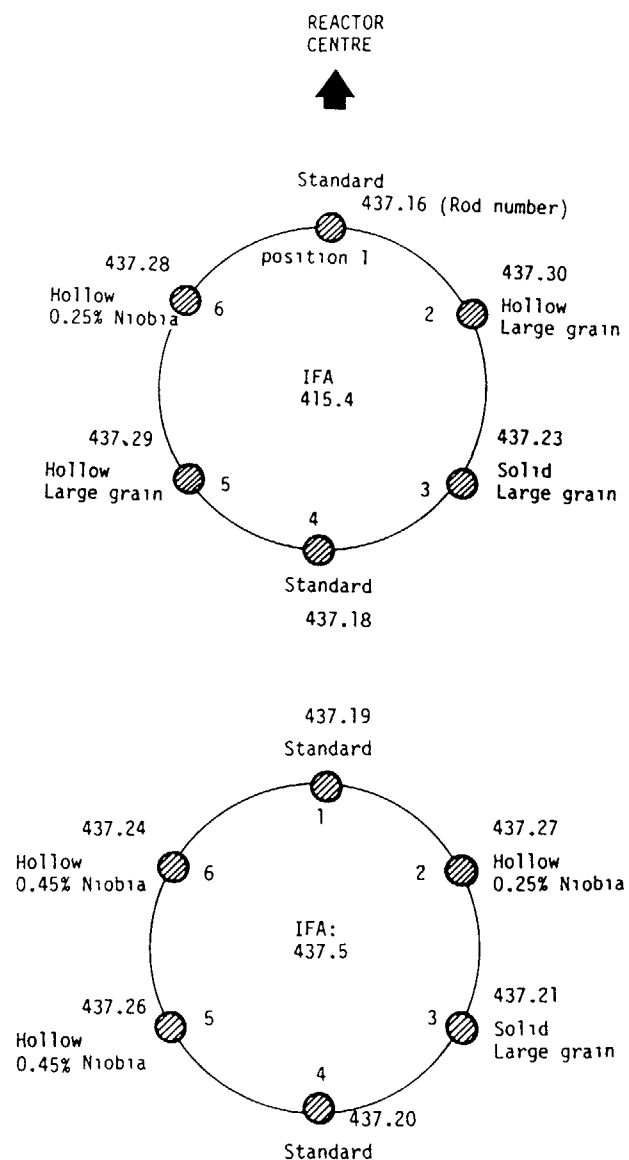


Figure 1 Location of Fuel Rods in Base Irradiation Rigs

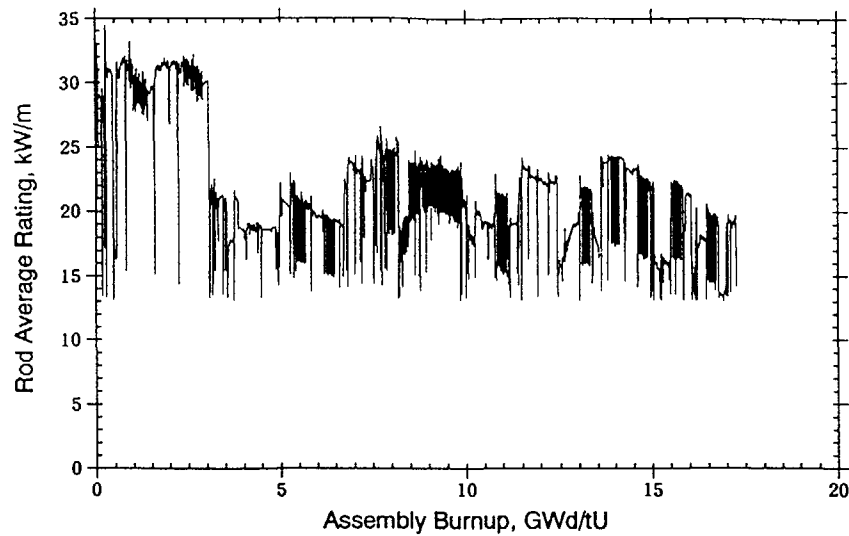


Figure 2 : Base Irradiation History for IFA-415.4

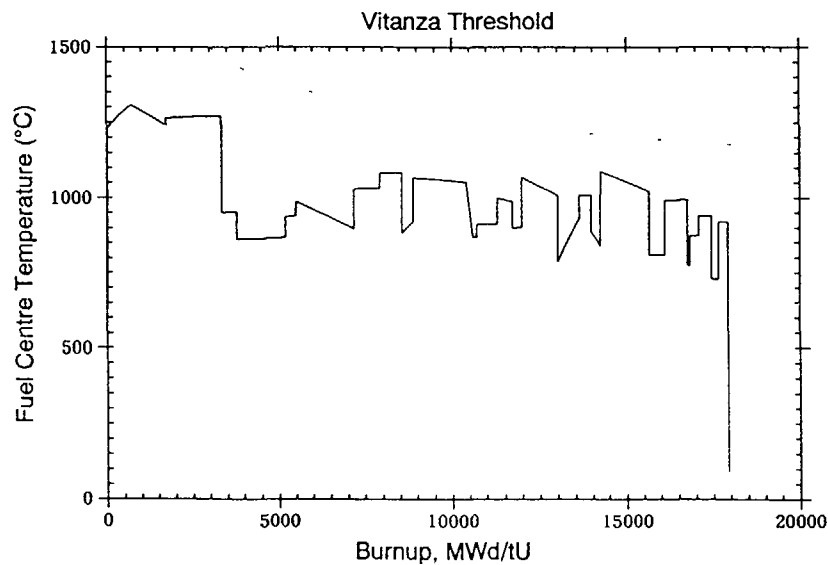


Figure 3 : Fuel Centre Temperatures for IFA-550.3 Rod 1

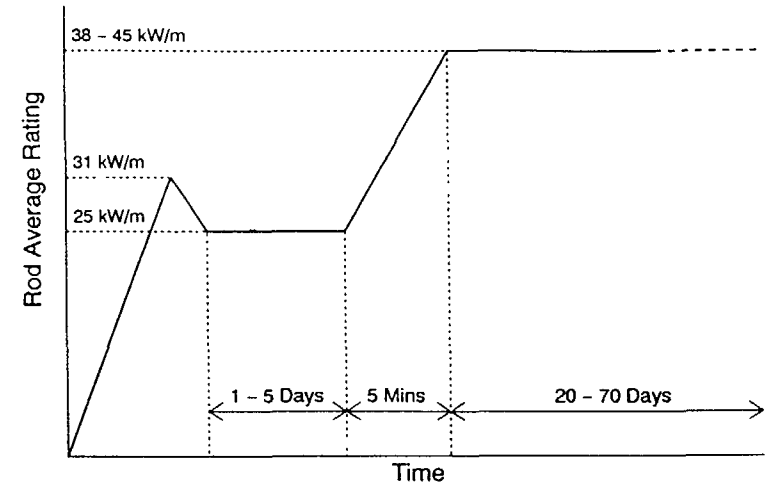


Figure 4 : Power Ramp Schematic

The rods were held at the high power level for between 20 and 70 days, and during this period measurements of internal pressure and rod diameter were made at intervals.

## 4. RESULTS

### 4.1 Fission Gas Release

From the measurements of internal pressure, the fission gas release in each rod was calculated and is plotted in Figs. 5 – 8. In most cases the rate of fission gas release was still declining at the end of the post-ramp period, up to 1700 hours in the second ramp test (Fig. 6). The increase for all three rods shown for the period 1000 – 1200 hours after the ramp in the fourth test (Fig. 8) is probably due to a small increase in rating at that time.

As expected, the solid large grain fuel shows a benefit over the standard fuel (Figs 5 and 8) and all annular large grain variants show further improvement.

### 4.2 Ridging

Measurements of clad diameter along the length of each rod at intervals in the post-ramp period showed the evolution and relaxation of ridging. The results for the standard and annular large grain fuel in the second ramp test are shown in Fig. 9.

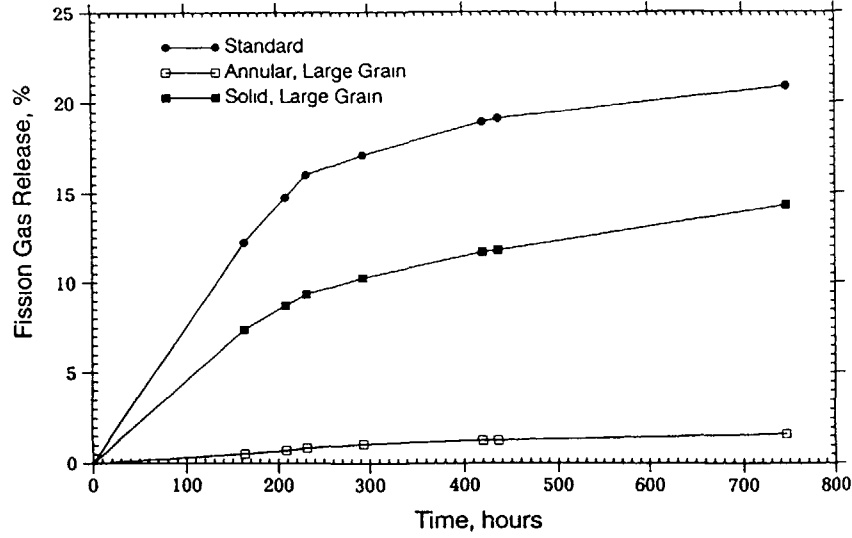


Figure 5 : Gas Release Inferred from Internal Pressure Measurements for Ramp Test 1

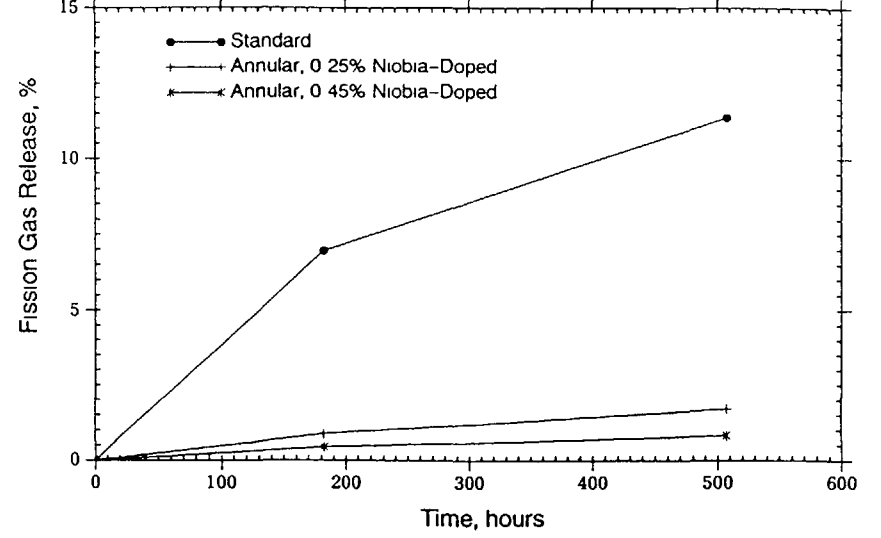


Figure 7 : Gas Release Inferred from Internal Pressure Measurements for Ramp Test 3

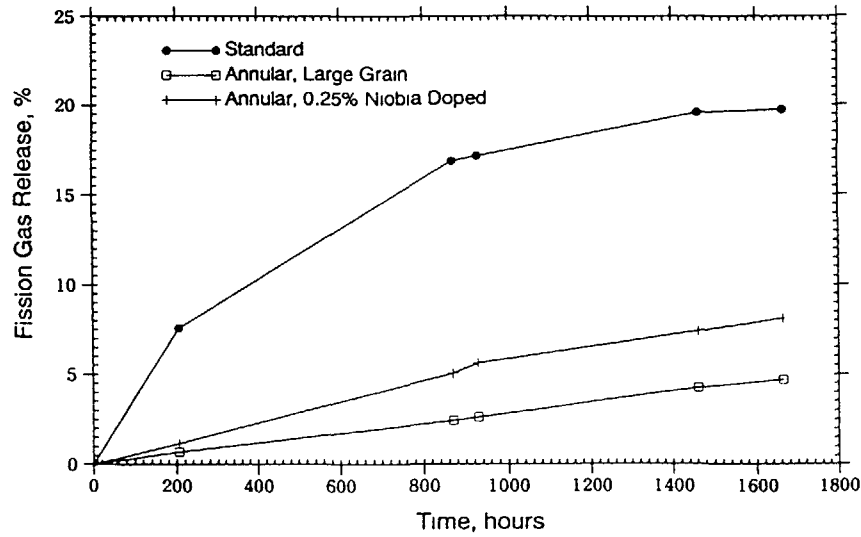


Figure 6 : Gas Release Inferred from Internal Pressure Measurements for Ramp Test 2

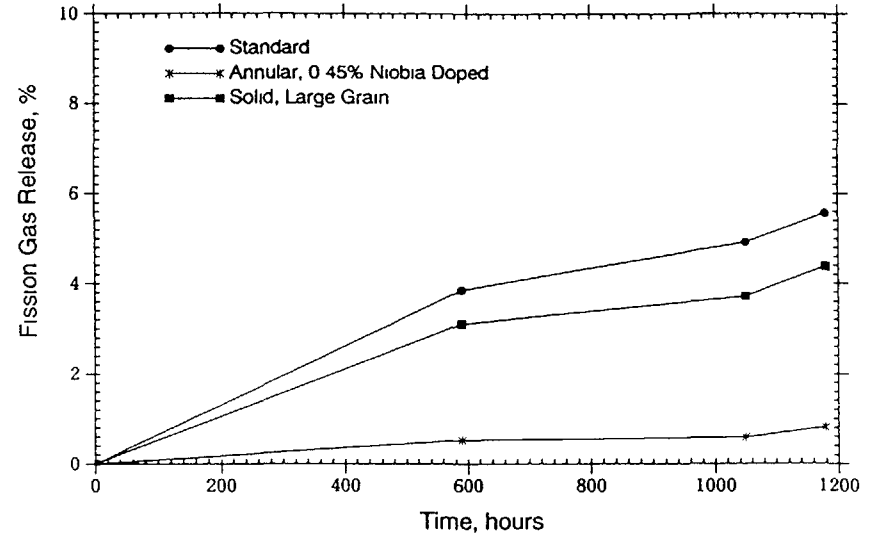


Figure 8 : Gas Release Inferred from Internal Pressure Measurements for Ramp Test 4

The results generally showed the ridging rising to a maximum value some hours after the ramp, before falling slowly towards the pre-ramp levels. The highest ridging was observed in the standard fuel, with the annular fuel variants all showing low ridging.

## 5. ANALYSIS

### 5.1 The ENIGMA Fuel Performance Code

The ENIGMA fuel performance code<sup>(1)</sup> is a state-of-the-art code jointly developed by British Nuclear Fuels plc and Nuclear Electric. It has been validated against a wide range of LWR data, including a database for fission gas release covering over 300 rods.

The gas release model is based upon the Booth treatment of diffusion from a sphere. A key component of the model is the treatment of gas in small intragranular bubbles. The nucleation and destruction model includes the effects of thermal resolution, so that a significant concentration of gas always remains in solution.

The arrival of fission gases to the grain boundaries is inhibited by the presence of an irradiation induced resolution process. This process operates by removing a proportion of gas atoms from the grain boundaries. The dynamic balance between diffusion to grain boundaries and irradiation induced resolution away from them sets up an effective barrier concentration. Incubation effects are handled using a novel treatment of the grain boundary in which the lenticular cavities are assumed to be tightly packed quasi-crystallites rather than equilibrium gas bubbles. Assuming irradiation induced resolution from these cavities, the broad features of the Vitanza interlinkage criterion are reproduced. Under conditions of large release, i.e. high temperatures, burnups and fast increases in temperature, enhanced gas releases are observed. The code incorporates a grain face bubble growth rate threshold above which transient grain face bubble interlinkage takes place, as distinct from grain edge bubble interlinkage. The criterion for enhanced release is derived from post-irradiation annealing test data.

### 5.2 Fission Gas Release

The ENIGMA calculations for the standard and large grain annular fuel are compared with the observations in Figs 10 to 13. With one exception, the magnitude of the post-ramp release is reasonably well predicted. The underprediction seen for the standard fuel case in Fig 12 is anomalous. As shown in Ref [1], the code is generally reliable in predicting fission gas release, the standard deviation on the ratio of prediction to measurement being slightly under  $\alpha/2$ .

The predicted time dependence of the release following the power ramp is in good agreement with the experimental results. The measured release levels follow the conventional square-root of time dependence, indicating a diffusive mechanism. The generally accurate predictions from ENIGMA provide good support for the magnitude of the gas diffusion coefficient used in the code.

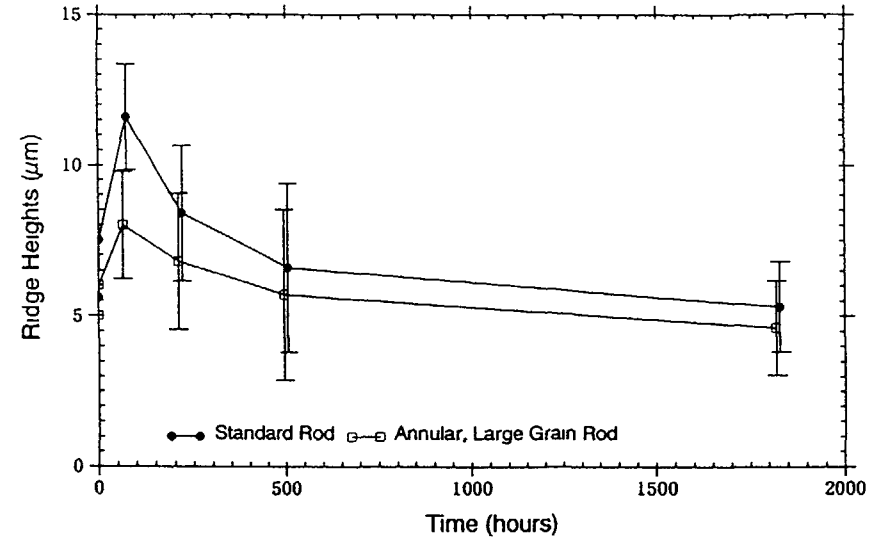


Figure 9 : Typical Ridge Height Measurements

### 5.3 Ridging

The ENIGMA predictions of the variation of clad ridge height with time are compared with the observations (from Fig 9) in Figs 14 and 15. Given that the measured ridges are small, around 5 to 11  $\mu\text{m}$ , and subject to several microns measurement uncertainty, the level of agreement between prediction and measurement is seen to be acceptable.

## 6 CONCLUSIONS

- (i) The increase of fission gas release following a power ramp does not saturate within several hundred hours after the ramp, for all the fuel types tested in the experiments described.
- (ii) Large-grain solid fuel shows a benefit over standard fuel, as expected, and large grain annular fuel (whether or not produced by niobia-doping) shows a further improvement.
- (iii) The ENIGMA code predicts well the magnitude and the variation with time of the post-ramp fission gas release, this confirms the validity of the fission gas release model in ENIGMA.
- (iv) The evolution and relaxation of ridging following a power ramp has been measured, and the benefit from annular fuel demonstrated.

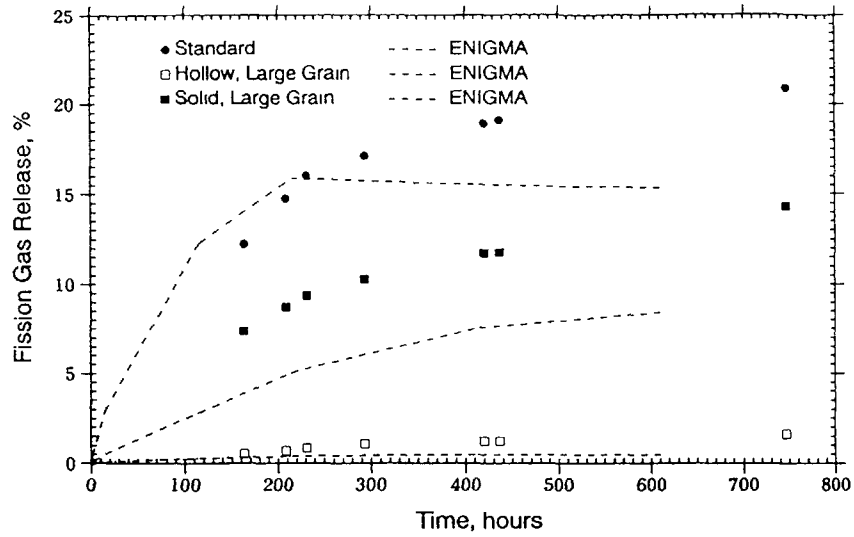


Figure 10 : Measured and Predicted Dynamic Gas Release for Ramp Test 1

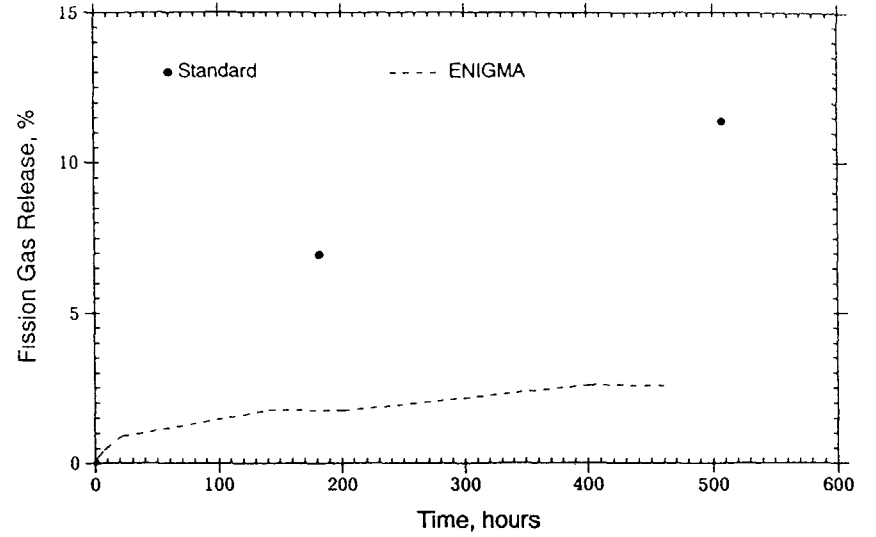


Figure 12 : Measured and Predicted Dynamic Gas Release for Ramp Test 3

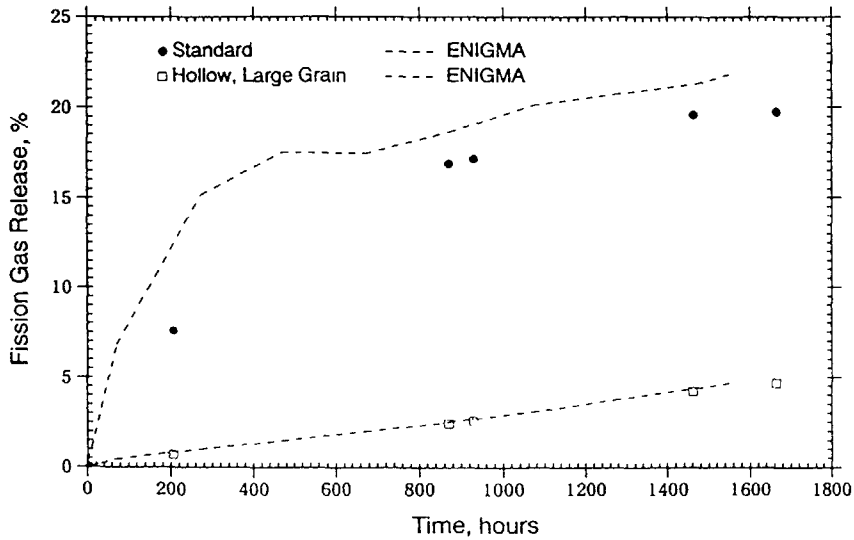


Figure 11 : Measured and Predicted Dynamic Gas Release for Ramp Test 2

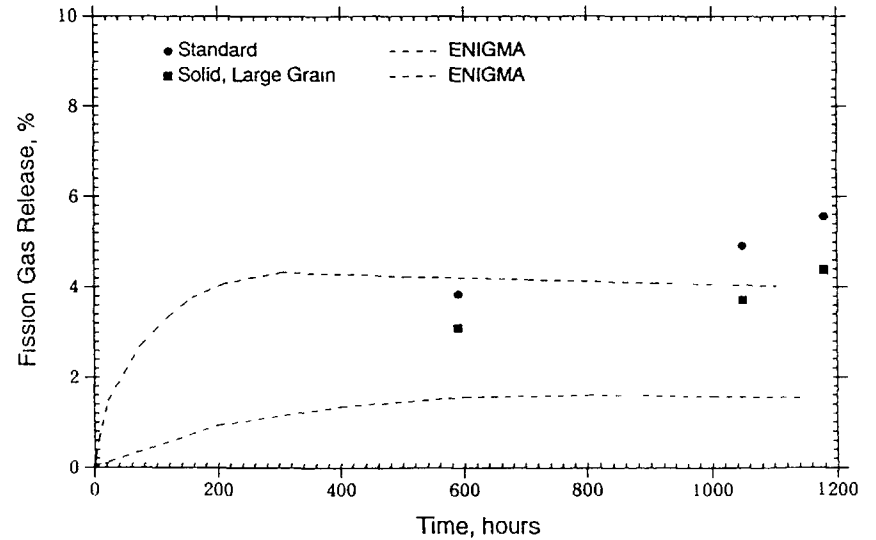


Figure 13 : Measured and Predicted Dynamic Gas Release for Ramp Test 4

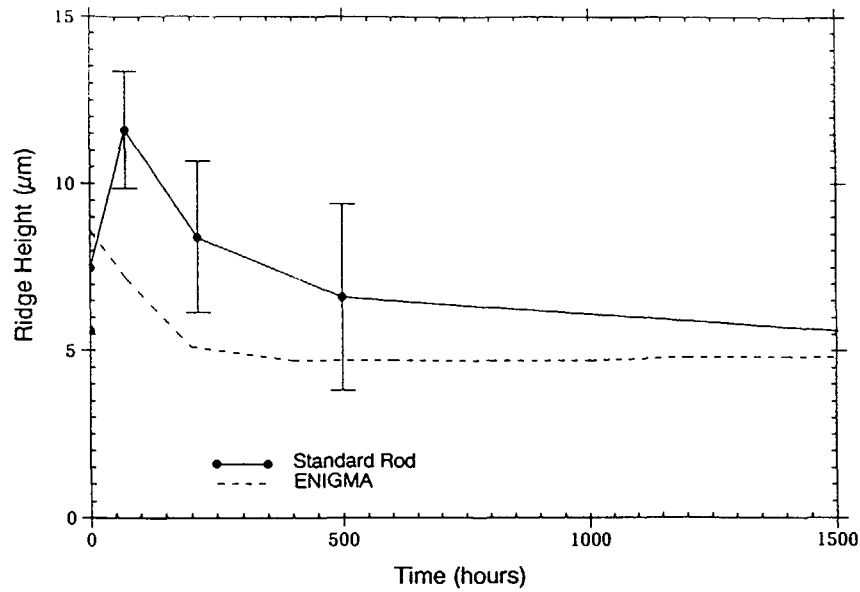


Figure 14 : ENIGMA Ridge Height Predictions for Ramp Test 2

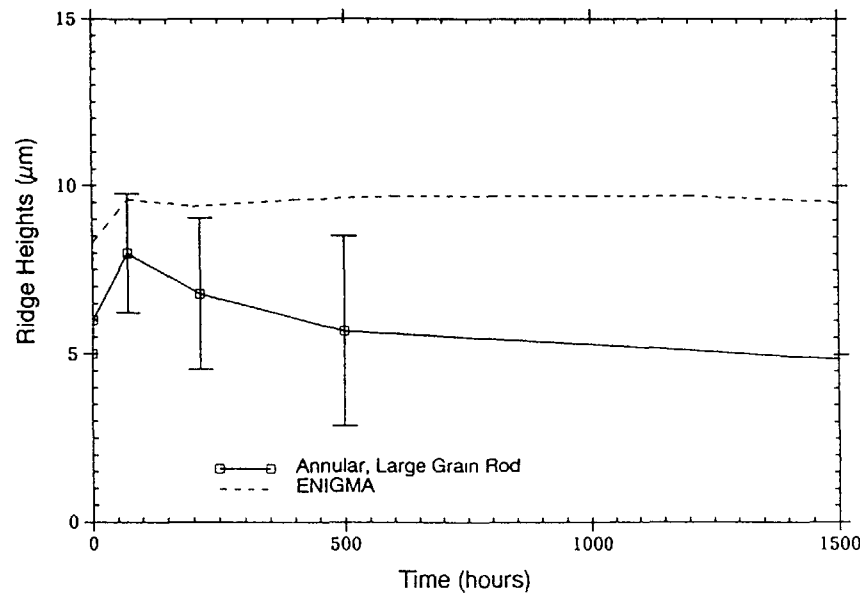


Figure 15 : ENIGMA Ridge Height Predictions for Ramp Test 2

#### ACKNOWLEDGEMENTS

The authors acknowledge the contribution of Mr C Vitanza of the Halden Reactor Project in the planning and execution of this successful set of ramp experiments which are particularly valuable in that on-line measurements were carried out during the test. M Smith of the Halden Project has supplied the results. The authors also acknowledge a major contribution to the funding of the experiments by the Electric Power Research Institute (EPRI) and are grateful to R Yang of EPRI for permission to publish the results.

#### REFERENCES

- [1] KILGOUR, W.J. et al., *Capabilities and Validation of the ENIGMA Fuel Performance Code*, ANS-ENS International Topical Meeting on LWR Fuel Performance, Avignon, France, April 21 - 24, 1991
- [2] VITANZA, C., GRAZIANI, U., FORDESTROMMEN, N.T., and VILPPONEN, K.O., *Fission Gas Release from In-Pile Pressure Measurements*, Halden Project Report HPR 221.10 (1978)

## FP GAS RELEASE BEHAVIOUR OF HIGH BURN-UP MOX FUELS FOR THERMAL REACTORS

K KAMIMURA

Power Reactor and Nuclear Fuel  
Development Corporation,  
Tokai, Ibaraki, Japan

### Abstract

Instrumented rig IFA-565 is now under irradiation in HBWR to investigate high burn-up MOX fuel behaviour for thermal reactors. The irradiation test of IFA 514 (former rig number for IFA-565) was performed from 1979 to 1988. The fission gas release behaviour for the MOX fuel rods of IFA-514/565 to the burn-up level of 41GWd/t MOX (47GWd/tM) has been analysed. The following observations are made:

Vitanga threshold for  $UO_2$  fuel is applicable to predict the onset of fission gas release for MOX fuel.

- There was no significant differences in fission gas release fraction between PNC MOX fuels and  $UO_2$  fuels at about 47GWd/tM.

Fission gas release fraction of hollow pellets might be smaller than that of solid pellets according to the In-pile data. It is necessary to confirm the result by using PIE data after the irradiation.

- PNC MOX fuels have achieved high burn-up as 47GWd/tM without failure.

### 1. INTRODUCTION

Power Reactor and Nuclear Fuel Development Corporation (PNC) has been Developing plutonium-uranium mixed oxide (MOX) fuels for fast breeder reactor (FBR), light water reactor (LWR), and advanced thermal reactor (ATR)[1]. Instrumented rig IFA-565 is now under irradiation in HBWR to investigate high burn-up MOX fuel behaviour for thermal reactors. The irradiation test of IFA-514 (former rig number for IFA-565) was performed from 1979 to 1988.

IFA-514 had one cluster with six fuel rods, which were 1380 mm in active length of  $5.8w/oPuO_2$ -Nat  $UO_2$  pellets. The purpose of IFA-514 irradiation test was to investigate the thermal and mechanical behaviour of MOX fuel and to see if its performance was different from uranium oxide fuel. The experimental parameters of IFA-514 were pellet shape (hollow pellet/solid pellet) and pellet surface treatment (ground pellet/as sintered pellet).

In 1989, non destructive post irradiation examination for six fuel rods of IFA-514 were performed. Three of them were reassembled to IFA-565 and re irradiation started in HBWR in 1990. Destructive examinations were performed on the other three fuel rods.

Irradiation conditions are summarized as follows:

	Solid Pellet	Hollow Pellet
Max Rod Average LHR(KW/m)	38	33
Rod Average Burn up(GWd/tM)	45	47

It is the purpose of this paper to present the fission gas release measurements in IFA-514/565. The analysis deals with the onset of fission gas release and burn-up-dependent release behaviour. The paper describes the results of the evaluation as follows:

- Comparison of the onset of fission gas release between MOX fuel and  $UO_2$  fuel
- Comparison of fission gas release between hollow pellet and solid pellet
- Comparison of the fission gas release fraction between MOX fuel and  $UO_2$  fuel

The experiments of IFA-514/565 are carried out as a part of joint research programme between PNC and Japan Atomic Energy Research Institute (JAERI) with the participation of the OECD Halden Reactor Project.

### 2 FUEL DESIGN AND IRRADIATION CONDITIONS

#### 2.1 Design of Rig

##### IFA-514

IFA-514 fuel assembly consists of six fuel rods which are mounted on a circle with the upper and lower tie plates, two spacers and three stay tubes. The fuel bundle is fixed to the shroud tube with a Zry 2 support tube which is located in the centre of the bundle. The six fuel rods have the same active length of 1380 mm and have instrumentations for in-pile measurements of fuel centreline temperature, plenum pressure, cladding elongation and fuel stack length change. The plenum pressure transducers are mounted on the top end plugs of Rod No. 1 and Rod No. 4. Rod No. 1 has

also a thermocouple from the bottom end To confirm the irradiation conditions, the rig is also instrumented with turbine type flow meter, thermocouples for coolant temperature measurements, neutron detectors and steam sampler for fuel failure detection

#### IFA-565

After non destructive post irradiation examination for six fuel rods of IFA-514 were performed, three of them were reassembled to IFA-565 The design of the clusters is similar to that of IFA-514

#### 2.2 Fuel Rod Specification

##### IFA-514

The fabrication data of IFA-514 fuel rods are given in Table I The six fuel rods have the same cladding dimensions as those of BWR 8x8 fuel assembly The fuel pellets are sintered of 5.8w/o PuO<sub>2</sub>-Nat UO<sub>2</sub> mechanically blended powder, 94% theoretical density, chamfered, and 10 mm long Pellet cladding diametral gaps are 240±20 μm. The pellets in the Rod No 1 and Rod No 2 were ground with centreless grinding The Rod No 4 and Rod No 6 contain hollow pellets, the inner diameter of which is 3.5 mm

##### IFA-565

IFA -565 consists of Rod No 3, 4 and 6

#### 2.3 Irradiation Conditions

TABLE II shows the irradiation data of IFA-514/565. IFA-514 was irradiated in the reactor from July 1979 until November 1988 The maximum average linear heat ratings (LHR) of Rod No. 1 and Rod No 4 were 38 and 33KW/m respectively The mean LHR averaged for burn-up of Rod No 1 and Rod No 4 were 24KW/m and 21KW/m respectively The rod average burn-up of Rod No 1 and Rod No 4 were 40GWd/t MOX (45GWd/tM) and 39GWd/t MOX (44GWd/tM) respectively Re-irradiation of IFA-565 started in November 1990, and maximum rod average burn-up for Rod No 4 is 41GWd/t MOX (47GWd/tM) The power histories of Rod No 1 and Rod No 4 are shown in Figure 1 and Figure 2

TABLE I FABRICATION DATA OF IFA-514/565 FUEL RODS

Parameter \ Rod No	1	2	3**	4**	5	6**
Instrumentation						
Upper	PF1	EF1	EF2	PF2	—	EF3
Lower	TF1	EC1	EC2	(EC4)**	TF2	EC3
Fuel Pellet						
Fabrication Method	MB*1	MB	MB	MB	MB	MB
Shape	Solid Chamfer Ground	Solid Chamfer Ground	Solid Chamfer AS*2	Hollow Chamfer AS	Solid Chamfer AS	Hollow Chamfer AS
Outer Dia. (mm)	10.54	10.57	10.57	10.55	10.56	10.55
Inner Dia. (mm)				3.5		3.5
Height (mm)	10.0	10.0	10.1	10.1	10.1	10.2
Density (%T.D.)	93.6	93.2	94.5	94.2	94.2	94.1
PuO <sub>2</sub> Enrich. (w/o)	5.8	5.8	5.9	5.9	5.8	5.9
**5U Enrich (w/o)	Nat. UO <sub>2</sub>					
O/W	1.99	1.98	1.98	1.99	1.99	1.98
Adsorbed Gas (μl/g)	<10	<10	<20	22	13	24
Moisture (μl/g)	<10	<10	<10	<10	<10	<10
Cladding	Zry-2					
Material						
Outer Dia. (mm)	12.53	12.53	12.53	12.53	12.53	12.53
Inner Dia. (mm)	10.80	10.80	10.80	10.80	10.80	10.80
Pellet/Clad Dia. Gap (μm)	260	220	230	240	240	250
Fuel Stack length (mm)	1380	1380	1379	1378	1379	1378
Filling Gas	He, late					

<Note>

- \*1: Mechanical Blending
- \*2: As-Sintered Pellet
- \*3: Re-Assembled to IFA-565

TABLE II IRRADIATION DATA OF IFA-514/565

Rod No.	1	2	3**	4**	5	6**
Fuel Pellet Type	Solid	Solid	Solid	Hollow	Solid	Hollow
Max Rod Average L.H.R. [KW/m]	38	37	36	33	36	33
Average Rod L.H.R. [KW/m]	24	24	23 (23)**	21 (21)**	23	21 (21)**
Rod Average Burn-up [GWd/t MOX]	40	40	38 (40)**	39 (41)**	38	39 (41)**

- \*1 Re-Assembled to IFA-565
- ( ) \*\* including IFA-565 as of April 1991

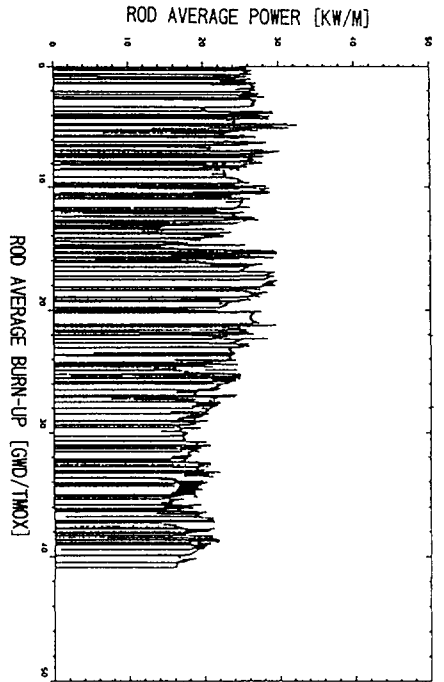


Fig 1 Rod Average Power History of IFA-514/565 Rod No 4

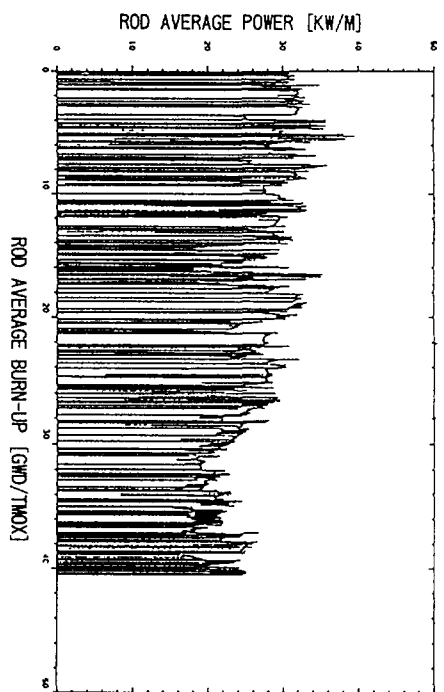


Fig 2 Rod Average Power History of IFA-514 Rod No 1

### 3 EXPERIMENTAL RESULTS AND ANALYSIS

#### 3.1 Plenum Pressure Measurement Results

Plenum pressures of fuel rods were measured on Rod 1 of IFA-514 and Rod 4 of IFA-514/565 by pressure transducers. Figure 3 shows the plenum pressure data normalized in the condition of zero power and 240°C. The plenum pressure data of Rod No 1 in the region above 28GWD/t MOX are not available because of the mechanical limit of the plenum pressure transducer. Nevertheless, the data derived from fission gas puncturing test is obtained. It is seen in figure 3 that the rod internal pressure in Rod No 1 (solid pellet) is much higher than in Rod No 4 (hollow pellet). Even though considering that the average LHR of Rod No 1 is relatively higher than that of Rod No 4, the internal pressure of Rod No 4 (hollow pellet) might be still lower than that of Rod No 1 (solid pellet). It might be caused by the difference of fuel temperature and free volume between the two rods.

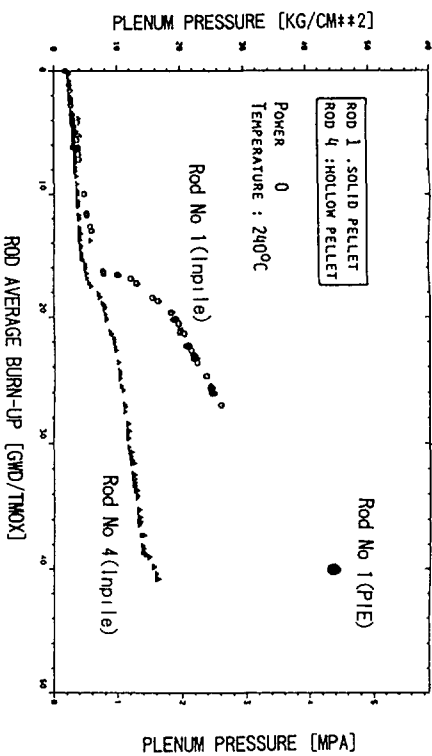


Fig 3 Plenum Pressure of IFA-514 as a Function of Burn-up

#### 3.2 Onset of Fission Gas Release

The plenum pressure in the region of burn-up < 24GWD/t MOX on Figure 3 is magnified as Figure 4

Fuel centerline temperature was measured on Rod No 1 by the in-fuel thermocouple. The peak fuel centerline temperatures derived from the measurement of thermocouple are plotted as a function of burn up together with the power histories in Figure 4. As Rod No 4 had no in fuel thermocouple, peak fuel centerline temperature of Rod No 4 was calculated by SIROD code.

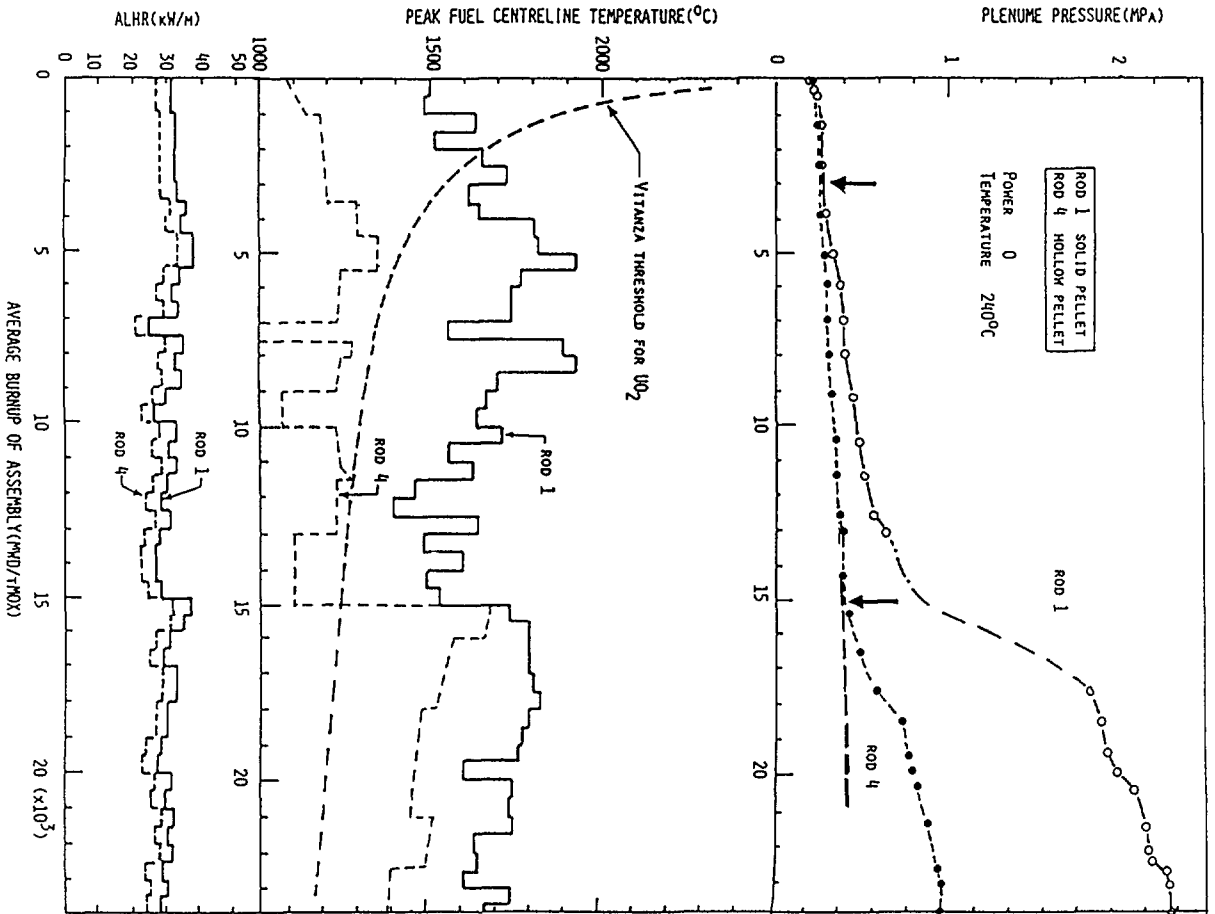


Fig 4 Comparison of fission gas release between solid pellet and hollow pellet (IFA 514)

The fission gas release does not occur from the beginning of the irradiation, but some burn up has to be accumulated before the release onset. This incubation period lasts longer at lower temperature. Vianza et al [3] proposed a prediction model for the onset of fission gas release of  $UO_2$  fuels. It is expressed by the following equation

$$\begin{aligned}
 \text{BUP}^* &= 5.0 \exp(9800/T_{cl}) \\
 \text{REL} &= 0 \quad \text{if burn up} \leq \text{BUP}^*
 \end{aligned}
 \tag{1}$$

where

BUP\* , threshold burn up of onset release (MWd/ $UO_2$ )

$T_{cl}$  , fuel centreline temperature ( $^{\circ}C$ )

The equation (1) is plotted in the middle part of Figure 4 in order to compare the release onset of MOX fuel with that of  $UO_2$  fuel.

It is seen in the upper part of Figure 4 that the plenum pressure increases gradually at lower burn up as shown by the broken line. It is caused by knock-out and recoil fission gas release mechanisms which are independent on temperature. The release onsets are shown by arrows when the abrupt plenum pressure increments occur. The incubation burn-ups marked by the arrows in Figure 4 agree well with the empirical  $UO_2$  fuel centreline temperature threshold by Vianza. This result means that the threshold burn up at which the release starts for these solid and hollow MOX fuel rods can be predicted by the model proposed for  $UO_2$  fuel. The release onset of the fuel rods in IFA-529 has already been analysed in the paper [2], and the same results has been obtained.

### 3.3 Comparison of Fission Gas Release between Hollow Pellet and Solid Pellet

Figure 5 shows the comparison of fission gas release between Rod No. 1 and Rod No. 4. The upper part of the figure shows the fission gas release fraction derived from the Figure 3 data. The middle and lower parts of the figure show the each power history. It is seen in Table 1 that there is no significant difference of fabrication specifications between Rod No. 1 and Rod No. 4 except the central hole.

For both Rod No. 1 (Solid Pellet) and Rod No. 4 (Hollow Pellet) the fission gas release is remarkable from 15GWd/t MOX. It is seen that the fission gas release fraction of Rod No. 1 keeps to increase until the end of life up to 23% at the burn up of 40GWd/t MOX. On the contrary, the fission gas release fraction of Rod No. 4 decreases slightly to reach 9% at the end of IFA 514 life. But at the beginning of the re-irradiation in IFA 565 the fission gas release fraction of Rod No. 4 increased slightly to reach 10%.

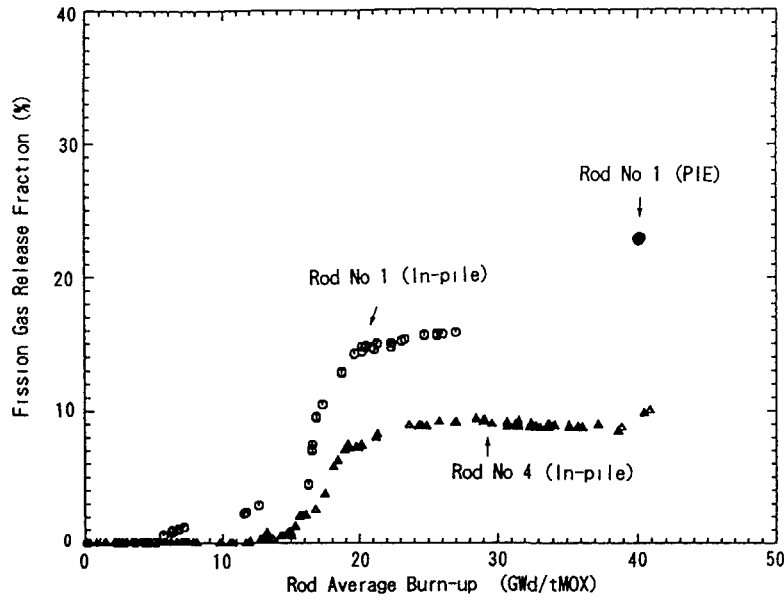


Fig 5 Fission Gas Release Fraction of IFA-514/565

The fission gas release fraction of Rod No 1 is much higher than that of Rod 4 at 40GWd/t MOX. Even if taking account of the difference of LHR, it seems the fission gas release fraction of Rod No 1 (solid pellet) is larger than that of Rod No 4 (hollow pellet). But it is necessary to confirm the In pile data by using PIE data after the irradiation.

3.4 Comparison of Fission Gas Release Fraction between MOX fuel and UO<sub>2</sub> Fuel

Figure 6 shows the burn up dependency of fission gas release fraction for BWR UO<sub>2</sub> fuels. The data of PNC MOX fuels for ATR and BWR are also plotted in Figure 6. The scattered region of PNC MOX fuel fission gas release fraction data is within that of UO<sub>2</sub> fuel. Fission gas release fraction In-pile and PIE data of Rod No 1 (Solid Pellet) and Rod No 4 (Hollow Pellet) of IFA 514/565 are drawn in the same figure. Those two lines are also located in the scattered region of UO<sub>2</sub> fission gas release fraction data. It is remarkable that even at high burn up of 40GWd/t MOX (45GWd/tM), fission gas release fraction of MOX fuel Rod No 1 is still low.

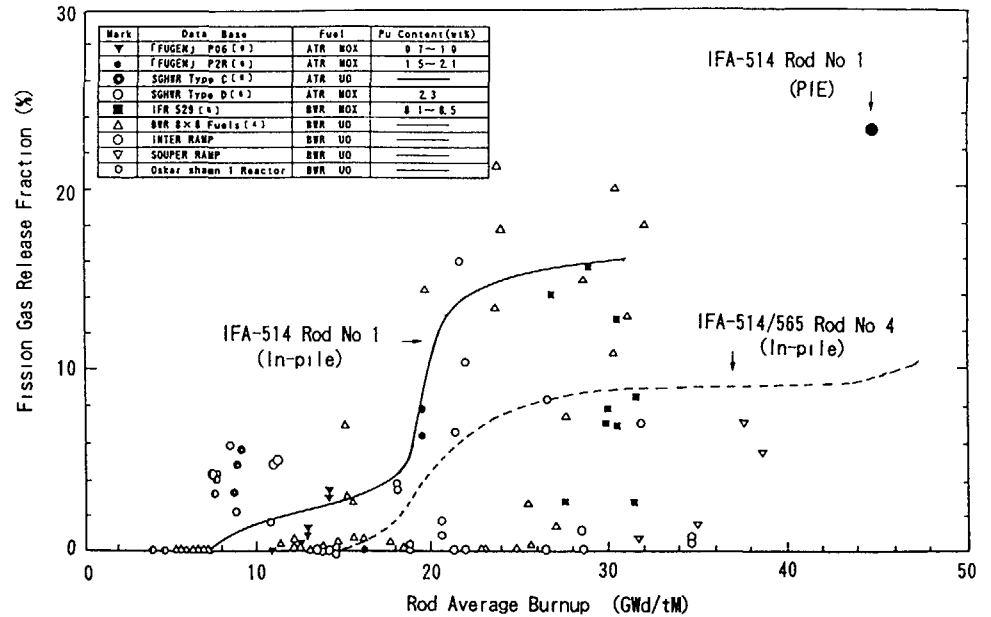


Fig 6 Fission Gas Release Fraction of UO<sub>2</sub> and MOX fuels as a Function of Burn-up

To compare the fission gas release fraction between different type of fuels, it is necessary to compare at the same linear heat rating.

Generally, fission gas release occurs above 10GWd/tM of burn up, and the maximum linear heat rating experienced above 10GWd/tM is most effective on fission gas release fraction.

A. Ohuchi et al. [5] made an analysis of measured UO<sub>2</sub> fission gas release fraction as a function of maximum linear heat rating ( $\geq 10$ GWd/tM). The result is depicted in Figure 7. In this figure, data of PNC MOX fuels irradiation experiments are also plotted. It is seen that fission gas release fraction data of PNC MOX fuels are located in the band of UO<sub>2</sub>.

4 CONCLUSIONS

The fission gas release behaviour for the MOX fuel rods of IFA 514/565 to burn up level of 41GWd/t MOX (47GWd/tM) has been analysed. The following observations are made:

UO <sub>2</sub> fuels [5]		
Grd	UO <sub>2</sub>	Burnup
○	UO <sub>2</sub>	12~17 GWd/tM
○	UO <sub>2</sub>	18~24 GWd/tM
⊙	UO <sub>2</sub>	22~30 GWd/tM

PNC MOX fuels [6]		
	Pu content (wt%)	Burnup (GWd/tM)
○	0.7 ~ 1.0	11 ~ 15
●	1.5 ~ 2.1	14 ~ 20
●	3.1 ~ 3.5	26 ~ 30
⊙	5.8	45
⊙	5.8	47

⊙1 : IFA-514 Rod1  
 ⊙2 : IFA-514 Rod4

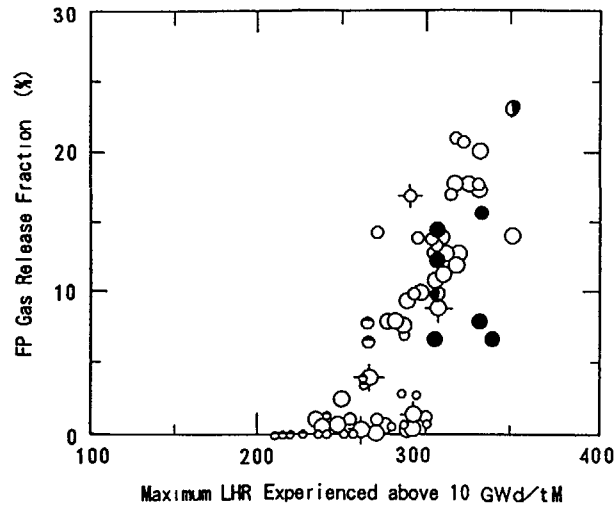


Fig. 7 Fission Gas Release Fraction of UO<sub>2</sub> and MOX Fuels as a Function of Maximum LHR Experienced above 10 GWd/tM

Vitanza threshold for UO<sub>2</sub> fuel is applicable to predict the onset of fission gas release for MOX fuel

There was no significant differences in fission gas release fraction between PNC MOX fuels and UO<sub>2</sub> fuels at about 47GWd/tM

Fission gas release fraction of hollow pellets might be smaller than that of solid pellets according to the In-pile data. It is necessary to confirm the result by using PIE data after irradiation

PNC MOX fuels have achieved high burn-up as 47GWd/tM without failure

## REFERENCES

- [1] Y. MISHIMA, "Japanese Fuel Study Related to Extended Burnup and Plutonium Recycling", IAEA Specialists' Meeting on Improved Utilization of Water Reactor Fuel with Special Emphasis on Extended Burnups and Plutonium Recycling, Mol, 1984
- [2] K. KAMIMURA, T. ABE and Y. YOKOUCHI, "Fission Gas Release Behaviour of MOX Fuel (IFA-514 and IFA-529)", Workshop Meeting on Fission Product Release, Halden, 19-20 September, 1985.
- [3] C. VITANZA, E. KOLSTAD and U. GRAZIANI, "Fission Gas Release from UO<sub>2</sub> Pellet Fuel at High Burn-up", ANS Topical Meeting on Light Water Reactor Fuel Performance, Portland, 1979.
- [4] T. Fujibayashi et al, "Proving Test on the Reliability for BWR 8×8 Fuel Assemblies in Japan", IAEA Specialists' Meeting on "Post Irradiation Examination and Experience", Tokyo, Japan 26-30 Nov. 1984.
- [5] A. Ohuchi et al, "Behavior of Gaseous and Volatile Fission Products in BWR Fuel Rods", IAEA Specialists' Meeting on "Post Irradiation Examination and Experience", Tokyo, Japan 26-30 Nov 1984
- [6] T. Kajiyama, K. Kamimura et al. "Irradiation Performance of MOX Fuel in Fugen". PNC Technical Review, No 67 Sep. 1988
- [7] T. Mishima, K. Kamimura et al. "Thermal and Mechanical Behaviours of MOX Fuel Rods" IAEA Technical Committee Meeting on Recycling of Plutonium and Uranium in Water Reactor Fuels, Cadarache, France, 13-16 Nov 1989

# FUEL ROD CHEMISTRY AND RELATED PROPERTIES

(Session 3)

**Chairmen**

**D.A. HOWL**  
United Kingdom

**R. MANZEL**  
Germany

# FISSION GAS RELEASE FROM HIGH BURNUP PWR FUELS UNDER TRANSIENT CONDITIONS

H. KANAZAWA, H. SASAJIMA, K. HOMMA,  
K. ICHISE, T. FUJISHIRO, T. YAMAHARA  
Tokai Research Establishment,  
Japan Atomic Energy Research Institute,  
Tokai, Ibaraki, Japan

## Abstract

Extensive research program on fission gas release behavior under accidental conditions, are in progress at Japan Atomic Energy Research Institute (JAERI). In this paper, the results obtained in experimental studies, including annealing tests, and in-pile experiments to simulate Reactivity Initiated Accident (RIA) conditions, are described and discussed.

## 1. INTRODUCTION

Extending the fuel burnup is an effective way to improve the economics of Light Water Reactor (LWR) operation. One of the important research subjects on the LWR fuel performance at extended burnup is to understand the fission gas release behavior during transient conditions. In-pile and out-of-pile transient experiments have been performed with high burnup fuels at JAERI.

The present paper describes the fission gas release behavior under (1) slow heat up conditions such as in a Loss of Coolant Accident (LOCA), using an electrical heating method (annealing test), and (2) RIA conditions using the Nuclear Safety Research Reactor (NSRR).

The objectives of the tests are to understand the fission gas release behavior during the transient conditions, and to obtain the quantitative information for computer modeling. The principal experimental parameters are annealing temperature and duration time for the annealing tests, and burnup of the fuel and an energy deposition for the RIA tests.

The test fuels used in this study were irradiated up to the burnup of 42 MWD/kgU in the commercial Pressurized Water Reactor (PWR) plant.

## 2. ANNEALING TEST

### 2.1 TEST APPARATUS AND PROCEDURE

Annealing test apparatus (so. called Out Gas Analyzer) was designed and installed in the hot cell of the Reactor Fuel Examination Facility (RFEF) at JAERI in 1987. The fuel pellets irradiated at the PWR power plant were heated up to 2000° C in the induction furnace under vacuum condition ( $1 \times 10^{-5}$  torr). Graphite was chosen for furnace materials, and it is powered by a high frequency generator. The furnace temperature is measured by optical pyrometers. The out-put from the pyrometers are fed to a controller to maintain the furnace temperature. Gas measuring units in the operating room, are connected with the furnace using stainless steel tubes. These units are set up in a box operated at a negative pressure for safety. The principal components of these units are :(1) a quadra-pole mass spectrometer; (2) vacuum pumps; (3) three sets of standard leaks for the calibration of the mass spectrometer; (4) gas reservoir tanks; (5) vacuum gauges and (6) pressure gauges.

To use in the annealing test, the irradiated pellets are removed from the fuel rods using a de-fueling system developed at Reactor Fuel Examination Facility (RFEF). In order to remove the fuel pellets from the cladding tube without any additional cracks during de-fueling process, the cladding tube is cut axially at two ridge lines. Released fission gases are collected in the gas reservoir tanks and the composition of released gases is measured by the mass spectrometer.

Annealing tests were performed using 2.5 grams of the specimen removed from the irradiated fuels. The specimens were heated up to target temperatures (1800° C, 1900° C, 2000° C) under vacuum condition. The released gases from the specimens were collected and measured at 10, 30, and 90 minutes. The heating rate of these tests was 6.6° C/sec.

### 2.2 RESULTS AND DISCUSSION

Under the temperature of 1800° C, krypton was continuously released up to 30 minutes. However, under the elevated temperature condition, i.e. 1900° C and 2000° C, all amount of krypton contained in the specimen was released within 30 minutes. Figure 1 shows the release rate of xenon as a function of annealing time. On this figure, the release rate means the

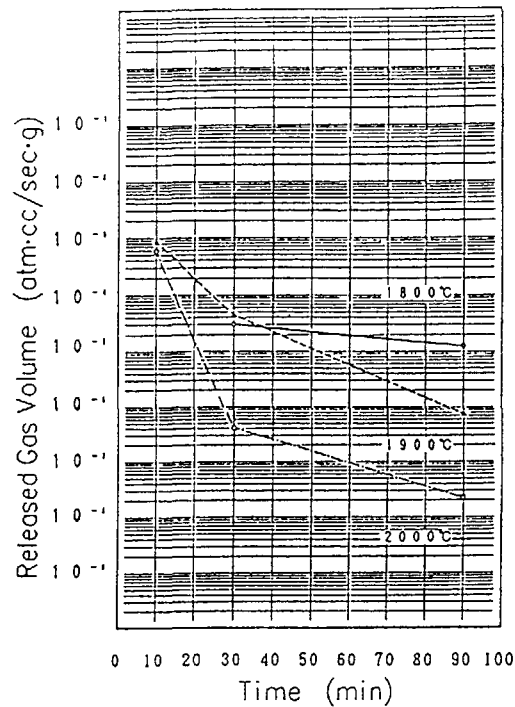


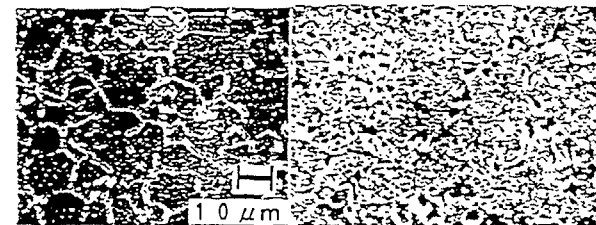
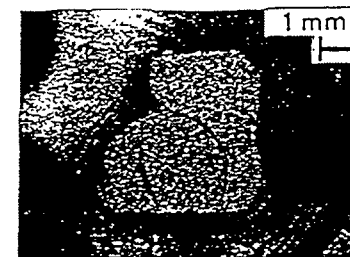
Fig. 1 The history of the released gas volume during the tests (Xe)

average value of the released volume during 0 to 10 minutes, 20 to 30 minutes and 80 to 90 minutes. As far as the test with 1800°C condition, the behavior of xenon release showed a similar tendency to that of krypton. In 1900°C and 2000°C conditions, the release of xenon was intensive during initial 10 minutes. Then, the release rate of xenon rapidly decreased and the amount of xenon measured at 90 minutes was much smaller than that at 10 minutes.

In the temperature of 1900°C or higher, the remained fission gases in the specimen were rapidly released. Under 1900°C condition, fission gas release rate (FGR) of the annealing tests up to 10 minutes was 73% for krypton and 47% for xenon, respectively. In case of 2000°C condition, FGR was 65% for krypton and 32% for xenon. The FGR could also be influenced by the location where the test specimen was taken from the pellet, since the amount of the retained fission gas was higher in the periphery of the pellet. It

could be expected that the specimen used in the test of 2000°C was taken from the inner reign of the pellet, then the FGR at 2000°C was lower than that of 1900°C condition. As stated previously, the released rate of fission gases was nearly constant at the test temperature of 1800°C. However significant change occurred when the temperature was elevated to 1900°C or higher. It can be noted that the threshold value of temperature in terms of intensive fission gas release exists between 1800°C and 1900°C. The release behavior of krypton differed from that of xenon at high temperature conditions. It could be thought that intergranular release of fission gases was controlled by diffusion. On the other hand, fission gases initially retained in the grain boundary were released in the beginning of the annealing tests by the burst release mechanism.

Microstructural examination and Electron Probe Micro Analyzer (EPMA) analysis were performed for the annealed pellet to observe the difference between the reference pellets. Figure 2 shows the observation results of optical microscope and Scanning Electron Microscope (SEM). On this observation the traces of fission gas bubbles appeared at intergranular and grain boundary.



BEFOR ANNEALING AFTER ANNEALING

Fig. 2 The results of microstructural observation

In the EPMA analysis, metallic phases composed by U, Ru, Rh, Mo, Tc, and Pd were observed at the peripheral region of the annealed specimens

### 3. FISSION GAS RELEASE UNDER RIA CONDITIONS

Experiments using burnup LWR fuel rods as test samples have been performed under simulated RIA conditions in NSRR. The objectives of the experiments are to understand the transient behavior of burnup fuel rods and to determine fuel failure thresholds under RIA conditions. The data on fission gas release are essential to understand the LWR fuel rod capability.

In contrast to the annealing tests presented in Chapter 2, the behavior of LWR fuel rod during RIA transients is characterized by very rapid fuel temperature increase, and very short duration of high temperature state. In addition, temperature distribution in the fuel rapidly changes especially in the early phase of the transient. It should be noted here that the maximum fuel temperatures attained in the RIA experiments described in this article were lower than those in the annealing tests.

This chapter presents the experimental results and FRAP-T6 predictions, mainly concerning the fission gas behavior under RIA conditions in NSRR.

#### 3.1. EXPERIMENT DESCRIPTION

LWR fuel rods used in the NSRR experiments were irradiated in the Mihama-Unit2 reactor(PWR) of Kansai Electric Power Co. to a local burnup of 39 MWd/kgU at the average linear heat rate of 18 kW/m (MH rod), and in the Genkai-Unit1 reactor(PWR) of Kyushu Electric Power Co. to a local burnup of 42 MWd/kgU at the average linear heat rate of 20 kW/m (GK rod). The fission gas release rates due to the irradiations in the commercial reactors were 0.17 % in MH rod and 0.43 % in GK rod, respectively.

The LWR fuel rods for the NSRR experiments were refabricated to short fuel segments. A schematic drawing of the test fuel rod is given in Figure 3. The rods were filled with pure helium of about 4 MPa. The use of pure helium instead of realistic mixture gas may have no significant effect on the fuel behavior because of the very low fission gas release rates before the RIA experiments. Instrumentation for the test fuel rod consists of thermocouple to measure cladding surface temperature, a rod internal pressure sensor, and the pellet stack and cladding tube elongation sensors

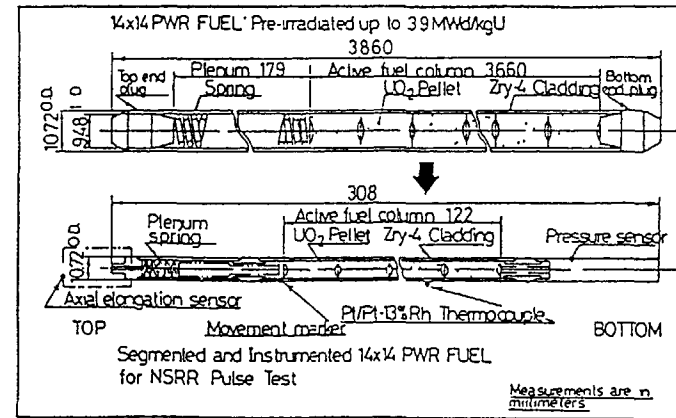


Fig. 3 Design of PWR fuel rod before (top) and after (bottom) refabrication

The test fuel rod was contained in a double-sealed capsule which was newly developed for the tests. The capsule, shown in Figure 4, was filled with stagnant water of ambient temperature and atmospheric pressure, and subjected to a pulse irradiation simulating an RIA transient in the NSRR.

Four RIA experiments, the tests MH-1 through MH-3 and GK-1, were conducted. Energy depositions in the test fuel rods ranged from 60 cal/g·fuel in MH-1 to 112 cal/g·fuel in GK-1, as shown in Table 1.

#### 3.2. EXPERIMENTAL RESULTS

Figure 5 shows the transient records of reactor power, core energy release, cladding surface temperature, rod internal pressure and cladding axial elongation measured in test MH-1. Table 1 gives the summary of the test results. No indication of the fuel failure was observed in all of the tests

As shown in Figure 5, the elongation behavior of the cladding tube followed the history of core energy release than that of cladding temperature. This suggests that the elongation of the cladding tube is mainly caused by pellet-cladding mechanical interaction (PCMI). This figure also shows the rapid increase of the rod internal pressure immediately after

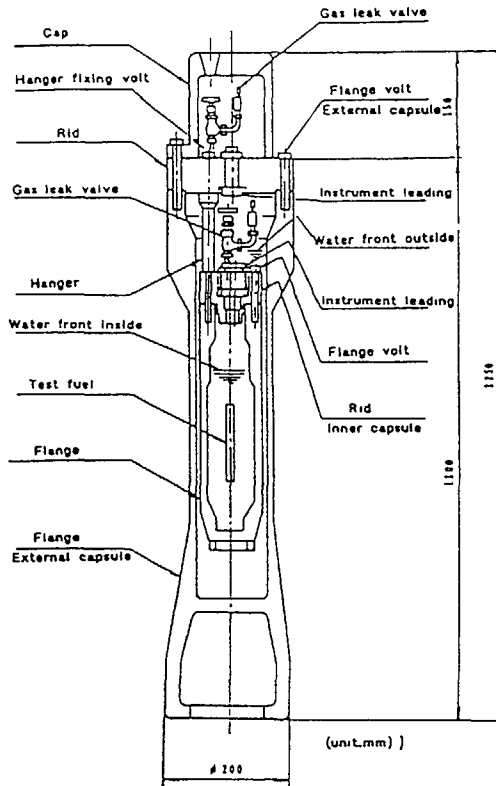


Fig. 4 Doubly shielded atmospheric pressure capsule (X-II type) for pulse irradiation of preirradiated PWR type fuel rod

the initiation of the pulse irradiation. This suggests that the burst release of fission gas occurred at the very early stage of the transient.

As listed in Table 1, measured fission gas releases during the pulse irradiation were from 3.7% to 4.3% in the test with MH rods, and 12.2% with GK rod. It can be noted that the fission gas release under RIA conditions were much higher than that observed during normal operation in the commercial PWRs.

Table 1 Summary of as-fabricated characteristics of the test fuel rods, and the test results

Test No	MH-1	MH-2	MH-3	GK-1			
Test fuel	Initial pellet enrichment (w/o)		2.6	3.4			
	Cladding material		Zircaloy-4				
	Assembly	Type	14x14 PWR				
		Filler gas (MPa)	4 (Helium)				
	Plenum volume (ml)		1.5				
Irradiation at power reactor	Reactor		Mihama	Genkai			
	Fuel burn-up (MWd/kgU)		39	42			
	Liner heat rate (kW/a)		18				
	F111 gas pressure at 0°C (MPa)		4.23	4.23	4.63	4.22	
	Plenum volume (cm <sup>3</sup> )		12.6				
	Fission gas release rate (%)		0.17		0.43		
Pulse irradiation	Pellet-cladding gap (μm)						
	Energy deposition (cal/g-fuel)		60	68	83	112	
	Peak fuel enthalpy (cal/g-fuel)		46	54	67	91	
	Max cladding surface temp (°C)		368	355	457	581	
	Pressure increase (MPa)		1.36	1.31	—	1.93	
	Peak cladding elongation (mm)		0.53	0.66	1.20	1.27	
	Peak cladding strain (%)		0.43	0.54	0.99	1.05	
	Peak stack elongation (mm)		—	0.84	1.49	1.16	
	Peak stack strain (%)		—	0.69	1.23	0.96	
	Fission gas release rate	Measured (%)		3.7	4.2	4.3	12.2
		FRAP-T6 Code (%)		0.25	0.25	0.51	5.61

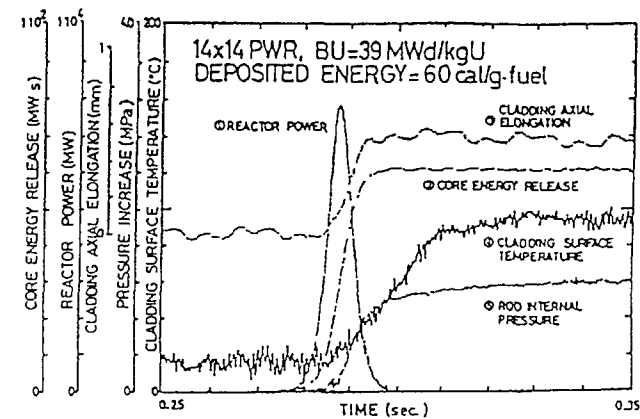


Fig. 5 Transient records during the RIA test MH-1

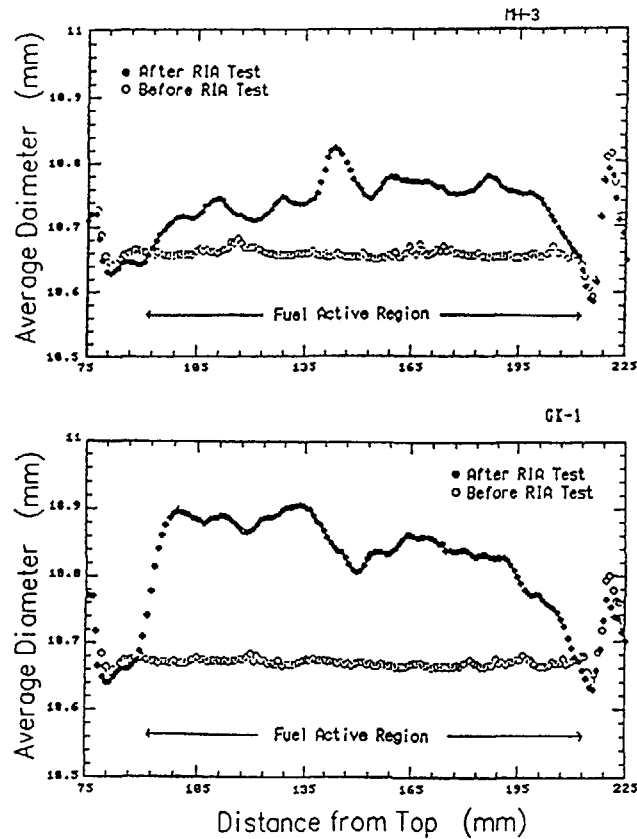


Fig. 6 Diametral profiles before and after the RIA transients for the MH-3 and the GK-1 rods.

The maximum cladding surface temperatures ranged from 82 °C to 184 °C in the tests with the MH rods. In the test with the GK rod, the maximum cladding surface temperature was 308 °C. The maximum cladding surface temperature and the cladding elongation increased according as the increase of energy deposition.

Figure 6 shows comparison of the diametral profiles along the active fuel region before and after the RIA transients in the tests MH-3 and Gk-1. As shown in the figure, after the transients, significant radial permanent deformation of the cladding tube was observed along at the active fuel

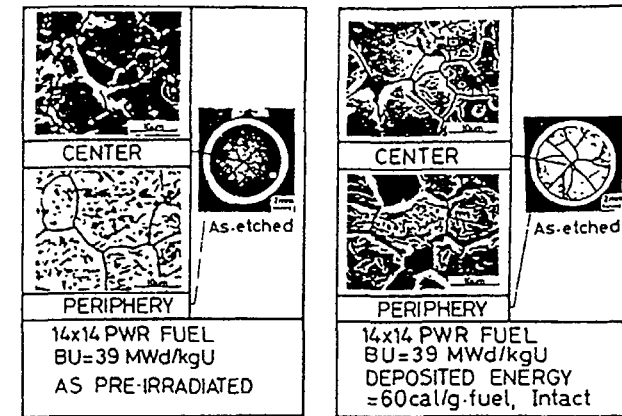


Fig. 7 Microscopic photographs of the fuel (a) before and (b) after pulse irradiation (Test MH-1)

region. The maximum permanent cladding hoop strain reached approximately 1 % in the test MH-3 and 3 % in the test GK-1, respectively.

Post NSRR test examinations of the test fuel rods indicated that grain boundary separation and microcrack generation took place within about 1 mm from the fuel periphery. Generation of the microcrack may be due to strong temperature gradient in the fuel periphery during the early stage of the transient. The cause of the grain boundary separation might be due to the early and significant release of the fission gas as discussed concerning in Figure 6. It can be considered that the most of released fission gas must have existed in the grain boundaries before the pulse irradiations because of the very short duration of the transient. Figure 7 shows the micrograph of the fuel sample taken from the MH-1 rod after the RIA transient test. The figure also includes the micrograph of the fuel sample taken from the reference rod which was not subjected to a pulse irradiation. On the fuel periphery, extensive grain boundary separation can be observed after the RIA transient with no significant grain growth. Figure 8 shows the micrograph of fuel samples taken from the GK-1 rod after the test. The rod showing the microcracks developed along the grain boundary on the fuel periphery during the RIA transients.

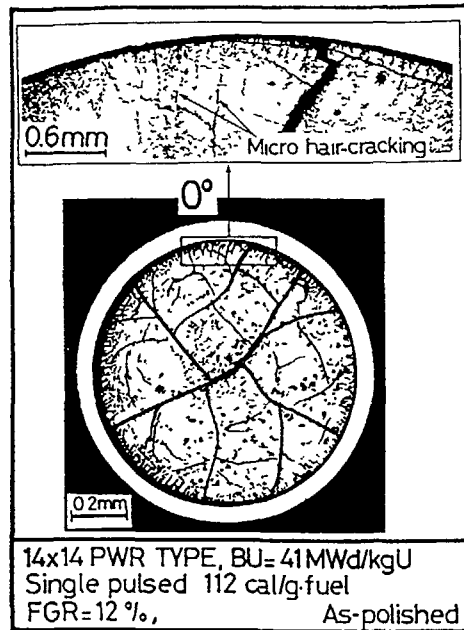


Fig. 8 Cross-sectional photograph of GK-1 test rod after pulse irradiation

### 3.3. ANALYSIS WITH FRAP-T6 CODE

FRAP-T6 (Fuel Rod Analysis Program-Transient) code was developed by Idaho National Engineering Laboratory (INEL) to mechanistically predict the performance of LWR fuel rods during operational transients and accidents. FRAP-T6 code incorporates the FASTGRASS model for the prediction of fission gas release [1,4]. The preliminary analysis was performed with FRAP-T6 concerning the fission gas behavior observed in the NSRR experiments with the burnup PWR fuel rods.

Figure 9 shows the calculated radial temperature profiles in the fuel for the test MH-3 at the several elapsed times after the initiation of the transient power burst. During the test, the maximum energy deposition occurs at the fuel pellet surface due to self-shielding effect, and the peak fuel temperature appears near the pellet surface at the early stage of the

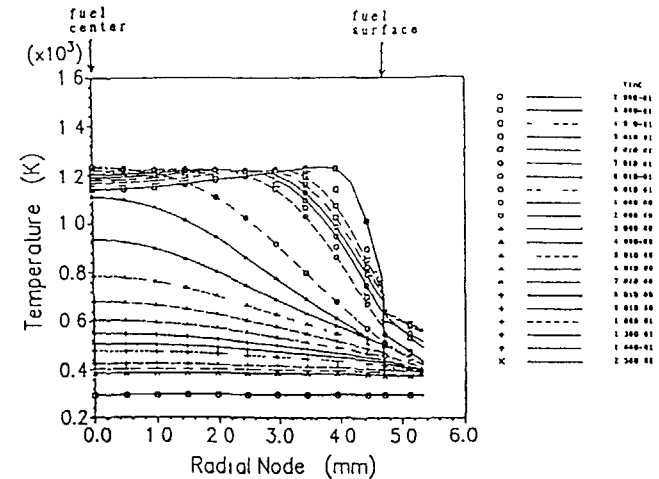


Fig. 9 Calculated fuel radial temperature profiles for several times after pulse irradiation in Test MH-3 (p/c gap  $30\ \mu\text{m}$ )

transient. Subsequently, strong thermal stress is generated in the fuel periphery due to rapid cooling of the fuel surface. This explains the generation of the microcracks on the fuel periphery.

Figure 10 shows the predicted and measured fission gas release rates as a function of energy deposition. The measured and predicted fission gas release rates increase with the increase of the energy deposition. The predicted fission gas release rates for the GK rods are higher than those for the MH rod. This is mainly due to the differences in the initial enrichment and irradiation conditions in the commercial PWRs. Higher burnup and higher liner heat rate during the irradiation for the GK rod result in large accumulation of fission gas in the grain boundaries. Higher initial enrichment means higher fraction of fission gas near the pellet periphery. Consequently, the GK rod has higher fission gas release rate than that of MH rod. The difference in the release rates between the GK and MH rods becomes larger at higher energy deposition.

Figure 10 also shows the significant difference between the measured and the predicted fission gas releases. Here, it can be pointed out that FRAP-T6 predicted much smaller permanent cladding hoop strain than the measured

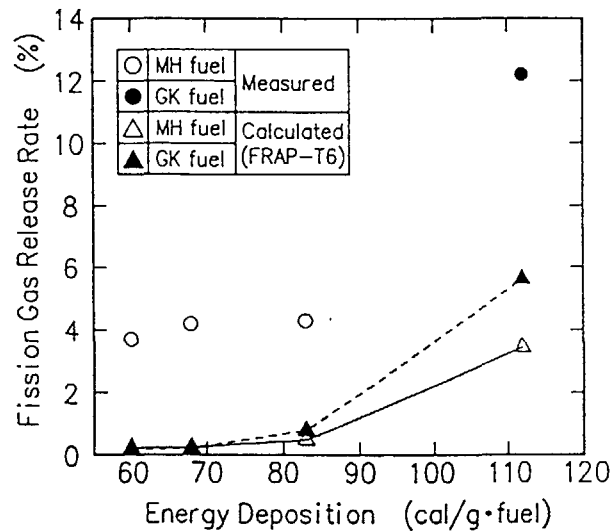


Fig. 10 Comparison of measured and calculated fission gas release rate under RIA conditions

For example, FRAP-T6 predicted  $\sim 0.001\%$  for the MH-3 rod and  $\sim 0.3\%$  for the GK-1 rod. The measured values were  $\sim 0.1\%$  for the MH-3 rod and  $\sim 3\%$  for the GK-1 rod. The predictions consider the conventional swelling of the fuel pellet due to fission gas release in addition to the thermal expansion. This suggests that the other effects such as grain boundary separation and the generation of the microcracks observed in the experiments must be taken into account more accurately for the prediction of the fuel behavior. These effects may also explain the above discrepancy on the fission gas release between the measurements and the predictions.

#### 4. SUMMARY

In the annealing tests, The released rate of fission gases was nearly constant at the test temperature of  $1800^\circ\text{C}$ . Significant change occurred when the temperature was elevated to  $1900^\circ\text{C}$  or higher.

The pulse irradiations experiments with burnup LWR fuel rods have been performed under simulated RIA conditions in the NSRR. As for the transient

fuel behavior including fission gas release, the analysis with FRAP-T6 was performed and compared with the experimental results. The major results obtained in the present study can be summarized as follows;

- (1) The fission gas release observed under RIA conditions was much higher than that during normal operation in a commercial PWR.
- (2) The fission gas release predicted with FRAP-T6 was lower than those of the measurements in the NSRR experiments.

#### ACKNOWLEDGEMENTS

The authors acknowledge the valuable advice from Mr. Y. Ichihashi, Mr. H. Amano and Dr. Soda, and wish to thank Mr. K. Ishijima, Dr. T. Fuketa and Mr. T. Nakamura for useful discussions. The authors would also like to thank staffs of the NSRR Operation Division for their assistance in performing the NSRR experiments. Finally, the authors wish to thank staffs of the Department of Hot Laboratories for their assistance in performing the PTEs.

#### REFERENCES

- [1] L. J. Siefken et al., FRAP-T6: A Computer Code for the Transient Analysis of Oxide Fuel Rods, NRC Report NUREG/CR-2148 (1981).
- [2] K. Ishijima et al., Behavior of Preirradiated LWR Fuel Rods under Reactivity Initiated Accident Conditions, IAEA, Cadarache (1992).
- [3] K. Yanagisawa et al., Studies of Transient Fission Product Gas Release and PCMI of PWR Fuel Preirradiated to  $39\text{ MWd/kgU}$ , International Topical Meeting on LWR Fuel Performance, Avignon (1991) 850-861.
- [4] J. Rest, GRASS-SST: A Comprehensive, Mechanistic Model for the Prediction of Fission-gas Behavior in  $\text{UO}_2$ -base Fuels during Steady-state and Transient Conditions, NUREG/CR-0202 (1978).
- [5] T. Fujishiro and T. Fuketa, NSRR Experimental Results on Fuel/Coolant Interaction during a Severe Reactivity Initiated Accident, Proc. 4th Int. Topl. Mtg. on Nucl. Reac. Thermal-Hydraulics (NURETH-4) October 10-13, Karlsruhe FRG, Vol. 1, 297-303 (1989).
- [6] P. E. MacDonald et al., Assessment of Light-Water-Reactor Fuel Damage During a Reactivity-Initiated Accident, Nuclear Safety, Vol. 21, No. 5 September-October (1980).

- [7] J Rest, The Prediction of Transient Fission-Gas Release and Fuel Microcracking under Severe Core-Accident Conditions, Nuclear Technology Vol 56, 553-564, March (1982)
- [8] M D Allen et al, Fission Product Release and Fuel Behavior of Irradiated Light Water Reactor Fuel under Severe Accident Conditions The ST-1 Experiment, Nuclear Technology, Vol 92, 214-228, November (1990)
- [9] M. F Osborne et al, Experimental Studies of Fission Product Release from Commercial Light Water Reactor Fuel under Accident Conditions, Nuclear Technology, Vol 78, 157-169, August (1987)

## FISSION PRODUCT BEHAVIOUR AND FUEL ROD CHEMISTRY AT EXTENDED BURNUP: RESULTS, MODELS AND PROGRAMMES OF ANALYTICAL EXPERIMENTS CARRIED OUT AT THE CEA, GRENOBLE

M CHARLES, L CAILLOT, P DEHAUDT, C LEMAIGNAN  
 Commissariat à l'énergie atomique,  
 Centre d'études nucléaires de Grenoble,  
 Grenoble, France

### Abstract

Of the analytical experiments carried out at CEA to study fuel behaviour at high burnups, special mention should be made of the study of the effects of moderate transients on fission gas release (importance of cracking associated with power variations), and SEM examination of fracture surface of various fuels (analysis of bubble populations and precipitates of associated metallic fission products)

Several factors must be considered when analysing the results radial specific power profile and its thermal effect, fission gas creation, oxygen balance density and open porosity, gaseous swelling. This paper describes the principle of various tools (calculations or experiments) used to obtain information on all these points

Finally, a brief discussion is given of the study programmes relating to the effect of O/M ratio on fuel behaviour and to the major problem of caesium retention

### 1 INTRODUCTION

A previous paper [1] gives a general view of the procedure adopted at CEA/Grenoble to improve knowledge of the behaviour of nuclear fuels as well as various results obtained

Note that the experimental study of this behaviour is based on the use of three main tools: an experimental pool type reactor (SILOE), a special laboratory for collection during irradiation and on line analysis of fission products released and a hot laboratory (LAMA). Another notable aspect of the organisation of this fuel behaviour research work is the fact that all aspects of the studies are integrated within a single team: design and preparation of fuels (advanced) study of the behaviour under irradiation, post irradiation examination, analysis of results and modelling

A significant example is given here of analytical irradiation experience aimed at obtaining a better understanding of the overall behaviour of a PWR type fuel under transient power conditions (CEA/EDF/FRAGEMA programme). The great importance of information obtained by hot laboratory microstructural studies is also stressed

Various tools are then presented which are invaluable for analysing the results obtained by describing the main behavioural parameters of a fuel

Finally, some information will be given on a number of major research projects

## 2. ANALYTICAL STUDIES ON HIGH BURNUP FUEL

### 2.1 Fission gas release under a moderate transient regime [2]

Two fuel rods were removed from assemblies irradiated in the Fessenheim 1 900 MWe PWR power plant. The first rod had reached a BU of 35 GWdT<sup>-1</sup>, and the second a BU of 50 GWdT<sup>-1</sup>. For both fuel rods, the irradiation histories in the power plant were typical of standard fuel rods. The rods were extracted from their fuel assembly and shipped to the CEA's hot laboratories at Saclay for remanufacturing: short lengths were cut and new end plugs with sweeping lines were welded at both ends of the rodlets. The rods were then sent to Grenoble for irradiation in the SILOE pool type reactor. The sweeping lines were connected to the fission product laboratory for fission gas sampling during irradiation and analysis.

The irradiations were performed in a pressurised loop with cladding temperatures controlled by nucleate boiling conditions. The irradiation in the experimental reactor led to an additional BU of 6 and 8 GWdT<sup>-1</sup> respectively. The power level was monitored using a series of self-powered detectors located in the periphery of the irradiation device. Moreover, every two or three pile cycles, gamma spectrography scanning of the rod was performed for an integral check of the power history.

The base irradiation was performed at a linear heat generation rate in the range 18-20 kWm<sup>-1</sup>, with transients lasting between 5 minutes and two days (most of them lasting 2 hours) at a LHGR never greater than 31 kWm<sup>-1</sup>.

The results obtained in [2] are summarised hereafter:

\* **Effect of burnup:** the two rods have a comparable behaviour. The major part of fission gas release occurs during the power transients (Fig. 1), although it was noted that the transients have a slightly greater effect on the rod at 50 GWdT<sup>-1</sup> (release of several % after the second transient) than on the rod at 35 GWdT<sup>-1</sup>.

\* **Effect of transient history and level:** the gas release associated with the transients depends on the plateau power more than on the time elapsing between two transients. For example, Fig. 1 shows that a transient at 25 kWm<sup>-1</sup> causes little release after two transients at 28 kWm<sup>-1</sup>.

\* **Effect of power variations and release mechanism:** the release of long-lived radioactive gases reaches a peak both when power is increased as when power is reduced.

The difference in behaviour of short-lived gases (no peak), as well as the shape of the network of cracks observed after irradiation, are indicative of a release through accumulation (at grain boundaries) cracking.

### 2.2 Fission product retention SEM microstructure examination

Fracture surfaces of three types of fuel of comparable density of 10.4 g cm<sup>-3</sup> were examined by scanning electron microscopy. The samples were as follows:

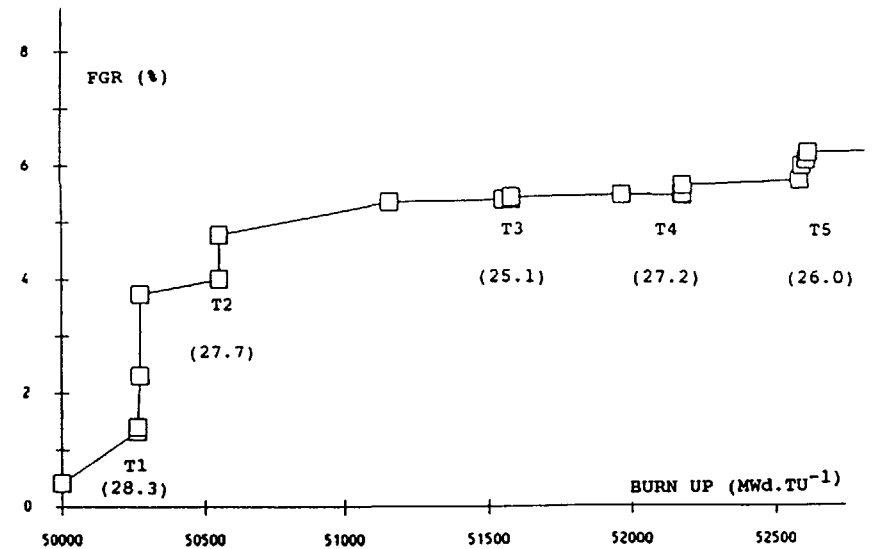


Fig. 1 : Fission gas release for the first 5 transients of the fuel rod irradiated up to 50 GWd/T (power level of the transient in kW m<sup>-1</sup>)

spheres of 1 mm diameter, irradiated up to 20 GWdT<sup>-1</sup> at 900°, 1200° and 1500°C, PWR type pellets irradiated at a burnup of the same order, with a centre-line temperature of about 1500°C,

- pellets taken from the 35-41 GWdT<sup>-1</sup> rodlet described in § 2.1 above

The effect of temperature on the nucleation, growth, coalescence and interconnection of intergranular bubbles is clearly visible in the types 1 and 2 fuels. The 3rd fuel shows a very high degree of porosity at the boundaries.

Numerous precipitates of metallic fission products associated with the bubbles were analysed. Usual compositions were found for the five metals (Mo, Ru, Tc, Rh, Pd), but also precipitates formed essentially of Ba - Zr (oxide form) and, for the fuel subjected to power transients, precipitates of the Pd, Sn (Mo, Ru, Tc) type. Further details may be obtained from reference [3].

## 3 SOME ANALYSIS TOOLS

### 3.1 Specific power radial profile inside the pellets

An adequate description of the variation in specific power radial profile with burnup is necessary in order to be able to calculate the fuel temperatures properly.

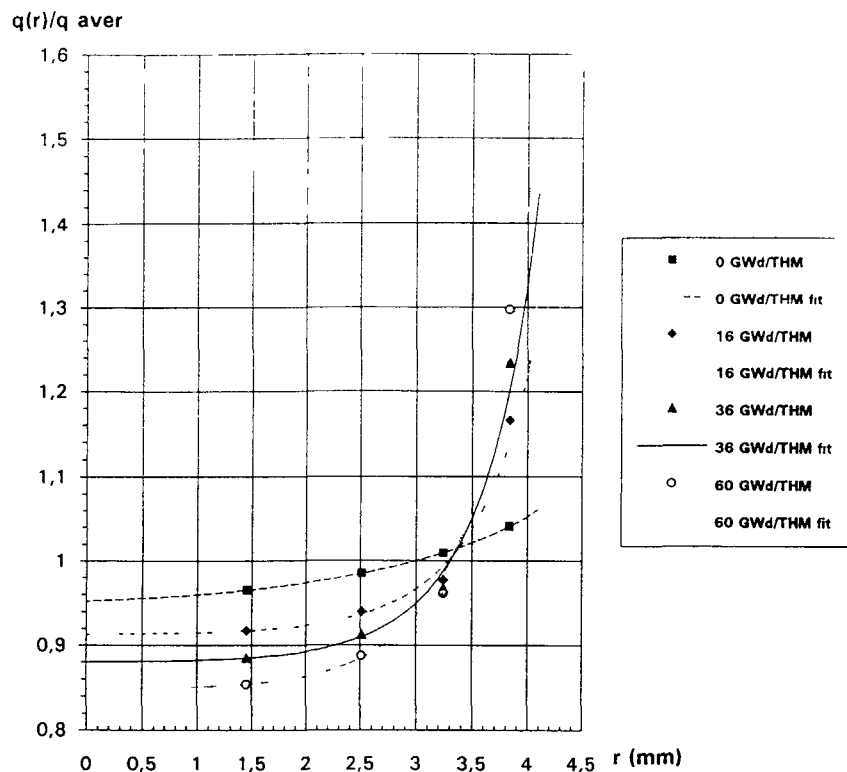


Fig. 2 : Relative radial variation of the specific power in a PWR fuel rod at various burnups

This point is not easy to deal with from a theoretical standpoint an analytical calculation as given in [4], albeit convenient, remains questionable (is diffusion theory suitable for dealing with this problem?) Processing by means of charts is not an easy matter in a computation code but it gives more satisfactory results provided that adequate neutronic methods are applied to describe the production of circumferential Pu in a PWR fuel rod. As an example, Fig. 2 shows how a computed profile was used on a fuel cut into 4 equal-volume zones [5] with a least square adjustment of a function of the following type

$$\frac{q(r)}{\bar{q}} = A + B \exp -C(a - r)^k$$

The calculation is performed for an initial  $^{235}\text{U}$  enrichment of 3.1% for burnups of 0, 16, 36 and 60  $\text{GWd}^{-1}$ . The coefficients A, B, C are burnup-dependent, k equals 0.93

\* Effect on the centre-line temperature all things being equal elsewhere, the drop in centre line temperature due to this effect alone must be taken into account about 35°C at 18  $\text{kWm}^{-1}$  and 100°C at 40  $\text{kWm}^{-1}$ . This only goes to show the great importance of using well-qualified neutronic calculation tools

### 3.2 Creation of fission gases

It is most important to calculate correctly the variation in composition of the mixture of stable gases released ( $\frac{X_c}{Kr}$  ratio). It is therefore advisable to make an accurate calculation of gas creation, taking into account the increasing part of the Pu fissions. A calculation of this type, based on the MARISE code, is described in [6]. It has recently been updated and developed to be applied to MOX fuels [7].

### 3.3 Oxygen balance in a fuel

This point is, of course, fundamental as the value of O/M governs the thermal conductivity of the fuel, its mechanical properties and the values controlling the behaviour of fission products (FP diffusion,  $\text{UO}_2$  surface energy)

The estimation method described here needs to be improved but nonetheless has the advantage of highlighting the importance of the Mo state for the problem. The four conventional FP groups are considered [8] and the most abundant of these were selected

- Mo, Ru, Tc, Rh, Pd (metals)
- Xe, Kr, I, Br
- Sr, Ba, Zr, Nb and the rare earths (dissolved oxides)
- Rb, Cs, Mo (precipitated oxides)

The creation of these FPs is calculated with the MARISE code which is briefly described in [6]. As a first step, it is assumed that there is no oxygen diffusion in the fuel. Allowance is made for binary oxides as well as CsI and a number of ternary oxides. The valency of the rare earths is adjusted on the equilibrium potential of  $\text{UO}_{2+x}$  - Mo/MoO<sub>2</sub>

In fact, the O/M values calculated lead to oxygen potentials greater than the Mo/MoO<sub>2</sub> potential. Now since Mo is always present in large quantities compared to O, it is plausible to consider that only a fraction of the Mo oxidises, thereby buffering the oxygen potential of  $\text{UO}_{2+x}$  to the value of the Mo/MoO<sub>2</sub> pair. This assumption is of great consequence since, if it is true, the value of x would be given by the oxygen potential of Mo/MoO<sub>2</sub>.

\* Testing the Mo/MoO<sub>2</sub> buffer pair assumption calculated fractions of metallic Mo were compared with those measured in the FP precipitates of the fuels quoted in § 2.2 and described in [3]. The following remarks can be made concerning the results, indicated in Fig. 3

in the comparison with TANGO, allowance must be made for the fact that the temperature in the  $\text{UO}_2$  spheres was between 1400 and 1500°C

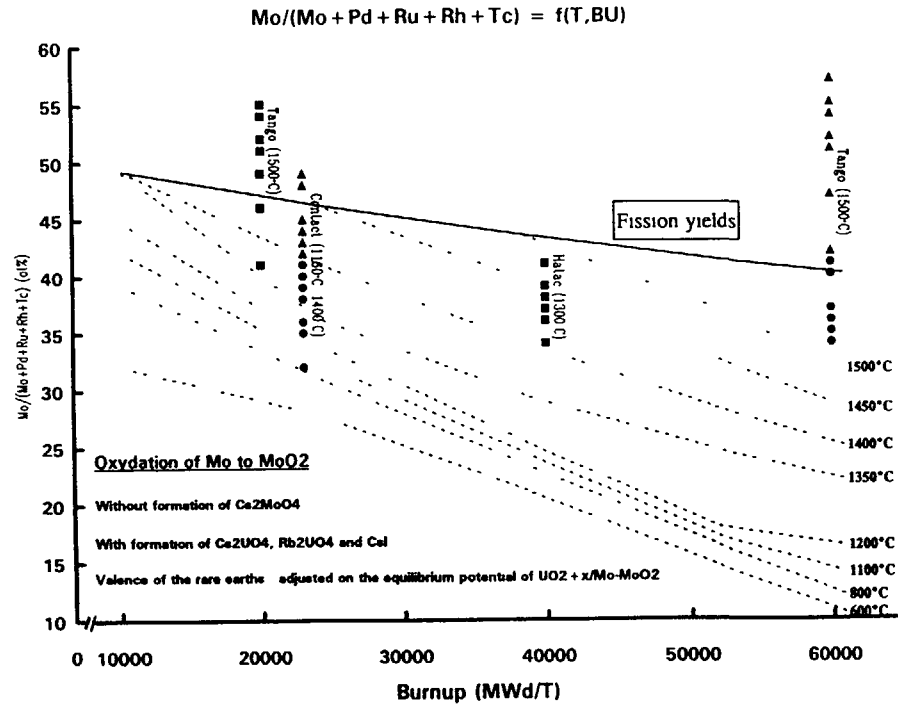


Fig. 3 : Percentage of Mo in metallic fission product precipitates.

- the HATAc results correspond to an ill-defined temperature (850 - 900°C base, 1250 - 1300°C plateau),
- there seems to be an interesting consistency with the CONTACT results (temperature between 1160 and 1400°C)

The calculations will be continued, with a more suitable list of compounds taken into account and attempting to define the effect of oxygen diffusion

### 3.4 Measurement of the density and open porosity of irradiated fuel

A method developed for non-irradiated fuel is currently being studied in the hot cell. The density is determined by a conventional technique involving vacuum impregnation (using a suitably selected liquid), and weighing of the dry mass and immersed mass. Then, by measuring the evaporation kinetics of the residual liquid film by weighing, the open porosity of the sample can be evaluated by suitable processing of the results.

During tests conducted with a non-irradiated fuel, this method gave comparable results to the conventional method by wiping.

### 3.5 Monitoring gaseous swelling of a fuel by diametral measurements

\* **The gaseous swelling phenomenon:** in high burnup fuel rods subjected to high-power transients, gaseous swelling becomes an important phenomenon. The fission gas atoms, supersaturated in the matrix, precipitate in the form of intra or intergranular bubbles, when the temperature is held at a high value, thereby contributing to the volume expansion of the fuel.

This swelling phenomenon has already been shown in the past on fuel rods removed from power reactors, the measurements having been taken after power ramps in an experimental reactor. An additional plastic deformation of the cladding was measured, as a result of the swelling, on fuel rods having reached a sufficient burnup, estimated at 50 GWdT<sup>1</sup> [9].

\* **The experiment:** in the programme presented here, a measurement system under irradiation is used for on-line monitoring of the diametral variation of a fuel rod, pre-irradiated in a PWR, subjected to a power transient, thereby gaining access to the swelling kinetics.

Given the possibilities of the irradiation device, the short rod, consisting of about 20 pellets of UO<sub>2</sub>, will be remanufactured using the FABRICE process.

The measurement system was developed within the context of analytical studies of the pellet-cladding mechanical interaction [10]. Integrated in the sample-holder of a GRIFFON device, which reproduces the PWR-type thermohydraulic irradiation conditions, this system is used to measure the diameter of a fuel rod along a generating line. A scheme for this system is shown on figure 4, together with an example of results obtained.

Its principle is based on the use of strain gauges. The deviation of two ceramic followers in contact with the cladding induces deformation of an elastic blade, instrumented with strain gauges, via two rigid rods. The entire assembly forms a mobile unit with drive system for travelling along the fuel rod. The voltages generated by the strain gauges are proportional to the diameters and are recorded after each follower displacement step. These measurement voltages are subsequently processed by reference to measurements taken on reference diameters fitted at the ends of the fuel rod. This systematic calibration each time a fuel rod profile is measured eliminates any risk of instrument drift under irradiation.

The accuracy obtained with this device, of the order of a micron, would seem to be sufficient for observing the gaseous swelling phenomenon, the order of magnitude of which is expected to be several dozen microns.

This experimental study will of course be supplemented by hot laboratory examinations, after irradiation, in order to establish links between macroscopic results under irradiation and microstructure changes in the fuel.

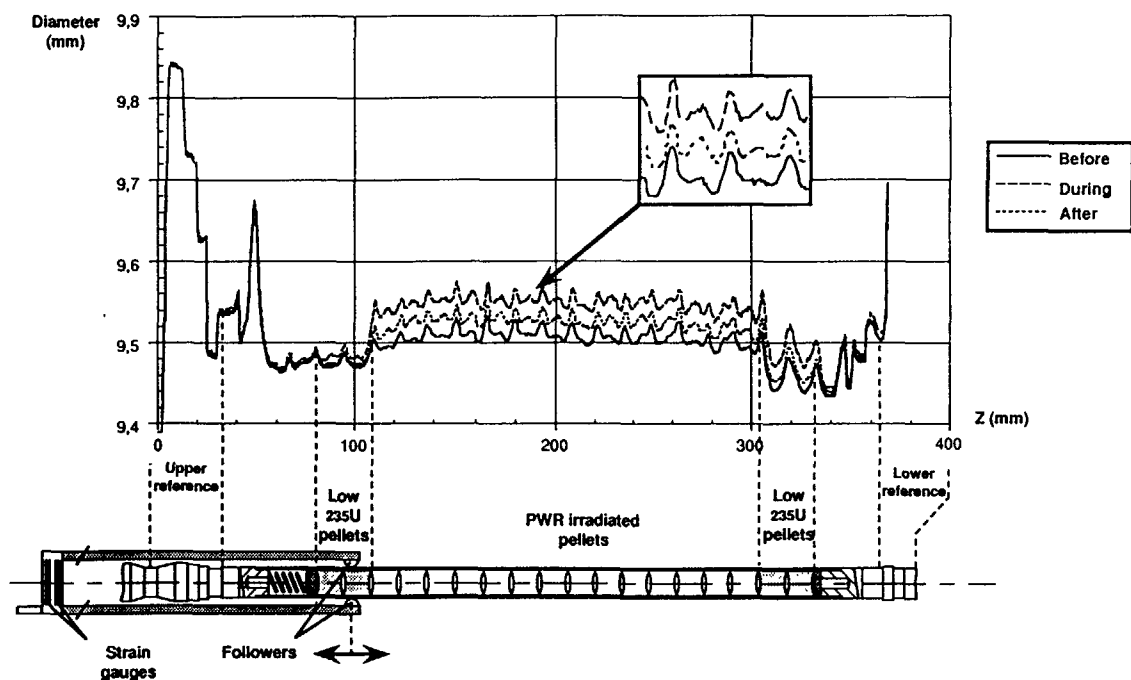


Fig. 4 : DECOR device - Diameter measurements (high power transient)

#### 4. RESEARCH PROJECTS

##### 4.1 Parametric study of the effect of O/M ratio of $UO_2$ on fission gas release

A parametric study was carried out on this subject. The experimental programme included four main stages:

- Fuel samples of different stoichiometry (up to 2.02) are prepared and accurately characterised (O/M measurement, microstructure observations).
- These samples are irradiated in a capsule in the SILOE reactor. The irradiation process, designed to accumulate fission gases in the matrix, is performed at a controlled temperature, sufficiently low to ensure that there is no release. Precautions were taken to restrict oxidation-reduction reactions likely to have an effect on the O/M ratio

- Samples having reached a sufficient burnup are transferred to the hot laboratory (LAMA) where they are subjected to heat treatment of variable duration and temperature.
- Finally, fine microstructure examinations (ceramographs, SEM, TEM) are performed to study the role of stoichiometry on release mechanisms, in the light of prior knowledge acquired after observations on high burnup fuels (TANGO, CONTACT, HATAC).

##### 4.2 Caesium retention inside the fuel

For retention outside the fuel, refer to reference [11].

Caesium retention inside the fuel is a delicate problem. As such, it is best to define efficiency domains rather than looking to achieve maximum retention in all cases.

The first stage involves defining potential compounds by an out-of-pile approach. The additives designed to form these compounds must be compatible with the fuel manufacturing process. The receiving compound, which must be thermally stable and insoluble in water, must be able to form under PWR operating conditions. Finally, it must be selective with respect to the caesium and must not prefer other fission products. These points are currently being studied for two types of compounds: caesium aluminosilicates and hollandites.

It will subsequently be necessary to run in-pile qualification tests on the selected products.

#### References

- [1] CHARLES, M and LEMAIGNAN, C, to be published, J Nucl Mater (1992)
- [2] PORROT, E, CHARLES, M, HAIRION, J P, LEMAIGNAN, C, FORAT C and MONTAGNON, F, Proceedings of the ANS/ENS International Topical Meeting on LWR Fuel Performance, Avignon (1991) p 558
- [3] CHARLES, M, CAILLOT, L, DEHAUDT, P and LEMAIGNAN, C, this Meeting, Session 4
- [4] PALMER I O, HESKETH, K W and JACKSON, P A, IAEA Report IWGFPT/13 (1983) p 347
- [5] SANTAMARINA, A, private communication (1987)
- [6] CHARLES, M, BRUET, M and CHENEBAULT, P, IAEA Report IWGFPT/19 (1984) p 429
- [7] PARRAT, D and BAUD, C, private communication, (1991)
- [8] KLEYKAMP, H, J Nucl Mater 131 (1985) 221
- [9] LEFEBVRE, F, JOSEPH, J and ROYER, J, IAEA Report IWGFPT/28 (1988) p 93
- [10] SOUCHON, F and CAILLOT, L, to be presented at the International Conference on Irradiation Technology, Saclay, 20-22 May 1992
- [11] BOCH, P, SEISS, M, VETTER, G and JACQUIN, M, to be published, J Nucl Mater (1992)

## IMPACT OF SYSTEMATIC STOICHIOMETRY DIFFERENCES AMONG BWR RODS ON FISSION GAS RELEASE

B. GRAPENGIESSER, D. SCHRIRE  
ABB Atom AB,  
Västerås, Sweden

#### Abstract

Fission gas release (FGR) in BWR fuel rods at normal powers and high burnup has proven to be very difficult to predict with high precision for every member in a large set of rods. ABB Atom has generated a data base of around 200 rods with several reactors represented. FGR has been carefully modelled as it is very sensitive to small variations in temperature close to the "Vitanza curve" and thus to powers close to normal values. Feedback through impact from fission gas released, including gas mixing, on fuel/cladding gap heat conductance adds to modelling difficulties. Small errors in detail in the power histories are mainly blamed for some quite large deviations between calculated and measured values. In the search for an explanation an obvious trend has been found that rods close to the control rod corner need the largest conservatism in the power history to match measured values. Impact from high reactivity neighbouring bundles, channel bow and void distribution in an assembly close to the top of an inserted control rod are possible causes of small overpowerings as compared to core physics results, especially in these rods.

In this paper quite another approach for the explanation of high FGR found in rods towards the control rod corner of the assembly is suggested, implying that differences in initial enrichment by a sequence of physical phenomena (presented below) have a strong impact on gas diffusion constant and FGR. Rods close to the control rod, especially the corner rod, are fabricated with a much lower initial enrichment than assembly average, to compensate for the greatly improved moderation, when the control rods are not inserted. Despite the lower enrichment, these rods typically reach the same burnup as assembly average at end of life, thus experiencing very similar linear heat ratings. For a low enrichment corner rod (typically 1.38% U-235) to reach the same EOL burnup (>40 MWd/kg U) as an interior rod (3.06% U-235) a much larger proportion of the total fissions must occur in Pu. The fission product yields for Pu are known to lead to an oxygen surplus (and thus hyperstoichiometry) compared to U-235 fission. Fission gas diffusion in  $UO_{2+x}$  is known to increase greatly with  $x$  (>2 orders of magnitude for  $x = 0 - 0,1$ ). In addition, increasing hyperstoichiometry reduces fuel thermal conductivity, thus further enhancing fission gas release.

An additional, although uncertain, enhancement may come from the redistribution of surplus oxygen in the temperature gradient. The part generated in the peripheral rim is probably stationary due to the low temperature, but in the more central parts there will be a surplus oxygen movement towards pellet centre according to some references in the literature.

Samples from a corner rod and an interior rod from an assembly with a burnup of about 40 MWd/kg U have been compared by EPMA for measurable differences in fission product concentrations, the O/M ratio and their radial profiles. Indications of enhanced diffusion controlled processes (FGR, fission product particles and microstructural changes) were observed in the corner rod. A simple model correction for this enrichment/stoichiometry effect is described with some typical results.

## INTRODUCTION

Fission gas release (FGR) in BWR fuel rods at normal powers and high burnup has proven to be very difficult to predict with high precision for every member in a large set of rods. ABB Atom has generated a data base of around 200 rods with several reactors represented. FGR has been carefully modelled as it is very sensitive to small variations in temperature close to the "Vitanza curve", and thus to powers close to normal maximum values. Feedback through impact from fission gas released, including gas mixing, on fuel/cladding gap heat conductance adds to modelling difficulties. Small errors in detail in the power histories are mainly blamed for some quite large deviations between calculated and measured values.

In the search for an explanation, an obvious trend has been found, that rods close to the control rod corner need the largest conservatism in the power history to match measured FGR values with the ABB Atom STAV-6 fuel performance program. Impact from high or low reactivity neighbouring bundles, as well as channel bow, are possible causes of small overpowerings as compared to core physics results, especially in these rods.

In this paper quite another approach for the explanation of high FGR found in rods towards the control rod corner of the assembly is suggested, implying that differences in initial enrichment due to a sequence of physical phenomena (presented below), have a strong impact on the fission gas diffusion constant and release. Rods close to the control rod, especially one corner rod, are fabricated with a much lower initial enrichment than assembly average, to compensate for the greatly improved moderation in the region, when the control rods are not inserted. Despite the lower enrichment, these rods typically reach assembly average burnup at end of life, thus experiencing very similar linear heat ratings. For a low enrichment corner rod (typically 1,38% U-235) to reach the same EOL burnup (>40 MWd/kg U) as an interior rod (typically 3,0 to 3,5 % U-235) a much larger proportion of the total fissions must occur in Pu. The fission product yields for Pu are known to lead to an oxygen surplus (and thus higher hyperstoichiometry) compared to U-235 fission. Fission gas diffusion in  $UO_{2+x}$  is known to increase greatly with  $x$  (> 2 orders of magnitude for  $x = 0 \rightarrow +0,1$ ). In addition, increasing hyperstoichiometry reduces fuel thermal conductivity, thus further enhancing fission gas release.

An additional, although uncertain, enhancement may come from the redistribution of surplus oxygen in the temperature gradient. The part

generated in the peripheral rim is probably stationary due to the low temperature, but in the more central parts there will be an oxygen movement towards the pellet centre, according to some references in the literature.

## 1. FISSION GAS RELEASE EXPERIENCE

Destructive hot cell, as well as nondestructive (Kr-85) methods have been used by ABB Atom to generate an extensive FGR data base for high burnup standard BWR-fuel rods. The latter method is very cost-effective as it is used in ordinary fuel storage pools, and after measurement the rods are reinserted into the assemblies for further use or ordinary back-end handling. Figure 1 illustrates the large scatter in results found. Of course peak powers rather late in life are a major parameter leading to high FGR, but this is not so easily illustrated due to the effect of positioning in the assembly. Figure 2 is chosen to exemplify that high releases often are found close to the water-rich corner of the assembly. The corresponding enrichment design, FGR and calculated internal burnup form factors are given in figures 3 and 4.

## 2. FISSIONS IN PLUTONIUM OR URANIUM

In a rod with the highest and most typical enrichment (e.g. 3,07 % U-235) about 80 % of the fissions have been produced by thermal fission in U-235 at a burnup of 10 MWd/kgU. At the other extreme, at a final burnup of about 35 MWd/kg U in the corner rod with the lowest enrichment (e.g. 1,18 % U-235) only 20 % of the fissions are due to thermal reactions in U-235 while the major part (about 70 %) comes from thermal fission in Pu-239. The typical development of the integrated proportion of Pu-239 fissions in different rods is given as a function of assembly burnup in Figure 5. It seems to differ most between enrichments at intermediate burnup.

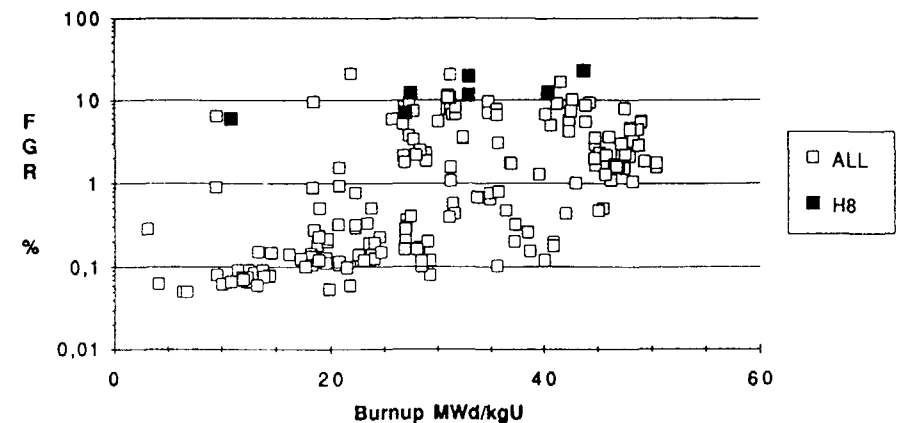


Fig 1. Fission Gas Release ABB Atom data base

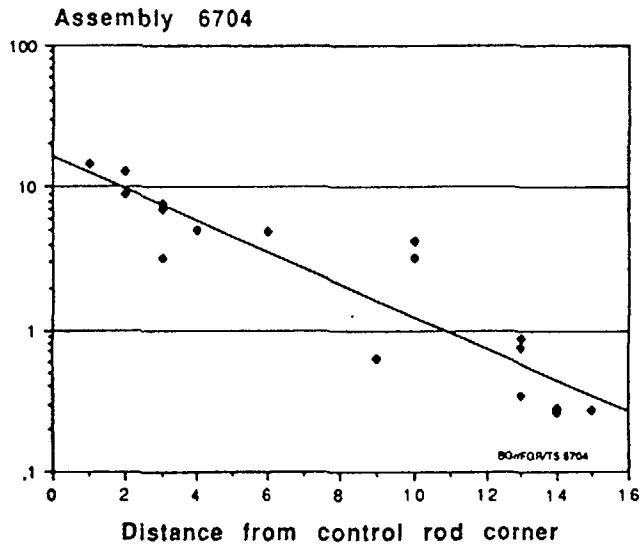


Fig 2. Measured FGR/Nominal FGR from STAV5

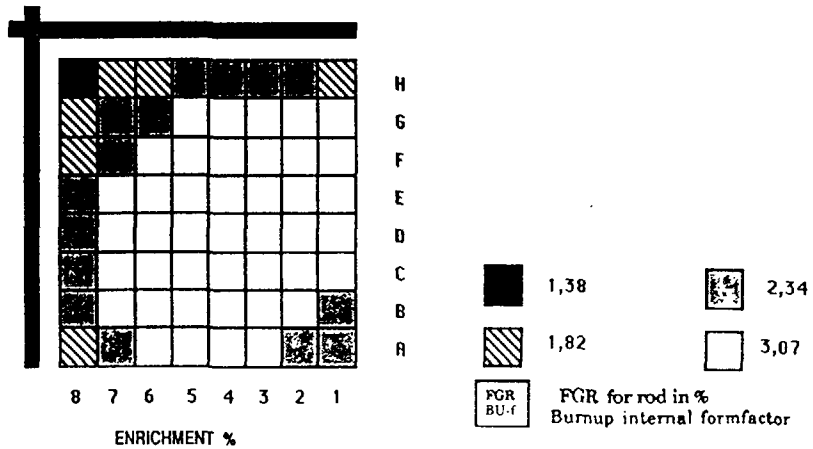


Fig 3. Example of ABB Atom BWR design

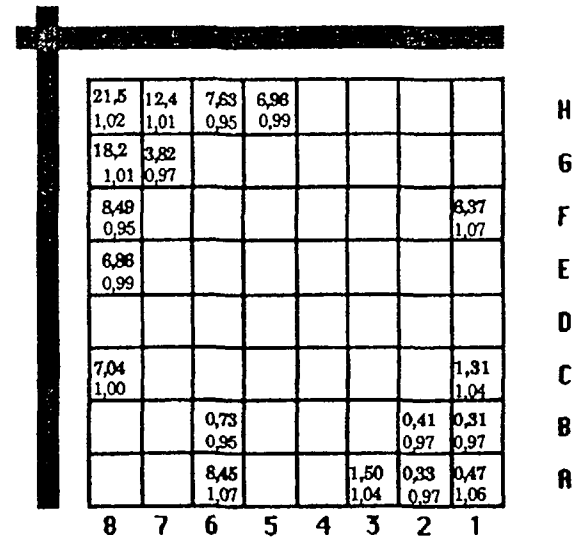


Fig 4. FGR and internal Burnup formfactor

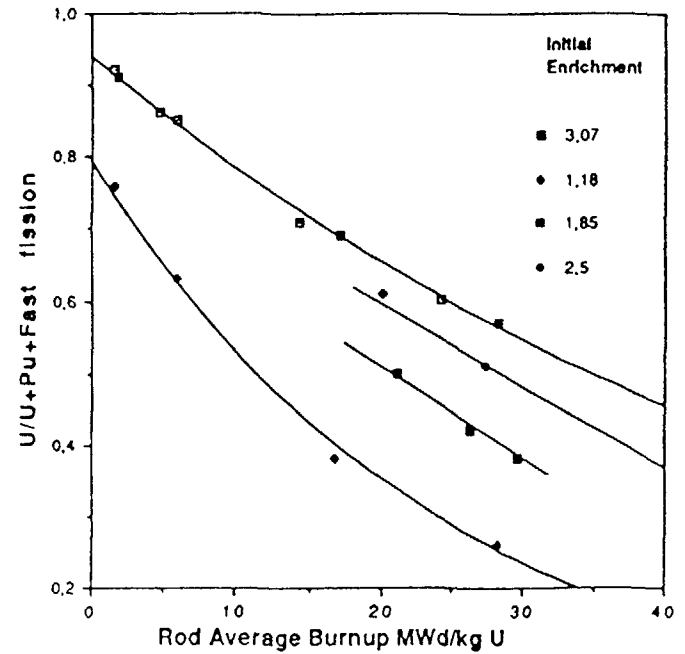


Fig 5. Ratio between integral number of fissions in U-235 and total number of fissions

Burnup rate scatter among rods is of minor importance with respect to the illustrated differences between rods. There are two main reasons behind the higher Pu-239 proportion in the corner rod.

- The lower enrichment makes it impossible to gain a large energy proportion from U-235.
- The higher neutron flux leads to a faster Pu-239 production rate.

It should also be noted that in a BWR the proportion of Pu production and burnup, relative to U-235, varies with the axial elevation in the rod, due to the increasing void fraction, and therefore harder neutron spectrum, towards the top of the core. This effect is exploited in spectral shift operation, whereby Pu is "bred" early in the reactor cycle, and "burned" later in the cycle.

### 3. DIFFERENCES IN ROD AVERAGE STOICHIOMETRY

There is quite a large difference in the fission yield distribution between fission in U-235 and Pu-239 (Figure 6). The increase in the light mass number fission yield peak by approximately 4 amu leads to a deficit in oxygen affinity of the

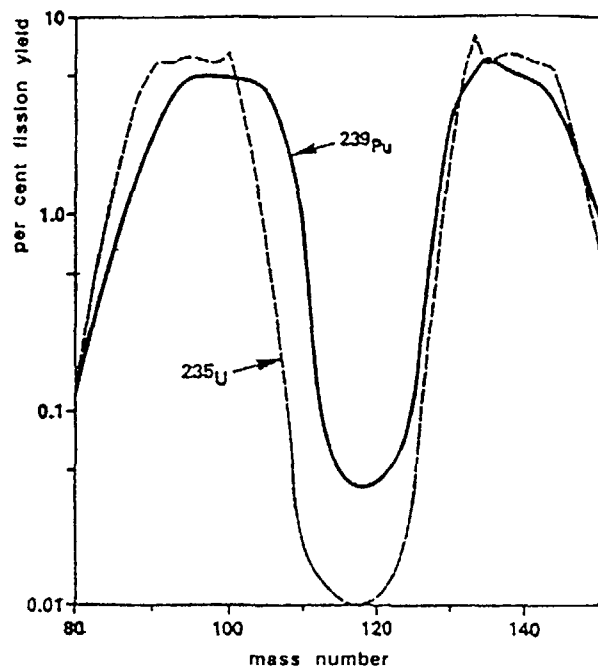


Fig 6.  $^{235}\text{U}$  and  $^{239}\text{Pu}$  mass yields for thermal neutron fission

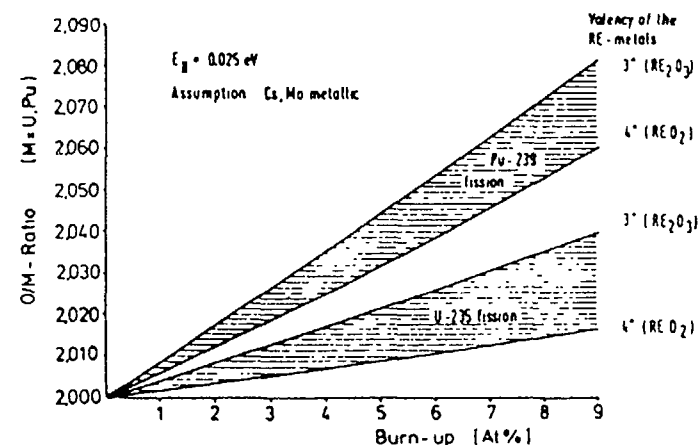


Fig 7. O/M-shift of the oxide fuel as a function of the burnup for the fission of U-235 and Pu-239

fission products as compared to the source atoms. The extra oxygen is bound as  $\text{UO}_{2+x}$  and according to Findlay [1] hyperstoichiometry ( $x$ ) increases seven times faster for Pu-239 fission than for U-235 fission. As plutonium has a lower valence ( $<4,0$ ) at an oxidation potential where the uranium valence is 4,0 the breeding into plutonium also leads to surplus oxygen, further increasing the oxygen potential.

For the case of fissioning in U-235 the small surplus oxygen amount is bound by such fission products that have an oxygen affinity close to  $\text{UO}_{2,000}$ . As long as U-235 dominates, when burnup proceeds, there is only an insignificant increase in oxygen potential or degree of hyperstoichiometry. The impact on material characteristics as a consequence of burnup is minor indeed for U-235 fission. In the case of Pu-239 fission on the other hand there is a considerable increase in stoichiometry.

A calculation for a corner rod at 35 MWd/kgU indicates  $\text{O}/\text{U} > 2,01$  according to [1] and  $\text{O}/\text{U} = 2,02$  according to [2] (see Figure 7). Compared to the as manufactured stoichiometry, or the amount of oxygen bound by the cladding bore, this hyperstoichiometry is quite considerable.

### 4. REDISTRIBUTION OF OXYGEN IN THERMAL GRADIENT

At high enough temperatures, surplus oxygen in  $\text{UO}_{2+x}$  tends to move up the temperature gradient in operating fuel pellets. This leads to a further O/U increase in the hot central part, while intermediate annular regions should be almost stoichiometric. Following Adamson's arguments [3], the O/U ratio in the pellet centre could easily reach 2,07 for the corner rod example (Figure 8).

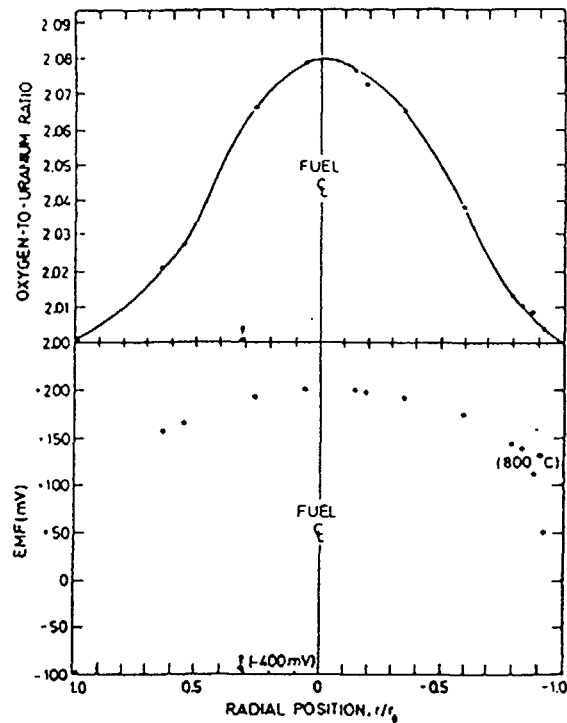


Fig 8. EMF probe results for section of Zircaloy-2 clad

However, there does not seem to be full consensus in the open literature on oxygen redistribution behaviour, especially regarding mechanisms - solid phase diffusion or transport by gaseous  $H_2/H_2O$  or  $CO/CO_2$  couples. All references do not fully agree with such a strong redistribution effect as indicated here.

PIE results have so far given no clear indication of thicker clad internal oxide layers in low enrichment corner rods than in higher enrichment rods from the same assemblies, probably due the solid-state kinetically limited (as opposed to thermodynamically limited) oxygen transfer mechanism from fuel to clad.

##### 5. DIFFUSION, HEAT CONDUCTANCE AND OTHER MATERIAL PROPERTIES OF INTEREST

Hyperstoichiometry is known to have a very strong impact on several material properties such as diffusion constants, creep behaviour and heat conductivity [4-6]. At 1200 °C there are indications that the Xe diffusion constant ( $D_{Xe}$ ) is as

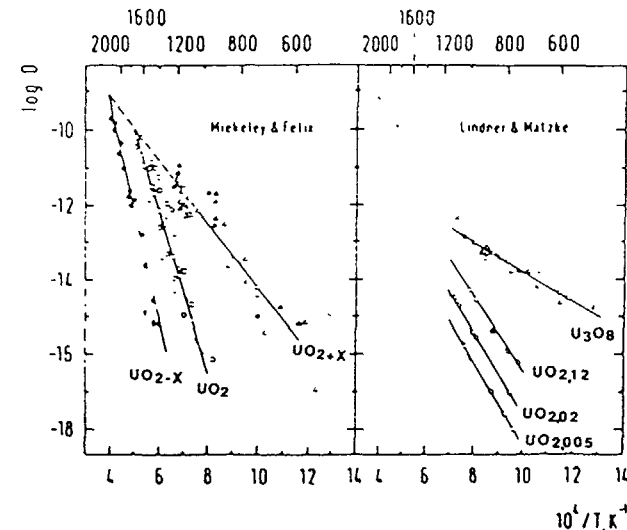


Fig 9. Xenon diffusion constant in hyperstoichiometric  $UO_{2+x}$

much as 2 to 3 orders of magnitude higher at an  $O/U = 2,07$  than at an  $O/U = 2,00$  which is equivalent to a centerline temperature increase of about 350 °C (Figure 9). When it comes to differences between rods it is only a question of degree of hyperstoichiometry at high burnup, and the diffusion constant differences are smaller.

Stoichiometry also has an impact on heat conductivity (Figure 10). In this respect the pellet centre does not matter as much as for the outer, cooler regions with a steeper temperature gradient, where no oxygen transport is expected. A rough estimate leads to an increase in centreline temperature of around 100 °C.

Creep behaviour is very strongly dependent on  $O/U$  as summarized e.g. by Bush [7] or Olander [8]. Grain growth and grain boundary sweeping are also mechanisms that may be expected to be influenced, and where hyperstoichiometry probably favours gas release.

##### 6. FGR MODELLING

Only limited modelling work considering this stoichiometry effect has been performed. The effect of oxygen redistribution in the temperature gradient, expected to increase the impact on FGR, was omitted in this modelling as it is somewhat uncertain and difficult to quantify as discussed above. Judged to be of less importance, the fuel heat conductivity difference was also omitted.

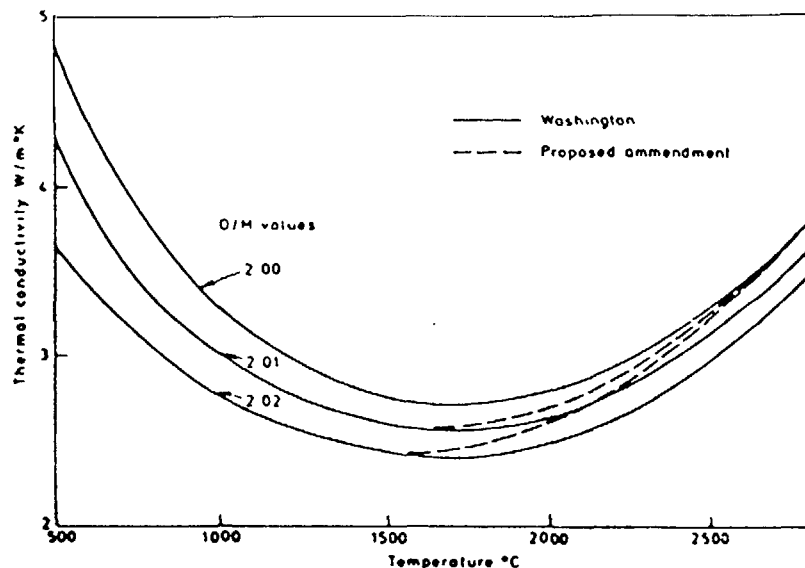


Fig 10. The thermal conductivity of fully dense hyperstoichiometric  $UO_2+x$

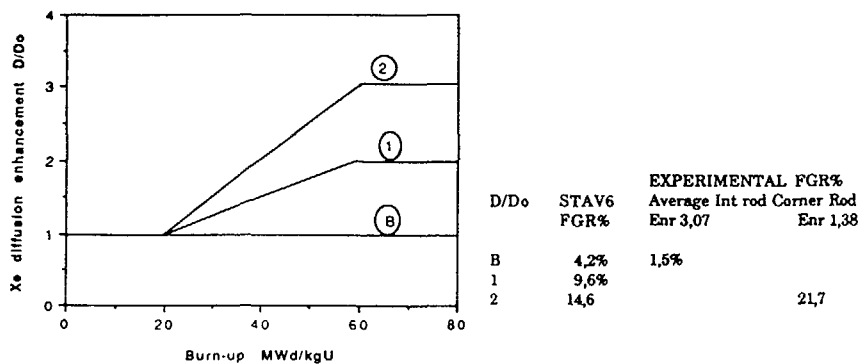


Fig 11. Diffusion enhancement for corner rod

The stoichiometry effect is introduced into the STAV-6 modelling by two simple options of fission gas diffusion constant ( $D_{Xe}$ ) enhancement, specified as burnup dependences. It is reasonable to await some burnup, say 20 MWd/kgU, without any impact. This would simulate the buffering capacity of some of the fission products. After that a linear increase was applied, up to 60 MWd/kgU, ending with diffusion coefficient enhancements of a factor two or three respectively. These values are intended to introduce the difference in diffusion constant between a corner rod and an average rod, considering the literature references to Xe diffusion enhancements at the stoichiometry levels which could be expected at this burnup. They are illustrated in Figure 11. The measured FGR in this corner rod was 21,7 %: the predicted FGR was 4,2 % without  $D_{Xe}$  enhancement, 9,6 % with 2x maximum enhancement and 14,6 % with 3x maximum enhancement. It is apparent from the power history for this rod that most of the release comes before 35 MWd/kgU when the assumed enhancement is  $< 1.7$ . A larger factor is thus motivated, but the experimental basis is as yet too uncertain to justify an accurate tuning of the model.

### 7. ADDITIONAL EXPERIMENTAL EVIDENCE

Samples from a corner rod and an interior rod from an assembly with a burnup of about 40 MWd/kg U have been compared by EPMA for measurable differences in fission product concentrations, the O/M ratio and their radial profiles. As can be seen in Figure 12, although the burnup in the two rods is the same (indicated by Nd/U-ratio) the proportion of Pu-fissions is higher in the corner rod (indicated by Ru/Nd-ratio). The rim effect is also very clearly seen.

The oxygen content and its radial variation were also determined to try to directly observe the small expected difference, although it was expected that the differences in the stoichiometry would probably not be observable with the EPMA technique. Most samples showed the expected radial slope (O/M increasing towards the pellet centre) despite a very large experimental uncertainty, but in some cases an opposite trend was seen. The average oxygen content was a little higher for the corner rods (see Figure 13). It was concluded, however, that EPMA was not a sufficiently sensitive technique for the purpose of detecting small differences in the O/M ratio in the different samples.

Indications of enhanced diffusion controlled processes (FGR, fission product particles and microstructural changes) were observed in the corner rods, as illustrated by the xenon profile in two rods of similar powers in Figure 14. This difference gives no proof of the cause, and even if powers are identical a difference in temperature may be the explanation rather than a difference in stoichiometry. Elements for which the redistribution is guided more by chemical than thermal behaviour should therefore be used to check for systematic stoichiometry effects. However, the general tendency for the H8 corner rod to have higher fission gas releases than other rods from the same assembly at the same burnup (and thus same lifetime averaged power) indicates that the stoichiometry effect is, indeed, a significant factor (see Figure 1).

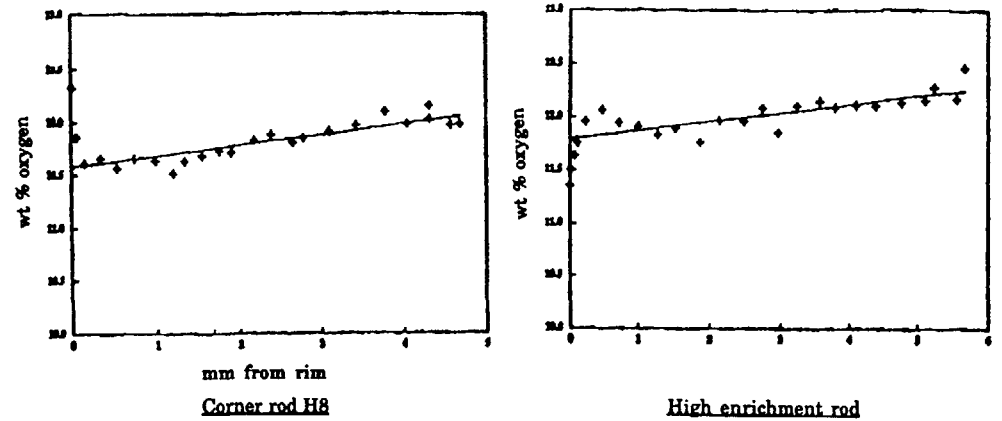
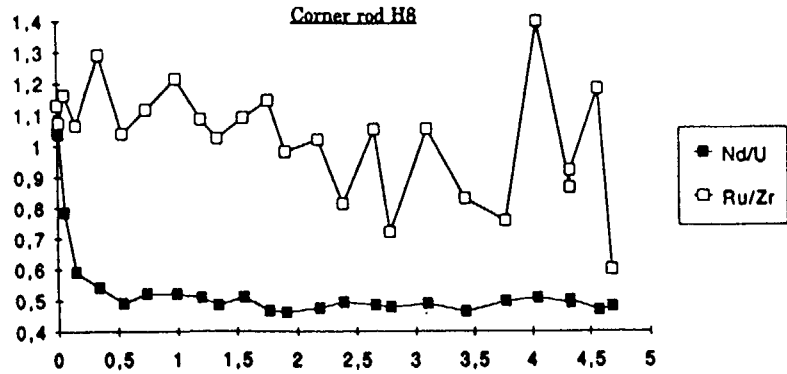


Fig 13. Oxygen profile by EPMA

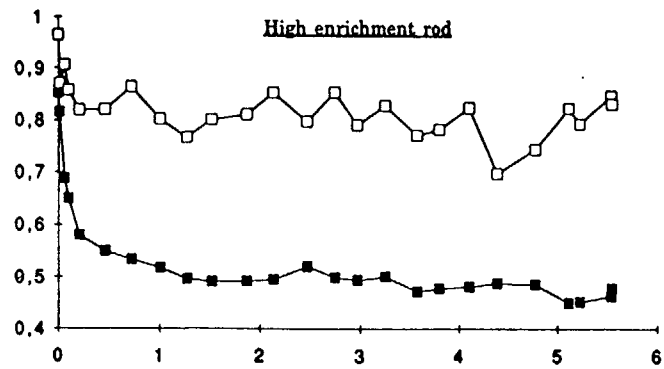
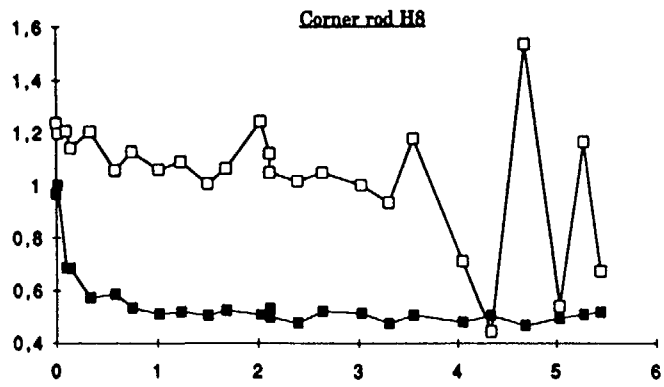


Fig 12. Element amount ratios by EPMA

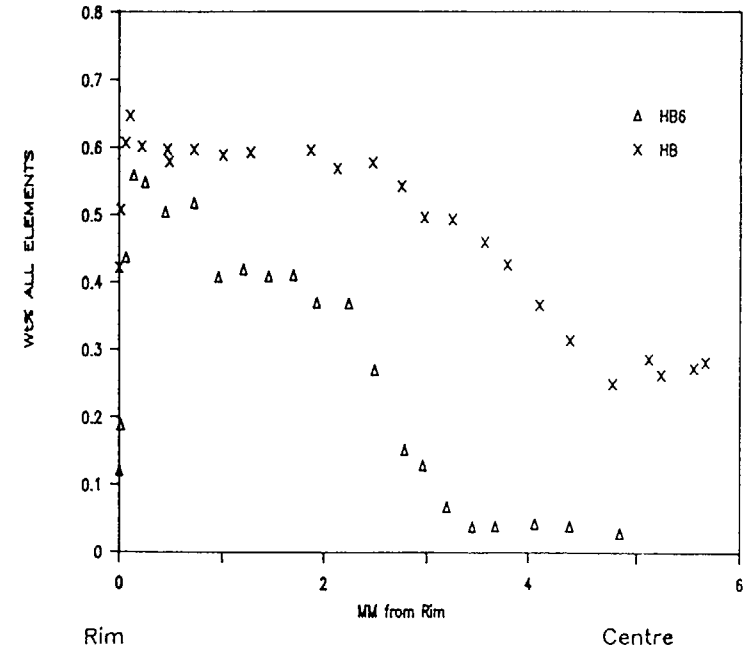


Fig 14. Xe profiles from peak burn-up positions for corner rod (HB6) and central rod (HB), showing marked displacement of the steeply falling part of curve towards the centre

Further work is planned to detect and, if possible quantify, the differences in the stoichiometry between the low enrichment corner rods and the higher enrichment rods. This will include lattice parameter measurements, as well as studies of the separate phases which form in the fuel. The phase studies will include an assessment of the extent of the acicular  $U_4O_9$  phase, as well as an investigation of the possible occurrence of the Ba-Zr-Sr rich perovskite phase, which has been observed in fast reactor fuel as well as Simfuel, and which may provide a clue as to the oxygen potential.

## 8. CONCLUSIONS

According to strictly physical reasoning, with each step experimentally well supported, BWR rods within an assembly are shown to be a heterogeneous group as regards material properties of the fuel (determined by the O/M ratio) after some burnup due to differences in the initial enrichment (between rods) and neutron flux spectrum (axially). Consequences of the stoichiometry dependence are usually swamped by the even stronger temperature dependence, and the difficulties of modelling in detail the complex power and thermal behaviour. The very large scatter found in FGR can be however be analysed in such a way as to support a suggested revision of the modelling of fuel material properties in most BWR fuel rod modelling so far. Other experimental support for the whole sequence may be found with the correct techniques, sensitive to the small differences in O/M, which lie behind the larger effects on the fuel behaviour.

## ACKNOWLEDGEMENTS

We are indebted to Dr John Pearce of AEA Technology Windscale Laboratories, who performed the EPMA measurements. The work was supported financially by Teollisuuden Voima Oy, Finland.

## REFERENCES

1. J.R. Findlay, "The Composition and Chemical State of Irradiated Oxide Reactor Fuel Material", IAEA PL 463/2
2. IAEA Specialists' Meeting on Internal Fuel Rod Chemistry, Erlangen, FRG, 23-25 Jan 1979, page 124.
3. Adamson et. al., Thermodynamics of Nuclear Materials, IAEA vol 1 SM 190/54, Wien, Austria, Oct 1974,
4. Hj. Matzke, "Gas Release Mechanisms in  $UO_2$  - A Critical Review", Radiation Effects 53 (1980) 219
5. Christensen et. al., "Uranium Dioxide Thermal Conductivity", Trans. Am. Nucl. Soc. 7(2), 390, 1964
6. D.G. Martin, "A Re-appraisal of the Thermal Conductivity of  $UO_2$  and Mixed (U, Pu) Oxide Fuels", Journal of Nuclear Material 110 (1982) 73-94
7. S.H. Bush, "Zirconium Clad Uranium Dioxide Fuel Element for Light Water Reactors", August 1973
8. D.R. Olander, "Fundamental Aspects of Nuclear Reactor Fuel Elements", ERDA Report TID-26711-P1, 1976

## RIM EFFECT OBSERVATIONS FROM THE THIRD RISØ FISSION GAS PROJECT

N. KJAER-PEDERSEN  
S. Levy Incorporated,  
Campbell, California,  
United States of America

### Abstract

The Third Riso Fission Gas Release Project was completed early 1991. The project was sponsored by a group of participants representing the world-wide nuclear industrial and scientific community. The analysis presented in this paper is based on an original data analysis sponsored by the Swedish Nuclear Inspectorate (SKI). This data analysis aimed at interpreting the temperature and fission gas release measurements of the project. Temperature measurements are available from both on-line thermocouple readings and determinations made in the hot cells based on local cesium concentrations. The temperature measurements made by the Risø staff indicate the typical existence at high burnup of a radial temperature profile that is highly "squared", i.e., shows a steep gradient close to the periphery, offset by a relatively flat appearance in the central part. Despite the "squaring", the central temperature measurements do not deviate to a large extent from values calculated by conventional methods. Along with the squared temperature profiles, a porous region has been detected in the fuel, close to the pellet periphery. This porous region exhibits a very high local porosity and a very small grain boundary bubble size. Fission gas release measurements are available from both pin puncturing and local retained gas determinations. The phenomena of the porous region are generally referred to as the "rim effect".

The present analysis attempts to a) relate the existence of the porous region to local burnup effects associated with the high-burnup power depression in the pellets and b) relate the observed squared temperature profile to the observed porosity levels at the rim and to the central power depression. In the original analysis, measured central temperatures were reconciled with data from the Halden Project. Also, the observed gas release levels were compared to levels measured in several of the Studsvik international fuel projects, which has led to the conclusion that the thermal gas release in the Riso experiments was consistent with that of those other experiments. In the present study, an empirical athermal porosity model for the rim is proposed, as well as a new porosity dependent model for the fuel thermal conductivity, particularly addressing the rim effect. The analysis indicates that the temperature increase through the rim, despite the steep gradient at the surface, is bounded by boundary bubble growth and coalescence. There are indications of a possible enhancement of the athermal gas release in the rim, which may play an indirect role in also enhancing the thermal gas release.

## 1. BACKGROUND

The Third Risø Fission Gas Project used a unique experimental technique to produce central temperature measurements in high burnup commercial LWR fuel. Commercial BWR and PWR fuel rods were refabricated in the Risø hot cells into short test rods, several of which were equipped with thermocouples and/or pressure gauges. In this way, thermocouple measurements were made available at a burnup level at which thermocouples inserted at zero burnup can not usually be reliably operated.

The refabrication technique was qualified through a number of experiments using fuel rod material from the batch of rods previously tested in the Second Risø Fission Gas Project. It was shown that previously tested performance parameters, such as gas release and dimensional and microstructural changes, were unaffected by the refabrication. The out-of-pile thermocouple calibration was assumed to be valid also under in-pile conditions, since the thermocouples had been exposed to no long term in-reactor irradiation.

The Risø experiments provided numerous sets of measurements of central temperature, local gas release and local heat rating. In addition, extensive hot cell investigations provided radial distributions of long- and short-lived fission product isotope concentrations to indicate burnup and power generation profiles, respectively, as well as local porosity volume and bubble size, and cesium concentrations; in particular, the radial location was established at which the cesium concentration profile started to drop off sharply toward the pellet center, presumably due to cesium boil-off, associated with a fixed temperature. It was observed that the outer pellet region, extending some 100-200 microns into the fuel (the "rim"), contained very large grain boundary porosity, consisting of very small bubbles. From the central temperatures, the cesium boil-off incipience location, and a calculated fuel surface temperature, it was possible to infer radial temperature profiles during overpower transients.

## 2. INTRODUCTION AND SUMMARY

The fuel central temperature measurements of the Risø project showed great mutual consistency. The comparison with data from other sources of experiments required careful consideration of a long range of operational parameters. After studies of the detailed documentation of the experimental conditions, including measuring equipment, calibrations, etc., the reliability of the data was confirmed.

Furthermore, the comparison of the Risø temperature data with similar data from the Halden Project showed that appropriately accounting for the operational differences between the Risø reactor and the Halden reactor leads to a reasonable reconciliation of the results from these two sources. Moreover, the comparison of the fission gas release data from the Risø project with fission gas release data from Studsvik experiments, which included the reduction of the data from both experimental sources to local

release values and local temperatures, showed excellent agreement. Thus, it has been established that thermal data from experiments performed in Halden, Risø and Studsvik seem to be generally consistent with each other.

Nonetheless, the presence in the Risø experiments of the "rim effect", as well as a strong radial power depression function, seems to have led to certain differences in the temperature measurements, relative to previous common experience. These conditions tend to create a "squared" temperature profile with a very steep slope at the pellet periphery and a correspondingly flat central portion. The term "rim effect" covers the combined effects of the precipitation of small gas bubbles in large numbers in a thin region extending 100-200 microns into the fuel from the periphery. The total volume of these small bubbles amounts to local porosities (gaseous swelling) in this relatively low temperature region, that may exceed 40 percent. Partial grain separation has also been observed in the rim region. The gas precipitation is probably driven by the strongly enhanced local burnup in the rim region, owing to the strong power depression confirmed to exist at the high cross-sectional burnup of approximately 45 MWd/kgU. The enhanced local burnup may reach 60 MWd/kgU, causing significant athermal release of gas atoms to the grain boundaries and, subsequently, to the rod free volume. This mechanism has been previously described in the literature, and the available data has been used in the present study to express the resulting athermal porosity contribution in a simple empirical model.

The porosity in the rim region has been identified as the cause of the steep slope of the temperature profile across that radial range. However, because of the strong power depression in the central part of the fuel, the rise of the temperature from the profile inflection point at the inner boundary of the rim and in the direction of the pellet center is reduced, so that the resulting central temperature may, in fact, be not dramatically different from the value that would be expected without the rim effect and without the strong power depression.

The strong power depression in the central region was not taken into account in early attempts to correct for the existence of the thermocouple bore. This may have led to an overestimation of the equivalent solid pellet temperature for the given heat rating.

The observed power depression is due to the depletion with burnup of the original  $U^{235}$  in the pellet interior along with a buildup of  $Pu^{239}$  at the periphery, and can be verified by transport theory calculations based on LWR lattice parameters.

Similar effects have not been reported in connection with Halden experiments, and would not be expected, since the (heavy water) flux spectrum in the Halden reactor is significantly different.

In Studsvik, the rim effect has not been specifically observed, certainly not in the bulk of the experiments from the international programs, where the burnup only in relatively few

cases reached levels of the order of 45 MWd/kgU. These cases, which might be affected by the rim effect, were excluded from the comparison of the thermal performance data.

In this paper, the temperature profiles measured in the Risø project are discussed in the light of the measured burnup and power generation profiles, as well as the measured porosity and bubble size in the rim zone.

The cesium boil-off temperature was not determined from literature data, but rather inferred from series of overpower tests at different heat ratings, using an extrapolation technique. This technique is based on plotting the measured central temperature versus the cesium boil-off location, the extrapolation of this curve to the radial location of the thermocouple bore indicates the cesium boil-off temperature.

The cesium boil off temperature and radial location establish a fixed point for the radial temperature profile, in addition to the central measurement. The fuel surface temperature can be calculated with reasonable accuracy, since the gap was closed during the overpower experiments. Thus, three points of the profile through the fuel pellet can be determined. Inferring the radial profile from this information invariably leads to a curve that exhibits a very steep slope close to the periphery. This can not be explained by the radial power depression, no matter how strong it appears to be. This is clear from the fact that the temperature gradient at the fuel surface is determined exclusively by the ratio of the heat flux and the thermal conductivity at that location. Since the surface heat flux is unchanged by the flux depression, the explanation has to be found in the thermal conductivity of the fuel within the rim region.

The many small bubbles on the grain surfaces in the rim region suggest a very dense covering of the individual grains. Geometric considerations suggest that bubbles of the size observed and which add up to the porosity volume observed, if arranged in a regular pattern, would indeed provide for practically complete coverage of the individual grain surfaces, i.e., a thin gaseous blanket may be envisaged around the grains, thermally insulating them from each other, thus causing a dramatic decline in the fuel thermal conductivity toward a limit set by, but not equal to, the conductivity of the fission gas. At higher temperatures, surface diffusion of the bubbles toward the grain edges is expected, based on well established experimental knowledge. This leads to bubble coalescence, i.e., the bubble size increases as a function of temperature. With a steep temperature gradient, bubble coalescence will occur within a short distance from the surface, and the porosity will no longer cover the grain surfaces effectively, which again causes the thermal conductivity to rapidly rise toward "normal" values, this trend is further enhanced by the decline of local porosity away from the surface, as a function of the steeply descending burnup profile.

Thus, the gas precipitation in small bubbles within the rim region can be seen as the cause of a dramatic reduction in thermal conductivity. This reduction, however, automatically recovers as the temperature is driven toward a level at which the small

bubbles can not exist. In fact, as an approximation it may be considered that this temperature level constitutes an effective new surface temperature that may be used for pellet temperature profile calculations when the rim effect is present (outside of the rim region itself), using the traditional thermal conductivity expression.

Based on simple considerations along the above lines, a multiplier to the fuel thermal conductivity can be formulated as a function of porosity, bubble size and grain size. An empirical expression for the saturated bubble size as a function of temperature can be obtained from numerous hot cell investigations reported in the literature. For the purpose of accounting for the rim effect, such expression need only be accurate at the low temperature end, since its influence on the conductivity ceases as soon as the bubble size has grown to a few microns. Thus, the proposed factor will not interfere with the factor normally used to account for the influence of the as fabricated porosity. A thermal conductivity model for UO<sub>2</sub> fuel, based on MATPRO data and the suggested rim porosity factor, along with the application of the appropriate power depression function, has been successfully applied to reproducing the temperature profiles observed in the Risø project.

### 3. DATA

The data analysis discussed here is largely limited to the Risø data. The previously performed data comparisons with Halden and Studsvik experiments are reported only in a summary way, for providing a better perspective of the Risø data.

#### 3.1 PRINCIPAL DATA ANALYZED

The Risø experiments included fuel manufactured by General Electric Company, Advanced Nuclear Fuels Company (presently Siemens Nuclear Company), and Risø National Laboratory. In this analysis, only experiments based on ANF fuel were included. The original data analysis, in which the Risø data were compared against data from other experimental facilities, included experiments based on fuel from all available manufacturing sources.

The Risø data are reported in References [1] and [2].

General materials data used to analyze the experiments were obtained from the MATPRO collection (Reference[3]).

#### 3.2 SUPPORTING DATA FROM OTHER EXPERIMENTS

The Halden experience included in the original analysis was derived from References [4] and [5]. The Studsvik experience included in that analysis was derived from References [6], [7] and [8].

## 4. ANALYSIS

### 4.1 ESTABLISHED THEORETICAL MODELING BASE

Since the principal objective of the present analysis is to understand the measured radial temperature profiles from the Risø experiments, the existing modeling base on which such task would normally be based is briefly discussed in the following.

#### 4.1.1 Radial power density and burnup profile

The radial power generation function, as depressed in the center of the fuel pellet, can only be properly calculated by transport theory methods. Such calculations have been carried out for LWR rods, and used to calibrate faster running methods based on two-group diffusion theory. Thus, numerical tools have been established for this part of the modeling activity, at least for LWR fuel to which this paper applies.

The theoretical calculations have been verified by comparison with power and burnup profiles determined from isotopic measurements in the Risø project. The agreement has been found to be excellent at the burnup level of 45 MWd/kgU. For ease of data analysis, the experimental profiles have been approximated by simple mathematical functions of the type:

$$P = P_{\min} + (P_{\max} - P_{\min}) \times \left( \frac{r}{r_0} \right)^{n_p} \quad (1)$$

and

$$bu = bu_{\min} + (bu_{\max} - bu_{\min}) \times \left( \frac{r}{r_0} \right)^{n_b}$$

where  $n_p$  and  $n_b$  are of the order of 12 and 10, respectively.

The max and min values are relative to the cross-sectional average and are approximately:

$$\begin{aligned} P_{\min} &= 0.945 \\ P_{\max} &= 1.430 \\ bu_{\min} &= 0.950 \\ bu_{\max} &= 1.300 \end{aligned}$$

at the 45 MWd/kgU burnup level. These values are characteristic of the actual initial enrichment of 3.0 percent, which is consistent with the calculations.

## 4.1.2 Fuel thermal conductivity according to MATPRO

The UO<sub>2</sub> thermal conductivity is given in the MATPRO collection as a rather complicated expression, giving a best fit to the available data. For data analyses, however, this expression is most practically approximated by a simpler analytical expression, such as

$$k(T, p, bu) = \frac{C}{B \times T + A + C_p \times p + C_b \times f(bu)} + D \times T^n \quad (2)$$

where T is temperature, p porosity, and bu is burnup at the local radial position

The constants have been determined (by fitting at zero porosity) to be

$$\begin{aligned} A &= 1.1 \\ B &= 0.0224 \\ C &= 93.0 \\ D &= 2.5 \times 10^{-14} \end{aligned}$$

This gives the conductivity in W/m/K. The power n in the "electronic" term is theoretically 3. However, the value 4 gives a much better fit to the MATPRO data.

The function f(BU) may be given as follows:

$$\begin{aligned} f(bu) &= C_x \times \left( \frac{bu - bu_x}{bu_0} \right)^{n_1} \quad \text{for } bu \geq bu_0 \\ &\text{and} \\ f(bu) &= \left( \frac{bu}{bu_0} \right)^{n_2} \quad \text{for } bu \leq bu_0 \end{aligned} \quad (3)$$

The constants in this expression are subject to fitting against data. The following values have been found reasonable:

$$\begin{aligned} bu_0 &= 10.0 \text{ (MWd/kgU)} \\ bu_x &= 7.5 \text{ (MWd/kgU)} \end{aligned}$$

$$\begin{aligned} C_x &= 2.0 \\ n_1 &= 0.5 \\ n_2 &= 2.0 \end{aligned}$$

The constants must be selected to provide continuity and differentiability across the region separator value, bu<sub>0</sub>.

The other constants of Equation 2 may be as follows:

$$\begin{aligned} C_p &= 56.0 \\ C_b &= 3.0 \end{aligned}$$

Without the burnup dependency, which is not given in MATPRO, Equation 2 provides a very good fit to the MATPRO expression. Note that it was found that the porosity correction can efficiently be placed as an adder to the denominator, along with the burnup correction.

## 4.2 EXTENSION OF MODELING BASE SUGGESTED BY DATA

## 4.2.1 Burnup-enhanced athermal gas release to grain boundaries

Pati et al. (Reference [9]) have analyzed post-irradiation data from a large number of commercial PWR rods, irradiated to burnup levels as high as 50-56 MWd/kgU, rod average. In particular, rods from the Calvert Cliffs and Fort Calhoun reactors provided very consistent data for fission gas release and rim porosity. A set of Fort Calhoun rods are reported to have shown a low temperature (athermal) gas release of between 0.56 and 1.33 percent, at a rod average burnup of approximately 52 MWd/kgU, while local cross-sections of the same rods at cross-sectional average burnup levels from 56 to 60 MWd/kgU, showed an average rim porosity level of 22.3 percent. For these cross-sections, the maximum local burnup in the rim was estimated at 93.7 MWd/kgU. This corresponds to a rim-to-average burnup ratio of approximately 1.56, which is consistent with values measured in the Risø project, as well as with transport theory calculations. The rim porosity of 22.3 percent is an average value, the variation across the rim region was not quantified in Reference [9], but a micrograph is shown to indicate a very steep variation. This is consistent with observations from the Risø project.

The following expression may be suggested to describe the small bubble porosity across the rim.

$$p(r, BU_{\max}) = p_0 \times \frac{g_0}{g} \times C \times \left( 1 - e^{-\left( \frac{BU_{\max}}{2 BU_r} \right)^3} \right) \times e^{-\frac{r_p - r}{b_{RP}} \times \frac{2 BU_r}{BU_{\max}}} \quad (4)$$

where

- $r$  = radial location (m)
- $BU_{max}$  = maximum local burnup, i.e., at location  $r = r_p$  (MWd/kgU)
- $p_0$  = a reference porosity, set to 0.20
- $g_0$  = a reference grain size (microns), set to 7
- $g$  = grain size in rim region (microns)
- $C$  = a constant, set to 2.25
- $BU_R$  = a reference burnup (MWd/kgU), set to 45.0
- $r_p$  = pellet radius (m)
- $\delta_{R0}$  = reference rim width (m), set to 0.0002

With the above choice of parameters, this expression approximately gives the measured average of 22.3 percent across the rim region

The expression has also been applied to the Risø rods and found to give realistic values

The grain size for the Fort Calhoun rods was reported to be 13 microns, for the Risø ANF rods it averaged 5.5 microns, while for the Risø GE rods at highest burnup it averaged 11.5 microns

The last factor of the porosity expression suggests an exponential variation away from the periphery, based on a given width of the rim region, this is justified because the data indicates a much steeper decline than can reasonably be directly associated with the radial variation of the local burnup function. A physically detailed theory is not available

#### 4.2.2 Role of bubble size in effect of athermal porosity

In Subsection 4.1 the  $UO_2$  thermal conductivity as a function of temperature at 100 percent theoretical density and no irradiation exposure has been discussed, the MATPRO expression has been named as representing the state of the art. It is pointed out that correcting for porosity and burnup effect is a matter of less consensus amongst researchers, nevertheless, an approximative mathematical form that permits a physically acceptable burnup correction was recommended, although the numerical values of critical constants were left to determination by benchmarking

It is generally agreed that the modest correction for as fabricated porosity and thermal gaseous swelling may be handled by one of several mathematical expressions like the one used in MATPRO, in particular, that this correction is insignificant at high temperature. An expression of the same magnitude as used in the MATPRO expression for porosity correction, but of a more convenient mathematical form was recommended in Subsection 4.1

The porosity from athermal swelling, the "rim effect" porosity, may have a much more pronounced effect on the thermal conductivity, since the very large number of very small bubbles that are required to make up the porosities of the order of 20-60 percent, as has been measured at the very periphery, can be shown to form such a dense population that virtual insulation of the fuel grains from each other may occur.

The chance that this will happen is expressed in terms of the "coverage factor", a number between zero and unity that indicates the degree of boundary saturation. The coverage factor depends on the bubble size. For a given grain size and burnup level there is a maximum possible athermal porosity, as suggested by Equation 4 above. When this porosity is reached, the coverage factor has reached its largest value for the given temperature. At higher temperatures, this value is much smaller than unity. At lower temperatures, smaller bubble sizes are expected, which increases the coverage factor for the given porosity. At a sufficiently low temperature, the coverage factor will reach unity. Based on the experimental evidence that the athermal porosity does develop in normal LWR operation, and that steep temperature gradients do occur at the fuel surface (i.e., dramatically reduced fuel thermal conductivity), it is concluded that the bubble size for athermal porosity at normal fuel surface temperatures is small enough to cause the coverage factor to reach unity at maximum porosity. This conclusion is specifically applied in the following subsections

#### 4.2.3 Bubble-size dependent model for conductivity vs porosity

The effect of boundary porosity on thermal conductivity can be treated in a first approximation on a purely geometric basis. If the bubbles are envisaged to be all of the same size and evenly distributed over the grain surface with a coverage factor of  $x$ , then the porosity can be expressed

$$p = \frac{1}{2} \frac{4\pi \left(\frac{g}{2}\right)^2}{\frac{4\pi}{3} \left(\frac{g}{2}\right)^3} \times \delta \times x = \frac{3\delta}{g} \times x \quad (5)$$

where

- $g$  = the grain diameter (microns)
- $\delta$  = the thickness of the gas layer (microns)

Alternatively, this relationship may be written

$$x = \frac{g p}{3\delta} \quad (6)$$

Note that, according to Equation 4, the product  $gp$  depends only on the burnup at the surface and the distance from the surface

The gas layer thickness is equivalent to the gas bubble diameter. However, for mathematical convenience we shall treat the bubbles as if they were cubic, thus we can obtain

$$r_b = \frac{g p}{3x} \times \sqrt[3]{\frac{3}{4\pi}} \quad (7)$$

where  $r_b$  is the bubble radius (microns)

The critical bubble size at which full grain surface coverage is achieved ( $x=1$ ) is

$$r_{b,1} = \frac{g_0 p_1}{3} \sqrt[3]{\frac{3}{4\pi}} \quad (8)$$

where  $p_1$  is a reference porosity level

Taking the reference porosity to be 30 percent, the critical bubble size becomes

$$r_{b,1} = \frac{7 \times 0.30}{3} \times \sqrt[3]{\frac{3}{4\pi}} = 0.4343 \text{ (microns)} \quad (9)$$

The assumption is now made, in accordance with the observations, that full coverage may occur at temperatures within the normal operating range of the pellet periphery, i.e., 600-900 K. The critical temperature level for bubble size  $r_{b,1}$  may be defined as  $T_1$ , i.e.

$$r_{b,1}(T_1) = 0.4343 \quad (10)$$

where  $T_1$  should be approximately 900-1000 K. The temperature dependency of the actual bubble radius is developed in the next subsection. At this point it is noticed that, for bubble sizes lower than  $r_{b,1}$ , corresponding to temperatures lower than  $T_1$ , or for porosities greater than the reference level  $p_1$ , coverage factors greater than unity will be

calculated. The original definition of the coverage factor is readily extended to cover this situation, which corresponds to multi-layer bubble conglomerations.

The expression for the thermal conductivity, based on coverage factor  $x$  and porosity  $p$ , is derived from a simple one-dimensional model of two slabs, one representing the fuel grain the other the boundary layer. It is practical to distinguish two cases: a)  $x < 1$  and b)  $x > 1$ .

a)  $x < 1$

$$k_{eff} = (k_f (1-x) + x k_g) \times \frac{1 + \frac{3x}{p}}{1 + \frac{3x}{p} \left(1 - x \frac{k_f - k_g}{k_f}\right)} \quad (11)$$

b)  $x \geq 1$

$$k_{eff} = k_f \times \frac{1 + \frac{p}{3}}{1 + \frac{p}{3} \times \frac{k_f}{k_g}} \quad (12)$$

It is readily verified that for  $x=1$  both expressions give the same result.

The maximum possible conductivity degradation due to the rim effect can be estimated from Equation 12.

With  $k_g$  to 0.00012 kW/m/K at 700 K, and  $k_f = 0.0048$  kW/m/K at the same temperature, the ratio  $k_f/k_g$  becomes 400, assuming further that the porosity is about 30 percent, the result is

$$k_{eff} = k_f \times 0.027 \quad (13)$$

While this indicates a severe degradation, the resulting (lowest perceived conductivity of the matrix) is still about ten times higher than the thermal conductivity of pure fission gas.

Risø results have suggested an average degradation of the conductivity over the rim region to 28 percent of normal conductivity. The result of Equation 13 (which would apply to the very edge) is in good agreement with this finding.

#### 4.2.4 Boundary bubble size versus temperature

The actual bubble size depends on the degree of saturation. The assumption is made that for incomplete saturation the bubble size will be reduced, but the number density of the bubbles will be that which corresponds to the maximum bubble size at saturation porosity. As shown above, a smaller saturation bubble size gives a higher coverage factor at a given porosity. The bubble diffusion along the grain surfaces, and eventual coalescence into larger bubbles at the grain edges, tends to reduce the coverage factor. This is taken into account by expressing the saturation bubble size as a function of temperature, as follows

$$r_b(T) = 0.1 + 16.0 \times e^{-1.8 \frac{1 - \frac{T}{3100}}{\frac{T}{3100}}} \quad (14)$$

This gives a bubble radius of 0.4343 microns at about 980 K, and a little over 10 microns at about 2500 K. The expression was obtained by matching observed bubble sizes under conditions of coalescence, it does not claim accuracy at higher temperatures, since it mainly serves the purpose of reflecting the reduction of the coverage factor as the temperature rises through the rim region.

#### 4.3 FITTING THE DATA WITH NEW POROSITY MODEL

The power and burnup profiles for a typical ANF fuel pin, ramped in the Risø project to about 40.0 kW/m, were established from Equations 1 and verified to match the experimentally determined profiles. Then, the athermal porosity model derived from the Pati data (Reference [9]) and expressed by Equation 4 was used to determine the radial porosity profile through the rim. Again, the calculated data were compared with the experimental results, establishing that the fit is clearly within the uncertainty.

The thermal conductivity expression of Equation 2, with the burnup correction term of Equation 3, and amended by the 'rim factor' suggested in Equations 11 and 12, was then used in a calculation of the temperature profile across the pellet. Documentation of this exercise is separately available in MATH-CAD file format from S. Levy Incorporated.

The geometrical dimensions were used that correspond to the Risø thermocouple bore design (pellet inner radius = 1.25 mm, outer radius = 4.5 mm). For a heat rating of 40 kW/m this exercise resulted in a calculated central temperature of 1900 K.

The Risø data indicates an experimental central temperature of 1840 K at the same heat rating. The Risø data also provides a temperature determination at the radial position of incipient cesium boil-off. The temperature at this point is about 1450-1500 K. Using these two radial fix-points together with an estimated pellet surface temperature of 700

K leads to the conclusion that the temperature profile must have a relative sharp knee in the range 900-1200 K. However, the radial location of the knee can not be accurately determined from the data.

While this agreement is very good, it should be borne in mind that the constants that determine the burnup correction to the fuel thermal conductivity of Equation 2 have no other basis for their selection than data such as the present. However, it must also be observed that the temperature at which the calculated radial temperature curve starts to bend over sharply (the "knee" that causes the "squared" profile), a value of approximately 900 K, in parametric studies has shown very little variability. According to the derivation of the rim porosity model, this is due to the increase with temperature of the boundary bubble size and corresponding decrease of the "coverage factor", which supports the observation that this temperature should be a near-constant value. Thus, the constancy of this temperature level supports the use of the data for estimating the magnitude of the effect of burnup on thermal conductivity.

## 5 CONCLUSION

The theoretical analysis of the Risø data has shown that the effect on the radial temperature profile of the rim effect can be explained in terms of the effect of the athermal porosity on the fuel thermal conductivity at low temperature. This effect seems to be self-eliminating at about 900 K, which may cause a sharp inflection of the temperature profile at that point, which would be a few hundred microns away from the pellet periphery. A detailed calculational method is suggested for the modeling of the rim effect, and is available in MATH-CAD format from S. Levy Incorporated. Furthermore, since the rim effect seems to be well quantifiable in terms of temperature, the Risø experiments also provide a means for estimating the magnitude of the thermal conductivity burnup correction at 45 MWd/kgU.

## ACKNOWLEDGEMENT

Thanks are due to the Swedish Nuclear Inspectorate (SKI) who supported the original analysis upon which the present work is based. Also, SKI kindly permitted the publication of this report.

## REFERENCES

- [1] The Third Risø Fission Gas Project, Final Report, RISØ FG P3 FINAL, Parts 1 and 2 and associated reports, March 1991.
- [2] The Risø Transient Fission Gas Release Project, Final Report, RISØ TFGP R29 Volumes 1 and 2, December 1986.

- [3] MATPRO-Version 11 (Revision 2), NUREG/CR-0497, TREE-1280, Rev 2, August 1981.
- [4] D.D. Lanning "Irradiation History and Final Postirradiation Data for IFA-432," Battelle Pacific Northwest Laboratory, NUREG/CR-4717, November 1986
- [5] M.E. Cunningham, E. Kolstad, C. Vitanza "Overview of Recent and Ongoing Extended Burnup Studies at the OECD Halden Reactor Project," IAEA Symposium, Stockholm, Sweden, 15-19 September, 1986 (IAEA-SM-288/34, 1987)
- [6] INTER-RAMP, Final Report, STUDEVIK-STIR-53, STUDEVIK, Sweden, August 1979
- [7] OVER-RAMP, Final Report, STUDEVIK-STOR-37, STUDEVIK, Sweden, May 1981.
- [8] SUPER-RAMP, Final Report, STUDEVIK-STSR-32, STUDEVIK, Sweden, December 1984.
- [9] S.R. Pati, A.M. Garde, L.J. Clink: "Contribution of Pellet Rim Porosity to Low-Temperature Fission Gas Release at Extended Burnups," ANS Topical Meeting on LWR Fuel Performance, Williamsburg, Virginia, April 17-20, 1988

## EXPERIMENTAL TECHNIQUES AND RESULTS RELATED TO HIGH BURN-UP INVESTIGATIONS AT THE OECD HALDEN REACTOR PROJECT

W. WIESENACK  
 OECD Halden Reactor Project,  
 Halden, Norway

### Abstract

Investigations of phenomena associated with extended or high burn up comprise a considerable part of the fuel & materials research programme carried out at the OECD Halden Reactor Project, reflecting the interests and priorities of the nuclear industry in this area. For this purpose, sensors, re-instrumentation techniques, irradiation rigs and data evaluation methods have been developed and successfully applied which allow tests to be conducted at extended burn up with high data quality.

Re-instrumentation of base irradiated fuel rods (50 MWd/kgU) with pressure transducers has been carried out with several rods, which were then subjected to high power, to study fission gas release. The results as well as those from another high burn-up test confirm the empirical fission gas release threshold developed at Halden, which predicts the onset of FGR to be at about 1100 °C at this burn-up. The related interlinkage-resintering effects can be studied in special assemblies allowing sweep-out and analysis of fission products.

Comprehensive investigations of fuel temperature data suggest a gradual degradation of UO<sub>2</sub> thermal conductivity with burn up. A special experiment is presently being irradiated to burn up beyond 60 MWd/kgU, where the accuracy of temperature measurements is maintained by utilising expansion thermometers, insensitive to irradiation induced decalibration. A preliminary evaluation of the temperature increase points to a UO<sub>2</sub> conductivity degradation of 35% at 50 MWd/kgUO<sub>2</sub> and 600 °C.

### 1. INTRODUCTION

The research programmes at the OECD Halden Reactor Project have for more than thirty years significantly contributed to the understanding of LWR fuel behaviour. They reflect the interests, priorities and long term goals of the nuclear industry. A prevailing subject at present is the adoption of extended burn up operation schemes aimed at an improved fuel cycle economy. This has important implications in many areas of fuel performance and necessitates an expansion of the knowledge base on current fuel.

In this paper, experimental techniques applied in high burn up investigations at the OECD Halden Reactor Project are described, and some particular results related to aspects of fuel rod behaviour are presented. They comprise the degradation of fuel thermal conductivity and fission gas release at high burn up.

## 2. EXPERIMENTAL TECHNIQUES RELATED TO HIGH BURN-UP

Investigations of fuel performance parameters at high burn-up have to overcome a number of obstacles

- many years of irradiation are required under 'normal' operation and testing conditions,
- the interaction of an increasing number of phenomena tends to become more and more complex,
- instrumentation must give reliable results and survive in a hostile environment for many years and at high fluences

The Halden Project has developed and applied experimental techniques and instrumentation which are able to mitigate these problems and make it possible to conduct high burn-up investigations in a tractable manner. They are briefly discussed in the following sections.

### 2.1 Re-instrumentation of irradiated segments

Re-instrumentation of fuel segments previously irradiated to high burn-ups has been used for several experiments. The sensors comprise pressure transducers, fuel thermocouples and cladding elongation detectors. Re-instrumentation with the latter is especially simple since it only requires the external fitting of a magnetic core to the segment, while the other two involve more elaborate techniques

#### - *Pressure transducers*

With this method, an instrumented head containing a bellows pressure transducer and a drill is welded onto the end plug of an irradiated rod. The drill is driven by external rotating magnets until a penetration into and gas communication with the fuelled section is achieved. The reaction of the bellows to pressure changes is picked up during further irradiation in the usual manner with an LVDT (linear voltage differential transformer). Continuous measurements of the internal gas pressure give precise information about the fission gas release as a function of time and burn-up. Results of a particular experiment are shown in section 3.1

#### - *Fuel thermocouples*

Re-instrumentation of irradiated fuel rods with fuel thermocouples is part of the current Halden Project programme. The technique, based on Risø experience, is fully implemented in the hot cell of Institutt for Energiteknikk at Kjeller, Norway, and has recently been demonstrated with the re-instrumentation of two rods pre-irradiated in the HBWR to 43 MWd/kgUO<sub>2</sub>

### 2.2 Expansion thermometer for high fluence operation

Refractory metal thermocouples (W-Re) suffer from a gradual transmutation of the alloys resulting in less EMF (less sensitivity) or an apparent temperature decrease. Although the

effect has been quantified [1] and a correction is automatically applied to HBWR data, this instrument behaviour constitutes an uncertainty. Expansion thermometers (ET), based on a Mo wire through the fuel stack and an outside LVDT to pick up its elongation with temperature, do not suffer from such a degradation and can therefore advantageously be used to obtain data at high burn-up and fluences. It is also possible to move segments equipped with ETs between test rigs without losing the temperature measuring capability as long as an outside LVDT is available.

Expansion thermometers have been successfully tested and applied in the HBWR and are presently being used in a high burn-up study which has reached 55 MWd/kgU.

### 2.3 Experiments to study separate effects

Most phenomena occurring in fuel rods during irradiation are interrelated, in particular via the influence of temperature. The dependences tend to become more complex with burn-up while uncertainties are increasing. The possibility to study some effects separately or in relative isolation is therefore of great advantage for fuel performance modelling. Of particular relevance for thermal properties and fission gas release investigations are the Halden Project's gas flow rigs. In these rigs, the gas contained in the fuel rods can be changed and the pressure can be varied. Volatile fission products can be swept out, cold trapped and analysed.

With this type of rig, a number of parameters can be assessed:

#### - *Gap size*

The hydraulic diameter or gap can be determined from the resistance that the fuel stack offers against the gas flow driven by a given differential pressure between the ends of a rod. Gradual gap closure with increasing burn-up has been verified by this method.

#### - *Effect of pressure on temperature*

The pressure and gas-type dependent temperature jump distance is an important parameter in fuel temperature calculation models. Variation of the fill gas pressure at constant power has a detectable effect on the fuel centre temperature measured simultaneously. This effect (decreasing temperature with increasing pressure) is more pronounced for helium than for argon or xenon, and increases with burn-up - probably due to more fuel cracking which creates a growing number of surfaces where the effect can take place.

#### - *Gas composition in the fuel-cladding gap*

By changing the gas in a rod, the separate effects of several parameters can be investigated. For fission gas release, the influence of temperature can be assessed while keeping the power density constant, thus separating thermal and athermal release. It is also possible to determine the influences of fuel vs gap heat conductance since mostly the latter is changed when replacing the gas filling, e.g. helium with argon.

### - Sweeping out and analysis of fission products

Volatile fission products swept out with the purging cover gas can be cold trapped and analysed using on-line  $\gamma$  ray spectrometry. The method allows the determination of release to birth ratios which are controlled by thermal and athermal diffusion processes. By analysing the release rates of several short lived isotopes, it is possible to assess the surface to volume ratio which is a sensitive indicator of grain boundary porosity interlinkage and resintering /2/

### 2.4 Fast burn-up accumulation

Burn-up representative of extended fuel cycle discharge values can be accumulated in an accelerated manner (about 20 MWd/kgUO<sub>2</sub> per year) by using highly enriched fuel and thin rods. Such an experiment is presently under irradiation in the HBWR and has reached about 50 MWd/kgUO<sub>2</sub>. Its purpose is the investigation of the fuel conductivity degradation effect and fission gas release at high burn up. Some results from this rig are presented in sections 3.2 and 3.3.

### 2.5 Noise analysis and utilisation of transient data

The technique of noise analysis is being used, in particular in conjunction with fuel thermal data, to monitor long-term changes which have an influence on fuel temperatures. These are essentially gap closure, fission gas release and conductivity changes which influence the time constant of the fuel. Also transient temperature data obtained with a recording system automatically activated during scrams, can be used to infer response (time constant) changes with burn-up. These techniques have the advantage of being independent of the exact power and temperature. They provide supplementary information to steady state analyses and usually corroborate the results obtained therefrom.

## 3. SOME RESULTS FROM HIGH BURN-UP STUDIES AT THE HBWR

Thermal performance of LWR fuel depends on many interrelated phenomena, two of which have received relatively more attention during recent years. These are an enhancement of fission gas release with burn up and the degradation of the UO<sub>2</sub> thermal conductivity. In this chapter, examples of HBWR experimental data related to these subjects are being presented. They comprise only a small part of the total available data base.

### 3.1 Fission gas release during a power increase in a re-instrumented fuel segment

For this experiment, a BWR type fuel rod segment which had been base irradiated to about 43 MWd/kgUO<sub>2</sub> average burn up, was re-instrumented with a bellows pressure transducer. The internal gas content was diluted to a 17% FG 83% He mixture. The rod was then subjected to high power operation.

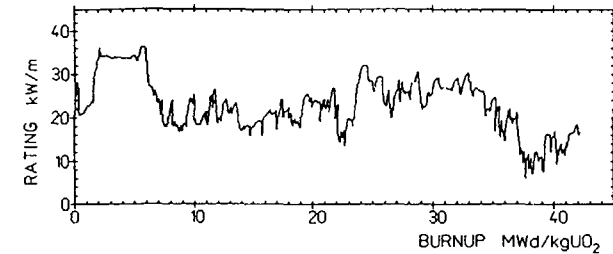


Fig 1 Base irradiation history of re-instrumented segment

### 3.1.1 Base irradiation

The base irradiation power history is shown in fig 1. As measured during the re-instrumentation process a fission gas release of 17 % occurred. A feature of the irradiation history is the operation at low power from 37 to 43 MWd/kgUO<sub>2</sub>, with values between 16 and 19 kW/m near the end. Calculated temperatures indicate that during this time the fuel was operated about 150 to 200 °C below the fission gas release threshold /1/. It is a general experience with Halden data that this kind of operation promotes the re-sintering process after previous FGR, gradually stopping further release as long as temperatures stay below the release threshold. In fact, exceeding the release threshold can be associated with (new) interlinkage and subsequent strong FGR. This pattern is also apparent in surface to volume ratio (S/V) measurements with the Halden Project's gas flow rigs /2/.

### 3.1.2 Development of pressure during power increase

The ramp test history is shown in fig 2. After an initial increase with normal speed, power was raised slowly over several days. Pressure increases are caused mainly by the changing coolant temperature together with some influence of the rod temperatures. The reduced data (zero power, 20 °C) show that the pressure is constant until about four days into the new irradiation when an increase can be observed. This is shown with a magnification in fig 3, where also other interesting details of the release behaviour appear. The wavy increase or change of slope can be associated with periods of increasing and constant power. The pressure jump at 9.5 days is connected to a power dip causing fuel cracking and some extra release.

### 3.1.3 Onset of fission gas release

By fitting portions of the reduced data in the vicinity of the presumed point of pressure increase and calculating the position of zero slope, the onset of fission gas release can be located at 4.3 days into the new irradiation. The corresponding temperature (calculated with rod average rating and burn up) is 1080 °C and coincides with the release threshold. Due to the power and burn up profile, some parts of the fuel are actually at temperatures above the threshold.

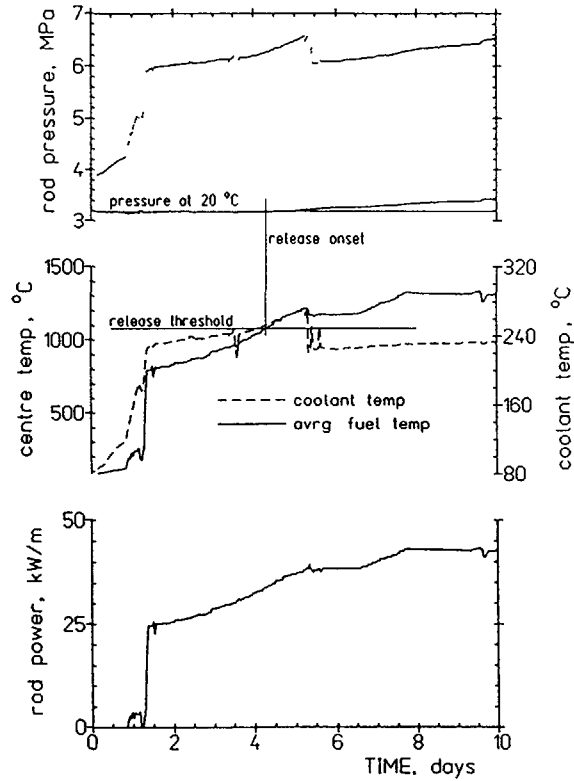


Fig 2 Pressure, temperatures and power during ramp test

This behaviour is in contrast to findings reported in /3/ where a much lower limit is presented. However, the data of this test are clearly related to thermal (diffusional) release, while the low release data of /3/ may also be associated with athermal diffusion processes. A proper control and definition of all parameters used in conjunction with the term *release threshold* is obviously required.

### 3.2 Pressure measurements in the ultra high burn-up rig

This rig, especially designed to study  $UO_2$  conductivity degradation and fission gas release at high burn up, has shown very good instrument performance. Measurements comprise internal rod pressure (2 rods) and fuel centre temperatures (4 rods, with expansion thermometers).

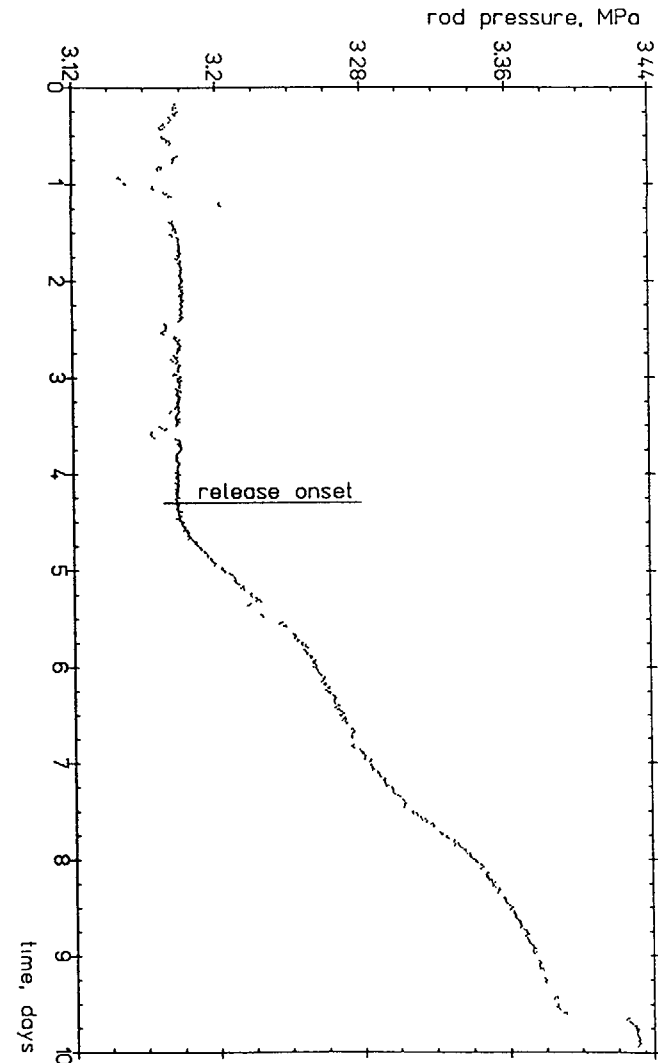


Fig 3 Rod pressure reduced to 20 °C, zero power, showing release onset at 4.3 days into the new irradiation

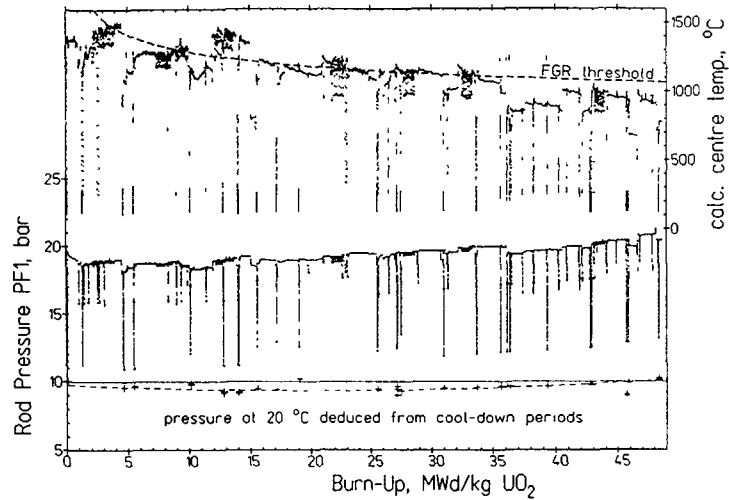


Fig. 4: Pressure and temperature history of Ultra-High-Burnup test. Temperatures are close to the release threshold, the small pressure increase can be explained with fuel swelling

The pressure and temperature history of one rod is shown in fig. 4. The lower part contains the result of a special data evaluation which, by using cool-down periods, eliminates any long-term sensor drift. These data points show an initial pressure reduction followed by an increase. This behaviour, in particular the increase, can be explained solely with dimensional changes of the fuel due to densification and swelling.

Calculated temperatures based on the measurements in the companion rods with expansion thermometers indicate that the rod has been operated close to or above the release threshold until about 36 MWd/kgUO<sub>2</sub> without showing definite signs of FGR (an order of magnitude increase of FGR is not uncommon when the release threshold is exceeded and interlinkage has started). In the high burn-up range temperatures stayed below the Halden FGR threshold, but considerably above the limit given in /3/. From these data (as well as from those shown in 3.1), a definite enhancement of FGR at high burn-up can therefore not be concluded.

### 3.3 Assessment of UO<sub>2</sub> conductivity degradation

An accurate characterisation of fuel temperature behaviour is a prerequisite for a satisfactory description of most phenomena occurring inside a rod during irradiation. Out-of-pile evidence /4/ as well as the more consistent rendering of experimental data suggest the inclusion of a burn-up dependent UO<sub>2</sub> conductivity correction in fuel performance codes. The effect of degrading  $\lambda_{UO_2}$  can also be seen in HBWR temperature data and has been reported in /2,5/ based on the evaluation of a variety of different fuels and rod designs. A special rig, intended

to study the phenomenon at high burn-up, has now reached 50 MWd/kgUO<sub>2</sub>, justifying an update of previous findings.

The temperature data, normalised to a constant rating of 25 kW/m (fig. 5), show an increase with burn-up. Conceded that fission gas release has not occurred (this is indicated by pressure measurements presented in section 3.2), conventional temperature calculation and gap conductance models will have difficulties in explaining this behaviour from first principles. Gap closure due to solid fission product swelling will rather lead to decreasing temperatures. A compensating effect in the fuel would help to rectify the situation.

The deduction of  $\lambda_{UO_2}$  degradation from fuel centre temperatures requires a model to separate the total measured  $\Delta T$  into the  $\Delta T$  across the gap (influence of gap conductance) and the  $\Delta T$  across the pellet (influence of  $\lambda_{UO_2}$ ). Gap conductance models can be very different, but it is nevertheless possible to give limits on the degradation effect (compare fig. 5).

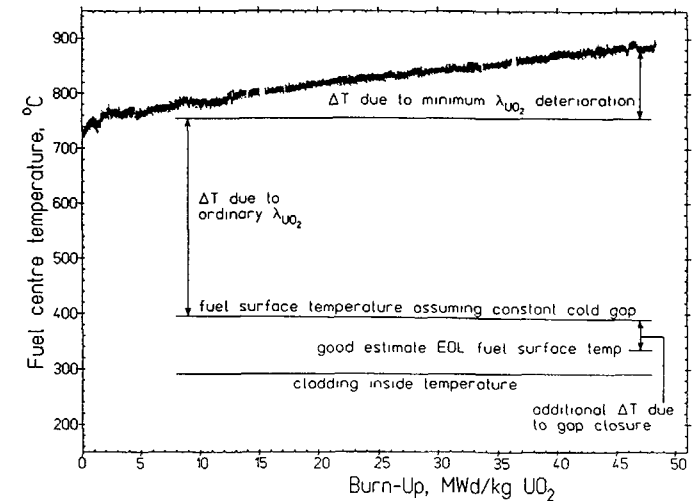


Fig. 5: Temperatures normalised to 25 kW/m show a gradual increase due to conductivity degradation

#### - Constant cold gap

This simplistic assumption does not consider gap closure due to fuel swelling.  $\lambda_{UO_2}$  degradation has only to account for the extra increase (after densification) of the centre temperature measured from the nearly constant pellet surface temperature. The value thus arrived at must be seen as the lower limit of the degradation effect and amounts to 26% at 600 °C and 50 MWd/kgUO<sub>2</sub> based on these data

- *Closing gap due to fuel swelling*

More realistic gap conductance models would assume gap closure due to relocation and fuel swelling. With an original cold diametral gap of 100  $\mu\text{m}$ , a pellet diameter of 5.92 mm and an assumed volumetric swelling rate of 0.1%/MWd/kgUO<sub>2</sub>, the hot gap at 50 MWd/kgUO<sub>2</sub> should be rather small (although the exact amount of densification is uncertain). The pellet surface temperature is therefore only slightly above the cladding inside temperature so that a larger  $\Delta T$  across the pellet must be accounted for by  $\lambda_{\text{UO}_2}$ . A good estimate value of 35% at 600 °C and 50 MWd/kgUO<sub>2</sub> is thus obtained.

By assuming a  $\Delta T$  between cladding and fuel of as little as 10 °C at current EOL, an upper limit of  $\lambda_{\text{UO}_2}$  degradation of 40% at 600 °C and 50 MWd/kgUO<sub>2</sub> can be derived.

- *Modelling considerations*

A correction C(burnup) was applied in the phonon term of conductivity:

$$\lambda_{\text{UO}_2}^{\text{phonon}} = 1/(A + B \cdot T + C(\text{burnup}))$$

It is in general not possible to derive the correction C independent of the gap conductance (and fuel densification) model, since C has to account for any remaining difference between measured and calculated temperatures. However, functional forms for C of D-burnup<sup>n</sup> invariably gave best results (1 $\sigma$  of about 4 °C mostly due to the noise in the data themselves) with exponents less than 1. This can be an indication of a saturation effect with increasing burn-up, and the values for the degradation given above should not simply be extrapolated or interpolated linearly. Also, it must be stressed that the correction cannot be used in existing models without a re-tuning (modification of gap conductance model) to the underlying data base. After all, the reference points remain unchanged and are given by the **measured fuel centre temperatures**. The inclusion of the conductivity degradation in fuel modelling codes is a way to arrive at a more satisfactory overall representation of the data base.

The ultra-high-burnup test, from which the data presented above originate, is an ongoing experiment which has reached a point where further irradiation and PIE can be expected to allow more definite and final conclusions both with respect to fission gas release and conductivity degradation. Meanwhile, the data and results obtained so far should be used with the care normally exercised in conjunction with R&D programmes still in progress.

#### 4. SUMMARY

For more than thirty years, the experimental work carried out at the OECD Halden Reactor Project has contributed significantly to the understanding of LWR fuel behaviour. Fuel rod re-instrumentation techniques for in-core pressure and temperature measurements, the development of sensors with reliable performance in a hostile environment under high fluences, the utilisation of gas flow rigs, and special data handling and evaluation methods all assist in the successful conduction of experiments related to high burn up effects.

Examples of rod internal pressure measurements at burn-ups of 43 to 48 MWd/kgUO<sub>2</sub> have been shown. They confirm fission gas release onset and interlinkage behaviour associated with the release threshold developed at Halden. An enhancement with burn-up cannot be concluded from these results.

Fuel temperature measurements made in the ultra-high-burnup test suggest a degradation of UO<sub>2</sub> thermal conductivity with exposure, reaching 35% at 50 MWd/kgUO<sub>2</sub> and 600 °C as a good estimate value. Lower and upper limits of this effect have been indicated as being 26% and 40%, respectively.

#### REFERENCES

- /1/ C. Vitanza, T. E. Sten: Assessment of fuel thermocouple decalibration during in-pile service, *Journal of Nuclear Materials* 139, 1986.
- /2/ E. Kolstad, C. Vitanza: Fuel rod and core materials investigations related to LWR extended burn-up operation, EMRS 1991 Fall Meeting, Strasbourg, France, November 1991.
- /3/ R. Manzel, R. Eberle: Fission gas release at high burnup and the influence of the pellet rim; International topical meeting on LWR fuel performance, Avignon, France, April 1991.
- /4/ H. Kleykamp: The chemical state of the fission products in oxide fuels; *Journal of Nuclear Materials* 131, 221-246, 1985.
- /5/ E. Kolstad, H. Devold, V. Tosi: High burn-up fuel behaviour studies by in-pile measurements, International topical meeting on LWR fuel performance, Avignon, France, April 1991.

## REVIEW OF STUDEVIK'S INTERNATIONAL FUEL R&D PROJECTS

M. GOUNES, S DJURLE, G LYSSELL, H MOGARD  
Studsvik Nuclear AB,  
Nykoping, Sweden

### Abstract

Since 1975, a series of international fuel R&D projects, primarily addressing the PCI/SSC failure phenomenon have been conducted under the management of STUDEVIK NUCLEAR. These projects have been pursued under the sponsorship of different groups of fuel vendors, nuclear power utilities, national R&D organizations and, in some cases, licensing authorities in Europe, Japan and the U.S. In most of the projects the clad failure occurrence was studied under power ramp conditions utilizing the special ramp test facilities of the R2 test reactor. The current projects are not limited to PCI/SSC studies but some of them also include other aspects of fuel performance, such as end-of-life rod overpressure. An overview of the nine projects that have been completed and six of the projects that are currently in progress or planned is given. During the late 1970's and 1980's the series of international ramp projects branched out in two directions. One series was initially concentrated on the PCI (Pellet-Cladding Interaction) phenomena under normal operational conditions in different types of BWR and PWR fuel rods subjected to increased burn-up under normal operational conditions. These projects were in a broad sense aimed at decreasing the fuel costs by increases in fuel utilization and reactor availability. The other series was concentrated on more safety-oriented issues, aimed at providing data for fuel-related safety considerations. The first-mentioned series includes the INTER-RAMP, OVER-RAMP, DEMO-RAMP I, SUPER-RAMP, SUPER-RAMP EXTENSION, SUPER-RAMP II/9x9 and SUPER-RAMP III projects. The second series includes the INTER-RAMP, DEMO-RAMP II, TRANS-RAMP I, TRANS-RAMP II, TRANS-RAMP III and TRANS-RAMP IV projects. Furthermore information is also given on the ROPE I, ROPE II and DEFEX projects.

### 1 RAMP RESISTANCE - BWR FUEL

The first of STUDEVIKS NUCLEAR's international fuel projects, INTER-RAMP, was executed in 1975-79 under the sponsorship of 14 organizations from 9 countries. The results has been described by Thomas [1] and Mogard et al. [2]. The main objectives of the program were to investigate systematically the failure propensity and associated phenomena of well-characterized BWR fuel rodlets when subjected to fast-over-power ramps under relevant and well-controlled experimental conditions

Table 1. Overview of STUDEVIK NUCLEAR's Completed International Power Ramp Test Projects 1975-86

Project (duration)	Fuel Type (No of rods)	Base Irradiation (Mwd/kg U)	Research Objectives
INTER-RAMP (1975-79)	BWR (20)	R2 (10-20)	Failure threshold Failure mechanism Clad heat treatment Modeling data
OVER-RAMP (1977-80)	PWR (39)	Obrigheim (10-30) BR-3, (15-25)	Failure threshold Design parameters Modeling data
DEMO-RAMP I (1979-82)	BWR (5)	Ringhals I (15)	PCI remedies (Annular, niobia doped pellets)
DEMO-RAMP II (1980-82)	BWR (8)	Wurgassen (25-29)	Failure threshold PCI damage by over-power transients
SUPER-RAMP (1980-83)	BWR (16)	Wurgassen (30-35) Monticello (30)	Failure threshold High burn-up effects PCI remedies Safe ramp rate Gd fuel
SUPER-RAMP EXTENSION (1984-86)	BWR (9)	Oskarshamn 2 (27-31)	Safe ramp rate
	PWR (4)	Obrigheim (33-45) BR-3 (28-33)	Design parameters Modeling data
TRANS-RAMP I (1982-84)	BWR (5)	Wurgassen (18)	Failure boundary Crack initiation and propagation Structural changes Fission gas release Modeling data
TRANS-RAMP II (1982-86)	PWR (7)	Zorita (30)	Failure boundary Crack initiation and propagation Structural changes Fission gas release Modeling data
SUPER-RAMP II/9x9 (1987-90)	BWR (4)	Desden (30)	PCI performance

Table 2. Overview of STUDESVIK NUCLEAR's Ongoing and Planned International Fuel R&D Projects

Project (duration)	Fuel Type (No of rods)	Base Irradiation (Mwd/kg U)	Research Objectives
ROPE I (1986-91)	BWR (4)	Ringhals (36)	Investigate clad creep-out as a function of rod overpressure
TRANS-RAMP IV (1989-91)	PWR (7)	Gravelines (20-25)	Influence of non-penetrating cracks on PCI failure resistance
ROPE II (1990-93)	PWR (6)	Ringhals Obrigheim (>40)	Same as ROPE I
Defect Fuel Degradation Experiment (NS*) 1992-95)	BWR (ND)* PWR (ND)*	ND (10-20)	Study secondary damage formation in fuel rods with simulated fretting defects
SUPER-RAMP III (NS, 1993-96)	PWR (ND)	ND (>40/>55)	PCI performance
TRANS-RAMP III (NS, 1993-95)	BWR (?)	ND	Same as TR IV

\*) NS = Not yet started  
ND = Not decided

A total of 20 8x8 type fuel rodlets made by ASEA-ATOM were tested by first being irradiated under cyclic power conditions in the R2 test reactor (the linear heat rate was alternated between about 25 and 40 kW/m every 65-70 days up to a burnup of about 10 or 20 Mwd/kgU) and then ramp tested to ramp terminal levels of mainly 40 to 50 kW/m. Failures developed when the ramp terminal level exceeded about 42 kW/m. Above 48 kW/m all rods failed. Two well-defined failure thresholds could be identified, one for the low-power irradiated rods and one for the high-power irradiated ones. No burnup dependence of the failure threshold was indicated within the range tested, 9 to 23 Mwd/kgU. Incipient (non-penetrating) cracks in the inner surface of the cladding were observed in some apparently non-defective fuel rods

The DEMO-RAMP I project was executed in 1979-82. The results have been described by Franklin et al [3]. The main objective of this program was to investigate the effects of two PCI remedies, annular pellets and niobia doping of the UO<sub>2</sub> on the ramp behavior, especially the fission-product release and the

pellet-cladding mechanical interaction (PCMI), of 8x8 type fuel rodlets made by BNFL and ASEA-ATOM. The use of hollow fuel pellets removed the hottest portion of the fuel and provided room into which the hot fuel could deform and the niobia doping gave large-grain, soft fuel pellets. The cladding of these rods originated from the same manufacturing lot as the cladding of the INTER-RAMP rods. The fuel rodlets were irradiated in a commercial power reactor to a burnup of about 15 Mwd/kgU, they were then ramp tested in the R2 test reactor. One of the rods was subjected to a "staircase" ramp, its power was increased in steps from 30 kW/m to 35, 40, ... 55, 60 kW/m. The remaining rods were ramped from 27.5 kW/m to between 46 and 61 kW/m. None of the rods failed

The SUPER-RAMP project was executed in 1980-83. The results have been described by Mogard & Heckermann [4] and Djurle [5]. The main objective of this project, which was co-sponsored by 20 organizations from 11 countries, was to make a valid contribution to the general understanding of the PCI phenomenon for commercial type LWR fuel rods at high burnup levels under power ramp conditions.

For the BWR subprogram\*) the more specific objectives were to

- Establish the PCI failure threshold for standard type test fuel rods on fast power ramping at burnup levels exceeding about 30 Mwd/kgU.
- Identify any change in failure propensity or failure mode as compared to the failure behavior at lower burnup levels.
- Establish a failure-safe reduced power ramp rate for passing through the PCI failure region.

The 16 8x8 type test fuel rods were produced by GE and KWU and had been base irradiated in commercial power reactors. Extensive pre- and post-ramp examinations were performed in STUDESVIK's and in KWU's hot cells. The power ramping was performed in the R2 test reactor. When the ramping was made from the low "conditioning" level of 18 kW/m the rods failed already beyond about 33 kW/m.

Extensive post-irradiation examinations were performed on the fuel rods tested.

In the SUPER-RAMP EXTENSION project, which was executed in 1984-86 9 further BWR fuel rods, manufactured by ASEA-ATOM and base irradiated in a commercial power reactor to about 30 Mwd/kgU, were ramp tested. The data have not yet been published.

\*) The PWR subprogram of the SUPER-RAMP project is discussed in Section 2 below

In the SUPER-RAMP II/9x9 project, executed in 1987-90, the failure boundary of ANF 9x9 type fuel rodlets, irradiated in a commercial power reactor to a burnup of 25 MWd/kgU, was determined.

The fuel rods were "conditioned" at 15 kW/m for 2 hours and then ramp tested to various ramp terminal levels for determination of the failure threshold. The ramp rate used was either 150+1300 W/cm,min (150 for the first part of the ramp) or about 100 W/cm,min. The fuel rods were then subjected to non-destructive and destructive examinations, including visual inspection, axial and radial gamma scanning, eddy current testing, profilometry, neutron radiography, gap squeeze measurements, fission gas release studies, clad inside inspection, metallography, ceramography, cladding hardness measurements, fuel density determination and burnup determination. The results have been described by Howe et al. [6].

## 2 RAMP RESISTANCE - PWR FUEL

The second of STUDSVIK NUCLEAR'S international fuel projects, OVER-RAMP, was executed in 1977-81. The results have been described by Hollowell et al. [7] and Djurle [8]. The overall objective was to increase the general understanding of the PCI phenomenon for commercial type PWR fuel rods under power ramp conditions. The main technical objectives were to

- Establish the power ramp failure threshold as a function of burnup.
- Determine the influence on the failure threshold of various design, material, pre-ramp irradiation and ramp testing parameters.
- Characterize failure mechanisms and pre-stages of fuel failure.
- Provide data for PCI failure analyses and predictive fuel modeling.

A total of 39 fuel rodlets, manufactured by KWU/CE and Westinghouse were first base irradiated, the KWU/CE rods in a commercial power reactor and the Westinghouse rods in BR3, a small power demonstration reactor, to burnups in the range 12 to 31 MWd/kgU and then ramped in the R2 test reactor. Among the rods there were nine groups with different combinations of design, material and base-irradiation parameters

The rods were ramp tested and extensive pre- and post-ramp examinations were performed in STUDSVIK's hot cells

In the SUPER-RAMP project, already discussed in Section 1 above, there was also a PWR subprogram. The objectives of that subprogram were to

- Establish the PCI failure threshold for standard type PWR test fuel rods on fast power ramping at burnup levels exceeding about 30 MWd/kgU and preferably 40 MWd/kgU.
- Identify any change in failure propensity or failure mode as compared to the failure behavior at lower burnup levels
- Establish any possible increase in failure resistance of selected candidate PCI remedy designs.

A total of 28 fuel rodlets, manufactured by KWU/CE and Westinghouse were base irradiated in the same reactors as those used in the OVER-RAMP project, discussed above. The rods could be divided into 6 groups including gadolinia fuel, fuel with large grain size pellets and fuel with annular pellets. The linear heat rating during the base irradiation varied considerably between the groups, from 9-21 kW/m to 20-27 kW/m. The burnups varied in the range 28-31 MWd/kgU to 41-45 MWd/kgU. The results appeared fully consistent within each group of fuel rods but showed large differences between groups. For some of the groups a comparison could be made with data from lower burnup fuel, tested in the OVER-RAMP project. The more important observations could be summarized as follows:

- The standard type PK1 and PK2 as well as the Gd-bearing PK4 rods all survived ramping up to the highest ramp terminal levels tested i.e. 48 - 50 kW/m. This PCI failure resistance seems surprising in view of the large clad strains and fission gas release fractions observed.
- The large grain PK6 rods failed beyond approximately 43 kW/m.
- The standard PW3 rods failed beyond approximately 38 kW/m.
- The annular PW 5 rods also failed beyond approximately 38 kW/m.
- No potentially life limiting high burnup effect was revealed as regards PCI behavior, since no declining trend in the PCI failure resistance was observed.

In order to investigate the difference between the various groups further in the SUPER-RAMP EXTENSION project, also discussed in Section 5 2 above, 4 further KWU rods were investigated. The results have not yet been published

There has been a considerable interest in the ramp resistance of PWR fuel after still higher burnups, above 40 or even above 55 MWd/kgU. Pre-project discussions regarding the prospective SUPER-RAMP III project are currently in progress

### 3 SAFETY-ORIENTED RAMP RESISTANCE STUDIES

In this series of fuel research projects (the INTER-RAMP, DEMO-RAMP II, TRANS-RAMP I, TRANS-RAMP II and TRANS-RAMP IV projects) it was demonstrated by means of power transient tests (intentionally interrupted power ramp tests) that when LWR test fuel rods were exposed to overpower ramps of increased severity, they exhibited a regular Pellet-Clad Interaction (PCI) failure progression. A higher transient peak power level resulted in an earlier fission product outleakage from the fuel rods. Stress corrosion cracks (SCC) initiated promptly on fast upramping, i.e. within the order of seconds and penetrated the cladding wall within about a minute. Depending on the actual power "over-shoot" and the time spent beyond the failure threshold, the transient passed consecutively through a number of power-time regions defining the progressive steps of the failure process.

Some of the LWR fault transients of the types that might be expected to occur once in a reactor year or once in a reactor lifetime carry a potential for causing PCI fuel clad damage or failure (i.e. through-wall crack penetration) on surpassing the PCI failure threshold. A question of prime concern is then whether a fast single transient of the type mentioned will result in fuel failure due to PCI, eventually followed by a release of radioactivity to the coolant.

In the INTER-RAMP (IR) Project, executed during 1975-79 [1,2], BWR fuel rods were subjected to power transients of varying "over-power" levels beyond the PCI failure threshold, where cladding failure and fission product release occur after a sufficient time. The results demonstrated a systematic time dependence of the fission product release to the coolant from the failed fuel rods. An increase in the power "over-shoot" of 5 kW/m caused a decrease of the time to fission product release by a factor of about 10.

In the DEMO-RAMP II (DRII) Project, 1980-1982 [9], BWR fuel rods of intermediate burnup levels were subjected to intentionally interrupted short-time power transients at linear heat ratings a few kW/m above the PCI failure threshold. The ramp rates were moderate, in the range of 40 to 220 W/cm, min. No cladding failures were detected after the transients but a large number of non-penetrating (incipient) cracks were observed. They had been formed very rapidly, within a minute. These cracks could be observed by destructive post-irradiation examinations only. The crack depths ranged from 10 to 60 percent of the cladding wall thickness.

In the TRANS-RAMP I (TRI) Project 1982-1984 [10], BWR fuel rods of intermediate burnup levels were subjected to simulated short time power reactor transients of a wide range of "over-powers" but at characteristic very fast ramp rates, in the range of 10 000 W/cm, min. The test results were similar to

the DR II results and permitted a tentative interpretation of the PCI failure progression in terms of well-separated power/time boundaries defining 1) crack initiation at the inside surface of the cladding, 2) through-wall crack penetration and 3) out-leakage of fission products to the coolant water.

In the TRANS-RAMP II (TRII) Project, 1984-1986 [11], PWR fuel rods of higher burnups, approximately 30 MWD/kgU, were subjected to short power transients corresponding to a steam line break event in PWRs. The PCI failure progression diagram obtained was quite similar to the one obtained from the TRI project for BWR fuel rods, indicating comparable times to failure for the two fuel designs, i.e. approximately one minute.

The time to initiation of SCC cracks was also found to be very much the same in the TRI and TRII projects, i.e. for both BWR and PWR designs, namely a few seconds after the transient passage of the PCI failure threshold.

However, the time to release of fission products to the coolant was seen to be strikingly different in the two projects. In the TRI project about 10-15 minutes elapsed between crack penetration and fission product release, while in the TRII project these events were actually coincident or separated by only a couple of minutes, depending on the severity of the transients. At the present stage of investigations it can not be firmly established whether this difference in time to fission product release is burnup related.

The crack initiation and penetration processes can only be detected by special hot cell laboratory or test reactor techniques. The delay of the fission product release indicates that in power reactors cladding failures that occur during fast transients and terminate before any outleakage of fission products may go undetected until manifested in later operational maneuvers.

In the TRANS-RAMP IV (TRIV) project, still in progress, the influence of non-penetrating (incipient) cladding cracks on the PCI failure resistance during an anticipated subsequent transient occurring later in life is studied.

Experience from the earlier STUDEVIK projects mentioned, as well as from power reactor operation, shows that non-penetrating cladding cracks form readily during certain short-time power transients and cracks initiate already within 5-10 seconds. However, it is conceivable that these non-penetrating (incipient) cracks will not propagate further during continued operation, owing to some passivation effect. The main purpose of the TRANS-RAMP IV project is to investigate experimentally the propensity for through-wall crack penetration of such initially non-penetrating (incipient) PCI cracks following a second power transient.

The irradiation tests were performed on 7 short fuel rodlets, refabricated from full-size PWR power reactor fuel rods. The rods had been irradiated to 20-25 MWd/kgU. Of these rods 3 were irradiated further in the R2 reactor after having been subjected to a first power ramp selected to give non-penetrating PCI cracks. After a continued base irradiation (of about 4 MWd/kgU) the rods were subjected to a second power ramp in order to determine the residual time to PCI failure. The rods are now undergoing a series of extensive non-destructive and destructive examinations.

A corresponding BWR project, TRANS-RAMP III, (TRIII) has been contemplated but is awaiting the completion of the TRIV project.

STUDSVIK NUCLEAR has also initiated some in-house R&D activities in this connection. There is a need for an improved LWR fuel design, resistant not only to operational power maneuvers but also to off-normal type high power transients. STUDSVIK NUCLEAR has been working on such a potential remedy design, rifled cladding, for many years [12, 13]. One approach, using a combination of rifled cladding and graphite coated fuel pellets under otherwise normal design conditions has so far demonstrated 100% failure resistance under very severe power transient test conditions. Two fuel rods were irradiated up to 10 MWd/kgU in the R2 reactor and were then subjected to power increases as follows: One rod by 35 kW/m up to 60 kW/m with a rate of power increase of 100 W/cm, min. The other rod was subjected to a power increase of 30 kW/m up to 58 kW/m with a rate of 3000 W/cm, min calorimetric power (10000 W/cm, min generated power). Adopting a hold time of 12 hrs no failures were experienced. The first rod was examined destructively with no signs of defects. A low fission gas release of only 9% was measured. The second rod, which had already been transient tested, was reinserted for a continued base irradiation up to 21 MWd/kgU, then it was again subjected to a transient under the same fast rate of power increase up to 58 kW/m. Again no failure occurred after a 12 hrs hold time. On both occasions the recorded diametral expansion was about 15 micrometers. After these double transient events the measured fission gas release still remained quite low, about 16%. Although the test results are few so far, the remedy approach adopted seems promising. Fuel modeling has also indicated superior behavior in this and other respects [14, 15].

#### 4 STUDIES OF "LIFT-OFF" PHENOMENA

When LWR fuel is used at higher and higher burnups the question of how the fuel might behave when the end-of-life rod internal pressure becomes greater than the system pressure attracts a considerable interest.

On one hand end-of-life overpressure might lead to clad outward creep and an increased pellet-clad gap with consequent feedback in the form of increased fuel temperature, further fission gas release, further increases in overpressure etc. On the other hand increased fuel swelling might offset this mechanism.

In connection with such considerations STUDSVIK NUCLEAR initiated the two international Rod Overpressure Experiments (the ROPE I and ROPE II projects). Before the start of the first of these projects a pilot experiment was performed as a limited in-house R&D activity in order to investigate the ability to detect the phenomena of interest: the ROPE Pre-project.

In the ROPE pre-project, which has been described by Schrire [16], two fuel rodlets from segmented fuel rods from the Oskarshamn 2 BWR with the same irradiation history (burnup up to 27 MWd/kgU) were used. One of the rodlets was refilled (pressurized with a gas mixture to simulate high end-of-life fission gas release), the other one was used as a reference. The primary objectives of the experiment were

- a) obtain some preliminary information on the behavior of BWR fuel rods operated with an internal pressure in excess of the system pressure
- b) estimate the magnitudes of the most important experimental parameters for the ROPE I project
- c) develop and test some of the experimental techniques to be used in the ROPE I project.

The test rods were characterized by gamma scanning, pellet-clad gap measurements and dimensional measurements (before and after the pressurization of the overpressure rod). The overpressure rod was then irradiated in an in-pile loop in the R2 test reactor for a total of 475 hrs. The peak linear heat rating during most of the experiment was about 30 kW/m. The loop system pressure was varied systematically between 80 and 140 bar. Noise analysis was carried out at each pressure level. Post-irradiation examination included the same type of measurements as before the irradiation as well as fission gas release measurements.

The main purpose of the experiment was to check the ability to perform the international projects planned. One of the conclusions drawn was that the ROPE I project should aim for a lower rod linear heat rating than that selected originally.

The purpose of the first of the international projects, ROPE I, was to investigate the behavior of BWR fuel rods. Three ABB-ATOM fuel rods, irradiated in the Ringhals 1 reactor to a burnup of 30.8 MWd/kgU were tested.

The irradiated fuel rods were pressurized to give hot internal pressures of approximately 185, 135 and 85 bars, respectively. The system pressure is 85 bars, so the rod overpressures were 100 bars, 50 bars and 0. The clad creepout and the time dependent changes in fuel rod conductance were investigated as functions of rod overpressure.

The fuel rods were irradiated one at a time during three 3-day cycles in an instrumented rig in an in-pile loop in the R2 reactor. During these cycles the fuel rod thermal response was determined on-line by noise analysis. Between the 3-day cycles the rods were irradiated together for a total of six 15-day cycles without the on-line measurements mentioned. In the intermissions between these cycles, profilometry measurements were performed in the R2 reactor pool. After irradiation, the rods underwent non-destructive and destructive examinations. The results have not yet been published.

In the second of these international projects, ROPE II, PWR fuel is being investigated in the same manner. This project has recently been started.

## 5 STUDIES OF DEFECT FUEL BEHAVIOR

A new type of project, the Defect Fuel Degradation Experiment (DEFEX), is currently under discussion. This project will consist of an experimental study in the R2 test reactor of secondary damage formation in BWR and PWR rods with simulated fretting defects. The project will be presented at an forthcoming IAEA meeting.

### REFERENCES

- [1] THOMAS G, The Studsvik INTER-RAMP Project: An International Power Ramp Experimental Program. J Nucl Materials 87(1979), p. 215-226. Also Proc KTG/ENS/JRC Meeting on Ramping and Load Following Behaviour of Reactor Fuel. Petten, The Netherlands, Nov 30 - Dec 1, 1978. H Röttger, (Ed.) (EUR 6623 EN, p. 95-106.)
- [2] MOGARD H et al., The Studsvik INTER-RAMP Project - An International Power Ramp Experimental Program. ANS Topical Meeting on LWR Fuel Performance. Portland, Oregon, USA, April 29 - May 3, 1979, p. 284-294. (DOE/ET/34007-1 )
- [3] FRANKLIN D G, DJURLE S, HOWL D, Performance of Niobium-Doped Fuel in Power-Ramp Tests. Nuclear Fuel Performance. Stratford-upon-Avon, UK, 25-29 March 1985. Proc BNES, London 1985. Vol 1, p 141-147

- [4] MOGARD H, HECKERMAN H, The International SUPER-RAMP Project at Studsvik Proc. ANS Topical Meeting on Light Water Reactor Fuel Performance, Orlando, Fla, USA, 21-24 April 1985. ANS, LaGrange Park, Ill 1985. (DOE/NE/34130-1, Vol.2, p 6-17 to 6-33).
- [5] DJURLE S, Final Report of the SUPER-RAMP Project. U.S. Department of Energy 1985. (DOE/ET/34032-1).
- [6] HOWE T, DJURLE S, LYSELL G, Ramp Testing of 9x9 BWR Fuel. ANS/ENS International Topical Meeting on LWR Fuel Performance, Fuel for the 90's, Avignon, France, 21-24 April 1991, p. 828-837.
- [7] HOLLOWELL T E, KNUDSEN P, MOGARD H, The International OVER-RAMP Project at Studsvik. Proc ANS Topical Meeting on LWR Extended Burnup - Fuel Performance and Utilization. Williamsburg, Va, USA, 4-8 April 1982, Vol. 1, p 4-5 to 4-18.
- [8] DJURLE S, The Studsvik OVER-RAMP Project. Studsvik Energiteknik AB, Sweden 1981. (STUDSVIK-STOR-37).
- [9] MOGARD H, KNAAB H, BERGENLID U, LYSELL G, The International DEMO-RAMP II Project at Studsvik. Nuclear Technology 69 (1985):2, p. 236-242.
- [10] MOGARD H et al., The International TRANS-RAMP I Fuel Project. IAEA Technical Committee Meeting on Fuel Rod Internal Chemistry and Fission Product Behaviour, Karlsruhe, FRG, 11-15 November, 1985. (IAEA IWGFPT/25, p. 157-167.)
- [11] MOGARD H, HOWL D A, GROUND M, The International TRANS-RAMP II Fuel Project - A Study of the Effects of Rapid Power Ramping on the PCI Resistance of PWR Fuel. ANS Topical Meeting on LWR Fuel Performance. Williamsburg, Va, USA, 17-20 April, 1988. p. 232-244.
- [12] MOGARD H et al., Irradiation Testing of an Advanced Fuel Cladding Designed for Load-Follow and Extended Burnup Operation. Studsvik Energiteknik AB, Sweden 1986. (STUDSVIK-86/1.)
- [13] MOGARD H, KJAER-PEDERSEN N, Improved PCI and FGR Performance of LWR Fuel Using Rifled Cladding IAEA Specialists' Meeting on Fuel Performance at High Burnup for Water Reactors, Studsvik, Sweden 5-8 June, 1990.(IWGFPT/36, p. 147-159.)
- [14] KJAER-PEDERSEN N, MOGARD H, Controlling Overall Fission Gas Release by Controlling Axial Gas Mixing IAEA Specialists' Meeting on Water Reactor Fuel Element Computer Modelling in Steady State, Transient and Accident Conditions Preston UK September 18-22, 1988

- [15] MONTGOMERY R O, RASHID Y R, KJAER-PEDERSEN N, Theoretical Evaluation of Rifled Cladding for LWR Fuel. Nucl. Eng. & Design 132(1992), p. 309-316.
- [16] SCHRIRE D, Rod Overpressure Experiment (ROPE) - Pre-Project. Studsvik Energiteknik AB, Sweden 1987. (STUDSVIK/NF(P)-87/43).

## METHODOLOGY OF IN-PILE EXPERIMENTS INCLUDING EXPERIMENTAL STUDIES OF VVER-1000 REFABRICATED FUELS AT THE MIR RESEARCH REACTOR

Yu.K. BIBILASHVILI\*, A.V. GRACHEV\*\*,  
V.V. NOVIKOV\*, V.P. SMIRNOV\*\*, A.V. SMIRNOV\*\*

\*All-Union Scientific Research Institute  
of Inorganic Materials,  
Moscow

\*\*Research Institute of Atomic Reactors,  
Dimotrovgrad  
Russian Federation

### Abstract

This paper gives some indications on the programme of reirradiation of WWER fuel which has been initiated in the experimental reactor MIR. It gives also a description of the process used for refabrication of fuel rods from power reactors.

### 1. INTRODUCTION

One of the main directions for improving VVER fuel cycle performance is to increase burn-up. At the first stage of strategy of reaching extended fuel burn-up an increase of burn-up to  $\sim 40$  MW.day/kg  $UO_2$  was considered (conversion from two year to three year cycle); at the next stage a further growth to  $\sim 55$  MW.day/kg  $UO_2$  was envisaged through the use of integral fuel burnable absorber. The realization of the plan is also to include

- studies of corrosion, fretting corrosion and irradiation induced growth and creep of cladding, including FA batches constituted for the fourth year of operation after a three year cycle;
- assessment of fuel reliability under transient conditions;
- investigation of fuel condition and FGR at high burn-up;
- validation of using integral fuels burnable absorber.

PCI can be expected not to result in severe events during fuel operation at extended burn-up since a decrease in average linear neat generation rate and small power variations due to reactivity decrease at those burn-ups do not increase the danger of fuel failure. However, the possible accumulation of cladding damage during operation with a considerable number of transients under conditions of an aggressive environment requires this phenomenon to be taken into account when validating fuel serviceability.

This circumstance makes it necessary to discuss the following directions of experimental investigations to validate fuel operation at extended burn-up:

- experimental fuel irradiation at power ramps according to a programme taking account of power load follow during a long-term operation of fuel;

- instrumented in-pile experiments with fuels refabricated from standard ones irradiated to high burn-up at NPP.

This programme embraces a wide range of issues: 1) requirements on in-pile irradiation conditions and changes in loads on fuels, 2) enumeration of characteristics to be controlled with adequate instrument provision, 3) development of technology for experimental fuel manufacture from standard NPP fuels, 4) post-irradiation investigations of fuels, validation and correction of computer codes etc.

## 2. CHOICE OF METHODS TO PROVIDE FOR INCREASE OF POWER AND ASSESSMENT OF POWER RAMP PARAMETERS

At the first stage of the work investigations were conducted to support "MIR" experiments with programmed heat rating variations in VVER-1000 type fuels. It is shown that the most favourable way of

power increase is to use reactor control elements taking account of the uniformity of load distribution on all fuel elements of an experimental FA. The maximum linear heat generation rates for fuels 4.4% enriched can reach 750 W/cm - 300 W/cm in the burn-up range  $\sim 10-30$  MW.day/kg while for fuels of 6.5% enrichment designed to study fuel behaviour at extended burn-up the maximum heat generation rates can rise to  $\sim 500$  W/cm at  $\sim 45$  MW.day/kg  $UO_2$ .

Investigations carried out in a physical reactor mock-up as well as in-pile experiments show that in principle a factor of 2-3 increase of power is feasible in experimental fuel assembly during a period not more than 10 min. To achieve this in the initial condition control elements that are close to loop channel must be lowered into a core while in the process of experiment they must be fully withdrawn during minimum possible time with the compensation by regulators sited in other core areas. Under conditions when regulators that are close to experimental channel are immersed the initial heat rating of experimental FA can be provided only if the loop channel is surrounded with "fresh" operating FAs. This results in a significant increase of efficiency of the indicated regulators and the need of a careful selection of automatic safety system elements designed for the compensation of the former at the initial stage of a reactor experiment. The needed maximum speed of a neutron flux redistribution required some changes to be introduced into the system governing control rods; their aim is to provide a quicker control of a reactor.

## 3. REFABRICATION AND TEST OF FUEL RODS

Aside from experimental fuel rods enriched to 4.4% and 6.5% the whole irradiation and testing cycle of which takes place in

"MIR" presently investigations have been started to study experimental fuels refabricated from standard NPP fuel elements irradiated to extended burn-up. Depending on the length the experimental fuel elements are divided into groups 0.25 m and 1 m long. The flow sheet of experimental fuel refabrication is shown below.

VVER-1000 fuels are selected for refabrication based on the results of non-destructive and destructive materials science investigations. The certificate for VVER-1000 fuel rod selected for refabrication contains the main data of plant-manufacturer, declared data on fuel operation history, characteristics of fuel and cladding, the extent and condition of a fuel-clad gap, condition of fuel column, pressure and composition of a filler gas, condition of welds and so on at the moment of refabrication.

The general refabrication flow sheet is as follows:

- selected fuel rod is cut into needed lengths in a hot chamber;
- from the ends of prepared fragments fuel is removed;
- cladding is prepared for welding;
- cladding is assembled with prepared end pieces;
- the first seam is welded and refabricated fuel rod is filled with helium;
- fuel fragment is subject to final sealing and the second seam is welded (if pressurized welding is used the fuel rod is filled with helium directly in a welding unit when it is filled with excess pressure);
- refabricated fuel element is subject to visual inspection and leak-tightness control.

Requirements on fuel element assemblage. The operation of fuel element fragments assembling with end-pieces-plugs involves placing

rod-type plugs inside cladding so that close contact could be provided between the plug and cladding.

Welding of irradiated fuel elements. It is accomplished using a remote semi-automated argon unit with a non-consumable electrode by circumferential seam or end fusion. If design plants and specifications for fuel elements contain special requirements, a fuel element is subject to drying prior to making the second seam before filling with helium.

Irradiated zirconium alloy claddings are only welded using a special additional nozzle to protect the weld against the environment. Temper colours on welds are not permitted.

If some defects of welded joints are revealed (the exception is single surface voids the size of which is not more than 7% of the seam section) welded joints are rejected. The second welding of joints is not allowed. Possible defects of welded joints are cracks, inclusions, large voids, poor penetration, metal splashing and so on.

The pressure required for welding is specified in design specifications for refabricated fuel.

Argon or helium gases are used as an operating environment.

Drying and helium impregnation of fragments. Drying of fuels is specially specified and accomplished in a unit in vacuo not less than  $1 \times 10^{-2}$  mm Hg.

Dried fuel fragments are impregnated by letting in helium at an excess pressure up to 0.1 atm and holding a fuel element in helium for 15 min. Before welding as impregnated fuel elements are not allowed to be held in air for more than 30 min.

Leak-tightness control. The leak-tightness of irradiated fuels is controlled with a helium mass-spectrometer by the high

pressure chamber method. The maximum permissible egress of helium from fuel rods is specified in design specifications.

The condition of refabricated fuels is assessed with non-destructive methods of investigation: gamma-scanning, eddy-current tests and profilometry of cladding, x-ray radiography, length measurement; visual inspection. The results are written down in a certificate for a refabricated fuel element and are subsequently used.

At present pilot batches of refabricated fuels have been produced. Using fuels of  $\sim 36$  MW.day/kg UO<sub>2</sub> burn-up preliminary experiments with power increases were conducted.

#### CONCLUSION

In the research reactor "MIR" experimental investigations were started to assess VVER fuel behaviour under various operating conditions, including also extended burn-up. A complex of work on design-physical modeling and instrumented support of VVER fuel studies are carried out.

Process of experimental fuel fabrication from standard irradiated fuels of NPPs has been worked out; it allows practically a retention of a filler gas and distribution of fuel fission products during operation. In-pile experiments with power ramps indicated their feasibility under specified conditions of programmed fuel loading in a wide range of fuel burn-up.

#### SOME EXPERIMENTAL RESULTS OF INVESTIGATIONS ON THE NUCLIDE COMPOSITION AND BURNUP FRACTION OF VVER-1000 STANDARD FUEL

A.V. SMIRNOV\*, A.P. CHETVERIKOV,  
V.V. NOVIKOV\*\*, V.N. PROSELKOV\*\*\*

\*Research Institute of Atomic Reactors,  
Dimitrovgrad

\*\*All Union Scientific Research Institute  
of Inorganic Materials,  
Moscow

\*\*\*I.V. Kurchatov Institute of Atomic Energy,  
Moscow

Russian Federation

#### Abstract

Fission and technological gases release into the free fuel rod volume has been measured by means of  $\mu$ -spectroscopy and mass-spectroscopy. Fuel rods for examination were taken from fuel assemblies with burnups ranging from 20 to 50 MW.d/Kg U.

It was found out that amount of fission gas release for intact fuel rods is not significant, e.g. the share of released Kr-85 has not exceeded 2.5%. In some cases the increased fission gas release was observed for defected fuel rods.

With the use of irradiation history data, information on fuel rod design and results of fuel rod parameters measurements in hot cells, calculations of fission gas release into rod free volume were carried out. Results of calculations and measurements were compared.

#### INTRODUCTION

Thermo-physical burnup calculations of fuel rods  $50 \frac{\text{MW d}}{\text{kg U}}$  and more, simulation of emergency situations and their consequences for the environment, evaluation of spent fuel reprocessing conditions and its long storage require experimentally authentic information about nuclide composition and burnup of the fuel and about distribution of transuranium elements (TUE) and fission products (FP).

Scientific and practical significance of this problem allowed within the programme of full-scale material science investigations of the VVER-1000 spent fuel assemblies, planning and determination of fuel burnup fraction and nuclide composition by mass spectrometry and radiochemical methods, research of TUE and FP distribution over the height and radius of the fuel column in a fuel rod, defining quantitative relationships between TUE FP accumulation and fuel burnup.

The results of performed investigations are presented in the paper.

#### FUEL CHARACTERISTICS AND RESEARCH METHODS

100 fuel with the initial enrichment 3.3, 3.6, 4.4 % for U-235 from 2 fuel assemblies of VVER-1000 was investigated. Fuel assembly N 4 has been operated in the fifth block of the New-Voronezh nuclear power plant (NPP) up to the design burnup  $\frac{\text{MW d}}{\text{kg U}}$  45. Fuel assembly N 6 in the first block of the South-Ukrainian NPP up to the design burnup  $\frac{\text{MW d}}{\text{kg U}}$  37.

The time of fuel cooling in assemblies N 4 and N 6 made up 3.4 and 4.3 years, respectively.

To investigate the nuclide composition and to determine the burnup over the fuel rod height, fuel specimens, 10 mm long, were selected from different levels of a fuel column.

To measure the burnup and nuclide composition there were selected samples over the fuel rod radius from the fuel column central part (level of 1970 mm from the fuel element bottom) only assemblies N 6 by drilling out the fuel using drills with a successively increasing diameter.

The fuel specimens were dissolved in nitric acid (concentration 8 mol/l) while heating for 3-5 hours. The methods of ion-exchange and extraction chromatography were used to extract uranium, plutonium, americium, cerium, cesium, cerium and neodymium for mass-spectrometry analysis. Isotopic composition of the extracted elements was determined at mass spectrometers. Loading of the element under analysis into the ions source made up 0.1-5  $\mu\text{g}$ . The concentration of these nuclides was found by means of isotopic dilution with mass spectrometric termination of the analysis. Standard solutions of these elements with U-235, Pu-242, Am-243, Cs-133, Ce-140 and Nd-146 enrichment up to 95-99.9 %, the concentration of which possessed the error of 0.5 % were used as marks. Cerium concentration was found by the alpha-spectrometry method combined with the mass spectrometry isotopic analysis.

Fuel burnup was defined by 2 methods:

according to change in isotopic relationships of heavy atoms (heavy atoms method (HAM)) and according to fission products accumulation (fission products method (FPM)). Use was made of the calculated equations of fuel isotopic composition change during fuel irradiation in the reactor for HAM burnup determination.

Isotopes of Cs (133 and 137), Ce (140 and 142) and Nd (143-146) were applied as monitors in calculating the FPM burnup.

Predecessors in these isotopes decay chain have short life. The chain with a mass number 144 including Ce-144 is an exception. In this case correction was introduced for Ce-144 content into the measured quantity of Ce-144 in fuel specimens by the moment of analysis.

Decay of Cs-137 was also taken into account by introducing the appropriate correction. Due to small value of the effect, influence of radiation capture on the burnup monitor accumulation was neglected except for Cs-133, Nd-143 and Nd-145. While determining the Cs-133 burnup a loss correction of this isotope in accordance with the measured Cs-134 content was introduced. The burnup for Nd isotopes was calculated proceeding from the total accumulation of Nd-143+144 and Nd-145+146. The value of efficient fission product releases—burnup monitors—was used during calculations.

#### EXPERIMENTAL RESULTS

Tabs. 1-5 present the results of burnup determination. It is clear that the full burnup values obtained by different methods within the errors agree between each other.

The burnup values at opposite ends of a fuel rod differ insignificantly and are considerably less than those in the centre of a fuel rod (fuel element N 11,307). This agrees well with the results of non destructive fuel rods investigations by gamma spectrometry methods (Fig.1).

Fig.2 shows the experimental results of burnup over the fuel rod radius from Tabs.3-5. Fuel burnup over the radius is not same. At the periphery the fuel burnup is 1.15-1.20 times higher than in the centre. Non-uniformity increases with growth of the fuel burnup.

Increase of fission fractions for U-238 and Pu-239 is observed in estimation of U-235, U-238, Pu-239 contributions

Table 1

Nuclides content and fuel specimens burnup of fuel assembly-N<sup>o</sup>6 by the end of irradiation, kg/t uranium (initial fuel U-235 enrichment 3.3%)

Parameter	Cut place (distance from the lower face)			
	Fuel element 11		Fuel element 253	
	1800 mm	100 mm	3420 mm	1970 mm
Burnup:				
PPM	47.5(9)*	29.1(6)	31.0(6)	39.9(8)
HAM	47(3)	29(2)	30(2)	38(2)
Including: U-235	22.26	17.18	17.19	18.48
U-238	2.94	1.75	1.82	2.36
Pu-239	18.80	8.80	9.56	14.88
Pu-241	2.84	0.79	0.94	1.96
Content of nuclides:				
U-235	6.14(5)	12.35(9)	11.58(7)	8.80(6)
U-236	4.20(4)	3.05(3)	3.81(4)	6.23(6)
U-238	932.1(9)	947.9(9)	946.9(10)	937.3(8)
Pu-238	0.190(9)	0.075(5)	0.066(3)	0.164(8)
Pu-239	5.57(7)	4.99(5)	4.91(6)	5.38(5)
Pu-240	2.39(2)	1.63(2)	1.70(2)	2.19(2)
Pu-241	1.56(2)	0.93(1)	0.96(1)	1.38(2)
Pu-242	0.74(1)	0.240(8)	0.280(6)	0.53(1)
sum	10.45(10)	7.86(8)	7.95(8)	9.64(10)
(Am-241) · 100	14	9	9	12
(Am-243) · 100	20.2(10)	4.4(2)	4.6(2)	13.3(7)
(Cm-242) · 100	2.2(12)	1.0(5)	1.2(6)	1.9(8)
(Cm-244) · 100	6.8(7)	0.55(6)	0.75(7)	3.4(4)
(Cm-245) · 100	0.48(15)	0.024(9)	-	-
(Cm-246) · 100	0.08(4)	0.0014(7)	-	-

\* Here and later the errors which values refer to the last significant figures of the corresponding magnitudes are presented in brackets. The errors are calculated for the confidence probability 0.95

Table 2  
Nuclides content and fuel specimens  
burnup of fuel assembly-№4 by the end of irradiation,  
kg/t uranium

Parameter	Cut place (distance from the lower face)					
	F/r 307 (3.6%)		F/r 317 (3.6%)		F/r 61 (4.4%)	F/r 257 (4.4%)
	1800mm	1070mm	3420mm	1850mm	1850mm	1850mm
<b>Burnup:</b>						
FPM	52.4(11)	53.1(12)	32.2(7)	53.9(12)	46.9(9)	51.0(11)
HAM	52(3)	53(3)	33(2)	52(3)	45(3)	50(3)
<b>Including:</b>						
U-235	26.11	26.31	18.41	26.95	26.20	28.25
U-238	3.44	3.49	2.16	3.45	2.96	3.29
Pu-239	18.09	18.54	10.11	17.72	13.34	15.36
Pu-241	4.27	4.36	2.22	4.04	2.65	3.25
<b>Content of nuclides:</b>						
U-235	4.35(3)	3.69(2)	13.03(10)	3.60(4)	11.74(9)	8.80(7)
U-236	4.92(3)	6.38(4)	4.11(4)	4.82(3)	5.33(6)	6.23(6)
U-238	927.5(8)	926.7(10)	941.5(7)	927.6(11)	927.1(10)	923.5(9)
Pu-238	0.31(2)	0.32(2)	0.110(6)	0.31(2)	0.27(2)	0.32(2)
Pu-239	5.00(5)	5.10(5)	5.11(5)	5.18(4)	5.64(6)	5.38(7)
Pu-240	2.62(3)	2.73(2)	1.77(2)	2.67(3)	2.29(3)	2.55(3)
Pu-241	1.64(2)	1.67(1)	1.05(1)	1.72(2)	1.51(2)	1.60(1)
Pu-242	1.12(1)	1.16(1)	0.260(4)	1.19(1)	0.560(9)	0.79(1)
sum	10.70(10)	10.98(11)	8.29(7)	11.07(10)	10.27(12)	10.64(14)
(Am-241)•100	17	16	6	21	10	14
(Am-243)•100	28.7(15)	29.1(14)	4.9(2)	30.9(16)	15.2(7)	20.8(10)
(Cm-242)•100	9(4)	9(4)	3.0(15)	9(5)	6(3)	6(3)
(Cm-244)•100	12.9(11)	11.7(10)	0.80(8)	13.1(12)	4.3(4)	7.8(10)
(Cm-245)•100	-	0.78(10)	0.034(12)	-	-	-
(Cm-246)•100	-	0.22(12)	0.0026(14)	-	-	-

Table 3  
Nuclides content and burnup of fuel assembly  
№5 specimens cut over the fuel element radius by the  
end of irradiation, kg/t uranium (fuel element 11, section 1).  
(Initial U-235 enrichment 3.3%, level of 1970 mm from the  
fuel element bottom)

Parameter	Cut place (distance from f/r axis)			
	1.1-2.5	2.5-3.05	3.05-3.65	3.45-3.85
<b>Burnup:</b>				
FPM	45.2(8)	48.2(9)	51.9(9)	54.5(10)
HAM	45.5(3)	45(3)	52(3)	55(4)
<b>Including:</b>				
U-235	21.50	22.47	23.26	23.49
U-238	2.31	3.00	3.28	3.50
Pu-239	17.74	19.93	21.87	23.89
Pu-241	2.69	3.26	3.60	4.04
<b>Content of nuclides:</b>				
U-235	6.05(5)	5.47(4)	4.05(4)	4.41(5)
U-236	4.90(3)	4.66(4)	4.45(5)	4.25(3)
U-238	933.7(8)	930.3(10)	926.5(9)	923.3(9)
Pu-238	0.27(2)	0.25(2)	0.27(2)	0.26(3)
Pu-239	5.38(5)	5.42(5)	5.91(6)	5.97(8)
Pu-240	2.42(3)	2.50(3)	2.73(2)	2.86(3)
Pu-241	1.35(1)	1.40(1)	1.55(1)	1.85(2)
Pu-242	0.760(9)	0.92(1)	1.00(1)	1.11(1)
sum	10.17(12)	10.49(9)	11.55(12)	12.07(13)
(Am-241)•100	10	11	13	16
(Am-243)•100	16.8(6)	18.2(9)	22.5(10)	28.1(15)
(Cm-242)•100	2.0(5)	2.2(11)	2.5(12)	2.5(14)
(Cm-244)•100	7.1(7)	3.5(5)	10.2(10)	12.0(11)
(Cm-245)•100	0.53(15)	0.54(21)	0.72(20)	0.90(27)
(Cm-246)•100	0.11(1)	0.11(1)	0.12(1)	0.12(1)

Table 4

Nuclides content and burnup of fuel assembly-N<sup>o</sup>6 specimens cut over the fuel element radius by the end of irradiation, kg/t uranium (fuel element 253, section 2). (Initial U-235 enrichment 3.3%, level 1970 mm from the fuel element bottom)

Parameter	Cut place (distance from f/r axis), mm		
	1.1 - 2.0	2.0 - 2.6	3.45 - 3.65
FPH	37.6(7)	41.0(9)	40.3(10)
HAM	30(2)	40(2)	44(2)
Including:			
U-235	19.99	20.12	20.56
U-238	2.36	2.51	2.75
Pu-239	13.90	15.49	17.97
Pu-241	1.70	2.03	2.57
Content of nuclides:			
U-235	8.17(7)	7.87(6)	7.55(7)
U-236	4.43(4)	4.61(4)	4.49(3)
U-238	939.2(10)	936.7(10)	932.4(9)
Pu-238	0.27(2)	0.21(2)	0.180(9)
Pu-239	5.44(5)	5.69(4)	6.17(6)
Pu-240	2.33(2)	2.35(2)	2.49(3)
Pu-241	1.33(1)	1.45(1)	1.64(2)
Pu-242	0.550(7)	0.610(5)	0.700(12)
sum	9.92(10)	10.31(9)	11.18(12)
(Am-241)*100	8	11	18
(Am-243)*100	9.0(5)	12.1(7)	21.2(10)
(Cm-242)*100	1.5(7)	2.0(10)	2.6(13)
(Cm-244)*100	5.9(6)	6.2(7)	8.5(7)
(Cm-245)*100	0.40(13)	0.42(14)	-
(Cm-246)*100	0.06(3)	0.06(3)	-

Table 5

Nuclides content and burnup of fuel assembly-N<sup>o</sup>6 specimens cut over the fuel element radius by the end of irradiation, kg/t uranium (fuel element 60, section 3). (Initial U-235 enrichment 3.3%, level 1970 mm from the fuel element bottom)

Parameter	Cut place (distance from f/r axis), mm			
	1.1-2.0	2.0-2.6	2.6-3.45	3.45-3.85
Burnup:				
FPM	41.1(8)	44.2(10)	46.0(10)	46.5(11)
HAM	42(3)	44(2)	46(3)	48(3)
Including:				
U-235	21.07	21.19	21.69	21.54
U-238	2.59	2.72	2.86	3.00
Pu-239	15.69	17.07	18.30	20.01
Pu-241	2.18	2.48	2.77	3.13
Content of nuclides:				
U-235	6.83(6)	6.53(6)	6.33(6)	6.40(4)
U-236	4.70(3)	4.87(4)	4.58(4)	4.66(3)
U-238	936.9(11)	934.6(9)	932.5(9)	929.4(10)
Pu-238	0.26(2)	0.27(2)	0.27(2)	0.28(2)
Pu-239	5.14(6)	5.37(5)	5.54(5)	5.88(6)
Pu-240	2.44(3)	2.51(3)	2.50(2)	2.60(3)
Pu-241	1.31(1)	1.38(1)	1.50(1)	1.62(2)
Pu-242	0.630(8)	0.710(9)	0.780(6)	0.850(5)
sum	9.78(11)	10.24(10)	10.59(11)	11.23(11)
(Am-241)*100	10.5	12	15	20
(Am-243)*100	11.7(6)	14.2(7)	18.1(9)	25.5(12)
(Cm-242)*100	1.2(6)	1.7(8)	2.4(12)	3.5(17)
(Cm-244)*100	6.4(7)	6.7(7)	7.6(8)	10.1(10)
(Cm-245)*100	0.53(15)	-	-	-
(Cm-246)*100	0.07(4)	-	-	-

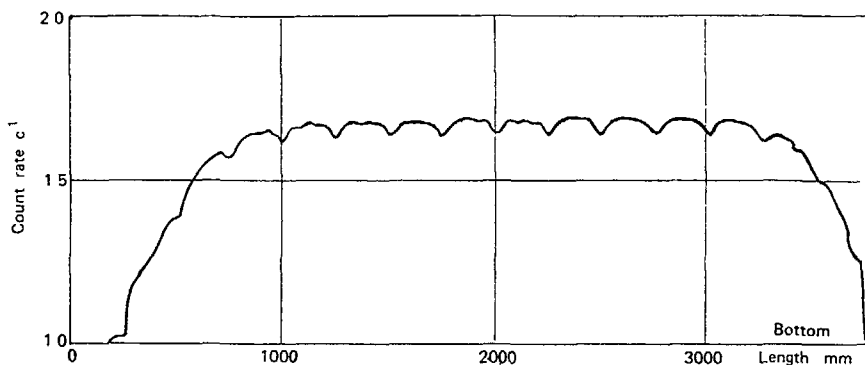


FIG 1 Distribution of Cs nuclide activity along fuel rod No. 159 of fuel assembly No. 4

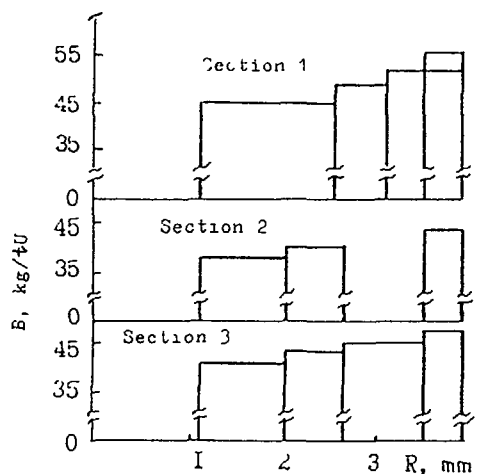
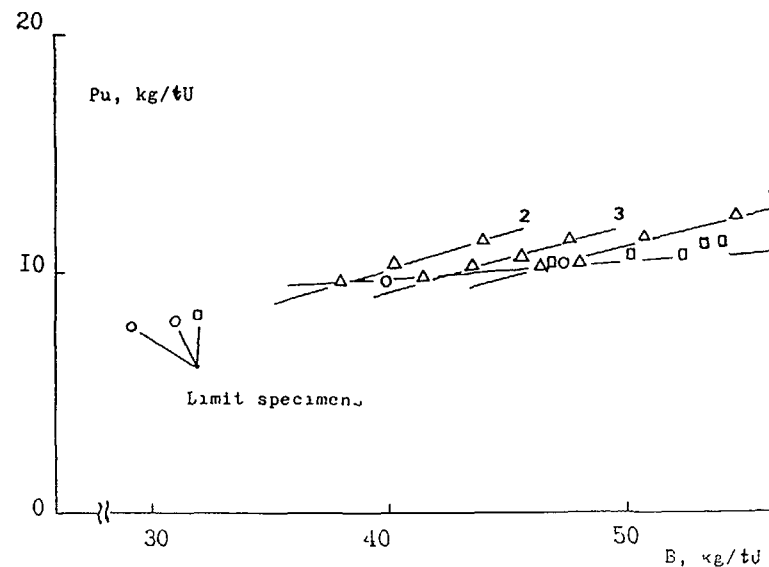


FIG 2 Experimental burnup distributions over the fuel element radius

to full burnup in movement towards the fuel rod centre over the height and outer layer over the fuel rod radius. Thus, the fission relationship of U-238 and Pu-239 to U-235 in the specimen from the centre is 1.13 and 1.25 times greater than in the limit specimen (fuel rod 307). These relationships

for specimens of the outer and inner fuel rod layers differ by a factor of 1.14 and 1.24, respectively (section 1). Pu accumulation (see Tables and Fig.3) in specimens over the fuel element height will rise with burnup growth and has a directly proportional character in the investigated burnups range. Specimens of limit fuel rod regions are an exception. Increase in Pu accumulation from the centre to the periphery of a fuel rod (Fig.4) is observed, this non-uniformity rising with burnup growth. This relationship is equal to 1.19 for section 1.



- - specimens of assembly 6,
- - specimens of assembly 4,
- △ - specimens of assembly 6 over the radius

FIG 3 Plutonium accumulation versus fuel burnup

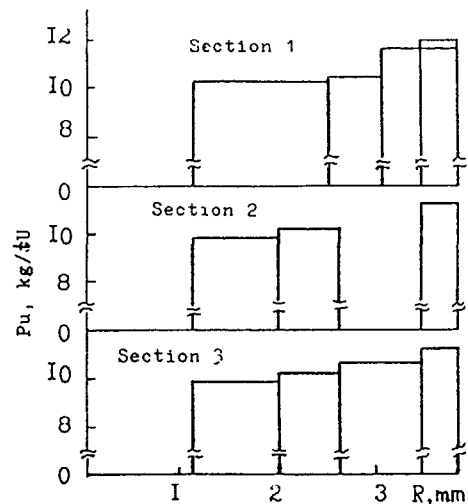


FIG. 4. Experimental distributions of plutonium accumulation over the fuel element radius.

Figs.5,6 show the regularities of separate Pu isotopes accumulation. In case of even isotopes, less accumulation values for VVER-1000 are observed.

Comparison of investigation results for Pu accumulation over the fuel rod height and radius versus the burnup fraction is of interest. If for even isotopes the dependence of accumulation on burnup is the same in the specimens selected both over the fuel rod height and radius, then fissionable Pu isotopes (Pu-239 and Pu-241) are characterized by abrupt accumulation growth from the centre to the periphery over the fuel rod radius. Thus, there is change of isotopic Pu composition along with increase in Pu accumulation from the centre to the periphery. This tendency is better illustrated in Figs.7,8.

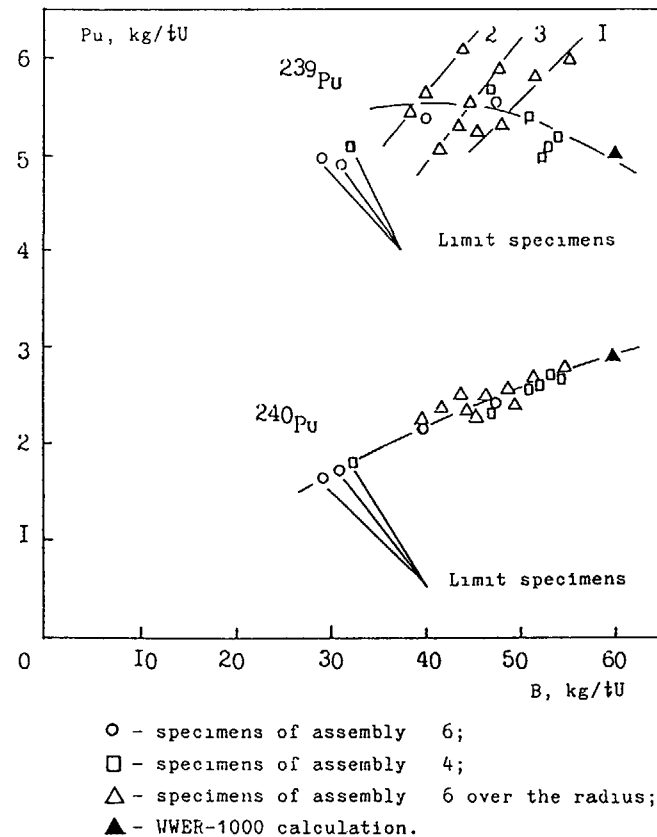


FIG. 5. Pu-239 and Pu-240 accumulation versus fuel burnup.

Increase of Pu accumulation from the fuel rod centre to the periphery leads to growth of fuel burnup. In this event such growth is mainly due to Pu isotopes fission. If burnup growth in the peripheral specimens as compared to central ones at the expense of U-235 fission makes up 7-10%, then Pu burnup rises by 25%. With small change in neutron flux over the fuel rod radius there is sharp growth of burnup at the expense of neutron Pu

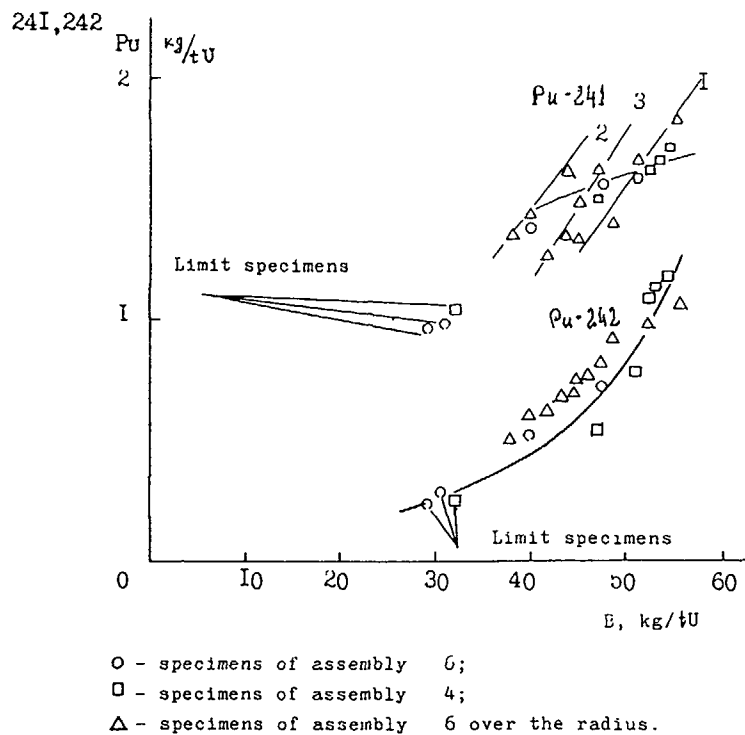


FIG. 6. Pu-241 and Pu-242 accumulation versus fuel burnup.

accumulation. Such a distribution of Pu over the fuel element radius affects the TOE distribution as well. As the table shows, accumulation of Am and Cm isotopes from the centre to the periphery rises by 50-70 %.

Analysis of the data over fuel rods height and radius results in the conclusion about similarity of fuel operating conditions in the centre of a fuel column and in limit regions of the fuel rod. So, accumulation of even Pu isotopes does not de-

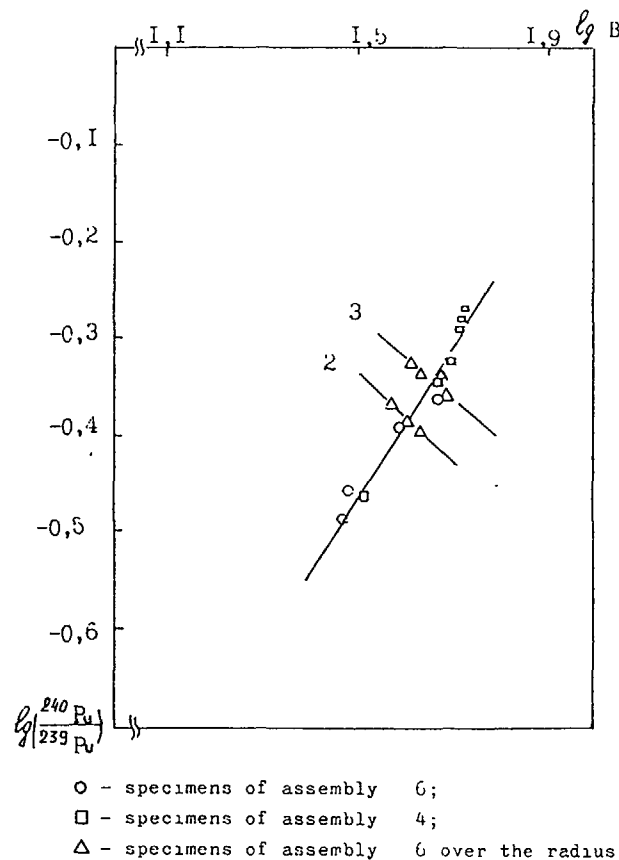


FIG. 7. Logarithms of the Pu-240 and Pu-239 atomic relationship versus logarithms of fuel burnup.

pend (see Figs. 5, 6) on the specimen location in the fuel element and reflects the common tendency of change in all specimens accumulation versus fuel burnup. Yet, accumulation of fissionable isotopes in limit specimens and inner part of the fuel column does not correspond to this tendency. Less accumulation of Pu-239

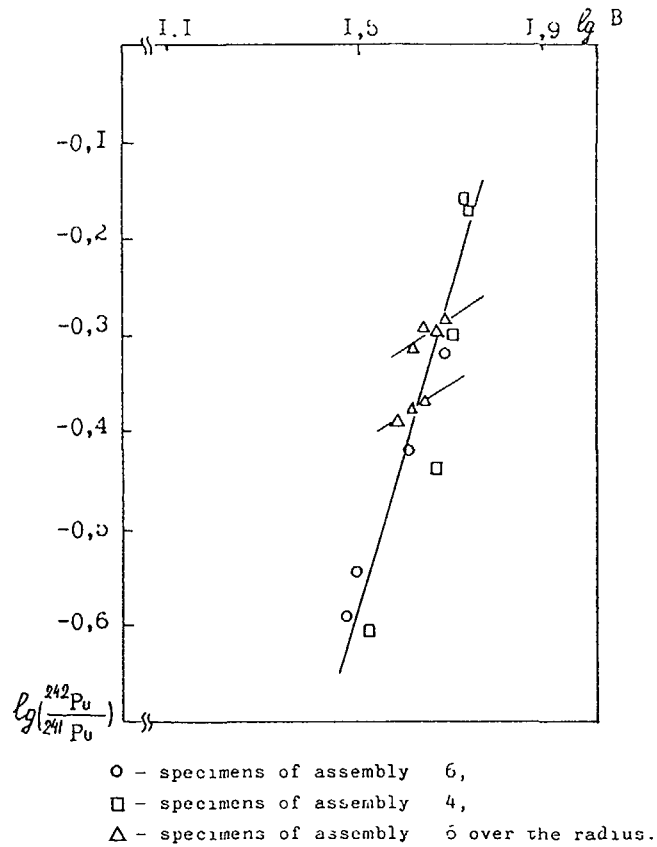


FIG. 8. Logarithms of the Pu-242 and Pu-241 atomic relationship versus logarithms of fuel burnup.

and Pu-241 in these specimens, to our mind, is caused by screening of thermal neutron flux.

Figs 9, 10 show dependencies of Cs-137 accumulation and Cs-134/Cs-137 ratio upon the burnup. These dependencies are important for non-destructive methods and allow the connection between the

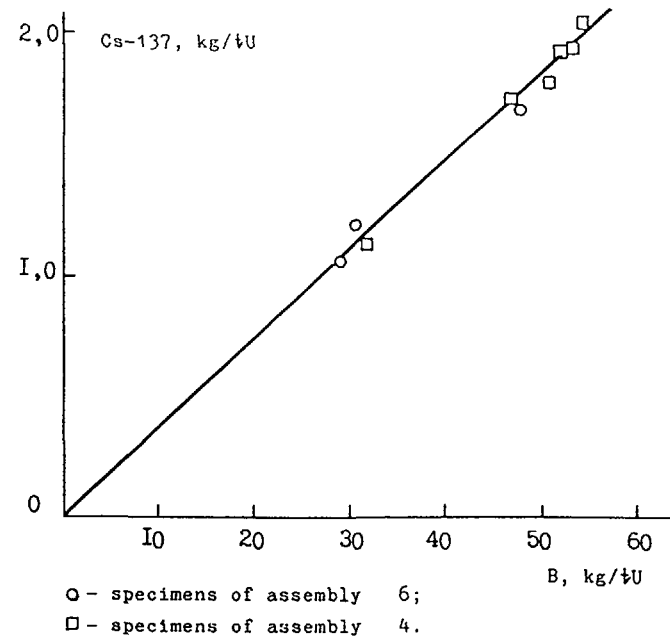


FIG. 9. Cs-137 accumulation versus fuel burnup.

burnup, Cs accumulation and the Cs isotopes ratio. The main restriction for this ratio application is the necessity to account irradiation history because of small half-life of Cs 134. As the figures show within the studied range of burnups, Cs-137 accumulation and Cs-134/Cs-137 ratio depend on burnup directly. In spite of burnup growth, the value of Cs-134/Cs-137 ratio changes negligibly which, in our opinion, means insignificant change of neutron flux. Slight inclination of straight lines 1, 2 and 3 is caused by change in Pu contribution to the total fissions number that leads to variation in effective releases of Cs-134 and Cs-137. And if for Cs-134 this variation is not

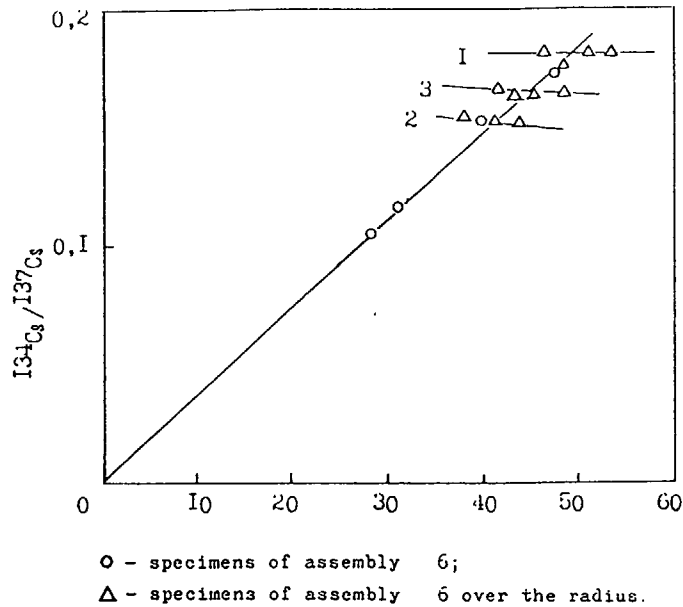


FIG. 10. Relationship of Cs-134/Cs-137 atoms quantity versus fuel burnup.

great (isotope release during fission of U-235 and U-239 6.72 % and 6.76 %, respectively), then for Cs-137 this change is of high importance (release 6.27 % and 6.48 %, respectively).

The regression equation  $B=0.37+27.02P$  connecting the burnup (B) with Cs-137 (P) accumulation is made on the basis of experimental data. Values of the equation parameters are calculated by the method of least squares.

Analogous dependence was gained for the Nd-145/Nd-146 relationship (Fig. 11). This pair of isotopes is widely used as a burnup monitor. Use of the total Nd 145 and Nd 146 accumulation is due to the necessary account of neutron capture by Nd 145 nuclei. The re-

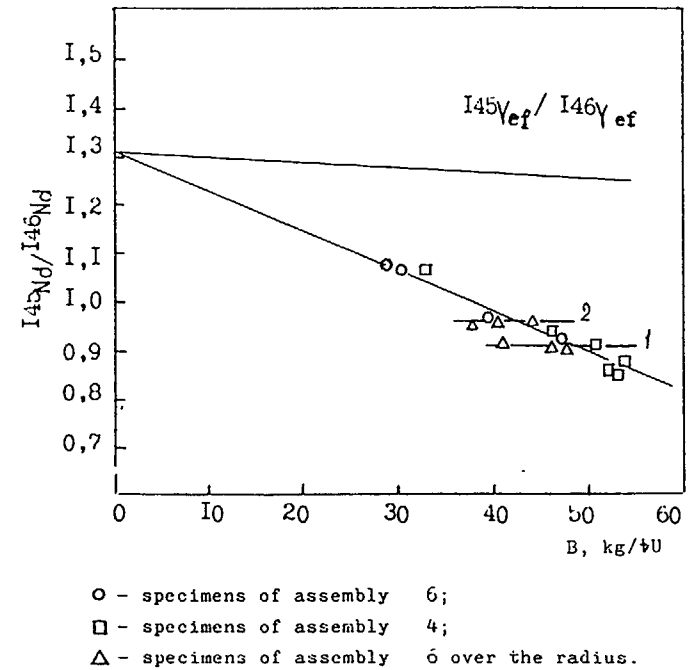


FIG. 11. Nd-145/Nd-146 atomic relationship versus fuel burnup.

lationship decreases with burnup growth, change is of a rectilinear. The straight line crosses the Y-axis in point 1.31, which corresponds to the ratio of Nd-145 and Nd-146 releases during U-235 fission. There is practically no modification in the relationship over the radius, and slight inclination of straight lines is caused as well as for cesium isotopes by change in effective releases of Nd-145 and Nd-146.

#### REFERENCE

1. Fudge A. In: Proc. IAEA Symp. "Reactor Burnup Physics" Vienna, 12-16 July 1973, p.239

**MODELLING AND MODELLING SUPPORT I**

**(Session 4)**

**Chairmen**

**M. GROUNES**

Sweden

**N. KJAER-PEDERSEN**

United States of America

## HOT CELL FISSION GAS RELEASE STUDIES ON UO<sub>2</sub>

M. COQUERELLE, D. BOTTOMLEY  
European Institute for Transuranium Elements,  
Commission of the European Communities,  
Joint Research Centre,  
Karlsruhe

### Abstract

UO<sub>2</sub> fuels irradiated at burn-up between 30 and 58 GWd/t and at average linear power ranging from 35 to 20 KWm<sup>-1</sup> have been investigated in the α,γ laboratory at the Institute for Transuranium Elements. The aim of this study was to determine the influence of increasing burn-up on fission gas release and the relationship between gas release and the fuel microstructure. A first study was undertaken by analysing fuel irradiated in power reactors and the results were reported at an IAEA technical meeting held at Studvik in 1990. Furthermore, an additional programme was developed aiming at a better understanding of the influence of burn-up, fuel grain size, oxygen potential and temperature on fission gas release.

Within the frame of this research our Institute carried out annealing tests in hot cells as part of the Research Programme of the Commission of the European Communities and of the international project High Burn-up Chemistry managed by Belgonucléaire.

In these experiments the release of <sup>85</sup>Kr is measured during the annealing of irradiated UO<sub>2</sub> samples under H<sub>2</sub>O:H<sub>2</sub> = 1:10, He/2%H<sub>2</sub>, and CO<sub>2</sub>:CO = 10:1 atmospheres. The fuel restructuring as a consequence of the annealing was analysed by optical microscopy and SEM. The analysed fuels were provided by three European nuclear fuel manufacturers: KWU-Siemens, BN and ASEA-ABB.

At the present time this study gives qualitative kinetic information on the influence of the different parameters chosen. The results support the view that an increase of the fission gas diffusion rate is caused by increasing burn-up and by annealing under oxidic atmospheres and by decreasing fuel grain size.

### 1. INTRODUCTION

The extension of fuel burn-up beyond previously prescribed levels has been proposed as a desirable means of improving uranium utilisation and minimising the amount of stored spent fuel. Therefore, it is necessary that the current knowledge base should be extended. Among the technical considerations related to LWR fuel performance at extended

burn-up the need to define fission gas release behaviour is probably the most important. This is primarily because large internal fuel rod pressure and high fuel temperature may not allow the maximum possible burn-up to be achieved.

The European Institute for Transuranium Elements has started a characterisation programme of UO<sub>2</sub> fuels irradiated to high burn-up (58 GWd/tU max.) in European power reactors. Some results of this study have been reported in a previous IAEA Technical Meeting [1].

Fission gas release is highly sensitive to fuel temperature and the uncertainties in this often quoted parameter increase with increase in burn-up. Among the interactive phenomena that effect fuel temperature and gas release, the ones of primary concern are fuel restructuring, fuel arching or densification, fuel chemical evolution and the chemistry of the inner cladding surface. A new study is underway where some parameters which influence the diffusion rate are analysed by annealing irradiated pieces of fuel in the hot cells. The goal is to obtain information, at least qualitatively, on the role played by parameters such as grain size, oxygen potential of the atmosphere surrounding the fuel and, of course, burn-up.

This report describes the experimental data collected up to the present time and the conclusions which can be drawn from it.

## 2. EXPERIMENTAL EQUIPMENT AND CONDITIONS

### 2.1 FUEL ROD DATA

This study is intended to quantify the fission gas release of irradiated UO<sub>2</sub> fuels supplied by three different fuel manufacturers (KWU, BN and ABB) by annealing segments of fuel pellets in the hot cell and to compare this behaviour as a function of grain size, burn-up and atmosphere. The analysed fuels were irradiated over 2, 3 and 4 cycles at a burn-up ranging from 31.8 to 58 GWd/tU in the Belgian BR-3 reactor (BN), in the Swiss Gösigen reactor (KWU) and in the Ringhals reactor (ABB).

Fuel and irradiation data are given in Table 1.

TABLE I. FUEL PELLET AND ROD DESIGN CHARACTERISTICS

Fuel	KWU	BN	ABB
Pellet density (%TD)	94.3-95	94.25	95.2
Grain size (µm)	6.5 - 7	11	40
Stoichiometry (O/M)	2.00	1.997	2.02
Pellet diameter (mm)	9.11	8.04	10.52
Burn-up (GWd/T)	31.5-53.2	58	53

The principal technique used is hot cell annealing of fuel under controlled oxygen potentials ( $\Delta G_{O_2}$  values), and to monitor the fission product release by measuring  $^{85}Kr$  evolved from the fuel. Examination of the fuel microstructures after annealing also aided the understanding of the fuel behaviour.

This work was done under the International program of High Burn-up Chemistry organised by Belgonucléaire in Brussels and also as a part of the research programme of the Commission of the European Communities.

## 2.2 HOT CELL ANNEALING AND FISSION GAS ANALYSIS EQUIPMENT

The furnace is a 1.5 kW high frequency induction coil (Cu coil - water cooled) that heats either a Pt-30 Rh (future experiments will use a ZrO<sub>2</sub> crucible) or a tungsten crucible (according to whether the heating is under oxidising or reducing atmospheres respectively). The crucible is supported on an Al<sub>2</sub>O<sub>3</sub> crucible holder, and this is enclosed in a quartz glass tube which is sealed top and bottom, and is joined to the gas lines from the glove box (see Fig. 1).

Temperature regulation is carried out by means of a Maurer infra-red pyrometer linked to a Eurotherm heating control (type 818) of the HF induction oven. The temperature profile of a particular run is preset by the operator in a Stange (St 234) Temperature/Process Controller that directs the Eurotherm oven controller.

The oven and gas line system is air-tight and can be evacuated or back-filled with a known atmosphere or gas mix using a mass flow controller (MKS 147 B) from the inlet lines.

For the reducing atmospheres the H<sub>2</sub>O:H<sub>2</sub> ratio of 1:10 was obtained by mixing N<sub>2</sub>-2%H<sub>2</sub> and N<sub>2</sub>-5%O<sub>2</sub> gases, while the oxidising atmosphere was made by mixing pure CO and CO<sub>2</sub> gases in the ratio 1:10 or using a ready-mixed CO/CO<sub>2</sub> (1:10) gas.

The mixed inlet gases (for description of these fuels see TUAR 86) are passed over an oxygen probe (Kent Taylor Z-FG O<sub>2</sub> probe) to monitor the oxygen potential, before passing over the crucible and sample (see Fig. 2). The gas is passed through activated charcoal traps to capture volatile fission products (e.g. Cs) before returning to the glove box to measure the  $^{85}Kr$  releases by passing through a NaI scintillation flow counter (Nuclear Enterprises linked to a Canberra 35+ multi-channel analyser), and then through a liquid N<sub>2</sub> cold trap to measure accumulated  $^{85}Kr$  releases quantitatively (using a Nuclear Enterprises NaI scintillation counter and NE scaler/ratemeter SR7). The gas was then exhausted back into the hot cell's ventilation system.

## 2.3 ANNEALING PROCEDURE

In preliminary tests, high (53.1 GWd/tU), medium (45.2 GWd/tU), and low (31.8 GWd/tU) burn-up fuels (KWU samples B4, B3 and B2 respectively) were subjected to anneals at 1500 °C for 1 hour or 1000 °C for

2 h or 48 h followed by 1 hour at 1500 °C (for description of these fuels see TUAR 86). These tests were carried out under strongly reducing conditions (He-2%H<sub>2</sub> flowing at 1 l mn<sup>-1</sup>) or reducing conditions (H<sub>2</sub>O:H<sub>2</sub> = 1:10 at 110 ml mn<sup>-1</sup>). The heat-up rate was approx. 25 °C mn<sup>-1</sup>.

The fuel samples of 0.1 - 0.3 g weight were selected from a 3 mm cut of the fuel to be as representative as possible of the fuels' structure.

Further tests were carried out with low and high burn-up KWU fuel (B2, B4) under reducing H<sub>2</sub>O/H<sub>2</sub> = 1:10 and oxidising (CO/CO<sub>2</sub> = 1:10) atmospheres at flow rates of 560 m/mn<sup>-1</sup>, heating to either 1000 °C or to 1500 °C directly for 1 hour, or heating to 1000 °C and rising in 100 °C steps (10 mins. rise time then 50 mins. hold time) for up to 1500 °C (stair-case profile).

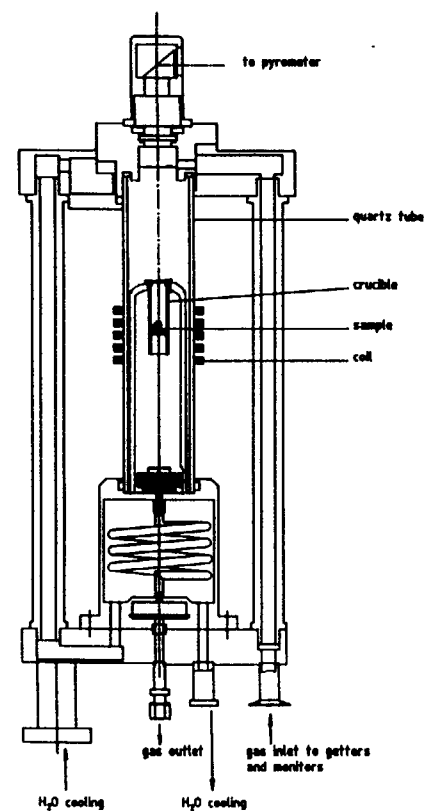


FIG. 1 HF Induction furnace for thermal annealing under controlled atmosphere

TABLE 2. <sup>85</sup>Kr RELEASES

				MCA imp/g	Trap imp/g
H <sub>2</sub> O/H <sub>2</sub>	1. BN	precooking only	⊕ ⊗	- 1.26x10 <sup>6</sup>	2,050 1,609
		precook + 1 h/1500°C	⊕ ⊗	88.4x10 <sup>6</sup> 32.5x10 <sup>6</sup>	72,728 31,188
		precook + 1000-1500°C 100 °C step	⊕ ⊗	- 15.7x10 <sup>6</sup>	25,067 19,344
		1 h/1500 °C	⊕	47.7x10 <sup>6</sup>	32,714
		1000-1500 °C 100 °C step	⊕ ⊗	28.7x10 <sup>6</sup> 25.8x10 <sup>6</sup>	21,917* (*1200-1500 °C) 16,724
		2. ABB	⊕ ⊗	5.08x10 <sup>6</sup> 11.1x10 <sup>6</sup>	4,333 (ramped) 7,500
	3. KWU	1000-1500 °C 100 °C step		47.3x10 <sup>6</sup>	5,133
		1000-1500 °C 100 °C step		356.13x10 <sup>6</sup>	41,091
CO/CO <sub>2</sub>	1. BN	1 h/1500 °C	⊕	48.2x10 <sup>6</sup>	-
		1000-1500°C in 100 °C steps	⊕	152.7x10 <sup>6</sup>	-
	2. ABB	⊕ ⊗	10.3x10 <sup>6</sup> 8.13x10 <sup>6</sup>	- -	
	3. KWU	1000-1500 °C 100 °C step		154.8x10 <sup>6</sup>	
		1000-1500 °C 100 °C step		362.2x10 <sup>6</sup>	

Abbrand KWU: (a) 31.5 GWd/t  
 (b) 53.1 GWd/t  
 BN: 58 GWd/t  
 ABB: 53 GWd/t

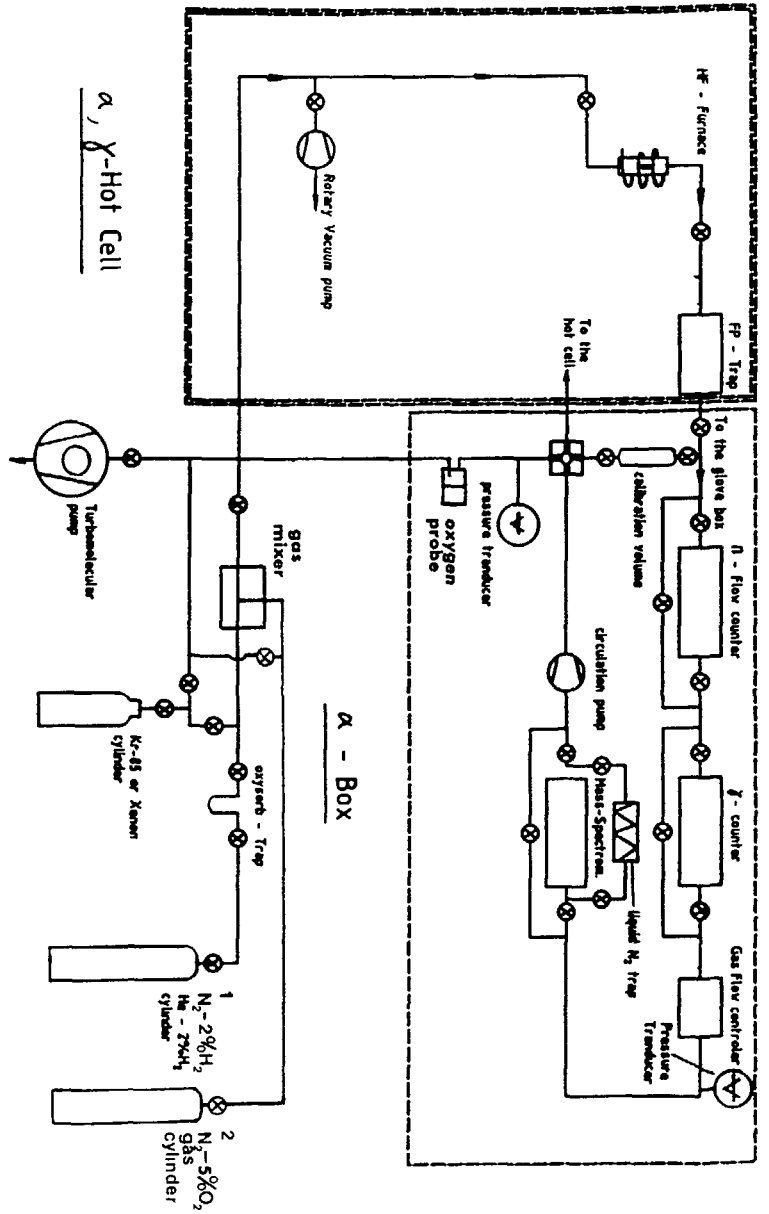


Fig. 2 Inlet and gas analysis lines for the HF induction furnace for determination of fission gas releases during thermal annealing

Final tests used Belgonucléaire fuel (burn-up 58 GWd/tU) and ABB fuel (burn-up) 53 GWd/tU under reducing conditions ( $H_2O:H_2 = 1:10$ ) and oxidizing conditions ( $CO:CO_2 = 1:10$ ) using similar temperature profiles. In addition, a baseline test of BN fuel was also performed with heating at 1000 °C for 48 hours under reducing conditions.

## 2.4 MICROSTRUCTURE ANALYSIS

Ceramographic examination (inc. porosity measurements) were made of cross-sections of the as-received material. In addition the surfaces of the heat-treated samples were examined by scanning electron microscopy (SEM). Energy dispersive analysis (EDX) will be performed on selected samples. These specimens have been re-mounted and polished, their examination under the optical microscope is underway. Future work will include residual gas analyses which will be made on the heat-treated samples as well as on the starting material to obtain the fission gas release ratios.

## 3. EXPERIMENTAL RESULTS

### 3.1 FISSION GAS RELEASES DURING ANNEALING

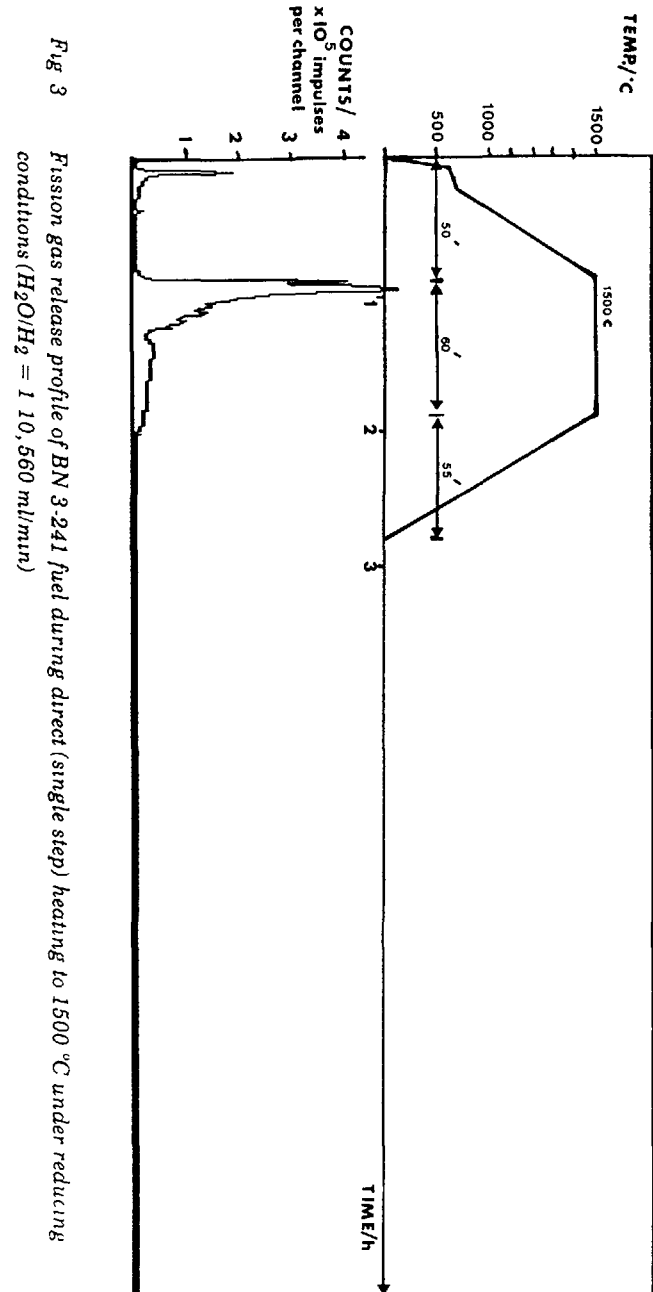
A list of the total  $^{85}Kr$  releases evaluated per gram of fuel are summarised in Table 2. This gives the flow counter measurements and where possible the cold trap measurements for the various profiles. Cold trap measurements were not possible for Kr and Xe releases under the oxidising  $CO/CO_2$  atmospheres (liquid  $N_2$  boils at -196 °C while  $CO_2$  sublines at -78.5 °C)

In general a small release was observed during the initial heat up at 700 - 850 °C. This usually represented from 6 % to 10 % of the total measured release. Thereafter with the direct (single step) heating to 1500 °C a second, and major, release was observed at approx. 1300 °C - 1400 °C (see Fig. 3). The exact temperature of release was difficult to determine because of the rapidity of the heating:  $\sim 50$  °C/min. For the staircase profile the major releases under reducing conditions occurred at 1300-1400 °C and 1400-1500 °C steps (see Fig. 4). The releases reached a sharp peak on attaining the hold temperature and then died away asymptotically.

On some occasions secondary, smaller outbursts were noted during the exponential decay phase of the release at hold temperature. These may result from microcrack formation. Thus there are sporadic burst events that modify a simple diffusion process.

At 1500 °C there was often a measurable background release at the end of the hold time, whereas at 1400 °C this background was relatively slight. The slowing heating rates were employed for the staircase profile to minimise thermal cracking effects compared to thermally activated diffusion processes.

Under oxidising conditions similar releases were seen, an initial low temperature, release at 700-800 °C, and then under single step heat-



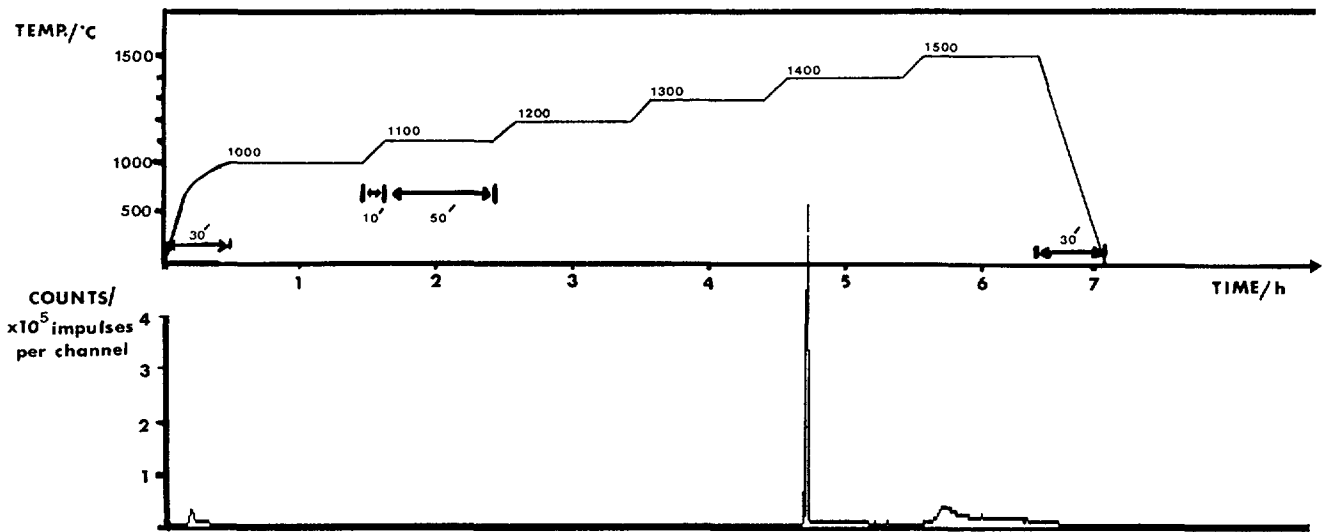


Fig. 4  $^{85}\text{Kr}$  gas release profile of BN 3-241 during a staircase anneal from 1000 °C - 1500 °C in 100 °C steps with 10 mins. rise time and 50 mins hold time under reducing conditions ( $\text{H}_2\text{O} \cdot \text{H}_2 = 1 \cdot 10, 560 \text{ ml/min}$ )

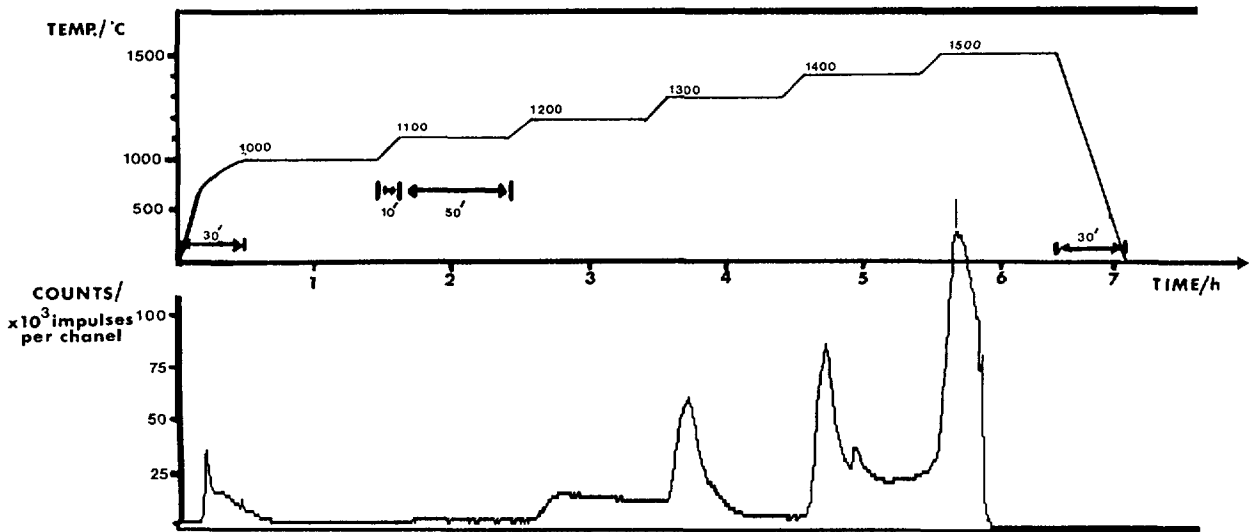
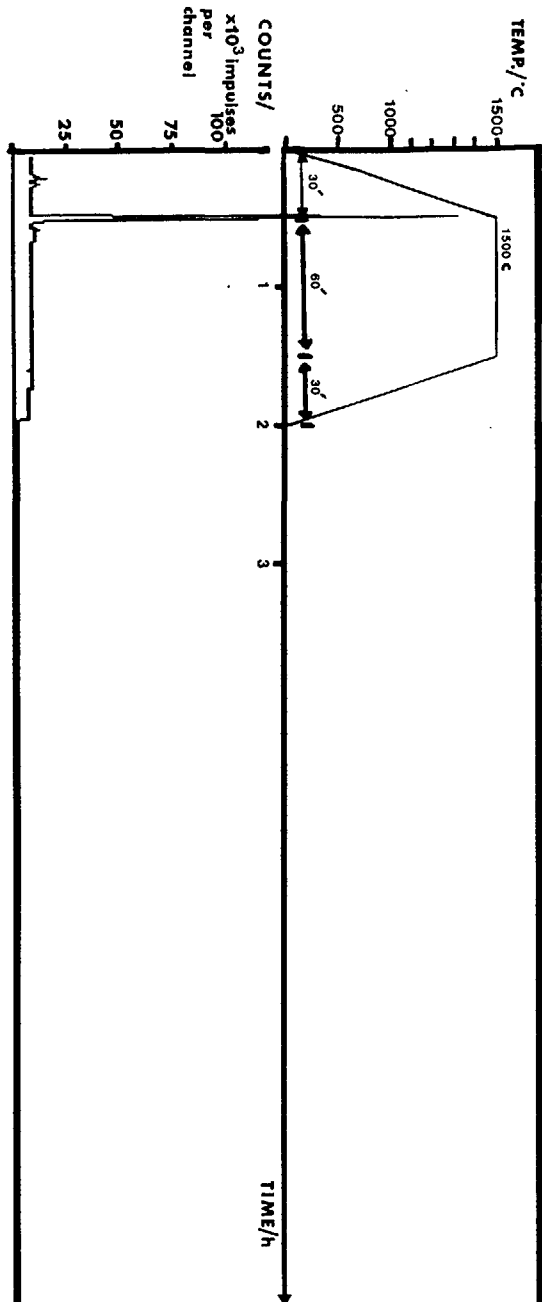


Fig. 5  $^{85}\text{Kr}$  gas release of BN 3-241 fuel during a staircase anneal from 1000 °C - 1500 °C in 100 °C steps with 10 mins rise time and 50 mins hold time under oxidising conditions ( $\text{CO}/\text{CO}_2 = 1 \cdot 10, 220 \text{ ml/min}$ )

Fig. 6  $^{85}\text{Kr}$  gas release profile of ABB 9K2-1 fuel during a direct (single step) heating to 1500 °C under reducing conditions ( $\text{H}_2\text{O}/\text{H}_2 = 1:10$ , 560 ml/min)



ing to 1500 °C a release on rising to 1400-1450 °C. The releases were similar in ratio and total amount to those observed during reducing conditions. By contrast the staircase anneals showed considerable greater (flow counter) total releases for the BN fuel and these appeared to commence approximately 100 °C lower (i.e. on rising to 1200 °C) (Fig. 5).

Total releases appeared to be slightly higher for the 'single step' BN specimens heated under reducing conditions as compared with the corresponding 'staircase' BN specimens. This may be attributable to the thermal stresses resulting from the more rapid and continuing heat up.

However the greatest differences were those observed with burn-up and, more strikingly, between fuels. The high (53.1 GWd/tU) burn-up KWU fuel released nearly 7 times more  $^{85}\text{Kr}$  as compared with the low (31.5 GWd/tU) burn-up KWU fuel under reducing conditions with a staircase heating profile.

This difference is reduced to only 2 times more  $^{85}\text{Kr}$  under oxidising conditions with the same profile. This indicates how oxidising conditions considerably help fission gas releases in longer (6 h) staircase tests for the low burn-up, but make little difference for the high burn-up fuel from KWU.

The comparison between BN fuel having staircase as compared with single step heating under oxidising conditions shows that the longer (6 h) staircase heating is required before the influence of oxidation on release is apparent.

At high burn-up the onset of releases (after initial (< 1000 °C) desorption) also commences at least 100 °C lower than for low burn-up fuels (i.e. ~ 1300 °C).

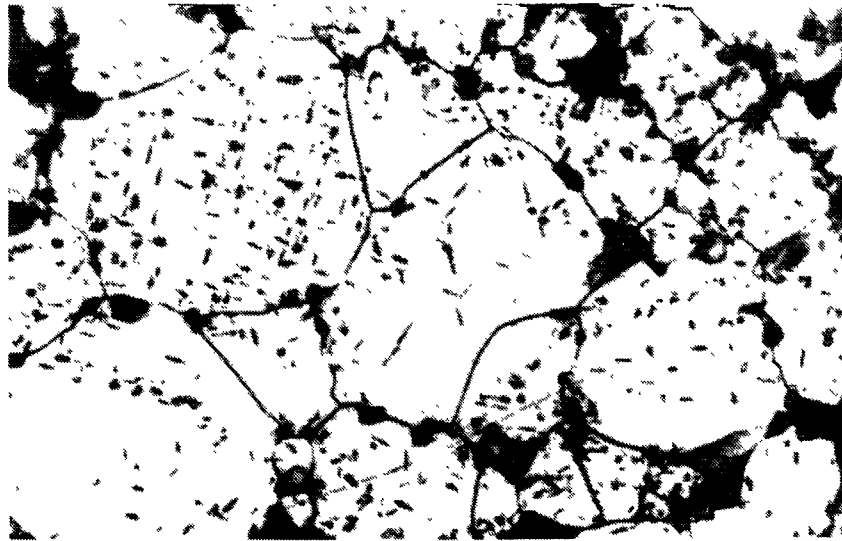
As expected the grain size of the fuels has a very significant difference on the release [2,3]. Compare BN fuel (Fig. 3) with ABB fuel (Fig. 6). ABB fuel appears to have the lowest releases with BN fuel next, then KWU fuel have the greatest releases. A ratio of total releases of approximately 1:4:8 is estimated for ABB:BN:KWU fuels assuming a staircase-type annealing under reducing conditions.

### 3.2 MICROSTRUCTURAL ANALYSIS

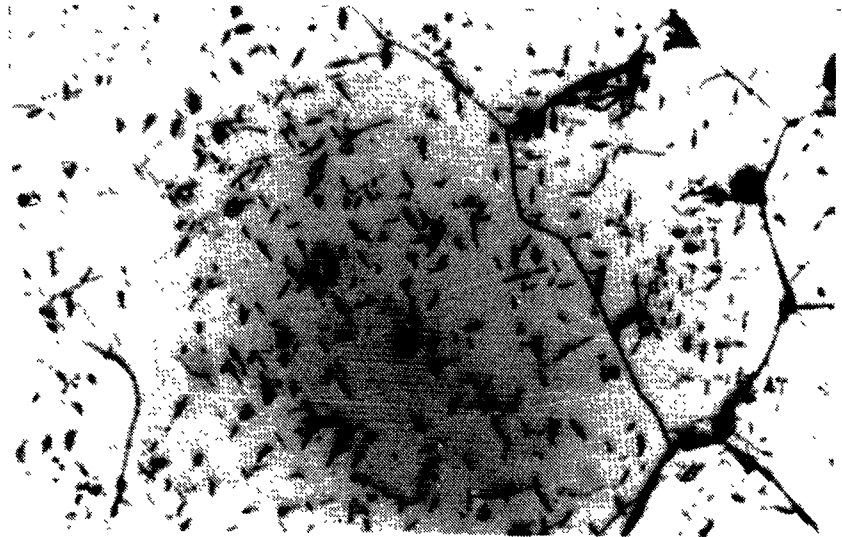
#### 3.2.1 Grain Size

The three fuels have differing microstructures particularly with respect to grain sizes. Thus:

- i) KWU fuel has 6/7  $\mu\text{m}$  mean grain diameter
- ii) BN fuel has 13  $\mu\text{m}$  mean grain diameter but with a binodal distribution:  $\approx 5 \mu\text{m}$  mean diameter with higher associated porosity; and larger grains 15-20  $\mu\text{m}$  of less porosity
- iii) ABB fuel with a mean grain diameter of 20.5  $\mu\text{m}$  (ranging from 9  $\mu\text{m}$  upto 65  $\mu\text{m}$  diameter).



a) BN3-241 (1100x),  $r/r_0 = 0.99$



b) ABB 9K2-1 (1100x),  $r/r_0 = 0.92$

FIG. 7 Optical micrographs ( $H_2SO_4/H_2O_2$  etched) of ABB 9K2-1 and BN3-241 fuels showing the acicular phase present in the as-received material in the outer part of the fuel. This had disappeared after precooking

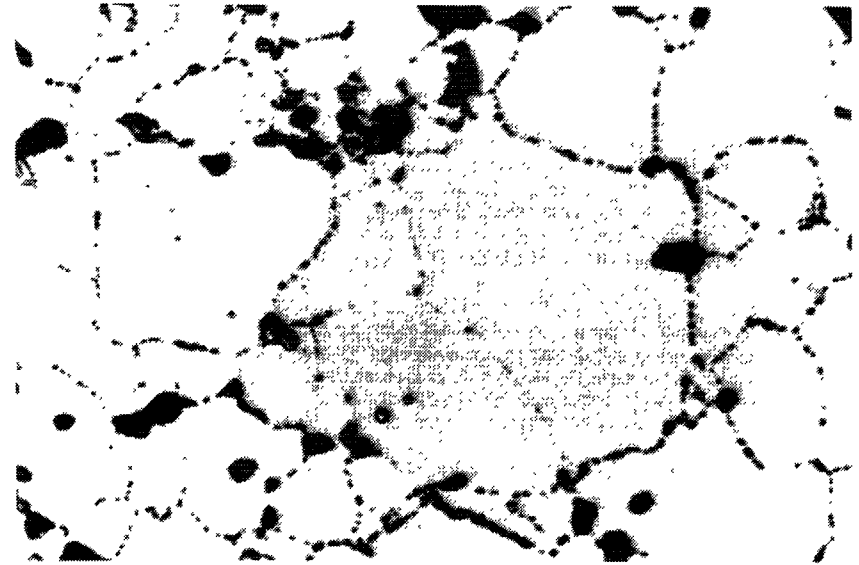


Fig. 8 Micrograph of BN 3-241 fuel after precooking at 1000 °C then staircase anneal to 1500 °C under reducing ( $H_2O/H_2$ ) atmosphere - see the grain boundary precipitates (1100x)

In addition only BN fuel displayed no porous outer rim which was present in the KWU and ABB fuels upto a maximum depth of 50  $\mu m$ .

### 3.2.2 $UO_2$ stoichiometry

Etching specifically for the  $U_4O_{9-x}$  phase was carried out for 2 fuels (ABB and BN) and an acicular phase appeared along two preferential orientations in the colder (outer) part of the fuel (e.g. in BN for  $r/r_0 > 0.87$ ) - see Fig. 7. This acicular phase disappeared after precooking for 48 h at 1000 °C under reducing conditions ( $H_2O:H_2 = 1:10$ ). This implies that the 3 fuels are slightly hyperstoichiometric after irradiation.

### 3.2.3 Porosity

The fuel has been examined by optical and electron microscopy after the various annealing treatments; the main feature of restructuring is the porosity which is modified in three major ways:

- i) there is always precipitation of intergranular porosity (Fig. 8)
- ii) their subsequent coalescence and formation of grain boundary channels (Fig. 9)
- iii) pore precipitation within the grains (Fig. 10)

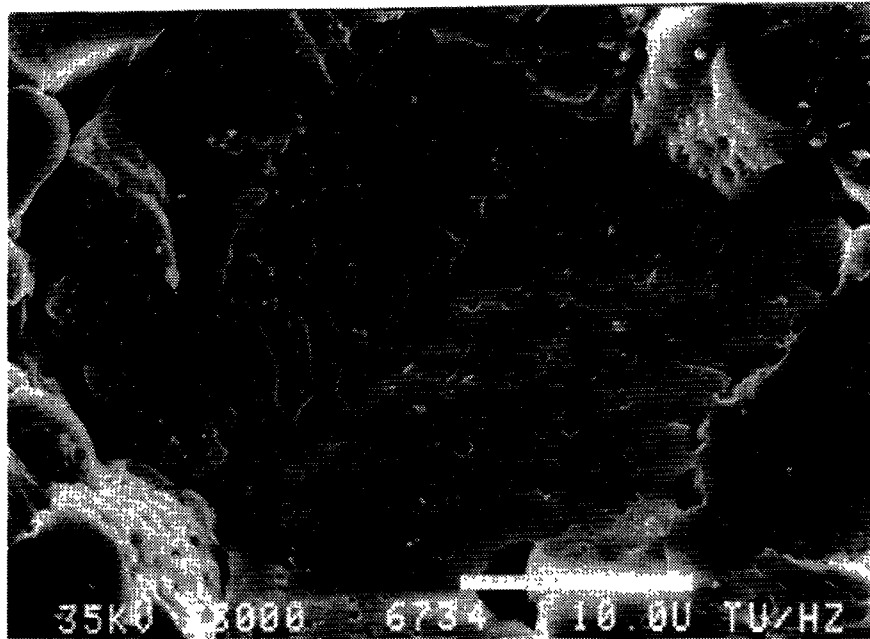


**Fig. 9** SEM micrograph of the BN 3-241 fuel after direct heating to 1500 °C under oxidising (CO/CO<sub>2</sub>) atmosphere (2000x) - see the grain boundary pore coalescence and channel formation

The intragranular pore formation and the coalescence at the grain boundary are increased (i.e. fewer but larger grain boundary pores) under oxidising (CO/CO<sub>2</sub> = 1:10) conditions and under rapid one-step heating under reducing conditions above 1300 °C.

At present stage of the work no quantitative evaluation of porosity is available but this is foreseen in the near future.

Nevertheless there appears to be a memory effect upon the fuels' microstructure with a) precooling and b) staircase annealing methods. During the initial (cooler) steps of precooling/annealing pore nucleation predominates and then during the hotter stages of the annealing pore growth is the major process. The low temperature annealing steps allow more nucleation than direct heating and therefore more numerous and finer grain boundary pores are formed. Under oxidising conditions the greatly enhanced numbers and size of intragranular pores implies a substantially increased gas mobility in the UO<sub>2</sub>. This additional oxygen in the fuel may be effective by altering the lattice structure and resulting in a higher effective diffusion coefficient.

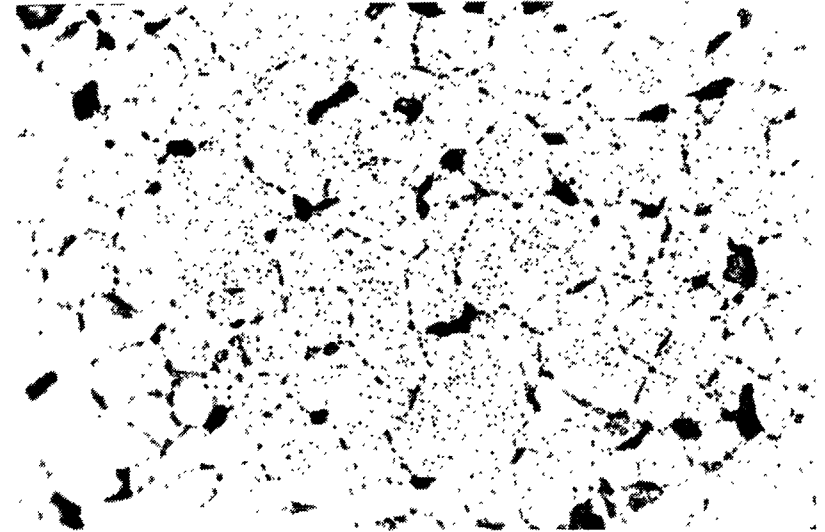


**Fig. 10** Optical micrograph of the BN 3-241 fuel after single step heating to 1500 °C (1 h) under oxidising (CO/CO<sub>2</sub> = 1:10) conditions - see the high density of intragranular pores (1100x)

#### 4. CONCLUSIONS

From the above results three main conclusions may be drawn:

a) As grain size increases, then there is a large decrease in the fission gas releases that result from the heat treatment. The grain surface area/volume ratio will be inversely proportional to the radius thus smaller grains mean more fission gas available at the grain boundaries and a greater possibility of release through the grain boundary interconnected pores/channels to the surface.

b) For the short annealing durations (upto 1 hour) of high burn-up fuel (ABB and BN) very little difference was seen between the oxidising (CO/CO<sub>2</sub>) and reducing (H<sub>2</sub>O/H<sub>2</sub>) conditions. However at longer annealing durations (staircase anneals (6 hours) of ABB and BN fuels) a considerable difference was seen between oxidising and reducing conditions. It is likely that at the longer duration there is sufficient time for the oxygen to diffuse in and affect the gas mobility. This effect is not seen in the KWU fuel, but these are the highest releases and in this case the grain size influence is likely to be the predominating factor.

c) The KWU fuel shows that the amount of fission product gas released under reducing conditions clearly increases with burn-up. There is also a kinetic effect as at high burn-up the onset of release seems to occur at 100 °C lower.

#### REFERENCES

- [1] COQUERELLE M., WALKER, C.T., UO<sub>2</sub> irradiated at extended burn-up in fission gas release and correlated structural features, Proc. of an IAEA Technical Committee Meeting, IWGRPT/36 held in Studvik, Sweden (1990), 110.
- [2] RONCHI Cl., Phys. processes and mechanism related to fission gas swelling in oxide type nuclear fuels, J. Nucl. Mater. 84, (1970), 79 p.55-84
- [3] RONCHI Cl., MATZKE, H.J. Calculations on the in-pile behaviour of fission gases in oxide fuels, 45, (1973), p.15-38

## FISSION-PRODUCT RELEASE KINETICS FROM CANDU AND LWR FUEL DURING HIGH-TEMPERATURE STEAM OXIDATION EXPERIMENTS

D.S. COX, Z. LIU, P.H. ELDER,  
C.E.L. HUNT, V.I. ARIMESCU\*  
AECL Research,  
Chalk River Laboratories,  
Chalk River, Ontario, Canada

#### Abstract

The kinetics of Cs and Kr releases from high-burnup CANDU and LWR fuel were measured in hot-cell annealing experiments (HCE-2 series) under simulated severe accident conditions. The Zircaloy-clad specimens were heated in an inert environment and then exposed to flowing steam or air at atmospheric pressure between 1350 and 1650°C. A simultaneous measurement of the oxidation rate of the fuel was made during these experiments. Both the CANDU and LWR fuels showed the same qualitative release behaviour. The Kr release kinetics could be divided into four different stages. During heating in inert conditions, a burst-release of Kr was detected starting at 1200 to 1400°C. The initiating temperature and the quantity of gas released in this stage was found to depend on the irradiation history. The second stage occurred only in fuel heated above 1400°C and could also be characterized as a burst-type release, although the peak rate and total quantity released in this stage increased with annealing temperature. A third peak of gas release occurred upon changing to an oxidizing environment. This peak was produced by a temperature escalation in the fuel resulting from exothermic oxidation of the Zircaloy. A final large gas release occurred after most of the Zircaloy cladding was oxidized, and presumably oxidation of the UO<sub>2</sub> was occurring. The kinetics of Cs release were similar to Kr except for lower Cs releases in the first stage, and a delay of several hundred to several thousand seconds relative to Kr, most notably in the first and fourth release stages. Differences and similarities between the CANDU and LWR results are discussed, and some of the HCE-2 data are compared to results from similar experiments conducted at the Oak Ridge National Laboratory.

#### 1. INTRODUCTION

The data presented in this paper were obtained as part of the Hot-Cell Experiment #2 (HCE-2), which is the most recent in a series of experiments in the Canadian out-reactor experimental program on severe accident fission-product source term research. The principal objectives of this program are to develop an understanding of the processes

---

\* IAEA fellow on attachment at AECL from Romania.

that control the release of fission products in accident conditions and to provide a database of fission product release kinetics for CANDU<sup>1</sup> fuel, from which rate equations and fission-product release models can be developed or validated

Experiments have been conducted at the Chalk River Laboratories (CRL) on fission-product release in accident conditions since 1985. Since many accident scenarios involve conditions that are oxidizing with respect to the  $UO_2$ , the emphasis of early and continuing work in the CRL program was to quantify the role of  $UO_2$  oxidation on fission-product release. The importance of oxygen potential on noble gas release kinetics had been demonstrated in pioneering work by Lindner and Matzke [1] and others [2,3]. This early work was extended to other fission products and a wider temperature range by oxidizing annealing tests on bare specimens of  $UO_2$  at CRL [4-8] and elsewhere [9,10].

Fission-product releases from bare  $UO_2$  specimens are very sensitive to changes in the oxygen potential of the surrounding environment. At high temperatures, the  $UO_2$  will rapidly oxidize or become reduced in response to changes in the surrounding atmosphere. As the oxygen potential in the  $UO_2$  changes, the chemical form, volatility and mobility of some fission products can be affected. Ruthenium is an example of an element that is rapidly released in an oxidizing atmosphere, but not in a reducing one [11]. Europium is an example of the opposite behaviour [12]. Rates of fission-product release can also be increased by oxidation or reduction of the  $UO_2$ , without changing the chemical form of the fission products, since diffusion rates are higher in nonstoichiometric uranium. Similarly, the solubility of fission products can be affected by the stoichiometry of the  $UO_2$  [13] and lead to higher releases.

The release rates from bare  $UO_2$  in oxidizing conditions are probably an upper-bound limit to those expected in an accident scenario, because the Zircaloy cladding can present a physical barrier to the release of fission products, even from severely damaged fuel. Also, the cladding is a sink for oxygen, which may retard oxidation of the  $UO_2$ .

Out-reactor annealing experiments on Zircaloy-clad light-water reactor (LWR) fuel specimens have also been conducted at the Oak Ridge National Laboratory (ORNL) as part of the HI and VI test programs (e.g., [14,15]). These tests, together with results of the HEVA program [16], constitute an extensive database for fission-product releases from Zircaloy-clad LWR fuels at high temperatures. Similar experiments have been conducted on CANDU fuels in the CRL program. Because of differences between CANDU and LWR fuels, a comparison was undertaken in the HCE-2 tests to assess the applicability of the existing LWR fission-product release data to CANDU accident analyses.

The differences between CANDU and LWR fuels are principally in the dimensions of the fuel and the fissile enrichment. In CANDU fuel, the  $UO_2$  is not enriched (0.7%  $U-235$ ), the pellet diameter is larger, and the Zircaloy sheath is thinner than for LWR fuel. The enrichment of LWR fuels results in a higher typical burnup. The dimensional dissimilarities result in different radial temperature profiles. The central temperature of

CANDU fuel can be higher than in LWR fuel operated at the same fission rate, since the  $UO_2$  diameter is larger, although this tends to be offset by higher  $UO_2$  sheath heat transfer in CANDU fuel, because the sheath collapses onto the  $UO_2$ , in comparison to the freestanding cladding in the LWR design.

The specific objective of the HCE-2 tests was to investigate isothermal fission-product releases from Zircaloy-clad CANDU and LWR fuels in steam and air environments in the temperature range 1350-1650°C. Fission-product release data were measured for several isotopes, including Cs-137, Cs-134, Kr-85, Rh-106 and Eu-154. A total of 20 individual tests were completed in HCE-2, 15 using Zircaloy-clad segments cut from fuel elements, and 5 tests using bare fragments of  $UO_2$ . Only a limited set of data, for Cs and Kr, will be presented in this paper, a more detailed description of all the HCE-2 test results will be available in future reports.

## 2 FUEL SPECIMENS

The  $UO_2$  specimens were taken from three different types of irradiated fuel: Bruce-type CANDU fuel irradiated in the NRU reactor (element AC-19 of Bundle XM) (457 MW·h/kg U), Bruce-type CANDU fuel irradiated in Unit-3 of the Bruce-A station (474 to 544 MW·h/kg U), and LWR fuel irradiated in the PWR Arkansas One station, Unit-2 (1375 MW·h/kg U). A description of the fuels is listed in Table I, including the results of post-irradiation gas puncture measurements for the Bruce-A fuel [17].

Zircaloy-clad specimens were obtained by cutting sections from both the LWR fuel rod and CANDU fuel elements. Zircaloy-4 end-caps were press-fitted on both ends of these fuel segments to make 'mini-elements'. Bare  $UO_2$  specimens were collected as fragments from the cut fuel. Prior to testing, all of the specimens were weighed. The weight of one end-cap was about 2.03 grams for the Bruce-type fuel samples and 1.58 grams for LWR fuel samples. The LWR mini-elements were cut from between about 533 and 648 mm from the bottom end of the fuel rod. The Bruce-A mini-elements were cut from near the element mid-plane (each element being about 500 mm long). Those from

Table I: Fuel Characteristics for the HCE-2 Tests

Fuel Bundle type or Rod	Fuel Element	Enrichment (wt% <sup>235</sup> U)	Burnup (MW·h/kg U)	Density (Mg/m <sup>3</sup> )	End-of-Life Power (kW/m)	Peak Power (kW/m)	Date of Discharge
Bruce XM	AC19	1.38	457	10.64	32	54	90-07-17
Bruce J03311W	7 <sup>a</sup>	Natural	544	10.70	33	59	88-06-28
Bruce J98315C	19 <sup>b</sup>	Natural	474	10.75	27	47	88-06-28
LWR TSLD95		3.5	1375	NA	NA	NA	88-02

<sup>a</sup> Outer element, 24.2% measured noble gas release after irradiation

<sup>b</sup> Intermediate element, 4.2% measured noble gas release after irradiation

<sup>1</sup> CANDU Canada Deuterium Uranium is a registered trademark

**Table II: Summary of the Specimen Characteristics and Test Conditions<sup>a</sup>**

Test	Fuel Type	Total Weight (g)	Sample Dimension(mm) <sup>b</sup>		Test Date	Environment	Test Temperature (°C)	Furnace Temp. at start of test (°C) <sup>c</sup>
			L	D				
<b>Mini-Elements</b>								
LM2	LWR	16.467	17	8.26	25/11/91	Steam	1350	70
LM3	LWR	16.875	20	8.26	28/11/91	Air	1650	650
LM5	LWR	16.878	20	8.26	26/11/91	Steam	1500	650
BM3	Bruce <sup>d</sup>	28.942	21	12.15	22/11/91	Steam	1500	650
BM5	Bruce <sup>e</sup>	30.205	22	12.15	21/11/91	Steam	1500	650
CM7	AC19	30.584	22	12.15	29/11/91	Steam	1650	1650 (fast ramp)
<b>Fragments</b>								
LF1	LWR	0.556	3 chips		9/11/91	Steam	1650	650

- <sup>a</sup> Limited to information on the tests described in this paper.
- <sup>b</sup> Calculated length L and nominal diameter D of UO<sub>2</sub>.
- <sup>c</sup> The furnace temperature at the time when the sample was loaded.
- <sup>d</sup> Outer element.
- <sup>e</sup> Intermediate element.

AC-19 were taken from locations over the entire element length. The specimen characteristics and the dimensions of the cut mini-elements are summarized in Table II for the tests reported in this paper.

### 3. EXPERIMENTAL APPARATUS AND PROCEDURE

The apparatus used in the HCE-2 experiment is illustrated in Figure 1. A tube furnace with molybdenum disilicide heating elements was used to heat the UO<sub>2</sub> specimens in a horizontal alumina tube. An alumina boat and push-rod was used for inserting and removing samples from the furnace. The specimen temperature was monitored with an R-type thermocouple located inside the push-rod. Two yttria-stabilized zirconia oxygen sensors at upstream and downstream locations in the furnace tube monitored the oxygen partial pressure and temperature of the flowing gases. These measurements were used to calculate the oxidation rate of the fuel specimens.

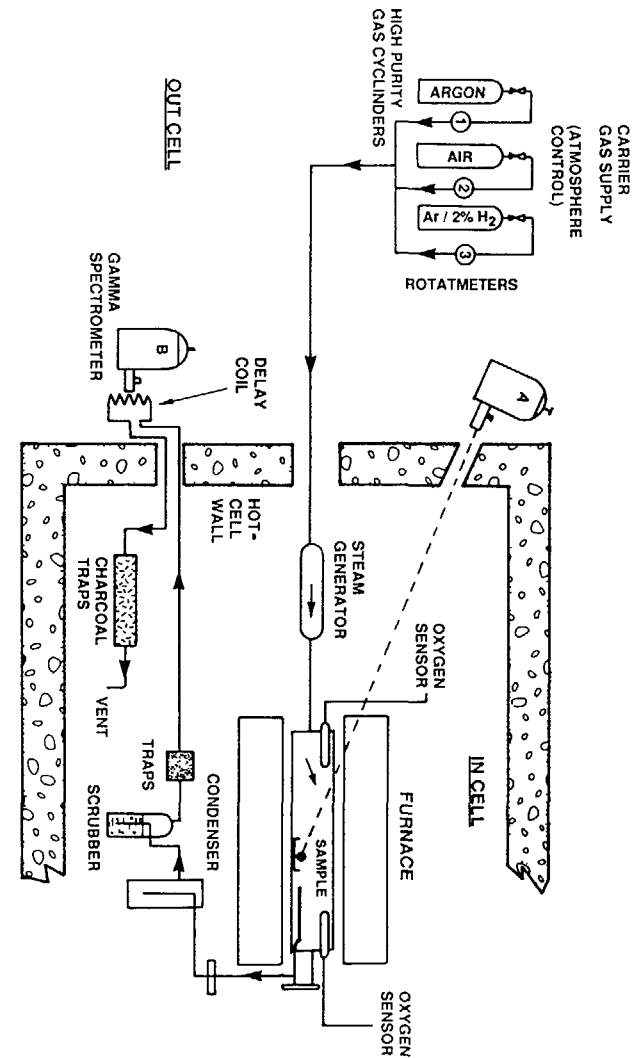


Figure 1: Schematic of experimental apparatus for HCE-2 tests.

After being released from the  $UO_2$ , the noble gas fission products were swept through the rig before venting into the hot-cell. All of the gases flowed sequentially through the furnace tube, steam condenser, iodine scrubber (bubbled through a solution of NaOH and  $Na_2S_2O_3$ ), moisture trap, out cell noble gas monitoring station, activated charcoal filter and water bubbler. Steam was produced by pumping distilled and de-ionized water with a calibrated positive displacement pump to a heated steam generator at a rate of 60 g/h. The steam was mixed with argon (flow rate of 100 STP mL/min) to act as a non-condensable carrier gas for transporting fission products beyond the steam condenser. In air oxidation tests, the flow rate was 200 STP mL/min.

The  $UO_2$  samples (either mini-elements or fragments) were placed in the alumina boat and pushed into the centre of the tube furnace in a flowing mixture of argon/2% $H_2$  (200 STP mL/min). For most tests, the furnace temperature was increased at a controlled rate after the sample reached the furnace centre-line. In test CM7, the specimen was pushed into the furnace, which was at the final testing temperature. The oxidizing environment (steam or air) was introduced after the sample reached the test temperature. All the test conditions were recorded every 15 seconds by a data acquisition system. After the tests, the specimens were removed from the furnace under an atmosphere of argon/2% $H_2$ . At the time of this report, ceramographic examinations of the post-test specimens were pending.

Two germanium gamma-ray spectrometers were used to measure fission-product activities during the tests. The first spectrometer was sighted directly at the fuel sample through a collimator in the ceiling of the hot-cell and was able to measure on-line changes in activity of Cs-137, Cs-134, Eu-154 and Rh-106. The low-yield gamma-ray of Kr-85 was measured by another spectrometer that viewed the out-cell monitoring station (see Figure 1). The gamma-ray spectra were collected for times ranging from 200 to 600 seconds throughout the tests.

## 4 DATA ANALYSIS

### 4.1 FISSION PRODUCT RELEASE KINETICS

A peak-search program was used to analyze the spectra collected by both of the gamma-ray spectrometers. This analysis permitted a re-calibration of the spectrum energy to correct for possible drift during the test. The release percentages,  $R(t)$ , of Cs, Eu and Rh were calculated from the count rates measured at the direct viewing spectrometer, using

$$R(t) = \left[ 1 - \frac{I(t)}{I(0)} \right] \times 100 \% \quad (1)$$

where  $I(0)$  was the standard count rate measured from the sample before the test and  $I(t)$  was the count rate during the spectra ending at time  $t$ . When necessary, the count rates

were normalized to a peak of an isotope that was not released (i.e., Eu-154). This latter correction was minor and accounted for a possible orientation difference of the specimen during the test relative to the standard count rate measurement.

The count rates from the out-cell spectrometer were used to calculate the Kr-85 activity measured during each spectra. This calculation took into account the measured efficiency of the spectrometer for 514 keV  $\gamma$ -rays, the  $\gamma$ -ray yield for Kr-85 and the time each unit volume of gas was visible to the spectrometer. This time was calculated from the non-condensable flow rates, including the effects of  $H_2$  production during oxidation of the Zircaloy by steam (see Section 4.2 below). The timing of these Kr-85 activities was then corrected for the transit time from the fuel to the out-cell spectrometer. Since no accurate measurements or calculations were yet available for the Kr-85 inventory of the LWR fuel, the Kr-85 release percentages were calculated by assuming that the final percentage releases of Kr and Cs were the same.

The Kr-85 inventories in the CANDU fuels were calculated using the FISSPROD 3 code and a detailed irradiation history. The calculated releases of Kr-85 were consistently 20 to 30% greater than the calculated inventories, indicating a systematic error in either the calculated inventory or the activity calculations. Because of this uncertainty, the fractional releases of Kr-85 for CANDU tests were also normalized to the final fractional release of Cs.

### 4.2 OXIDATION KINETICS

The rate of oxygen consumption by the fuel specimens was determined from the measured oxygen partial pressure ( $PO_2$ ) at the upstream and downstream oxygen sensors in the furnace. The  $PO_2$  at each sensor was calculated from the measured sensor temperature and voltage. By assuming equilibrium between  $H_2O$ ,  $H_2$  and  $O_2$ , the  $PO_2$  values were used to calculate the rates of oxygen consumption and hydrogen production inside the furnace, as a function of the molar flow rates of steam and argon, total pressure and temperature of the specimen. Details of this technique are given elsewhere [18]. The  $H_2$  production rates were used in the calculation of non-condensable flow rates at the Kr-85 monitoring station.

## 5 RESULTS

The oxidation kinetics for all of the HCE-2 specimens were determined using the output from oxygen sensors as described above. For all of the mini-element specimens, oxygen was consumed primarily by the Zircaloy (90 to 95%), the remainder being due to  $UO_2$  oxidation. Therefore, the overall kinetics primarily reflect oxidation of the Zircaloy. The oxidation kinetics were compared directly with the fission product release kinetics, since the oxidation state of the specimens influenced the measured releases.

Figure 2 shows an example of the calculated oxidation kinetics for the LWR mini-element test LM2 (1350°C in steam). The plot shows the rate of  $H_2$  production (mol/s) and the cumulative weight gain (mg) during the test. Complete oxidation of the Zircaloy would consume 2090 mg of oxygen, and  $UO_2$  oxidation to the equilibrium value of  $UO_{2.188}$

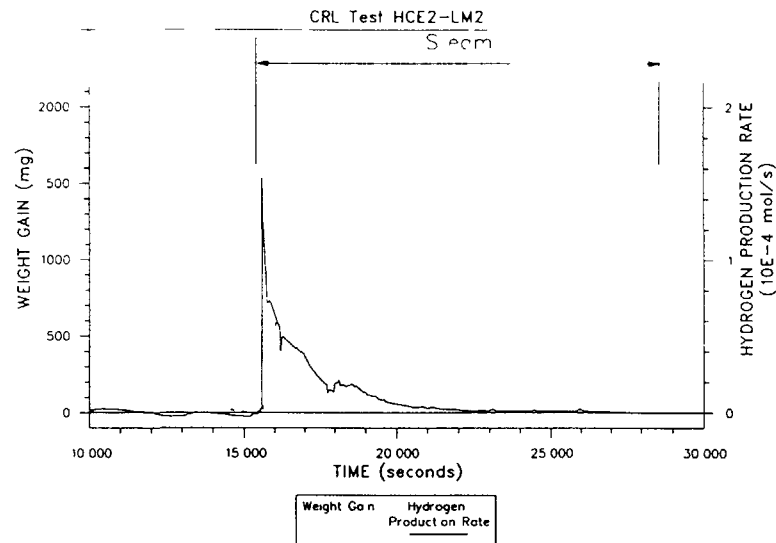


Figure 2 Weight gain kinetics and hydrogen production rates in LWR mini-element test HCE2-LM2 (1500°C steam)

would require 95 mg. The calculated weight gain at the end of the test was 2160 mg, indicating almost complete oxidation. As expected for these conditions, the oxidation was rapid. The time required to oxidize 50% of the specimen was about 1260 s.

### 5.1 LWR FUEL

Figures 3-5 show plots of Kr-85 release rates during three of the LWR mini-element tests. The Kr release rates can be characterized by a series of up to four separate peaks. In all of the LWR tests, Kr started to release during heating in the argon/2% $H_2$  at a temperature of about 1200°C.

Test LM2 (steam at 1350°C, Figure 3) was heated at 5°C/min and the maximum of the first peak was at about 1300°C. After reaching isothermal conditions at 1350°C, the release rate dropped continuously until steam was introduced at about 15,400 s. A small increase in the release rate occurred when steam was started. This was coincident with a rise in the specimen temperature due to oxidative heating. About 2000 s after the introduction of steam, the release rate increased rapidly and remained high for a period of about 3000 s. The first peak in test LM2 was 26% of the Kr inventory (normalized to Cs). The oxidation calculations indicate that  $75 \pm 5\%$  of the Zircaloy was oxidized at the start of the last peak (see Figure 2).

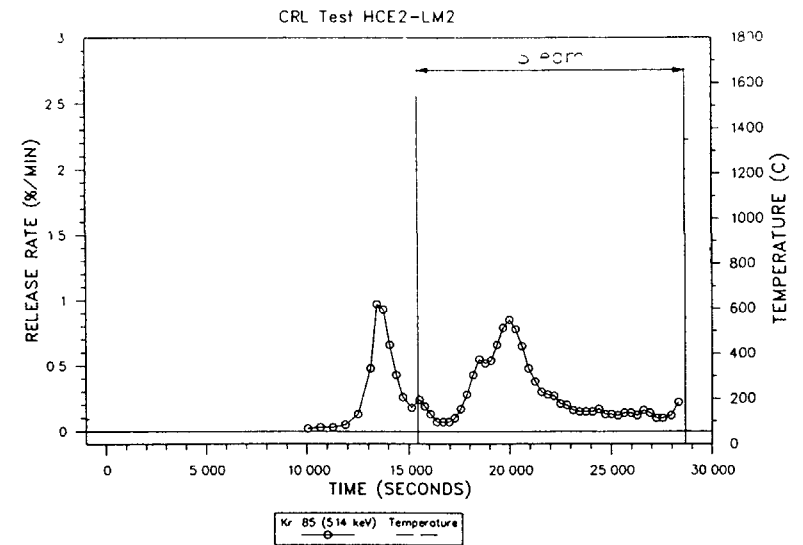


Figure 3 Release rate behaviour of Kr-85 for LWR mini-element test HCE2-LM2

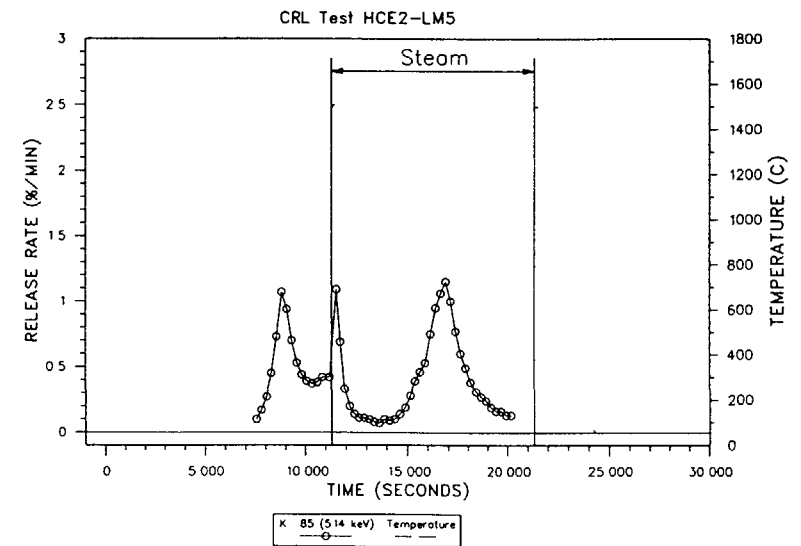


Figure 4 Release rate behaviour of Kr-85 for LWR mini element test HCE2-LM5

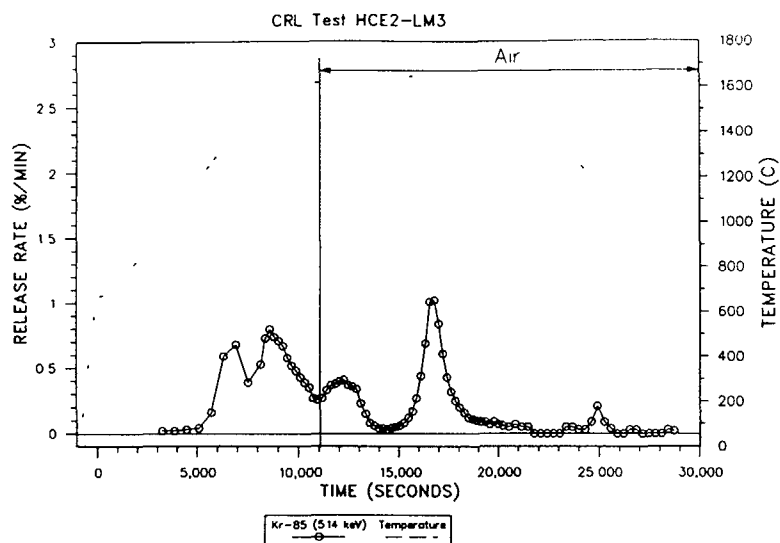


Figure 5: Release rate behaviour of Kr-85 for LWR mini-element test HCE2-LM3.

Test LM5 (steam at 1500°C, Figure 4) was heated at 5°C/min and the first peak in Kr release was almost identical to LM2 (same shape and maximum at 1300°C). As the fuel was heated above 1300°C, the release rate decreased until 1450°C was reached. The release rate was slowly increasing prior to the start of steam at about 11 400 s. A rapid increase in the Kr release rate occurred when steam was introduced, producing a peak of about 600 s in duration. The release rate decreased to a low value until a final increase in rate occurred about 2500 s after steam was introduced. This final peak lasted about 2500 s. The first peak was 27% of the Kr-85 inventory (normalized to Cs). About 85% of the Zircaloy had been oxidized at the start of the last peak in Kr release rate.

Test LM3 (air at 1650°C, Figure 5) was heated at 7°C/min. The first peak of Kr release was similar to LM2 and LM5, although the spectra were collected every 600 s (compared to 300 s in LM2 and LM5), yielding poor time resolution early in this test. The maximum occurred between 1300 and 1400°C. The first peak was 25% of the normalized Kr-85 inventory. This peak was followed by a second large and broad peak, beginning when the fuel temperature exceeded about 1500°C. The introduction of air at about 11 000 s produced a small but broad peak, lasting about 2000 s. A fourth peak in release rate occurred 4000 s after air was started, when the Zircaloy was about 80% oxidized. An additional small peak was measured late in the test upon cooling below about 1200°C. This may have coincided with the phase transformation from  $UO_{2+x}$  to  $U_3O_8$ .

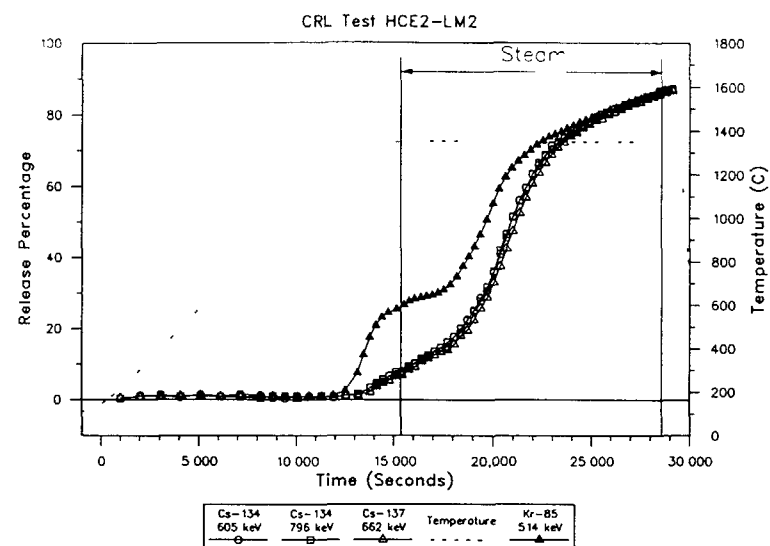


Figure 6: Cumulative release behaviour of Cs and Kr for LWR mini-element test HCE2-LM2.

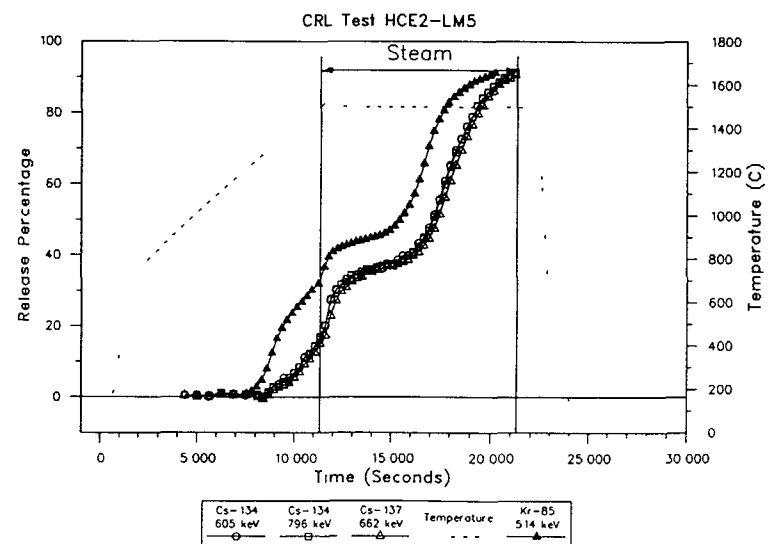


Figure 7: Cumulative release behaviour of Cs and Kr for LWR mini-element test HCE2-LM5.

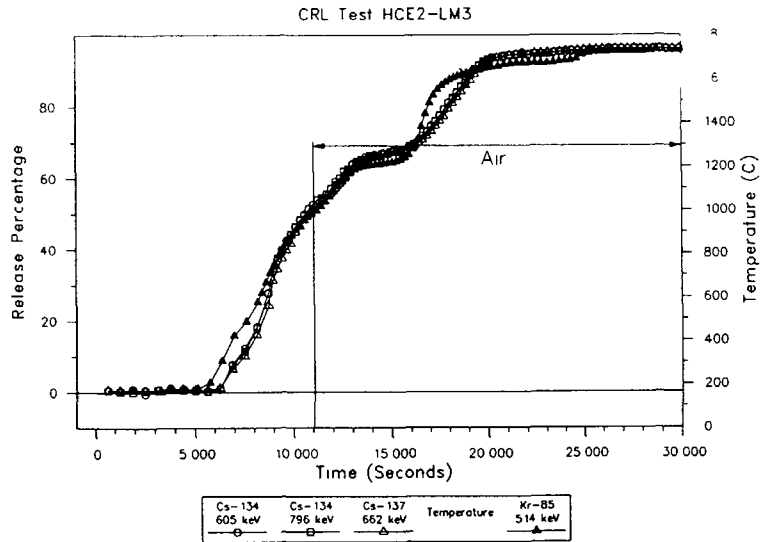


Figure 8: Cumulative release behaviour of Cs and Kr for LWR mini-element test HCE2-LM3.

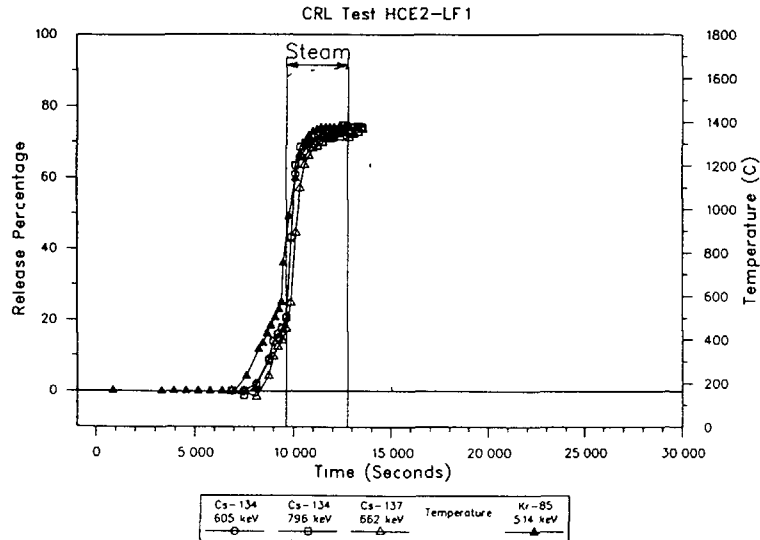


Figure 9: Cumulative release behaviour of Cs and Kr for test HCE2-LF1 (LWR UO<sub>2</sub> fragment).

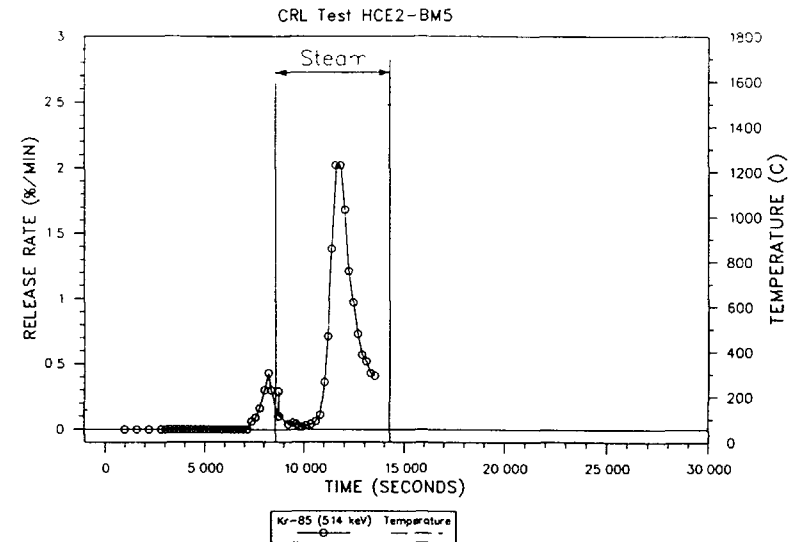


Figure 10: Release rate behaviour of Kr-85 for CANDU mini-element test HCE2-BM5.

Figures 6-8 show the kinetics of cumulative Kr and Cs release for test LM2, LM5 and LM3. A comparison of the Cs and Kr kinetics during the inert heating period of tests LM2 and LM5 (both 5°C/min) showed excellent reproducibility. The Kr releases were higher than Cs during this period. The difference between Cs and Kr releases diminished with increasing temperatures. Above about 1550°C, Cs and Kr release rates were very similar, although in periods of rapid release the Kr preceded the Cs by several hundred seconds. Test LM3 (Figure 8) was heated at 7°C/min and showed less difference between Cs and Kr kinetics during the inert period, although Kr was preceding Cs by about 600 s. The releases beginning at 17 000 s (5000 s after introducing air) were much more rapid and slightly earlier for Kr relative to Cs.

Figure 9 shows the kinetics of Kr and Cs release from a bare fragment of LWR fuel (test LF1 at 1650°C in steam). This test was heated at 7°C/min, so it can be compared with the results of LM3 (Figure 8) during the inert period. Kr was released from the fragment starting at about 1400°C and Cs was released at 1500°C (about 800 s later). These threshold temperatures were about 200°C higher than for the mini-element test LM3. When steam was introduced to the fragment, there was an immediate increase in the release rates of both Kr and Cs. During steam exposure, Cs was only slightly delayed relative to Kr (less than 300 s).

## 5.2 CANDU FUEL

Test BM5 (1500°C, steam) was from an intermediate element of the Bruce-A fuel. Figure 10 shows the Kr-85 release rates measured during this test. An initial peak in the

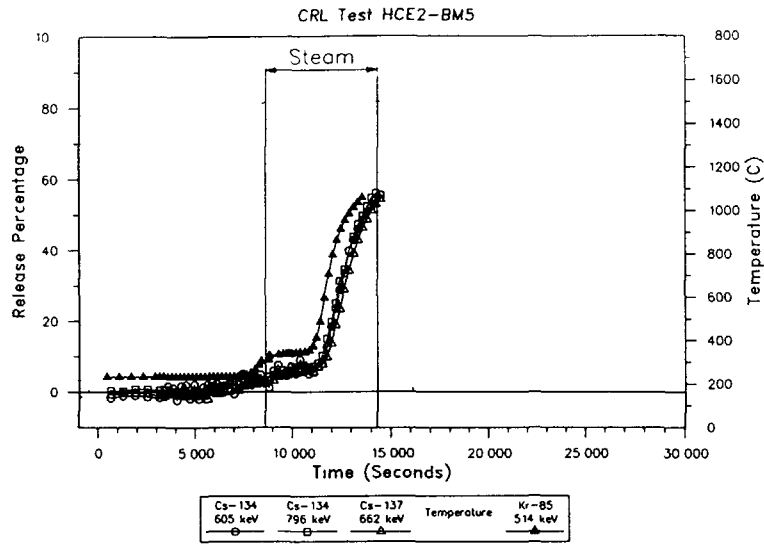


Figure 11: Cumulative release behaviour of Cs and Kr for CANDU mini-element test HCE2-BM5

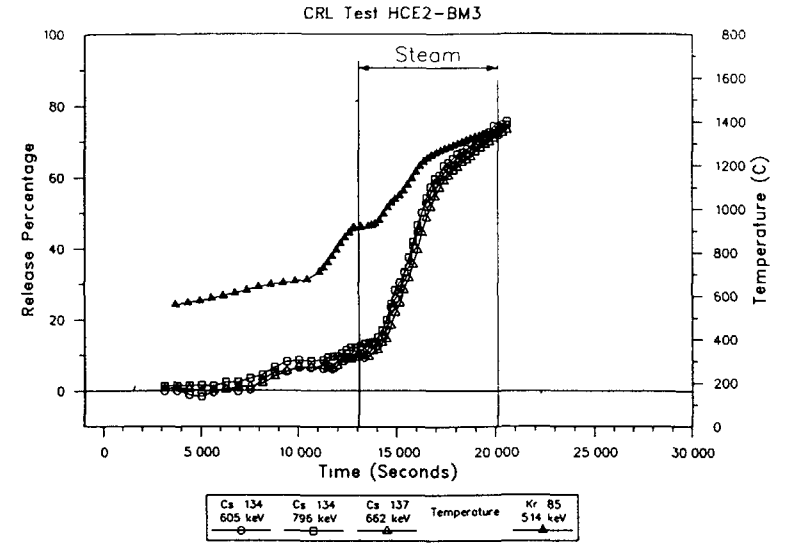


Figure 13: Cumulative release behaviour of Cs and Kr for CANDU mini-element test HCE2-BM3.

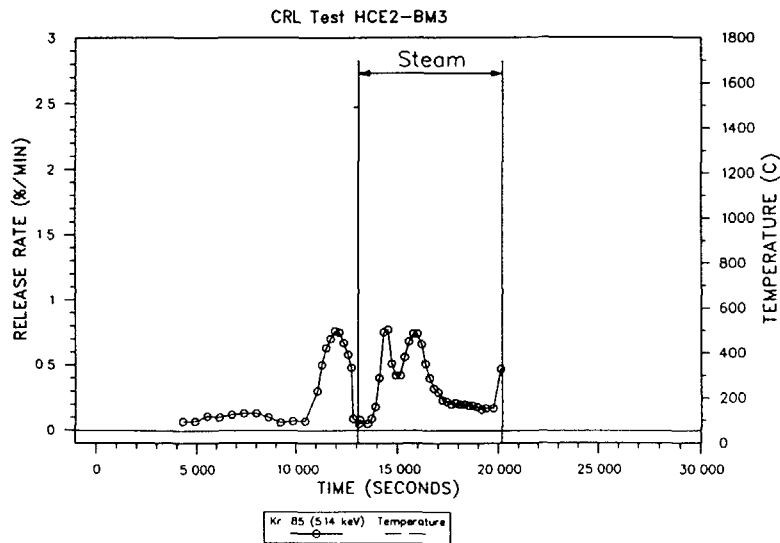


Figure 12: Release rate behaviour of Kr-85 for CANDU mini-element test HCE2-BM3

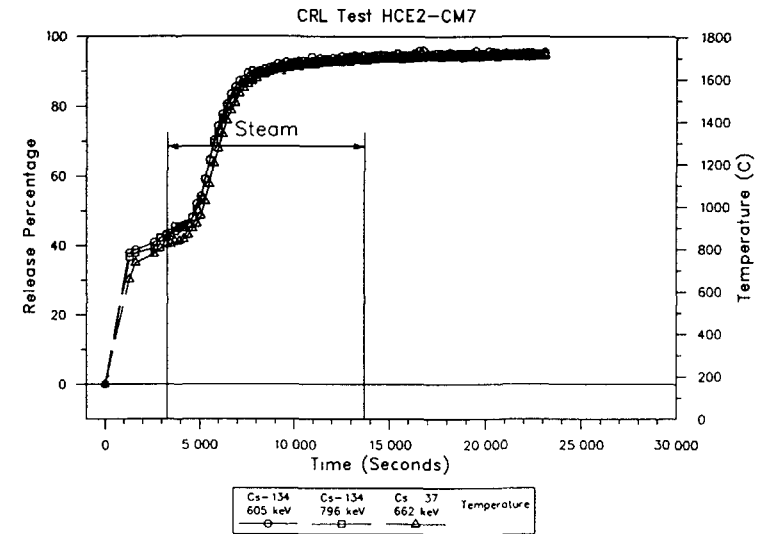


Figure 14: Cumulative release behaviour of Cs for CANDU mini-element test HCE2-CM7

release rate occurred during inert heating, starting at about 1350°C. The maximum rate for this peak occurred when the fuel reached 1500°C, then the rate decreased for the next 2000 s, except for a small spike when steam was introduced. The first peak accounted for 7.5% of the Kr-85 inventory (normalized to Cs). A large amount of Kr was released beginning about 2000 s after steam was introduced. The start of this peak was consistent with 80% of the sheath being oxidized. Figure 11 compares the Cs and Kr kinetics for test BM5, including the 4.2% measured gap release of noble gases, which would have been released during preparation of the mini-element. The Cs releases in the inert period occurred more slowly than the Kr releases, but the shape of the kinetics was similar.

Test BM3 (1500°C, steam) was an outer element from the Bruce-A fuel. Figure 12 shows the Kr-85 release rates that were measured during the test. A small amount of Kr was released during the entire heating period, beginning at 1000°C. A large peak in the rate started at about 1350-1400°C during heating and reached a maximum rate at the end of the temperature ramp to 1500°C. The rate then decreased for about 1000 s and remained at a low value for a further 1000 s. There was no obvious effect on the Kr release rates when steam was started. A sharp increase in the release rate occurred about 1000 s after steam was introduced, leading to a pair of overlapping peaks and a slowly decreasing release rate at the end of the test. Figure 13 shows the Cs and Kr release kinetics for test BM3. The measured post-irradiation gap inventory of noble gases was 24.2%, and this is reflected in the Kr plot. The final value of Kr release was normalized to Cs. During heating above 1300°C, the Kr release rate was much higher than the Cs, and the Kr preceded the Cs after steam was introduced.

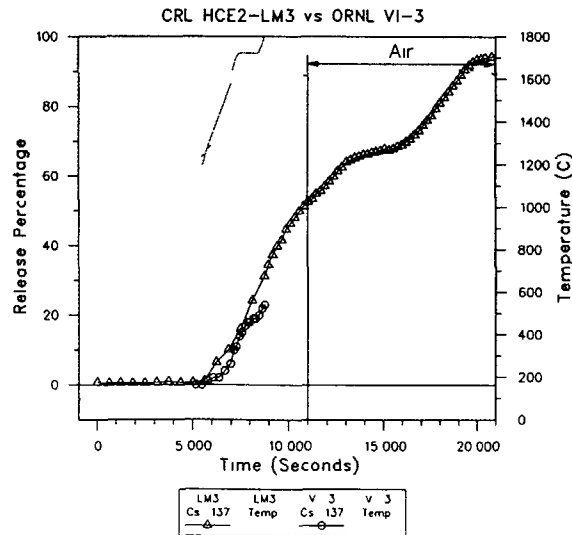


Figure 15 Comparison of cumulative release behaviour and temperatures for tests HCE2 LM3 and ORNL VI-3

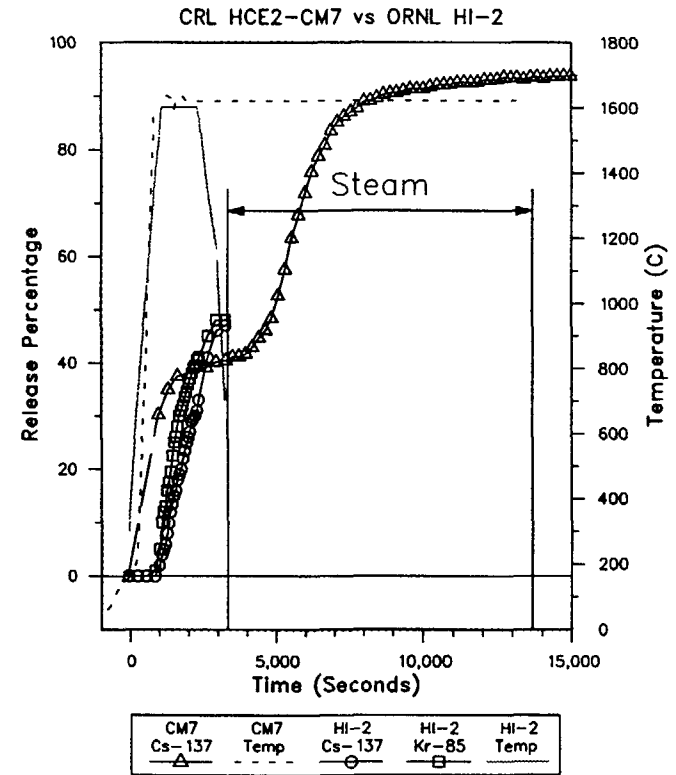


Figure 16 Comparison of cumulative release behaviour and temperatures for tests HCE2-CM7 and ORNL HI-2

Test CM7 (1600°C in steam, Figure 14) was conducted by pushing the specimen into the hot furnace, and it therefore experienced a faster temperature increase than the other CANDU specimens. The heating rate in this test was about 120°C/min. Between 30 and 40% of the Cs was released by the time the sample reached 1600°C. Kr data was not obtained during the temperature ramp because the gas flow was not directed to the delay coil during this period. After reaching 1600°C, the Cs release rate decreased to an approximately constant value for about 4000 s. There was a large increase in the release rate about 1500 s after steam was introduced, and 95% of the Cs was eventually released.

### 5.3 COMPARISON WITH ORNL RESULTS

Figure 15 shows the Cs-137 cumulative release kinetics for HCE 2 test LM3 (1650°C, air) compared with the ORNL test VI-3 [15]. In VI 3, the fuel sample was

heated to 1700°C, held for twenty minutes and then heated again to above 2000°C. For comparison purposes, the results of VI-3 are shown only until the start of the second heating period. During the entire VI-3 test, steam was flowing in the system at 1.5 STP L/min. The Zircaloy-clad fuel specimen (with Zircaloy end-caps) used in VI-3 was from the BR3 reactor and had a burnup of 1008 MW·h/kg U. This is a lower burnup than the specimen in test LM3 (1375 MW·h/kg U). The CRL and ORNL plots in Figure 15 were superimposed so that their temperatures coincided at 1300°C, which was close to the temperature of initial release for both tests.

A rapid release was observed during heating in both VI-3 and LM3. Both also showed a small decrease in release rate once a constant temperature was reached (at 7500 s in VI-3 and at ~10 000 s in LM3). The release rate increased in VI-3 when further heating started. During the heating period in which similar releases were observed, steam was flowing in the VI-3 test and argon/2%H<sub>2</sub> was flowing in the LM3 test.

In Figure 16, ORNL test HI-2 [14] was chosen for comparison with CRL test CM7 because both had similar high heating rates (> 80°C/min) and a test temperature of 1600°C. The entire HI-2 test was conducted in flowing steam (1.0 STP L/min). The fuel specimen was held at this temperature for 20 min and then cooled. The fuel specimen was from H.B. Robinson and had a burnup of 672 MW·h/kg U, compared to 457 MW·h/kg U for the CM7 sample. As with VI-3, the specimen was Zircaloy-clad and had Zircaloy end-caps.

A comparison of HI-2 and CM7 (Figure 16) showed that in both tests there was a rapid release rate during heating that continued for between 1000 and 2000 s after a constant temperature was reached. The same behaviour was seen with CM7 in inert conditions, as with HI-2 in steam. CM7 also showed a second period of rapid release about 2000 s after the introduction of steam. The time duration of HI-2 was too short to see whether a similar release might have occurred.

## 6. DISCUSSION

### 6.1. CRL LWR TESTS

In all of the LWR mini-element tests, four distinct peaks in Kr release rates could be identified. The first peak was a burst-type release; it always started at 1200°C, and it accounted for between 25 and 27% of the Kr-85 inventory. This suggests that it may have originated from grain-boundary venting upon heating. The size of the second peak was sensitive to temperature, and only occurred above 1400°C. This may represent a diffusional release from the grains, but, like the first peak, the release was not sustained. The diminishing rate may be due to coalescence of Kr to form bubbles within the grains, and hence a reduction in Kr mobility. The third peak coincided with the introduction of steam or air. In steam, the peak was a sharp burst, and in air the peak was broader. The cause of this peak may be cracking of the fuel in response to the temperature escalation due to the chemical heat of Zircaloy oxidation, or perhaps the temperature escalation itself. The broader peak in air tests is consistent with measurements that indicated slower

oxidation in air compared to steam, due to a lower supply rate of oxidant for the conditions in HCE-2. The fourth peak occurred following a delay period after the introduction of steam or air. Except in cases where the Zircaloy end-caps were loose on the mini-element, the delay period corresponded to the time required to oxidize more than 75% of the Zircaloy. After such a time, the oxidation rate had dropped by about one order of magnitude. With a lower oxidation rate, the local gas-phase oxygen potential near the surface of the UO<sub>2</sub> and adjacent to the oxidizing Zircaloy would be higher than under conditions of rapid oxidation, due to O<sub>2</sub> depletion (in air) or H<sub>2</sub> production (in steam). The higher oxygen potential would make UO<sub>2</sub> oxidation more favourable, and this in turn may be the cause for the final increases in release rate.

Cs releases from mini-elements were similar to the Kr releases, except in the inert heating period, where the rates were much lower than Kr. Above 1500°C, however, the Cs release rates were almost equivalent to Kr if a delay of about 500 s was included for the Cs. The Cs release after oxidation was also delayed relative to the Kr.

Kr and Cs releases from bare UO<sub>2</sub> fragments were very similar, and the Cs was not delayed relative to the Kr. This suggests that the Zircaloy cladding played a role in retarding the Cs releases from mini-elements. Also, steam oxidation of bare fragments produced an immediate increase in the release rate, and the rate was higher from a fragment than from an oxidized mini-element at the same temperature. A surprising result was an increase in the threshold temperature for release of both Cs and Kr from the bare UO<sub>2</sub> relative to mini-elements. This is not understood, but it could be speculated that the fragments originated from the central portion of the fuel, and were therefore representative of a higher operating temperature than the mini-element specimen.

### 6.2. CANDU FUEL TESTS

Both Kr and Cs releases from the CANDU fuels tested were qualitatively similar to the behaviour described above for the LWR fuel. However, results from the CANDU specimens showed large differences that were related to the fuel-element power levels. Low power ratings (from intermediate elements) produced only a small release of both Cs and Kr during the inert heating period (7.5% Kr and 5% Cs in test BM5). This was much less than for an outer element under the same conditions (22% Kr and 10% Cs in test BM3). The threshold temperatures for Kr release were between 1350 and 1400°C in all of the Bruce-A CANDU fuels, independent of element power. The threshold temperature for Cs release was about 1200°C for all of the CANDU specimens.

Post-irradiation measurements of the noble gas volumes in the Bruce-A CANDU fuel indicated that 4% (BM5, intermediate element) and 24% (BM3, outer element) of the stable noble gases were released during irradiation (i.e., released to the gap). This gas would have been released from the fuel element when it was cut to make mini-element specimens. The Cs that was released during irradiation would probably have remained in the mini-elements after cutting because of its low volatility in the cold fuel. It is possible that this Cs would be available for release in the annealing tests upon heating the mini-elements to a sufficiently high temperature, such that the condensed Cs compounds were volatile. Based on the half-life dependence of isotopic releases, the gap release fraction of

Cs-134 and Cs-137 should be similar to the stable noble gas releases. The results of tests BM3 and BM5, however, showed Cs releases during heating that were much lower than the gap release fractions for noble gases. This could indicate that either some Cs was released from the fuel element when it was cut into mini-elements, or else some of the Cs released to the gap had formed a low-volatility compound and remained in the mini-element during heating up to 1500°C.

### 6.3. COMPARISON OF CANDU AND LWR RELEASES

The CANDU and LWR release characteristics can be compared in tests LM5 and BM3 (Figures 4 vs 12 and 7 vs 13). Both of these tests were heated at 5°C/min to 1500°C, then exposed to steam. The Cs releases from the CANDU fuel began at about 1200°C compared to 1350°C for the LWR fuel, but the rate was much lower from the CANDU fuel. The temperature rise at the start of steam oxidation produced a measurable increase in the release rates from the LWR fuel, but minimal effect for the CANDU specimen. This may be due to the larger Zr/VO<sub>2</sub> ratio for the LWR specimens, which may have produced a more severe thermal transient due to the oxidation. Also, the LWR specimens may have been more susceptible to cracking in the thermal transient, since the higher-powered CANDU fuel was already extensively cracked during irradiation. The Kr releases were more difficult to compare because the amount released during irradiation was unknown for the LWR fuel. However, Figures 4 and 12 show that the large Kr peak released during inert heating started at 1200°C in the LWR fuel and at 1400°C in the CANDU fuel. This may be related to the maximum temperature reached during irradiation, which was higher in the CANDU fuel.

The measured differences between CANDU and LWR releases can probably be attributed to differences in burnup, operating power and the ratio of Zr/VO<sub>2</sub> in the specimens tested. Further speculation must await the results of post-test ceramography and electron microscopy to observe the microstructures, cracking patterns and porosity.

### 6.4. COMPARISON WITH ORNL RESULTS

Direct comparison of the release rates and cumulative releases during the ORNL tests and the HCE-2 tests could be misleading because of a number of factors. The irradiation history and size of the fuel specimens used in the ORNL tests were different from the LWR fuel specimens used in HCE-2. Also, the heating rates, annealing times, and oxidant flow rates were different between the tests compared here. However, note that: (1) there was a similar release during heating for tests with similar heating rates, regardless of the environmental conditions (oxidizing or inert), and (2) the short annealing times in the ORNL tests did not produce the second increase in rapid (oxidative) releases that were observed in all of the HCE-2 tests.

## 7. CONCLUSIONS

The kinetics of fission-product release from high-burnup CANDU and LWR fuels were measured in the HCE-2 annealing experiments. Zircaloy-clad specimens or bare VO<sub>2</sub>

fragments were heated in an inert environment and then exposed to flowing steam or air at atmospheric pressure between 1350 and 1650°C. A simultaneous measurement of the oxidation rate of the fuel was made during these experiments.

The Kr release kinetics could be divided into four different stages. During heating in inert conditions, a burst-release of Kr was detected starting at 1200 to 1400°C. The initiating temperature and the quantity of gas released in this stage was found to depend on the irradiation history. The second stage occurred only in fuel heated above 1400°C and could also be characterized as a burst-type release, although the peak rate and total quantity released in this stage increased with annealing temperature. A third peak of gas release occurred upon changing to an oxidizing environment. This peak was produced by a temperature escalation in the fuel resulting from exothermic oxidation of the Zircaloy. A final large gas release occurred after most of the Zircaloy cladding was oxidized, and presumably oxidation of the VO<sub>2</sub> was occurring.

In general, the kinetics of Cs release were similar to Kr, except for lower Cs releases in the first stage, and a delay of several hundred to several thousand seconds relative to Kr, most notably in the first and fourth release stages. The impaired Cs releases in the first stage may be due to the formation of low-volatility compounds after Cs was released from the VO<sub>2</sub> during irradiation. The Cs delay relative to Kr during oxidation of the mini-element specimens was attributed to the presence of the Zircaloy, since this delay was not measured in other tests on bare VO<sub>2</sub> specimens.

Differences between the CANDU and LWR results should be attributed to the different irradiation histories for the fuels tested, and perhaps the different ratio of Zr/VO<sub>2</sub> in the LWR and CANDU specimens.

Some of the HCE-2 results were compared with similar tests from the ORNL HI and VI experiments. In general the comparison produced similar results; however, a detailed comparison of the release rates and cumulative releases could be misleading because of differences in the irradiation history and size of the fuel specimens, the heating rates, annealing times, and oxidant flow rates. Further studies with LWR and CANDU fuels at similar burnup should be conducted to investigate the applicability of LWR data to CANDU fuel behaviour under postulated accident scenarios.

## ACKNOWLEDGEMENTS

Funding for this work was provided by the CANDU Owners Group R&D Program: Working Party No. 08, WPIR No. 492. R.D. Barrand, R.F. O'Connor and G.W. Wood are acknowledged for equipment design and operation, and N.A. Keller for gamma spectroscopy support. The staff of the Universal Cells are acknowledged for their assistance during the testing. G.P. Smith, Jr., of ABB-Combustion Engineering, and the US DOE, are acknowledged for allowing us to use the high-burnup LWR fuel samples in these tests. M.R. Floyd of Ontario Hydro is acknowledged for providing the Bruce-A fuel with irradiation histories and gas puncture results. F.C. Iglesias of Ontario Hydro is acknowledged for helpful discussions during the planning of these tests.

## REFERENCES

- [1] LINDNER, R., MATZKE, H.J., Z. Naturforschg, 14a 582 (1959).
- [2] LEWIS, W.B., MACEWEN, J.R., STEVENS, W.H., HART, R.G., Fission gas behaviour in  $UO_2$  fuel, (Third UN Int. Conf., Geneva, August 1964) and AECL report AECL-2019.
- [3] MIEKELEY, W., FELIX, F.W., Effect of stoichiometry on diffusion of xenon in  $UO_2$ , J. Nucl. Mat., 42 297 (1972).
- [4] HUNT, C.E.L., et al., The release and transport of fission products during oxidation of  $UO_2$  in air, (Proc. 192nd ACS Symposium on Chemical Phenomena Associated With Radioactivity Releases During Severe Nuclear Plant Accidents Anaheim, September 7-12, 1986), report NUREG/CP-0078.
- [5] IGLESIAS, F.C., et al.,  $UO_2$  oxidation and fission product release, (Workshop on Chemical Reactivity of Oxide Fuel, Berkeley, UK, April 1987).
- [6] COX, D.S., et al., Fission product release from  $UO_2$  in air during temperature ramps, (Proc. 8th Conf. Can. Nucl. Soc. St. John NB, Canada, June 1987).
- [7] HUNT, C.E.L., et al.,  $UO_2$  oxidation in air or steam - release or retention of the fission products Ru, Ba, Ce, Eu, Sb and Nb, (Proc. 8th Conf. Can. Nucl. Soc. St. John NB, Canada, June 1987).
- [8] HUNT, C.E.L., IGLESIAS, F.C., COX, D.S., Measured release kinetics of iodine and cesium from  $UO_2$  at high temperatures under reactor accident conditions, in "Fission product transport processes in reactor accidents," J.T. Rogers, ed., Hemisphere Publishing, (Proc. ICHMT Seminar on Fission Product Transport Processes in Reactor Accidents, Dubrovnik, Yugoslavia, 1989), pp. 257.
- [9] SHIBA, K., Fission iodine and xenon release from the  $UO_2-U_3O_8$  system with emphasis on radiation damage, J. Nucl. Mat. 57 271 (1975).
- [10] PEEHS, M., KASPAR, G., Experimental investigations of Cs and I release from irradiated  $UO_2$ , High-Temp.-High Press. 14 517 (1982).
- [11] IGLESIAS, F.C., HUNT, C.E.L., GARISTO, F., COX, D.S., Ruthenium release kinetics from uranium oxides, in "Fission product transport processes in reactor accidents," J.T. Rogers, ed., Hemisphere Publishing, (Proc. ICHMT Seminar on Fission Product Transport Processes in Reactor Accidents, Dubrovnik, Yugoslavia, 1989).
- [12] OSBORNE, M.F., LORENZ, R.A., COLLINS, J.L., Atmospheric effects on fission product behaviour at severe LWR accident conditions, (Proc. Int. Topical Meeting on Safety of Thermal Reactors, Portland Oregon, July 1991), pub. American Nuclear Society.
- [13] GRIMES, R.W., CATLOW, C.R.A., The stability of fission products in uranium dioxide, Phil. Trans. R. Soc. Lond. A 335 609-634 (1991).
- [14] OSBORNE, M.F., LORENZ, R.A., TRAVIS, J.R., WEBSTER, C.S., NORWOOD, K.S., Data summary report for fission product release test HI-2, report NUREG/CR-3171 (ORNL/TM-8667) 1984.
- [15] OSBORNE, M.F. et al., Data summary report for fission product release test VI-3, report NUREG/CR-5480 (ORNL/TM-11399) 1990.
- [16] MATHIOT, A., LEMARIOS, G., WARLOP, R., Analysis of fission product release during a simulated severe fuel damage accident: the HEVA program, (Proc. IAEA technical committee meeting on fuel behaviour and fission product release in off-normal and accident conditions, Vienna, November 1986).
- [17] FLOYD, M.R., NOVAK, J., TRUANT, P.T., Fission-product release in fuel performing to extended burnups in Ontario Hydro nuclear generating stations, this meeting.
- [18] COX, D.S., O'CONNOR, R.F., SMELTZER, W.W., "Measurement of oxidation/reduction kinetics to 2100°C using non-contact solid-state electrolytes", (Proc. 8<sup>th</sup> Int. Conf. Solid State Ionics, Lake Louise, Oct. 1991) accepted for publication in J. Solid State Ionics.

## THERMAL CONDUCTIVITY AND GAS RELEASE FROM SIMFUEL

P.G. LUCUTA\*, R.A. VERRALL\*,  
H. MATZKE\*\*, I.J. HASTINGS\*

\*AECL Research,  
Chalk River Laboratories,  
Chalk River, Ontario, Canada

\*\*European Institute for Transuranium Elements,  
Commission of the European Communities,  
Joint Research Centre,  
Karlsruhe

### Abstract

SIMFUEL --SIMulated high-burnup UO<sub>2</sub>, FUEL-- replicates the chemical state and microstructure of irradiated fuel. Non-radioactive elements in amounts equivalent to given burnup compositions are added to UO<sub>2</sub> powder. The preparation route features high-energy grinding and spray drying to achieve homogeneous dispersion on a submicrometre scale, and sintering to provide atomic-scale mixing. This leads to a phase structure representative of high-burnup fuels having operated at high temperatures. Extensive characterization shows solute fission-product atoms dissolved in the oxide matrix, spherical metallic Mo-Ru-Pd-Rh precipitates and ceramic phases.

Thermal properties of UO<sub>2</sub> at high temperature are among the most important parameters in assessing fuel behaviour at high burnup. Changes in thermal conductivity occur in the fuel during irradiation as fission gas bubbles form and solid fission products (dissolved and precipitated) build up. The thermal diffusivity and specific heat of SIMFUEL were measured between 25 and 1500°C, at two laboratories using two different techniques, with good agreement. These data were combined to obtain thermal conductivity. The conductivity of 3 and 8 at% burnup SIMFUEL was lower than for "pure" UO<sub>2</sub> by 29 and 45% at room temperature, and by 6 and 15% at 1500°C. The decrease in thermal conductivity was approximately linear with burnup. An increase in central fuel temperature of about 200°C was roughly estimated from the change in thermal conductivity reduction of 3 at% burnup SIMFUEL for a linear power of 45 kW/m, assuming no influence from gas bubbles.

Isochronal and isothermal release of ion-implanted krypton from UO<sub>2</sub> and SIMFUEL specimens were measured under reducing conditions for gas concentrations which led to temporary trapping of the gas due to gas-defect interactions. Results for these conditions showed somewhat higher release rates from SIMFUEL. For example, at 1400°C the release data from UO<sub>2</sub> and 8 at% burnup SIMFUEL corresponded to an increase by a factor of 7 in the effective diffusion coefficient. For comparison, the increase of 200°C, in central temperature 1500°C, would lead to a 3 times larger change in the diffusion coefficient.

## 1. INTRODUCTION

Extending burnup has been identified as a practical means of improving the economics of water-reactor operation, via improved fuel utilization and reduced spent-fuel volumes. Current development work at AECL in support of the CANDU<sup>1</sup> reactor is focusing on fuel cycles (slightly-enriched and recovered uranium) using the new CANFLEX fuel bundle [1-4]. In examining life-limiting factors at extended burnup, increased fission-product mobility and gas release rank among the most important.

Studies of irradiated fuels provide important data on the thermodynamics and chemistry of the fission products at high burnup. However, the associated high costs and practical difficulties have limited the number of these studies. Simulated high-burnup fuel, termed SIMFUEL represents a convenient way to contribute to the data base. Most of the data used in computer models, even for long irradiation times, were obtained on unirradiated UO<sub>2</sub> or by empirical fitting to the results of post-irradiation examinations. Thus, measurements on SIMFUEL of properties such as fission-product mobility and thermal conductivity can improve this situation.

At extended burnup, there is experimental evidence that fission-gas release is higher than would be expected from low-burnup extrapolation, or from computer codes developed so far. A decrease in the fuel thermal conductivity is a possible indirect reason for this enhanced release at high burnup. Heat transfer degradation, particularly in the fuel-sheath gap, could also contribute to higher fuel-operating temperatures. The only reported study on irradiated high-burnup fuels, by Daniel and Cohen [5], showed a marked decrease in thermal conductivity at high burnup compared to the fresh fuel. Their data for 4 at% burnup<sup>2</sup>, analyzed by Marchandise [6], showed a difference of 27% at 500°C compared to unirradiated fuel, decreasing to 10% at 1500°C. These are measurements that include all changes in the fuel induced by irradiation: dissolved and precipitated fission products, changes in stoichiometry, displacement of the atoms in the lattice, and fission-gas bubbles and cracks. The decrease of the thermal conductivity was also shown by several experiments who have measured the effect of a single additive to UO<sub>2</sub> -- gadolinia [7-9], yttria [10], different rare earths [11]. All additives decreased the conductivity and the reduction was proportional to the amount of the additive. Schmitz et al. [12] fabricated simulated (U,Pu)O<sub>2</sub> fuel with eight additives at an equivalent burnup of 16 at%, and showed that between 500 and 800°C, the conductivity of the high-burnup simulated fuel was comparable to pure (U,Pu)O<sub>2</sub> when the O/M ratio was 1.97, but was 30% lower when the ratio was 2.0. A similar experiment by Runfors [13] with UO<sub>2</sub> doped with oxides of zirconium, rare earths, and alkaline earths (both forerunners of SIMFUEL) indicated a degradation in conductivity by 18% compared to pure UO<sub>2</sub> between 500 and 1000°C.

<sup>1</sup> CANada Deuterium Uranium

<sup>2</sup> 1 at% burnup = 225 MW.h/kg U = 9375 MW d/t U

Fission-gas release from operating fuel is a complex process, depending not only on temperature, temperature transients, microstructure and O/M ratio of the fuel, but also on gas concentration. Release to the fuel-to-sheath gap depends on intragranular diffusion to grain boundaries, accumulation of the gas at the boundaries and venting to the gap via tunnels or, more likely, via the mechanical cracking which accompanies a temperature transient. Intragranular gas concentrations, in-reactor, are strongly dependent on the local operating fuel temperature.

This paper describes briefly the concept of simulated high-burnup  $\text{UO}_2$ -based fuel -- termed SIMFUEL. It also presents the results on thermal conductivity of 3 and 8 at% SIMFUEL, calculated from thermal diffusivity and specific heat measurements. The results are compared to those obtained from pure  $\text{UO}_2$ . Gas-release experiments from ion-implanted SIMFUEL provide useful data to assess the diffusion within the grains.

## 2. SIMFUEL CONCEPT

For the last few years, a program has been in place at Chalk River Laboratories in cooperation with the Institute for Transuranium Elements and Whiteshell Lab. to

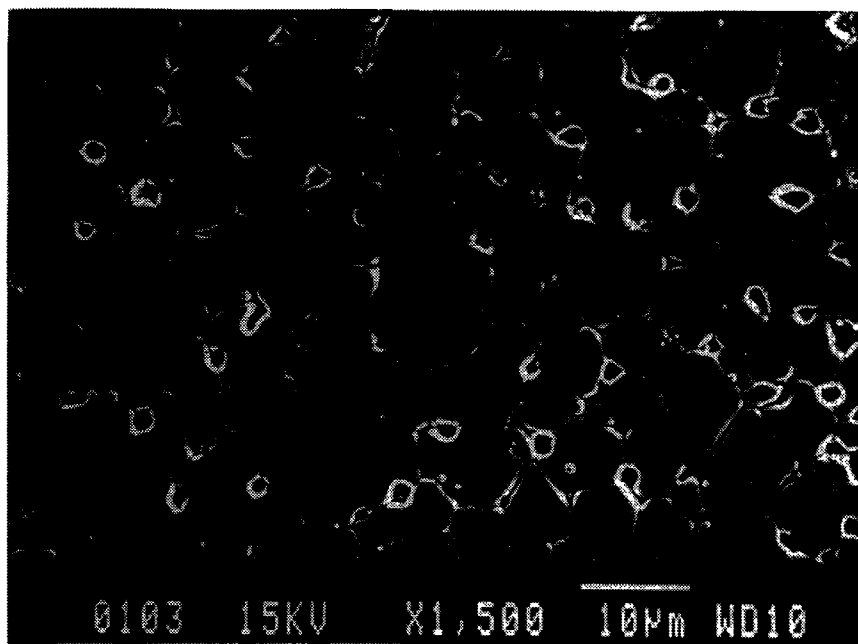


Figure 1. Secondary electron image of polished and etched surface showing matrix grains with solute La and Nd.

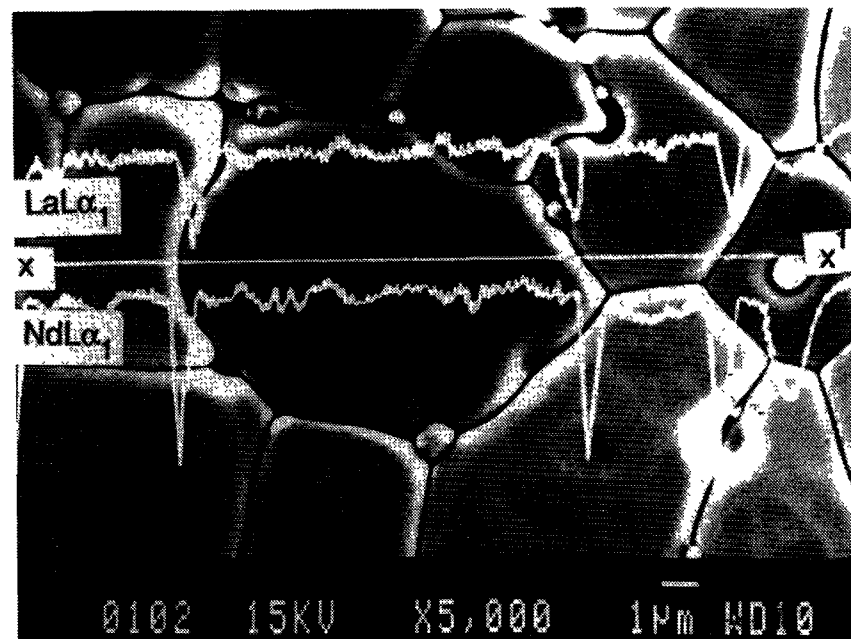


Figure 2. SEM image of polished, thermally etched SIMFUEL surface with spherical metallic precipitates.

fabricate and test SIMFUEL. The burnup is simulated by doping  $\text{UO}_2$  with stable additives in an appropriate amount. Because gases and volatiles are not added, the microstructure does not contain bubbles observed in irradiated fuel. We have previously reported the fabrication procedure of  $\text{UO}_2$ -based SIMFUEL with an equivalent burnup of 3 and 8 at% [14-16].

To replicate the complex structure of high-burnup fuel, it is necessary to achieve very fine and uniform dispersion of all added fission products and to reach phase equilibrium during SIMFUEL preparation. This implies that SIMFUEL constituents must be mixed homogeneously on a submicrometer scale and then heated to a sufficiently high temperature to achieve homogeneity on an atomic level by diffusion. So, vacuum dried, high purity (99.999%) oxides were dry mixed with  $\text{UO}_2$  powder. High-energy, wet attrition-ball milling was used to achieve a uniform fine dispersion.

A spray-drying step served to lock the selected composition (corresponding to burnups of 3 and 8 at%) into granules. Conventional precompaction, granulation, pressing and sintering at  $1700^\circ\text{C}$  for 2 hours in flowing  $\text{H}_2$  yielded a structure typical of a fuel that has operated at high temperature where solid phase precipitates and gas bubbles form.

Extensive characterization [15-17] demonstrated the equivalence of the microstructure and phase structure of SIMFUEL to irradiated high-burnup fuel. All classes of fission products (except the gases and volatiles) were found in SIMFUEL. The  $\text{UO}_2$  matrix contained fully or partially dissolved oxides (e.g., Nd, La, Ce, Y, Sr, Zr, - Figure 1). Spherical metallic Mo-Ru-Pd-Rh precipitates were uniformly dispersed throughout the matrix (Figure 2) and a fine perovskite phase of the  $(\text{Ba,Sr})_2\text{ZrO}_3$ -type was also seen at matrix grain boundaries.

Due to the absence of fission-gas bubbles, SIMFUEL yields the *intrinsic* thermal conductivity of the material. The use of SIMFUEL for thermal conductivity measurements has a number of advantages:

- Permits easy and reliable measurements due to the absence of high radioactivity.
- Provides relatively large samples, well characterized and free of cracks, for thermal diffusivity measurements.

Intragranular gas mobility at extended burnup can be investigated using ion-implanted SIMFUEL specimens [18-24]. The implanted doses can be easily controlled and ion distribution can be characterized [25]. A high implantation dose corresponds qualitatively to fuel at high burnup that has been operating at low temperature and experiences only limited intragranular-gas migration. Medium and low implantation doses correspond qualitatively to fuel of low-burnup, or, to a certain extent, high-burnup fuel that has been operating at higher temperatures and experiences substantial intragranular gas migration. Intrinsic undisturbed diffusion of single gas atoms only occurs at very low gas concentrations (0.1 appm), corresponding to short reactor irradiations of up to a few days only. At higher gas concentrations, the gas atoms, which are largely insoluble in the matrix, interact with lattice defects and different types of radiation damage [18]. They also interact with each other, forming clusters of a few atoms. At high concentrations, they precipitate into bubbles. Such gas atoms trapped at defects or clusters or precipitated into bubbles are temporarily immobilized, thus significantly reducing the "effective" diffusion coefficient (their mobility within the fuel) by up to a factor of  $10^3$ . The present tests, performed in the absence of fission, are reproducing the effect of non-volatile fission products on gas diffusion within  $\text{UO}_2$  grains.

### 3. THERMAL CONDUCTIVITY OF SIMFUEL

#### 3.1 Experimental

The thermal conductivity  $\lambda$  for 3 and 8 at% SIMFUEL was calculated by combining the measured values of thermal diffusivity  $\alpha$ , specific heat  $c_p$  and density  $\rho$ :

$$\lambda = \alpha c_p \rho \quad (1)$$

Thermal diffusivity was measured by laser-flash (25 - 1500°C) and modulated electron-beam (900 - 1600°C) methods [26] at two different laboratories with good agreement. In both methods, the thermal diffusivity is determined from the rear-surface temperature history after the front surface of the sample was heated by the

beam. The measurements for both methods were performed in vacuum. A second set of laser-flash measurements were performed in a low pressure, high-purity argon atmosphere. The results showed good reproducibility for multiple tests on a single specimen.

The specific heat of SIMFUEL and "pure"  $\text{UO}_2$  was measured between 25 and 600°C, using a standard Perkin-Elmer Model DSC-2 Differential Scanning Calorimeter (DSC) with sapphire as a reference material. The standard and sample, both encapsulated in pans, were subjected to the same heat flux, and the differential power required to heat the sample at the same rate as the standard was recorded. From the masses of the sapphire standard and pans, the differential power, and the known specific heat of the sapphire, the specific heat of SIMFUEL specimens was computed. For higher temperatures, in the range of 400 to 1400°C, the specific heat of SIMFUEL specimens was calculated from enthalpy data, measured using a Netzsch 404 calorimeter.

The density of SIMFUEL at room temperature was measured by standard immersion techniques. Density variation with temperature of the SIMFUEL was accounted for using the thermal expansion coefficient of  $\text{UO}_2$  ( $10 \times 10^{-6} \text{ K}^{-1}$  [26]). All thermal conductivity values were normalized to fully dense specimens by using the Loeb equation:

$$\lambda = \lambda_{\text{TD}}(1 - \beta P) \quad (2)$$

where P is the pore volume fraction, the subscript TD means fully dense sample. Theoretical densities of 10.96, 10.81 and 10.58 were used for "pure"  $\text{UO}_2$ , 3 and 8at% burnup SIMFUEL [26]. For  $\beta$  the temperature dependence:  $\beta(T) = 2.58 - 0.58 \cdot 10^{-3} T$  was used. Similar results were obtained using the Eucken-Maxwell porosity correction equation.

#### 3.2. Results and Discussion

Thermal conductivities of  $\text{UO}_2$  and, 3 and 8 at% equivalent burnup SIMFUEL, normalized to fully dense (100% TD), are given in Table 1 for various temperatures between 25 and 1500°C. They are also plotted in Figure 3. The results show a significant degradation of the thermal conductivity of SIMFUEL compared to that of "pure"  $\text{UO}_2$ . At room temperatures, the thermal conductivities of 3 and 8 at% burnup SIMFUEL are 71 and 53% that of pure  $\text{UO}_2$ . At 1500°C, the differences are smaller: 94 and 85% for 3 and 8 at% SIMFUEL, compared to  $\text{UO}_2$ . Most of the difference in thermal conductivity of SIMFUEL compared to fresh  $\text{UO}_2$  is due to the decrease in thermal diffusivity; specific heat had only a small effect (less than 3% difference between  $\text{UO}_2$  and 8% burnup SIMFUEL) and it is in the opposite direction [26].

Intuitively, the metallic precipitates should increase thermal conductivity of SIMFUEL. However, reduction is caused primarily by the dissolved fission products and possibly by the ceramic phase precipitates. Because the volume fraction of is ceramic phase is very small, it will have only a small effect. This is in good qualitative agreement with the single additive tests [7-11]. Compared to thermal

Table I Thermal conductivities of fully dense  $UO_2$  and SIMFUEL with an equivalent burnup of 3 and 8 at% between room temperature and  $1500^{\circ}C$

Temperature ( $^{\circ}C$ )	Thermal Conductivity ( $W/m^{\circ}C$ )		
	$UO_2$	3 at% SIMFUEL	8 at% SIMFUEL
25	8 281	5 773	4 413
100	7 837	5 567	4 307
200	6 994	5 182	4 081
300	6 121	4 771	3 845
400	5 511	4 336	3 656
500	4 971	4 044	3 463
600	4 670	3 832	3 209
700	4 069	3 498	3 014
800	3 750	3 232	2 866
900	3 445	3 024	2 692
1000	3 211	2 877	2 564
1200	2 889	2 560	2 318
1400	2 519	2 275	2 076
1500	2 353	2 190	1 984

conductivities reported for 4 at% burnup irradiated fuel [5], these results for SIMFUEL, interpolated to 4 at% burnup, show less reduction. We obtained a reduction by 16%, 10% and 8% at 500, 1000 and  $1500^{\circ}C$ , compared to 27%, 16% and 10% reported for irradiated fuel [8] at the same temperatures. This is reasonable agreement considering the two different techniques of measurements and the fact that the irradiated fuel contained gas bubbles.

The thermal resistivities ( $R = 1/\lambda$ ) of  $UO_2$  and SIMFUEL are shown in Fig 4. As obtained by Fukushima et al [9-11] for the single additive tests, the resistivity varies linearly with temperature for each SIMFUEL burnup.

$$R = A + B T \tag{3}$$

The parameters A and B for each burnup were determined by fitting the data to straight lines. Van Vliet and Haas [27] predicted that the parameter A would be

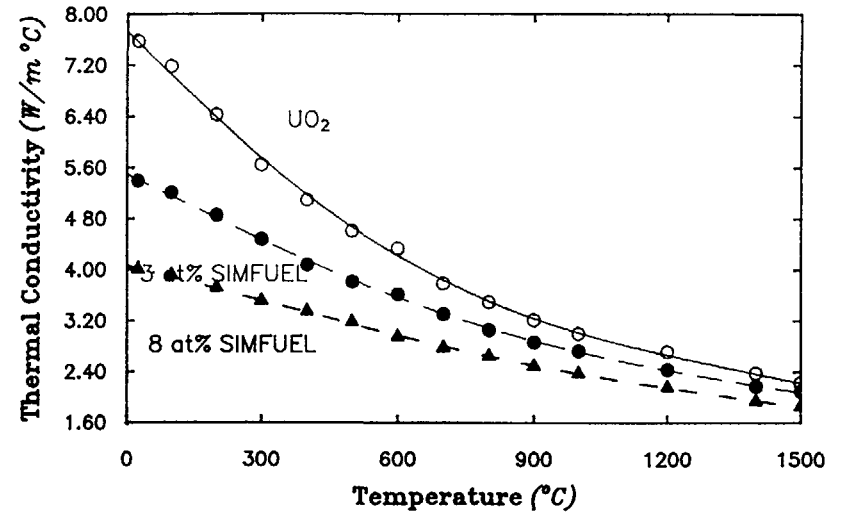


Figure 3 Thermal conductivity of  $UO_2$  and SIMFUEL (3 and 8 at% burnup) as a function of the temperature. The plotted values were normalized to 95% of the theoretical density.

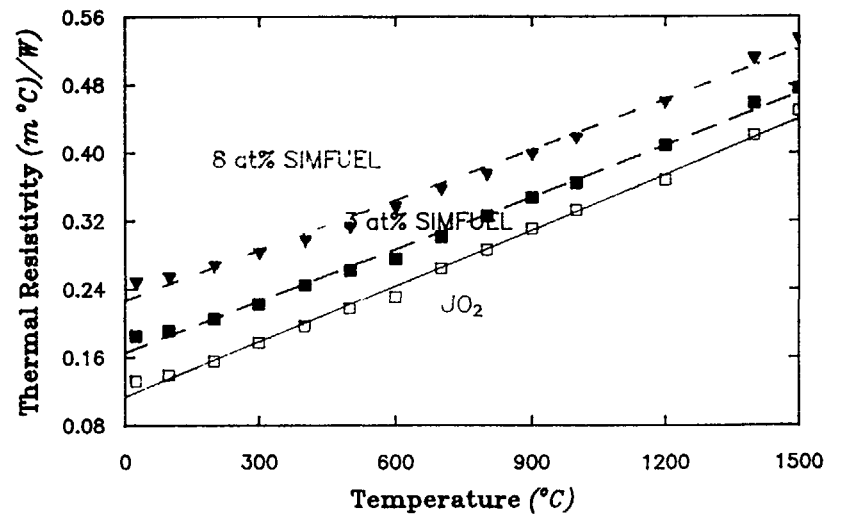


Figure 4 Thermal Resistivity of  $UO_2$  and SIMFUEL showing a linear dependence with the temperature.

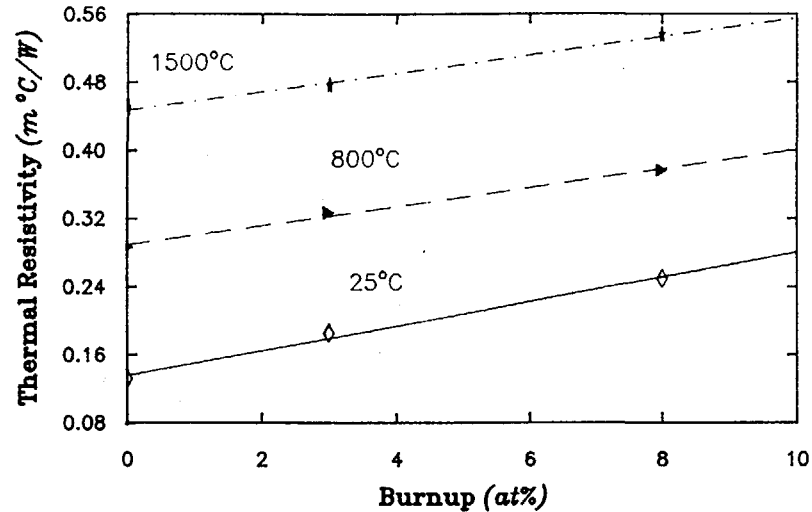


Figure 5. Thermal Resistivity as a function of the burnup.

linearly dependent on burnup, while B would be largely independent of burnup. Analysis of our results yields:

$$R = [0.053 + (0.016 \pm 0.0015) b] + [2.2 - (0.005 \pm 0.002) b] 10^{-4} T \quad (4)$$

where R is expressed in mK/W and b is the burnup in at%. This is good agreement with van Vliet and Haas [27], indicating that most of the burnup dependence is in the temperature-independent parameter, phonon-defect interaction term. Figure 5 is a plot of the thermal resistivity versus burnup for three selected temperatures, showing linear variation.

The central temperature  $T_c$  of the fuel can be approximately calculated for a given linear rating  $\chi$  and a given surface temperature  $T_s$  from the conductivity integral:

$$\chi = 4\pi \int_{T_s}^{T_c} \lambda dT \quad (5)$$

For a typical CANDU reactor linear power of 45 kW/m, the central temperature obtained from (5) using our data (no gas bubbles) is about 200°C higher for 3 at% burnup SIMFUEL than for the "pure" UO<sub>2</sub>. This predicted increase in fuel operating temperatures due to the changes in the *intrinsic* thermal conductivity is a possible reason for enhanced gas-release observed at high burnup, especially in those fuels that have not undergone high-temperature transients. We recommend incorporation of our SIMFUEL data in fuel modelling codes, to determine sensitivity and the effect on gas release.

## 4. KRYPTON RELEASE FROM SIMFUEL

### 4.1 Experimental

Discs of UO<sub>2</sub> and SIMFUEL were sliced from the sintered pellets and were carefully polished with emery paper and diamond paste to 0.05 μm. All samples were pre-annealed in reducing conditions at 1400 - 1500°C to remove polishing damage at the surface. This is necessary to obtain release, not affected by microcracks, dislocations or by the recovery of the mechanical polishing damage [28].

The polished surfaces were implanted with radioactive Kr-85 at an energy of 40 keV using the Chalk River electromagnetic mass separator. Doses of about 10<sup>12</sup> ions/cm<sup>2</sup> were obtained this way.<sup>3</sup> To achieve a second, much higher dose of about 10<sup>16</sup> ions/cm<sup>2</sup>, some samples were pre-implanted with stable Kr-84, before labelling with Kr-85. The two doses represent high and low temperature regions of high burnup fuel. In physical terms, the two doses represent conditions of trapping without bubble formation (10<sup>12</sup> ions/cm<sup>2</sup>) and conditions of extensive bubble formation (10<sup>16</sup> ions/cm<sup>2</sup>).

Release measurements were made by annealing the ion-implanted specimens in a reducing atmosphere (Ar + 8% H<sub>2</sub>), beginning at 250°C, and increasing the temperature in steps of 100°C, up to 1500°C. Each anneal lasted 15 min. The specimens were removed from the furnace and the remaining activity of Kr-85 was measured in a proportional counter. In addition, isothermal anneals were performed by annealing specimens at a constant temperature (e.g. 1500°C), and counting the remaining Kr-85 at selected intervals.

### 4.2 Results and Discussion

Typical results on Kr-release are shown in Figures 6 and 7. Figure 6 shows the isochronal release of Kr-85 (dose 10<sup>12</sup> ions/cm<sup>2</sup>) from UO<sub>2</sub> and from 3 and 8% burnup SIMFUEL with. No significant release is observed below 1000°C. Release starts above 1000°C which is the normal onset temperature for implanted UO<sub>2</sub> using these energies and doses. Due to the short diffusion distances (10-20 nm) and the absence of grain boundary effects, gas-release temperatures are generally slightly lower for ion-implanted specimens than for reactor-irradiated specimens. Even if the diffusion coefficients are the same, the release temperatures will be lower in ion-implantation studies because of the shorter diffusion distances. At higher temperatures, there was enhanced release for 3 and 8 at% SIMFUEL, compared with that from UO<sub>2</sub>. The higher release from SIMFUEL shows that trapping of gas at radiation damage is somewhat less efficient in SIMFUEL than in UO<sub>2</sub> at the high temperatures. As indicated by the arrow in Fig. 6, the difference in effective diffusion coefficients is a factor of 7 at 1500°C.

<sup>3</sup> This dose is termed "medium" because it is possible to implant doses of 10<sup>11</sup> ions/cm<sup>2</sup>, or lower, of Xe [18]. This is not possible with Kr in our present experimental arrangement.

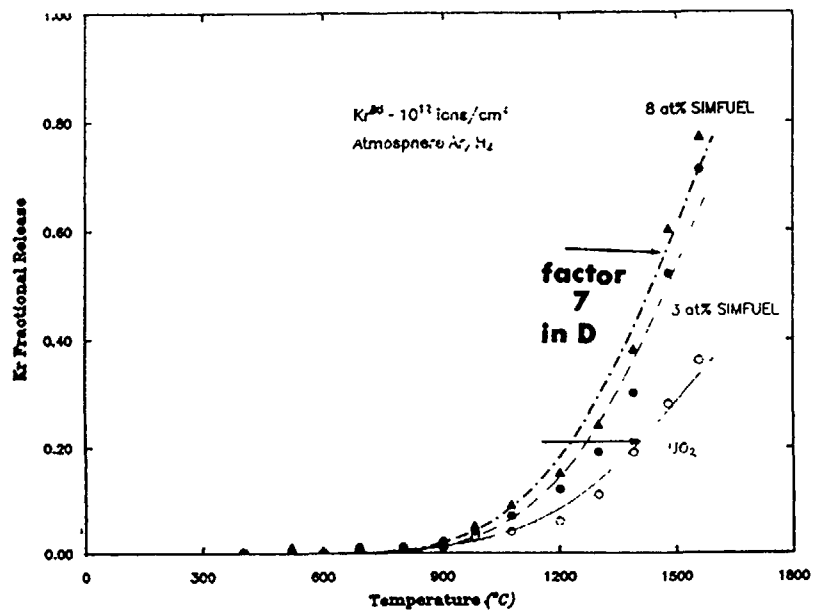


Figure 6. Isochronal Kr-release from medium-dose implanted  $UO_2$  and SIMFUEL (3 and 8 at% equivalent burnup) measured under reducing conditions. Estimated increase by a factor of 7 in diffusion coefficient value is shown.

Figure 7 gives results from 3 at% SIMFUEL and  $UO_2$  for isothermal anneals at  $1500^\circ C$  in a reducing atmosphere. The medium-dose of implanted Kr ( $10^{12}$  ions/cm<sup>2</sup>) at the energy used (40 KeV) corresponds to a gas concentration of about  $10^{-3}$  at% at which gas bubble formation does not occur, but gas trapping at radiation-induced lattice defects is already causing most of the gas to diffuse slower than in a perfect  $UO_2$  lattice [18]. Figure 7 represents a composite release curve with a fast release stage at the beginning, as shown in the lowest part of the figure by the dashed line. This stage, representative of the single-gas-atom diffusion without trapping (high diffusion coefficient), is typical for implantations at 40 keV since a fraction of the gas located near the surface can be always released without becoming trapped. The second part of the release curves represents gas diffusion in the presence of trapping and yields the effective diffusion coefficient of the gas in operating nuclear fuel [22]. It is constant with time (straight lines in the middle and upper part of the Figure 7).

Because the implantation distances are small, release fractions are larger for ion-implanted specimens than for similar experiments on irradiated fuel. Considering the diffusion coefficients obtained, the corresponding percentage of gas release for the

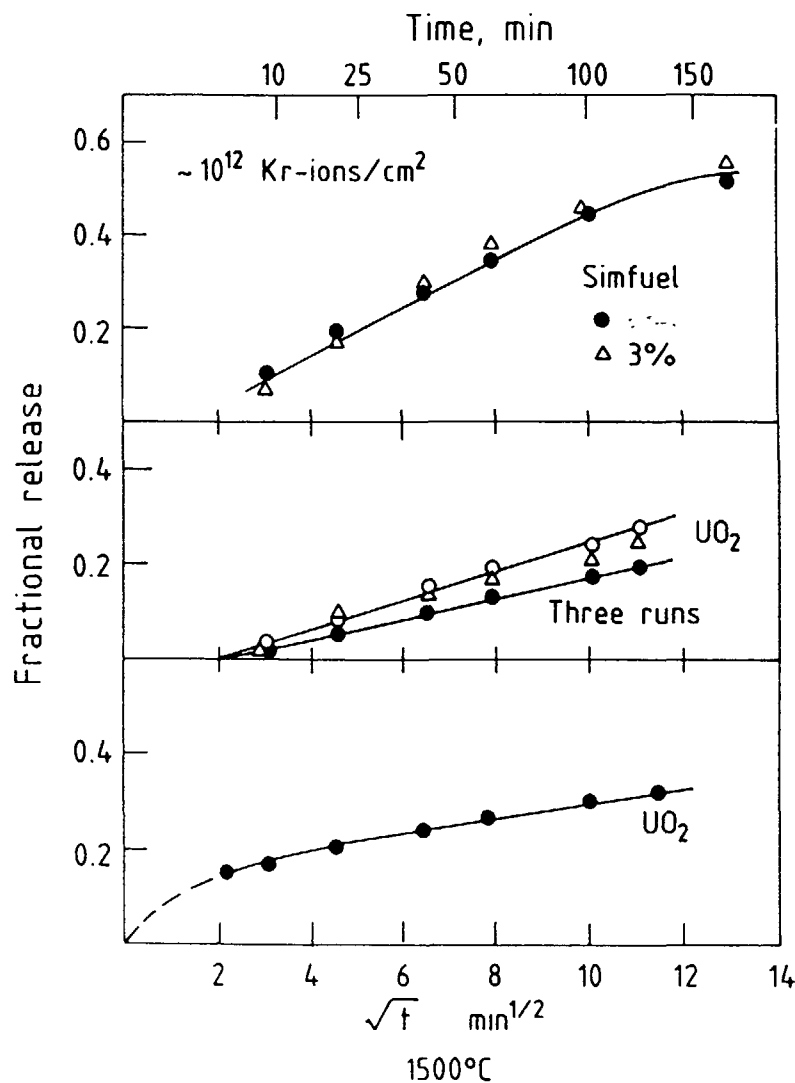


Figure 7. Isothermal medium-dose Kr release from  $UO_2$  and 3 and 8 at% burnup SIMFUEL at  $1500^\circ C$  under reducing conditions. The lower part (a) shows a typical as-measured release curve for  $UO_2$ . The two upper parts show the release results for  $UO_2$  (b) and SIMFUEL (c) following subtraction of the fast release in the first anneal step of 5 min duration (dashed curve in the lower part)

anneal conditions in Fig. 7 would be 1.1% for reactor irradiated  $UO_2$  and 1.5% for reactor irradiated SIMFUEL. Similar results were obtained for the high gas concentrations and anneals under reducing conditions. The presence of non-volatile fission products in  $UO_2$  is thus predicted not to cause a dramatic increase in gas release at high temperatures.

## 5. CONCLUSIONS

In summary:

- SIMFUEL with an equivalent burnup of 3 and 8 at% has been fabricated and shown to be a good replica of high-burnup  $UO_2$  fuels, not including gas bubbles.
- The thermal conductivity of SIMFUEL was reduced, compared with that of undoped  $UO_2$ , and the effect was larger at low temperatures.
- Releases from SIMFUEL at 1400°C were higher than from pure  $UO_2$ . For a  $UO_2$  fuel of 8 at% burnup, gas diffusion coefficients at 1500°C should be increased by a factor of 7, which will only slightly increase the gas release.

An immediate application is to insert the measured conductivities into fuel performance models and evaluate the effect on central temperature and fission-gas release.

## ACKNOWLEDGEMENTS

This work was jointly funded by CANDU Owners Group, AECL Research, and the Institute for Transuranium Elements(CEC). The contributions of R.E. Taylor and H. Groot from Purdue University (West Lafayette, Indiana), H.A. Tasman and D. Pellotiero from the European Institute for Transuranium Elements and P. Hayward from AECL Research (Whiteshell Laboratories, Manitoba), for thermal diffusivity and specific heat capacity measurements are gratefully acknowledged.

## REFERENCES

1. R. Green, P.G. Boczar and I.J. Hastings, "Advanced Fuel Cycles For CANDU Reactors," 28<sup>th</sup> Annual Conference of the CNA, Winnipeg, Manitoba, 1988 June 12-15; also AECL report AECL-9755 (1988).
2. P.G. Boczar, I.J. Hastings and A. Celli, "Recycling in CANDU of Uranium and/or Plutonium from Spent LWR Fuel," IAEA Technical Committee Meeting on Recycling Plutonium and Uranium in Water Reactor Fuels, Cadarache, France, 1989 Nov. 13-16; also AECL report AECL-10018 (1989).
3. I.J. Hastings, P.G. Boczar and A.D. Lane, "CANFLEX - An Advanced Bundle Design for Introducing Slightly-Enriched Uranium in CANDU," Intl. Symp. on Uranium and Electricity (The Complete Nuclear Fuel Cycle), Saskatoon, Saskatchewan, 1988 Sept. 18-21, CNS; also AECL report AECL-9766 (1988).
4. I.J. Hastings, A.D. Lane and P.G. Boczar, "CANFLEX - An Advanced Fuel Bundle for CANDU," Intl. Conf. on Availability Improvements in Nuclear Plants, Madrid, Spain, 1989 April 10-14; also AECL report AECL-9929 (1989).
5. R.C. Daniel and I. Cohen, Bettis Atomic Power Report WAPD-246 (1964).
6. H. Marchandise, Commission of the European Communities Report EUR-4568 f (1970).
7. S.D. Preston, C. Barrett, P. Fassina, K.C. Mills and N. Zaghini, High Temp.-High Press., 21 (1989) 287.
8. M. Hirai, J. Nucl. Mater., 173 (1990) 247.
9. S. Fukushima, T. Ohmichi, A. Maeda and H. Watanabe, J. Nucl. Mater. 102 (1981) 30.
10. S. Fukushima, T. Ohmichi, A. Maeda and H. Watanabe, J. Nucl. Mater. 105 (1982) 201.
11. S. Fukushima, T. Ohmichi, A. Maeda and M. Handa, J. Nucl. Mater. 114 (1983) 312.
12. F. Schmitz, G. Dean, M. Housseau, F. Keroulas and J.C. van Craeynest, Proc. Intern. Meeting on Fast Reactor Fuel and Fuel Elements, Eds. M. Dalle Donne, K. Kummerer and K. Schroeder GfK Karlsruhe (1970) 396.
13. U. Runfors, ENEA Fuels and Material Specialist Meeting on Fast Gas-Cooled Breeders, Stockholm, (1969), quoted by G. Fayl and K. Hansen, Risø Report No. 269 (1972).
14. R.A. Verrall, I.J. Hastings, P.G. Lucuta, Hj. Matzke and B.J. Palmer, "Preparation and Applications of Simulated High-Burnup Fuel," Proc. 11<sup>th</sup> Annual Conf. of the CNA, Toronto June 3-8 1990; also AECL report AECL-10217 (1990).
15. P.G. Lucuta, B.J. Palmer, Hj. Matzke and D.S. Hartwig, "Preparation and Characterization of SIMFUEL: Simulated CANDU High-Burnup Nuclear Fuel," Proc. Second Int. Conf. CANDU Fuel, Ed. I.J. Hastings, CNS, Toronto (1989) 132; also AECL Report, AECL-10117 (1989).
16. P.G. Lucuta, R.A. Verrall, Hj. Matzke and B. Palmer, J.Nucl.Mater. 178 (1991) 48

- 17 Hj Matzke, P G Lucuta and R A Verrall, *J Nucl. Mater* 185 (1991) 292.
- 18 Hj Matzke, *Rad Effects* 53 (1980) 219
- 19 R A Verrall, I.J. Hastings, D H Rose, Hj Matzke and I L F Ray, "Fission Gas Mobility in  $UO_2$ , Simulating High Burnup of 700 MWH/kgU," *Proc Second Int. Conf. CANDU Fuel*, Ed I J Hastings, CNS, Toronto (1989) 132, also AECL Report, AECL-10117 (1989)
20. Hj. Matzke and R.A. Verrall, *J. Nucl. Mater.* 182 (1991) 261
- 21 Hj. Matzke, I.L.F. Ray and R.A. Verrall, "Diffusion and Behaviour of Iodine and Rubidium in  $UO_2$  and  $ThO_2$ ," *IAEA, Vienna, IWGFPT/27* (1987) 183.
22. R.A. Verrall, Hj. Matzke, T. Ogawa and B.J.F. Palmer, "Iodine Rubidium and Krypton Release and Bubble Formation in Oxide Fuels," *Proc. Int. Conf. CANDU Fuel*, Ed. I.J. Hastings, CNS, Toronto (1986) 558.
23. T. Ogawa, R.A. Verrall, D.M. Schreiter and O.M. Westcott, "Dose effect on release of Ion-Implanted Noble Gases from Oxide Fuel," *Proc. Int. Conf. CANDU Fuel*, Ed. I.J. Hastings, CNS, Toronto (1986).
24. T. Ogawa, R.A. Verrall, Hj. Matzke and P. G. Lucuta, "Release of Ion-Implanted Kr From  $(Th,U)O_2$  - Effect of Matrix Oxidation," *Proc. Int. Conf. Non-Stoichiometric Compounds*, Tokyo, Dec. 1990, *Solid State Ionics* 49 (1991) 211
25. W.H. Hocking, R.A. Verrall, P. G. Lucuta and Hj. Matzke, "Depth Profiling Studies of Ion-Implanted Cesium and Rubidium in SIMFUEL and Uranium Dioxide," to be published - *Rad. Effects*
26. P.G. Lucuta, Hj. Matzke, R.A. Verrall and H.A. Tasman. "Thermal Conductivity of SIMFUEL," *E-MRS Fall Meeting, Symposium E, Strasbourg* Nov. 5-8 1991, to be published - *J. Nucl. Mater.*
- 27 J van Vliet and D Haas, 6<sup>th</sup> Post-SMIRT Seminar on Mathematical/Mechanical Modelling of Reactor Fuel Elements, Kappel, Switzerland, August 1987

## INTERGRANULAR FISSION GAS BUBBLES AND SOLID PRECIPITATES IN $UO_2$ IRRADIATED AT HIGH BURNUP IN VARIOUS CONDITIONS

M. CHARLES, G. EMINET, C. LEMAIGNAN  
Commissariat à l'énergie atomique,  
Centre d'études nucléaires de Grenoble,  
Grenoble, France

### Abstract

With a view to gaining a better understanding of fission gas release mechanisms at high burnups, the microstructures of three types of nuclear fuel of initial density close to  $10.4 \text{ g cm}^{-3}$  were studied: spheres of 1 mm diameter irradiated up to 20 GWd/THM at 900, 1200 and 1500°C, pellets of PWR type irradiated to 22 GWd/THM, with centre-line temperature of the order of 1500°C, and PWR pellets irradiated to 35 GWd/THM in a power reactor and then subjected to a number of transients between 200 and 300  $\text{W cm}^{-1}$  in an experimental reactor

SEM examination of fracture surfaces of these various fuels shows that, below 900°C, no bubbles are visible. At 1200°C, the nucleation of intergranular bubbles is clearly apparent, accompanied by metallic precipitates. At 1400 - 1500°C, apart from a tendency for grain growth, it was found that the bubbles coalesce to a considerable degree, with accompanying start of porosity interconnection and formation of tunnels at grain edges. In cases where power transients were applied, this interconnection phenomenon is particularly marked in areas having reached 1300°C in the plateau phase.

The metallic precipitates associated with the bubbles were analysed by the EDS SEM system. Three classes of precipitates were distinguished, with a typical composition being given for each of them.

These results must be supplemented by ceramographs and TEM examination.

### 1. INTRODUCTION

To ensure best possible use of nuclear fuel at high burnup, fission gas release must be more efficiently controlled, not just during stable operation, but also under load following conditions. It is therefore necessary to have more detailed knowledge of release mechanisms and fuel microstructure.

This paper deals with this aspect. It concerns the microstructure examinations made on  $UO_2$  fuel rods irradiated in various experimental programmes. Conducted in the SILOE experimental reactor at the Grenoble Research Centre of the CEA, these programmes have already been presented in terms of overall fuel behaviour (temperature, swelling, fission gas release). This paper gives the results of observations made by scanning electron microscopy (SEM) on bubble populations found at grain boundaries, and on their associated metallic fission product precipitates.

## 2. DESCRIPTION OF FUELS STUDIED

### 2.1 TANGO programme [1]

The purpose of this programme was to study the swelling of  $\text{UO}_2$  under irradiation and under quasi-isothermal, stress-free conditions. Three parameters were taken into consideration: initial density of the oxide, temperature, and burnup reached. To this effect,  $\text{UO}_2$  spheres of 1 mm diameter and of different densities (10.11, 10.43 and  $10.78 \text{ g.cm}^{-3}$ ) were irradiated at temperatures of 900, 1200 and  $1500^\circ\text{C}$  at burnups of 20, 40 and 60 GWd/THM. At high burnups, some difficulties were encountered in recovering certain batches of spheres, related to a fuel decohesion phenomenon. Consideration is given here only to results at 20 GWd/THM and for a density of  $10.43 \text{ g.cm}^{-3}$ : these spheres were irradiated at  $900^\circ\text{C}$ ,  $1200^\circ\text{C}$  and  $1500^\circ\text{C}$ . Other results (40 GWd/THM and 60 GWd/THM at  $1500^\circ\text{C}$ ) are presented in [2].

### 2.2 CONTACT Programme [3], [4] (CEA-FRAGEMA collaboration)

This programme consisted in irradiating PWR experimental fuel rods (approx. 7 cm long) in order to measure the centre-line temperature (thermocouple), stable and radioactive fission gas release (sweeping lines and special analysis lab) and the gap closure (pressure drop through the fissile column). Linear heat generating rate was  $25 \text{ kW.m}^{-1}$  (up to 12 GWd/THM) and  $40 \text{ kW.m}^{-1}$  (up to 22 GWd/THM). Samples of material irradiated at the latter level could thus be compared with the TANGO fuel, since temperature range was comparable.

### 2.3 HATAC Programme [5], [6] (CEA/EDF/FRAGEMA collaboration)

In this programme, experimental fuel rods (about 30 cm long) were remanufactured from fuel rods taken from the Fessenheim reactor (burnup of 35 and 50 GWd/THM). These rods were then subjected to a series of ten moderate power transients of the load following type ( $20$  to  $30 \text{ kW.m}^{-1}$ ), and the release of stable and radioactive fission gases was measured. This programme demonstrated the importance of fuel cracking during power variations (power increase and decrease). In this instance, fuel at 35 GWd/THM (41 GWd/THM after the series of power transients) was studied, although comparisons are difficult in this case because, on one hand, the base fuel (35 GWd/THM before re-irradiation) has not yet been studied and, on the other hand, the TANGO fuel available at 40 GWd/THM had operated at a higher temperature than the HATAC fuel.

### 2.4 SEM examination of fracture surfaces [7]

The scanning electron microscope was installed in a shielded cell in the hot lab (LAMA). TANGO fuel spheres were fractured using a special device (micrometer). In the CONTACT and HATAC pellets, micro core samples were prepared (0.3 to 2 mm diameter, approximately 2 mm long) by an ultrasonic technique. In this way, it was possible to take three micro core samples over the pellet radius.

Qualitative and quantitative analyses were carried out by dispersive energy spectrometry. Allowance was made for the disturbances caused by sample radioactivity.

## 3. MICROSTRUCTURE OF GRAIN BOUNDARIES

### 3.1 Results at 20 GWd/THM and at various temperatures

A detailed study of the results obtained on TANGO fuel is available in [2]. A brief overview of the well-known scenario [8] is given below:

- at  $T = 900^\circ\text{C}$ , no visible bubbles on grain boundaries,
- at  $T = 1200^\circ\text{C}$ , numerous, irregular-shaped bubbles are observed associated with metallic precipitates,
- at  $T = 1500^\circ\text{C}$ , numerous spherical bubbles can be seen, with coalescence, interconnection and formation of tunnels at grain edges.

The micro core samples taken on the CONTACT fuel were used to study the following temperatures (estimated from the temperature measurement):  $840^\circ$ ,  $1200^\circ$  and  $1400^\circ\text{C}$  for a burnup of 22 GWd/THM. The results are comparable to those obtained with the TANGO fuel.

- At  $840^\circ\text{C}$  (fig. 1): no bubbles, but (as with TANGO fuel) a beginning of gas accumulation between grains.
- At  $1200^\circ\text{C}$  (fig. 2): bubble nucleation has started, associated with the presence of precipitates. The irregular shape of the bubbles in question is worth noting and seems to be imposed by the presence of the precipitates. This could indicate that the precipitates were present before the bubbles, although this important question must be studied in more detail.

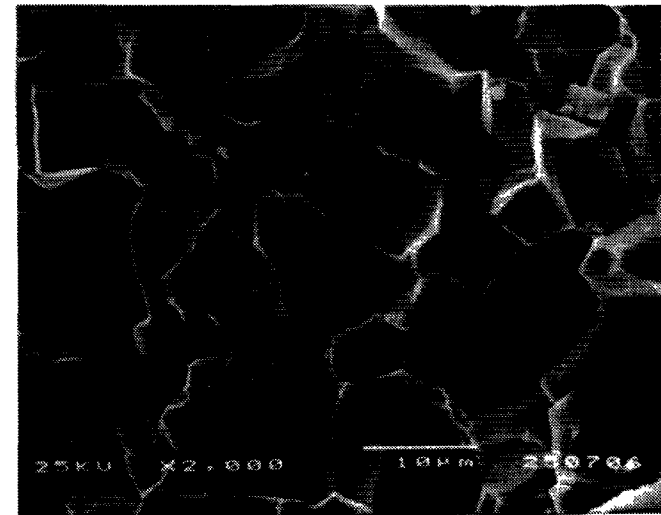
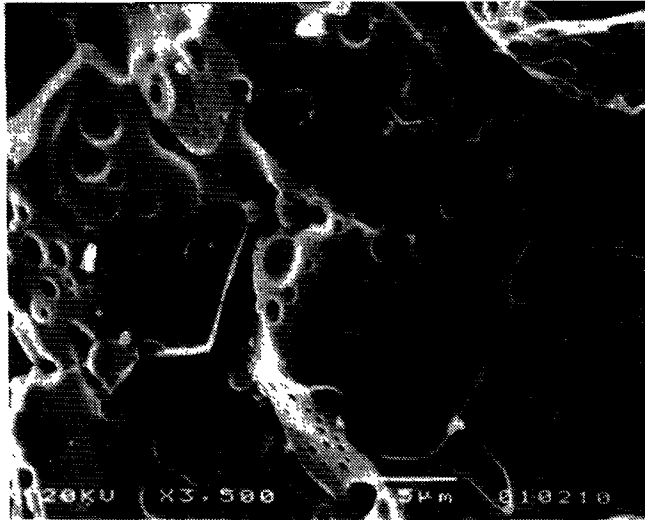


Fig. 1 : Microstructure of grain boundaries in  $\text{UO}_2$   
22 GWd/THM -  $840^\circ\text{C}$



**Fig. 2 : Microstructure of grain boundaries in UO<sub>2</sub>  
22 GWd/THM - 1200 °C**



**Fig. 3 : Microstructure of grain boundaries in UO<sub>2</sub>  
22 GWd/THM - 1400 °C**

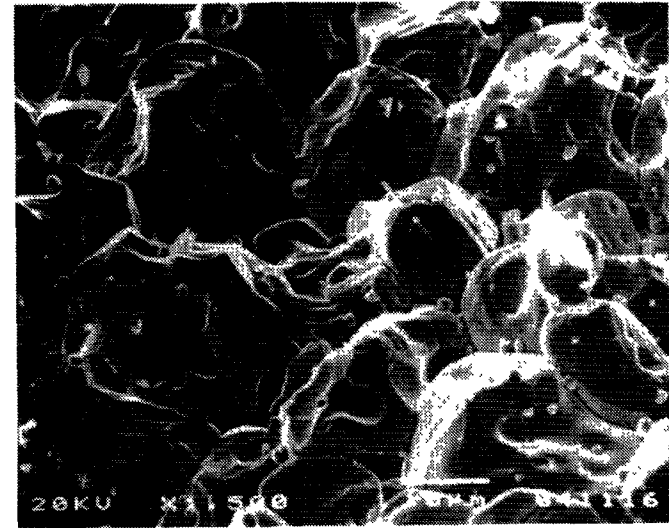


**Fig. 4 : Microstructure of grain boundaries in UO<sub>2</sub>  
41 GWd/THM - 900 °C (1300 °C)  
(+ transients)**

- At 1400°C (fig. 3): configuration already described. There is a tendency for some of the grains to reach a size of the order of 20 µm. This value is equivalent to that measured in the TANGO programme (24 µm at 20 GWd/THM and 1500°C), although more systematically than in the CONTACT programme. This phenomenon must be taken into account in assessing the change in intergranular bubbles and precipitates.  
A more detailed analysis of grain size will be performed on ceramographs.

N.B.: In TANGO at 1500°C, the following grain size values were obtained:  
at 40 GWd/THM: 29 µm and at 60 GWd/THM: 32 µm.

### 3.2 Results at 35-41 GWd/THM (transients)

It is important at the outset to mention that:

- the thermal history of the samples is complex (transients); an estimate of the centre-line temperatures reached gives 850 - 900°C in base irradiation and 1250 - 1300°C at the plateau,
- compared to the previous cases, the burnup is not the same and the fuel observation at 35 GWd/THM before the transients is currently in progress and will have to be integrated in the analysis.

TABLE I - METALLIC PRECIPITATES (COMPOSITION IN AT%)  
TANGO 1500°C

$\tau$ Gwd/THM	Mo	Ru	Tc	Rh	Pd	Sn	Ag	Cd	Sr	Ba	Zr
20	49	29	16	5	3						
40	47	27	18	6	3						
	35	33	16	9	3						
60	51	27	16	6	2						
	37	36	15	9	3						

TABLE II - METALLIC PRECIPITATES (COMPOSITION IN AT%)  
CONTACT - 22 GWD/THM

T °C	Mo	Ru	Tc	Rh	Pd	Sn	Ag	Cd	Sr	Ba	Zr
1160	45	29	12	6	9						
	39	35	13	8	21						
1300	43	30	14	7	6						
	36	39	15	11	8						
										79	21
1400	43	31	14	7	4						
	36	35	13	10	6						
										78	22

TABLE III METALLIC PRECIPITATES (COMPOSITION IN AT%)  
HATAC 900 (1300°C)

Mo	Ru	Tc	Rh	Pd	Sn	Ag	Cd	Sr	Ba	Zr
46	27	10	4	12						
37	32	11	4	16						
7	5	2		61	12	5	4	1		

Nevertheless, the high level of porosity in the grain boundaries (interconnections) in the centre-line zone (fig 4) is worth noting and can be related to the increase in fission product release which characterised this experiment [6]

### 3.3 Projects

- \* Apart from the additional examinations referred to above, work is progressing on developing a technique for preparing thin films of irradiated fuel so that TEM may be used to examine the fuels studied by SEM
- \* Systematic characterisation of the bubble population (size, density), similar to that started for TANGO [2] should provide a means of determining the order of magnitude of a highly important phenomenon the re-resolution rate of bubbles by fission spikes [5]

## 4. METALLIC PRECIPITATES

The EDS SEM system was used to analyse a great number (~50) of precipitates of the various fuels studied. The results of this analysis are given in tables I to III in the form of typical compositions. Notwithstanding the statistical problem involved in the observations, three major classes of precipitates can be distinguished

- Mo, Ru, Tc, Rh and Pd with one or two compositions which do not appear to be particularly affected by the irradiation conditions and are compatible with known results [9], [10],
- Ba - Zr (80 at% - 20 at%), in oxide form, (CONTACT fuel at 1300 - 1400°C),
- (Mo, Ru, Tc) Pd, Sn with Pd 60 - 70 at% and Sn in appreciable quantities (10 - 15%) (HATAC fuel)

Knowledge of these compositions is of great use in validating considerations developed to determine the oxygen balance in an irradiated fuel [11]

A more detailed analysis of these precipitates is planned by means of TEM studies

### References

- [1] KAUFFMANN, Y, MORLEVAT, J P, JANVIER, J C, BRUET, M, IAEA Specialists' Meeting on Water Reactor Fuel Element Performance Computer Modelling, Blackpool (1980)
- [2] EMINET, G, Thesis, CNAM, Paris (1985)
- [3] CHARLES, M, ABASSIN, J J, BARON, D, BRUET M, MELIN, P, IAEA Report IWGFPT/13 (1982), 447
- [4] CHARLES M, CHENEBAULT, P, MELIN P, ANS Topical Meeting on Light Water Reactor Fuel Performance, Orlando (1985)

- [5] CHARLES, M, SIMMONS, J, LEMAIGNAN, C, IAEA TCM on Modelling of Water Reactor Fuel Elements in normal, transient and accidental conditions, Preston (1988)
- [6] PORROT, E, CHARLES, M, HAIRION, J P, LEMAIGNAN, C, FORAT C, MONTAGNON, F, International Topical Meeting on LWR Fuel Performance, Avignon (1991)
- [7] EMINET, G, FAURE, Y, European Working Group on Hot Laboratories, Barnwood (1991)
- [8] CHARLES, M, Ann Chim Fr (Materials Science), 10 (1985) 415
- [9] KLEYKAMP, H, J Nucl Mater 131 (1985) 221
- [10] LUCUTA, P G et al, J Nucl Mater 178 (1991) 48
- [11] CHARLES, M et al, this Meeting, Session 3

## FGR MODEL IMPROVEMENT FOR HIGH BURNUP FUEL ANALYSIS

K. MORI, H. IKEDA, N. FURUYA  
Nuclear Fuel Industries Limited,  
Osaka, Japan

### Abstract

NFI has developed and has been utilizing FPAC code (Fuel Performance Analysis Code) to analyze fuel behavior. Two main models in FPAC were revised in 1988 to expand the capability of the code based on the available high burnup fuel data at that time. Fission gas release from pellets (FGR) is modelled in FPAC based on diffusion theory. Diffusion constant in the model is consist of three terms K1, K2 and K3. K1 models the gas channels through grain boundaries and was revised to be more sensitive to fuel temperature. K2 models FGR enhancement by burnup increase and was adjusted to be less sensitive to burnup. K3 models the gas channels through open porosities. As a total, these constants were adjusted to minimize the error of code prediction.

New pellet relocation model was introduced into the code to predict the fuel temperature and clad deformation accurately. FGR is sensitive to fuel temperature and the code prediction is closely related with these models.

The accuracy of the improved code was evaluated. FGR, clad OD, fuel temperature and inner pressure which were calculated by FPAC, were compared with available test data. These results were submitted to licensing authorities and code revision for licensing was accepted.

It was confirmed later that the revised FGR model could also predict the FGR of gadolinia bearing fuel correctly.

New design criteria for fuel rod inner pressure was accepted at the same time. A design limit was set at the value which does not increase the pellet clad gap during a normal reactor operation. The design value was calculated by the code, taking a code error into account. The code was used for analyses of NFI PWR fuel for burnup extension.

The demo fuel assemblies were irradiated in Ohi-1 for four cycles and attained the burnup of max 48 GWd/t (fuel rod). Hot cell PIE was performed at a facility in JAERI and was completed in 1991. The accuracy of the code in high burnup range was verified again by PIE data. FGR was low though high burnup was attained. This confirmed again that the fuel temperature is a more dominant factor in FGR than burnup increase. But pellet rim effects must be an important factor for higher burnup fuel evaluation.

## 1. Introduction

The accurate evaluation of fuel behavior is an important issue to achieve high burnup. Nuclear Fuel Industries, Ltd. (NFI) developed and has been utilizing a computer code "FPAC" (Fuel Performance Analysis Code) to analyze PWR fuel behavior.

FPAC code improvement was started when Japanese PWR utilities made a plan to extend fuel burnup up to 48 GWd/t (Fuel assembly). The objective of the improvement was set to expand the applicable burnup range of the code over this value. To achieve this objective, the models for fuel temperature calculation and fission gas release (FGR) were mainly studied, since these items have the largest effect on fuel behavior.

This paper describes the FGR model improvement and presents verification data which NFI has obtained so far.

## 2. History

A new FGR model for high burnup fuel was proposed by the USNRC in 1978<sup>(1)</sup>. NFI checked the validity of the model and introduced this model into FPAC. EPRI presented their opinion in 1979 that the NRC model was too sensitive to a burnup effect<sup>(2)</sup> and we also evaluated that the FGR model was too conservative for LWR fuel.

NFI surveyed the published models at that time and selected the KWU model<sup>(3)</sup> as a basis for revised model, since the KWU model was based on maximum available data. FGR data of high burnup LWR fuel was limited to KWU data at that time.

NFI revised parameters in the model to minimize the error of code prediction, using available data including proprietary data from the HBEP (High Burnup Effects Program).

A process to extend the fuel burnup in Japan is shown in Fig.-1. The first step to attain high burnup was a demo fuel irradiation in Ohi Unit 1 of Kansai Electric Power Company (Kansai).

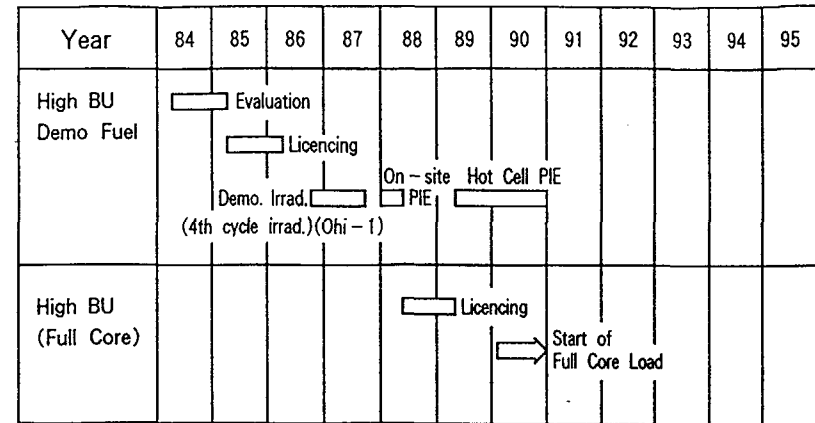


Fig.-1 Burnup Extension Plan

The improved FPAC was used to confirm demo fuel integrity as a reference and the original FPAC was used for the demo fuel design, since the improved FPAC was under licensing review.

After an approval of the improved FPAC by the licensing authority, the code was used to design high burnup fuel. The pre-pressurization of high burnup fuel was reduced to satisfy new design criteria for higher fuel rod pressure. The new design criteria precludes the increase of pellet-clad gap size during normal operation.

## 3. Model Description

FPAC is a computer code which analyzes fuel behavior during normal reactor operation. In order to predict FGR correctly, an accurate temperature calculation is required, since FGR is largely dependent on fuel temperature.

The original FPAC was found to be conservative in predicting fuel temperature, therefore fuel relocation model was introduced for reduction of conservatism in the temperature calculation. In

Table-1 Data for FGR Model Improvement

• HBEP	(Task-2)
• Zorita	(WH Program)
• BR-3	(WH Program)
• Oconee-1	(B & W Program)

this model, pellet clad gap was dealt with differently between the mechanical and thermal calculations. Only in the temperature calculation, pellet clad gap size was reduced.

In the next step, the KWU FGR model was introduced. The FGR model presented by KWU is described below briefly.

$$\frac{df(t)}{dt} = Kg(t)$$

where f: Amount of gas release

g: Gas concentration at the grain boundaries

The factor K is split up into three factors K1, K2 and K3. These factors were optimized to minimize the prediction errors by data shown in Table-1.

K1 models the gas channels through grain boundaries and is a function of temperature. The low temperature region of the constant represents FGR mechanisms of recoil and knock-out. K1 was revised to be more sensitive to fuel temperature in the higher temperature region.

K2 models FGR enhancement by burnup increment and is a function of burnup. K2 was revised to be less sensitive to burnup.

K3 models the gas channels through open porosity and is a function of a quantity of open porosity and not changed from the original KWU model.

#### 4. Code Verification

The code accuracy was verified with available data. We selected the verification data with two criteria, that is, the data should be from standard LWR fuel and all the necessary input data for verification is available. FPAC was verified with fuel behavior data such as FGR, clad OD, fuel temperature, inner pressure, and pellet densities. Fuel temperature was verified mainly by Halden Project data.

FGR was verified by data shown in Table-2. These FGR data are plotted against fuel burnup in Fig.-2. The relation between burnup and maximum fuel rod power are shown in Fig.-3. The data cover the power which high burnup fuel will experience in a power reactor.

It was confirmed that the improved FPAC had reduced the errors in fuel behavior prediction. But for gadolinia bearing fuel, FPAC had a tendency to predict a slightly higher FGR. Accuracy of FPAC prediction was improved when a best fit thermal conductivity of gadolinia bearing fuel was introduced into the code, as shown in Fig.-4.

Table-2 Additional Verification Data for Improved FPAC

• HBEP	(Task-3)
• TRIBULATION	
• GAIN Program	
• NFIR	
• High Burnup Demo Fuel	(NFI)
• Gadolinia Demo Fuel	(NFI)
• High Performance Demo Fuel	(NFI)

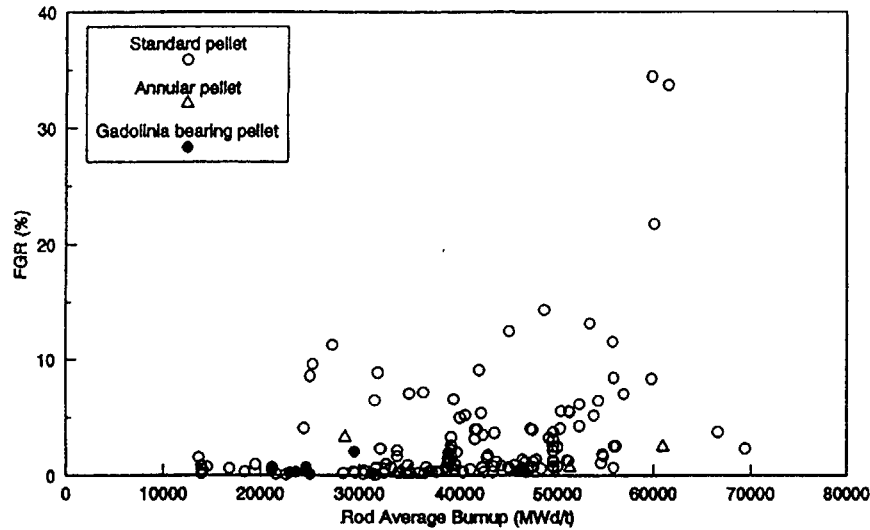


Fig.-2 Relationship between FGR and burnup

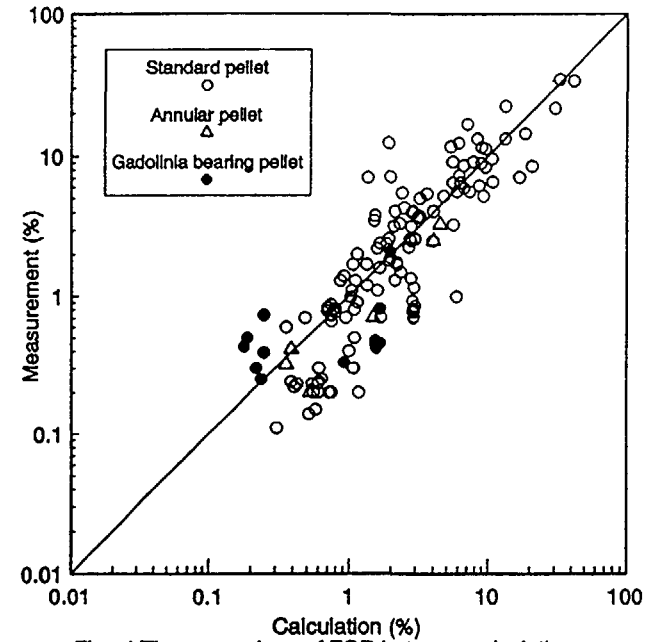


Fig.-4 The comparison of FGR between calculation and measurement

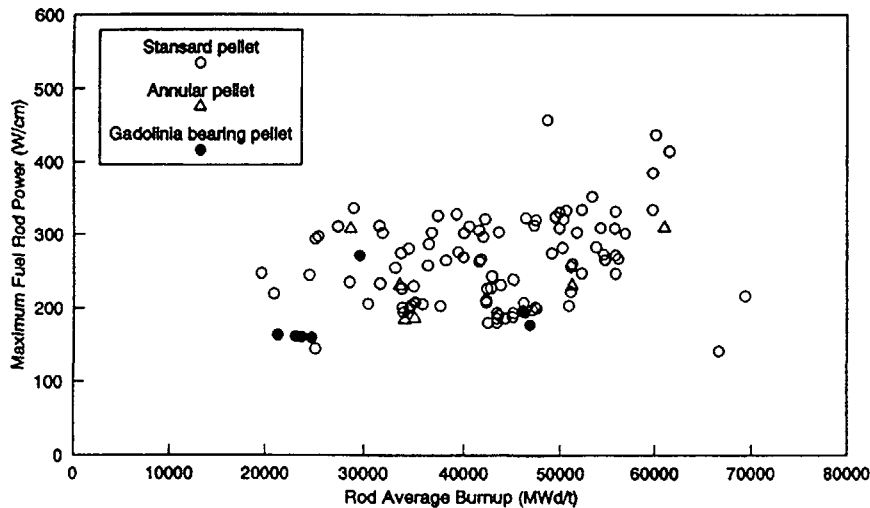


Fig.-3 The range of FGR data as a relation between burnup and maximum fuel power

Calculations with various parameters were done to evaluate their effects on FGR. FGR is enhanced with burnup increment when fuel power is high. If the fuel rod power is low, FGR stays at a low value as shown in Fig.-5. Also the effect of pre-pressurization is simulated as shown in Fig.-6. The calculation shows that non-pre-pressurization causes a large thermal feed back. Even pre-pressurization with a small value reduces FGR considerably. The effects of pre-pressurization saturate at high pressure. The effect of an annular size was surveyed and shown in Fig.-7. This figure shows that an annular size of 10% volume is practically optimum, because a larger size will reduce the uranium inventory too much.

5 FGR Data of NFI Fuel

The FGR data for NFI fuel were obtained from following three programs.

- (1) Gadolinia bearing demo fuel<sup>(4)</sup>
- (2) High burnup demo fuel<sup>(4)</sup>
- (3) High performance demo fuel

The programs (1) and (2) were joint studies with the Japanese 5 PWR operating utilities. The program (3) was organized by NUPEC (Nuclear Power Engineering Corporation) All the fuel assemblies were irradiated in power reactors of Kansai. All the hot cell PIE was performed at JAERI (Japan Atomic Energy Research Institute) in Tokai-mura.

The data on gadolinia bearing pellets from test reactors will be available in the near future

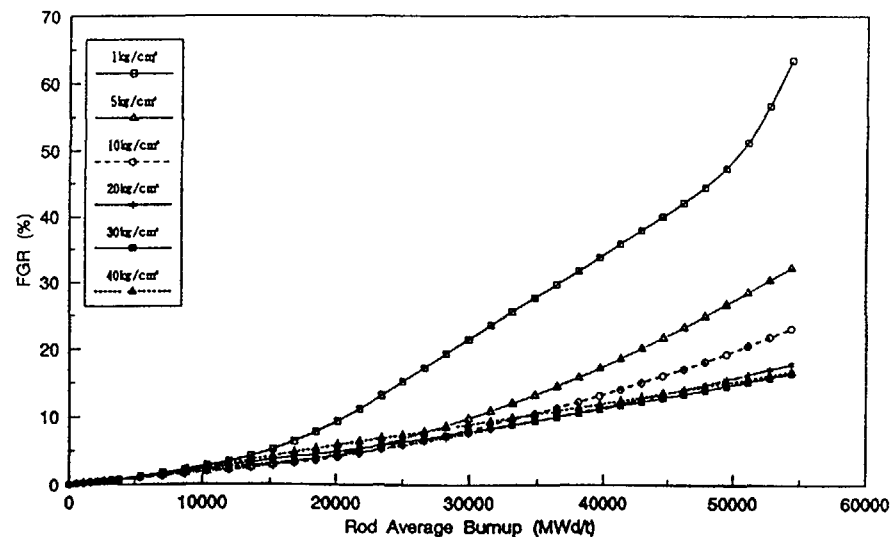


Fig.-6 FGR Calculation with various pre-pressurations

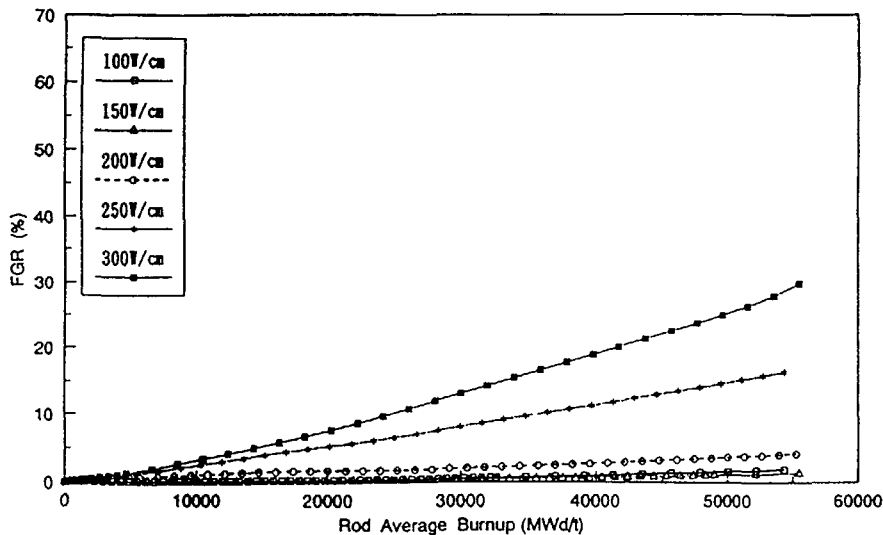


Fig-5 FGR calculation with various constant powers

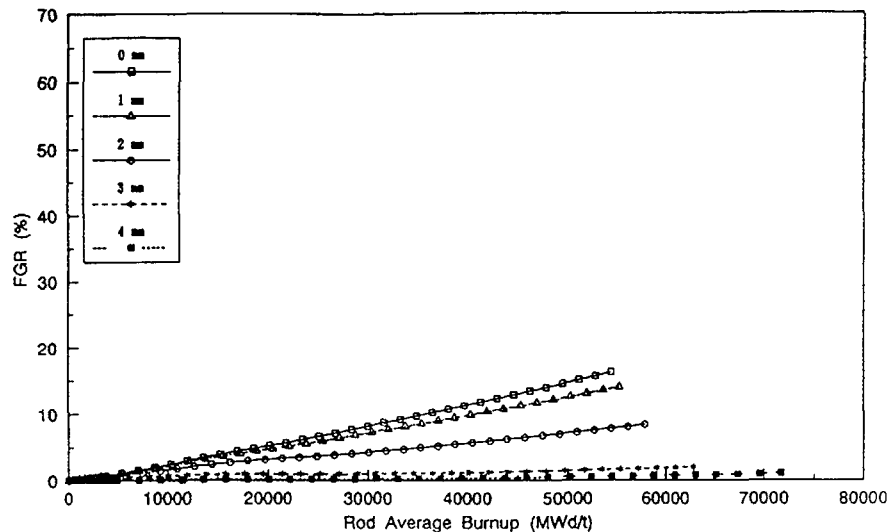


Fig -7 FGR Calculation with various annular diameter

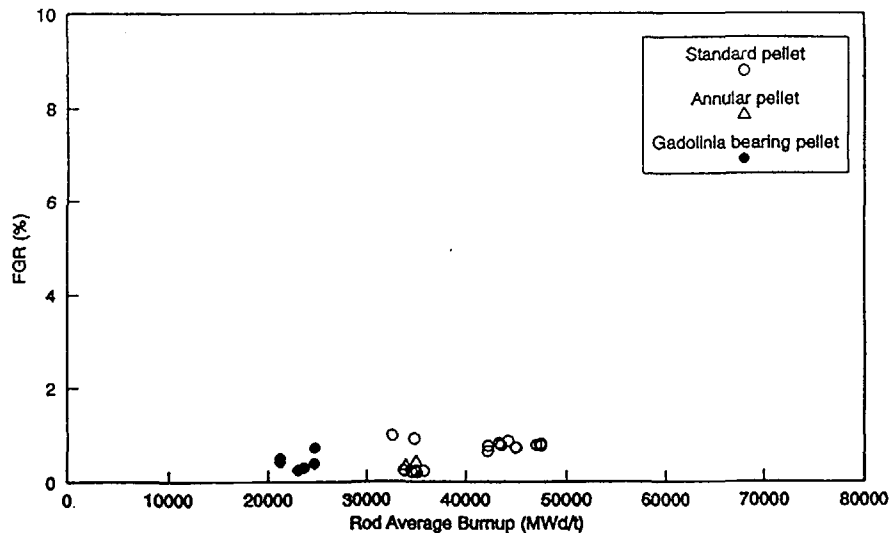


Fig.-8 Relationship Between FGR and Burnup

Relationship between FGR and burnup is shown in Fig.-8. All the FGR values are low and burnup enhancement effect is not observed. This again confirms the fact that the fuel temperature is a dominant factor to FGR.

These data include pellets from standard fabrication products, annular pellets and gadolinia bearing pellets. There are no clear differences in FGR among these pellets. Annular pellets were expected to reduce FGR but the measured values were slightly higher than standard pellets. This may be only an error of the measurement, or the increase of pellet surface area which accelerated recoil and knock-out mechanisms.

#### 6. Pellet Improvement for FGR Reduction

NFI is developing two kinds of pellets to reduce FGR. Both kinds of pellets aim to increase the diffusion distance of FP gas to

grain boundaries by a large grain size. The effects of a grain size on FGR has been shown by OVER-RAMP testing<sup>(6)</sup>. Large grain size is obtained by sintering in an oxygenate atmosphere without an additive<sup>(7)</sup>. Another kind of pellet is fabricated with an additive. These improved pellets were fully tested out-of-pile and FGR reduction will be confirmed by a test now under irradiation in a power reactor. Also irradiation in a test reactor will start this year.

#### 7. Future Model Development

NFI is planning to expand the code applicability mainly in two ways. One is to extend the burnup limit to even higher region. For this purpose, NFI is collecting higher burnup FGR data and studying the models shown in Table-3.

In a higher burnup region, a rim effect may be important. The pellet samples from high burnup demo fuel had shown only a slight rim region at approximately 50 GWd/t. This means that the direct contribution of a rim region to FGR may be small compared with

Table - 3 Models for Future Improvement

- |                                    |
|------------------------------------|
| 1. Rim Effect                      |
| 2. Effect of Power Cycling         |
| 3. He - gas Production             |
| • High Burnup                      |
| • MOX Fuel                         |
| 4. He - gas Resolution into Pellet |
| 5. Axial Gas Migration             |

other mechanisms. If the characteristics at the rim region, such as thermal conductivity, change greatly, the effects to FGR may be important at higher burnup.

Another is a revision for MOX fuels. Current available data shows that the FGR may depend on the fabrication process.

The models will be revised or introduced into the FPAC code after surveying the available data.

#### 8. Summary

It was confirmed that FPAC is able to predict fuel performance at high burnup. The FGR data base for NFI fuel is increasing. It will be necessary to study and survey available data to expand the code applicability even more.

#### Acknowledgements

The authors express their thanks to the engineers of Kansai Electric and other PWR operating utilities, and NUPEC for their support in the study program.

#### References

- (1) R. O. Meyer, C. E. Beyer, J. C. Voglewede "Fission-Gas Release from Fuel at High Burnup" Nucl. Safety vol. 19 No. 6 699-708 (1978)
- (2) H. Ocken, J. T. A. Roberts "Letter to the Editor: Comments on "Fission-Gas Release from Fuel at High Burnup" in Vol. 19, No. 6" Nucl. Safety Vol. 20, No. 4 (1979) 417-421
- (3) W. Hering "The KWU Fission Gas Release Model for LWR Fuel Rods" J. Nucl. Matr. 114 (1983) 41-49
- (4) M. Yokote, K. Mori, S. Kobayashi "Gadolinia Fuel Usage and Demonstration Program in Japan" Int. Topical Meeting on LWR Fuel Performance April 21-24 (1991) Avignon France

(5) Y. Matsuoka, K. Mori, A. Oe, T. Yokoyama "High Burnup Demo Fuel PIE" Transaction of ENC '90 (1990)

(6) EPRI NP-3150-SR "LWR Core Materials Performance Program: Progress in 1981-1982" (1983)

(7) K. Kawanishi, K. Watarumi "Control of  $UO_2$  Microstructure by Oxidation-Reduction Sintering Method" Paper No. P-118 of Int. Symp. on Advanced Nuclear Energy Research-Roles and Direction of Materials Science in Nuclear Technology- Mito Japan (1992)

# MODELING CANDU-TYPE FUEL BEHAVIOUR DURING EXTENDED BURNUP IRRADIATIONS USING A REVISED VERSION OF THE ELESIM CODE

V.I. ARIMESCU\*, W.R. RICHMOND  
AECL Research,  
Chalk River Laboratories,  
Chalk River, Ontario, Canada

## Abstract

The high burnup data base for CANDU fuel includes several cases from both power station and experimental reactor irradiations, with achieved burnups of up to 800 MW.h/kgU. The power history for each of these cases is different, encompassing low steady-state, declining, and power-ramps.

This variety offers a good opportunity to check the models of fuel behaviour, and to identify areas for improvement. The main parameters for comparing calculated versus measured data are the fission gas release and the sheath hoop strain. Good agreement of calculated values of these two parameters with experimental data indicates that the global behaviour of the fuel element is adequately simulated by our codes.

The ELESIM computer code was used as the simulation tool. The models for fission gas release, swelling and for fuel pellet expansion were thoroughly analysed. Changes were proposed for both models. The fuel pellet expansion model was modified to account for gaseous swelling, which becomes very important at high burnups. As well, the mathematics of the fission gas release model was upgraded for the diffusional release of fission gas atoms to the grain boundaries.

A revised version of the ELESIM computer code was used to simulate the cases from the high burnup data-base. Satisfactory agreement was found for most cases. The discrepancies are discussed in view of alternative mechanisms that can operate and be enhanced at high burnup. These include stoichiometry changes with burn up that affects fission gas release, and also outer pellet rim fission gas release by a grain boundary diffusion process.

The main conclusion of this study is that the revised version of the ELESIM code is able to simulate with reasonable accuracy high burnup as well as low burnup CANDU fuel. This includes irradiations of steady-state, declining, or ramped fuel power histories with a prolonged hold at high power. However, future improvements to ELESIM are needed to model fuel power histories with short dwell times at a high terminal ramp power.

\* IAEA fellow on attachment at AECL from Romania.

## 1 INTRODUCTION

There is a strong incentive to operate fuel elements to extended burnup, because of increased fuel consumption efficiency and also to reduce spent fuel volumes[1]. To achieve this objective, both experimental and theoretical activities are needed to assure good fuel performance for extended burnup irradiations. This paper presents recent modelling developments and comparisons with experimental data.

The extended burnup database for CANDU fuel (burnup greater than 300 MWh/kgU, and up to about 900 MWh/kgU) comprises about 100 individual element cases from 16 fuel bundles and 4 single elements, irradiated in both power stations[2] and a research reactor. There is a variety of power histories; typical examples are shown in Figures 1 to 3. In addition, there is a large database for CANDU normal operating burnup (up to 300 MWh/kgU), that includes about 120 cases.

The fuel-element performance computer code ELESIM[3,4] was developed to simulate CANDU fuel behaviour during normal operating conditions. Several versions have been developed over time by adding new features or by changing different models. ELESIM contains both CANDU-specific and generic fuel behaviour models and features. Specific to CANDU fuel are: radial flux depression factors (calculated for CANDU neutron spectra), Zircaloy sheath mechanical constitutive equation, gap heat transfer coefficient (because of collapsible sheath, the thermal gap can be considered as zero), and densification correlation[4]. Of general applicability are the models for fission-gas release and swelling[5], pellet dimensional changes, and temperature calculation[6].

When applied to extended burnup cases, the current version of ELESIM has been found to significantly underpredict both fission-gas release and permanent sheath strains[7]. There is reasonable agreement between prediction and measurement for the normal burnup data, although a tendency toward underprediction still exists. These observations suggest that either additional phenomena related to extended burnup behaviour need to be accounted for, or the existing models are not sufficiently accurate or consistent to predict the normal enhancement of modeled processes with increasing burnup.

Work is currently underway to improve the capability of ELESIM to better predict the behaviour of CANDU fuel at extended burnups. The approach being taken is to first re-examine existing component models to ensure that they are self-consistent and sufficiently accurate over the entire burnup range (i.e., up to 1000 Mwh/kgU), and then, if necessary, to consider adding new models or modifying existing ones to account for burnup-dependent effects not yet considered.

This paper presents some results from the first part of the exercise. Specifically, the current fission-product release,

POWER HISTORIES FOR BUNDLES  
J24518C AND DG063

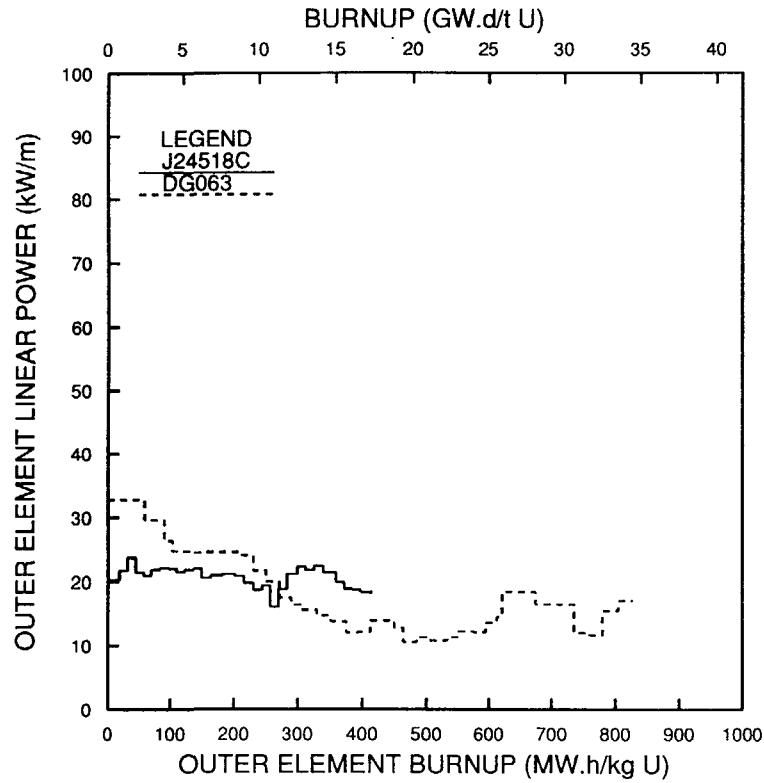


FIGURE 1 - Quasi-constant power history extended burnup irradiation.

POWER HISTORIES FOR BUNDLES  
J03311W AND J24546C

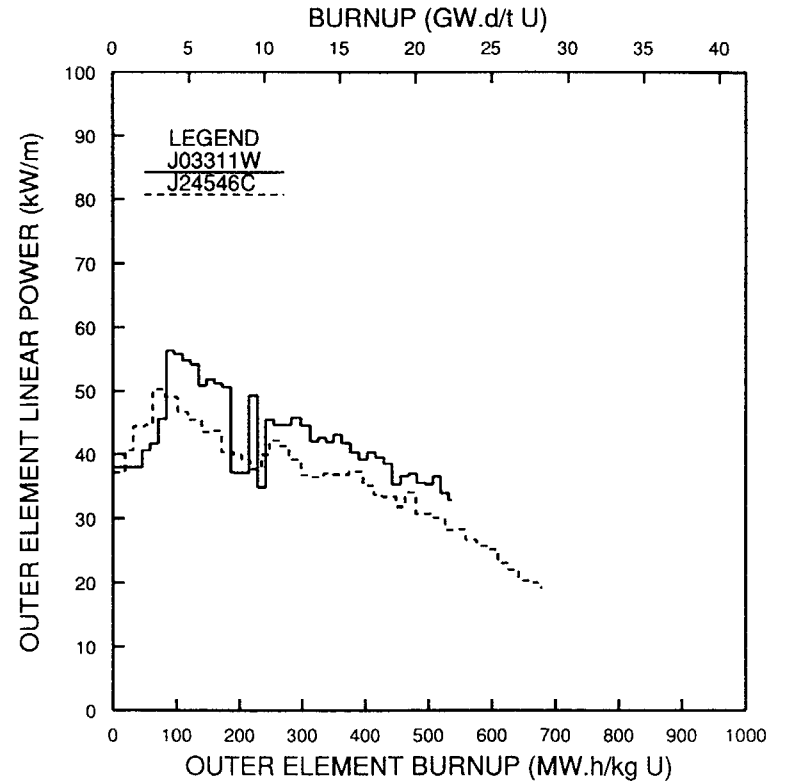


FIGURE 2 - Declining power history extended burnup irradiation.

## POWER HISTORIES FOR BUNDLES J64703C, KE, AND KF

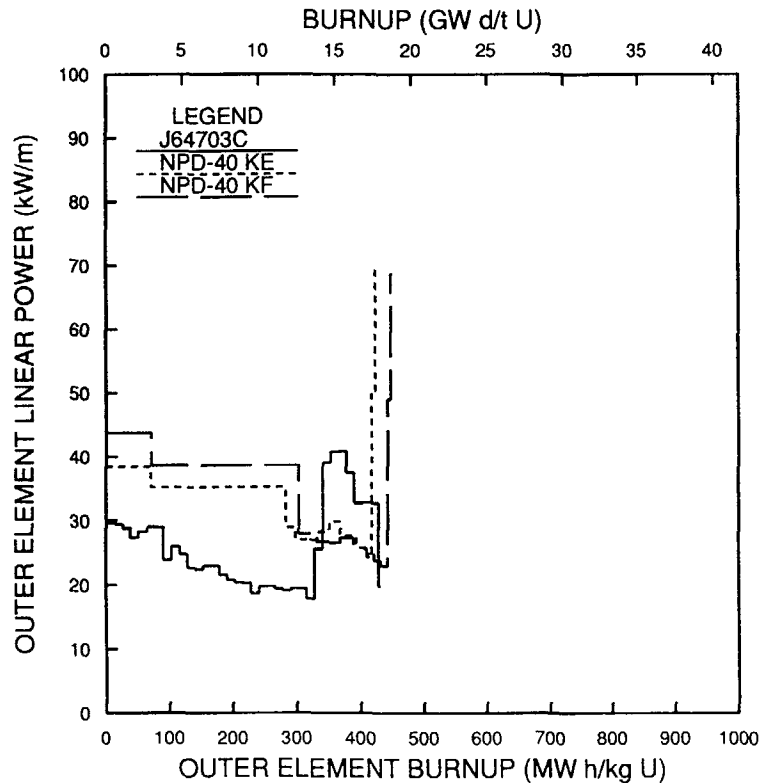


FIGURE 3 - Quasi-constant power history extended burnup irradiation followed by a power ramp

swelling, and dimensional change models were assessed and changes made. These changes were incorporated into a revised version of ELESIM and comparisons were made against the database. These results, with particular emphasis on the extended burnup cases, are presented and discussed.

### 2.0 FISSION-GAS RELEASE AND SWELLING MODEL

The ELESIM fission-gas release and swelling model[8] can be termed as semi-mechanistic. Three main stages of fission-gas release to the free voidage are taken into account: diffusional transport and sweeping collection of the fission-gas atoms to the grain boundary, formation of intergranular bubbles on grain faces and edges, and venting of the gas to the free voidage.

While this general picture is widely accepted, specific data are either still missing or there is a large spread in the reported data range for particular processes, such as diffusion inside the grains and intragranular bubbles mobility. As well, the complexity of the problem imposes some restrictions on the extent of detail in the model so that it can be implemented in a general fuel performance code. Consequently, certain assumptions and simplifications were made throughout the model.

Because the model is presented in detail in Reference[8], only the most important parameters are emphasized here. A general feature is related to the fact that the global code as well as the component models are steady-state ones, thus some simplifications are made by neglecting the transient evolution of different processes.

The intragranular diffusion of the gas atoms is treated by using an effective diffusion coefficient, and by idealizing the grain shape as an equivalent sphere. No modelling of intragranular bubbles is attempted, but their presence is implicitly accounted for in the effective diffusion coefficient. A thorough analysis of the treatment of the diffusional process inside the grain revealed certain inconsistencies that were corrected, as described in Section 2.1. Further, the values of the diffusion coefficient for different temperature ranges, and how this affects the final fission-gas release, is discussed in Section 4.1.

The other way for the fission-gas atoms to arrive at the grain boundary is by grain-boundary sweeping resulting from grain growth. This can be as important as diffusion in some cases. Fission-gas atoms arriving at the grain boundary are assumed to enter intergranular bubbles. This leads to gaseous swelling, the extent of which depends on the criterion used for the retention capacity of the grain boundary. Changes to this stage of the model are described in Section 2.2.

Although there is a strong intercorrelation between the various phenomena taking place in a fuel element, the model for fission-gas release and swelling is most affected by the stress state of the pellet. This is because the hydrostatic stress is a key factor in

calculating the intergranular bubble radius. Basically, it is assumed that the central plastic core, if one exists (the extent of the plastic core is based on the plasticity temperature concept[6]), is subjected to only the gas pressure, while the outer cracked region of the pellet is also subjected to the fuel-sheath interface force, which is focused toward the base of the crack wedge.

### 2.1 DIFFUSION OF GAS ATOMS TO GRAIN BOUNDARY.

The diffusion of gas atoms to the grain boundary can be described by the following equation, treating the grains as spheres of radius  $a$ :

$$\delta C(r,t)/\delta t = (D/r)\delta^2[r.C(r,t)]/\delta r^2 + \beta(t) \quad (2.1)$$

where  $C(r,t)$  is the gas atom concentration,  $D$  is the effective diffusion coefficient, which depends on the local temperature, and  $\beta$  is the source term, calculated as the volumetric fission rate multiplied by the fission yield for fission-gas atoms.

As the diffusion coefficient and the source term are varying in time according to the changing power history, the approach taken in Reference[8] is to solve equation (2.1) for a given time-increment, with all the parameters being treated as constant during the increment. Therefore, the initial and boundary conditions are:

$$C(r,0) = C_0 \quad (2.2)$$

$$C(a,t) = 0 \quad (2.3)$$

$$C(0,t) = \text{finite}, \delta C(0,t)/\delta r = 0 \quad (2.4)$$

where  $C_0$  is the concentration of gas atoms at the beginning of the time increment, assumed uniformly distributed across the grain, while the grain boundary is considered as a perfect sink as described by equation (2.3), and  $t$  is the time elapsed from the beginning of the increment.

To calculate the net release during the time increment, the current model considers separately the "new gas" born and partially released during the increment and the "old gas" present at the start of the increment and partially released during the increment.

The "old gas" released during the time interval is calculated as follows. Using the solution to the diffusion equation for zero production with finite non-zero initial concentration,  $C_0$ , and the total fractional release,  $f_0$ , at the end of the previous time interval, an effective time,  $t_0$ , is calculated. This is done by assuming the temperature, and therefore the diffusion coefficient, is kept constant at the current value. The same relationship is then used to calculate  $f_1$ , the effective fractional release of the "old gas" at the end of the time increment (i.e., at  $t=t_0+\Delta t$ ). The net fractional release of the old gas during the time interval is then simply calculated as  $\Delta f_0 = f_1 - f_0$ .

To calculate the fractional release,  $\Delta f_n$ , of the "new gas" born during the time interval, the solution of the diffusion equation with production and zero initial concentration is used. Once this is done, the net fission-gas release is calculated by summing up the contributions from the old and new gas, and the total net fractional release is computed by normalizing by the total fission-gas produced up to the end of the time interval. It can be shown that the above procedure for calculating the fractional release of the old gas will lead to an underprediction of fission-gas release to the grain boundary. This underprediction can vary from 10% to 30%, depending on the power history.

It is not necessary to follow the above approach since the "old gas" fractional release equation can be applied to a time step, independent of what happened before. All that is needed is an estimate of the "old gas" concentration at the beginning of the time step. The following is a recommended procedure that results in a more accurate and consistent calculation of the "old gas" fractional release during a time step.

To solve equation (2.1), the solution is written as the sum of two parts, as follows:

$$C(r,t) = U(r,t) + V(r,t) \quad (2.5)$$

where  $U(r,t)$  satisfies the equation:

$$\delta U/\delta t = (D/r)\delta^2(r.U)/\delta r^2 + \beta \quad (2.6)$$

$$U(r,0) = 0 \quad (2.7)$$

$$U(a,t) = 0 \quad (2.8)$$

while  $V(r,t)$  is the solution of:

$$\delta V/\delta t = (D/r)\delta^2(r.V)/\delta r^2 \quad (2.9)$$

$$V(r,0) = C_0 \quad (2.10)$$

$$V(a,t) = 0 \quad (2.11)$$

$U(r,t)$  can be interpreted as the "new gas", which is born during the time-increment, while  $V(r,t)$  can be interpreted as the "old gas", which was present at the beginning of the time increment inside the grain.

The solutions of the two equations are used to derive the flux of gas atoms to the boundary. After integrating this flux for the respective time step, the percentage release is obtained by dividing by the total new gas produced in the case of  $U$ , and by the initial total old gas inside the grain, in the case of  $V$ . The relations describing the fractional release for the two cases are presented in [8].

To specify the value of the initial gas concentration at the beginning of the time increment, which is needed for the "old gas" calculation, an assumption has to be made regarding its radial distribution inside the grain. There are two extremes: a uniform radial distribution, and an asymptotic, steady-state one. The first one has been used here. A comparison of the fractional release relations corresponding to these two limiting cases indicates that the difference between them is not significant, particularly in view of the wide scatter of data for the effective diffusion coefficient. Therefore, it is considered that for steady-state calculations the procedure outlined above is sufficiently accurate.

In summary, the new procedure consists of first evaluating  $C_{old}$ , the initial old gas concentration for the present time-step, as:

$$C_{old} = C_{p0} - C_{r0} \quad (2.12)$$

where  $C_{p0}$  is the total amount produced and  $C_{r0}$  is the total amount released, and then calculating  $C_r$ , the "old gas" atoms released to the grain boundary during that time-step from:

$$C_r = C_{old} \cdot f_o(\delta t) \quad (2.15)$$

where  $f_o(\delta t)$  is the fractional release of the "old gas" during the time-step  $\delta t$ . This is then summed up with the contributions from the "new gas" and from the sweeping process to calculate the total release to the grain boundary.

## 2.2 GAS ATOMS ON THE GRAIN BOUNDARY

The second part of the model addresses the gas atoms arriving at the grain boundary. These are assumed to reside in a given number of bubbles per unit of grain-boundary area, per unit volume of fuel. The grain-boundary area per unit volume is a calculated parameter. Because each grain boundary is shared by two adjacent grains, the total grain-boundary area must be divided by two, a factor not considered in the current model. This inconsistency, which has been corrected in the revised version, resulted in a doubling of the maximum retention of gas atoms on the grain boundary, thereby diminishing release to the free voidage.

The current model assumes that bubbles have a spherical shape and are of equal size. An important parameter of the model is the number of bubbles per unit area of grain boundary, which is assumed to remain constant. The value of this parameter has been inferred from metallographic studies at AECL[9], and is confirmed by recent data[10]. Using this constant and calculating the bubble radius as dictated by the bubble gas content, surface tension and hydrostatic restraint, the detailed modelling of bubble nucleation and coalescence can be avoided. If this parameter has an adequate value, the average bubble size and grain-boundary retention capacity can be well characterized, even if the detailed processes are not modelled. This is especially true for steady-state

condition, where arguments can be given in favour of the evolution of a uniform bubble size distribution on the grain faces[11].

More important is the shape of the bubbles, which is in fact lenticular instead of spherical. Therefore, the revised code treats intergranular bubbles as having a lenticular shape, while keeping the number of bubbles per unit grain-boundary area the same as before. With the 45-degree interfacial angle, this change accounts for a decrease of grain-boundary retention capacity of about 66%, compared to that for the same number of spherical bubbles.

The balance made to account for gas atoms residing on the grain boundary, those released to free voidage, and those collected by the grain boundary by diffusion and sweeping, is confusing and inconsistent in the current model. Excess gas atoms are allowed to be vented even if the maximum retention capacity is not yet attained. The revised version includes a change to allow venting to the free voidage only when saturation of the grain boundary is calculated to occur.

One assumption of the current model is that if saturation occurs, the excess gas atoms arriving at the boundary are allowed to be released to the free voidage, via interlinked tunnels. This assumption was originally introduced because no model for the formation and stability of edge tunnels was available. Physical considerations make this assumption somewhat arbitrary. It was replaced in the revised version by the assumption that the venting of the gas atoms to the free voidage will proceed until the pressure inside the bubbles equals the gas pressure in the free voidage. The same idea is considered by Kogai et al. [12], who also include an equation to describe the kinetics of the venting. For steady-state calculations, such venting kinetics is not considered important, and therefore is not included here.

## 3.0 SIMPLIFIED STRESS-STRAIN MODEL OF THE PELLETT

A detailed mechanical calculation for the pellet is very complex. It is advantageous to consider model simplifications, if possible. Two facts can be taken into account to simplify the calculation. First, experimental evidence[13] suggests that there is quite a steep transition from rigid to plastic behaviour of  $UO_2$ ; thus the use of the so-called "plasticity temperature" to delineate this transition. Second, the usual radial temperature gradient, and the relatively low rupture modulus of  $UO_2$ , are such that the outer rigid zone of the pellet will be cracked, and thus the thermal stress relieved. These considerations have led to a simple three-zone model of the pellet[14,15], with a separate calculation for dimensional changes[6,16], and with the stress computed as described in Section 2.0.

In the current model, the basis for evaluating the dimensional changes of each of the hundred annuli that the pellet is divided into is to sum up the contributions of thermal expansion,

densification, solid swelling and gaseous swelling. Although each one of these processes is evaluated independently, the swelling is taken into account only when it becomes greater (on the basis of percentage porosity) than the porosity remaining after densification.

A modification has been made in the revised version of ELESIM to algebraically add dimensional changes resulting from densification, gaseous swelling, thermal expansion and solid swelling. The rationale for this change is that not only are these processes independently evaluated, but they are also physically distinct.

#### 4.0 RESULTS AND DISCUSSION

Comparison of fission-gas release predictions by the current version of ELESIM against the normal and extended burnup database

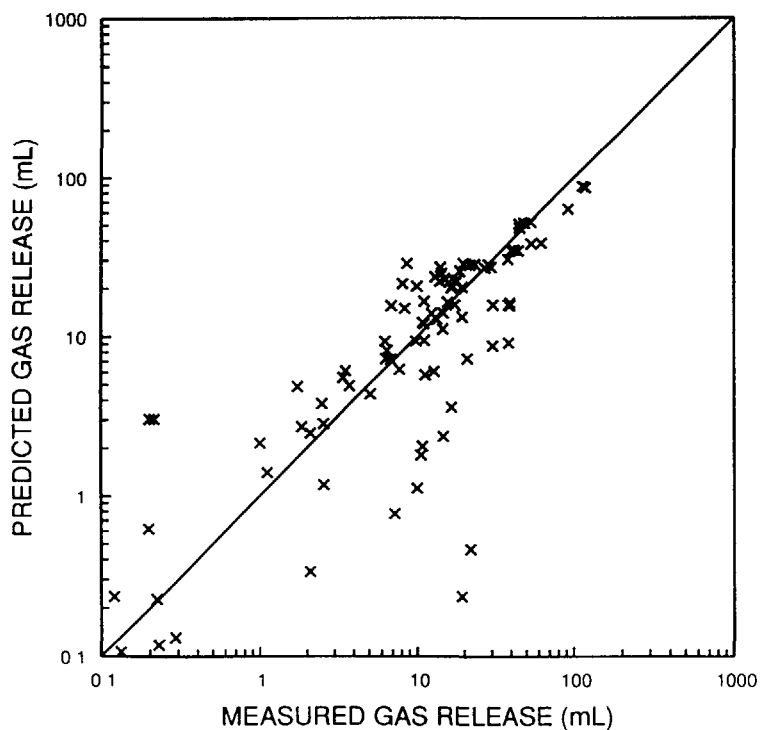


FIGURE 4 - Comparison between measured and predicted fission gas releases using the current version of ELESIM for the normal burnup database (burnup up to 300 MW.h/kgU).

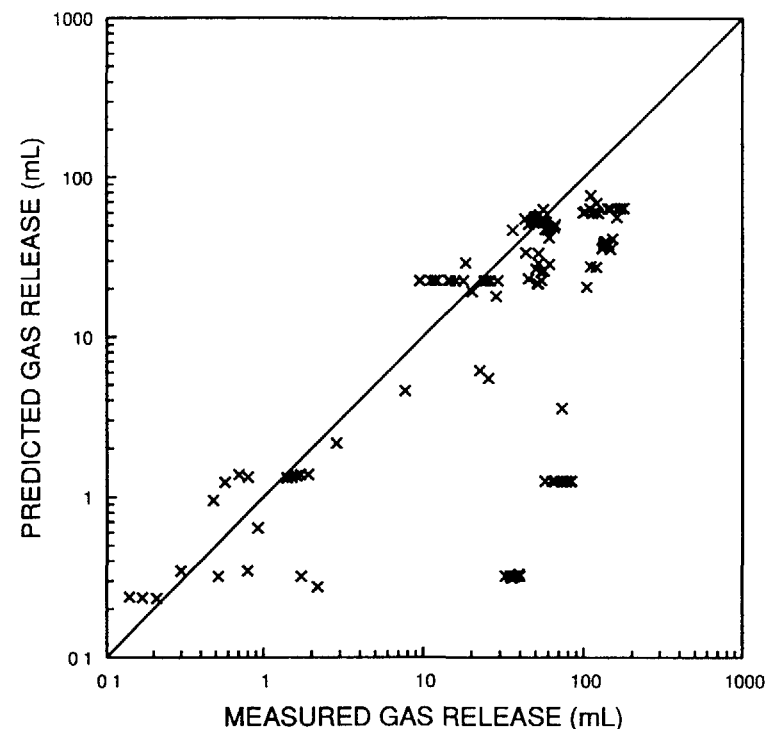


FIGURE 5 - Comparison between measured and predicted fission gas releases using the current version of ELESIM for the extended burnup database (burnups between 300 and 1000 MW.h/kgU).

are presented in Figures 4, 5 and 8. A tendency to underpredict the normal burnup cases is apparent, while the extended burnup cases are strongly underpredicted, especially for high release values. Figure 10 shows that the sheath strains for the extended burnup case are considerably less than the measured values, being compressive for most of the cases, while measured strains are highly tensile.

This situation is improved considerably when using the revised version of the code. Figure 6 shows the results of fission-gas release for the normal burnup database. The points are in a narrower band around the bisector line (perfect agreement), with a tendency to overpredict a number of cases. The overprediction for most of the cases is largely related to the high fission-gas

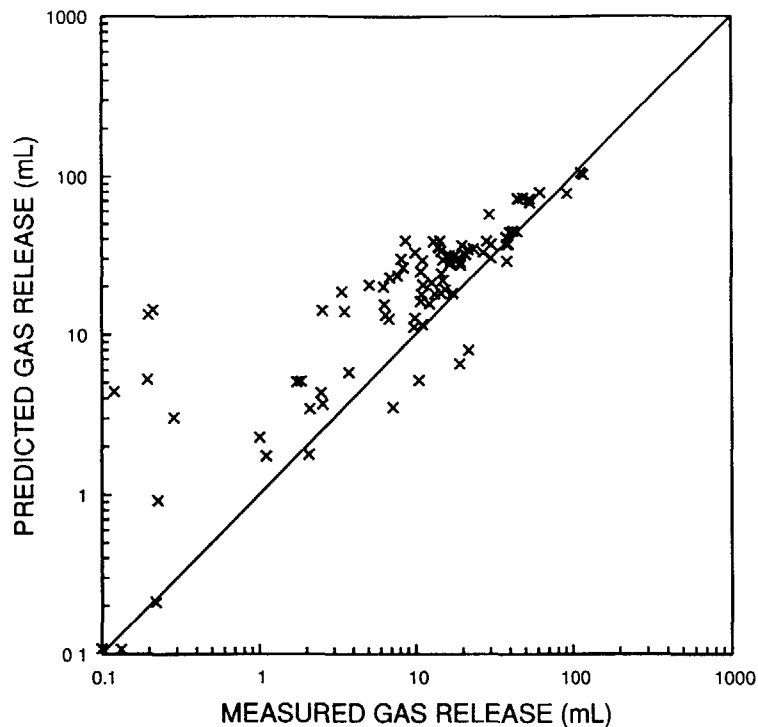


FIGURE 6 - Comparison between measured and predicted fission gas releases using the revised version of ELESIM for the normal burnup database.

release predicted in the centre columnar region that develops at high power ratings. It is believed that the sweeping correlation used for this region is causing too large a release (close to 100%). A revision of the treatment of this region is envisaged for the future.

In general, the sheath strains for the normal burnup range are also better predicted.

Improved agreement is obtained for the extended burnup database. The results of the revised version of ELESIM for fission-gas release are presented in Figure 7.1, and for sheath permanent strain (average at mid-pellet) in Figure 11. Except for the values for very low measured fission-gas release (less than 2 mL STP,

which represents less than about 1% fission-gas release), the data is grouped around the line of perfect agreement. These low release data are discussed below. At the other end, there are data involving large releases (see Figure 9), where an underprediction by a factor of 2 is noticed. The elements related to this situation are part of two NPD bundles irradiated at low power in the NPD reactor, and then ramped in NRU to very high terminal powers (about 70 Kw/m) for a short time. It is likely that the underprediction for these cases can be attributed to transient characteristics not yet modelled in the steady-state code, or to an underestimate of the low-power operation during the steady-state portion of the irradiation.

The cases where a very large overprediction is noticed (up to 20-fold) are all related to very low power irradiations. Some of the

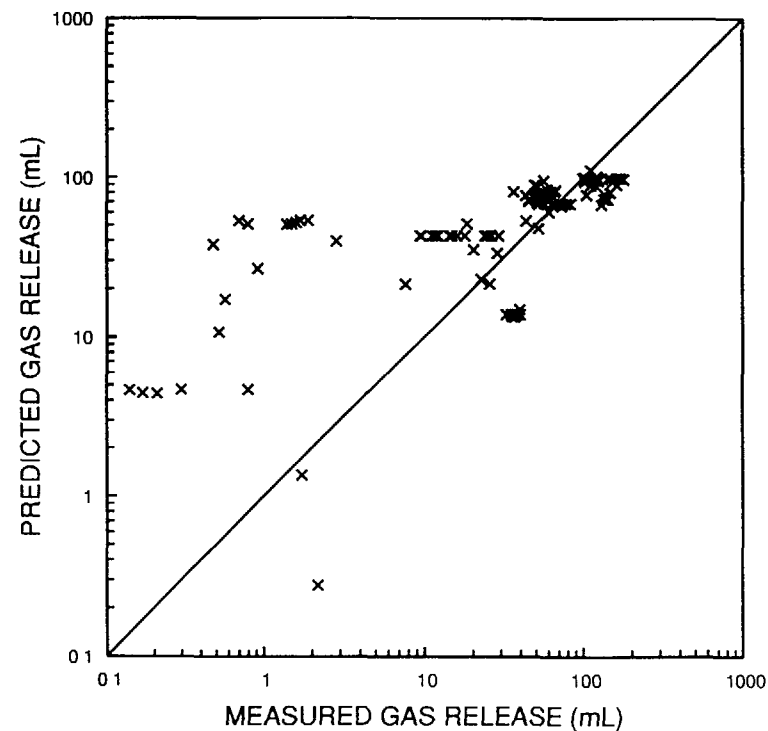


FIGURE 7.1 - Comparison between measured and predicted fission gas releases using the revised version of ELESIM for the extended burnup database.

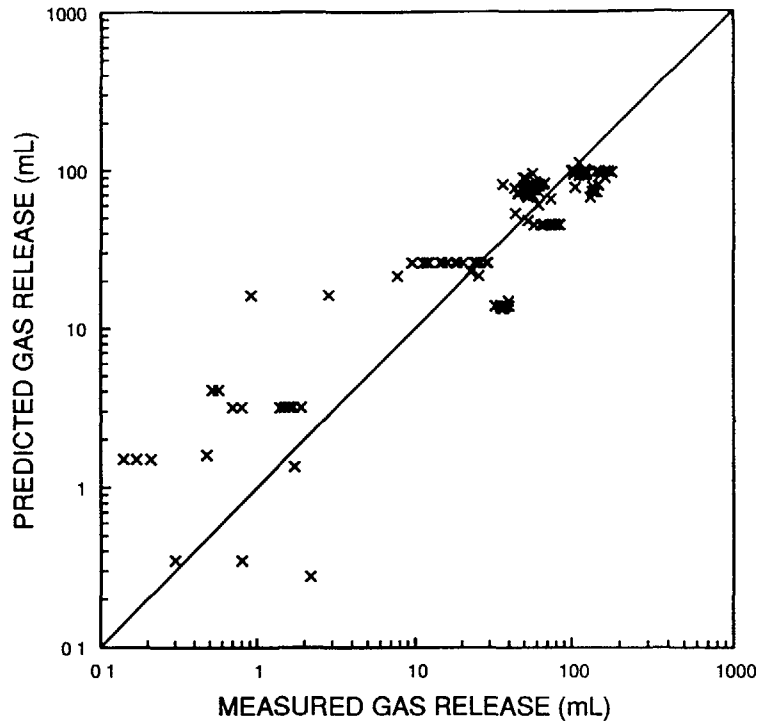


FIGURE 7.2 - Comparison between measured and predicted fission gas releases using the revised version of ELESIM for the extended burnup database and using the reduced low temperature diffusion coefficient (see Section 4.1).

elements associated with this situation are intermediate or inner elements from bundles that exhibited large fission-gas release from the outer elements, which were well predicted by the revised code. Both power and burnup are less for intermediate and inner elements. The power level is, however, more important, because it dictates the temperature in the pellet. The main parameter of the fission-gas release model affected to a significant extent is the diffusion coefficient.

#### 4.1 SENSITIVITY OF FISSION-GAS RELEASE TO DIFFUSION COEFFICIENT

In analyzing the large overprediction for the low releases, it was noticed that the average pellet centre temperature for these cases

was predicted to be 800-900 K. The overprediction was thus related to the value of the diffusion coefficient in this low temperature range. The initial fission-gas release model[8] uses Findlay's diffusion coefficient[17], but with a minimum value corresponding to a temperature of 1273 K. The argument for the use of this lower limit is an irradiation-enhancement of diffusion, which is an athermal process that depends on fissioning rate[8,18].

The revised version of ELESIM does not include the factor-of-3 increase in the diffusion coefficient[8], which was invoked when fine-tuning the code, and justified on the basis of the observed spread in the measured diffusion coefficient.

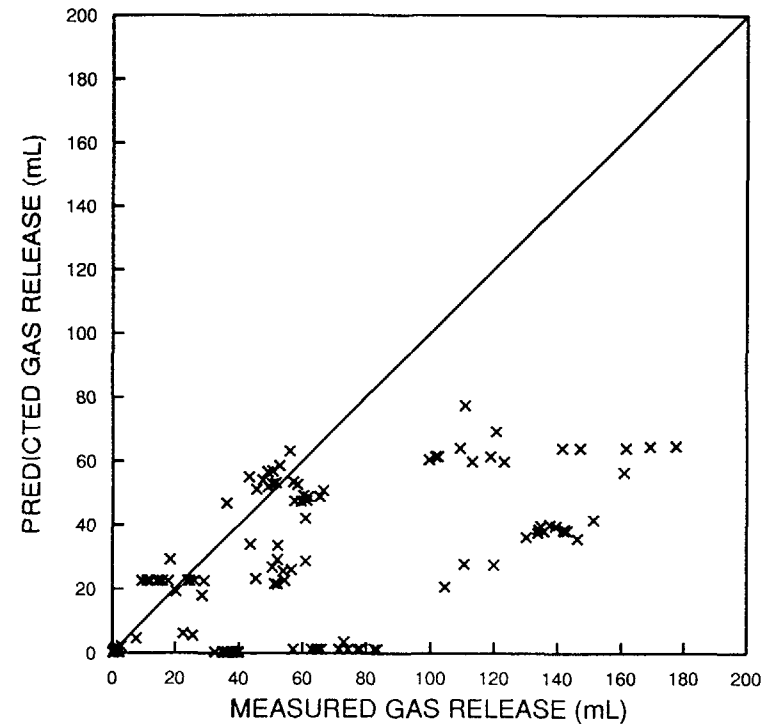


FIGURE 8 - Comparison of the current version of ELESIM prediction of fission gas release against the extended burnup data

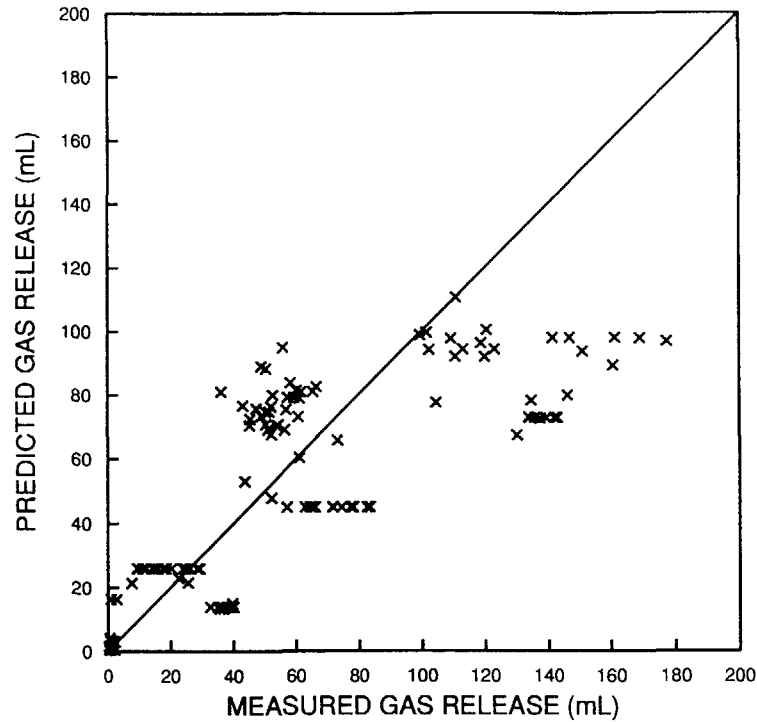


FIGURE 9 - Comparison of the revised version of ELESIM prediction of fission gas release against the extended burnup data.

The sensitivity of fission-gas release to this low-temperature irradiation-enhancement threshold was investigated to a limited extent. To this end, the cut-off temperature was decreased by 5%, which decreased the diffusion coefficient by 3-4 times for the temperature range below 1200 K. The results are presented in Figures 7.2 and 9, showing that the overprediction is eliminated, while the high release predicted for the higher-temperature outer elements is not affected.

A brief survey of the literature brought up the following arguments to support this change to the diffusion coefficient at the low-temperature range.

First, the irradiation-enhanced athermal plateau was originally detected and measured for metal diffusion (U or Pu in uranium

oxides). Fission-gas atoms can have the same value of the irradiation-enhanced diffusion coefficient as the metal, or less, depending on what process is operative. In fact, in a recent paper[19], Matzke suggests a lower value for fission-gas atoms, and indicates a value for Xe, measured in uranium carbide, that is three orders of magnitude lower than that of the metal. Further, there is some support from Findlay's original data for the effective diffusion coefficient of Kr-85, which does not show a low-temperature limit down to temperatures of about 1073 K.

Second, is a large scatter in the values of the diffusion coefficient reported in the literature. Part of this large scatter is due to the testing of different materials (small differences in U/O ratio can significantly affect the result) at different test conditions, and to different data evaluation methods[19].

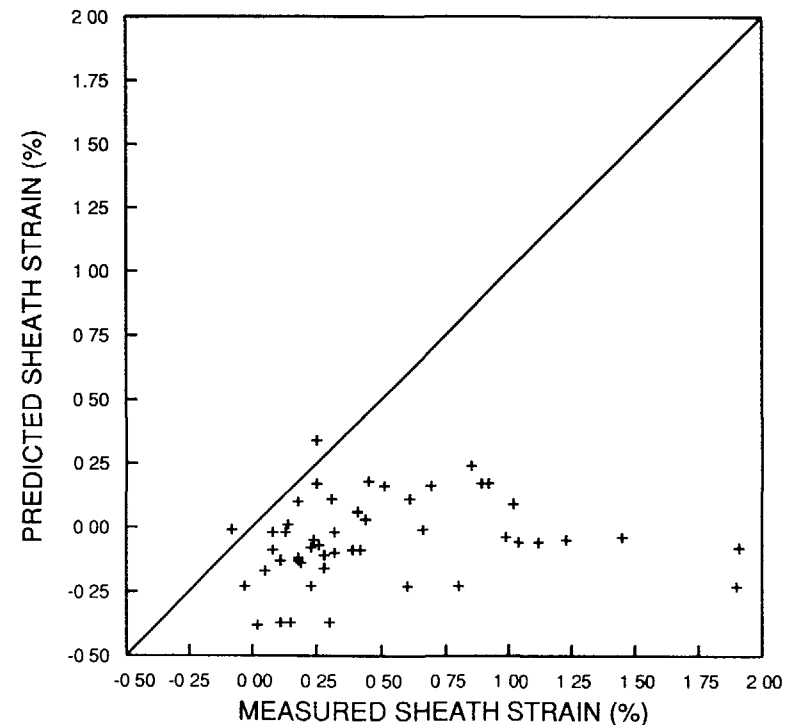


FIGURE 10 - Comparison between measured and predicted average mid-pellet permanent strains using the current version of ELESIM for the extended burnup database.

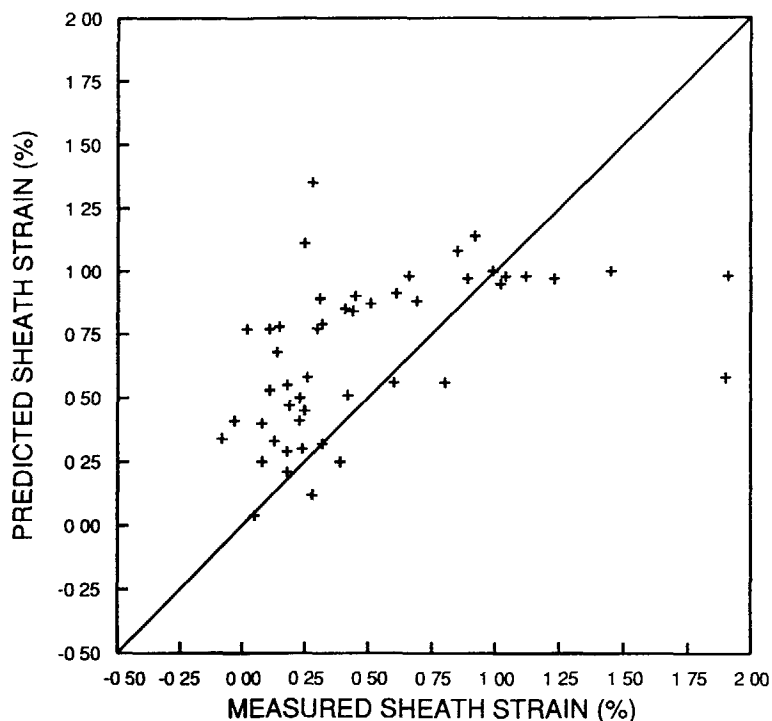


FIGURE 11 - Comparison between measured and predicted average mid-pellet permanent strains using the revised version of ELESIM for the extended burnup database.

Therefore, it is felt that the low-temperature irradiation enhancement plateau should be further decreased. More studies are necessary to find the best fit to the data, the present value adopted being only an attempt.

#### 4.2 CONCLUSIONS

As part of a first step in developing an extended burnup capability for the ELESIM code, several component models were reviewed. Changes were made to the models for fission-gas release in the grains and on the grain boundaries, as well as to the models for swelling and pellet dimensional changes.

When incorporated into a revised version of the ELESIM code, improved predictions of both fission-gas release and average mid-

pellet permanent strain were obtained, particularly for the extended burnup data. The need was identified to further examine relationships for the diffusion coefficient, as well as for the treatment of release in the columnar grain region.

Future work will entail a more detailed assessment of these two areas, together with an examination of the extent of thermal conductivity degradation in extended burnup CANDU fuel, particularly that having higher densities.

#### ACKNOWLEDGEMENTS

The above work was funded by the CANDU Owners Group (COG) as part of its Fuel Technology Program on Extended Burnup. Numerous discussions with L.N. Carlucci have been of great help.

#### REFERENCES

- [1] Green R.E., Boczar P.G., Hastings I.J., "Advanced fuel cycles for CANDU reactors", in Proceedings of the 28th Annual Conference of the Canadian Nuclear Society, Winnipeg, 1988, also AECL-9755
- [2] Floyd M.R., Novak J., Truant P.T., "Fission product release in fuel performing to extended burnups in Ontario Hydro nuclear generating stations", this meeting
- [3] Notley M.J.F., A computer program to predict the performances of  $UO_2$  fuel elements irradiated at high power outputs to a burnup of 10000 Mwd/mtU, Nucl. App. and Tech. 9 (1970) 195.
- [4] Notley M.J.F., A computer program to predict the performance of  $UO_2$  fuel elements, Nuc. Tech. 44 (1979) 445.
- [5] Notley M.J.F., Campbell F.R., Hastings I.J., Sills H.E., "Fuel modelling: gap conductivity, gas bubble swelling and fission gas release", AECL-5787.
- [6] Notley M.J.F., Calculation of fission-product gas pressures in operating  $UO_2$  fuel elements, Nuc. App. 3 (1967) 334.
- [7] Hains A.J., Novak J., "Ontario Hydro high burnup power reactor fuel performance", Proceedings "Second international conference on CANDU fuel", Pembroke, Canada, 1989.
- [8] Notley M.J.F., Hastings I.J., "A microstructure-dependent model for fission product gas release and swelling in  $UO_2$  fuel", AECL-5838, 1979.
- [9] Hastings I.J., Notley M.J.F., Rose D.H., Irradiation-induced volume changes in commercial  $UO_2$  fuel: comparison with model prediction, J. of Nuc. Mat. 75 (1978) 301.

- [10] Kashibe S., Une K., Effects of temperature cycling and heating rate on fission gas release of BWR fuels, *J. of Nuc. Scie. and Tech.*, 28, 12 (1991) 1090.
- [11] Tucker M.O., The spacing of intergranular fission gas bubbles in irradiated  $UO_2$ , *J. of Nuc. Mat.*, 74 (1978) 34.
- [12] Kogai T., Ito K., Iwano Y., The effect of cladding restraint on fission gas release behaviour, *J. of Nuc. Mat.* 158 (1988) 64.
- [13] Olander D.R., "Fundamental aspects of nuclear reactor fuel elements", TID-26711-P1, NTIS Springfield VA 22161 1976
- [14] Gittus J.H., Theoretical analysis of the strains produced in nuclear fuel cladding tubes by the expansion of cracked cylindrical fuel pellets, *Nuc. Eng. Des.* 18 (1972) 69.
- [15] Lassmann K., URANUS-a computer programme for the thermal and mechanical analysis of the fuel rods in a nuclear reactor, *Nuc. Eng. des.* 45 (1978) 325.
- [16] Notley M.J.F., Bain A.S., Robertson J.A.L., "The longitudinal and diametral expansions of  $UO_2$  fuel elements", AECL-2143 1964.
- [17] Findlay J.R., "BNES conference on chemical nuclear data", Canterbury 1971 91.
- [18] Matzke H.J., Gas release mechanisms in  $UO_2$ -a critical review, *Rad. Effects* 53 (1980) 219.
- [19] Matzke H.J., "Fundamental aspects of inert gas behaviour in nuclear fuels:oxides, carbides and nitrides", in "Fundamental aspects of inert gases in solids", edited by Donnelly S.E. and Evans J.H., Plenum Press, New York 1991.

## IMPROVEMENT OF ELESIM CANDU FUEL PERFORMANCE ANALYSIS CODE

### *Fission product gas release, fuel densification and neutron flux depression*

H.C. SUK, W. HWANG, B.G. KIM,  
K.S. KIM, Y.H. HEO  
Korea Atomic Energy Research Institute,  
Daeduk, Republic of Korea

#### Abstract

*KAERI has developed two major models which are a comprehensive fission gas release model and a mechanistic fuel densification model, and has expanded the ELESIM data base of neutron flux depression in fuel. Based on MATPRO-Version 11(Rev. 2), it has also updated the material properties such as fuel thermal conductivity, clad elastic moduli and clad thermal expansion used in ELESIM code of which most material properties are originated from MATPRO-Version 9[5]. Using the KAERI developed models, the expanded data base, and the updated material properties, KAERI has improved the ELESIM Computer Code and then the improved version of ELESIM has been designated as KAFEP(AERI/AECL Fuel Element Performance Analysis). The KAFEP code was verified through comparison with fission gas release experimental data taken from AECL and KAERI irradiation tests*

#### 1. INTRODUCTION

KAERI (Korea Atomic Energy Research Institute) has conducted on KAERI/AECL(Atomic Energy of Canada Limited) Joint "CANFLEX (CANdu FLEXible)" Fuel Development Program since February 1991. The CANFLEX fuel is a CANDU advanced fuel bundle and is consisted of 43 elements with 2 pin sizes. The CANFLEX fuel bundle with, for example, 1.2 % slightly enriched uranium dioxide fuel can be irradiated up to the core average discharge burnup of about 21000 MWd/MtU which is three times higher than that of the current CANDU 37-element bundle with natural uranium dioxide fuel.

As one of the CANFLEX Development Program, KAERI has improved the ELESIM Computer Code[1] designed for CANDU fuel element design and performance analysis, since AECL transferred the ELESIM code to KAERI in 1983 as a part of KAERI Fuel Verification Agreement between KAERI and AECL. In order to conveniently describe and distinguish the versions of ELESIM code in this report, the KAERI version of the code would be liked to be called KAFEP(AERI/AECL Fuel Element Performance Analysis) since it is based on AECL version of the code, while the AECL version shall be called ELESIM as its original name.

KAERI has developed two major models which are a comprehensive fission gas release model[2, 3] and a mechanistic fuel densification model[4], and has expanded the ELESIM

data base of neutron flux depression in fuel Based on MATPRO-Version 11(Rev 2)[4], it has also updated the material properties such as fuel thermal conductivity, clad elastic moduli and clad thermal expansion used in ELESIM-MOD10 code[1] of which most material properties are originated from MATPRO Version 9[5]

**2. INTERGRANULAR FISSION GAS RELEASE MODEL**

The ELESIM code includes Notley and Hastings' microstructure dependent fission gas release model[6] Their model incorporates the relevant physical processes such as fission gas diffusion, bubble and grain boundary movement, intergranular bubble formation and interlinkage

In KAERI, as a modelling of intergranular fission gas bubble behaviour, a comprehensive fission product gas release from UO<sub>2</sub> fuel has been modelled and programmed into the ELESIM code by considering the behaviour of multiple bubble sizes on the fuel grain boundary in terms of relevant physical parameters, while the ELESIM considers only a single bubble size at the grain boundary The KAFEP model takes an approach similar to that of Gruber[7], but it extends to account for bubble migration and coalescence, critical bubble size, which depends on the thermal gradient on the grain boundary, and the lenticular shape of the bubbles Those bubbles that exceed the critical bubble size are assumed to be left on the grain boundary and to migrate along the thermal gradient until they encounter free voidages. The KAFEP model also considers the specific condition of the gas stored at the grain boundaries and, in addition, allows an assessment of gas bubble swelling at the grain boundary, including the effect of restraint on bubble size The intragranular fission gas behaviour is modelled by adopted Booth's classical diffusion theory[8, 9] Under steady-state or slowly varying conditions, the pressure caused by the fission gas within the gas bubbles is in equilibrium with the surface tension of the bubbles[10, 11] Thus, the gas pressure in intergranular bubbles is assumed to be balanced by the surface energy and any externally applied hydrostatic stress under steady state

**2.1 Critical Bubble Size on the Grain Boundary**

An experimental examination[12] showed that the grain boundary bubbles at equilibrium took up a lenticular shape consisting of two hemispherical caps suited either side of the plane of the boundary as shown in Fig 2 1-1

Based Shewmon report[13] on the movement of grain boundary bubble in a temperature gradient to biasing of the jumps of each atom by means of a force on each atom, the critical bubble radius, r<sub>gb</sub>, for grain boundary pull-off in UO<sub>2</sub> fuel is derived as

$$r_{gb} = \left[ \frac{\Omega \gamma_{gb} T}{2 Q (dT/dx)} \right]^{1/2} \quad (2-1)$$

where

- Ω = atomic volume
- T = temperature (K)
- (dT/dx) = thermal gradient in the x direction in the pore
- γ<sub>gb</sub> = grain boundary surface tension
- Q = heat of transport for matrix atoms

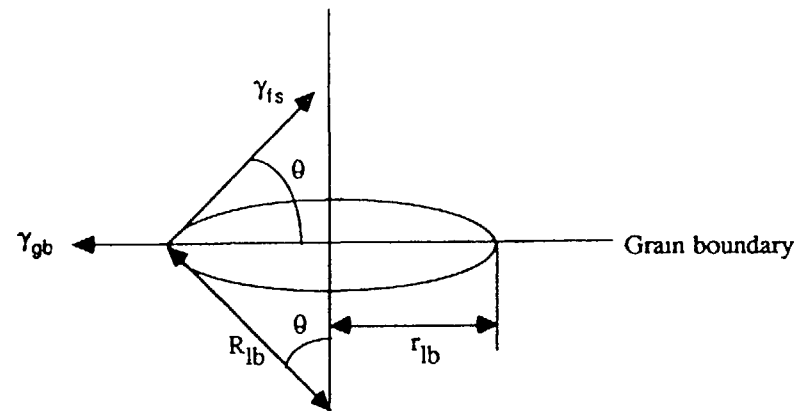


FIG 2 1-1 Lenticular shape of a grain boundary bubble

In Eq (2-1), the thermal gradient in the bubble has been assumed to be 3/2 of the microscopic thermal gradient and the angle φ of the lenticular shaped bubble assumed to be attained a maximum at 45°

**2.2 Bubble Size Distribution for Gas Bubble Coalescence at the Grain Boundary**

To estimate the amount of gas released from the grain boundary and the amount of gas that remains, it is necessary to determine the bubble size distribution on the grain boundary using the number of gas atom diffuse from inside the grains

Assuming that bubble mobility arises from the diffusion of atoms of the solid around the solid-gas interface, Gruber[7] treated two cases (i) the bubble growth by random migration coalescence for a fixed number of gas atoms, (ii) the bubble growth by biased migration coalescence for a fixed number of gas atoms Baroody[13] subsequently indicated that a large numerical error existed in Gruber's calculation for random migration coalescence Baroody introduced essentially the same assumptions as did Gruber and gave the major attention to situations where pore mobility results from surface diffusion

In this report, it is also assumed the same one as did Gruber who consider two groups of particles characterized by diffusion coefficients D<sub>i</sub> and D<sub>j</sub> and equated for the number ΔF<sub>ij</sub> of coalescence between i and j bubbles in Δt

$$\Delta F_{ij} = 4\pi D_{ij} R_{ij} F_i F_j \left\{ 1 + \left[ \frac{R_{ij}}{\pi D_{ij}} \right]^{1/2} \right\} \Delta t \quad (2-2)$$

where

$$D_{ij} = D_i + D_j = 0.301 D_s \alpha_o^4 (r_i^4 + r_j^4)$$

$$R = 8.3134 \text{ J/mol-K}$$

$F_i, F_j$  = numbers of each type of particle per unit volume,

$\alpha_o$  = lattice constant of  $\text{UO}_2$

$D_s$  = Surface diffusion coefficient ( $\text{cm}^2/\text{sec}$ ) =  $5.4 \times 10^5 \exp(-108000/RT)$

$R_y$  = distance between the centers of two particles when they begin to interact strongly, which is taken to be the sum of the bubble radii  $r_i + r_j$  for bubble coalescence

Each collision in the appearance of one  $i$  and  $j$  bubble and the formation of one  $(i+j)$  bubble. Assuming that all bubbles were initially monatomic, for the time interval between

$t_i$  and  $t_{i+1}$  for  $i$  bubble containing  $n_i$  gas atoms, the average number,  $\bar{f}_i$ , of bubbles per gas atom per unit volume is obtained from Eq (2-2) and then the effective number,  $f_i$ , of bubbles for a median atom size at a given bubble size group is given the following equation as detailed in References 2 and 3

$$\bar{f}_i = 0.23 m \tau^{-4/5} \int_0^{n_i} \{ \exp[0.7(n \tau^{2/5} - 0.5)] [\sinh \sqrt{1.12 n \tau^{2/5} - 0.5}] \} dn \quad (2-3A)$$

$$f_i = \bar{f}_i m_{gb} \left[ \sum_{\text{size range}} \bar{f}_i \frac{(n_i + n_{i+1})}{2} \right]^{-1} \quad (2-3B)$$

where

$\tau$  = reduced time as a dimensionless parameter  $\equiv 91.725 \alpha_o^4 D_s m (\gamma_{gb}/kT)^{3/2} t$

$m = m_{gb}/Et$  = number of gas atoms per unit volume around the grain-boundary surface

$m_{gb}$  = number of gas atoms per unit area on the grain boundary

$E_t$  = effective thickness of the grain boundary

$\gamma_{gb}$  = grain boundary surface tension

$t$  = time

Eq (2-3A) can be calculated by using the Gaussian integration formula which appropriate the definite integral by the expression

$$\int_1^i f(x) dx = w_0 f(x_0) + w_1 f(x_1) + \dots + w_n f(x_n) = \sum_{k=1}^n w_k f(x_k) \quad (2-4)$$

where  $w_0, w_1, \dots, w_n$  are the weighting coefficients and  $x_0, x_1, \dots, x_n$  are the associated points

### 2.3 Bubble Saturation on the Grain Boundary and Bubble Tunneling at Grain Edge

Based on a simple cubic structure in two dimensions, the critical fraction of the grain boundary area occupied by bubbles when interlinking first occurs is [14]

$$\left( \frac{r_{sb}}{r_{sg}} \right)_{crit}^2 = \frac{\pi r_{sb}^2}{(2 r_{sb})^2} = \frac{\pi}{4} \quad (2-5)$$

where

$r_{sb}$  = radius of spherical gas bubble,

$r_{sg}$  = radius of the circular unit cells of the grain boundary

To determine the bubble saturation condition at the grain boundary, the lenticular bubble is considered to be real bubble shape on the grain boundary because an experimental observation is reported by Reybikids et al [12]. The radius  $r_{sb}$  of spherical bubble can be expressed with respect to the lenticular curvature  $R_{lb}$  and  $r_{lb}$  of intergranular bubble as shown in Fig 2-1-1

$$R_{lb} = \exp\left[\frac{1}{3} \ln\left(\frac{r_{sb}}{\alpha}\right)\right]^3 \quad (2-6)$$

$$r_{lb} = \sin \phi \exp\left[\frac{1}{3} \ln\left(\frac{r_{sb}}{\alpha}\right)\right]^3 \quad (2-7)$$

The gas atoms from the grain form lenticular grain boundary bubbles, which can grow until they interlink. Tunnels subsequently form at grain edges as given by the combination of Equation (2-5) with Equations (2-6) and (2-7), that is, the saturation condition for a unit area of grain boundary is given by

$$\frac{1}{4} = \sum_{\text{size range}} (r_{lb})^2 f_i \quad (2-8)$$

and gas ultimately escape to voidage, such as fuel cracks or a plenum, within the fuel element

### 2.4 Fission Gas Swelling

If the bubbles are smaller than the critical pull-off size  $r_{gb}$ , they are considered to be the grain boundary inventory. The KAFEPa code calculates grain-boundary saturation of gas bubbles by dealing directly with the calculated lenticular-shaped size distribution and determines the sum of the volumes of the bubbles trapped on the grain boundary, and then calculates the fractional swelling due to the bubbles on the grain boundaries. The van der Waals gas law is used to calculate the fission gas swelling. It is noted that, in the KAFEPa code, the total fission induced swelling in the fuel is obtained by adding the fission gas swelling with solid fission product swelling.

### 2.5 Model Application and Results

Table 1 shows the major differences between the single-bubble-size model of the ELESIM code and the multiple bubble-size model of the KAFEPa code. The present fission gas model installed in the KAFEPa code was verified [2, 3] through comparison with experimental data taken from AECL and KAERI irradiation tests. The KAFEPa code slightly well predicts the absolute magnitude and trend of fission gas release in comparison with ELESIM as shown in Fig 2-5-1.

Table 1 Difference Between ELESIM and KAFEPA Fission Gas Release Models

Parameter	KAFEPA Code	ELESIM Code
1 Fission Gas Release Model		
- Bubbler shape on grain boundary	Lenticular with a dihedral angle of $100^\circ$	Spherical
Diffusion Coefficient ( $m^2/s$ )	$D = 7.8 \times 10^{-2} \exp\left[-\frac{288 \text{ kJ/mol}}{R(T/10^3)}\right]$	$D = C \times 7.8 \times 10^{-2} \exp\left[-\frac{288 \text{ kJ/mol}}{R(T/10^3)}\right]$ where C is an arbitrary factor of 3
Bubble behaviour on grain boundary	Moving by random and biased driving force	- Stationary
- Saturation condition at grain boundary	- Critical size and saturation condition for lenticular bubble	Fixed max density with single bubble size Max size & max density for a single spherical bubble size
2 Fuel densification model		
- Model	Mechanistic	Empirical (The void consumption due to densification varies with temperature)
3 Neutron flux depression data base		
Pellet diameter	8.0 ~ 19.5 mm	12.15 ~ 19.5 mm
Fuel enrichment	0.711 ~ 6 wt% U 235	0.711 ~ 6 wt% U 235
Fuel burnup	0 ~ 800 MWh/kgU	0 ~ 200 MWh/kgU
4 Fuel material properties	Mostly based on MATPRO Version 9	Mostly based on MATPRO Version 11 (Rev 2)

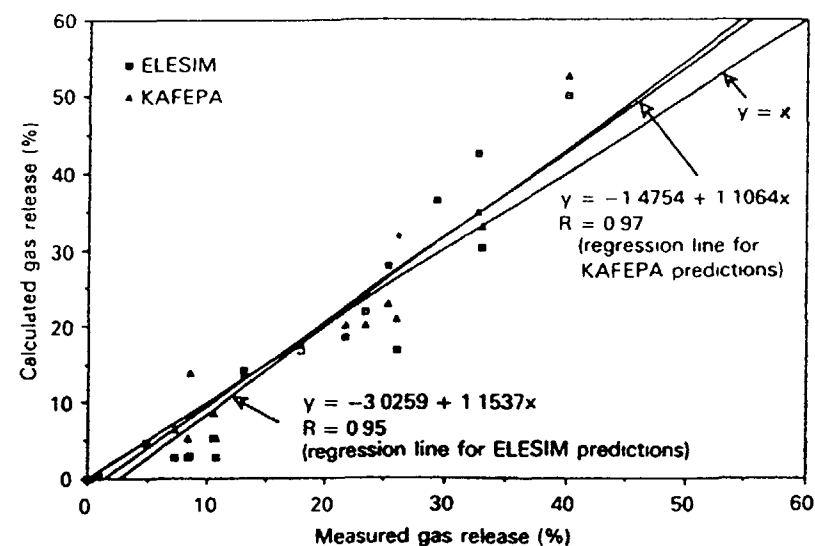


FIG 2.5-1 Comparison between measured end-of-life fission gas release and KAFEPA and ELESIM predictions for the verification of the fission gas release model

### 3 MECHANISTIC MODEL FOR IN-REACTOR DENSIFICATION OF $UO_2$

Reviewing [17] of previous works on  $UO_2$  fuel densification and considering vacancy generation and migration in grain and sink at grain boundary, KAERI [17] has developed a mechanistic densification model which is dependent on  $UO_2$  temperature and microstructure based on Assmann and Shehler's model [18]. This densification model is a function of time, fission rate, temperature,  $UO_2$  density, pore size distribution and grain size. The resultant equation derived in the present model which is different from Assmann and Shehler's resultant equations for four fuel temperature regions as described below can be applied directly for all pellet temperatures.

#### 3.1 Rate Equation and its Integration Method for In-Reactors Pore Shrinkage of Coarse Pores

The  $UO_2$  fuel densification is in principle, a two-step mechanism: (i) generation of an excess vacancy concentration around the pores and (ii) partial migration of these vacancies to the grain boundary. We can consider that first generation and reabsorption of single vacancies at or close to the surface of the pore; second migration of excess vacancies to the grain boundary.

The rate equation for the shrinkage of the pore radius is given by Assmann and Stehle [18]

$$\frac{dr}{dt} = - \frac{(D_v^{th} + D_v^{irr}) r_g}{r (r_g - r)} \times \frac{\frac{\gamma \Omega D}{r k T g a} + \frac{\lambda \omega F}{3} (C_s - C_T)}{D_v^{th} \frac{1}{2 g a} + \frac{(D_v^{th} + D_v^{irr}) r_g}{r (r_g - r)} + \frac{\lambda \omega F}{3}} \quad (3-1)$$

where

- r = pore radius
- t = time
- λ = fission spike length
- ω = UO<sub>2</sub> volume (5 x 10<sup>19</sup> cm<sup>3</sup>)
- k = Boltzmann constant
- a = lattice parameter of UO<sub>2</sub>
- C<sub>s</sub> = saturation concentration of vacancies of UO<sub>2</sub>
- D<sub>s</sub> = self-diffusion coefficient of uranium in UO<sub>2</sub>
- D<sub>v</sub><sup>th</sup> = thermal vacancy diffusion coefficient
- D<sub>v</sub><sup>irr</sup> = irradiation induced vacancy diffusion coefficient
- r<sub>g</sub> = grain radius
- γ = surface tension of UO<sub>2</sub>
- Ω = vacancy volume
- g = numerical parameter
- T = temperature
- F = fission rate
- C<sub>T</sub> = thermal vacancy concentration

Characterizing the UO<sub>2</sub> fuel temperatures as four regions such as region I of low temperature below 450 °C, region II of moderately low temperatures between 450 and 750

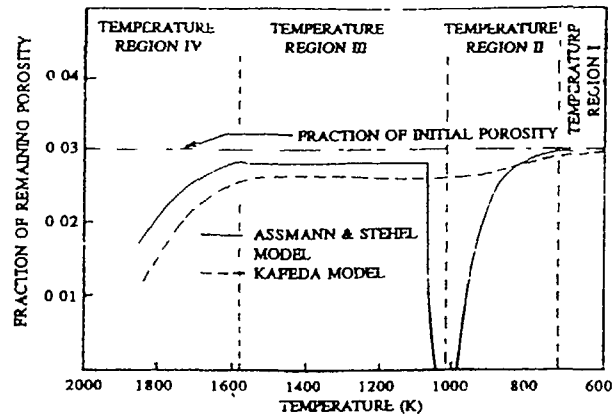


FIG 3-1-1 Distribution of remaining porosity at 40 MW h/kg U

°C, region III of moderately high temperatures between 750 and 1300 °C, region IV of high temperature above 1300 °C as did by Assmann and Stehle, we have evaluated the Assmann and Stehle's modelling of coarse pore [17] and then we can find the discontinuity of the distribution of remaining porosity as a function of temperature in the regions I and II as shown in Fig 3-1-1

The initial intragranular porosity can be divided into two groups such as fine pores and coarse pores. The coarse porosity can be further characterized by five size ranges, such as used in this work. Coarse pores keep their identity and show a continuous shrinkage of the pore radius. For this region, fission-induced fuel density changes can be expressed for pore only by equations for average porosity, whereas the behaviour of coarse pores can be expressed by an equation for the individual pore radii.

To calculate how the sintering porosity distribution changes with time and power requires the solution of the non-linear differential Equation (3-1).

For  $r \ll r_g$ , and  $C_T \ll C_s$ , Eq (3-1) can be simplified to

$$\frac{dr}{dt} = - \frac{D_v(S + Zr)}{r(D_v + Br)} \quad (3-2)$$

where  $B = \frac{D_v^{th}}{2ag} + \frac{\lambda \omega F}{3}$ ,  $Z = \frac{\lambda \omega F C_s}{3}$ ,  $S = \frac{\gamma \Omega D}{k T a g}$  and  $D_v = D_v^{th} + D_v^{irr}$

In order to integrate Eq (3-2) from pore radii  $r_0$  and  $r_1$ , we can rearrange the equation as

$$\int_{r_0}^{r_1} \frac{r[1 + (B r/D_v)]}{(S + Zr)} dr = - \Delta t \quad (3-3)$$

Integrating Eq (3-3), we obtain the following results,

$$\frac{1}{Z^2} [(S + Zr) - S \ln(S + Zr)]_{r_0}^{r_1} + \frac{B}{D_v Z^3} \left[ \frac{(Zr + S)^2}{2} - 2S(Zr + S) + S^2 \ln(Zr + S) \right]_{r_0}^{r_1} = - \Delta t \quad (3-4)$$

The quadratic relationship in  $r_1$  can be solved by known methods

$$A_1 r_1^2 + A_2 r_1 + A_3 = 0 \quad (3-4)$$

where  $A_1 = \frac{ZB}{2}$ ,

$$A_2 = -(SB - ZD_v)$$

$$A_3 = - \left[ (D_v S - \frac{BS^2}{Z}) \ln(S + Zr_0) + A_1 r_0^2 + A_1 r_0 - (D_v S - \frac{BS^2}{Z}) \ln(S + Zr_1) - \Delta t Z^2 D_v \right]$$

Therefore if we used a generalization of the Newton Raphson method we can obtain the final radius of the pore in the above equation. Using Equation (3-4) with the constant

parameters or formula summarized in Reference 17, we can obtain the distribution of remaining porosity as a function of temperature as shown in Fig 3 1 1

3.2 Modelling of Fine Pore

It is assumed that a population of very fine pores (radius  $r_p$ , density  $Z_p$ ) and a second population of coarse pores (radius  $r_c$ , density  $Z_c$ ) are presented inside a  $UO_2$  grain with radius  $r_g$ . It is also assumed that the volume,  $p$ , of the fine sized porosity inside a grain is homogeneously distributed within the matrix. Under steady condition a certain concentration of vacancies in excess of the thermal equilibrium is maintained in the  $UO_2$  matrix because of the continuous input of vacancies from the atomization of the fine pores by fission spikes. Most of the vacancies generated by a single event, they are coalesced to a new pore or they can grow the coarse pore. Because they are trapped by coarse pores, only a small fraction of vacancies migrate to the grain boundaries. Nevertheless, because of the large number of vacancies generated by one event and the large number of events per unit time, the contribution of fine pores to the initial densification rate is considerable. Physically, the problem can be treated as a diffusion problem with a homogeneous source of vacancies inside the grain, a densification effective sink at the grain boundary, and ineffective sinks at the surface of the coarse pores inside the grain. So far the disappearance of the very fine pores has been treated only in the high temperature region, that is, under the assumption that the vacancy diffusion rate is rather and, therefore, the kinetics are purely controlled by the athermal vacancy generation rate[19]

For the vacancy diffusion coefficient,  $D_v$ , large at high temperatures, the grain size large and pore concentration high ( $a r_g \ll 1$ ) where  $a$  is the lattice constant, the fraction of the vacancies reach the grain boundary,  $f$ , is approximately given by[21]

$$f = \frac{1}{1 + (4\pi/3)Z_c r_c r_g / \sqrt{4\pi(Z_c r_c + Z_p r_p)}} \quad (3-5)$$

The densification is therefore given by[17]

$$\frac{\Delta V}{V_o} = f p_o [1 - \exp(-\Omega_{sp} \eta t)] \quad (3-6)$$

and then the coarse pore growth in case of well sintered fuel is given for the fractional amount,  $\Delta f_g$ , of the vacancies absorbed by coarse pore[17]

$$\frac{\Delta f_g}{V_o} = (1 - f) P_o [1 - \exp(-\Omega_{sp} \eta t)] \quad (3-7)$$

where  $P_o$  = fraction of porosity and  $\eta = 2 \times 10^{-4} [r_g \sqrt{4\pi(Z_c r_c + Z_p r_p)}]^{-1}$

For the vacancy diffusion coefficient  $D_v$  small at low temperatures ( $a r_g \gg 1$ ) the average porosity,  $\bar{P}$ , is approximately given by[17]

$$\bar{P} = P_o \left(1 - \frac{3}{2r_g} \sqrt{\frac{\Omega_{sp} \eta C_s D_s}{P_o F}} Ft\right)^2 \quad (3-8)$$

The time,  $t_o$ , needed for the disappearance of the fine sized porosity is

$$t_o = \frac{2 r_g}{3} \sqrt{\frac{P_o}{F \Omega_{sp} C_s D_v}} \quad (3-9)$$

Eqs (3-8) and (3-9) clearly show the influence of the grain size on the densification. Similarly, as shown previously for coarse size fractions, the shrinkage is smaller for large grain material than for small grain material. According to the temperature dependence of the vacancy diffusion coefficient,  $D_v$ , the pore shrinkage rate depends also on temperature.

3.3 Model Application and Results

Table 1 shows the major differences between the empirical model of the ELESIM code and the mechanistic model of the KAFEPa code. The present densification model is consisted of parameters of which input data are irradiation period, fission rate, pellet temperature and  $UO_2$  density, pore size distribution, and grain size, while the ELESIM Code calculated the densification through that the void consumption due to densification varies with temperature. The present densification model installed in the KAFEPa code was verified[17] through comparison with experimental data taken from AECL irradiation tests with Pickering fuel of

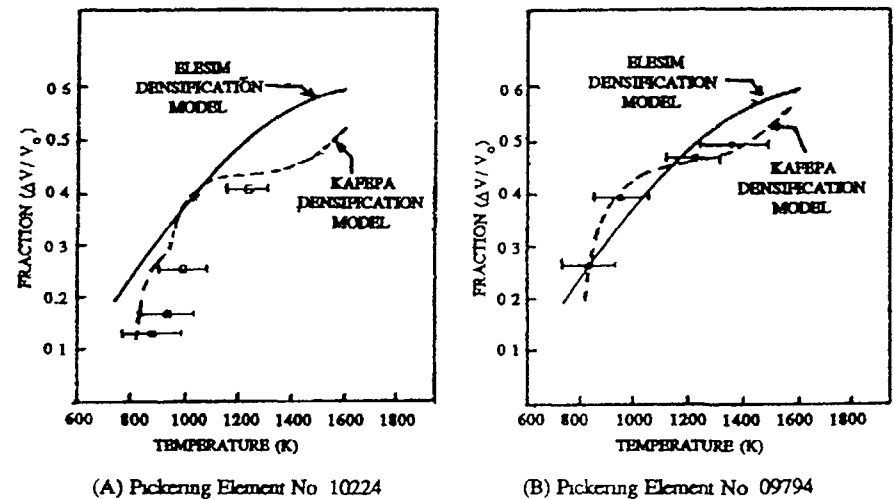


FIG 3 3-2 Volume fraction ( $\Delta V/V_o$ ) as a function of temperature for Pickering element numbers 10224 and 09794 irradiated to  $200 \pm 15$  MW h/kg U

10.2, 10.4, 10.6 and 10.7 Mg/cm<sup>3</sup> initial densities [23]. The KAFEPAC codes predicted the fuel densification for Pickering elements as shown in Fig. 3.3.2. As shown in these figures, the KAFEPAC code well predicts the absolute magnitude and trend of fuel densification in comparison with ELESIM.

#### 4. DATA BASE EXPANSION OF NEUTRON FLUX DEPRESSION IN FUEL AND UPDATING OF THE MATERIAL PROPERTIES IN ELESIM CODE

KAERI has updated the ELESIM data base of neutron flux depression in fuel and the material properties such as fuel thermal conductivity, clad elastic moduli and clad thermal expansion in order to more accurately analyze and predict the in-pile behaviour of a CANFLEX extended fuel element.

In CANDU reactor, the thermal neutron flux decreases as one moves towards the center of fuel due to neutron absorption in the fuel. As irradiation proceeds the original fissile atoms are depleted in the fuel, fission products build up and new fissile atoms are formed. Since these processes are dependent on the neutron flux level and spectrum, the local fission rate within the fuel pellet will vary with burnup. The Pu-239 formed in UO<sub>2</sub> pellet during irradiation in thermal reactors is nonuniformly distributed. The radial distribution of plutonium formed by thermal neutron capture is governed by the radial thermal neutron flux distribution [21]. In practice, the buildup of plutonium atoms near the fuel surface has the greatest effect on the CANDU reactor fuel which is used natural uranium and produces higher fission rates at the surface as burnup proceeds.

An accurate and fast running model for calculating radial power profile, through fuel life, in both solid and annular pellets for existing and advanced CANDU-PHWR fuel has been developed in KAERI, where the radial power profile is slightly lower than that of the original ELESIM data table when normalized to unity at the pellet surface. This model contains resultant flux depression equations and neutron depression data table for the CANDU pellets with the diameter of 8.0 to 19.5 mm and enrichment of 0.71 - 6.0 wt% U-235 in total uranium, over a burnup range of 0 to 35000 MWd/MTU.

For a solid cylindrical fuel, the applicable neutron flux depression is expressed by [23, 24]

$$\phi_r = \phi_o \{ I_0(\kappa r) + \beta \exp[\lambda(r - a)] \} \quad (4-1)$$

where  $\phi_r$  = neutron flux at radius  $r$  (number of neutrons/cm<sup>2</sup>-sec)

$\phi_o$  = neutron flux at the center (radius  $r = 0$ ) (number of neutrons/cm<sup>2</sup>-sec)

$I_0$  = zero-order modified Bessel function of first kind

$r$  = coordinate in radial direction (mm)

$a$  = radius of pellet (mm)

$\kappa$  = the neutron inverse diffusion length

$\beta, \lambda$  = empirical parameters in the neutron flux depression term

and the rate of heat generation,  $h_r$ , in the fuel pellet radius  $r$  which is proportional to the neutron flux is given by

$$h_r = h_o \{ I_0(\kappa r) + \beta \exp[\lambda(r - a)] \} \quad (4-2)$$

where  $h_o$  = heat generation rate at the center (radius  $r = 0$ ) (number of neutrons/cm<sup>2</sup>-sec)

For an annular fuel, the applicable neutron flux depression is expressed by [23, 24]

$$\phi_r = \phi_o \left\{ I_0(\kappa r) + \frac{I_1(\kappa r)}{K_1(\kappa r)} K_0(\kappa r) + \beta \exp[\lambda(r - a)] \right\} \quad (4-3)$$

where  $I_1$  = first-order modified Bessel function of first kind

$K_0$  = zero-order modified Bessel function of second kind

$K_1$  = first-order modified Bessel function of second kind

and the rate of heat generation,  $h_r$ , in the fuel pellet radius  $r$  is given by

$$h_r = h_o \left\{ I_0(\kappa r) + \frac{I_1(\kappa r)}{K_1(\kappa r)} K_0(\kappa r) + \beta \exp[\lambda(r - a)] \right\} \quad (4-4)$$

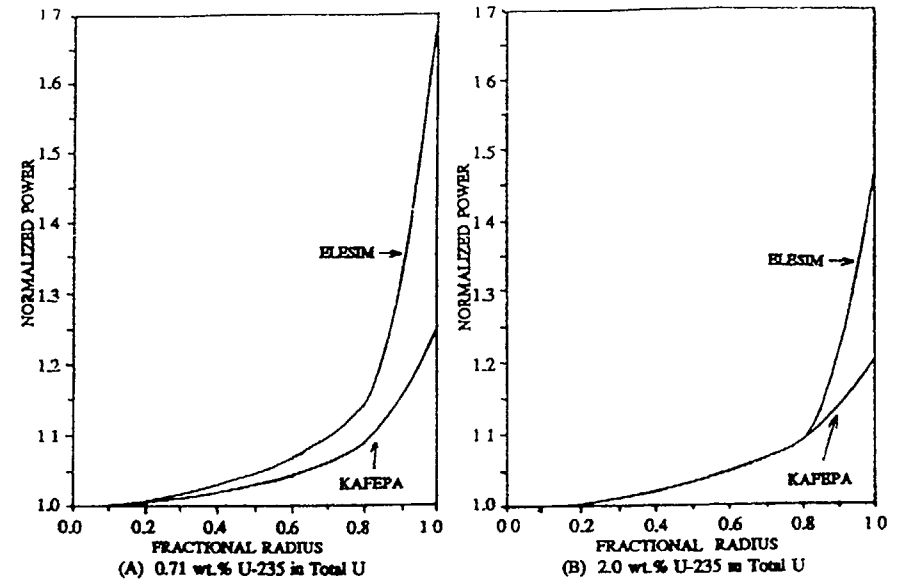


FIG. 4.1 Comparison of the radial power profiles by ELESIM and KAFEPAC codes. Pellet diameter = 12.15 mm and burnup = 120 MW h/kg U.

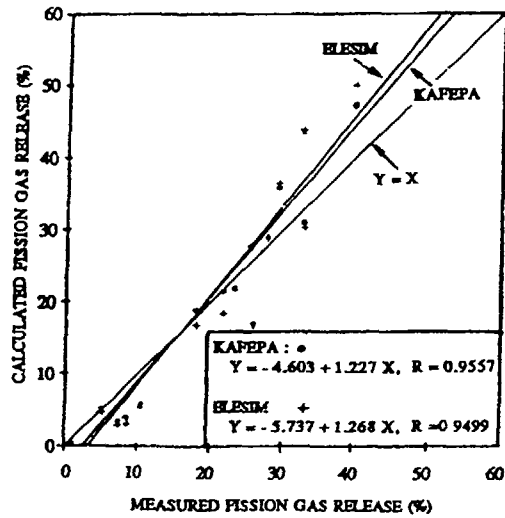


FIG 4 2 Comparison between measured end-of-life fission gas release data and KAFEPA and ELESIM predictions for the verification of neutron flux depression data base

The HAMMER physics code is a heterogeneous lattice analysis code with depletion using heterogeneous analysis by the multipgroup method of exponentials. In connection with the use of HAMMER physics code for the calculation of  $\kappa$ ,  $\beta$  and  $\lambda$ , Eq (4-4) can be expressed as[23]

$$\frac{\bar{h}(r_2^2 - r_1^2)}{2} = h_0 \left\{ \frac{r_2 I_1(\kappa r_2) - I_1(\kappa r_1)}{\kappa} - \frac{h_0 \beta}{\lambda} \{ r_2 \exp[\lambda(r_2 - a)] - r_1 \exp[\lambda(r_1 - a)] \} - \frac{\exp(\lambda(r_2 - a)) - \exp(\lambda(r_1 - a))}{\gamma} \right\} \quad (4-5)$$

The parameters  $\kappa$ ,  $\beta$  and  $\lambda$  for the relative heat generation rate equation (4 5) were derived by fitting them to fission heat profile calculated by the HAMMER physics code. Here, As the present purpose, the HAMMER physics code's input data such as isotope composition and concentration, effective neutron temperature and material buckling were obtained from references [22, 23 24]. In order to obtain the values of  $h_0$ ,  $\kappa$ ,  $\beta$  and  $\lambda$  which are the functions of fuel burnup, enrichment and pellet diameter, NL2INT subroutine[25] was used to fit the curve equation (4 5). When the input parameters of fuel enrichment, pellet diameter

and final burnup are specified, multi-variate interpolation routines obtain the values of  $\kappa$ ,  $\beta$  and  $\lambda$  as a function of burnup for the particular case, and store the arrays into KAFEPA code. The value of  $\kappa$ ,  $\beta$  and  $\lambda$  are then obtained at each burnup history point by one-dimensional interpolation from the data stored in the arrays.

Table 1 shows the major differences between the ELESIM code's data base and the KAFEPA code's data base. Figs 4-1 show the differences in radial profiles, based on both the ELESIM and KAFEPA codes' neutron flux depression data bases. Using the ELESIM and KAFEPA codes data bases, Figs 4 2 shows the predictions of fission gas releases for experimental data and indicates that KAFEPA code gives a slightly better prediction than the ELESIM code's prediction.

Based on MATPRO Version 11(Rev 2)[4], it also has updated the material properties such as fuel thermal conductivity, clad elastic moduli and clad thermal expansion used in ELESIM-MOD10 code[1] of which most material properties are originated from MATPRO-Version 9[5]. The updated material properties installed in the KAFEPA code was verified[2, 3] through comparison with experimental fission gas release data taken from AECL and KAERI irradiation tests. This verification gave that the KAFEPA code well predicts the absolute magnitude and trend of fission gas release in comparison with ELESIM code.

### 5. DISCUSSION AND CONCLUSIONS

Table 1 summarizes the major differences between the ELESIM and KAFEPA codes. The KAFEPA code is installed with the present fission gas release and densification models, the expanded neutron flux depression data base, and the updated properties of fuel and clad materials.

As shown in Fig 2 5-1, KAFEPA code predicts the fission gas releases that are in reasonable agreement with a wide variety of the experimental data, while the ELESIM code gives predictions that are slightly more scattered than the KAFEPA code's predictions. These results also show that the behaviour of multiple-bubble size distribution on grain boundary appears to be a very important phenomena in fission gas release from  $UO_2$  fuel. It is noted that the Notley and Hastings model was modified to increase to fission gas release so that measured and predicted fission gas release were, on average, equivalent, since their model was in ELESIM code as a fuel design code. This was done by arbitrarily increasing the diffusion coefficient by a factor of 3. However, incorporating the present intergranular bubble model for fission gas release into the KAFEPA code, the tuning factor of 3 is not desired as no arbitrary quantities are used in the present model.

As shown in Fig 3 3 2, The KAFEPA code predicts the fuel densifications of which fraction is a trend in the experimental behaviour while the ELESIM densification algorithm predicts the fraction which is monotonically raised with increasing temperature. The fuel densification model used in KAFEPA code is based on the Assmann and Stehle model which is introduced the pore and spike interaction and suggests the rate equation and the relationships for four regions of fuel temperatures. The Assmann and Stehle model are not only observed

some discrepancies with experimental data but also gives some discontinuities at the boundaries of each temperature region. However, to overcome such discrepancies and discontinuities, the present integral method of Assmann and Stehle's rate equation results to predict the fuel densification to overcome such discrepancies and discontinuities in the Assmann and Stehle model. The present fuel densification is a function of time, fission rate, temperature, fuel density, pore size distribution and grain size, and requires the input data of each pore size distribution for each fuel type. So it appears that the initial pore size distribution is the most important parameter which determines the fuel densification rate. It is noted that, in the ELESIM code, the void consumption due to fuel densification simply varies temperature for a given fractional porosity of manufactured pellet.

In addition, the expanded data base of neutron flux depression in fuel and the updated properties of fuel and clad are employed in the KAFEPa code. These data base and properties give a slight improvement for the prediction of fuel performance as shown in the prediction of fission gas release.

As closing in this report, it is concluded that, since KAFEPa code has well predicted the absolute magnitude and trend of fission gas release in comparison with experimental data and ELESIM code's predictions, (1) the behaviour of a multiple-bubble-size distribution in the present model appears to be an important phenomenon in fission gas release from  $UO_2$  fuel, (2) the initial pore size distribution is the most important parameter which determines the fuel densification rate, (3) the expanded data base of neutron flux depression in fuel and the updated properties of fuel and clad with respect to those in ELESIM code also give to help better prediction of CANDU fuel performance.

#### REFERENCES

- 1 M J F. NOTLEY, "ELESIM A Computer Code for Predicting the Performance of Nuclear Fuel Element", Nucl Appl Tech 44(1979) 445-450
- 2 H C SUK, W HWANG, J H PARK, B G KIM, K S SIM, and C J JEONG, "Improvement of CANDU Fuel Performance Analysis ELESIM MOD10", presented at Int. Conf. CANDU Fuel, Chalk River, Canada, October 1986
- 3 W HWANG, H C SUK and W M JAE, "Comprehensive Fission Gas Release Model Considering Multiple Bubble Sizes on the Grain Boundary Under Steady State Conditions", Nucl Tech 9(1991)314
- 4 MATPRO-Version 11 (Revision 2), "A Handbook of Materials Properties for Use in the Analysis of Light Water Reactor Fuel Rod Behaviour", compiled and edited by D L HAGRMAN, G A REYMAN, and R E MASON, NUREG/CR-0479, TREE-1280, Rev 2, R3 and R4, EG & G Idaho, Aug 1981
- 5 MATPRO-Version 9, "A Handbook of Materials Properties for Use in the Analysis of Light Water Reactor Fuel Rod Behaviour", compiled and edited by P E MacDONALD et al, TREE NUREG 1005, EG & G Idaho, Dec 1976
- 6 M J F NOTLEY and I J HASTINGS, "Microstructure-Dependent Model for Fission Product Gas Release and Swelling in  $UO_2$  Fuel", Nucl Eng and Des 56(1980) 163
- 7 E E GRUBER, "Calculated Size Distributions for Gas Bubble Migration and Coalescence in Solids", J Appl Phys, 38, 1, (1967) 243
- 8 A H BOOTH, "A Suggested Method for Calculating the Diffusion of Radioactive Rare Gas Fission Products from  $UO_2$  Fuel Elements and a Discussion of Proposed In-Reactor Experiments That May be Used to Test its Validity", AECL 700 (DCI 127), Atomic Energy Canada Limited, (1957)
- 9 A H BOOTH, "A Method for Calculating Fission Gas Diffusion from  $UO_2$  Fuel and its Application to the X-2-f Loop Test", CRDC 721, AECL 700 (DCI-127), Atomic Energy Canada Limited, (1957)
- 10 C C DOLLINS and M JURSCICH, "Swelling and Gas Release in Oxide Fuels During Fast Temperature Transients", J Nucl Mater 107(1982)46
- 11 J M GRIESMEYER, W G STEELE, D OKRENT, S H CHIEN, and A R WAZZAN, "A Nonequilibrium Analysis of Fission Gas Release and Bubble Freezing During Fast Reactor Transient", Tran Am Nucl Soc, 23(1976)174
- 12 G L REYNOLDS, W B BEERE and P T SAWBRIDGE, "The Effect of Fission Product on the Ratio of Grain Boundary Energy to Surface Energy in Irradiated Uranium Dioxide", J Nucl Mat 41(1971)112
- 13 E M BRAOODY, "Calculations on the Collisional Coalescence of Gas Bubbles in Solids", J App Phys 38(1967)4893
- 14 D R OLANDER, "Fundamental Aspects of Nuclear Reactor Fuel Elements", TID-26711-1P1, Atomic Energy Commission (1976)
- 15 S R MacEWEN and I J HASTINGS, "A Model for In-Reactor Densification of  $UO_2$ ", AECL-4993, Atomic Energy Canada Limited, Sept. 1974
- 16 M D FRESHLEY, D W BRITTE, J L DANIEL and P E HART, "Irradiation-Induced Densification of  $UO_2$  Fuel Pellet", J Nucl Mat 62(1976) 138-166
- 17 W HWANG, K S SEO and H C SUK, "A Mechanistic Model for In-Reactor Densification of  $UO_2$ ", J Kor Nucl Soc, 17(1985)116
- 18 H ASSMANN and H STEHEL, "Thermal and In-Reactor Densification of  $UO_2$  Mechanisms and Experimental Results", Nucl Eng and Des 48(1978) 49-67
- 19 H STEHEL and H ASSMANN, "In-Reactor  $UO_2$  Densification", Nucl Mat 61(1976) 326-329
- 20 I J HASTINGS and L E EVANS, "Densification Algorithm for Irradiated  $UO_2$  Fuel", J Am Cera Soc, 62 (1979)
- 21 H CALSEN and D N SAH, "Radial Concentration and Effect on Temperature of Plutonium Formed in  $UO_2$  During Irradiation", Nucl Tech 55(1981) p
- 22 U HESSE, "Verification of the OREST(HAMMER-ORIGIN) Depletion Program System Using Post-Irradiation Analysis of Fuel Assemblies 168, 170, 171 and 176 from the Obninsk Reactor, ORNL/TR-88/20, p 1-32, May 1984
- 23 W HWANG, H C SUK and W M JAE, "A Model for Predicting the Radial Power Profile in CANDU PHWR Fuel Pellet", J Kor Nucl Soc 23(1991)445-456
- 24 E HELLSTRAND, "Measurement of the Effective Resonance Integral in Uranium Metal and Oxide in Different Geometries", J Appl Phys, 28(1957)1493
- 25 J E DENNIS, D M GAY and R E WELSH, "Algorithm 573 NL2SOL: An Adaptive Nonlinear Least-Squares Algorithm (E4)", ACM Transactions on Mathematical Software, Vol 7 No 3, Sept 1981

## MODELLING AND MODELLING SUPPORT II

(Session 5)

**Chairmen**

**M. CHARLES**

France

**F. IGLESIAS**

Canada

**EVALUATION OF MEASURED HIGH BURNUP FUEL TEMPERATURE AT RISØ PROJECT PHASE 3**

S. KITAJIMA, M. KINOSHITA  
 Central Research Institute of Electric Power Industry,  
 Tokyo, Japan

**Abstract**

We developed an effective thermal conductivity model of pellet which includes effects of open spaces in pellet and fission product solid solution.

At RISØ project phase 3, measured fuel central temperature indicated that the effective thermal conductivity of pellet decreased as burnup increase. This project also examined the relation of filled gas component and fuel temperature.

We evaluated RISØ data utilizing the fuel performance evaluation code involving the model, and found out that the effective thermal conductivity of pellet decreased about 25% at 40 MWd/kgUO<sub>2</sub>. The code could simulate that observed temperature drop of Xenon filled rod after fission gas burst release at RISØ project. And the analyses of the RISØ data show that contribution of the open spaces for the thermal conductivity degradation is more than 30% of the total degradation.

**1. Introduction**

In order to improve the economy of nuclear power generation, fuel burnup extension is an effective measure and related technological development is in progress. However high burnup fuels may behave differently from that at usual burnup. Therefore the fuel reliability indicators, such as fuel temperature and rod internal gas pressure, should be closely investigated.

The aim of the RISØ project phase 3[1] was to obtain fuel performance data during power transient at high burnup. In this project totally 15 fuels were supplied to the transient tests. Many fuel rods had instrumentations of a thermocouple and a pressure transducer, and central fuel temperature and rod internal pressure are measured during transients. The results indicates degradation of fuel thermal conductivity and enhancement of fission gas release at high burnup.

The fuel temperature is determined by fuel thermal resistance and liner heat rating. The thermal resistance is composed of that of fuel pellet, pellet-cladding gap and cladding wall. Fig.1-1 illustrates the schematic view of fuel thermal resistance, that is inverse of the thermal conductance, during irradiation. This fuel resistance may composed of two major parts;(1)fuel matrix, and (2)open spaces between fuel matrix. The latter includes large macroscopic cracks and microgaps which may exist due to grain boundary separation. From view of the fuel behavior, the resistance of fuel matrix is only dependent on fuel burnup and affects only on static fuel performance. On the other hand the resistance due to microgap depends on gas composition in the open space and gives additional dynamic effects during transient. Therefore the evaluation of this latter component may contribute to fuel design improvements and recommendations for reactor operation

We have developed a fuel performance evaluation code, the EIMUS [2], involving above two mechanisms in order to describe the thermal conductivity decrease at high burnup. We evaluated the fuel central temperature data of RISØ project phase 3, utilizing the modified code.

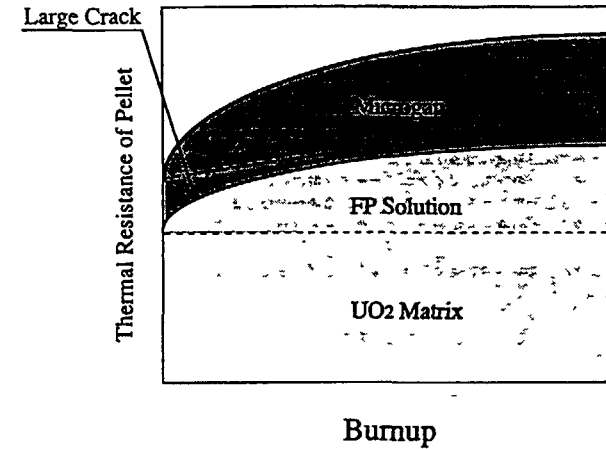


Fig.1-1 Schematic view of fuel thermal conductivity degradation.

**2. Modeling of Effective Thermal Conductivity**

The degradation mechanism of the fuel thermal conductivity at high burnup could be categorized as (1) static mechanism, and (2) dynamic mechanism. The thermal conductivity degradation of the static mechanism depend only on burnup. On the other hand, that of the dynamic mechanism depends on gas component and gas pressure in fuel rod, that changes significantly during reactor operation especially at transients.

Details of mathematical framework is described in the previous paper[3]. We divided pellet radius into  $N_r$  segments and calculated the average effective thermal conductivity at each segment (Fig.2-1).

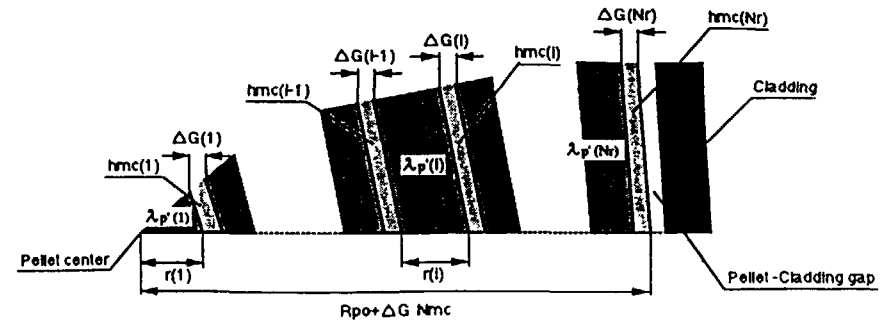


Fig.2-1 Schematic Diagram of the Microgap model

2.1. Static Mechanism

Most of the produced solid fission products may be in solution at normal LWR fuel condition. The quantity of the solid solution is proportional to burnup, and it reduces thermal conductivity of the UO<sub>2</sub> matrix. This is because change of the lattice constant reduces the heat conduction by phonon scattering. The thermal conductivity of UO<sub>2</sub> matrix involving the soluble fission product was theoretically analyzed by Klemens[4]. Then Ishimoto [5] adapted the equation for UO<sub>2</sub>, that is given by

$$\lambda_p'(i) = \lambda_p(i) \frac{\tan^{-1}(2.40 \cdot (\lambda_p(i) \cdot x)^{0.5})}{2.40 \cdot (\lambda_p(i) \cdot x)^{0.5}} \quad (1)$$

where  $\lambda_p$  is thermal conductivity of unirradiated UO<sub>2</sub> matrix and  $x$  is fraction of the solid solution of fission products. We assumed that the increase rate of the fraction is 0.1% per 10 MWd/kgUO<sub>2</sub>. This corresponds that all solid fission products are in solution and may give the upper limit for the conductivity degradation by this mechanism.

2.2. Dynamic Mechanism

Fig.2-2 shows that a pellet is divided into several fragments by the thermal strain at initial stages of power generation and the pellet fragments relocate in radial direction. Because the large cracks occurring at these stages are mainly in radial direction, the cracks may not be significant thermal barrier. At the same time the pellet-cladding gap (PC gap) is reduced by the pellet relocation and the total thermal resistance for rod is reduced during these initial stages (Fig.1-1).

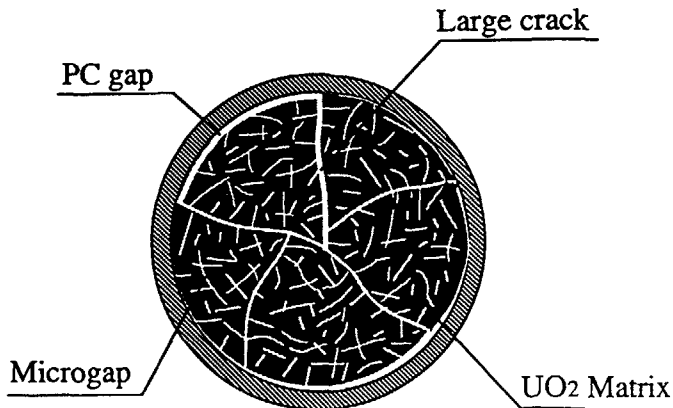


Fig.2-2 Typical Behavior of Pellet at high burnup.

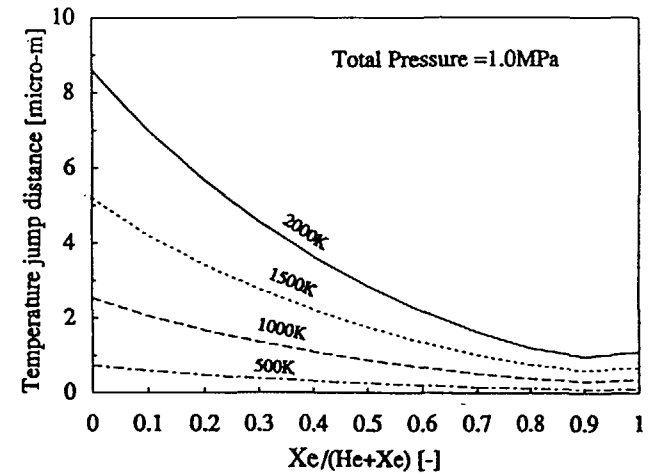


Fig.2-3 Temperature jump distance mixed gas of He and Xe.

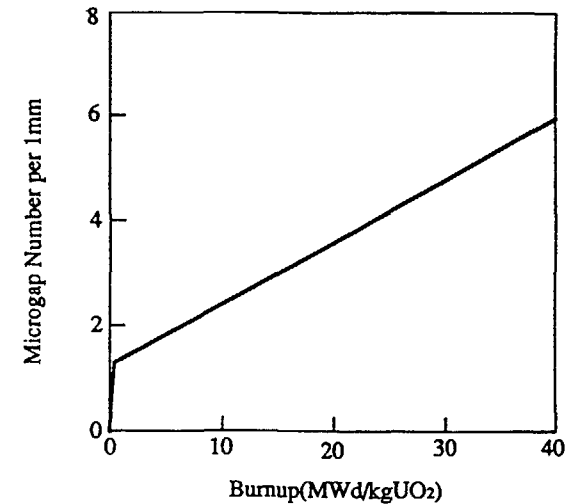


Fig.2-4 Derived MicrogapNumber Per 1mm.

Grain boundary separations, which could be generated by the development of grain boundary gas bubbles, may take place as burnup increase. If the separated grain boundaries are connected to the rod free volume, these open space in pellets may have the same gas composition as that of plenum gas. Because the thermal conductivity of gas is less than that of UO<sub>2</sub> matrix, grain boundary separations causes the thermal conductivity degradation of pellet.

In our analysis model the microgaps are assumed to distribute uniformly in pellet radial cross-section. Direction of microgaps are mapped into two components that are radial and the circumferential directions. For our analysis the thermal barrier due to the radial component could be neglected.

The solid-gas temperature jump takes place at interfaces of the UO<sub>2</sub> matrix and the gas. Therefore the thermal conductance at circumferential microgaps of segment *i*,  $h_{mc}(i)$ , is given by

$$h_{mc}(i) = \frac{\lambda_{ga}(i)}{(g_1(i) + g_2(i) + \Delta G)} \quad (2)$$

where  $\Delta G$  is a microgap width and  $g_1(i)$  and  $g_2(i)$  are temperature jump distances (TJDs) of mixed gas in pellets and rods. We adapted a TJD formula which was theoretically developed by Loyalka[6]. The TJD is inversely proportional to gas pressure, and depends on gas component and temperature. Fig.2-3 shows the TJD of mixed gas composed of Helium and Xenon where the total pressure is 1.0MPa. Comparing TJD's at the same gas pressure condition, they increase as the fraction of Helium or the gas temperature increases. This effects become remarkable when the fuel rod is at high linear heat rating or it has low internal gas pressure. In equation (2) the width of microgap is set to be very narrow, that is 0.45micro-m. This value was deduced from analyses of the RISO data described in the following sections.

The effective thermal conductivity of pellet at segment *i* is given by

$$\lambda_{ef}(i) = \frac{R_{po} + \Delta G \cdot N_{mc}}{\frac{R_{po}}{\lambda_{p'}(i)} + \frac{N_{mc}}{h_{mc}(i)}} \quad (3)$$

where  $R_{po}$  is a pellet radius and  $N_{mc}$  is the microgap number per pellet radius. We implemented these models in the fuel performance evaluation code, EIMUS and applied the models for verification.

The number of microgaps was estimated from experiments different from RISO project. The temperature data from a special experimental rig, IFA504, of OECD Halden project[7] was utilized. It has instrumented fuel rod with two thermocouples and two pressure gages at the top and bottom and the rod internal gas can be exchanged during irradiation. IFA504's experimental data indicated that fuel central temperature decreased as rod gas pressure is increased. This temperature decrease becomes more significant as burnup increases. We evaluated this behavior utilizing the modified code and estimated the number of microgaps as shown in Fig.2-4.

### 3. Transient Test of RISO Project Phase 3

The RISO project phase 3 comprised totally 15 rods of both PWR and BWR designs and they were supplied for transient tests. PWR designed rods were fabricated by Advanced Nuclear Fuels (ANF) and BWR designed rods were fabricated by General Electric (GE) and also by RISO National Laboratory. 10 rods were refabricated at the RISO after base irradiations, and were instrumented with a thermocouple and a pressure

Table 3-1 Refabrication data and irradiation conditions of instrumented rods

	Fabrication	Filled gas (MPa)	Burn-up (MWd/kgUO <sub>2</sub> )	Pellet Diameter (cm)	PCMI at TC position	FP release (%)
AN3	ANF	He 1.47	41.3	0.905	hard	35.5
AN4	ANF	Xe 0.092	42.7	0.905	hard	40.9
AN10	ANF	He 0.61	44.6	0.905	hard	25.1
GE2	GE	He 0.66	43.2	1.04	soft	24.6
GE4	GE	He 0.66	21.5	1.04	soft	27.0
II3	GE	He 0.68	15.6	1.09	soft	17.4
II5	RISO	He 0.64	47.7	1.26	hard	10.6

transducer to measure fuel central temperature and rod internal pressure during transient tests.

Refabrication data and irradiation conditions are shown in Table3-1. Almost all of the refabricated rods were filled with Helium gas. An ANF rod and a RISO rod, which failed during a transient test, were filled with Xenon gas. The initial gas pressure of Xenon filled rod were relatively lower than Helium filled rods. The burnups of ANF rods are around 40MWd/kgUO<sub>2</sub>. On the other hand GE fuels had a burnup range from 15 to 45 MWd/kgUO<sub>2</sub>.

The diameter measurements indicated that ANF rods (AN3,AN4,AN10) experienced hard PC contact during transient tests as a result of large creep down of around 100 μm during base irradiations. RISO rods (II3,II5) experienced hard PC contact during base irradiations and transients. On the other hand, GE rods (II3,GE2,GE4,GE6) did not experience hard PC contact of thermocouple position at least, except II2 which failed during a transient test.

ANF and GE fuels showed little fission gas release during base irradiations. However RISO fuels experienced fission gas release during base irradiations as a result of high heat rating. At similar temperature, ANF fuels released more fission gas than GE and RISO fuels during transient tests. And only ANF fuels were showed gas release of approximately 6% at very low heat rating, that is below 170W/cm. The different behavior of GE and ANF rods could be due to own characteristics of the pellets. Time dependence of the measured rod internal pressures indicated that fission gas release to the free volume dose not follow the diffusion rule and the burst release occurred when the power goes down for a short time (dip). This behavior can be interpreted by two stage mechanism. The fission gas diffusively moves from UO<sub>2</sub> matrix to grain boundary. The grain boundary becomes large storage for the gas especially if pellets are constrained by large hydraulic pressure due to hard PC contact. The burst release occurs from this storage to the open space. This grain boundary corresponds to the microgap which has little or no connection to the open volume.

Analyzing the measured fuel central temperatures, they are higher than predicted if thermal conductivity of unirradiated UO<sub>2</sub> is used for the calculation. The analysis results indicate that the effective thermal conductivity of pellet decreases about 25% at 40 MWd/kgUO<sub>2</sub>. During the transient tests, at constant heat rating, fuel central temperature

variations were observed. Details of the observation are presented in the next section. As these variations have different time constants, the background mechanism may not be unique.

#### 4. Analysis of Transient Tests

Firstly we analyze the Xenon filled rod in which gas mixing effect can be ignored. AN4 was an only Xenon filled rod which was instrumented with a thermocouple and a pressure transducer. The measured temperature of AN4 decreased during constant heat rating, and this behavior was more remarkable at low heat rating. We make use of the measured internal pressure as inputs for fuel temperature calculation. This is because the gas pressure is an important parameter for the microgap model to determine the effective thermal conductivity. Fig.4-1 shows the comparison of measured and calculated temperature of AN4. The figure indicates that the calculated temperature agrees well with the measured temperature in broad range of heat rating (220-375W/cm at a thermocouple position). This result induces that the assumed thermal conductivity is reasonable for a Xenon filled rod in broad temperature range. The calculated temperature behavior agrees well with the observed temperature decrease. In the code, the temperature decrease of a Xenon filled rod comes from following sequence of the mechanisms.

1. Gas pressure of microgaps increases by fission gas release.
2. TJDs decrease by the gas pressure increase at microgaps.
3. The effective thermal conductivity of pellet increases as the TJDs decrease.

The calculated temperature decrease during the constant heat rating is remarkable at low internal gas pressure. This decrease qualitatively agrees with the observation. This result induces that the microgap model is necessary in order to describe the effective thermal conductivity decrease at high burnup.

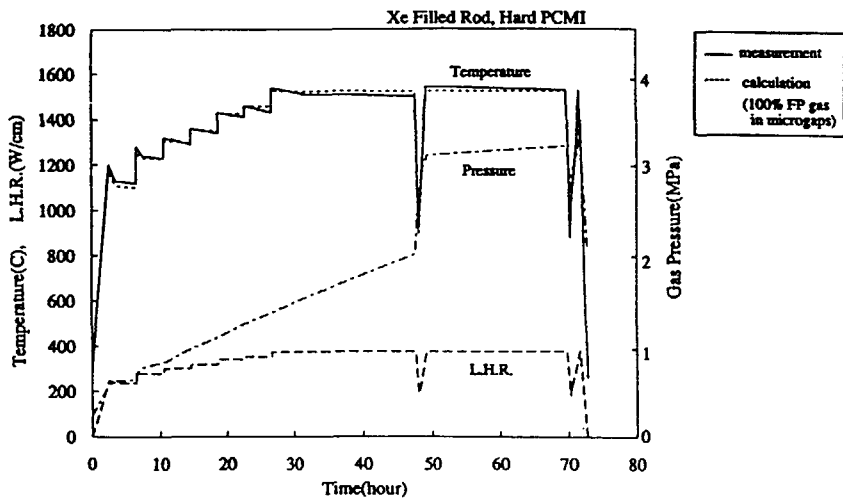


Fig.4-1 Power,Pressure and Temperature History of AN4.

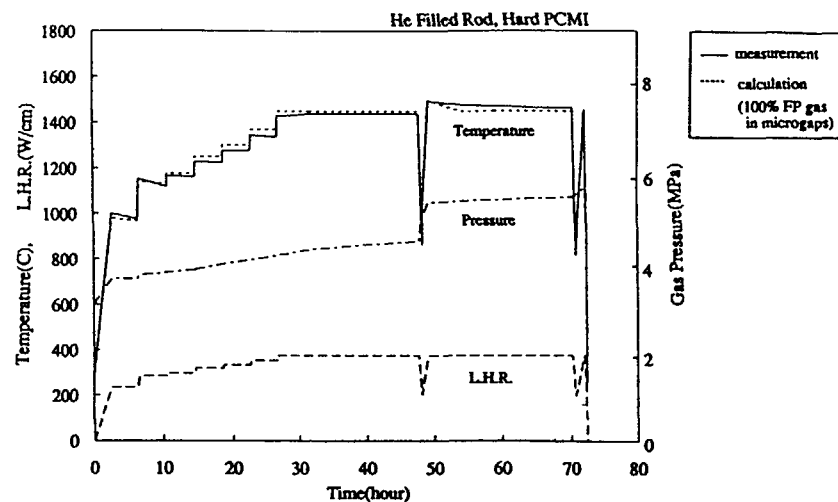


Fig.4-2 Power,Pressure and Temperature History of AN3

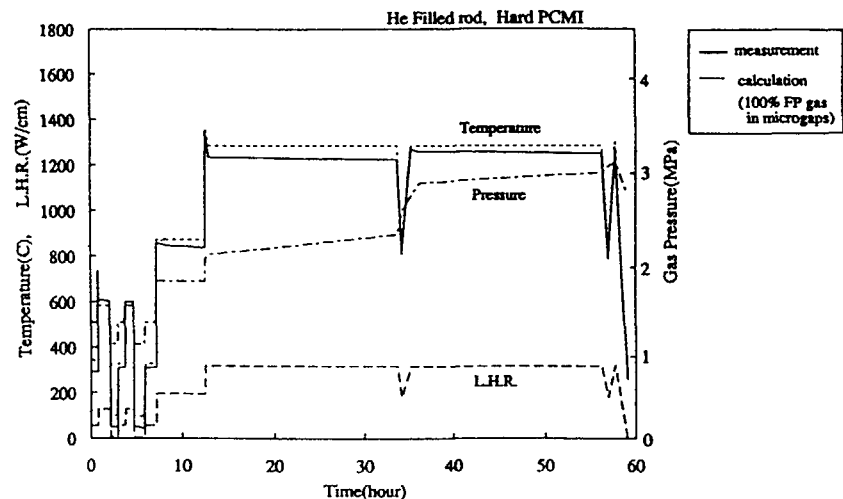


Fig.4-3 Power,Pressure and Temperature History of AN10

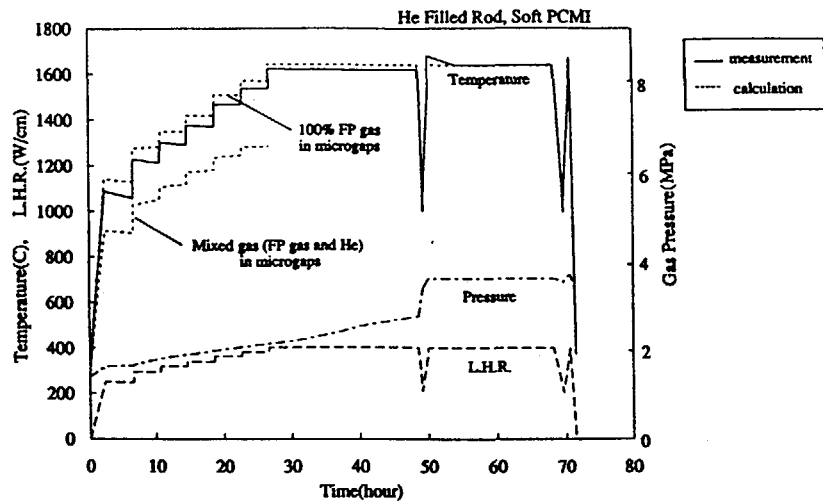


Fig.4-4 Power, Pressure and Temperature History of GE2

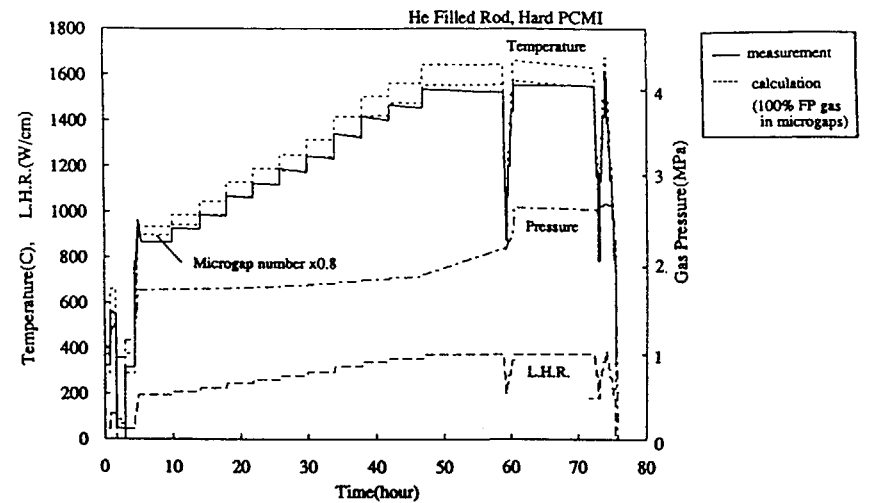


Fig.4-6 Power, Pressure and Temperature History of IIS

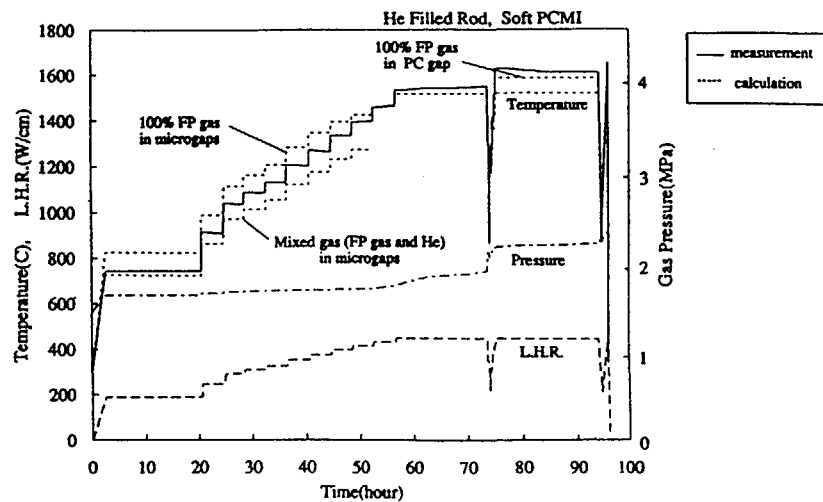


Fig.4-5 Power, Pressure and Temperature History of IIS

Secondly we analyze Helium filled rods with the same fabrication, that are AN3 and AN10. These rods have the same pellets as Xenon filled AN4. The measured temperatures of AN3 and AN10, having much better thermal conductance at PC gap, are lower than that of AN4 at all range of heat rating. For these Helium filled rods, we assumed that microgaps are completely filled with fission gas during whole tests because diffusional mixing in microgaps could be negligible if the gas release is continuously taking place. On the other hand, fission gas in pellet-cladding gap could be mixed with plenum gas which has large fraction of Helium filled at refabrication. Fig.4-2 and Fig.4-3 show the comparison of calculated and measured temperatures of AN3 and AN10. Calculated temperatures agree well with measured temperatures in general. The results indicate that the assumption of gas composition in microgaps is valid for AN3 and AN10. Both AN3 and AN10 indicate that measured temperatures after the first dip are higher than before the first dip. The calculation does show the same behavior for AN3 because the fission gas fraction increases in pellet-cladding gap by the burst release. The axial fission gas transport model in the code is effectively utilized in these calculations[8]. However, the calculation does not show the same behavior for AN10. This could be because the code does not correctly evaluate the hydraulic diameter of AN10 at the burst release.

Thirdly we analyze BWR designed GE and RISO fuels. Although GE fuels have a similar diameter as ANF fuels, RISO fuels have a larger diameter than ANF fuels. Fig.4-4 and Fig.4-5 show the comparisons of measured and calculated temperatures of GE fuels, that are GE2 and IIS3. The calculation was made assuming the microgaps are filled only with fission gas as previous calculations for ANF fuels. The calculated temperatures agree with the measured temperatures at high heat rating before the first dip. In this

condition the released fission gas could be enough to fill the microgaps. These results are indicating that the code with microgap model is able to predict fuel temperature at high heat rating for different fabricated fuels. However, for GE fuels at low power and at the fission gas burst release, calculated results have some discrepancy. Because the fuels have a burnup range between 15-45 MWd/kgUO<sub>2</sub>, it is confirmed that the modified code can predict observed burnup dependence.

Fig.4-6 shows the comparison of measured and calculated temperatures of II5 (RISO fuel). The calculated temperature is about 100C higher than the measured temperature. It is supposed that the temperature difference is caused by a large pellet diameter of II5. We calculated a fuel temperature of II5, assuming the microgap number per pellet radius of RISO fuel is approximately the same as that of ANF fuels. If we assume that the microgap number per unit length is 0.8 times that of other fabricated fuels, the calculated temperature could fit to the measured temperature.

The data from these transient tests of PWR, BWR and RISO fuels, especially the maximum temperature and dynamic temperature variation were evaluated by the thermal conductivity degradation model and the calculational results were in good agreement with the data. In these analyses we assumed that the thermal conductivity degradation was composed of static solid solution mechanism and dynamic microgap mechanism. The analyses revealed that contribution of the microgap in the total degradation is approximately 50% for these transient tests.

## 5. Discussion

The calculated temperatures of AN3, AN4, AN10 and II5 are in good agreement with the measured temperatures in the range from low power of 200W/cm to the maximum power of 400W/cm. The measured rod diameters for these rods indicate that they had pellet-cladding contact at the thermocouple position even at low power during transients. Therefore it is plausible that the diffusional mixing of the gas in microgaps and that in the plenum is very slow and the gas in microgaps are only fission gas during the transients. On the other hand, the calculated temperatures of GE2 and II3 are notably lower than the measured temperatures at low heat rating. The measured rod diameters indicated that these fuels did not have a hard pellet cladding contact at the thermocouple position. Therefore, as shown Fig.4-4 and Fig.4-5, we did additional temperature calculation for GE2 and II3, assuming that gas in the microgaps are filled by the gas of the pellet-cladding gap. Then the calculated temperatures become lower than the measured temperatures for whole range of heat rating. The results indicate that, in these rods, fission gas in microgaps was partly mixed with Helium which was filled at refabrications. This analysis indicates that the fast mixing between microgaps and free volume may take place when mechanical PC contact is not significant.

The rod II3 in Fig 4-5 shows that the temperature after the first dip is 100C higher than that before the first dip. It is considered that the PC gap of this rod was totally filled by fission gas as a result of the burst release due to the power dip. The pellet cladding gap could be nearly closed after the first dip and kept out the gas exchange. The calculated temperature, assuming the pellet cladding gap is filled only with fission gas, is in good agreement with the measured temperature increase as shown in the figure.

In these analyses, we assumed that the microgap have an uniform distribution in pellet radial cross-section. However the microgaps may develop significantly around the pellet rim region at high burnup. In such a case the radial temperature profile will become more flat near pellet center. And the code, with uniformly distributed microgap model verified against central hole temperature, may over-estimate the center temperature of solid pellet.

The thermal conductivity degradation model, which was utilized here, is composed of solid solution and microgap mechanisms. The effect of solid solution is based on Ishimoto's correlation which was confirmed by SIMFUEL experiments[5]. The concept

of the microgap covers geometrical thermal barrier such as cracks, separated grain boundaries, and planar fault in grains. However the microgap model in this analysis is the one which has connection of gas transport to the open volume. The parameters of the model are number density, width of the microgap and the gas composition and the pressure. The number density was fixed to fit the data from the gas flow rig at Halden Project. The width has not significant effect if the microgap is filled by Helium. This is due to long TJD of Helium as shown in Fig.2-3 and eq.(2). When the microgap is filled by Xenon the width has certain effect. We fixed the width to fit temperature data from Xenon filled rod of Halden Project. The calculational results using this width agrees well with the data from Xenon rod of the RISO Project. The microgaps with assumed width of 0.45 μm are difficult to be observed by usual metallography. However it is considered that these planar microgaps are only the mechanism for the degradation other than the degradation in fuel matrix. The dynamic behavior of the temperatures in the RISO Project is explained by the gas composition and pressure in the microgaps.

## 6 Conclusion

We have developed an effective thermal conductivity model for fuel performance analysis code which include the dynamic microgap and the static solid solution models. Evaluating the temperature data of RISO project phase 3, the code with the model can simulate observed dynamic behavior at high burnup power transient.

The calculated temperature of Xenon filled rod agrees well with the measured temperature. The model can predict the temperatures of Helium filled rods, if the gas component in microgaps is properly provided.

The evaluation of RISO Project data confirmed that significant fraction of the high burnup thermal conductivity degradation is due to the microgap mechanism.

## Nomenclature

$\lambda p'(i)$	Thermal conductivity of UO <sub>2</sub> matrix including with FP solid solution [W/m K]
$\lambda p(i)$	Thermal conductivity of unirradiated UO <sub>2</sub> matrix [W/m K]
$x$	Concentration of solid solution FP [at%]
$h_{mc}(i)$	Thermal conductance of microgaps [W/m <sup>2</sup> K]
$g_1(i), g_2(i)$	Temperature jump distance between solid and gas phases [m]
$\Delta G$	Microgap width [m]
$\lambda_{ef}(i)$	Effective thermal conductivity of a pellet [W/m K]
$R_{po}$	Radial length of a pellet [m]
$N_{ac}$	Microgap number [-]

## References

- [1]RISO Materials Department,RISO-FGP3-FINAL,Pt.1,The Third RISO Fission Gas Project, March(1991)
- [2]M Kinoshita,Development of High Burn-up Fuel Analysis Code EIMUS, CRIEPI Report ET88002, July 1988.
- [3]S Kitajima,T Matsumura,M Kinoshita,Reduction of Effective Thermal Conductivity in High Burn-up Fuels, IAEA Technical Committee Meeting on Fuel Performance at High Burnup for Water Reactors, Nykoping, Sweden, 5-8 June, 1990
- [4]P G Klemens, Physical Review,119,507(1960)
- [5]S Ishimoto,M Hirai and K Ito, The Twelfth Japan Symposium on Thermophysical Properties,A304(1991)

- [6] S K Loyalka, Nuclear Technology, A Model for Gap Conductance in Nuclear Fuel Rods, Vol. 53, 220, May (1982)
- [7] J A Turnbull, A D Applehans, OECD Halden Reactor Project, Fuel Behavior Inferred from Internal Gas Flow and Temperature Measurements made at the Beginning-of-Life of IFA-504, HPR273, (1981)
- [8] M Kinoshita, Evaluation of Axial Fission Gas Transport in Power Ramping Experiment, IAEA Specialists' Meeting on Water Reactor Fuel Performance Computer Modelling, Windermere, England, April (1984), also published in Res mechanica, 19(3)1986

## A SIMPLE FISSION GAS RELEASE/ GASEOUS SWELLING MODEL

T KOGAI  
Nippon Nuclear Fuel Development Company Ltd,  
Ibaraki, Japan

### Abstract

A model was developed to evaluate fission gas release and gaseous swelling of LWR fuels. The model described gas atom behavior via transport of gas atoms from in-grain to grain boundary sites, formation of intergranular gas bubbles, and release of gas atoms to the rod free volume. The release consisted of two competing mechanisms, i.e. bubble growth and pellet microcracking. The microcracking used tensile stress in a pellet fragment as its index.

Agreement, which validated the overall model formulation, was got between the calculated and measured fission gas releases. The abrupt gas release observed at power reduction was simulated by the microcracking model. Comparison of the gas atom retention distribution showed that the model correctly responded to the temperature rise and simulated the EPMA measured profile satisfactorily.

### 1 INTRODUCTION

Generated fission gas atoms in fuel grains move to grain boundaries and then to the rod free volume. Fission gas bubbles, precipitated on grain boundaries, induce pellet swelling and the released gas leads to a rise in rod internal pressure. Both may be hazardous to fuel rod performance especially at extended burnup. Therefore, it is crucial to understand and evaluate fission gas release and gaseous swelling to develop high burnup fuel.

We have developed a simple model to evaluate fission gas release rate and the amount of gaseous swelling by adopting the minimum number of parameters required. The model does not deal with intragranular gas bubbles, but treats their effects on gas release indirectly by considering an effective gas atom diffusion coefficient. It should be possible to express gaseous swelling with good accuracy this way since no data have shown that intragranular gas bubbles contribute more to gaseous swelling than intergranular ones. Although 7% intragranular gas bubble swelling has been reported for a pellet of ca. 40GWd/tU burnup[1], the size of these

bubbles was limited to the mid-radius position, and the volume averaged swelling was not more than 2%, i.e. a quarter of the gaseous swelling on grain boundaries.

The results of monitoring on-power rod internal pressure in the Risø Transient Fission Gas Project[2] showed a sluggish gas release at a high power hold, and an abrupt one at a down-ramp. Based on a proposal that these two types of gas release are brought about by different pathways, we have conceived one mechanism induced by the growth of intergranular gas bubbles and another by microcracking in a pellet to release gas from the grain boundary. Microcracking is ascribed to thermal stress in the pellet. The effect of power ramp rate is explicitly expressed by dealing with stress relaxation via creep, and that enables direct model verification by irradiation data.

The next section explains the structure of the model, section three gives its mathematical description, and section four summarizes results of the model verification work.

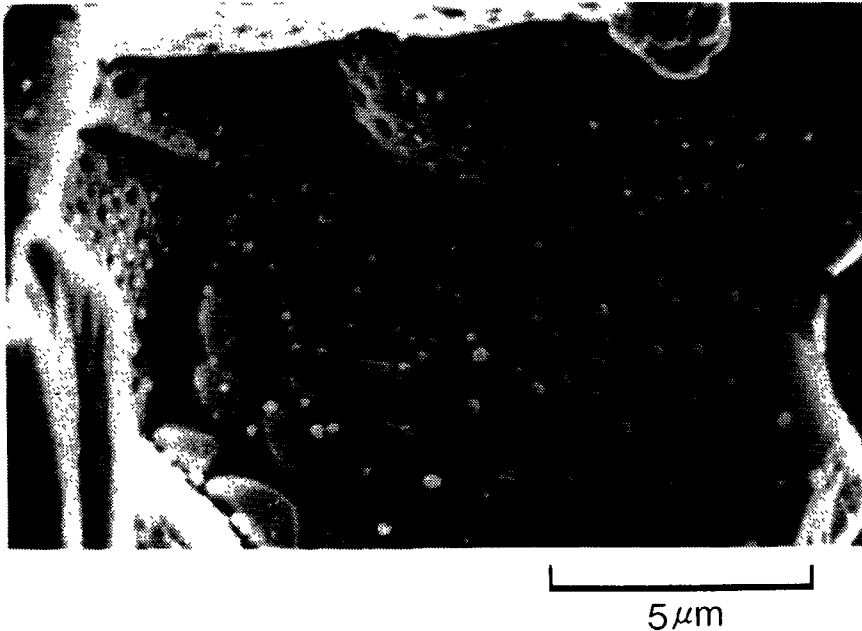


Photo 1. Fracture Surface of Pellet after Bump Test at 30GWd/tU<sup>(2)</sup>

## 2. MODEL STRUCTURE

Photo 1 shows a fractograph of a pellet which experienced a high power operation at high burnup[3]. Numerous gas bubbles exist on the grain boundaries, and interlinked gas bubbles are seen at the positions where grains intersect. These observations of pellet condition are consistent with the following proposed gas release process.

Fission gas atoms generated in fuel grains diffuse to grain boundaries, repeating trapping by and re-resolution from intragranular gas bubbles[4]. Also, gas atoms in the vicinity of the grain boundaries are swept out to the boundaries by grain growth. Although a part of the gas atoms reaching the grain boundaries return to the grain interior by irradiation[4], most of them contribute to the formation of intergranular gas bubbles which induce a volume increase of the pellet (gaseous swelling). Intergranular gas bubbles grow with the inflow of gas atoms, and interlink with adjacent bubbles to form gas release paths. Gas release via these paths reduces internal pressure of the bubbles. When gas release outweighs the supply of gas atoms to the bubbles, growth halts and is followed by shrinkage and disappearance of bubbles. The size of the intergranular gas bubbles is determined by a balance between the supply of gas atoms from the grain interior and their release to the rod free volume.

We have modeled this process as follows. The diffusion of fission gas atoms in grains is ascribed to a concentration distribution in the radial direction of a spherically simplified grain. Sweep-out rate of gas atoms is proportional to the product of grain growth rate and average gas atom concentration in the grain. Once fission gas atoms have reached the grain boundaries, they form intergranular gas bubbles, and the internal pressure of each bubble is balanced by the sum of the hydrostatic pressure imposed on the pellet and surface tension. Gas atoms in intergranular gas bubbles obey the ideal gas law, and the area density of the intergranular gas bubbles is constant regardless of grain size.

Gas release from intergranular gas bubbles to the rod free volume is assumed to take place via a hypothetical thin tube. This idea has evolved from the observation that a sluggish gas release at a high power hold[2] resembles a gas leak through a pinhole. The gas flow conductance of the tube is described as a function of the bubble radius and stress in the pellet. This formulation allows gas release to be depicted by increasing the conductance through shortening of the tube with bubble growth and thickening of the tube with pellet microcracking. Here, stress in the pellet is used as an index representing the extent of cracking. This stress is determined by modelling a constrained pellet fragment by a finite element method and providing the fragment with the temperature distribution existing in the pellet. This pellet fragment model is able to calculate creep relaxation of stress to express the effects of ramp rate and crack healing on fission gas release

### 3 MATHEMATICAL DESCRIPTION

#### 3.1 Basic equations for gas atom transport

In order to represent the generation process for fission gas atoms in the grain interior and their release to the rod free volume, the model considers three regions, i.e., grain, intergranular gas bubble, and free volume, and deals with the transport of gas atoms between them using the following equations

The rate of change of the average gas atom concentration in a grain,  $c_a$ , is given as follows

$$\dot{c}_a = c_g - 3c_a \frac{\dot{r}_g}{r_g} \quad (1)$$

Here,  $\dot{c}_g$  is rate of change of the average gas atom concentration obtained when grain size is fixed,  $3c_a r_g / r_g$  is equivalent concentration of the amount of gas atoms swept out due to grain size change, and  $r_g$  is grain radius. The first term on the RHS of equation 1 describes the concentration change of gas atoms due to in-grain diffusion, and the second one describes the change when all the gas atoms in the region through which a grain boundary passes are swept out to the grain boundary.

The balance of inflow and outflow of gas atoms on grain boundaries is described as follows

$$m_{gb} = K_g - c_a - m_{ex} \quad (2)$$

Here,  $m_{gb}$  is rate of change of the number of gas atoms in intergranular gas bubbles,  $K_g$  is gas atom generation rate, and  $m_{ex}$  is rate of change of the number of gas atoms in the rod free volume per unit volume of a grain. The difference between the first and second terms of the RHS is the number of outflowing in-grain gas atoms, and it equals the number of inflowing gas atoms to the intergranular gas bubbles. The gas atom generation rate in the grain,  $K_g$ , is given by the following equation

$$K_g = y f_D \quad (3)$$

Here,  $y$  is yield of fission gas atoms and  $f_D$  is fission density.

The gas release rate to rod free volume,  $m_{ex}$ , is given as follows

$$m_{ex} = \beta P_{gb}^2 \quad (4)$$

Here  $\beta$  is a parameter to express the ability of a gas to flow to the rod free volume and  $P_{gb}$  is internal pressure of an intergranular gas bubble. Using the square of pressure is derived from the kinetics of an ideal gas flowing through a thin tube. As described later,  $\beta$  is defined as a function of the

size of the intergranular gas bubble and the thermal stress generated in the pellet.

By using the gas release rate  $m_{ex}$  obtained by equation 4, we get a fractional gas release  $f_{gr}$  as follows

$$f_{gr} = \frac{\int_0^t m_{ex} dt}{\int_0^t K_g dt} \quad (5)$$

where  $t$  is time.

#### 3.2 Transport of gas atoms from in grain to grain boundary sites

The change of gas atom concentration in a grain is calculated by the following diffusion equation

$$\frac{\partial c_g}{\partial t} = \frac{1}{r_g^2} \frac{\partial}{\partial r_g} (D_g r_g^2 \frac{\partial c_g}{\partial r_g}) + K_g \quad (6)$$

It is assumed that a grain is a sphere and the gas atom distribution is spherically symmetric.

While quite a few methods have been reported to solve the above equation numerically, we employ one by Matthews and Wood[5], which has superior performance for the combined aspect of accuracy and computational time[6]. This method transforms equation 6 into the equivalent variational equation 7 according to Euler's theorem, and yields in grain gas atom concentration as a solution of an extremum problem

$$\delta \int_0^{r_g} \left[ \frac{D_g}{2} \left( \frac{dc_g}{dr} \right)^2 + (c_g - K_g) c_g \right] r^2 dr = 0 \quad (7)$$

In the solution scheme of the above equation, a spherical grain is divided into two concentric regions, and gas atom concentration  $c_g$  is represented by a quadratic function for each region. Application of three boundary conditions, i.e., the gas atom concentration gradient being zero at the grain center, continuity of gas atom concentration at the boundary of the two regions, and gas atom concentration being zero at the grain surface converts equation 7 into the following

$$\left( [C] + \frac{D_g}{4r_g^2} [K] \Delta t \right) \{c_i\} = [C] \{c_i\}^o + K_g \Delta t \{F\} \quad (8)$$

Here,  $\{c_i\}$  is an unknown fission gas atom concentration vector, and the elements are the concentrations at normalized radii of 0.4, 0.8 and 0.9,  $[C]$  and  $[K]$  are known coefficient matrices and  $\{F\}$  is a vector obtained when the partial derivative of the integrand in equation 7 is taken for each  $c_i$  ( $i = 1-3$ ).  $D_g$  is a diffusion coefficient and  $\Delta t$  is time increment. Discretization of the time domain is performed by the backward Euler approximation. The superscript  $^o$  implies the value at the start of a time step.

The average gas atom concentration  $\bar{c}_g$ , without considering the effect of grain growth, is described as follows by using gas atom concentration  $\{c_i\}$

$$\bar{c}_g = \frac{3}{r_g^3} \int_0^{r_g} c_g r^2 dr = [D]\{c_i\} \quad (9)$$

Here,  $[D]$  is a known coefficient matrix obtained by integrating the shape functions for the gas atom concentration distribution. The gas atom concentration  $\{c_i\}$  is obtained by solving equation 8

An average gas atom concentration  $c_a$ , which considers the effect of grain growth, is given as follows by substituting the rate of change of average gas atom concentration without the effect of grain growth  $\bar{c}_g$  into equation 1

$$(1 + 3\Delta t \frac{r_g}{r_g})c_a = [D](\{c_i\} - \{c_i\}^o) + c_a^o \quad (10)$$

The  $\bar{c}_g$  is obtained by applying the backward Euler approximation to  $\bar{c}_g$  given by equation 9

The number of gas atoms in the intergranular gas bubble at the end of a time step  $m_{gb}$  is given by the following equation after substituting equations 1 and 4 into equation 2

$$m_{gb} = K_g \Delta t - [D](\{c_i\} - \{c_i\}^o) + 3c_a \Delta t \frac{r_g}{r_g} - \beta P_{gb}^2 \Delta t + m_{gb}^o \quad (11)$$

Here,  $m_{gb}^o$  is the amount of gas atoms at the start of a time step

The number of gas atoms in the rod free volume at the end of a time step  $m_{ex}$  is given by the following equation

$$m_{ex} = \beta P_{gb}^2 \Delta t + m_{ex}^o \quad (12)$$

The above equation is obtained by discretizing equation 4 with regard to time

### 3.3 Intergranular gas bubble swelling

The balance of forces acting vertically onto the surface of an intergranular gas bubble is described as follows

$$P_{gb} = P_h + \frac{2\gamma}{r_{gb}} \quad (13)$$

where  $P_h$  is hydrostatic pressure imposed on the pellet and  $\gamma$  is surface tension

The equation to give the radius of an intergranular gas bubble  $r_{gb}$  is obtained as follows by substituting the equation of state for the ideal gas into equation 13

$$P_h r_{gb}^3 + 2\gamma r_{gb}^2 - \frac{3n_{gb} k T}{4\pi} = 0 \quad (14)$$

Here,  $k$  is the Boltzmann constant and  $T$  is absolute temperature. The  $n_{gb}$  is the number of gas atoms contained in a single intergranular gas bubble, and it is given by

$$n_{gb} = \frac{2m_{gb} r_g}{3N_{gb}} \quad (15)$$

where  $N_{gb}$  is area density of the intergranular gas bubbles, which is constant regardless of grain size

Gaseous swelling  $\Delta V/V$  is calculated by the following equation, using the intergranular gas bubble radius  $r_{gb}$

$$\Delta V/V = \frac{2\pi N_{gb} r_{gb}^3}{r_g} \quad (16)$$

### 3.4 Gas release from grain boundary to rod free volume

Gas release from the grain boundary to the rod free volume is modelled to take place through a thin columnar tube connecting both regions. The gas kinetics indicates that the gas release rate in a thin tube is proportional to the square of the pressure of an intergranular gas bubble (equation 4). The model defines this proportionality constant  $\beta$  as follows

$$\beta = \max(\beta_1, \beta_2) \quad (17)$$

Here,  $\beta_1$  is a function of the radius of the intergranular gas bubble and  $\beta_2$  is a function of the tensile stress in the pellet fragment. Equation 17 means that the larger value of the two should be adopted. These functions are explained in the following subsections

#### 3.4.1 Bubble interlinkage factor $\beta_1$

The bubble interlinkage factor  $\beta_1$  expresses the interlinkage of bubbles by their growth, and is given as

$$\beta_1 = a \{1 - \exp(-(\frac{r_{gb}}{r_{gb}^*})^n)\} \quad (18)$$

where  $a$ ,  $n$ , and  $r_{gb}^*$  are model parameters. This function increases monotonically with bubble radius. Its value approaches zero when the bubble size diminishes, which expresses the latent period to fission gas release. This model has evolved from EPMA observation of gas retention[1] in which gas release is seen in the region where the grain boundary coverage by bubbles is less than 20%.

### 3.4.2 Pellet cracking factor $\beta_2$

The pellet cracking factor  $\beta_2$  expresses the effects of microcrack generation in the pellet, and is given by the following equation

$$\beta_2 = b\sigma_t \quad (19)$$

where the  $b$  is a model parameter and  $\sigma_t$  is tensile stress acting on the pellet. This tensile stress is obtained by providing a temperature gradient for the saucer-shaped pellet fragment model shown in figure 1(a). This model is formulated as follows by a finite element method.

The  $r$ - and  $z$  direction nodal displacements  $u_s$  and  $v_s$ , respectively, of a finite element of the pellet fragment, as shown in figure 1(b), are defined by

$$\begin{aligned} u_s &= u_1 \frac{z(z-c)}{2c^2} - u_2 \frac{(z+c)(z-c)}{c^2} + u_3 \frac{(z+c)z}{2c^2}, \\ v_s &= v_1 \frac{z(z-c)}{2c^2} + v_3 \frac{(z+c)z}{2c^2} \end{aligned} \quad (20)$$

where  $u_1, u_2, u_3$ , and  $v_1, v_3$  are  $r$  and  $z$ -direction nodal displacements at the periphery of the pellet fragment, respectively,  $c$  is the half thickness of the fragment, and  $z$  is the  $z$ -direction coordinate. The above equation generates stress in the pellet fragment by constraint of bending through restricting the pellet fragment to maintain flat surfaces at both ends.

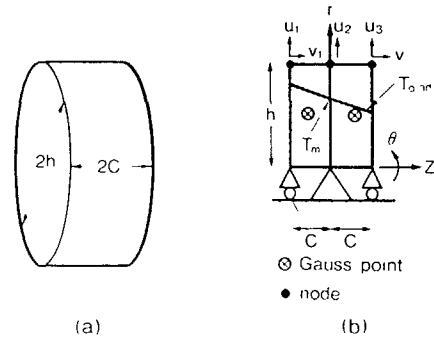


Figure 1 Saucer-shaped Finite Element Model of Pellet Fragment

The  $r$  and  $z$ -direction displacements inside the pellet fragment are defined as

$$\begin{aligned} u &= \frac{r}{h} u_s, \\ v &= v_s \end{aligned} \quad (21)$$

where  $r$  is the  $r$  direction coordinate and  $h$  is the radius of the pellet fragment. The  $r$  direction displacement is assumed to be proportional to the distance from the center, and the  $z$ -direction displacement is independent of the  $r$ -direction coordinate.

Total strain of the pellet fragment is given by (22),

$$\{\varepsilon\} = [B]\{u\}, \quad (22)$$

in which  $\{\varepsilon\}$  is a strain vector,  $\{u\}$ , a displacement vector, and  $[B]$ , a shape matrix of the finite element, all having the following definitions

$$\{\varepsilon\} = \begin{Bmatrix} \varepsilon_r \\ \varepsilon_\theta \\ \varepsilon_z \\ \gamma_{rz} \end{Bmatrix}$$

$$\{u\} = \begin{Bmatrix} u_1 \\ u_2 \\ u_3 \\ v_1 \\ v_3 \end{Bmatrix}$$

$$[B] = \frac{1}{hc^2} \begin{bmatrix} z(z-c)/2 & -(z+c)(z-c) & (z+c)(z-c)/2 & 0 & 0 \\ z(z-c)/2 & -(z+c)(z-c) & (z+c)(z-c)/2 & 0 & 0 \\ 0 & 0 & 0 & h(2z-c)/2 & h(2z+c)/2 \\ r(2z-c)/2 & 2z & r(2z+c)/2 & 0 & 0 \end{bmatrix}$$

The balance of forces acting on the pellet fragment is given as follows

$$\int [B]^T \{\sigma_{n+1}\} dV = \{F_{n+1}\} \quad (23)$$

Here  $\{\sigma_{n+1}\}$  and  $\{F_{n+1}\}$  are stress and load vectors at time  $t_{n+1}$  respectively. The load acting on the pellet fragment is given by the following equation as equivalent nodal forces calculated from the hydrostatic pressure

$$\{F_{n+1}\} = P_h \begin{Bmatrix} \Delta/6 \\ 2\Delta/3 \\ \Delta/6 \\ \Delta \\ \Delta \end{Bmatrix} \quad (24)$$

where  $\Delta'$  and  $\Delta$  are areas at the side surface and bottom surface per radian, respectively

Hook's law (constitutive equation) is given by (25),

$$\{\sigma_{n+1}\} = [D](\{\varepsilon_{n+1}\} - \{\varepsilon_{n+1}^c\} - \{\varepsilon_{n+1}^o\}) \quad (25)$$

in which  $\{\varepsilon_{n+1}\}$ ,  $\{\varepsilon_{n+1}^c\}$ , and  $\{\varepsilon_{n+1}^o\}$  are a strain vector, a creep strain vector, and a thermal strain vector at time  $t_{n+1}$ , respectively, and  $[D]$  is a stress-strain matrix

The temperature distribution in the pellet, which is the source for thermal strain generation in the pellet fragment, is given by the following equation

$$T = T_{\text{grad}} z + T_m \quad (26)$$

Here,  $T_{\text{grad}}$  is temperature gradient, and  $T_m$ , temperature at the center of the pellet fragment thickness direction (figure 1(b))

Since creep strain and stress are non-linear relationships, we apply the Newton-Raphson method to these variables, and describe the stress vector  $\{\sigma_{n+1}\}$  and the creep strain vector  $\{\varepsilon_{n+1}^c\}$  as follows

$$\begin{aligned} \{\sigma_{n+1}\} &= \{\sigma_{n+1}^i\} + \{\delta\sigma_{n+1}^{i+1}\}, \\ \{\varepsilon_{n+1}^c\} &= \{\varepsilon_{n+1}^{c,i}\} + \left\{\frac{\delta\varepsilon^c}{\delta\sigma}\right\}\{\delta\sigma_{n+1}^{i+1}\} \end{aligned} \quad (27)$$

where  $i$  is an iteration number. The above equation adds the correction term obtained by the  $i+1$  th iteration to the stress and strain obtained at the  $i$  th iteration

Substitution of equation 28 into equation 25, and then equation 25 into equation 23 yields the following stiffness equation

$$\begin{aligned} \int [B]^T [\tilde{D}] [B] \{u_{n+1}^{i+1}\} dv = \\ \{F_{n+1}\} - \int [B]^T \{\sigma_{n+1}^i\} dv + \\ \int [B]^T [\tilde{D}] (\{\varepsilon_{n+1}^{c,i}\} + \{\varepsilon_{n+1}^o\} + [D]^{-1} \{\sigma_{n+1}^i\}) dv \end{aligned} \quad (28)$$

Here

$$[D] = ([D]^{-1} + \left\{\frac{\delta}{\delta\sigma}\right\})^{-1}$$

The model constructs equation 29 to obtain the displacement vector  $\{u_{n+1}^{i+1}\}$  first, substitutes the vector into equation 22 to get the total strain vector  $\{\varepsilon_{n+1}\}$ , and then substitutes this strain vector into equation 25 to obtain the stress vector  $\{\sigma_{n+1}\}$ . This procedure is repeated until the change of  $\{\sigma_{n+1}\}$  becomes smaller than a predetermined value

After confirmation of the convergence of stress, the following hydrostatic stress is obtained by using the calculated stress components

$$\sigma_H = \frac{\sigma_r + \sigma_\theta + \sigma_z}{3} \quad (29)$$

Here,  $\sigma_r$ ,  $\sigma_\theta$ , and  $\sigma_z$  are  $r$ ,  $\theta$ , and  $z$  direction components of stress, respectively

The tensile stress  $\sigma_t$  to obtain pellet crack factor  $\beta_2$  (equation 19) is determined as follows with the above hydrostatic stress,

$$\sigma_t = \begin{cases} \max(\sigma_H^1, \sigma_H^2) - \sigma_H^o & \text{if } \max(\sigma_H^1, \sigma_H^2) \geq \sigma_H^o \\ 0 & \text{if } \max(\sigma_H^1, \sigma_H^2) < \sigma_H^o \end{cases} \quad (30)$$

and  $\sigma_H^1$  and  $\sigma_H^2$  are hydrostatic pressures calculated at the two Gauss points (figure 1(b)). The  $\sigma_H^o$  expresses a threshold value for microcracking, and is positive

## 4 VERIFICATION RESULTS

### 4.1 Selection of fuel rods

Fuel rods for the model verification were selected by considering irradiation conditions and data availability. The irradiation conditions were set so as to cover fission gas behavior at extended burnup and/or under flexible operation and included

- irradiation to high burnup in commercial reactors,
- high power irradiation in test reactors and
- ramp irradiation in test reactors

Ramp irradiation was selected to examine the effects of PCMI constraint. Verification items were as follows

- fission gas release (PIE and on power)
- fission gas retention distribution and
- porosity distribution

Eighteen fuel rods (six full length rods and twelve short length test rods) were selected having burnups ranging from 15 to 55GWd/tU (thermal power) from 150 to 580W/cm<sup>2</sup> and fission gas release from 1 to 30%

#### 4.2 Generation of input history data

History data on fission density, fuel temperature, and pellet hydrostatic pressure are required to run the model. Fission density was determined from rod power. Temperature and hydrostatic pressure were estimated as follows:

##### 4.2.1 Fuel temperature

Fuel temperature predicted by a fuel performance analysis code was corrected by considering the degradation of pellet thermal conductivity with burnup and the decrease of gap conductance by gas release. This correction was repeated until the calculated grain growth roughly matched the measured. The difference due to using different grain growth models amounted to ca. 100°C as fuel centerline temperature.

##### 4.2.2 Pellet hydrostatic pressure

Hydrostatic pressure in the pellet was calculated by assuming that the observed cladding deformations were due to creep [2]. The equivalent stress of cladding was then converted to the pellet hydrostatic pressure by assuming a bridging radius of 0.7.

#### 4.3 Comparison with experiments

We started model verification by comparing calculated gas release with the PIE values. Figure 2 shows the best-fit results obtained by tuning the model parameters in equations 18, 19, and 30. Bars attached to each solid circle were obtained by assuming  $\pm 10\%$  error for the input temperature. Fair agreement between the calculations and measurements was got, validating the overall model formulation. Exceptions were the rods exposed to intense PCMI, for which a systematic overestimation was observed. If fuel pellets are under PCMI restraint, gas atoms reside on grain boundaries accordingly [2]. This prolonged residence might allow re-solution of gas atoms from the grain boundary [4] to reduce the amount of gas release.

We then proceeded to look at how the model behaved regarding power changing conditions. Some results are shown in figure 3. This rod underwent a bump power rise after a low power base irradiation up to ca. 29 GWd/tU. As shown in figure 3(a), several intentional power reductions were included in the test, and the rod showed an abrupt gas release each time. We could simulate this gas release via the microcracking model by adjusting the reduction level of the hydrostatic pressure. Fuel pellets experience various patterns for changes in temperature and hydrostatic pressure which means that microstructure in pellets may also change in time. The result showed that the model could describe the effects on gas release for microstructural change.

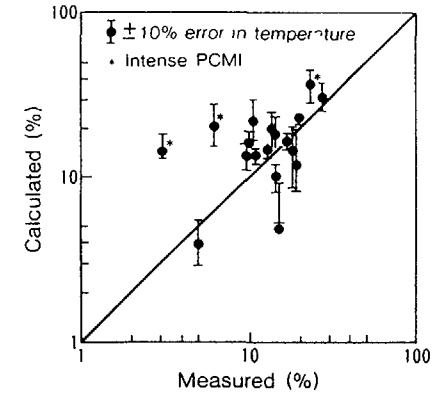


Figure 2 Comparison of Fission Gas Release

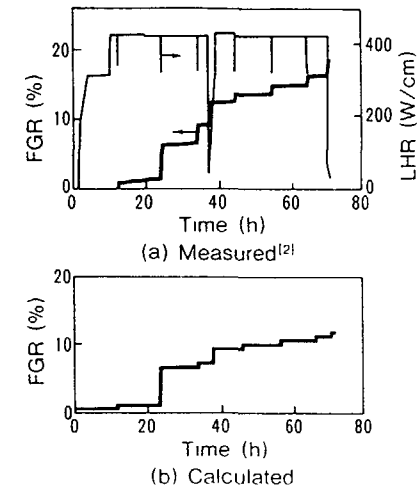


Figure 3 Comparison of Time Response in Bump Fission Gas Release

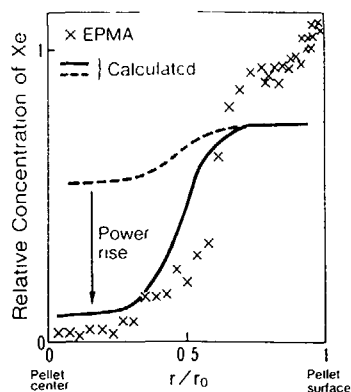


Figure 4 Comparison of Gas Atom Retention

Calculated in-grain gas atom retention is compared with the measured in figure 4. The distribution of retention, i.e., reversed gas release, is a good index by which to examine the performance of a gas release model [8]. The gas release response to temperature increase was reasonable, and the final retention profile simulated the EPMA profile well. The sharp rise at the pellet periphery, observed in the EPMA profile, may be caused by local burnup buildup due to epithermal fission, and the model would be able to simulate this by considering a radial power profile, which was assumed to be flat for the present analysis.

We found in comparison of the porosity distribution that the model made a significant overestimation near the pellet center in some cases. This observed discrepancy may suggest a need for modification of the swelling model, such as introduction of swelling saturation.

## 5 CONCLUSIONS

A fission gas release/gaseous swelling model was developed.

(1) The model described fission gas behavior via transport of gas atoms from in grain to grain boundary sites, formation of intergranular gas bubbles, and gas release from the grain boundary to the rod free volume. The gas release was modeled with two different mechanisms: growth of the gas bubbles and microcracking of the pellet. The microcracking was assumed to be induced by thermal strain, and tensile stress in a pellet fragment was used as its index.

(2) Predicted input temperature was corrected by considering the degradation of both pellet thermal conductivity and gap conductance, and this was checked against grain growth. Input hydrostatic pressure was produced by assuming that the observed deformations of cladding were due to creep.

(3) The calculated fission gas release exhibited fair agreement with the measured, to validate the overall model formulation.

(4) The abrupt gas release observed at a power reduction was simulated well by the microcracking model.

(5) Comparison of the gas atom retention distribution showed that the model correctly responded to the rise of temperature and simulated the measured retention distribution well.

(6) Overestimation of gaseous swelling at the pellet center suggested the possible need for a modification in its treatment.

## REFERENCES

- [1] MOGENSEN, M, et al, "Local fission gas release and swelling in water reactor fuel during slow power transients", *J Nucl Mater* **131** (1985) 162-171.
- [2] KOGAI, T, et al, "Cladding deformation due to gas bubble swelling of UO<sub>2</sub> pellet in bump test", *J Nucl Sci Tech* **27**(11) (1990) 1017-1027.
- [3] KNAPPIK, P, WALKER, C T, "SEM investigation of gas bubble nucleation and growth in the pin section STR018 20", Risø TFGP R24 (1986).
- [4] SPEIGHT, M V, "A calculation on the migration of fission gas in material exhibiting precipitation and re solution of gas atoms under irradiation", *Nucl Sci Eng* **37** (1969) 180-185.
- [5] MATTHEWS, J R, WOOD, M H, "An efficient method for calculating diffusive flow to a spherical boundary", *Nucl Eng Des* **56** (1980) 439-443.
- [6] ELTON, P T, LASSMANN, K, "Calculational methods for diffusional gas release", *Nucl Eng Des* **101** (1987) 259-265.
- [7] KNUDSEN, P, et al, "Fission gas release in high burnup fuel during power transients", ANS Topical Mtg on LWR Fuel Performance, April 17-20 (1988) Williamsburg, Virginia.
- [8] WALKER, C T, et al, "The DCOM blind problem on fission gas release: the predictions of the TRANSURANUS and FUTURE codes", *Nucl Eng Des* **117** (1989) 211-233.

# AN APPROACH TO MODELLING FUEL BEHAVIOUR USING DATA FROM SOME INTERNATIONAL HIGH BURNUP FUEL PROGRAMMES

L.-Å. NORDSTROM, C. OTT  
Paul Scherrer Institute,  
Villigen, Switzerland

## Abstract

The well-defined fuel rod tests from the international research programmes TRIBULATION and High Burnup Effects Programme have provided a large amount of fuel performance data for computer code verification and validation. This report describes the calculation approach used to simulate the fuel rod deformations and fission gas release focused on some rods irradiated to high burnups. The TRANSURANUS computer code was used for the calculations.

In a first phase the fuel densification input parameter as well as the fuel swelling and clad creep-down rates have been adjusted in order to reproduce the measured end-of-life clad dimensional changes. The agreement was very good. The experimental fission gas releases were then compared with the values predicted by three different models. Besides the standard model URGAS also the Halden model as well as one from FRAMATOME were implemented in TRANSURANUS. A significant discrepancy was found not only between the different models but also against the measured fission gas release values.

The achieved result was discussed and some conclusions from this first step on the way to develop a new model at PSI to be used with TRANSURANUS were drawn.

## 1. INTRODUCTION

As would be expected some difficulties can arise in modelling high burn up fuel behaviour using models usually validated using fuels of moderate burn up. In comparison to the end of life (EOL) values which can be measured, these usually appear as deviations of the calculated values from the fission gas release, which is a monitor of the lifetime thermal behaviour of the fuel, and also measured rod diametral and length changes.

Here, using the extensive data produced by the HIGH BURNUP EFFECTS PROGRAMME and the TRIBULATION programmes, the standard TRANSURANUS code is being adapted as a first step to try and accommodate the high burnup influences.

The TRANSURANUS fuel rod code is one of a number of comprehensive codes developed over recent years and made available to researchers and fuel designers. It was selected as a code for general use at PSI after an evaluation exercise involving other similar codes [1]. TRANSURANUS was developed initially at the Kernforschungszentrum Karlsruhe (as URANUS) and later at the European Institute for Transuranium Elements - EITE (as TRANSURANUS) by Dr Klaus Lassmann and co-workers [2]. It was chosen by PSI for being a flexible, modular code with many built-in model choices according to the problem to be solved, it could handle both Light Water Reactor as well as Fast Reactor Fuels in steady state or unsteady state (transient) conditions, with different fuel and cladding materials of interest to PSI, it was well supported by its original developer and in use by a number of renowned fuel organisations, safety authorities and utilities. Not the least TRANSURANUS was a code built up and verified on results of international fuel experiments and was not a fuel vendor code having models of relevance only to one or other vendor's fuel designs and materials.

## 2. IRRADIATION

It goes without saying that a code such as TRANSURANUS is only as good as the input data which is fed into it. Only when complete and accurate data on the fuel rod design, materials and materials property data is available, the correctness of the models can be judged. The user must also be aware of the validity of the subroutines (models) in the code and the range of fuel rod results against which the models were validated.

Further the validity of a code is also strongly dependent on an accurate knowledge of the conditions in the reactor (the time dependent power variations over life, coolant flows and temperatures, etc.). Finally the accuracies of the EOL measurements with which the code predictions are compared should be known. This too is often difficult given the problems of making measurements and analyses on irradiated fuel rods either in the reactor pool or in shielded hot cell facilities (Post Irradiation Examination-PIE). A useful source of data on fuel behaviour is the number of special experiments carried out in power or materials testing reactors on well characterised fuel rods.

### 2.1 The Fuel Research Programme HBEP-TVO

The HBEP (High Burnup Effects Programme) was an international research programme [3], running from 1978 to 1990 and managed by Battelle, Pacific Northwest Laboratories (BNWL). The objective (of TASK 3) was to provide well-characterized data on the effects of fuel temperature, burnup, power history and different fuel characteristics with an emphasis on Fission Gas Release (FGR). In this report we examine some of the nine commercial BWR fuel rods manufactured by ABB-ATOM and irradiated in the Finnish TVO-1 reactor. All nine of the full-length (3.7 m) rods were typical ABB-ATOM commercial BWR rods (solid pellet, 0.4 MPa fill gas pressure).

The TVO-1 rods were irradiated for a total of five or six reactor cycles. Peak-in-life linear heat generation rate (LHGR) values occurred during the first and third operating cycles, with maximum rod-average LHGR values being approximately 18 to 27 kW/m. Rod average burnups ranged from 44 to 50 MWd/kgUO<sub>2</sub>. The particular interest in modelling these rods is the wide spread of FGR at closely similar burnup under ostensibly similar irradiation conditions, ranging from 0.3 to 16.7%.

The characterization, irradiation history and PIE are well documented and constitute a suitable basis for fuel behaviour modelling.

The rods considered in this report have the test matrix numbers A1/8 4, A3/6 4, H5/27 4 and F1/3 6.

## 2.2 The Fuel Research Programme TRIBULATION

The international TRIBULATION research programme (Tests Relative to High Burnup Limitations Arising from Transient Incidents Occurring Normally in LWRs) ran from 1980 to 1989 and was organised by Belgonucléaire [4]

As its title implies, mid-life transients (ANSI class II criteria) were applied to selected rods to determine any effect on reaching a high burnup of the order of 70 GWd/tUO<sub>2</sub>. As well as demonstrating no deleterious effect of mid life class II transients, the programme provided a large amount of fuel and performance data for code verification. In all, 48 rods from four different vendors were irradiated in the BR-3 PWR (and BR-2 MTR for the transient tests)

The non-destructive examinations made at Mol included visual examination, eddy current testing, neutron radiography, gross gamma scanning, profilometry and length measurement. The destructive exams made at various laboratories included rod puncture and fission gas analyses, fuel ceramography, retained fission gas and burnup analysis

The rods considered in this report have the test matrix numbers, 15, 27, 33 and 39

## 3 FUEL BEHAVIOUR MODELLING USING TRANSURANUS

Since the TRANSURANUS code has a great flexibility with many options for choosing different sub-models, the first step was usually to adjust some of the model parameters to obtain the basic values of burnup, rod (and fuel) elongations and profilometry close to the EOL measured results. This was done in order to form a sound basis for following the modelling of gap closure, fuel temperatures and hence FGR

### 3.1 Burnup

The first step was to use the given power history and compare the calculated burnup with the published EOL values. For both the programmes we had access to detailed irradiation data on computer-diskettes, from ABB-ATOM and Belgonucléaire respectively. As recommended by BNW [5], we had to increase this power history for the TVO-rods with + 15 % for the five cycle-rods and + 11 % for the six-cycle-rods. In this way the values obtained with TRANSURANUS covered the best-estimate rod-average burnups as derived by BNW very well. For TRIBULATION rods the agreement on burnup was very good.

### 3.2 Cladding Elongation

The measurements of the EOL cladding elongation could be carried out very accurately so the next step was to reach these experimental values.

The cladding growth has been modelled using the MATPRO [6] swelling correlation for Zircaloy, built in as a choice in TRANSURANUS. The variable in this correlation is the neutron fluence and the cladding length is calculated according to the following expression

$$\Delta L/L = 1.407 \times 10^{-16} [e^{240} 8/T] (\phi t)^{0.5} (1.3 fz) (1+2 cw)$$

where  $\Delta L/L$  is the fractional cladding change in length

$T$  is the cladding temperature (K)

$\phi t$  is the fluence of the fast neutrons,  $E > 1$  MeV ( $n/m^2$ )

$fz$  is the texture factor for the tubing axis (0.05)

$cw$  is the cold work factor

The model only gives the axial strain due to irradiation induced swelling, the radial and tangential components are set to zero. In addition, the multiplication factor 2 of the cold work factor is questionable and here the entire expression  $(1 + 2 cw)$  has been adjusted.

### 3.3 Fuel Swelling and Clad Outer Diameter Changes

The first parameter concerned is the minimum porosity of the fuel at the end of the fuel densification, a phenomena which occurs early in life and leads to shrinkage of the fuel column. The empirical model selected calculates the sinter porosity as a function of the burnup according to the following relationship,

$$P_{bu} = P_{oo} + (P_o - P_{oo}) e^{-\frac{5 bu}{bu_o}}$$

where  $P_{bu}$  is the sinter porosity

$P_{oo}$  is the minimum porosity (input data)

$P_o$  is the fabrication porosity (input data)

$bu_o$  is the burnup constant (input data)

$bu$  is the average burnup in the slice

After this initial fuel restructuring the positive volume increase in the fuel caused by solid and gaseous fission product has been modelled by considering the linear correlation proposed by Lassmann and Moreno [7]

$$\Delta (\Delta V/V) = S \Delta bu$$

where  $S$  is the swelling rate (1/at %)

$\Delta bu$  is the burnup increment during time step  $\Delta t$

In this model the gaseous swelling is not considered separately but is included in  $S$ . The standard value (0.01) of  $S$  was found to be too high and was adapted to match the observed swelling rates.

In order to get the correct cladding profilometry for the TRIBULATION rods at the end of the irradiation phase two coefficients ( $k_1$  and  $k_2$ ) were introduced in the expression of the local creep rate and adjusted. The general correlation for the local creep rate can then be written as

$$\dot{\epsilon} = k_1 \dot{\epsilon}_t + k_2 \dot{\epsilon}_\phi$$

where  $\dot{\epsilon}_t$  is the thermal creep rate

$\dot{\epsilon}_\phi$  is the irradiation creep rate

The coefficient  $k_1$  multiplies the local thermal creep rate and has been determined to obtain the hoop strains as observed in the hottest part of the fuel column whereas the  $k_2$  factor has been adjusted to describe the experimental clad strains observed in the upper and lower parts of the fuel rod. For the HBEP TVO rods the introduction of  $k_1$  and  $k_2$  was not necessary.

It is not possible to report here on all the numerical values considered for the different materials but it must be pointed out that the temperatures, deformations and fission gas behaviour cannot be calculated in isolation without making certain assumptions.

## 4 FISSION GAS RELEASE

The release of fission gases from the fuel has important consequences for the thermal behaviour of the fuel rods since fuel temperatures rises in response to contamination of the fuel cladding gap by xenon and krypton. One consequence of this thermal feedback effect is an increase in gas release and an increasing internal gas pressure. In the integral fuel rod performance codes the fission gas released into the fuel/clad gap is a vital parameter. A clear understanding of the fission gas release processes is of first importance for the modellers because of its direct influence on many aspects of the fuel rod behaviour.

### 4.1 Fission Gas Release Mechanisms

The release into the free volume of the fuel rod of the gas atoms produced is currently considered as a two stage process. In a first stage, the gas atoms produced by fission inside the grains migrate by some mechanisms to the grain boundaries. In a second step, the atoms migrate from these boundaries to the free surface of the fuel from which they are released to the free volumes of the fuel pin.

The diffusion of the gaseous products towards the grain boundaries has shown to be strongly dependent on the local temperature with a temperature threshold. For fuel pin sections operating below the temperature threshold, the athermal release mechanisms (recoil and knockout) are predominant. Because the athermal fission gas release processes affect only the outer layer of the fuel surface, the fraction of gas released is dependent on the open porosity of the fuel and remains quite small at least at low burnup. The athermal fission gas release increases continuously with average fuel rod burnup, an acceleration of this mechanism is observed above 45 GWd/tUO<sub>2</sub> due to the contribution of the so-called rim area which is characterised by a high density of fission products and porosities due to high local burnup (up to 1.3 % at 55 GWd/tUO<sub>2</sub> [10]).

During the second stage of the release, that is the transport from the grain boundaries to the rod free volume, the atoms leaving the grains tend to accumulate at the grain boundaries where they form bubbles. It is widely acknowledged that the bubbles formed are then expected to grow until they become large enough for interlinking and coalescence to occur over large distances thereby providing a path for the release to the plenum. Experimental observations have shown that this "incubation" period is strongly temperature-dependent and they are in disagreement with treatments based on diffusion theory which predict release from zero burnup.

### 4.2 Fission Gas Release Models

In parallel with the standard TRANSURANUS fission gas release model, the well-known HALDEN threshold approach as well as a model from FRAMATOME on gas release has also been implemented in the integral fuel rod behaviour code.

In the standard URGAS model [8], the stable fission gases xenon and krypton diffuse through the grains and collect on the grain boundaries, where they accumulate in bubbles until the maximum capacity of the grain boundary is reached. The attenuation of gas mobility due to intragranular trapping and resolution from fission gas bubbles is described by the so-called effective diffusion coefficient.

Some of the input values for the URGAS model are still in the test phase. We used as the saturation limit for grain boundary gas a numerical value of 0.00001 (μmol/mm<sup>2</sup>).

On the contrary to the URGAS model, which is based on a diffusion process, the empirical Halden fission gas release model, derived from data obtained in the low and intermediate burnup range, predicts that some burnup has to be accumulated in the fuel before fission gas release starts. This incubation period is calculated according to [9]

$$buh = 5 * \exp(9800/T)$$

where buh is the burnup at which release starts (MWd/tUO<sub>2</sub>)  
T is the fuel centreline temperature (C)

The fraction of gas released (fgr) is calculated by

$$\begin{aligned} fgr &= 0 && \text{if } bu \leq buh \\ fgr &= (T/1800) ** 5 && \text{if } bu > buh \text{ and for } T \leq 1800 \text{ C} \\ fgr &= 1 && \text{if } bu > buh \text{ and for } T > 1800 \text{ C} \end{aligned}$$

FRAMATOME has developed a model [10], which includes three terms to describe the FGR mechanisms, athermal release, thermal release as well as gas release achieved by transients.

The athermal term is burnup dependent and considers the initial fuel open porosity as follows

$$fgr = A \exp(B \cdot bu^2) + C \cdot \ln(9 + \text{oporos})$$

where fgr is the local fission gas release fraction  
bu is the local fuel burnup  
oporos is the open porosity (input data)  
A, B, C fitting coefficients

The thermal term is represented by a network of hyperbolic tangent functions as follows

$$fgr = (\text{TANH}(bu * G - F) + (\text{TANH}(F)) / (1 + \text{TANH}(F)))$$

where bu is local burnup  
G = (A \* TK - B) / C  
F = D \* TK + E  
TK = local fuel temperature  
fgr = local fraction released  
A, B, C, D, E fitting coefficients

The transient part of the model was not implemented as none of the rods presented in this report were ramped.

One after another, all three models have been tested to model the fission gas release of the selected fuel rods.

## 5 RESULTS

For the eight considered rods (four from each TRIBULATION and HBEP TVO), the values predicted with TRANSURANUS were compared with the experimental results. The comparison considers the EOL cladding length and outer diameter average changes as well as the fuel FGR.

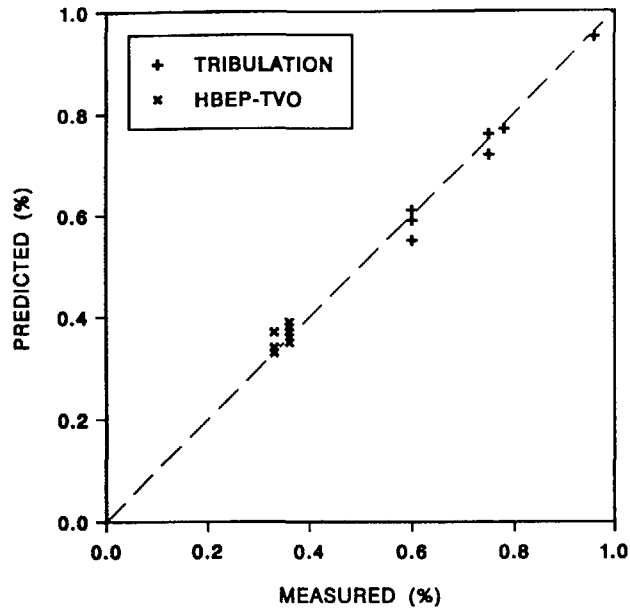


FIG. 1. Cladding elongation at EOL. Predicted vs measured values.

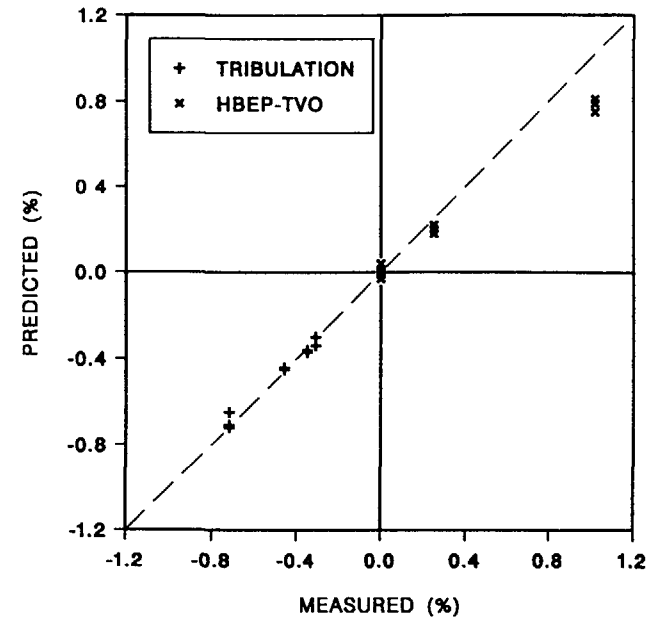


FIG. 2. Cladding average hoop strains at EOL. Predicted vs meas. values.

### 5.1 Cladding elongation at EOL

Figure 1 shows the calculated against the measured values. For each rod three values are given, one for each FGR model considered. These three values are very close to each other or even identical, as would be expected. For all rods and each FGR model the agreement is very good.

### 5.2 Cladding average hoop strains at EOL

The fuel rod claddings were Zircaloy-4 with a thickness of about 0.6 mm for the TRIBULATION and Zircaloy-2 with 0.8 mm for the HBEP-TVO rods.

Figure 2 shows the predicted against the measured values from each FGR-model for each fuel rod. In contrary to the HBEP fuel rods which show cladding creep out at EOL, the TRIBULATION rods show a strong creep down. Except for one rod the agreement is very good. The exception is the rod HBEP-TVO A1/8-4, with a large difference between the published value, 1.02%, and the value which can be evaluated from the profilometry provided by BNW, about 0.75%, which we choose as the reference value.

### 5.3 Integral fission gas release

FGR experimental results have been made by puncturing the plenum. Figure 3 shows a comparison between measured and predicted FGR using all three considered models. The derivation of FGR using the empirical Halden equation based on a threshold approach, depends only on the fuel temperature and burnup. Figure 4 shows for three rods the mid rod fuel centreline temperature compared with the Halden threshold approach for 1% FGR. The predicted values are consistent with these curves as the FGR is 0.0%, 0.8% and 2.1% for Rod No. 39, 15 and 27 respectively (compare Figure 3). The average fuel rod burnup ranges between 51 and 56 MWd/tUO<sub>2</sub> for the TRIBULATION and between 45 and 49 MWd/tUO<sub>2</sub> for the HBEP fuel rods.

Both Halden and URGAS models underpredict systematically the FGR with values on a low level while FRAMATOME model mostly overpredicts the fission gas release particularly the athermal component.

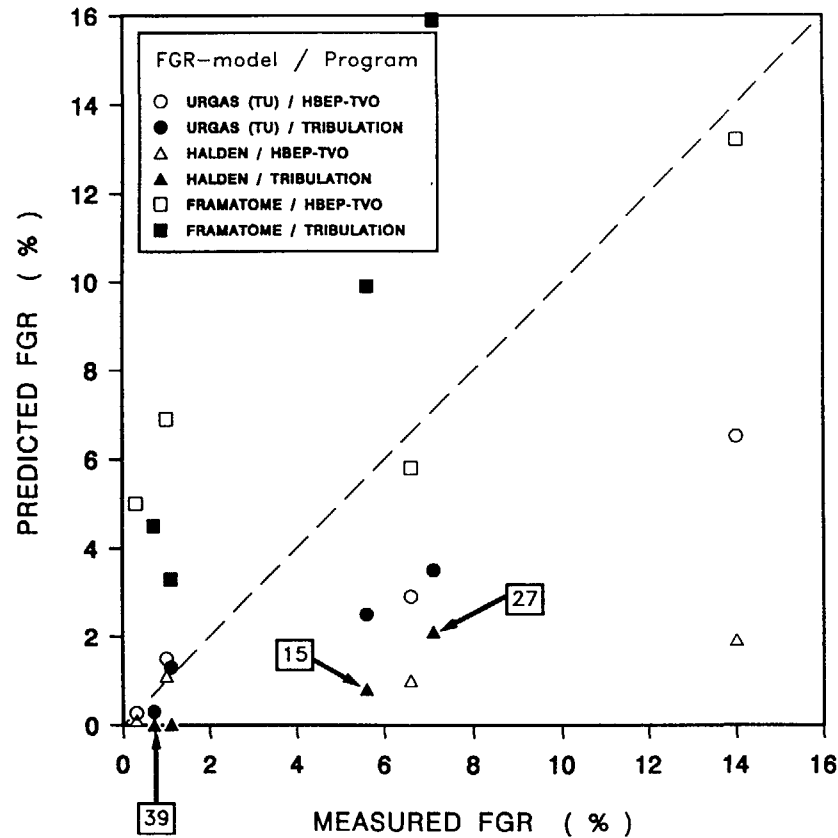


FIG. 3. Integral Fission Gas Release for some TRIBULATION and HBEP-TVO Rods, calculated with different models. 3 TRIBULATION Rods (No 15, 27 and 39 resp.) calculated with the Halden FGR model are specified for the comparison with FIG. 4.

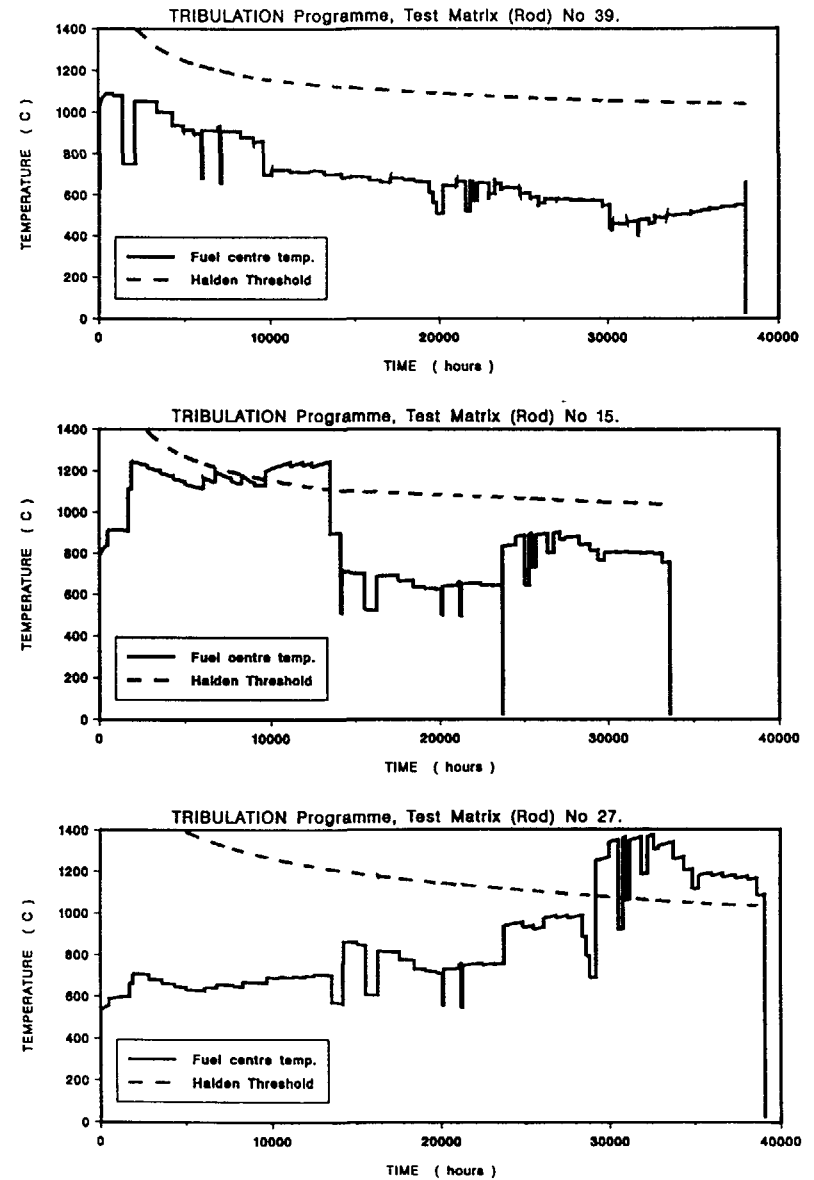


FIG. 4. Fuel Centreline Temperature for 3 TRIBULATION Rods compared with the Halden FGR Threshold [9] over Irradiation Time.

## 6. DISCUSSION

With the objective to develop detailed submodels in order to be able to describe the fuel rod behaviour, fundamental aspects such as fuel temperatures and fuel/clad dimensions must be calculated correctly before, for example, the detailed modelling of FGR mechanisms can be addressed. By this comparison all three FGR models underlay the same frame-work (TRANSURANUS code), i.e. the same temperature calculation mechanism. A comparison of the rod temperatures over the irradiation time calculated in connection with the three different FGR models show no significant difference. Under the assumption of a correct calculated fuel rod temperature, the effective diffusion coefficient as used in the URGAS model seems not to be adequate for the modelling of fuel FGR at high burnup or at least the work on this model has to continue. The next step should then be a parametric study of the sensitivity of this coefficient on the FGR. The Halden model was originally given for burnups up to about 40 MWd/tUO<sub>2</sub>. The result presented here shows that a simple extrapolation of the FGR threshold to higher burnups becomes questionable as already mentioned in [11].

During the work to try to develop an adequate FGR model, the necessity to consider several model components for the calculation of the fraction FGR becomes evident, in order to be able to simulate the different mechanisms involved. In this context the FRAMATOME model has advantages not only with the possibility to consider the fuel open porosity as input, but also to adapt the athermal and thermal FGR terms independent of each other. The implementation of this model in TRANSURANUS as a first step didn't bring satisfactory results, but we think that an refitting of the model parameters would help further.

It is also obvious that calculations have to be done against a far larger experimental data base than used for this report. On the other hand, due to the various uncertainties of some code input data, only, after using the statistical version of the code, can the correctness of the fission gas release model be judged.

A very good agreement with the experimental rod deformations was achieved through changing parameters in the different models (Fig. 1 and 2). The next step will be to examine these changes to determine what could be the physical basis supporting this, especially in relation to high burnup properties. Features needing further examination are the possible fuel batch-to-batch differences in O/M-ratio, affecting the diffusion rates in the fuel, and the degradation of the thermal conductivity for (especially) high burnups.

## 7. CONCLUSION

The evaluation of different FGR models shown in this report is the first step to develop a new model at PSI to be used inside TRANSURANUS.

The international research programmes maintain a very large data base on EOL results but spare information on fuel temperatures during irradiation. With Switzerland as a new member of the Halden Reactor Project, we hope to find adequate experimental result on this in the Halden Fuel Data Base.

TRANSURANUS is a very flexible and modern structured code, which allows for changing of models, submodels and correlations as well as being very suitable to predict all of the different geometrical experimental results used.

The statistical version of TRANSURANUS, lately available at PSI, will be an essential help to deal with uncertainties of the basic input data as for example the LHGR for the HBEP-TVO as described in 3.1.

## REFERENCES

- [1] H.K. Kohl, L-Å. Nordström, C. Ott, R.W. Stratton, "A Modern Fuel Behaviour Code for PSI", TM-43-90-40, (1991).
- [2] K. Lassmann, H. Blank, "Modelling of Fuel Rod Behaviour and Recent Advances of the TRANSURANUS code" Nucl. Eng. Design, 106, 291-313, (1988).
- [3] J.O. BARNER, "High Burnup Effects Program-Final Report", HBEP-61 Final, Battelle (*Pacific Northwest Laboratories*), April 1990
- [4] M. Lippens, D. Boulanger, "TRIBULATION, Final Report." Belgonucléaire, TR 89/79, (1989).
- [5] M. Cunningham, BNW, private communication/Letter for PSI, July 1989
- [6] MATPRO version 11, "A Handbook of Material Properties for Use in the Analysis of LWR Fuel Rod Behaviour" NUREG/CR TREE-1280), (1979).
- [7] K. Lassmann, A. Moreno, "The Light Water Reactor Version of the URANUS code", Atomkernenergie, Bd. 30, Lfg3, 207-215, (1977)
- [8] P.T. Elton, K. Lassmann, "Calculational Methods for Diffusional Gas Release", Nucl. Eng. and Design 101 (1987) 259-265, (1987).
- [9] C. Vitanza, et al, "Fission gas release from in-pile pressure measurements", Enlarged HPG Meeting on Water Reactor Fuel Performance and Application of Process Computers in Reactor Operation, Loen, Norway, (1978).
- [10] D. Baron, et al, "Framatome Experience on Fission Gas Release under Base and Transient Operating Conditions", Proceedings of the Intl. Topical Meeting on LWR fuel performance, ANS, Williamsburg, April 1988
- [11] R. Manzel, R. Eberle, "Fission Gas Release at High Burnup and the Influence of the Pellet Rim", Proceedings of the Intl. Topical Meeting on LWR Fuel Performance, Avignon, April 1991

# FUEL PERFORMANCE MODELING OF HIGH BURNUP FUEL

S.H. SHANN, L.F. VAN SWAM  
Siemens Nuclear Power Corporation,  
Richland, Washington,  
United States of America

## Abstract

A Siemens Nuclear Power Corporation (SNP) developed fuel performance code with its diffusion controlled fission gas release model was modified for high burnup application. The modeling changes included a modification of fuel thermal conductivity, addition of the pellet rim effect, and modifications of the fission gas release model.

With the data obtained in the High Burnup Effects Program, various aspects of the code were validated:

- Prediction of retained gas inside fuel grain versus EPMA (electron probe microanalysis) measured Xe data
- Prediction of total retained gas (inside grain and in grain boundary) versus XRF (X-ray fluorescence) measured Xe data
- Prediction of Pu production versus EPMA measured Pu/U data
- Prediction of radial burnup distribution versus EPMA measured Nd data

The validation results indicate that the modified code accurately accounts for the fuel pellet rim effect and with a high degree of accuracy predicts the pellet burnup profile, retained fission gas, and fission gas released to the rod free volume up to high burnup.

## 1. INTRODUCTION

Fuel performance computer codes and fission gas release models within these codes have typically been applied to burnup levels that are being reached by current reload fuel assemblies and rods, i.e., to fuel rods approaching burnups of 55 to 60 MWd/kgU. Well benchmarked fuel performance computer codes can provide accurate predictions of fission gas release up to these burnups.

Since significant physical and chemical changes take place in higher burnup UO<sub>2</sub> fuel, adjustment of the fission gas release models and associated models that affect the fission gas release rate is required to obtain accurate fission gas release predictions for higher burnup fuel rods. The High Burnup Effects Program (HBEP)<sup>(1)</sup> has provided important postirradiation performance data to permit adjustments of the fuel performance models for application to higher burnup fuel.

This paper describes a modified fission gas release model for high burnup fuel and modifications to other sub-models that affect the fission gas release rate. The modified models have been benchmarked against the available HBEP data.

## 2. MODEL DESCRIPTION

To extend the applicability of the fuel performance codes to higher burnup levels and to obtain accurate fission gas release predictions up to high burnup, modifications were made to the fission gas release model and the UO<sub>2</sub> thermal conductivity sub-model. A new model was introduced to properly represent the effects due to the development of a higher than pellet average burnup pellet rim which becomes more pronounced as burnup progresses.

### 2.1 FISSION GAS RELEASE MODEL

The RODEX series of fuel performance computer codes have been developed by Siemens Nuclear Power Corporation (SNP) for design and licensing calculations. The RODEX codes incorporate a diffusion controlled fission gas release model. Modifications have been made to the fission gas release model to extend the prediction capability of the RODEX codes to higher burnup. These modifications include (a) separation of the grain boundary into grain face and grain edge regions with separate and different properties and effective fission gas diffusion rates and (b) coupling of gaseous swelling effects and gas release.

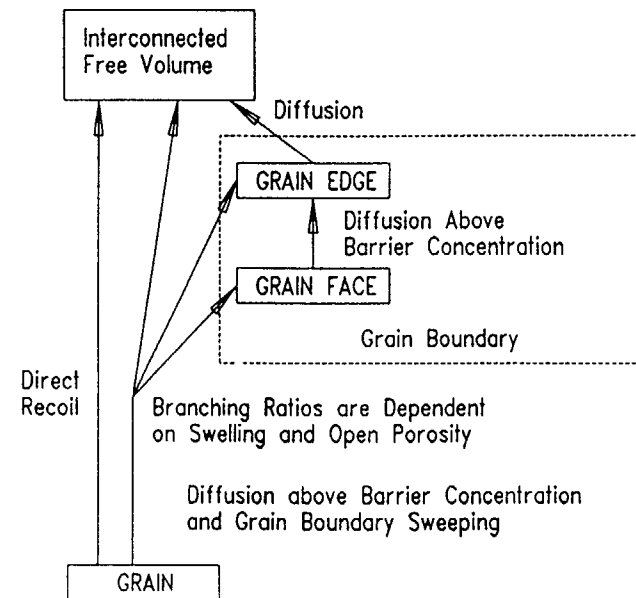


FIGURE 1. Fission gas release model

The phenomena incorporated into the high burnup gas release models are

- diffusion of fission gas from grain to grain boundary (grain face, grain edge and open porosity) controlled by a resolution barrier
- diffusion from grain face to grain edge controlled by a grain face saturation concentration
- release from the grain edge to interconnected free volume
- direct (recoil) release to open porosity
- grain boundary sweeping release due to grain growth or grain restructuring

Figure 1 presents in graphic form the process of fission gas release as it is envisioned to take place in  $UO_2$  fuel pellets up to high burnup. Diffusion, grain boundary sweeping and direct recoil are the major mechanisms which transfer fission gas out of  $UO_2$  grains.

#### 2.1.1 Diffusion From Grain to Grain Boundary

Fission gas is transferred from the grain interior to the grain boundary through diffusion. The resolution of fission gas accumulated at the grain boundary is simulated as a barrier resisting the escape of fission gas from the grains; the more fission gas that has been accumulated at the grain boundary, the greater the barrier. The barrier height is increased by high fission density and reduced by high diffusion rates. The modeling of diffusion and resolution effects is based on the work by Collins and Hargreaves<sup>(2)</sup>. The effective diffusion coefficient depends on the fission rate as modelled in the COMETHE code<sup>(3)</sup>.

A fission gas atom may reach the boundary of a grain at the grain face (area in contact with another grain), at the grain edge (area in contact with two other grains), or at the surface in direct contact with the free volume. The fraction of gas atoms that reaches the boundary at a grain edge is gaseous swelling dependent. The fraction that reaches the boundary at the area of interconnected free volume is open porosity dependent. The remaining fraction of fission gas atoms, that which crosses the grain boundary at the grain face area, remains at the grain face where the atoms may coalesce in fission gas bubbles. Assuming a tetrakaidecahedron fuel grain shape, Tucker<sup>(4)</sup> established a relationship between the volumetric swelling and the surface area coverage of grain edge porosity. The calculation of the probability of a fission gas atom reaching one of the three areas (branching ratio) follows Tucker's geometric concept and treats swelling and open porosity as grain edge bubbles.

#### 2.1.2 Diffusion From Grain Face to Grain Edge

As in White and Tucker's model<sup>(5)</sup>, grain face bubbles serve as intermediate storage sites for fission gas until a saturation limit is reached. The saturation limit concentration is dependent on the hydrostatic pressure on the fuel pellet or pellet fragments<sup>(5)</sup>. The external pressure on the fuel material is assumed to be equal to the sum of the compressive mean stress (mechanical stress from cladding and/or other pellet fragments) and the rod internal gas pressure. When the grain face saturation limit is exceeded, the excess gas diffuses from the grain faces to the grain edges.

#### 2.1.3 Release From Grain Edge

Fission gas transfer from the grain edge to the free volume is diffusion dependent. The diffusion length is open porosity and gaseous swelling dependent; the higher the open porosity or gaseous swelling, the shorter the diffusion length and the faster the release.

#### 2.1.4 Direct Recoil

Fission gas release due to direct recoil can occur in a thin surface layer of fuel adjacent to open porosity. The direct recoil model assumes that open porosity has a large radius of curvature compared to the range of fission fragments. With the assumption that the direction of fission fragments paths are isotropically oriented, one fourth of the fission gas atoms generated in the surface boundary layer of 10 microns thickness will intersect the surface and result in release<sup>(6)</sup>.

#### 2.1.5 Grain Boundary Sweeping

Grain boundary sweeping is based on the equiaxed grain growth model proposed by Ainscough, et al.<sup>(7)</sup> As the grain grows, the moving grain boundary sweeps all fission atoms in its path. A swept gas atom may reach the grain face, the grain edge, or interconnected open porosity when it reaches the grain boundary. The branching ratios of the swept gas atoms are the same as that for the diffusion process (described in the second paragraph of Section 2.1.1). The resistance to grain growth due to pinning of grain boundary by fission products is also considered<sup>(7)</sup>.

### 2.2 THERMAL CONDUCTIVITY MODEL

Fission products generated during irradiation affect the thermal conductivity of the fuel ( $UO_2$  plus fission products). The fission products and their effect on thermal conductivity are treated as if they were rare earth elements. Measured  $UO_2$ - $Gd_2O_3$  thermal conductivity data are used to calculate the fission product induced thermal conductivity degradation. Calculated fuel rod center line temperatures were benchmarked to achieve a best estimate representation of the available measured data.

### 2.3 RIM EFFECT MODEL

The accuracy of a diffusion controlled fission gas release model depends on an accurate calculation of fuel pellet temperature and, therefore, on a knowledge of the fuel thermal conductivity and the temperature profile from the pellet centerline to the pellet edge. Due to the rim effect discussed earlier, the fuel thermal conductivity will be affected and vary as a function of the pellet radius.

The RODEX computer code uses a two group fast running radial power and burnup profile model which has been described previously<sup>(8)</sup> to determine the rim effect and to calculate the burnup as a function of pellet radius.

The calculated burnup profile in conjunction with the thermal conductivity model described in Section 2.2 provides an accurate prediction of fuel temperature profile from pellet edge to pellet centerline up to high fuel burnup levels.

The High Burnup Effect Program (HBEP) found that high gas release occurred at high burnup pellet periphery. An empirical model published by HBEP was also included in the code.

### 3 VALIDATION RESULTS

#### 3.1 DATA BASE USED IN VALIDATION ANALYSIS

Measured postirradiation data from the High Burnup Effects Program (HBEP) have been used to validate the modified fuel performance code. Data is available for fuel with rod average burnups up to 70 MWd/kgU. In addition to end of life released fission gas to the rod free volume, the types of microstructure data used in validating the models include:

- EPMA (electron probe microanalysis) measured Xe data
- XRF (X ray fluorescence) measured Xe data
- EPMA measured Pu/U data
- EPMA measured Nd data

EPMA measures the Xe concentration in a small area of the fuel with a shallow penetration depth (<1 micron). XRF measures the Xe level to a greater depth (~20 microns). The EPMA measured Xe can be considered to represent the fission gas retained inside the fuel grains. The XRF measured value represents the "total" gas retained (inside the grain and in the grain boundary). Measurements have been made in various axial and radial regions in fuel rods. The computer code was validated for fuel regions that experienced different LHGRs and hence different temperatures. The dependence of the gas release model on temperature and operating conditions was validated.

TABLE 1 GAS RELEASE VALIDATION RESULTS FOR SEVERAL HBEP RODS

Rod ID	Rod Average Burnup [MWd/kgU]	Measured Gas Release [%]	Calculated Gas Release [%]
3 138	56	2.6	4.0
BSM 27	57	7.1	7.6
BK363	67	3.8	4.2
BK365	69	2.4	5.3

The rim effect is an important phenomenon that becomes more pronounced at high burnup. The radial distribution of the EPMA measured Pu to U ratio data is a good indicator of the rim effect. Comparison of the calculated Pu to U ratio with the measured Pu to U ratio as a function of pellet radius determines whether the computer code properly predicts the higher Pu generation near the pellet rim.

The EPMA measured Nd data is a good indicator of relative local burnup. The code was validated with the EPMA measured Nd data in various radial and axial regions. It evaluates whether the computer code properly calculates the pellet radial burnup profile.

#### 3.2 FISSION GAS RELEASE VALIDATION RESULTS

The modified fuel performance code has been validated against the measured rod release data. The calculated results agreed well with the measurements. As an example, Table 1 shows the validation results for several high burnup rods.

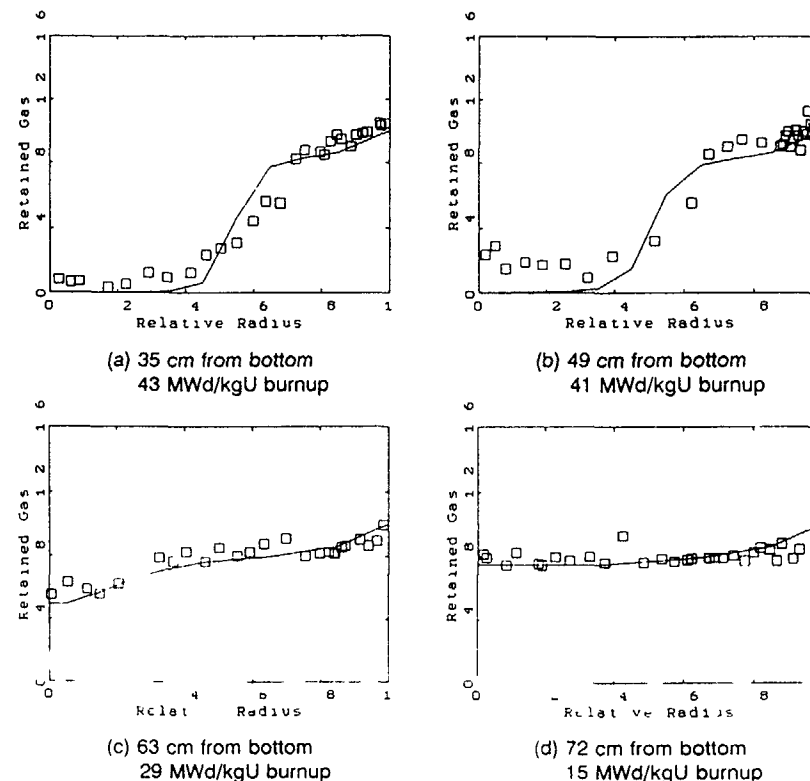


FIGURE 2 Validation results, EPMA measured Xe data for HBEP Rod 5D17-4

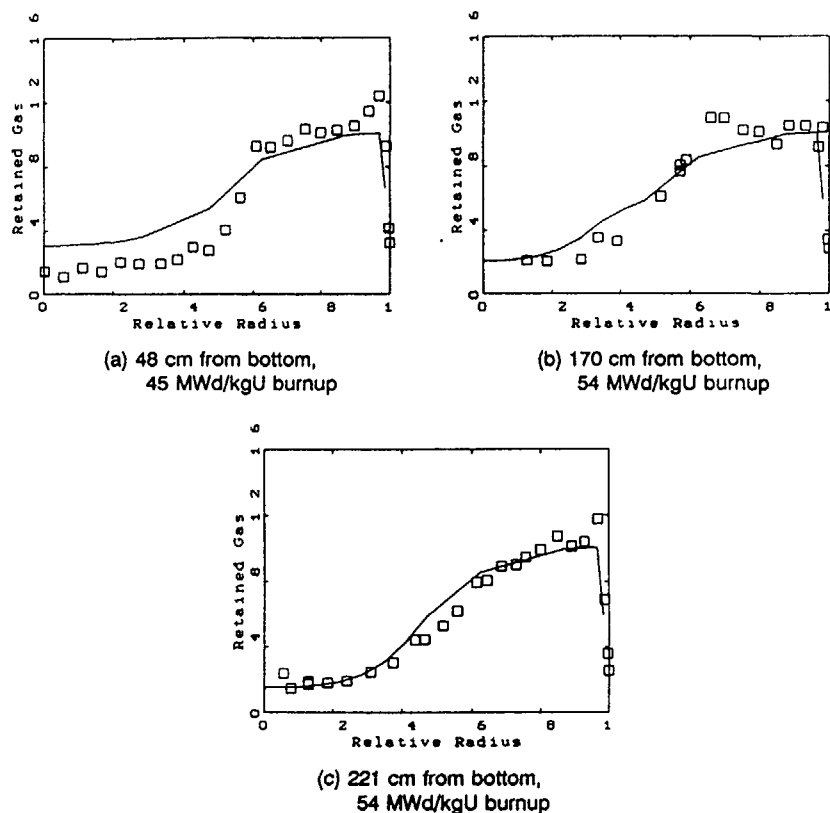


FIGURE 3. Validation results, EPMA measured Xe data for HBEP Rod H8-36-4.

### 3.3 RETAINED FISSION GAS VALIDATION RESULTS

#### 3.3.1 EPMA Xe Data

Figure 2 displays the validation results for HBEP rod 5D17-4. This BWR fuel rod had an end-of-life rod average burnup of 32 MWd/kgU. Curves in the figure present the calculated retained fission gas inside the grain, and the symbols present the EPMA measured Xe data. For the four axial regions where measurements were made, the code results agreed well with the EPMA measured retained fission gas as a function of radial profile. Different axial/radial fuel regions experienced different temperatures and LHGRs. The agreement between calculated and measured values confirms that the model has the correct temperature and LHGR dependence.

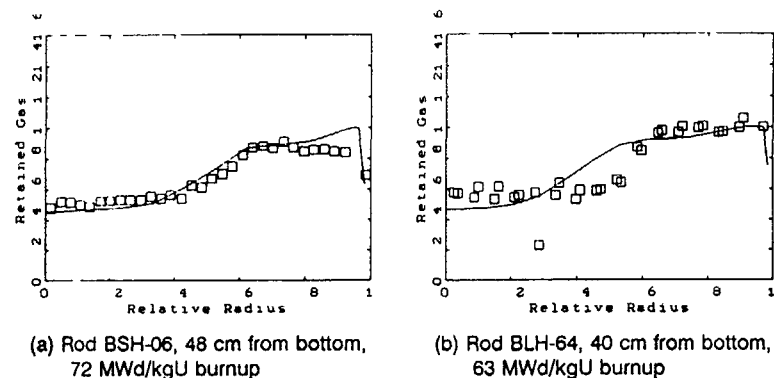


FIGURE 4. Validation results, XRF measured Xe data for HBEP rods BSH-06 and BLH-6X

Figure 3 shows the validation results for HBEP rod H8-36-4. This rod had a rod average burnup of 47 MWd/kgU. This figure also shows a good agreement between calculated and measured retained gas in various axial regions, and indicates that the model has the correct temperature and LHGR dependence.

#### 3.3.2 XRF Xe Data

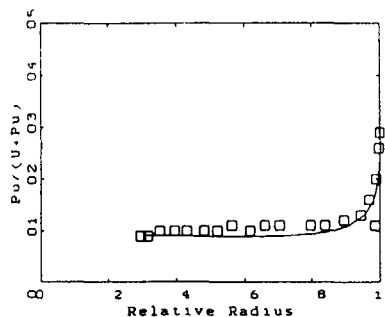
Figure 4 compares the calculated total retained gas (inside grain and in grain boundary) with the XRF measured Xe data. For both rods, BSH-06 and BLH-64, the code gave good predictions of the grain and grain boundary retained gas distribution. The rod average burnup for these rods was respectively 60 and 52 MWd/kgU.

### 3.4 VALIDATION RESULTS FOR PLUTONIUM AND URANIUM DATA

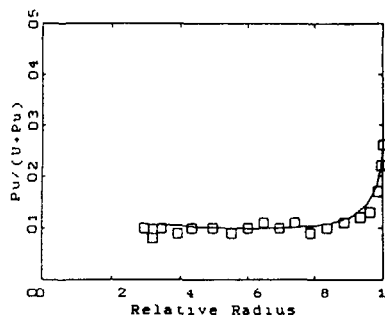
Figure 5 presents the predicted and measured Pu production as a function of pellet radius for HBEP rod BK365 with a rod average burnup of 69 MWd/kgU. This rod was chosen to be presented here because it contained the specimen which experienced the highest burnup among all HBEP data. Figure 5 plots the Pu/U ratio versus relative radial location. The measured Pu/U ratios are EPMA data. The code results agreed well with the measurements at three axial locations in the fuel rod. The model properly simulated the high Pu production near the pellet rim.

### 3.5 VALIDATION RESULTS FOR NEODYMIUM DATA

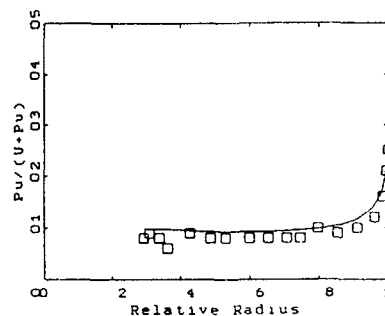
Figure 6 plots the calculated and measured radial burnup profiles for HBEP rod BK365. The measured burnup is determined through EPMA Nd data. The code gave good radial burnup profile predictions at all three axial locations. Figures 5 and 6 confirm that the code contains a reliable rim effect prediction model.



(a) 15 cm from bottom, 51 MWd/kgU burnup



(b) 46 cm from bottom, 85 MWd/kgU Burnup

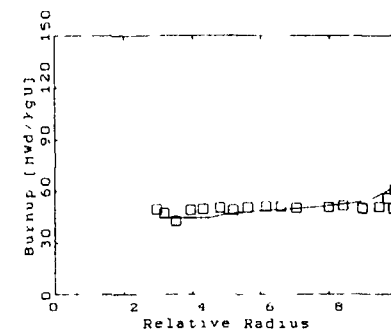


(c) 86 cm from bottom, 59 MWd/kgU Burnup

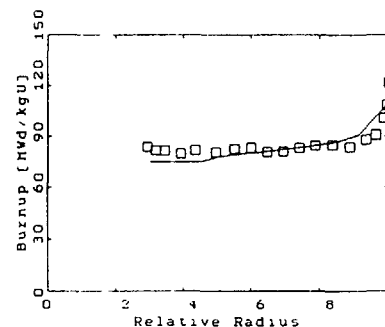
FIGURE 5. Validation results, EMA measured Pu/U data for HBE rod BK365

#### 4. CONCLUSION

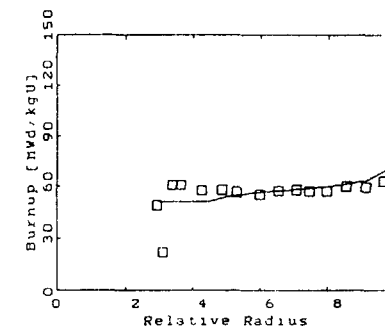
An SNP developed fuel performance code with its diffusion controlled fission gas release model was modified for use to high burnup. Modelling changes included a modification of fuel thermal conductivity, addition of the pellet rim effect, and modifications to the fission gas release model. Various aspects of the code were validated with the data obtained in the High Burnup Effects Program. The validation results indicate that the modified code accurately accounts for the fuel pellet rim effect and with a high degree of accuracy predicts the pellet burnup profile and fission gas release up to high burnup.



(a) 15 cm from bottom, 51 MWd/kgU Burnup



(b) 46 cm from bottom, 85 MWd/kgU Burnup



(c) 86 cm from bottom, 59 MWd/kgU Burnup

FIGURE 6. Validation results, EPMA measured Nd data for HBEP rod BK365.

#### REFERENCES

- [1] J O Barner, M E Cunningham, M D Freshley, and D D Lanning "Relationship between Microstructure and Fission Gas Release in High Burnup  $UO_2$  Fuel with Emphasis on the Rim Region," ANS/ENS International Topical Meeting on LWR Fuel Performance, Avignon, France 1991
- [2] D A Collins and R Hargreaves, "A Quantitative Model for Fission Gas Release and Swelling in Irradiated Uranium Dioxide," Journal of British Nuclear Energy Society, 15, 311 (1976)

- [3] R. Christensen, "SPEAR Fuel Reliability Code System, General Description" EPRI NP-1378, pp 5-21, 1980
- [4] M. O. Tucker, "A Simple Description of Interconnected Grain Edge Porosity" Journal of Nuclear Materials, 79, 199 (1979)
- [5] R. J. White and M. O. Tucker, "A New Fission Gas Release Model," Journal of Nuclear Materials, 118, 1 (1983)
- [6] D. R. Olander, "Fundamental Aspects of Nuclear Reactor Fuel Elements," TID-26711 P1, Section 15.3 (1976)
- [7] T. B. Ainscough, B. W. Oldfield, and J. O. Wave, "Isothermal Grain Growth Kinetics in Sintered UO<sub>2</sub> Pellets," Journal of Nuclear Materials, 49, 117 (1973)
- [8] S. H. Shann, K. R. Merckx, C. W. Lindenmeier, C. C. Lee, and A. H. Robinson, "A Two Group Radial Power Distribution Prediction Model," ANS/ENS International Topical Meeting on LWR Fuel Performance, Avignon, France, 1991

## DISCUSSION BETWEEN S.H. SHANN AND M. MOGENSEN

### S.H. Shann.

We appreciate the careful work and analysis by Mr. Mogensen et al. presented in the paper entitled "Fission Gas Release Below 20 kWm<sup>-1</sup> in Transient Tested Water Reactor Fuel at Extended Burnup". We would, however, like to point out the following observations that provide alternative explanations for the observed low power fission gas release in some ANF fuel rods as observed in the Risø tests:

- (1) The CB series fuel pins of the Risø-3 project had fuel with a grain size of 6 μm, which is very small (and incidentally atypical of current standard production) and much less than the grain size in the other rods tested. It is well known that small grain size fuel shows higher fission gas release than larger grain fuel at a given LHGR.
- (2) The paper stated that the gas released at lower power had been stored in larger pores (greater than 50 μm in size). A calculation has been performed to determine how much fission gas can be stored in these pores. The gas overpressure in bubbles as large as 50 μm is small. Even if it is assumed that big pores occupy 1% of the pellet volume (measured total porosity at mid-radius is 1.1%), and that the pores contain only Xe and Kr, and that all the pores are vented under transient, the calculation showed that, at most, these big pores can account for only 1.9% fission gas release, which is much less than the 5-7% claimed in the paper. The resulting pressure increase would be far smaller than that measured in the tests with refabricated rods.
- (3) The paper stated that rod CB11 was not refabricated and was submitted to a bump test up to 16.9 kW/m average power (20.4 kW/m peak power). The puncture gave a fractional fission gas release of 5.1%. Through an electron probe microanalysis (EPMA) study, C.T. Walker, B. Cremer, and W. Ziehl (European Institute for Transuranium Elements) determined that only 0.1% was released thermally in pellet centre, and that the majority of released gas was from pellet periphery or rim. They compared the EPMA of rod CB11 with that of low-release sibling rod CB7 (both rods fabricated by ANF) irradiated under the same conditions and determined that the two concentration profiles differ only by the xenon concentration in the rim zone. This is clearly shown in Figure 4 of the paper. Due to neutron self-shielding in the fuel pellet, pellet periphery experiences higher neutron flux than pellet centre. <sup>83</sup>Kr and <sup>131</sup>Xe have much higher thermal neutron absorption cross sections than <sup>84</sup>Kr and <sup>132</sup>Xe, respectively. Thus the CB11 puncture gas is expected to have lower <sup>83</sup>Kr/<sup>84</sup>Kr and <sup>131</sup>Xe/<sup>132</sup>Xe ratios than the puncture gas from all other tests in which thermally released gases were from the pellet centre region, which explains the observed isotope ratios reported in Table V of Mr. Mogensen's paper.

As already stated, the fuel of the CB series fuel pins was characterized by small grain size (6 μm) and a high as fabricated porosity. At burnups as high as 42,000 MWd/tm this gives a porous and loose structure of the fuel at the rim of the pellets. When submitted to even a moderate power transient up to a power higher than the end-of-life power, a high hoop stress in the pellet rim

(TEM study results of I.L.F. Ray, et al., European Institute for Transuranium Elements) can lead to cold creep of the fuel (small-grain fuel has higher creep than large-grain fuel) and to local release of the gas retained on the grain boundary.

### M. Mogensen:

We at Risø agree that other explanations of the low power release than the one given in our paper on "Fission Gas Release Below 20 Kw m<sup>-1</sup> in Transient Tested Water Reactor Fuel at Extended Burnup" might be possible.

There are, however, two important aspects which S.H. Shann has overlooked in his analysis. It is clearly explained in our paper like in Mr. Shann's comments that a lower Xe concentration in the rim zone in CB11-2, compared to the base irradiated pin, was not found in the fuel of all the other low power releasing pins which were also examined by EPMA. This means that this phenomenon is probably not associated with the low power release. Secondly, S.H. Shann in his discussion of the isotopic ratios overlooked the fact that the gas which had the highest ratios was not from the centre of the fuel, but from retained gas extracted by dissolving a full pellet size sample (see first line in Table V of our paper). This means that we still think that the explanation given in the paper is so far the best one.

Furthermore, the basis for S.H. Shann's statement that the gas overpressure in bubbles as large as 50 μm is small, is probably not generally true. The overpressure could be high or low depending on the mechanism and the circumstances causing the porosity.

Finally, we agree that it should be realized that the ANF fuel in the Risø-3 project was not of a standard type, and this was already clearly stated in Section 2 of our paper.

**LIST OF PARTICIPANTS**

**BELGIUM**

Mertens, L Fuel and Materials Division  
Belgonucléaire S A  
rue du Champ de Mars, 25  
B-1050 Bruxelles

**CANADA**

Boczar, P G AECL Research  
Chalk River Laboratories  
Chalk River, Ontario K0J 1J0

Carter, T J AECL - CRL, Station 63  
Chalk River Laboratories  
Chalk River, Ontario K0J 1J0

Cox, D S AECL Research  
Chalk River Laboratories  
Chalk River, Ontario K0J 1J0

Elder, P H AECL Research  
Chalk River Laboratories  
Chalk River, Ontario K0J 1J0

Fehrenbach, P J AECL Research  
Chalk River Laboratories  
Chalk River, Ontario K0J 1J0

Floyd, M R Ontario Hydro  
Attached to Chalk River Labs  
Chalk River, Ontario K0J 1J0

Hastings, I Atomic Energy of Canada Ltd  
(Chairman) 344 Slater Street  
Ottawa, Ontario K1A 0S4

Hu R Hydro Quebec  
6600, Cote-des Neiges, bureau 215  
Montreal Quebec H3S 2A9

Hunt, C E L AECL Research  
Chalk River Laboratories  
Chalk River Ontario K0J 1J0

Iglesias F Ontario Hydro  
700 University Avenue  
Location H11 E14  
Toronto Ontario M5G 1X6

**CANADA (cont )**

Lewis, B J Royal Military College of Canada  
Dept Chemistry & Chemical Eng  
Kingston, Ontario K7K 5L0

Liu, Z AECL Research  
Chalk River Laboratories  
Chalk River, Ontario K0J 1J0

Lucuta, P G AECL Research  
Chalk River Laboratories  
Chalk River, Ontario K0J 1J0

MacDonald, L AECL  
P O Box 1046, Station B  
270 Albert St  
Ottawa, Ontario K1P 5S9

Reid, P. Ontario Hydro  
700 University Avenue  
Location H11 E13  
Toronto, Ontario M5G 1X6

Richmond, W R AECL Research  
Chalk River Laboratories  
Chalk River, Ontario K0J 1J0

Tayal, M ACL - CANDU  
2251 Speakman Drive, AP2F4  
Mississauga, Ontario L5K 1B2

Verrall, R AECL Research  
Chalk River Laboratories  
Chalk River, Ontario K0J 1J0

Veeder, J AECL (CRL)  
Chalk River Laboratories  
Chalk River, Ontario K0J 1J0

Walker, J R AECL Research  
Chalk River Laboratories  
Chalk River, Ontario K0J 1J0

**DENMARK**

Mogensen, M Materials Department  
Risø National Laboratory  
DK-4000 Roskilde

**FINLAND**

Kelppe, S

Technical Research Centre  
of Finland VTT  
P O Box 208  
SF-02151 Espoo

**FRANCE**

Charles, M

Commissariat à l'Energie Atomique  
CENG/DTP-SECC  
BP 85X  
F-38041 Grenoble Cedex

Forat, C

FRAGEMA/  
FRAMATOME Nuclear Fuel Division  
10 rue Juliette Recamier  
F-69006 Lyon

Kapusta, B.

Commissariat à l'Energie Atomique  
CEA Centre d'Etudes de Saclay  
DMI/SETIC/LECR, Bat 460  
F-91191 Gif-sur-Yvette Cedex

Permezel, P

Electricité de France  
EDF/SEPTEN  
12/14 Avenue Dutriévoz  
F-69628 Villeurbanne Cedex

**GERMANY**

Manzel, R.

Siemens A.G., KWU Group  
Siemens AG, KWU BT4  
P O Box 3220  
D-8520 Erlangen, FRG

**JAPAN**

Aoki, T

Nuclear Power Engineering Center  
Nuclear Fuel Department  
Shuwakamiyacho Bldg 4-3-13  
Toranomon, Minato-ku, Tokyo, 105

Kamimura, K

Power Reactor and Nuclear  
Fuel Development Corporation  
4-33 Muramitsu  
Tokai-mura, Naka gun  
Ibaraki ken, 319-11

**JAPAN (cont )**

Kanazawa, H

Japan Atomic Energy Research Institute  
2-4 Shirakat-shirane  
Tokai-mura, Naka gun  
Ibaraki-ken, 319-11

Kitajima, S

Central Research Institute  
of Electric Power Industry  
11-1, Iwato Kita, 2-Chome  
Komae-shi, Tokyo 201

Kogai, T

Nippon Nuclear Fuel Development  
Co., Ltd  
Narita-cho, Oarai-machi  
2163 Higashi-Ibaraki-gun  
Ibaraki-ken, 311-13

Koizumi, S

Toshiba Corporation  
Nuclear Fuel Engineering Sec.  
ISOGO Nuclear Engineering Center  
8, Shinsugita-cho, Isogo-ku  
Yokohama, 235

Mori, K

Nuclear Fuel Industries Ltd  
930, Okaza-Noda, Kumatoricho  
Sennangun  
Osaka City, 550

Sasajima, H

Reactivity Accident Laboratory  
Japan Atomic Energy Research  
Institute  
Tokai Research Establishment  
2 4 Shirakata-shirane  
Tokai-mura, Naka-gun  
Ibaraki-ken 319-11

Yamawaki, M

Nuclear Engineering Research  
Laboratory  
University of Tokyo  
91 Shirakata, Tokai-mura  
Ibaraki-ken, 319-11

**KOREA, REPUBLIC OF**

Suk, Ho Chun

Heavy Water Reactor Fuel  
Development Department  
Korea Atomic Energy Research  
Institute (KAERI)  
P O Box 7  
Daeduk Danji Daejeon 305 353

**NORWAY**

Wiesenack W

OECD Halden Reactor Project  
P O Box 173  
N-1751 Halden**ROMANIA**

Arimescu, V I

AECL Research  
Chalk River Laboratories  
Chalk River, Ontario K0J 1J0

Gheorghiu, C

CRNL Ontario Canada  
Institute for Nuclear Research  
P O Box 78  
0300 Pitesti**RUSSIAN FEDERATION**

Novikov, V V

All-Union Scientific Research Institute  
of Inorganic Materials  
St Rogov 5  
123060 Moscow

Smirnov, A V

Research Institute of Atomic Reactors  
433510 Dimitrovgrad  
Ulyanovsk Region

Proselkov, V N

I V Kurchatov Institute of Atomic Energy  
Moscow**SPAIN**

Mendez-Martin, F J

CIEMAT  
Avda Complutense, 22  
E 28040 Madrid**SWEDEN**

In de Betou, J

Swedish Nuclear Power  
Inspectorate  
P O Box 27106  
S 102 52 Stockholm

Grapengiesser, B A

ABB Atom AB  
S 721 63 Vasteras

Grounes M

Studsвик Nuclear AB  
S 611 82 Nykoping**SWITZERLAND**

Nordstrom, L A

Paul Scherrer Institute  
CH 5232 Villigen**UNITED KINGDOM**

Howl, D A

British Nuclear Fuels plc  
Springfields Works, Salwick  
Preston, Lancashire PR4 0XJ

Rothwell J P

HSE - Nuclear Safety Division  
St Peters House  
Balliol Road  
Bootle, Merseyside  
L20 3LZ**UNITED STATES OF AMERICA**

Kjaer-Pedersen, N

S Levy Incorporated  
3425 South Bascom Avenue  
Campbell, CA 95008

Shann, S H

Siemens Nuclear Power Corporation  
2101 Horn Rapids Road  
P O Box 130  
Richland, Washington 99352**COMMISSION OF THE EUROPEAN COMMUNITIES**

Coquerelle, M

Commission of the European  
Communities  
Joint Research Centre  
Institute for Transuranium Elements  
Postfach 2340  
D-W 7500 Karlsruhe, Germany**INTERNATIONAL ATOMIC ENERGY AGENCY (IAEA)**Chantoin, P  
(*Scientific Secretary*)Division of Nuclear Fuel Cycle  
and Waste Management  
International Atomic Energy Agency  
Wagramerstrasse 5  
A-1400 Vienna  
P O Box 100  
Austria